UNCLASSIFIED

AD NUMBER
AD370030
CLASSIFICATION CHANGES
TO: **UNCLASSIFIED**
FROM: **SECRET//RESTRICTED DATA**
LIMITATION CHANGES
TO: **Approved for public release; distribution is unlimited.**
FROM: **Distribution authorized to U.S. Gov't. agencies and their contractors; Administrative/Operational Use; JAN 1962. Other requests shall be referred to Aeronautical Systems Division, Wright-Patterson AFB, OH 45433. Restricted Data.**
AUTHORITY
OSD/WHS memo dtd 17 Mar 2016; OSD/WHS memo dtd 17 Mar 2016

THIS PAGE IS UNCLASSIFIED

DEPARTMENT OF DEFENSE
WASHINGTON HEADQUARTERS SERVICES
1155 DEFENSE PENTAGON
WASHINGTON, DC 20301-1155

MAR 17 2016

MEMORANDUM FOR DEFENSE TECHNICAL INFORMATION CENTER
(ATTN: DTIC-OQ INFORMATION SECURITY)
8725 JOHN J. KINGMAN ROAD, SUITE 0944
FORT BELVOIR, VA 22060-6218

SUBJECT: OSD MDR Case 13-M-3705

We have reviewed the attached document in consultation with the Department of Energy and Department of the Air Force and have declassified it in full. If you have any questions please contact Mr. John D. Smith by phone at 571-372-0482 or by email at john.d.smith887.civ@mail.mil, john.d.smith887.civ@mail.smil.mil, or john.smith@osdj.ic.gov.

George R. Sturgis
Deputy Chief, Records and Declassification Division

Attachments:
1. MDR request w/ document list
2. Document 7

#7

DECLASSIFIED IN FULL
Authority: EO 13526
Chief, Records & Declass Div, WHS
Date: MAY 29 2015

DEPARTMENT OF ENERGY DECLASSIFICATION REVIEW

1ST Review Date: Oct 17, 2013	DETERMINATION (CIRCLE NUMBER(S))
Authority: ☐ DC ☒ DD	1. CLASSIFICATION RETAINED
Name: G W Brothers	2. CLASSIFICATION CHANGED TO: NSI
2ND Review Date: 10/24/2013	3. CONTAINS NO DOE CLASSIFIED INFO
Authority: DD	4. COORDINATE WITH:
Name: S. Fivozinsky	5. CLASSIFICATION CANCELED
	6. CLASSIFIED INFO BRACKETED
	7. OTHER (SPECIFY):

SECURITY MARKING

~~The classified or limited status of this report appl s to each page, unless otherwise marked.~~

~~Separate page printouts MUST be marked accordingly.~~

~~THIS DOCUMENT CONTAINS INFORMATION AFFECTING THE NATIONAL DEF ISE OF THE UNITED STATES WITHIN THE MEANING OF THE ESPIONAGE LAWS, T LE 18, U.S.C., SECTIONS 793 AND 794. THE TRANSMISSION OR THE REVELA ON OF ITS CONTENTS IN ANY MANNER TO AN UNAUTHORIZED PERSON IS PROHI TED BY LAW.~~

~~NOTICE: When government or other drawings, specifications or ther data are used for any purpose other than in connection with a efi-nitely related government procurement operation, the U. S. Gov rnment thereby incurs no responsibility, nor any obligation whatsoeve ; and the fact that the Government may have formulated, furnished, c in any way supplied the said drawings, specifications, or other data s not to be regarded by implication or otherwise as in any manner li ensing the holder or any other person or corporation, or conveying ar rights or permission to manufacture, use or sell any patented inventi n that may in any way be related thereto.~~

5 U.S.C §552
+

Office of the Secretary of Defense
Chief, RDD, ESD, WHS
Date: 29 MAY 2015 Authority: EO 13526
Declassify: X Deny in Full: ____
Declassify in Part: ____
Reason: ____
MDR: 13 -M- 3705

R-5
13-M-3705

370020

AD No.

DDC FILE COPY

355 | 5

(NASA CR OR TMX OR AD NUMBER) | (CATEGORY)

Page determined to be Unclassified
Reviewed Chief, RDD, WHS
IAW EO 13526, Section 3.5
Date: MAY 2 9 2015

DDC

VAN NUYS, CALIFORNIA

~~SECRET - Restricted Data~~
~~Atomic Energy Act of 1954~~

370030

AD No 370030
DDC FILE COPY

THE Marquardt CORPORATION

VAN NUYS, CALIFORNIA

~~SECRET - Restricted Data~~
~~Atomic Energy Act of 1954~~

115155

30 JANUARY, 1962

REPORT 5876

COPY NO. 52

(TITLE -- UNCLASSIFIED)
ANNUAL REPORT FOR 1961
NUCLEAR RAMJET PROPULSION SYSTEM
PROJECT PLUTO

Contract AF 33(616)-7857

28598

DECLASSIFIED IN FULL
Authority: EO 13526
Chief, Records & Declass Div, WHS
Date: MAY 2 9 2015

(11) DATE 30 Jan[redacted]962, (13) 346 p. (14) [redacted] 5876

Number of Pages: 346 and xviii

~~RESTRICTED DATA~~

~~THIS DOCUMENT CONTAINS RESTRICTED DATA AS DEFINED IN THE ATOMIC ENERGY ACT OF 1954. ITS TRANSMITTAL OR THE DISCLOSURE OF ITS CONTENTS IN ANY MANNER TO AN UNAUTHORIZED PERSON IS PROHIBITED.~~

~~SECRET RESTRICTED DATA~~

~~ATOMIC ENERGY ACT OF 1954~~

~~EXCLUDED FROM AUTOMATIC REGRADING: DOD DIR 5200.10 DOES NOT APPLY~~

(Title -- Unclassified)

(9) ANNUAL REP[redacted]T. [redacted] 1 Feb-31 Dec 61.

(6) NUCLEAR RAMJET PROPULSION SYSTEM

PROJECT PLUTO (U). (8)

[redacted] (15) AF 33(616)-7857

[redacted] AF-254 (16)

APPROVED BY

A. O. Mooneyham, Jr.

Senior Project Engineer,

Pluto Project

~~This document contains information affecting the National Defense of the United States within the meaning of the Espionage Laws ... in any manner to an unauthorized person is prohibited by law.~~

SECRET CONTROL

95

30

Register

Copy No. 5

~~SECRET RESTRICTED DATA~~

~~ATOMIC ENERGY ACT OF 1954~~

THE Marquardt CORPORATION

VAN NUYS, CALIFORNIA

28398

(218 350)

MAC A1798

Previous page was blank, therefore not filmed.

DATE (11) 30 January 1962, (13) 346 p. REPORT (14) 5876

Number of Pages: 346 and xviii

~~RESTRICTED DATA~~

~~THIS DOCUMENT CONTAINS RESTRICTED DATA AS DEFINED IN THE ATOMIC ENERGY ACT OF 1954. ITS TRANSMITTAL OR THE DISCLOSURE OF ITS CONTENTS IN ANY MANNER TO AN UNAUTHORIZED PERSON IS PROHIBITED.~~

~~SECRET RESTRICTED DATA~~

~~ATOMIC ENERGY ACT OF 1954~~

~~EXCLUDED FROM AUTOMATIC REGRADING; DOD DIR 5200.10 DOES NOT APPLY~~

(Title -- Unclassified)

(9) ANNUAL REPORT, 1 Feb-31 Dec 61.

(6) NUCLEAR RAMJET PROPULSION SYSTEM PROJECT PLUTO (U). (8)

~~Contract~~ (15) AF 33(616)-7857

~~Project~~ AF-254 (16)

APPROVED BY

A. O. Mooneyham Jr.
Senior Project Engineer,
Pluto Project

~~This document contains information affecting the National Defense of the [illegible] in any manner to [illegible] is prohibited by law.~~

SECRET Marquardt [illegible] 39.5 Register Copy No. 2 CONTROL

~~SECRET RESTRICTED DATA~~

~~ATOMIC ENERGY ACT OF 1954~~

28398

THE Marquardt CORPORATION

VAN NUYS, CALIFORNIA

(218 350)

MAC A1770

FOREWORD

This report is submitted in compliance with applicable paragraphs of Air Force Contract AF 33(616)-7857 for the period 1 February through 31 December 1961.

ABSTRACT

Results of studies conducted during the period 1 February through 31 December 1961 on Project Pluto are presented. A major portion of discussion is directed toward integration of the components of the propulsion system. Included are the results of studies involving mechanical design and structural analyses, performance evaluation, materials research, control system analysis, and facilities planning investigations.

(Unclassified Abstract)

CONTENTS

Previous page was blank, therefore not filmed.

ILLUSTRATIONS

ILLUSTRATIONS (Continued)

DECLASSIFIED IN FULL
Authority EO 13526
Chief, Records & Declass Div, WHS
Date: MAY 2 9 2015

ILLUSTRATIONS (Continued)

ILLUSTRATIONS (Continued)

ILLUSTRATIONS (Continued)

ILLUSTRATIONS (Continued)

ILLUSTRATIONS (Continued)

ILLUSTRATIONS (Continued)

TABLES

TABLES (Continued)

1.0 INTRODUCTION

The Marquardt Corporation, under U. S. Air Force Cont ct AF33 (616)-7857, is engaged in a program of applied research on nuclea ramjet propulsion systems (Project Pluto). This report summarizes tech ical progress for the period 1 February 1961 through 31 December 1961.

Under the provisions of the contract, Marquardt is respo ible for the technological advancement of propulsion system nonnuclear co ponents necessary to the ultimate design, development, and testing of a fli t prototype nuclear ramjet engine. Lawrence Radiation Laboratory, und AEC contract, has responsibility for development of a flight-worthy reacto An important program milestone was achieved in 1961 with the successf operation of the Tory IIA reactor. Designed and built by the Lawrence Radi ion Laboratory (LRL), the Tory IIA reactor achieved or surpassed all desig and test objectives, thereby establishing the feasibility of a high power den ty, high-temperature, air-cooled reactor. The flight-type reactor, design ed Tory IIC, is presently being fabricated by LRL and is scheduled for test g early in 1963.

As propulsion system contractor for the Air Force, Marq ardt's efforts during 1961 were directed toward establishing performance a d preliminary design of an integrated propulsion system based on the Tory I reactor.

Sufficient analytical and experimental data have been acc ulated to describe a propulsion system capable of fulfilling a prescribed Air Force mission (ADO-11). As evidence of the potential offered by the Pluto p opulsion system, the Air Force has elected in 1962 to pursue a program ai ed at early ground testing of a flight prototype engine--the first major step to rd the timely acquisition of a SLAM vehicle.

2.0 SUMMARY

Nuclear ramjet performance studies performed durin 1961 were published in the form of four performance bulletins, Performance ulletin No. 4 being an integral part (Section 3.3) of this summary report. The f st bulletin presented preliminary design point performance characteristics of . propulsion system (designated the Marquardt Model MA50-XCA) utilizing the ' ory IIC reactor. The second bulletin contained revised Model MA50-XCA rformance characteristics consistent with newly acquired Tory IIC reactor da . In addition, the second bulletin described the performance effects associa d with a 2500° F isothermal reactor wall temperature and the effects of inc asing the Tory IIC reactor diameter. The diameter scaling effects were use by the aerothermodynamics contractor to perform a first iteration of the reac r size necessary to perform the ADO-11 mission. The basic Model MA50-XC design point performance characteristics contained in the second bulletin listed he engine thrust as 39,700 pounds and the thrust coefficient as 0.200. For a isothermal wall, the thrust increased to 43,860 pounds and the thrust coefficie t went up to 0.221.

Performance Bulletin No. 3 was devoted to the perfor ance analysis of an engine capable of performing the ADO-11 mission. his propulsion system, with a reactor of increased diameter and decreased l gth, is identified as the Model MA50-XDA ramjet. The reactor diameter as increased from 57 to 63 inches, and 4 inches of the forward reflector and 4 i hes of the aft fueled core were removed. The net jet thrust of the system is), 000 pounds.

Performance Bulletin No. 4 represents a departure f m previous bulletins in that it is devoted to the prediction of potential perform ce gains achieved through reasonable advancements in Tory IIC technology. Advancements included modifications in basic Tory IIC geometry and changes in c sign criteria. Optimization of reactor length, reduction in the number of tie rods a change fuel element tube diameter, modification of the power profile, and n increase in the beryllia elastic thermal stress limit are among the effects vestigated. The most significant performance gains (up to 5 percent increase i thrust) were those resulting from changes in power profile and thermal stress l nits.

Exit nozzle model tests were successfully completed, with experimental data being obtained for forced convection and ejector type n zzles. Nozzle velocity coefficients greater than 0.98 were documented for ea nozzle configuration tested, thus verifying the value of 0.98 used in past perf rmance studies, and supporting the conviction that the Model MA50-XCA p formance characteristics are entirely realistic.

The aerodynamic coupling test, also successfully completed, ve -fied within 5 percent the calculated effects of imposed pressure profiles on reactor tube weight flow distributions. The effects of reactor-nozzle couplin length were documented, and data were obtained that substantiate the effectiv ness of the reactor as a flow straightener. On the basis of this test a slightly greater separation distance is required between reactor and nozzle.

The inlet model test program proceeded on schedule, up until m l- December 1961. Installation of the model in the Langley Field wind tunnel, originally scheduled for 18 December, was delayed by facility problems. Tw inlet configurations will be tested, the basic Pluto inlet and an alternate inlet mutually agreed upon by Marquardt and the aerothermodynamics contractor. Initial experimental data will become available about 1 February, 1962.

The mechanical and structural problems concerning the installa on and support of the reactor in a minimum diameter airframe have been investi gated both analytically and experimentally. The concept of a lateral support s- tem utilizing pre-loaded springs has been studied in the light of four differen spring configurations. High-temperature deflection and vibration tests were er- formed on Belleville and corrugated springs, and an analysis of reactor vibra tion modes was made to aid in the establishment of design criteria and the sp :- ification of input data for test programs. An experimental vibration test is under way to evaluate proposed engine-airframe lateral attachment systems. In these tests a full scale 10-inch thick, lateral section containing a simulated c re matrix, peripheral shell, and suspension system will be subjected to vibratic tests at typical operating temperatures (1300° F). The first system to be tes d utilizes corrugated springs. Initial test results should be available about 1 March, 1962.

In the area of propulsion system controls, emphasis has been placed on high-temperature actuator and electronic component development. Sixty hours of ambient temperature testing and 1 1/2 hours of high-temperatu e testing (1000° F) were accumulated on the 40-inch-stroke high-speed pneumat : actuator. Closed loop operation indicated satisfactory performance at air su ply pressures as low as 40 psia. A closed loop uncompensated frequency respon of 9 cps was obtained under ambient conditions. Compensating networks are being added to increase the frequency response to 15 cps.

Analyses were made of the dynamic response characteristics of ne nuclear instrumentation in the engine ground control system to provide basic information for reactor start up studies. It was indicated that no serious sta l- ity problems exist, and power can be increased from source level to 0.1 perc nt of full power with a step ln n command and an inverse period override.

Very promising results were obtained from the electr ics irradia-tion test performed in August 1961 at General Dynamics/Fort Wortl The magnetic amplifier circuits incorporating General Electric ZJ225 d des exhibi-ted good radiation resistance. One circuit operated satisfactorily t an integrated dose of 2×10^{15} nvt, a dose in excess of that expected during a typi il mission. On the strength of results obtained from this first irradiation test, set of second generation circuits and components was prepared for anothe irradiation test to be performed in January 1962. These second generation cir iits employ ZJ225 diodes that have been specially prepared and individually sel ted. The diodes were subjected to screening tests (including preliminary low vel gamma and neutron irradiation) to insure uniformity and maximum reliabil r. These circuits are expected to operate satisfactorily to integrated neutron osages well beyond requirements for Pluto applications.

Ground test facility studies have been aimed at the est olishment of facility performance and design criteria, the delineation of mini um facility requirements, and the assessment of the economies associated witl various air supply systems. Facility performance criteria have been revised t account for changes in engine test planning and facility utilization. Present em iasis points to the use of the facility for testing of flight engines only, with run- me capabil-ities based on simulation of maximum anticipated run time at full r ctor power. Sustained full power operation is assumed to occur for a maximum 90 minutes during the dash portion of the mission profile. This installed capal ity allows simulation of a complete mission trajectory in two separate test ru .

Facility cost estimates have been made for a variety air storage schemes and run times. A cost of $21.9 million is estimated for a ninimal facility capable of simulating a Mach 3.0 sea level dash of 90-minu duration. This facility is based on the use of underground air storage, a mini ium of ex-haust handling equipment, continuous vitiated air heating, and the s aring of certain Tory IIC facilities.

Phase I of the Underground Air Storage Experiment w concluded with the completion of the core drilling program and submittal to th AEC of final drawings and specifications for the experimental chamber. T core drilling program confirmed the existence of suitable rock structure it a point approximately 8500 feet east-southeast of the Tory test point. Tes chamber construction is scheduled to begin early in 1962.

DECLASSIFIED IN FULL
Authority: EO 13526
Chief, Records & Declass Div, WHS
Date: MAY 2 9 2015

3.0 PROPULSION SYSTEM DESIGN AND ANALYSIS

3.1 TORY IIC DESIGN DATA

The Marquardt Model MA50-XCA propulsion system present · being considered for nuclear ramjet application utilizes a Tory IIC type reacto . Responsibility for Tory IIC reactor development and testing is vested in the awrence Radiation Laboratory (LRL), prime contractor for the Atomic Energy Commission.

Information relative to the Tory IIC configuration, performa ce, materials, etc., has been published by LRL in the Tory IIC Data Book (Re erence 1). Data revisions are issued periodically by LRL and incorporated in pr pulsion system design and performance analyses.

Table 1 presents basic performance data for the Tory C reactor revised to 16 November 1961. It should be remembered that these da a are preliminary in nature. Continuing optimization studies in combination w h applicable experimental information will result ultimately in a firm reactor pecification.

3.2 PERFORMANCE ANALYSIS

3.2.1 Propulsion System Performance

Status

The Model MA50-XCA propulsion system incorporates a var ible geometry external-internal compression inlet, an S-shaped subsonic diffu r duct, the Tory IIC type reactor, and a fixed convergent-divergent exit nozzle. The design point Mach number is 2.8 at an altitude of 1,000 feet for the ANA Hot Day condition.

At the beginning of the year it was generally recognized that propulsion system incorporating the Tory IIC reactor would provide insufficient rust to propel a missile capable of performing the ADO No. 11 mission. In pril, a coordination meeting was held at Aeronautical System Division (ASD), yton, Ohio, for the purpose of defining mutually acceptable areas of responsibilit and investigation. At this meeting it was decided that the performance of a sy em utilizing Tory IIC reactor technology should be studied under what could be called Phase I. Tory IIC technology, including such items as reactor comp ent materials and fabrication techniques, structural concepts, maximum desi wall

TABLE 1

TORY IIC PERFORMANCE

Minimum total reactor assembly flow area		1060 sq in.
Fueled channel flow area	848.7 sq in.	
Tie rod peripheral channel flow area	13.3 sq in.	
Side reflector channel flow area	34.5 sq in.	
Standard tie rod flow area	28.3 sq in.	
Control tie rod flow area	11.7 sq in.	
Side support flow area	123.4 sq in.	
Fueled tube hole diameter		0.227 sq in.
Fueled channel L/D ratio (length includes forward and aft reflectors and 1 1/2-inch thick base block)		283
Missile condition simulated, Mach number at 1000 feet		2.8
Total reactor flow rate		1672 pps
Fueled tube flow rate (83.67%)	1399 pps	
Side reflector tube flow rate (1.48%)	25 pps	
Tie rod peripheral tube flow rate (1.14%)	19 pps	
Standard tie rod flow rate (4.67%)	78 pps	
Control tie rod flow rate (3.07%)	51 pps	
Side support annulus flow rate (5.97%)	100 pps	
Flow rate per fueled tube		0.067 pps
Average exit stagnation temperature		1987° F
Maximum fueled tube wall temperature		2500° F
Maximum fueled tube internal temperature		2564° F
Total reactor power		510 Mw
Power per fueled channel		23.88 Mw
Average fueled tube material power density*		21.9 Mw/cu
Maximum fueled tube material power density		26.19 Mw/c ft
Maximum volumetric power density*		12.31 Mw/c ft
Fueled tube entrance Mach number		0.215
Fueled tube exit Mach number		0.457
Fueled tube entrance stagnation temperature		946° F
Fueled tube exit stagnation temperature		2157° F
Fueled tube entrance stagnation pressure		322 psia
Fueled tube exit stagnation pressure**		230 psia
Stagnation pressure drop across reactor		92 psi
Expected reactor stagnation pressure loss		7.2%
Entrance loss	0.4%	
Tube offset loss	1.8%	
Exit loss	5.0%	
Fueled tube maximum thermal stress		15,200 psi

* Based on active core volume
** Not corrected for "Expected Reactor Stagnation Pressure Loss"

temperature, fuel element power density, and cooling airflows was t b pre-served under Phase I. To account for the inadequate thrust level, th reactor diameter would be allowed to grow to meet the mission requirements The aero-thermodynamics contractor stated that the missile-propulsion syster combination would be sized by about September 1961. Under Phase II, poten al performance gains to be realized through improvement of Tory IIC technol y were to be studied.

Phase I performance prediction of the propulsion system in rporating the Tory IIC type reactor was completed with the publication of the fi st three Performance Bulletins. Phase II is represented by Performance Bu etin No. 4, which is an integral part of this report.

Analytical Approach

Reactor neutronic, dimensional, and performance data have een taken wherever possible from the Tory IIC Data Book prepared by LRL. I rquardt IBM performance programs have incorporated this reactor informati n together with the inlet performance data of Figure 1 and the assumption of e-dimensional exit nozzle flow with a 98 percent velocity coefficient. The pr cedure has been to airflow-optimize the propulsion system to provide a maximu thrust per unit reactor frontal area at the design point for a maximum reactor ll temperature of 2500°F. Side support cooling airflow rate, as specified by RL, is collected at the exit of the pressure shell and passed through the nozzle oolant channels. The drag associated with the side support-nozzle combin on has been included in the net jet thrust. Engine installation drag, composed of nlet supersonic spillage drag, inlet bleed drag, and engine bypass drag necess ry for engine-inlet airflow matching, has been specified. By agreement, t airframe contractor will determine and account for the other installational dr items.

Performance Bulletin No. 1*

Performance Bulletin No. 1 contains the initial performanc analysis of the Model MA50-XCA propulsion system. In the course of the analy s it was necessary for Marquardt to generate input information on void fracti s and equivalent flow diameters of the front grid and side support sections s well as nuclear heat generation rates in nonnuclear components. These dat vere not contained in the Tory IIC Data Book at that time. At the design poin a net jet thrust coefficient of 0.195 was determined. The net jet thrust coeffi ent-minus-inlet bleed drag was found to be 0.173, or within 1.2 percent of the I L value.

*Reference 2.

ESTIMATED PERFORMANCE OF BASIC INLET FOR MA50-XCA ENGINE

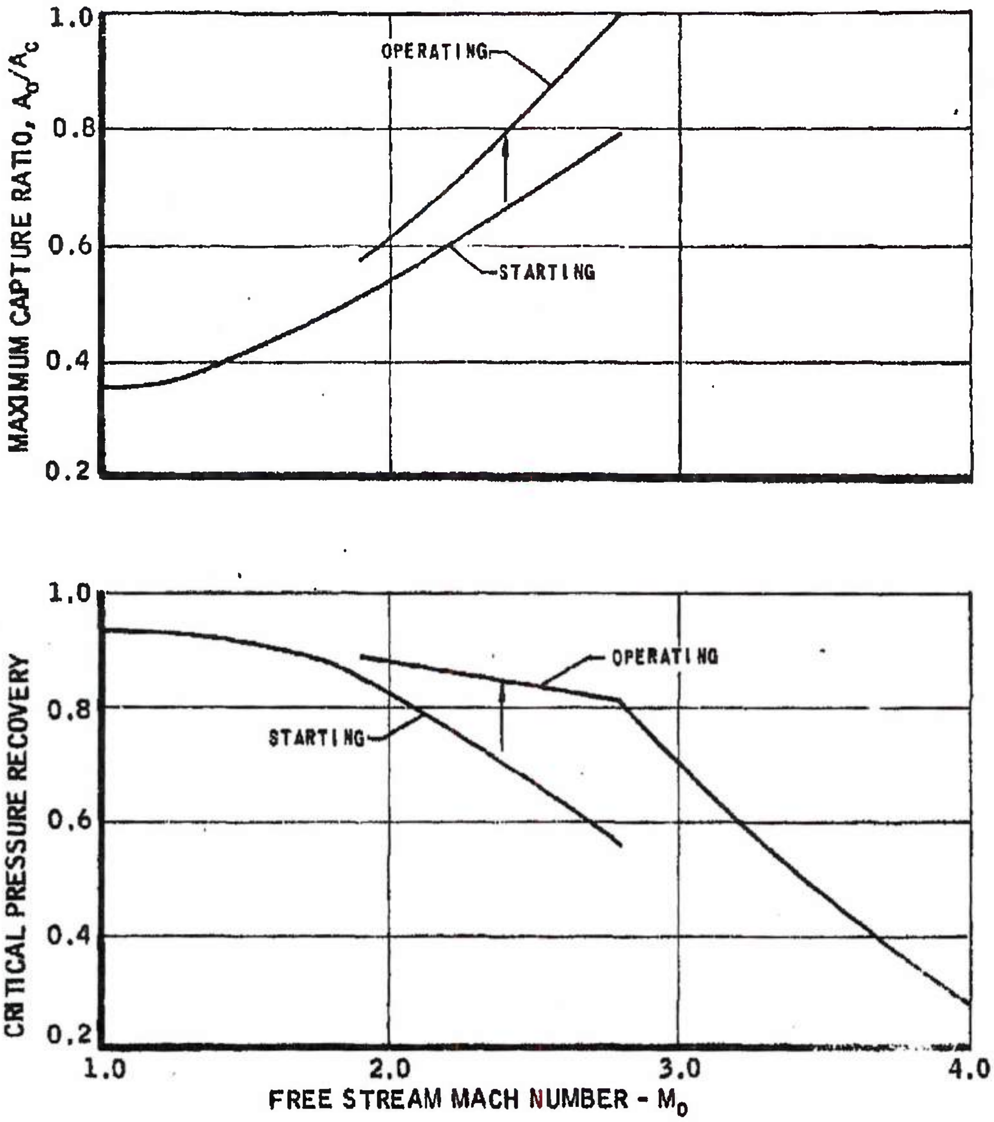

Performance data on jet thrust coefficient, reactor thermal · ·wer, inlet pressure recovery and airflow ratio, and installed drag were determi ·d for a range of day conditions at an altitude of 1,000 feet and for the Standar Day condition at 30,000 feet. These data are included in Figures 2 through 9. The effect of inlet pressure recovery on the net jet thrust coefficient was tablished for Standard Day conditions and is presented in Figures 10 and 11. Near the design point, a 1.7 percent change in thrust coefficient per percent ch nge in pressure recovery is indicated for the Model MA50-XCA propulsion s stem.

Included in the bulletins was a brief study of the performance gains to be realized by raising the reactor wall temperature above the present 25 0°F design point. Two analyses were conducted, one in which only the reactor te nperature was changed and the other in which the inlet and exit were resized for he higher temperature. In Figure 12, the maximum reactor wall temperature as increased 200°F while maintaining the Model MA50-XCA sized inlet and exit areas. At Mach numbers below 2.87 the inlet is forced to operate subcritical . In Figure 13 the inlet and exit were resized for the higher temperature These data indicate a 6.5 percent change in thrust coefficient per 100°F cha e in reactor wall temperature. These studies, while bordering on Phase II, vere meant only to indicate performance trends. LRL has not as yet indicated co currence in temperatures greater than 2500°F.

Performance Bulletin No. 2*

With receipt of the revised Tory IIC Data Book, input inform tion became available on side support, void fraction, and equivalent flow hydraulic diameter as well as nuclear heat generation in nonnuclear components. Using this new information, the performance predictions for the Model MA50-XCA propul on system were revised and published in Performance Bulletin No. 2. The desi . point aero-thermodynamic performance characteristics are compared in Table 2. The first column indicates the performance of the Model MA50-XCA syste as determined in Performance Bulletin No. 1. The second column contains d a from Performance Bulletin No. 2. It can be seen that the inputs from the revi d Tory IIC Data Book resulted in relatively small changes. The net jet thrust co fficient increased from 0.195 to 0.200. This change in performance was due p ncipally to a revision of the momentum drag losses in the side support-nozzle sy em.

At the request of the aerothermodynamics contractor, the se ond bulletin extended the altitude performance data for the Standard Day condit n. These data, presented in Figures 14 and 15, are based on the same assun tions as those presented in Performance Bulletin No. 1. At the request of the aerothermodynamics contractor, the effect of scaling the Tory IIC reactor to lar r diameters

*Reference 3

~~SECRET RESTRICTED DATA~~
~~ATOMIC ENERGY ACT OF 1954~~

ESTIMATED THRUST COEFFICIENT OF MA50-XCA RAMJET
AT ALTITUDE OF 1000 FEET
MAXIMUM WALL TEMPERATURE = 2960°R

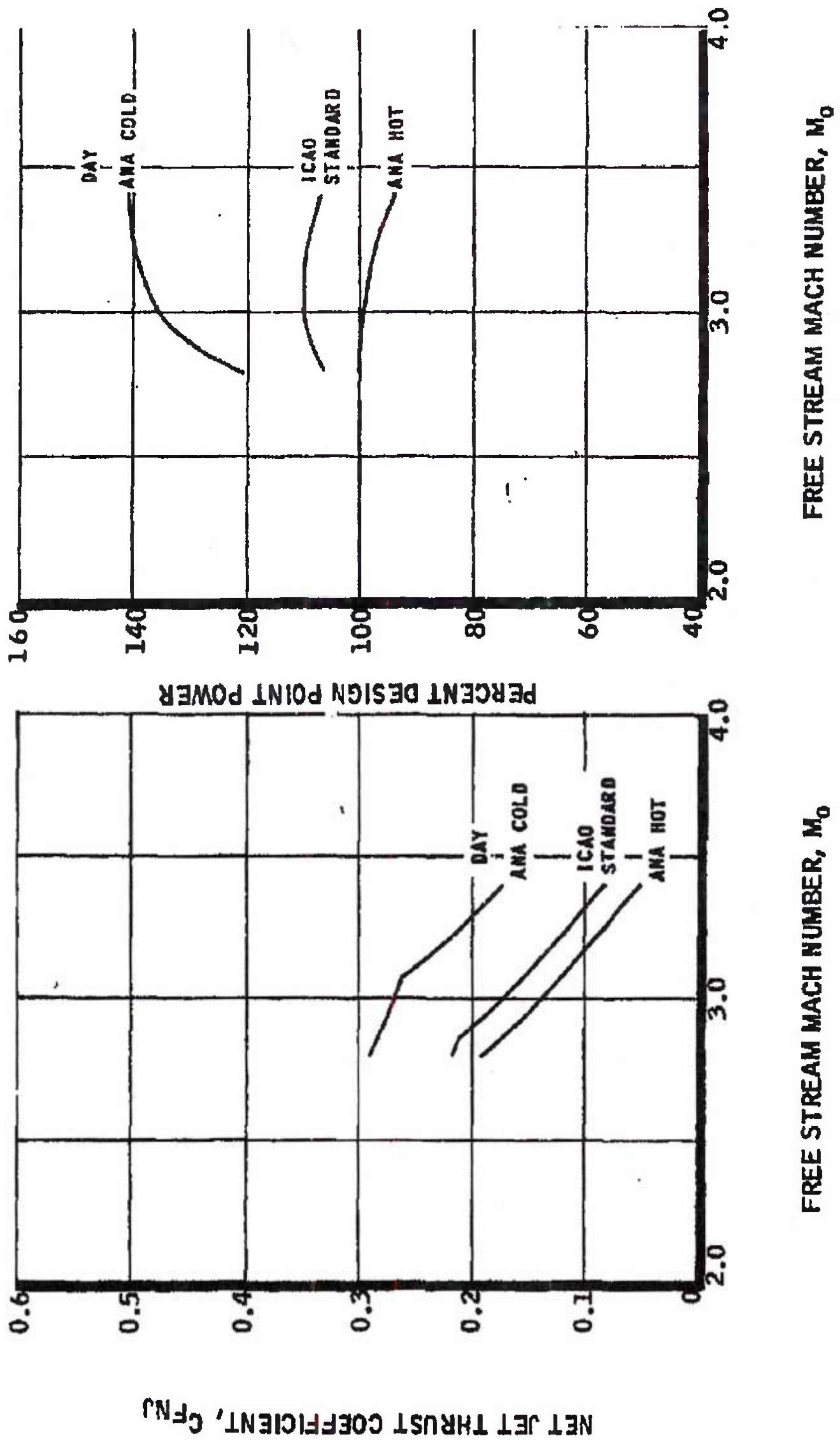

~~SECRET RESTRICTED DATA~~

ESTIMATED THRUST COEFFICIENT OF MA50-XCA RAMJET
AT ALTITUDE OF 30,000 FEET
MAXIMUM WALL TEMPERATURE = 2960°R

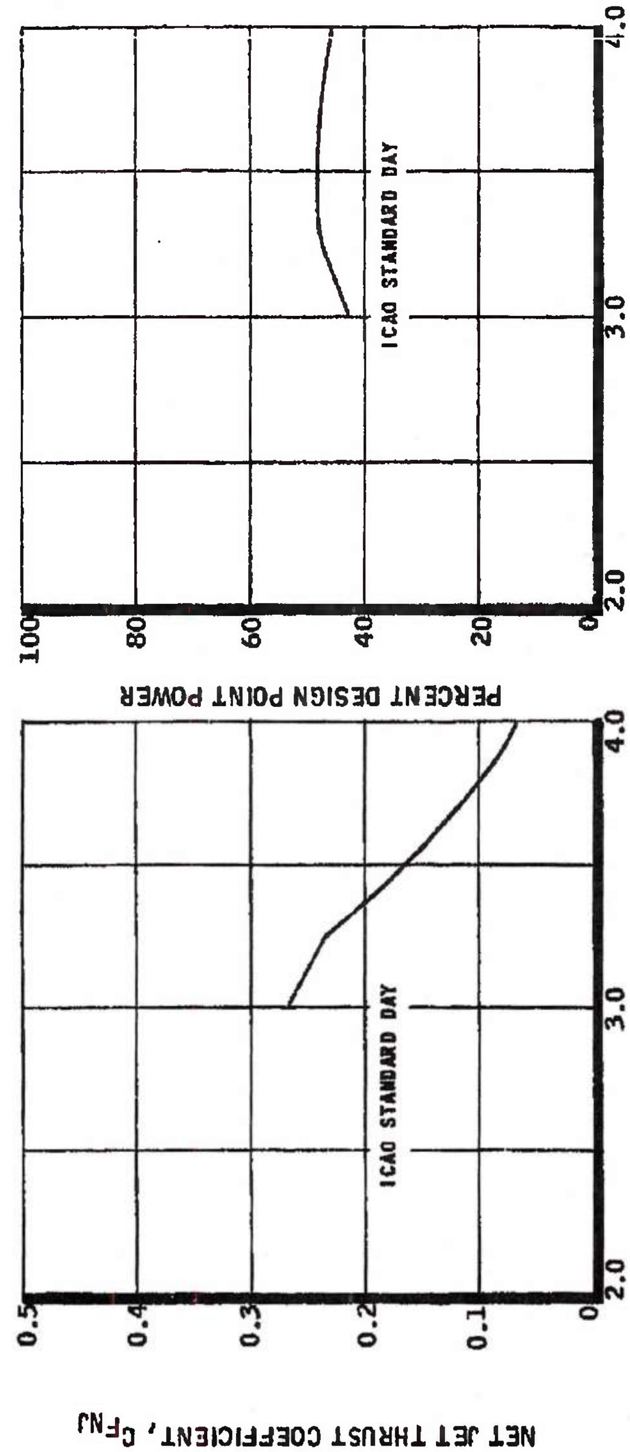

FIGURE 3

INLET PRESSURE RECOVERY OF MA50-XCA RAMJET
AT ALTITUDE OF 1000 FEET
MAXIMUM WALL TEMPERATURE = 2960°R

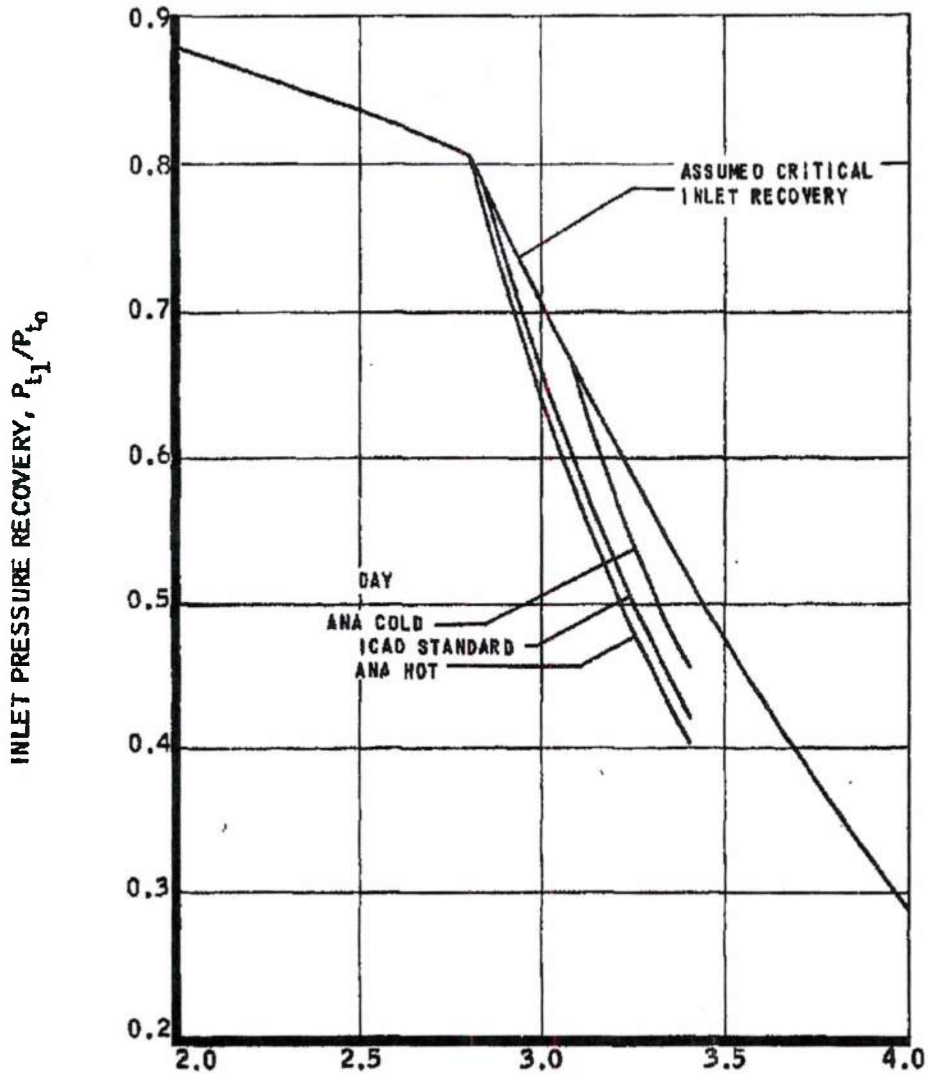

FREE STREAM MACH NUMBER, M_0

INLET PRESSURE RECOVERY OF MA50-XCA RAMJET AT

ALTITUDE OF 30,000 FEET

MAXIMUM WALL TEMPERATURE = 2960°R

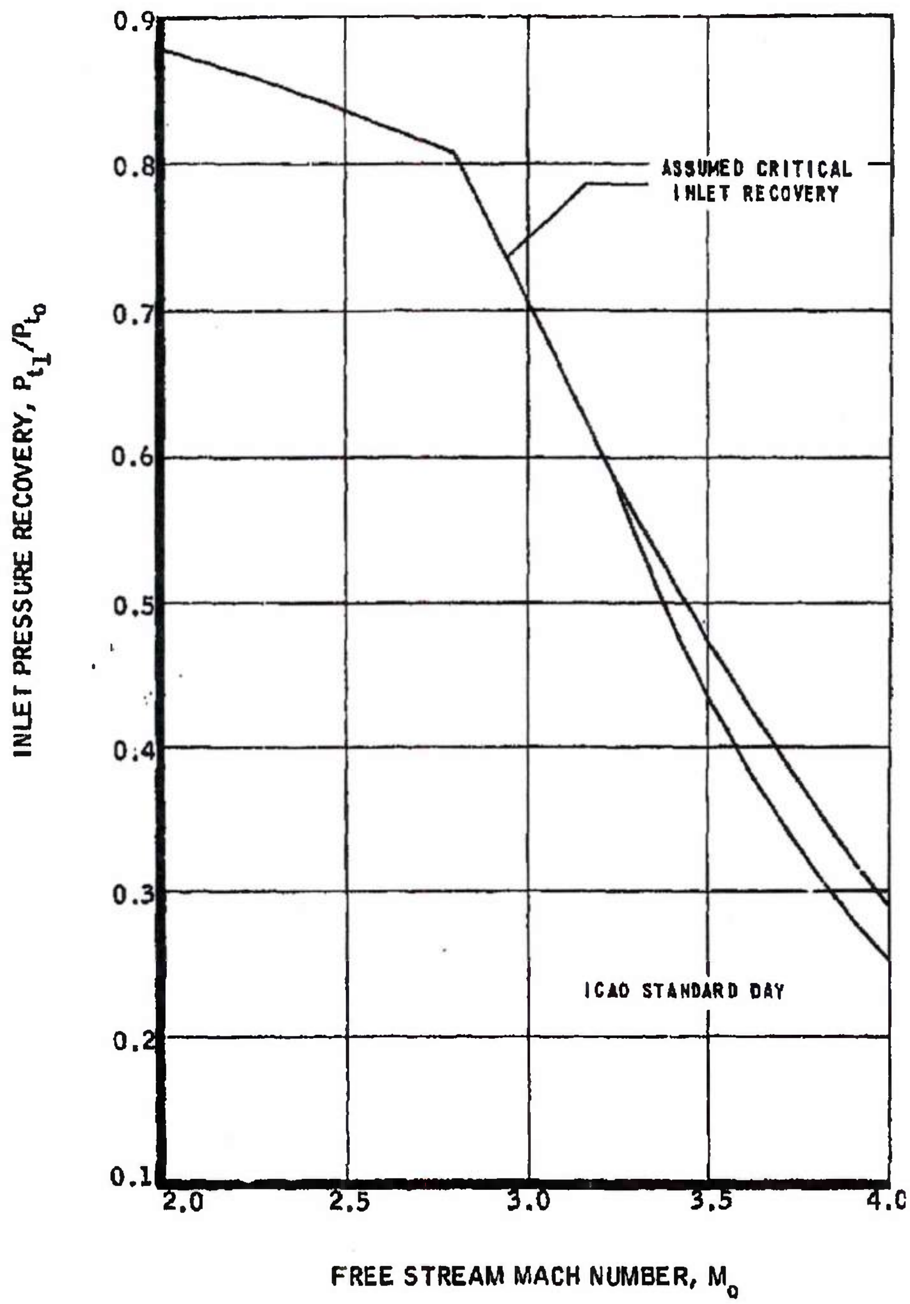

FREE STREAM CAPTURE AREA RATIO OF MA50-XCA RAMJET
AT ALTITUDE OF 1000 FEET
MAXIMUM WALL TEMPERATURE = 2960°R

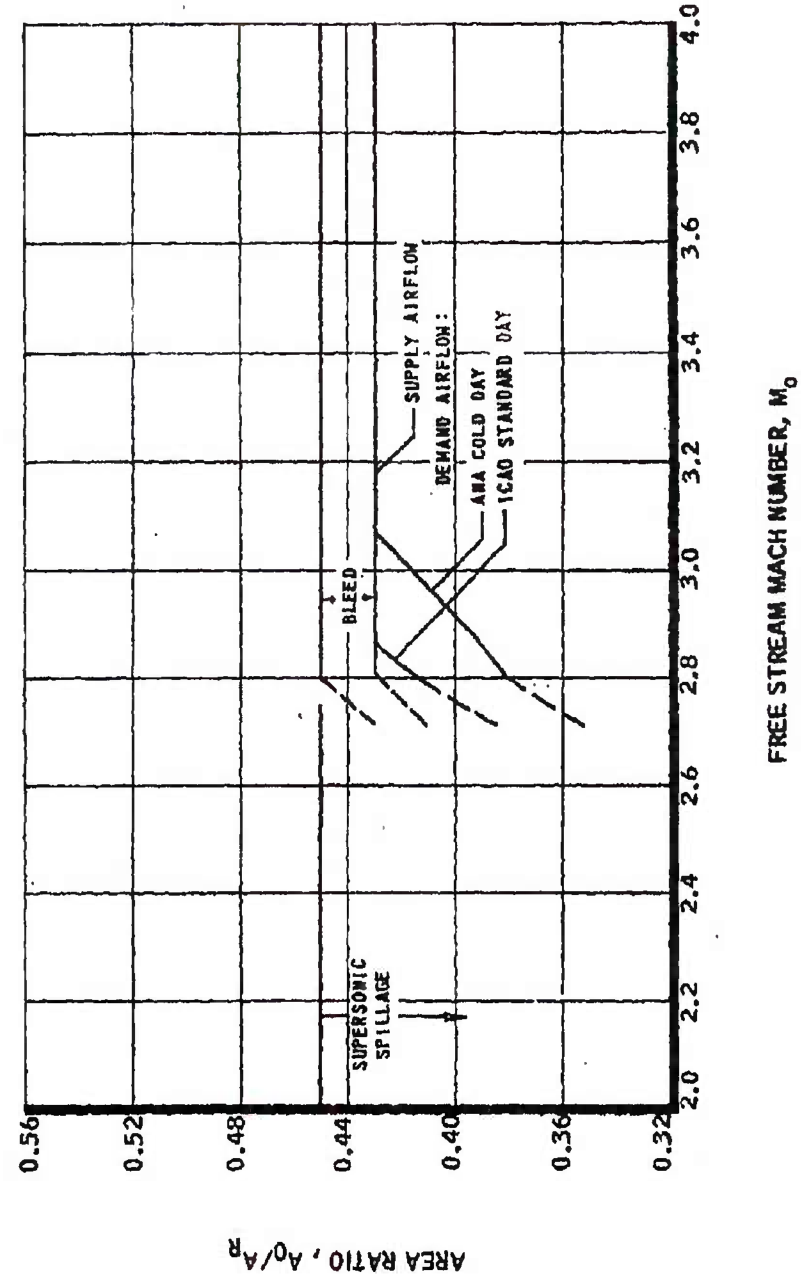

THE Marquardt CORPORATION
VAN NUYS, CALIFORNIA

~~SECRET RESTRICTED DATA~~
~~ATOMIC ENERGY ACT OF 1954~~

ORT 5876

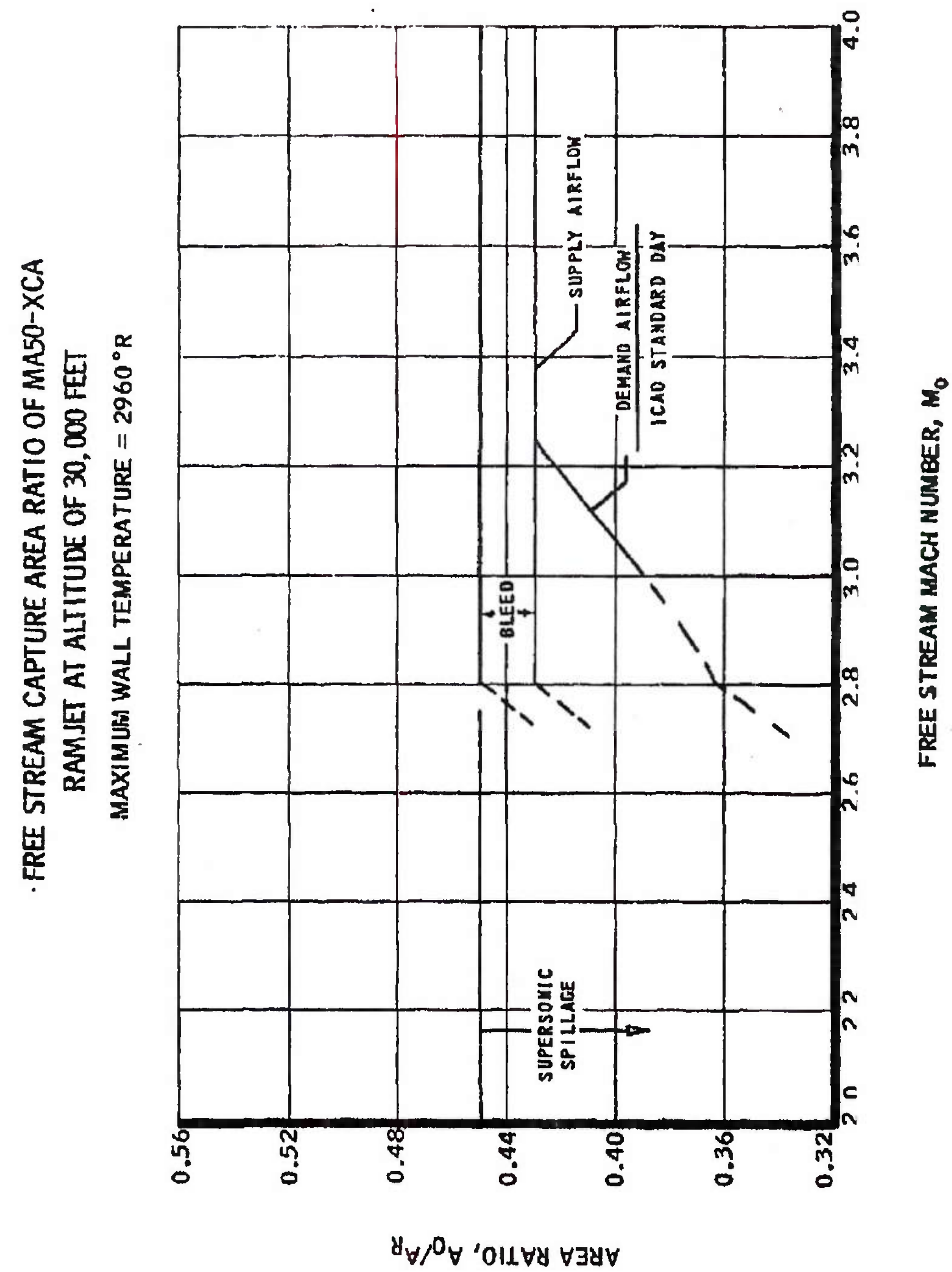

~~SECRET RESTRICTED DATA~~

N22E372 ~~ATOMIC ENERGY ACT OF 1954~~ FIGURE 7

DRAG OF MA50-XCA RAMJET ENGINE INSTALLATION
AT ALTITUDE OF 1000 FEET

MAXIMUM WALL TEMPERATURE = 2960°R

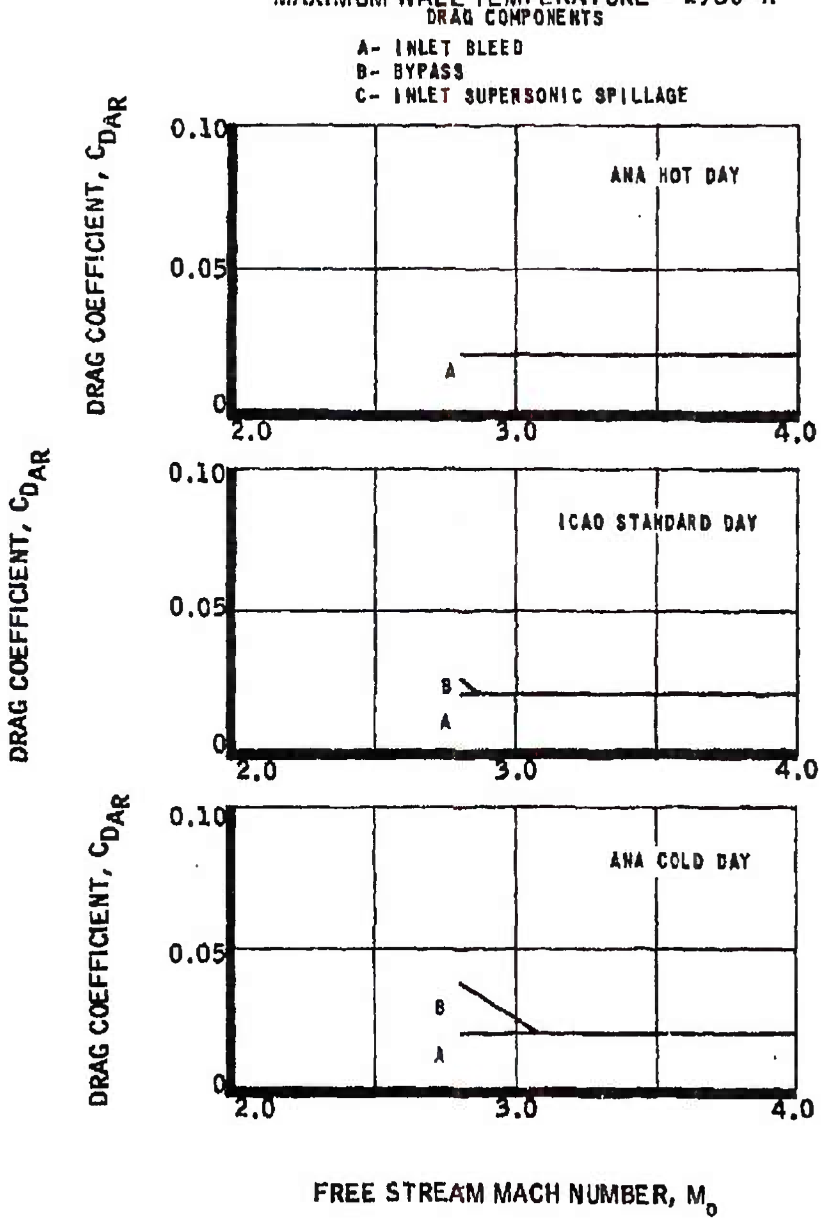

DRAG OF MA50-XCA RAMJET ENGINE INSTALLATIO AT
ALTITUDE OF 30,000 FEET

MAXIMUM WALL TEMPERATURE = 2960°R

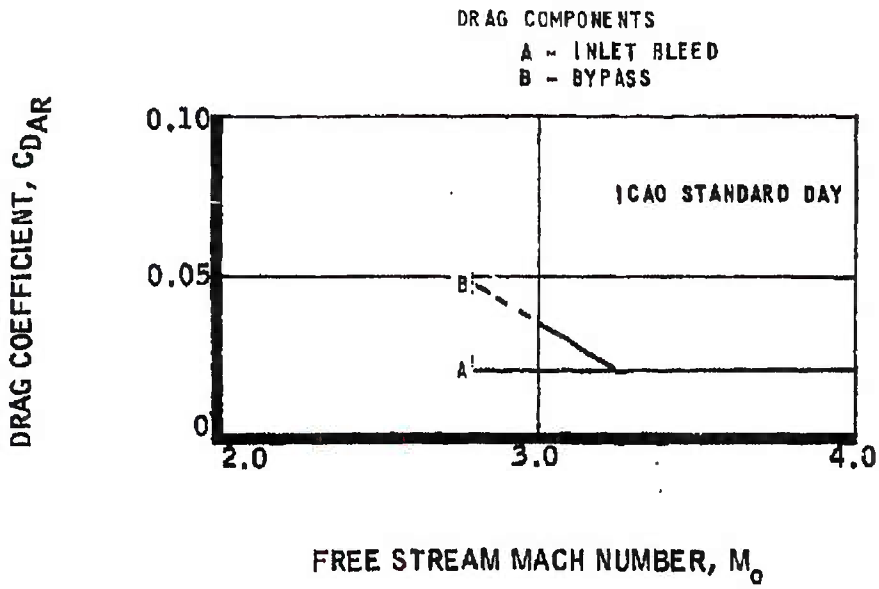

EFFECT OF INLET PRESSURE RECOVERY OF MA50-XCA RAMJET

AT ALTITUDE OF 1000 FEET

MAXIMUM WALL TEMPERATURE = 2960°R

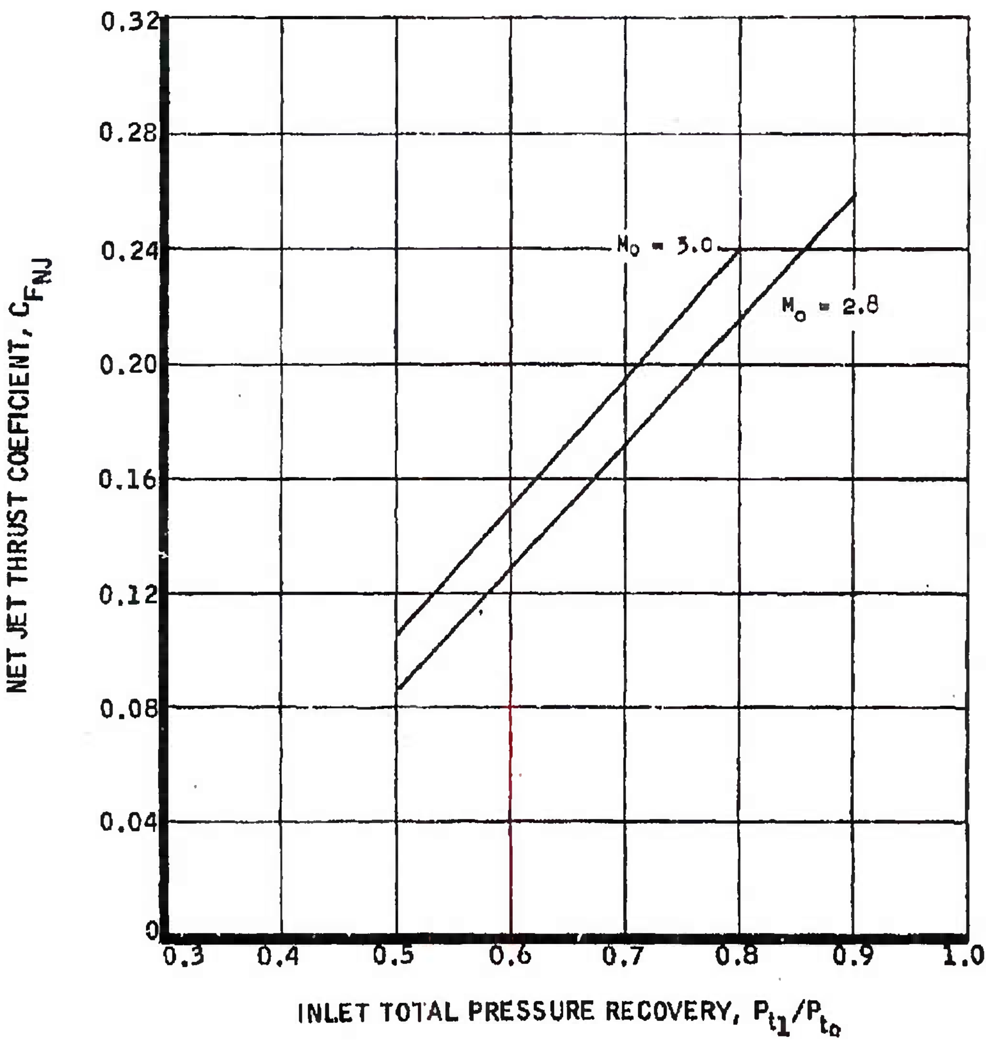

EFFECT OF INLET PRESSURE RECOVERY OF MA50-XCA RAMJET

AT ALTITUDE OF 30,000 FEET

MAXIMUM WALL TEMPERATURE = 2960°R

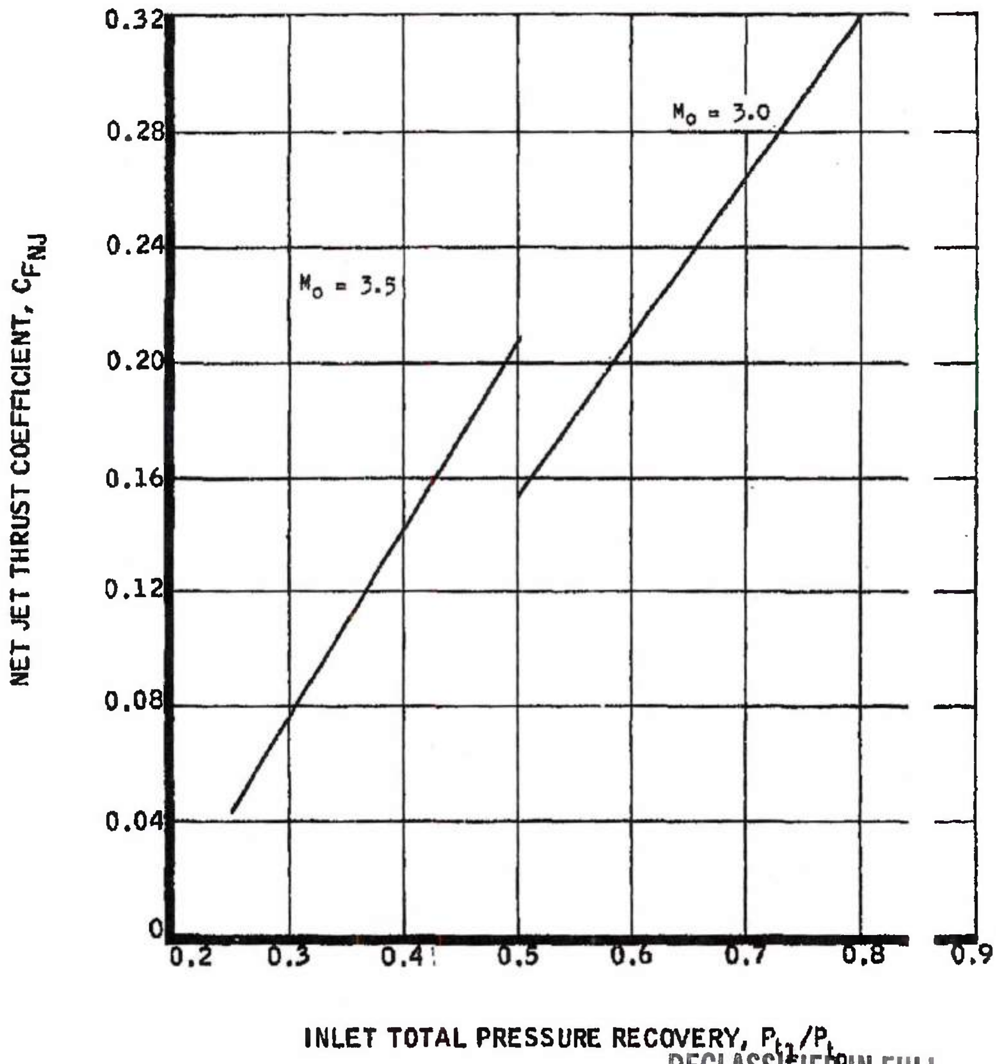

DECLASSIFIED IN FULL
Authority: EO 13526
Chief, Records & Declass Div, WHS
Date: MAY 2 9 2015

~~SECRET RESTRICTED DATA~~
~~ATOMIC ENERGY ACT OF 1954~~

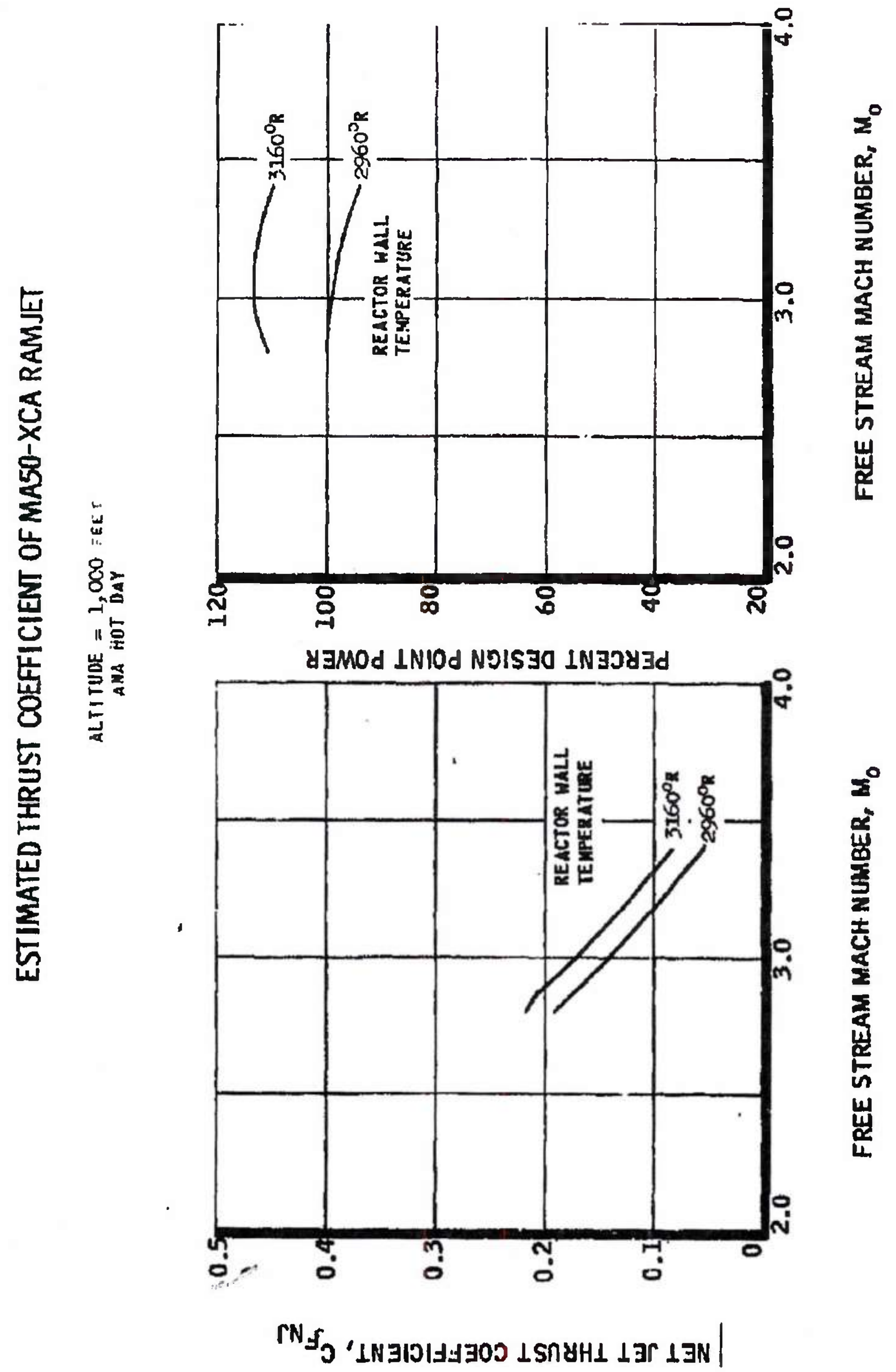

~~SECRET RESTRICTED DATA~~

~~SECRET RESTRICTED DATA~~
~~ATOMIC ENERGY ACT OF 1954~~

EFFECT OF WALL TEMPERATURE ON NET JET THRUST COEFFICIENT AT DESIGN POINT

NOTE: A. OPTIMIZED INLET AND EXIT
B. TORY IIC - 1 REACTOR SCALED TO 3160°R. (DIFFERENTIAL NEUTRONIC EFFECTS BETWEEN T_W = 2960°R TO T_W = 3160°R NOT INCLUDED)

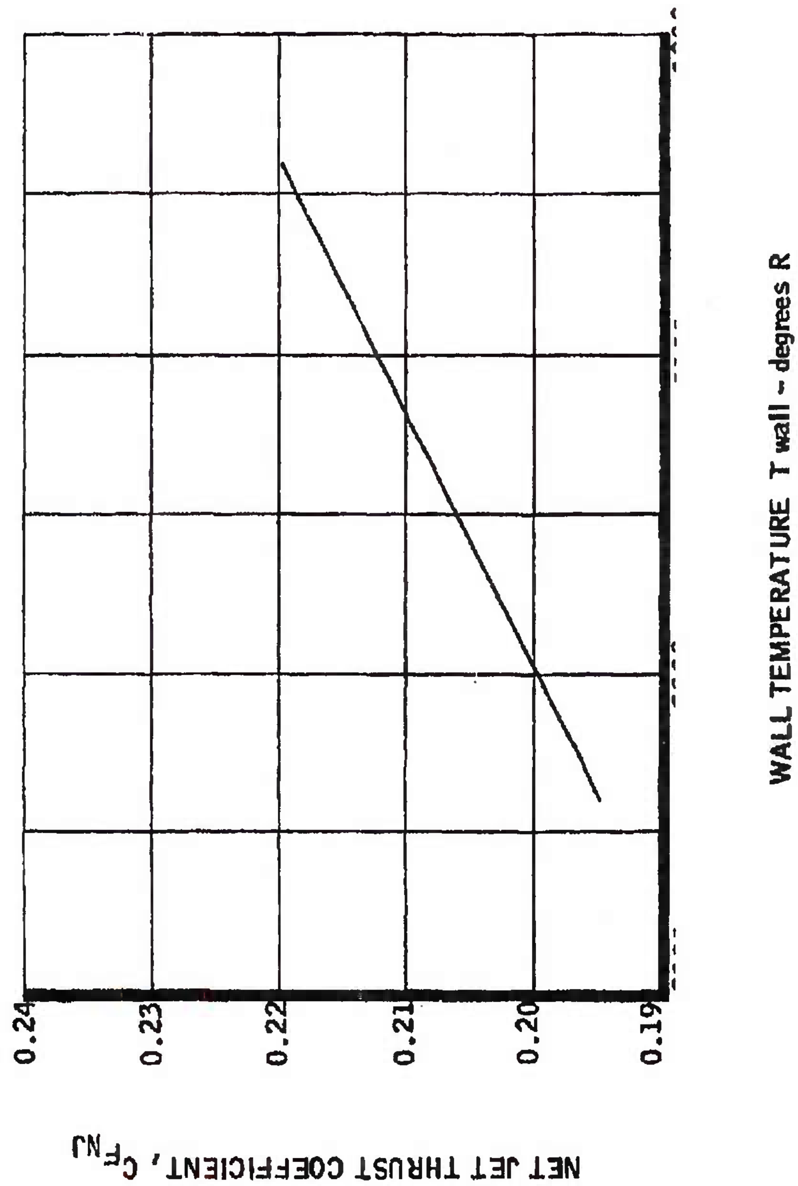

~~SECRET RESTRICTED DATA~~
~~ATOMIC ENERGY ACT OF 1954~~

TABLE 2

COMPARISON OF AEROTHERMODYNAMIC PERFORMANCE CHARACTERISTICS AT THE DESIGN POINT

(Mach 2.8; ANA Hot Day Temperature; Altitude, 1000 feet)

Parameter	MA50-XCA	MA50-XCA (Revised)	MA50-[illegible]CA (Isother[illegible]al)
Reactor Air Flow, W_a, lb/sec	1,577	1,577	1,53[illegible]
Side Support Cooling Air Flow, W_{a_c}, lb/sec	113	113	11[illegible]
Inlet Total Pressure, P_{t_o}, psia	393	393	39[illegible]
Inlet Total Temperature, T_{t_o}, °R	1,402	1,402	1,40[illegible]
Inlet Recovery, P_{t_1}/P_{t_o}	0.807	0.807	0.80[illegible]
Core Inlet Mach Number, M_3	0.23	0.23	0.2[illegible]
Core Tube Diameter, ft	0.0189	0.0189	0.018[illegible]
Maximum Core Wall Temperature, T_w, °R	2,960	2,960	2,96[illegible]
Total Reactor Power, Q, Mw	518	518	568
Reactor Ceramic Average Void Fraction	0.416	0.416	0.41[illegible]
Reactor Exit (mixed) Total Temperature, T_{t_4}, °R	2,522	2,520	2,65[illegible]
Reactor Pressure Recovery, P_{t_4}'/P_{t_1}	0.678	0.678	0.671
Reactor Diameter, D_R, in.	57	57	57
Reactor Length, L_R, in.	62.7	62.7	62.7
Reactor Area, A_R, ft^2	17.72	17.72	17.72
Nozzle Throat Area, A_5, ft^2	4.94	4.94	4.97
Nozzle Exit Area, A_6, ft^2	12.74	12.74	12.86
Cowl Area, A_c, ft^2	7.97	7.97	7.78
Exhaust Nozzle Velocity Coefficient, C_V	0.98	0.98	0.98
Thrust Coefficient, $C_{F_{A_R}}$ (Full Expansion)	0.195	0.200	0.221
Thrust, F, (Full Expansion), lb	38,640	39,700	43,860

~~SECRET RESTRICTED DATA~~
~~ATOMIC ENERGY ACT OF 1954~~

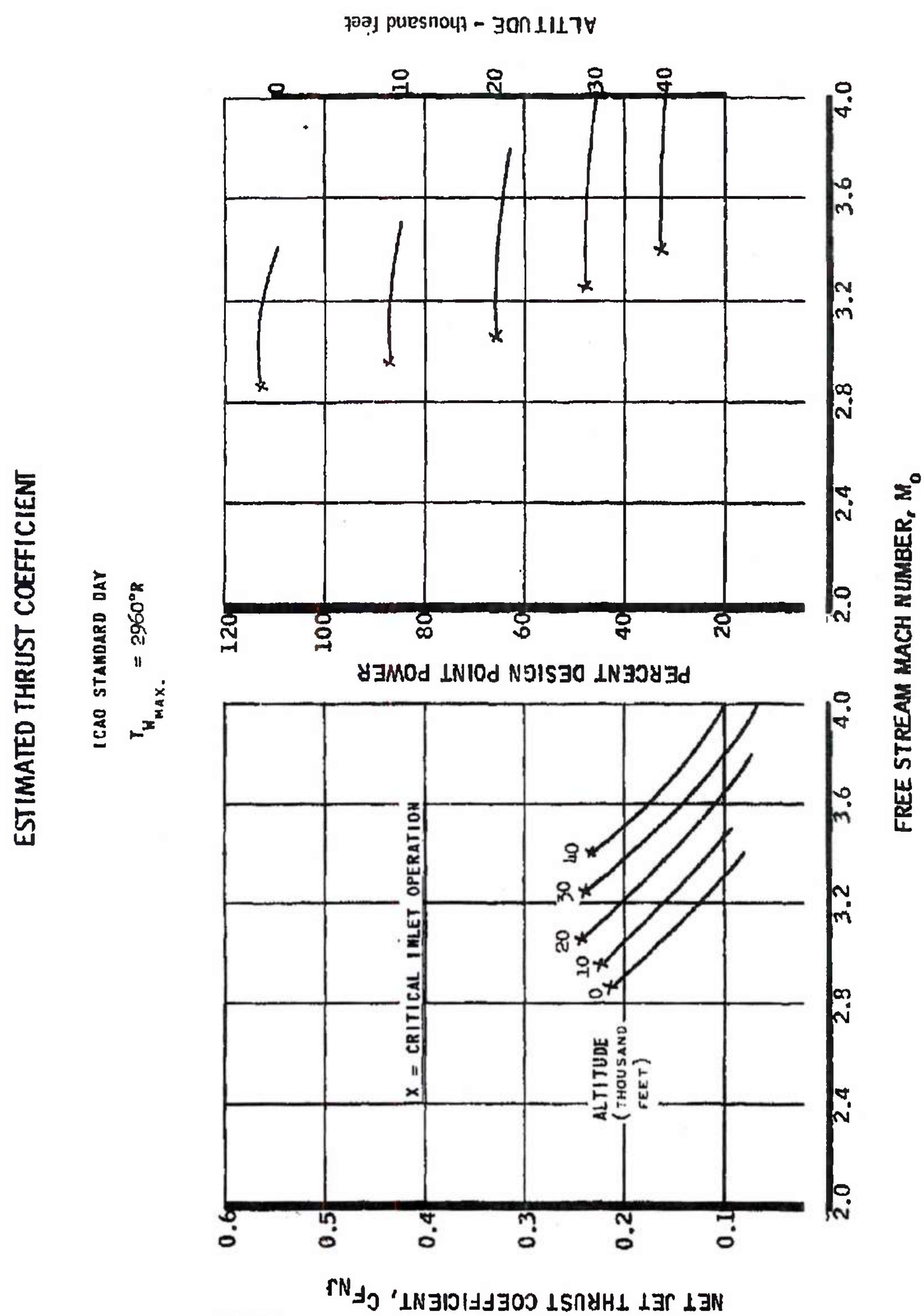

MAC A473

INLET PRESSURE RECOVERY

ICAO STANDARD DAY
$T_{W_{MAX.}} = 2960°R$

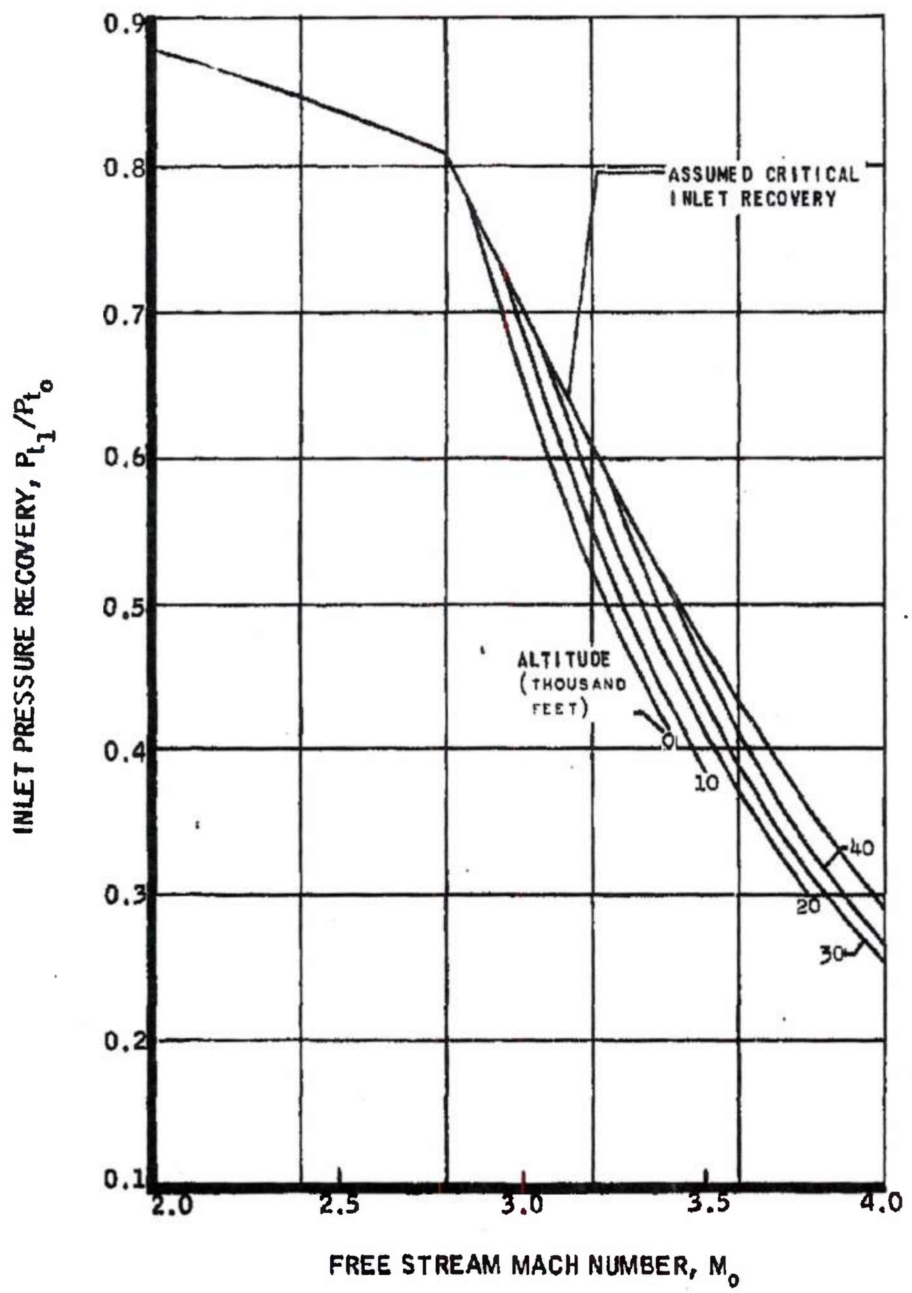

was also presented. This information, however, was found to be in rror and was subsequently corrected in Performance Bulletin No. 3.

The final item presented in Performance Bulletin No. 2 wa a study of the potential performance gains associated with a 2500°F isotherma wall in the Tory IIC reactor. Results of the study, based on the Model MA50-X A system geometry, are given in the third column of Table 2 . A potenti thrust gain of 10 percent is indicated. Achieving this performance would neces tate a 65 percent increase in the maximum power density in the core. LRL h s indicated a desire not to increase power density until problems relating to fue element thermal stress are more clearly defined. Additional study of the ae othermo-dynamics of the isothermal core indicated that a large weight reduct n could be achieved without incurring a performance penalty by reducing the cc e length 9 percent.

Performance Bulletin No. 3*

The reactor diameter scaling curve presented in Performa e Bulletin No. 2 was revised, and the corrected data were given to the aerothe modynamics contractor. This information permitted the aerothermodynamics cc ractor to perform a first iteration on the reactor diameter necessary to satis the performance requirements of the ADO No. 11 mission. This diameter, m ually agreed upon by LRL, Marquardt, and the aerothermodynamics contr ctor, was set at 63 inches as compared to 57 inches for the basic Tory IIC rea or. This change in reactor diameter, combined with other modifications, res ted in a propulsion system sufficiently different from the Model MA50-XCA warrant a separate identification. Accordingly, this system has been designat l as the Model MA50-XDA. The size scaling curve is presented in Figure . The following assumptions were made in deriving this curve. The curve re resents propulsion systems optimized for airflow to yield maximum thrust coef cient. The core power profile and the nuclear heat generation rates in nonnucle r components were considered to be independent of core diameter. Reflector hickness and tube geometries for all components were unchanged. The number o ie tubes and the projected frontal area of fueled core were increased as the squa of the ceramic diameter. The unfueled region about each tie rod and the nur er of control rods were unchanged. The side support gap was maintained at 1.56 nches. In addition to the increased diameter, the core was reduced in length f m 62.7 to 54.6 inches. The maximum wall temperature and reactor power de ity remained at the Tory IIC values. LRL has indicated concurrence in the ab e-noted changes to the basic Tory IIC reactor.

* Reference 4

EFFECT OF REACTOR DIAMETER INCREASE ON NET JET THRUST COEFFICIENT
(ERRATA SHEET FOR FIGURE 5 OF PERFORMANCE BULLETIN NO. 2)
(TORY IIC REACTOR LENGTH)

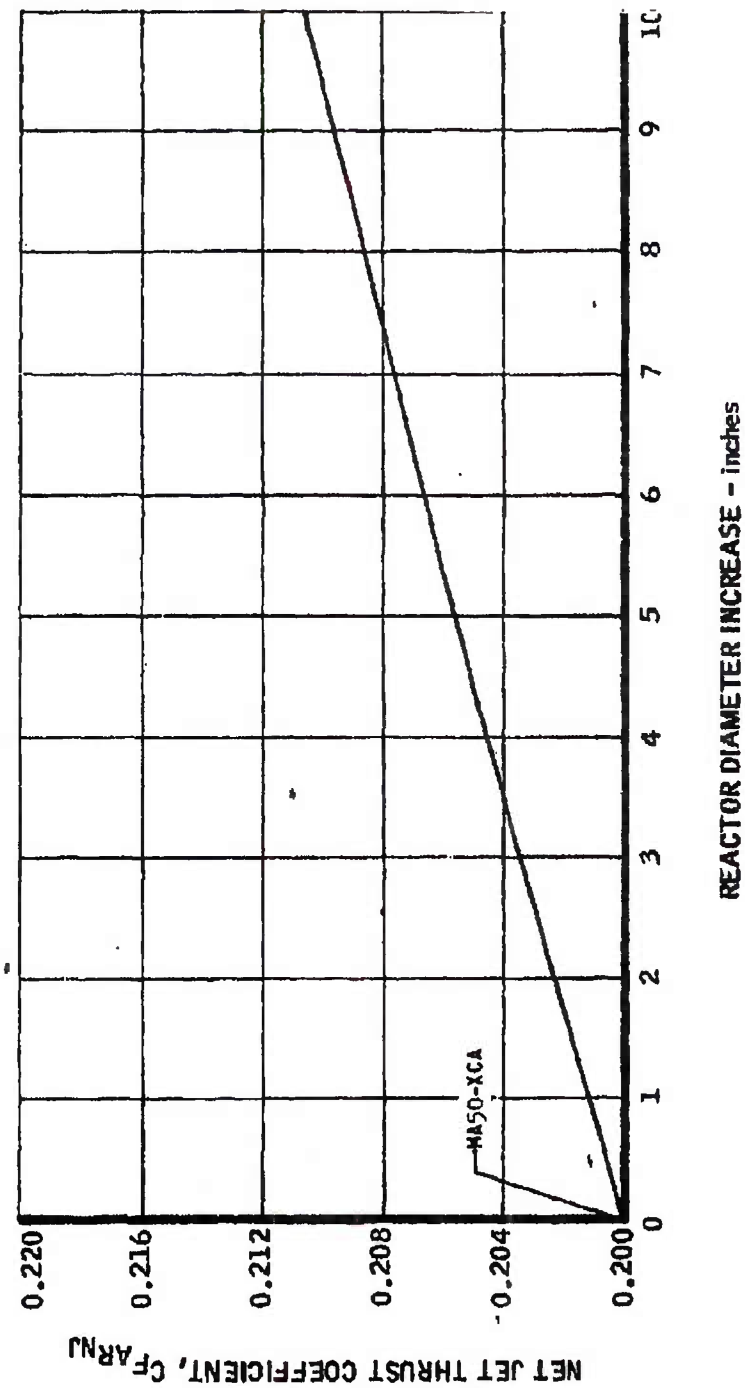

The design point aerothermodynamic properties of the Model I A50-XDA propulsion system are presented in Table 3 . The thrust coefficie : has increased to 0.207, or 3-1/2 percent above the basic Model MA50-XCA t rust coefficient. This thrust gain was achieved in spite of an allowance of 2.2 inches for side support spring area gaps as compared to the 1.56-inch gap all· ted for the Model MA50-XCA. The effect of the side support gap allowance ma be noted by comparing Figure 17 to Figure 16. Figure 17 presents the revis l size scaling curve assuming a variable gap thickness with increased reacto: diameter. It will be noted that this curve is much flatter than that presented in Fi ıre 16 wherein the gap was maintained at 1.56 inches. A comparison of these wo figures also indicates that a 3 percent thrust gain was achieved simply / shortening the Model MA50-XCA system as previously discussed. It is beli ·ed that the reactor scaling relationships utilizing the variable side support gap (Figure 17) is the more realistic of the two methods and will be utilize in all future analyses.

Net jet thrust, reactor thermal power, inlet pressure recover and airflow ratio, and installed drag were determined for altitudes of 1,000 ar 30,000 feet and are presented in Figures 18 through 24 for the Model MA50- DA system.

Performance Bulletin No. 4

With publication of the first three Performance Bulletins, Pha : I of the performance work utilizing Tory IIC technology was concluded. Perfoi ıance Bulletin No. 4, included as Section 3.3 of this report, represents initia Phase II performance studies, which are predicated on advancements in Tory II· technology. The advances considered are as follows:

(1) A modification in the core power profile. By modifying th core power profile, thrust performance can be improved without exceeding .e Tory IIC design limits of 15,000-psi elastic thermal stress and 2500°F maxi .um wall temperature. There follows an explanation of this improvement in thru t performance. With the present Tory IIC power profile, the 15,000-psi therm l stress limit is achieved at one location near the center of the core. At positic s closer to the front of the core, the thermal stress falls off to lower values bec use of increased thermal conductivity through the fuel element at the lower te pera- tures. Similarly, at the rear of the reactor the wall temperature is le than the 2500°F limit. Figure 25 presents a comparison of relative power cur :s for the isothermal wall reactor, the Tory IIC reactor, and the revised profile r the Tory IIC, which more nearly fits the limiting conditions on elastic ther al stress

TABLE 3

MA50-XDA AEROTHERMODYNAMIC PERFORMANCE CHARACTERISTICS AT THE DESIGN POINT

(Mach 2.8; ANA Hot Day Temperature; Altitude, 1000 feet)

Parameter	MA50-XDA
Reactor Air Flow, W_a, pps	2,012
Side Support Cooling Air Flow, W_{a_c}, pps	120
Inlet Total Pressure, P_{t_o}, psia	393
Inlet Total Temperature, T_{t_o}, ^oR	1,402
Inlet Recovery, P_t/P_{t_o}	0.807
Core Inlet Mach Number, M_3	0.235
Core Tube Diameter, ft	0.0189
Maximum Core Wall Temperature, T_W, ^oR	2,960
Total Reactor Power, Q, Mw	654
Reactor Ceramic Average Void Fraction	0.421
Reactor Exit (Mixed) Total Temperature, T_{t_4}, ^oR	2,510
Reactor Pressure Recovery, P_{t_4}/P_{t_1}	0.683
Reactor Diameter, D_R, in.	63
Reactor Length, L_R, in.	54.6
Reactor Area, A_R, sq ft	21.63
Nozzle Throat Area, A_5, sq ft	6.2
Nozzle Exit Area, A_6, sq ft	16.09
Cowl Area, A_c, sq ft	10.05
Exhaust Nozzle Velocity Coefficient, C_V	0.98
Thrust Coefficient, $C_{F_{A_R}}$, (Full expansion)	0.207
Thrust, F, (Full expansion), lbs	50,200

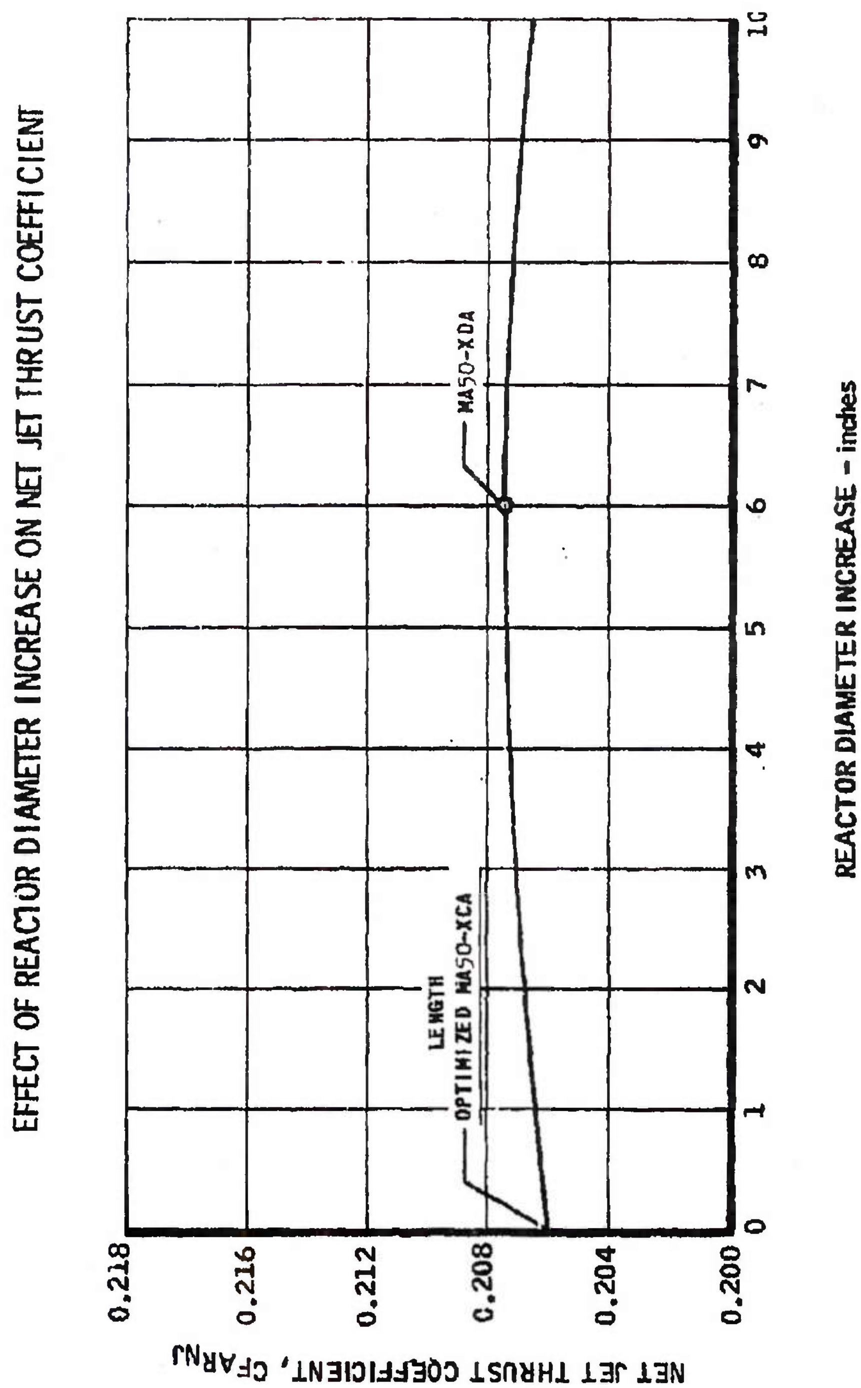
EFFECT OF REACTOR DIAMETER INCREASE ON NET JET THRUST COEFFICIENT
MA50-XDA
LENGTH
OPTIMIZED MA50-XCA
0
1
2
3
4
5
6
7
8
9
10
REACTOR DIAMETER INCREASE - inches
0.218
0.216
0.212
0.208
0.204
0.200
NET JET THRUST COEFFICIENT, CFARNJ

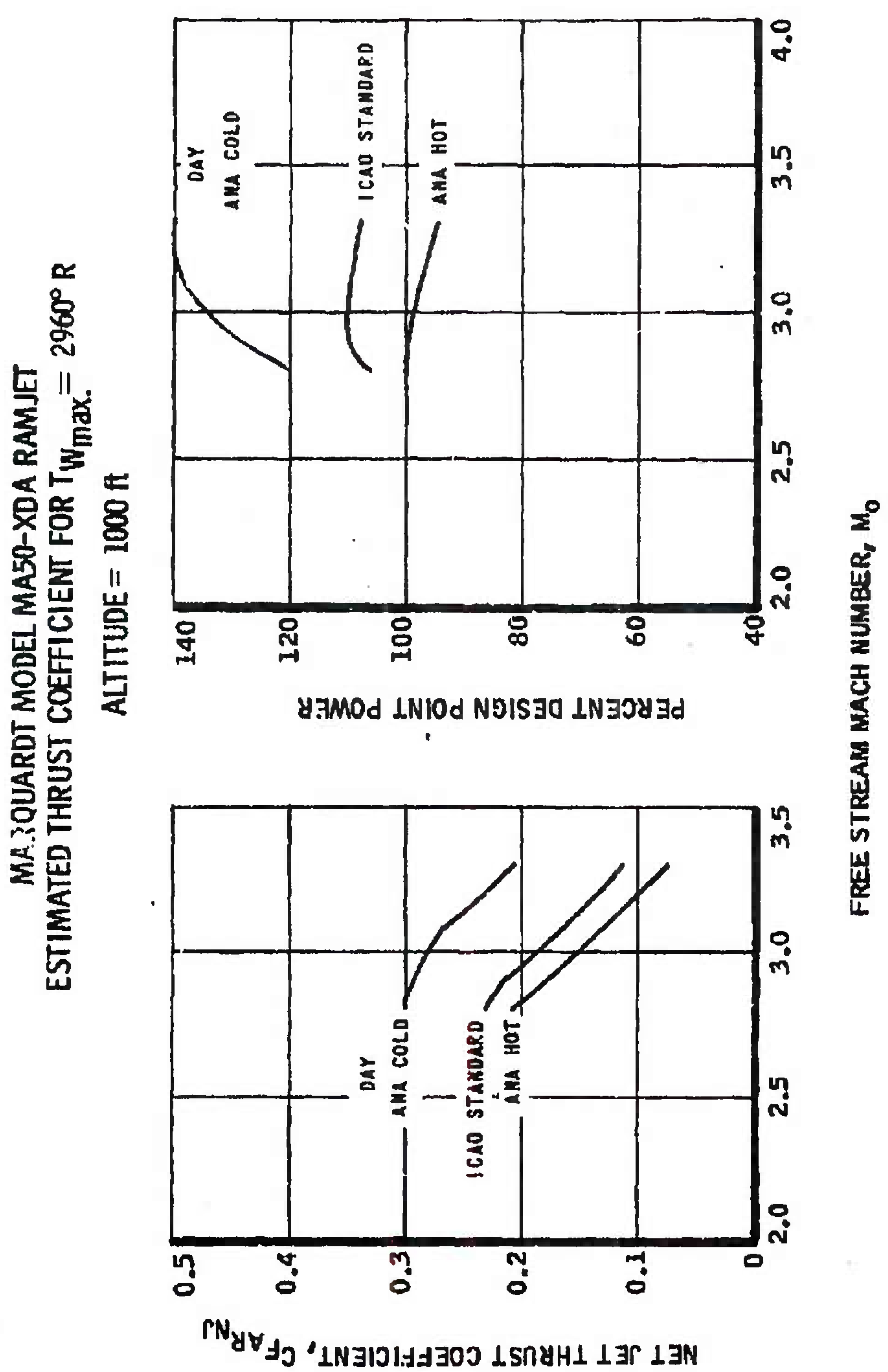
MARQUARDT MODEL MA50-XDA RAMJET
ESTIMATED THRUST COEFFICIENT FOR $T_{W_{max.}} = 2960°$ R
ALTITUDE = 1000 ft
DAY
ANA COLD
ICAO STANDARD
ANA HOT
PERCENT DESIGN POINT POWER
140
120
100
80
60
40
2.0
2.5
3.0
3.5
4.0
NET JET THRUST COEFFICIENT, $C_{F_{A R_{NJ}}}$
0.5
0.4
0.3
0.2
0.1
0
FREE STREAM MACH NUMBER, M_0

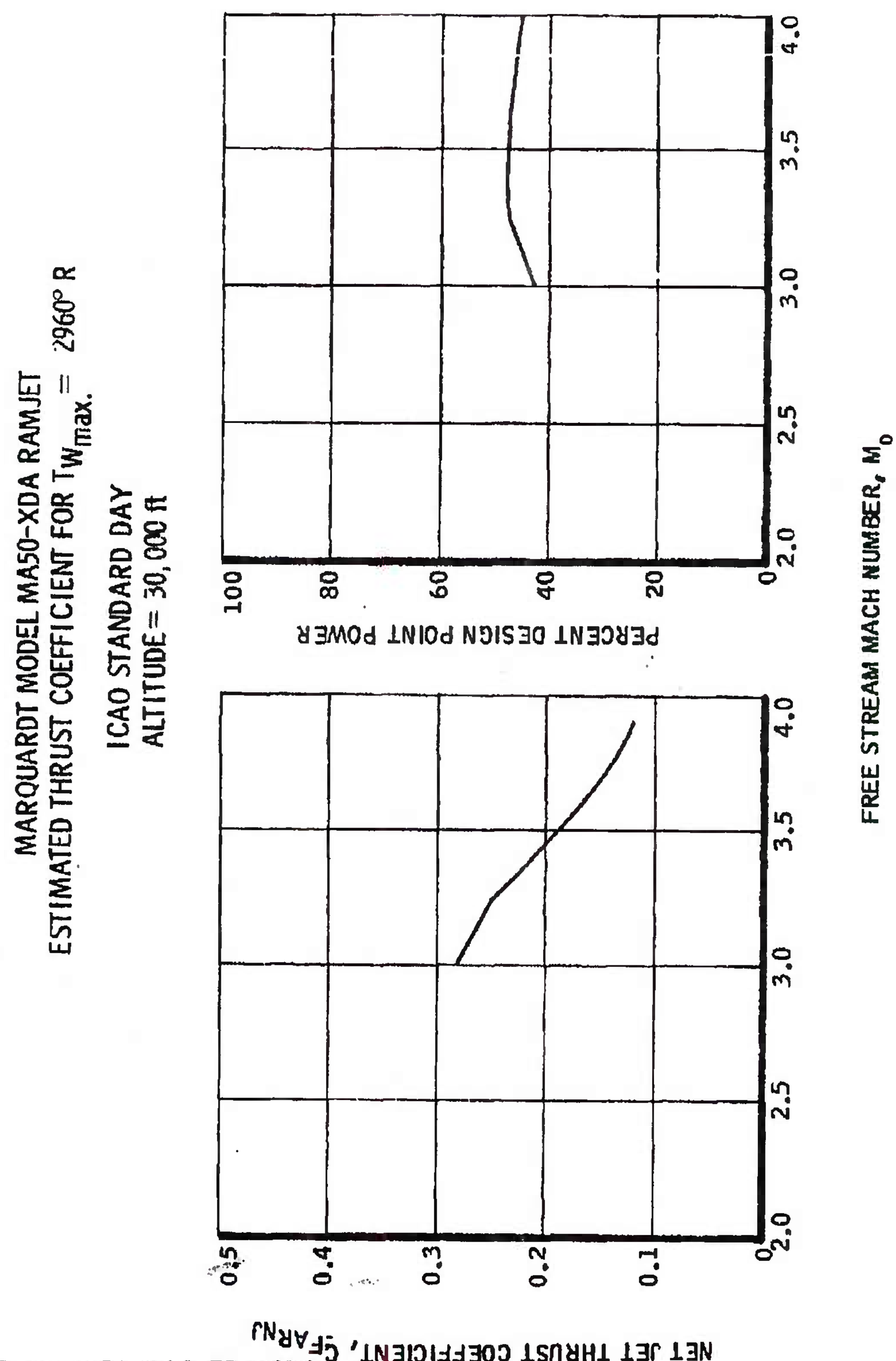
MARQUARDT MODEL MA50-XDA RAMJET
ESTIMATED THRUST COEFFICIENT FOR $T_{W_{max.}}$ = 2960° R
ICAO STANDARD DAY
ALTITUDE = 30,000 ft
PERCENT DESIGN POINT POWER
100
80
60
40
20
0
2.0
2.5
3.0
3.5
4.0
NET JET THRUST COEFFICIENT, $C_{F_{ARN_J}}$
0.5
0.4
0.3
0.2
0.1
0
FREE STREAM MACH NUMBER, M_0

MARQUARDT MODEL MA50 XDA RAMJET
INLET PRESSURE RECOVERY
ALTITUDE = 1000 ft
$T_{W_{max.}}$ = 2960° R

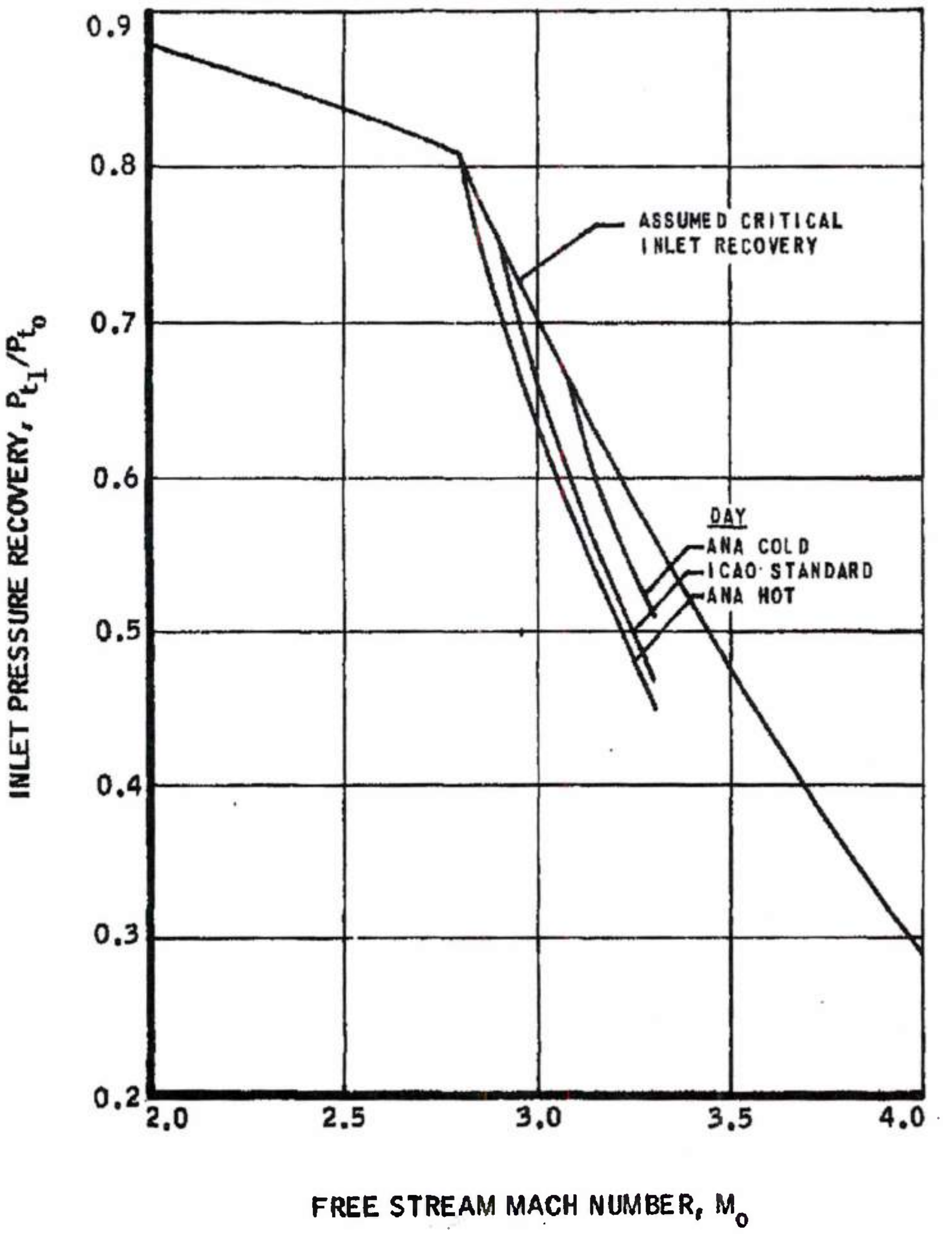

MARQUARDT MODEL MA50-XDA RAMJET INLET PRESSURE RECOVERY

ALTITUDE 30,000 ft

$T_{W_{max.}} = 2960° R$

ICAO STANDARD DAY

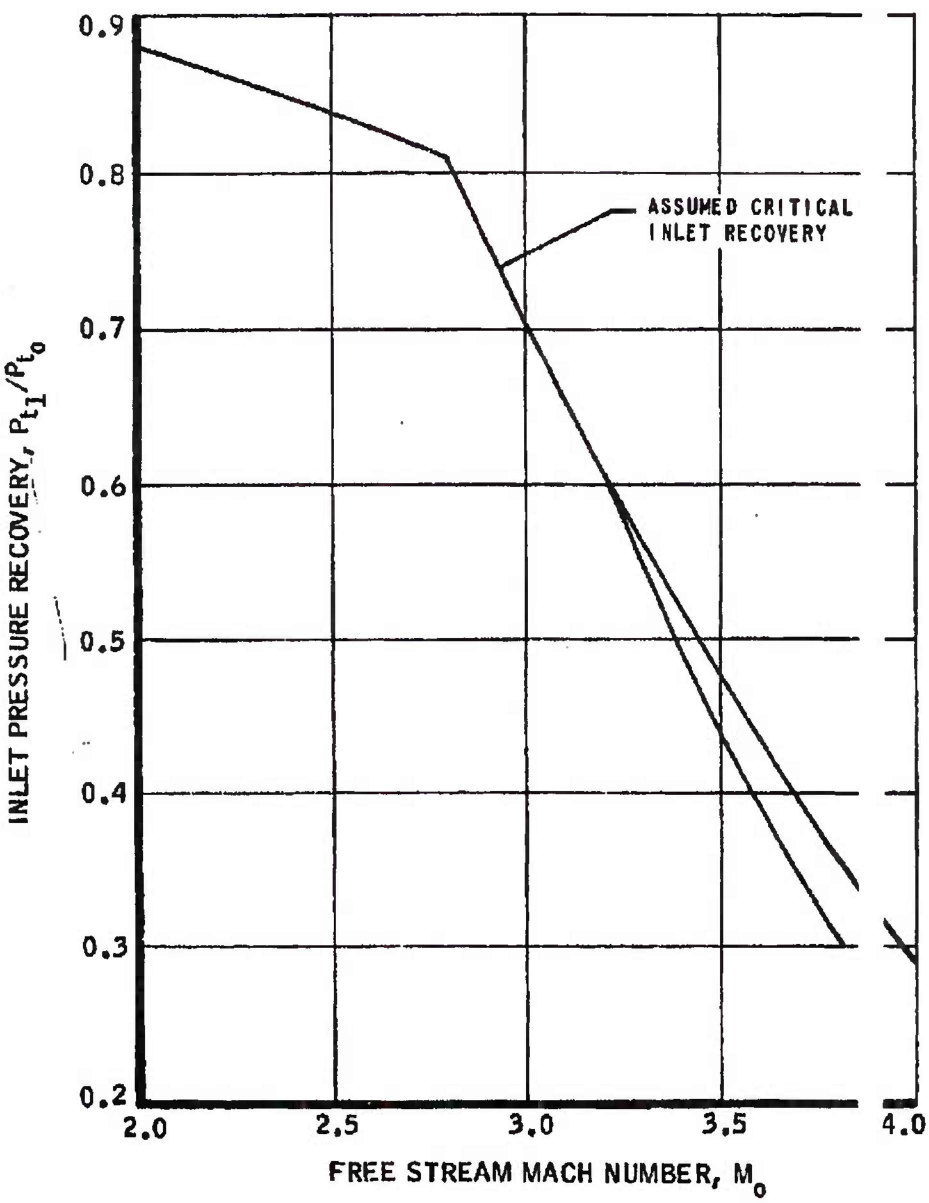

FIGURE 21

MARQUARDT MODEL MA50-XDA RAMJET
FREE STREAM CAPTURE AREA RATIO
$T_{W_{max.}} = 2960° R$

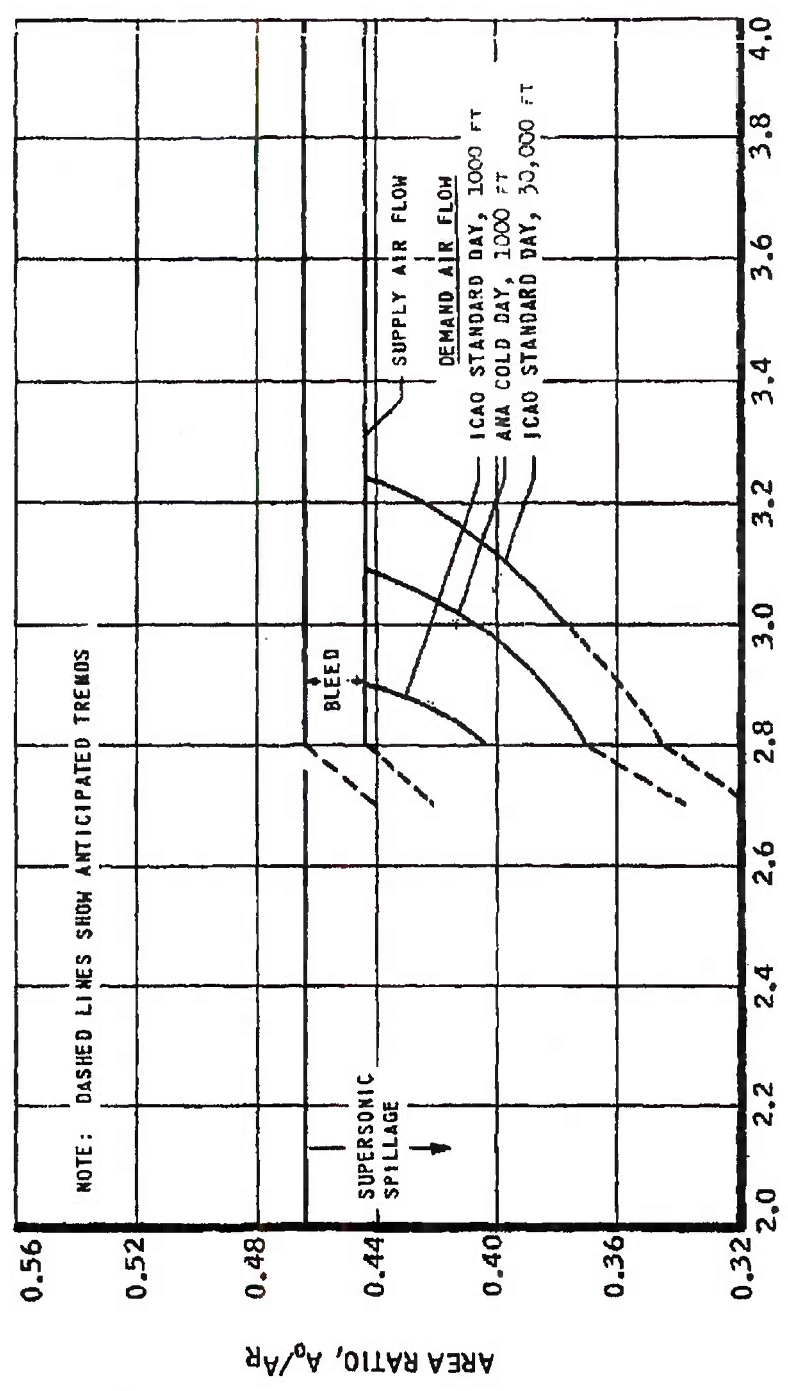

MARQUARDT MODEL MA50-XDA RAMJET
DRAG OF ENGINE INSTALLATION
ALTITUDE = 1000 ft
$T_{W_{max.}}$ = 2960° R

DRAG COMPONENTS
A - INLET BLEED
B - BYPASS

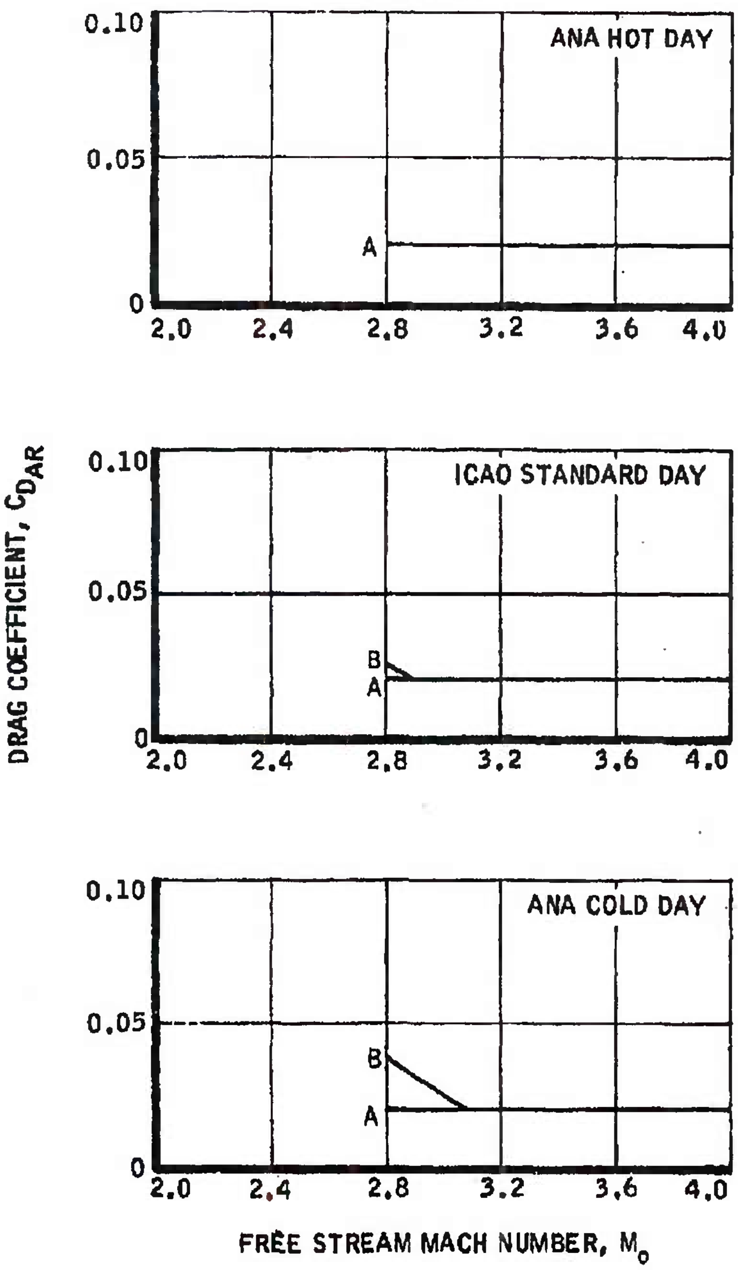

~~SECRET RESTRICTED DATA~~
~~ATOMIC ENERGY ACT OF 1954~~

MARQUARDT MODEL MA50-XDA RAMJET
DRAG OF ENGINE INSTALLATION
ALTITUDE = 30,000 ft
$T_{W_{max.}}$ = 2960° R

DRAG COMPONENTS
A = INLET BLEED
B = BYPASS

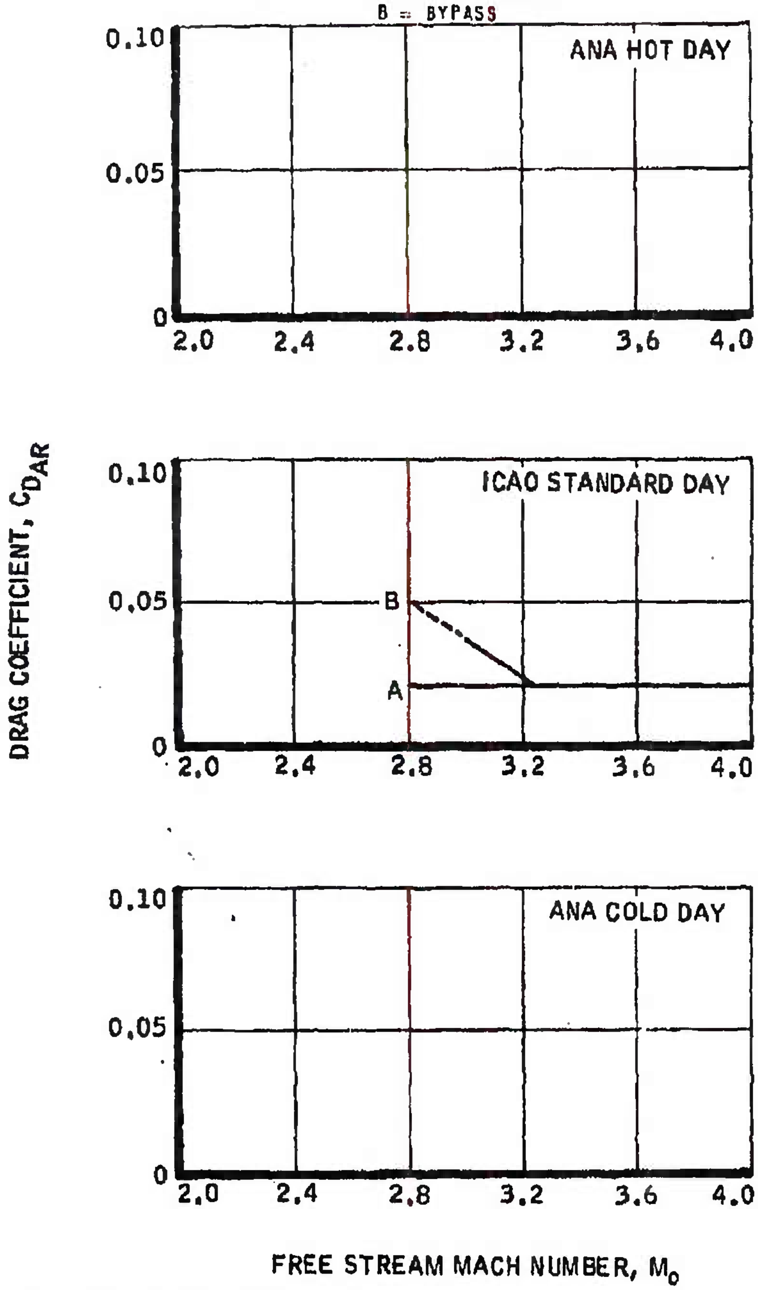

~~SECRET RESTRICTED DATA~~

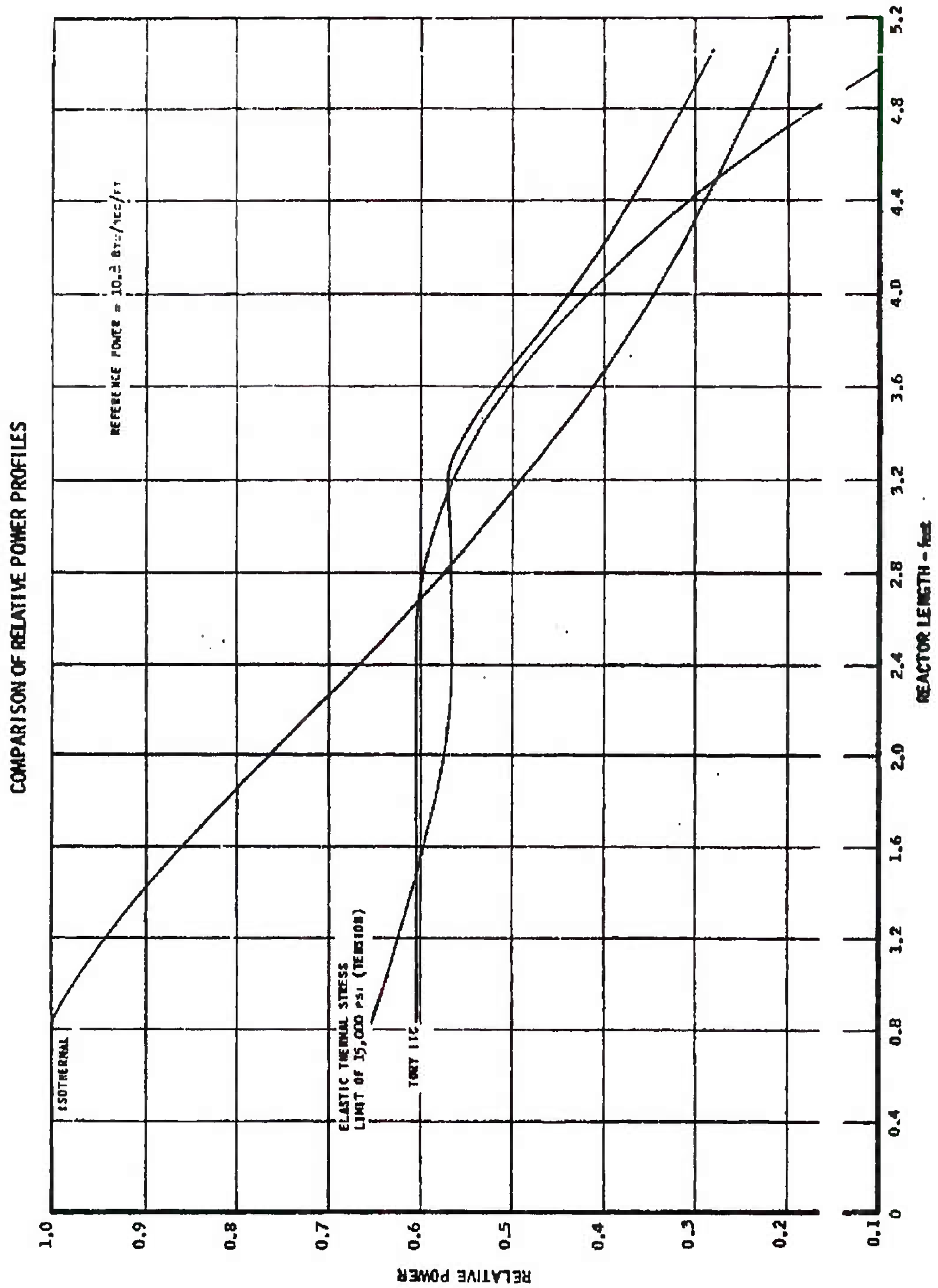

MAC A673

FIGURE 25

and wall temperature. This change in power profile results in an improvei ent of thrust coefficient of 2.5 percent for the basic Model MA50-XCA propulsi n system.

(2) A change similar to (1) above, wherein the elastic thermal st: ss is raised to 18,000 psi. The change in power profile for this core results a 5 percent increase in thrust coefficient for the basic Model MA50-XCA. T s increase in elastic thermal stress limit is considered feasible on the basis f successful operation of the Tory IIC core at thermal stresses above 20,000 psi.

(3) A change in the number of tie tubes. The number of tie tubes or the Tory IIC is determined principally by the diameter of the billet used for th Tory IIC base plate. LRL now believes that advancements in fabrication techniq s may permit an increase in billet diameter from 5 to 9 inches. Inasmuch a the present tie tube design point temperature is relatively low, LRL believes t number of tie tubes may be reduced by the ratio of the billet diameters (5/9). When the number of tie tubes is reduced, the reactor frontal area previous occupied by tie tube and unfueled region is replaced by fueled core tubes. reduction in the number of tie tubes as outlined above will permit a thrust co- efficient increase of 2.5 percent for the basic Model MA50-XCA propulsion system.

(4) An increase in the fueled core tube diameter. A fueled core tu e di- ameter increase from 0.227 to 0.230 inches, for the same fuel element siz , in- creases the core void fraction by 2.5 percent. This change results in a 1 p rcent increase in thrust coefficient for the basic Model MA50-XCA propulsion sy sm.

(5) A reduction in the cooling airflow per tube. Inasmuch as the Tory IIC tie tubes are running cool (1250°F), the cooling airflow per tube may b re- duced. This reduction has been accomplished by reducing the inside diame r of the tie tube while keeping other tie tube dimensions and geometry fixed. A e- duction of tie tube inside diameter to 0.325 inches increases the tie tube te per- ature to 1650°F, and the thrust coefficient change is 0.5 percent. This ch ge is invalidated when the number of tie tubes is reduced, as in Item (3) above.

LRL has indicated feasibility concurrence on the changes listed ab ve. Future work will include analysis of effects on propulsion system performa ce of combining individual concepts to determine whether individual results a additive and to determine the most feasible manner of increasing system p for- mance. Mechanical design, heat transfer, structural analysis, and neutro c studies will be made in areas showing the most promising performance gai s.

3.2.2 Inlet Survey and Performance Analysis

The design considerations for the nuclear ramjet propulsio system are unique. The air temperature rise across the reactor is limited by t maximum permissible operating temperature of the reactor core material. Tl low heat addition per unit frontal area of the reactor and the characteristicall large reactor pressure drops are indicative of low thrust coefficients. In pa :icular, the installed thrust-over-missile drag margin is low and is therefore qu e sensitive to inlet pressure recovery and installed drag characteristics.

The requirement for maximum inlet pressure recovery con ined with low drag is met by the use of internal contraction. Unfortunately, tl internal contraction inlet required some form of variable geometry to permi nlet starting (swallowing of terminal shock) as well as internal bleed to maint n high pressure recovery. The 1961 program has been directed towards experi iental verification of assumed inlet pressure recoveries, required bleed rates inlet airflow characteristics, and installed drag characteristics.

The original objective of the 1961 experimental program, a presented in Reference 5, was the design and fabrication of two small scale i et models. It was planned that the first inlet be tested during 1961 and the secon in 1962. Inlet design for both models was to be based upon the external-inter l compression type described in Reference 6. (This inlet has demonstrated g od pressure recovery characteristics for modest bleed rates, and is easily contr led as to variable spike position as well as internal shock position-bypass ope ation). The inlets were to be underslung beneath the missile body and to incorpo te the S-shaped subsonic diffuser ducting. The first inlet was to be axially s nmetric as far as the supersonic compression surfaces were concerned, while t e second inlet was to be asymmetric and partially wrapped about the lower fu lage contour. The choice between the two inlet configurations was to be bas upon calculation of a net thrust-minus-installed drag value using the pressu recovery and drag measurements obtained.

On 18 April 1961, a coordination meeting was held at ASD, ayton, Ohio, with the aerothermodynamics contractor and Marquardt as participa s. At this meeting it was ruled that the experimental inlet test program be a jc it effort between Marquardt and the aerothermodynamics contractor. Lines fo: the aerodynamic models were to be mutually agreeable. Marquardt was giv the responsibility for model design and fabrication and performance of the test rogram including data reduction. As a result of these decisions, coordination ieetings were held between Marquardt and the aerothermodynamics contract for the purpose of establishing test inlet configurations. The principal change in the original test plan has been the elimination of the design and fabrication of the asymmetric inlet and the substitution of an alternate axisymmetric inlet. Th alternate inlet was selected on the basis of less sensitivity to angles of attack and yaw than the basic inlet.

Lines for the basic inlet are shown schematical in Figure 26. Through the use of a finite initial cone followed by an isentropic turning surfa e, external supersonic compression from Mach 2.8 to about Mach 2.2 is achiev with only a 1 percent loss in total pressure. Additional supersonic compress on as well as supersonic turning are effected internally. This is accomplished the reflection of two finite oblique shocks off the cowl in conjunction with a fl h bleed slot on the centerbody. The bleed slot removes the boundary layer pri to the adverse pressure gradient associated with the internal compression. A t ns- lating spike is used to permit inlet start and to obtain high pressure recovery during off-design operation while minimizing drag. To use an inlet of this ty effectively, the configuration must be optimized on a net thrust-minus-drag basis. An optimization procedure was performed in Reference 7 wherein th pressure recovery (and, therefore, thrust) of several combinations of isentr ic turning, cowl angles, and attendant cowl drags were determined. The result of this study are shown in Figure 27 . The net thrust-minus-cowl drag is show as a function of cone surface Mach number and flow turning at the cowl.

This optimization study for the basic inlet was revised in Reference to account for more realistic subsonic diffuser losses. This revision permit d increased flow turning at the cowl and therefore improved cowl drag. The ne thrust-minus-cowl drag of Figure 27 was increased from 0.233 to 0.240 by is analysis. The final basic inlet configuration is summarized by the following parameters (see Figure 26):

θ_1	14.48°	θ_3	5.14°
θ_2	20.97°	θ_4	4.86°
ϕ	25.97°	M_3	1.72
M_{S_1}	2.37	M_4	1.37
M_{S_2}	2.13	M_5	0.753
$\overline{M_2}$	2.17	Bleed	4.5 percent

Estimated performance for the basic inlet is shown in Figure 1 , a a function of free stream Mach number for conditions of zero angle of attack ar yaw. This performance is based upon the spike position variation shown in Figure 28. During boost, the spike is translated forward 6 inches to reduce the

AXISYMMETRIC, EXTERNAL-INTERNAL COMPRESSION INLET

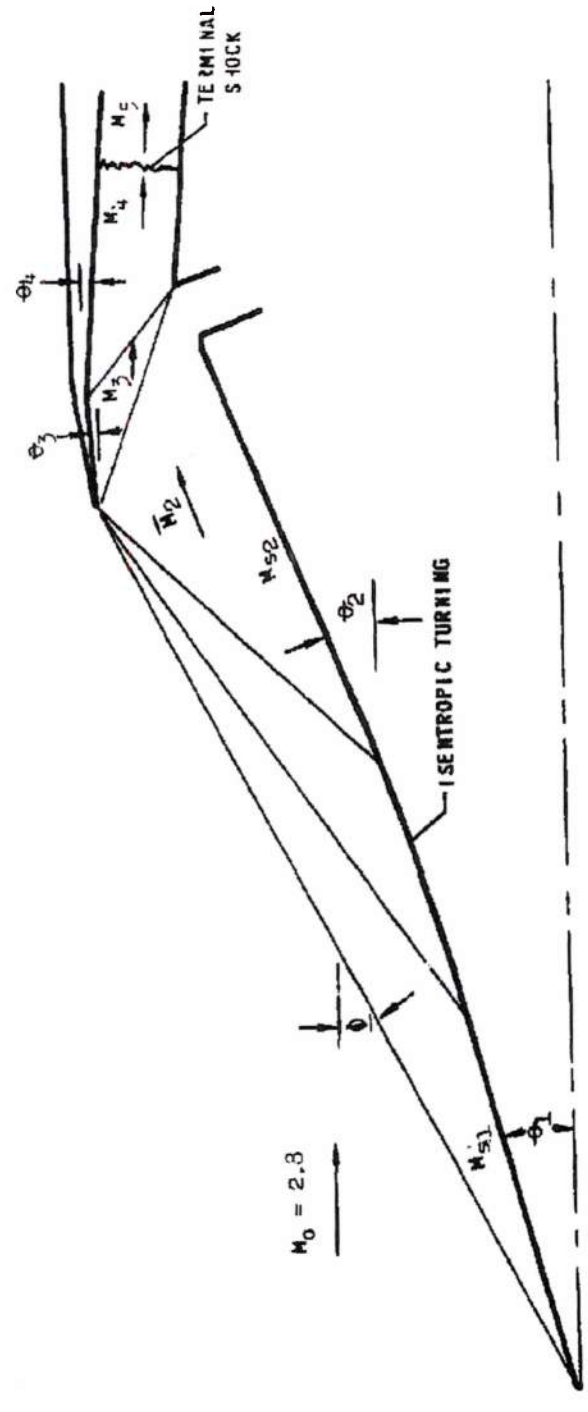

OPTIMIZATION OF MACH 2.8 AXISYMMETRIC INLET

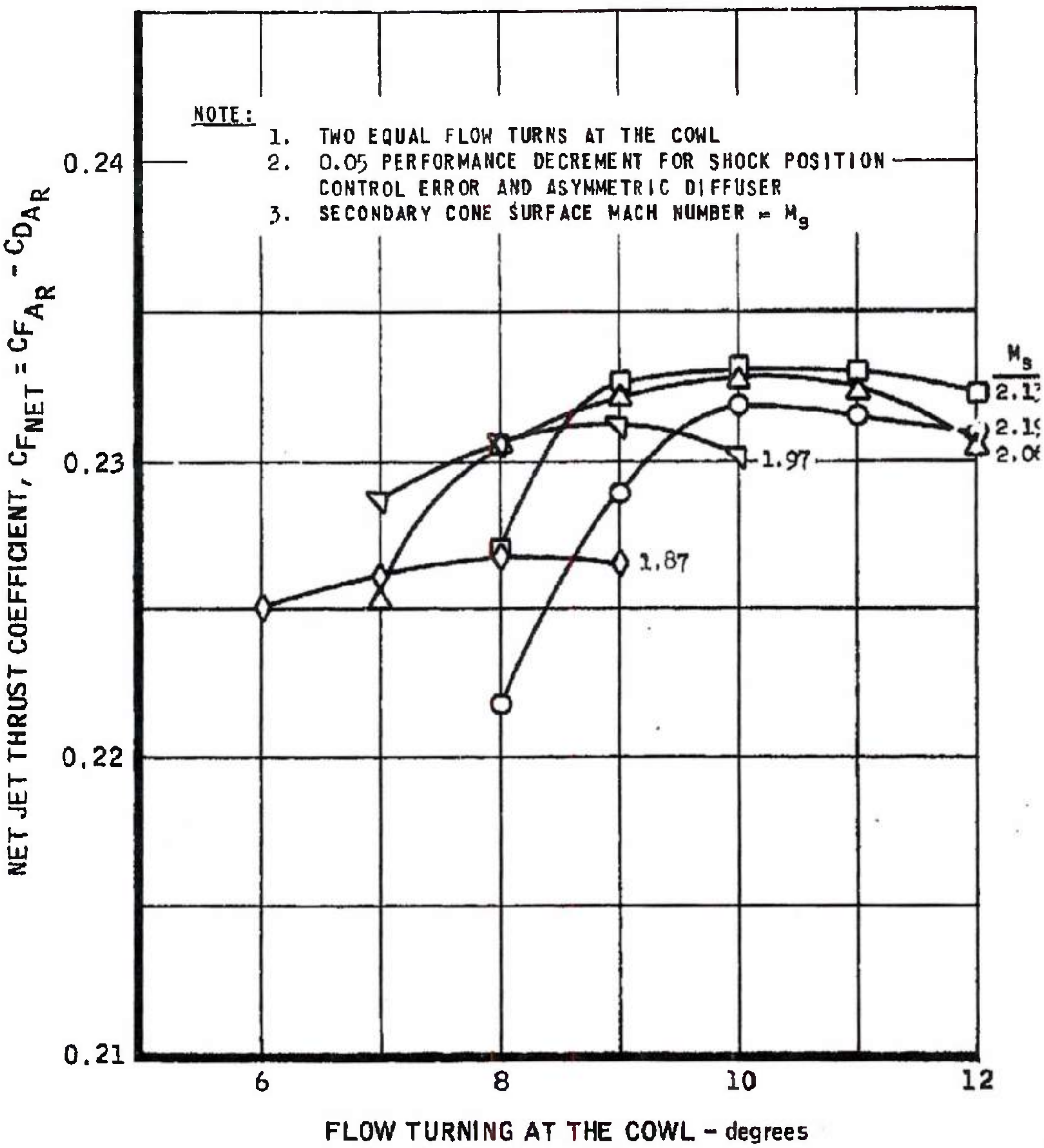

VARIABLE INLET OPERATION
AT 0° ANGLE OF ATTACK AND YAW

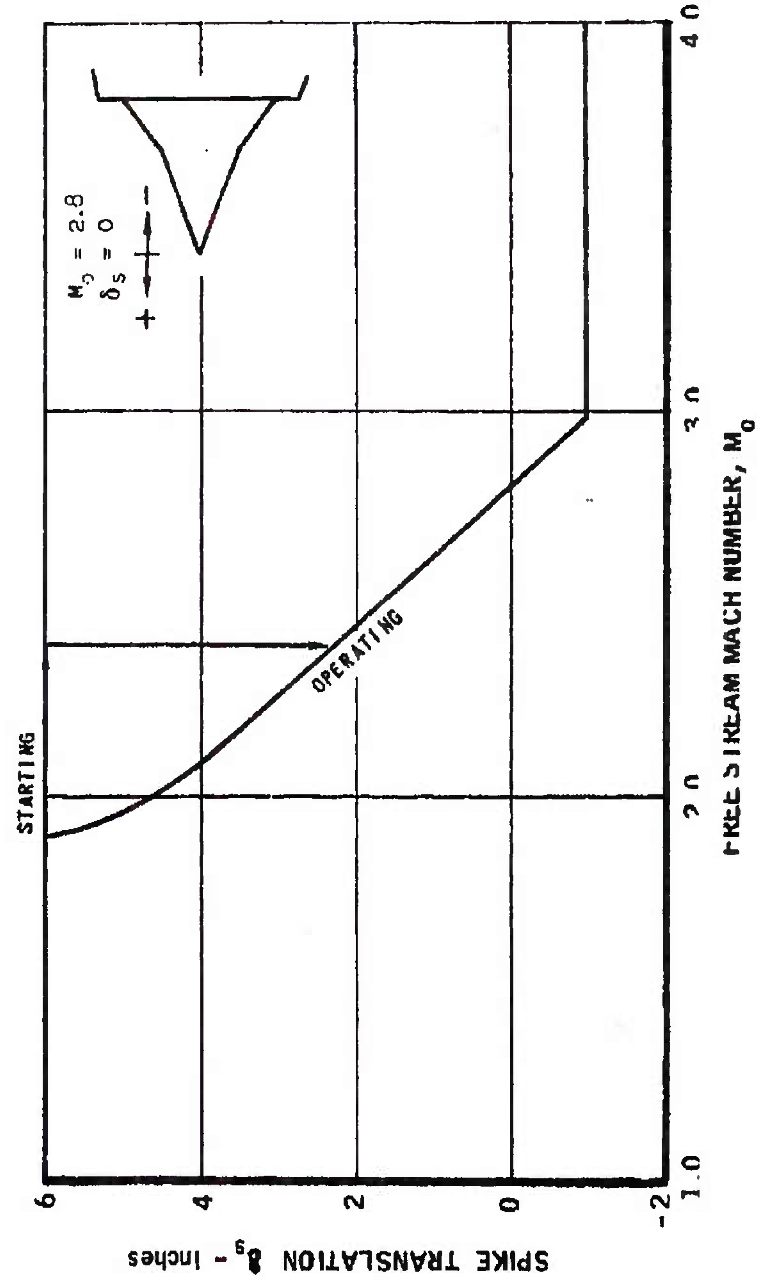

internal contraction, as indicated in Figure 29. In this position the inlet wi swallow the terminal shock at a free stream Mach number of about 2.4 Foll ing this, the inlet spike position is varied continuously (operating line) betwe Mach 3.0 and 1.9 to keep the first lip shock on the rim of the centerbody ble slot.

Details of the alternate inlet have been agreed upon by representati s of Chance Vought and Marquardt. This inlet differs from the basic inlet in t t the compression fan from the inlet spike will not be focused on the lip but ra er will be spread out and reflected from the cowl inner surface. The comparis of the inlet types is shown schematically in Figure 30. The alternate inlet i longer and has a shallower initial cowl angle. It is anticipated that the alter te inlet will require less bleed and will be less sensitive to perturbations in ang of attack and yaw. Its performance at zero angle of attack and yaw is expect to be about equivalent to the basic inlet. The inlet test program is further di cussed in Section 3.8.1

3.2.3 Exhaust Nozzle Aerodynamics

The Marquardt role of integrating the propulsion system into a pred table, reliable, and efficient system has required a concentrated effort on th exit nozzle during 1961. This effort is prompted by the inherently low thrust to-drag margin of the missile system, which imposes stringent requirements o the accuracy of nozzle performance predictions. Nozzle efficiency must be high a 98 percent velocity coefficient is assumed for calculation purposes), nozzle ag loads must be known, and nozzle cooling air must be handled efficiently. It is recognized that experimental tests of the exhaust nozzle were necessary to supply the required design information. The nozzle length-to-area ratio sel ted for the installation must be based upon net thrust-minus-installed drag char ter-istics rather than upon nozzle jet thrust alone. Thus, efficient handling of e ine and exit nozzle cooling air must be accomplished, and nozzle shroud boattail nd base drags must be considered in establishing the overall exit nozzle geomet .

The types of nozzle configurations analyzed during the year are sho in Figure 31. In Figure 31A the engine cooling air between the reactor and pressure vessel is mixed with the reactor air and passed through a common nozzle. The engine cooling airflow must be throttled to prevent flow starvati through the reactor. While this configuration has about the same net jet thru as the other configurations studied (see Section 3.8.2), analysis of this syste was limited pending the demonstration of successful coatings necessary for t radiation cooled nozzle. In Figure 31B the engine cooling air is collected

VARIATION OF INLET AREA RATIO WITH SPIKE TRANSLATION

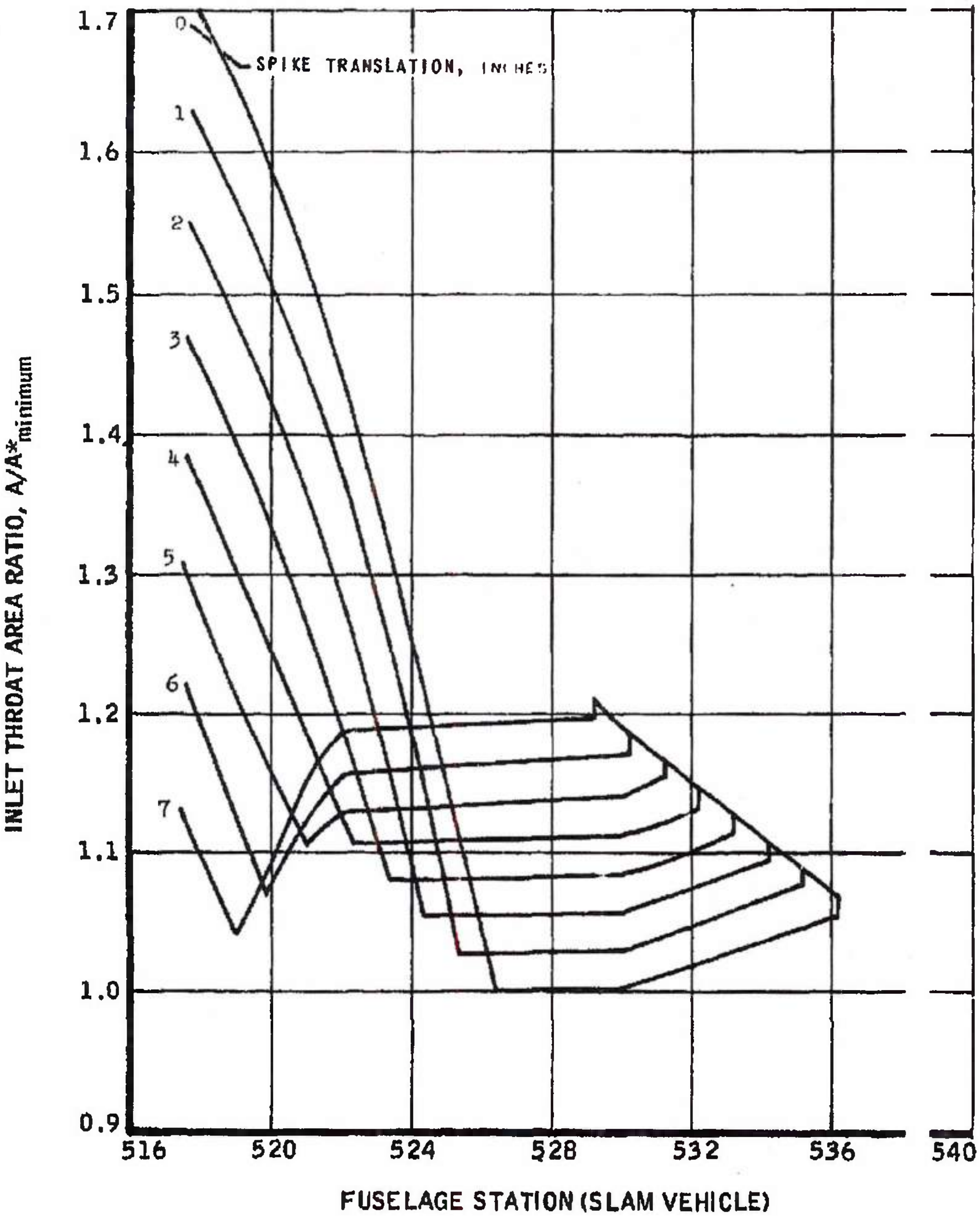

COMPARISON OF INLET TYPES

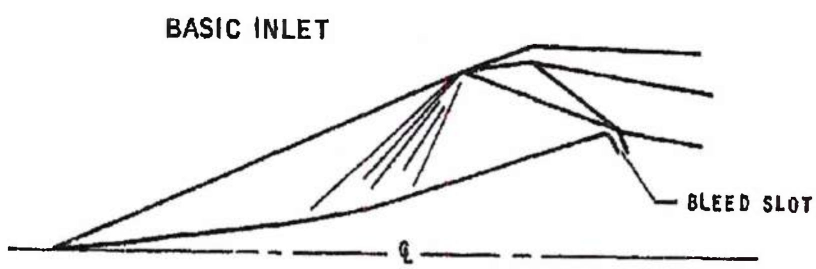

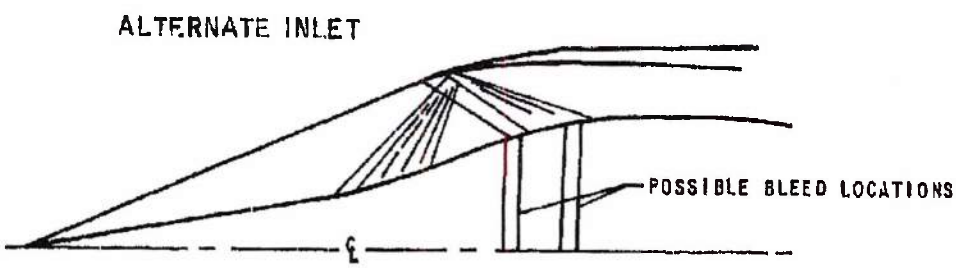

TYPICAL EXHAUST NOZZLE INSTALLATIONS

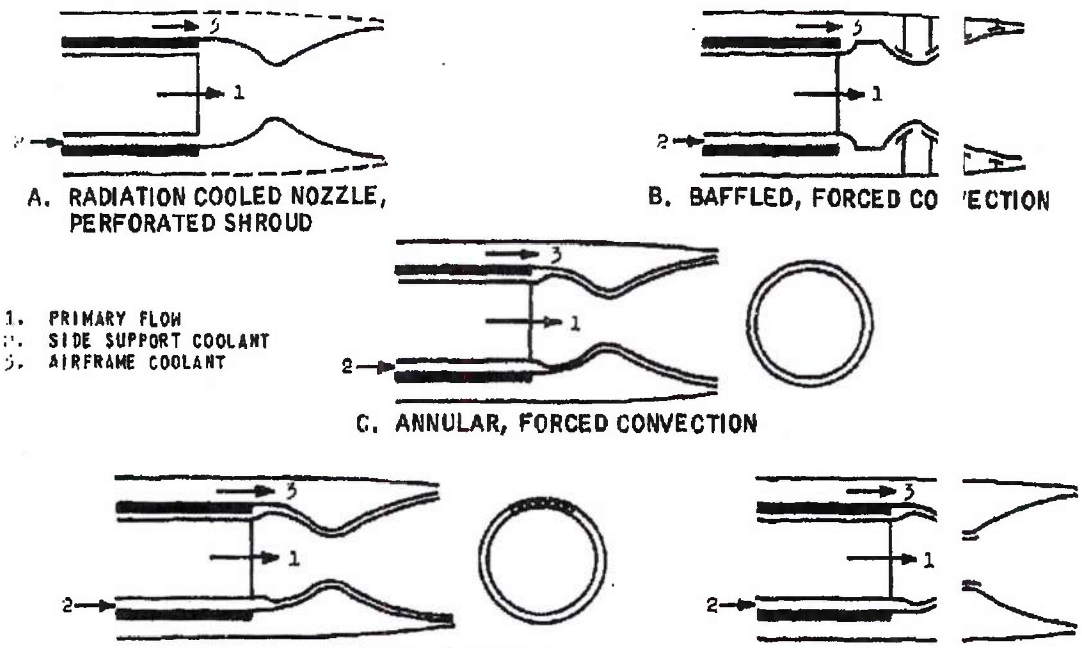

A. RADIATION COOLED NOZZLE, PERFORATED SHROUD

B. BAFFLED, FORCED CO 'ECTION

C. ANNULAR, FORCED CONVECTION

D. TUBULAR, FORCED CONVECTION

E. EJECT(

exterior to the nozzle and is baffled to provide cooling at critical areas of th nozzle. This forced convection cooling scheme was eliminated in favor of tl configuration of Figure 31C, because it appeared that the pressure drop of t cooling air was exces ive. The configuration of Figure 31C employs forced convection in an annular passage and performs the function of the baffled ar nge-ment more efficiently. Figure 31D shows a forced convection model in whic the nozzle wall is formed from small coolant channels similar to those used in gen-eratively cooled rocket nozzles. Finally, configuration 31E indicates anoth approach in which the engine cooling air is used to supply the secondary flov of an ejector type nozzle. Film cooling is used on the divergent portion of the nozzle.

Nozzle Sizing

In order to design, test, and evaluate exhaust nozzle models during he 1961 time period, it was necessary to make a preliminary study of the nozzl configuration to establish basic nozzle sizing relationships. From the Mode MA50-XCA propulsion system optimization at design point, it was determin that the effective nozzle area expansion is 2.58 for a fully expanded nozzle v th an operating pressure ratio of 15.2. These data also indicated that the influ nce coefficient of the nozzle on the Model MA50-XCA propulsion system perforn nce was 4.8 percent change in thrust for each percent of nozzle velocity coeffici nt. A nozzle-boattail optimization was performed in Reference 8, wherein it wa established that the optimum installation on a net jet thrust-minus-boattail c ag basis would call for a nozzle overexpansion of about 13.2 percent as shown i Figure 32. The cooling air drag losses were neglected in this analysis inas much as this drag is essentially constant for a given type of configuration.

Nozzle Aerodynamic Lines

Nozzle aerodynamic lines from the method of characteristics were determined as presented in Reference 9. Nozzles both longer and shorter t an the basic nozzle were described for test, because it was believed that knowl lge of the variation of the internal nozzle performance with nozzle length would d in future nozzle configuration studies. Characteristics of the forced convec on primary nozzle are listed in Table 4, and nozzle coordinates are specified Figure 33. The annular type coolant passage of Figure 31C was designed f testing with the basic nozzle to establish the pressure drop relations for suc a system. The tubular nozzle configuration of Figure 31D could not be tested ue to the small scale of the models. The ejector type configuration of Figure E was designed and is shown in Figure 34. This nozzle is again the same len h and has the same area ratio as the basic optimized nozzle. Model tests of t ese

NOZZLE-BOATTAIL OPTIMIZATION FOR MA50-XCA ENGINE AT DESIGN POINT

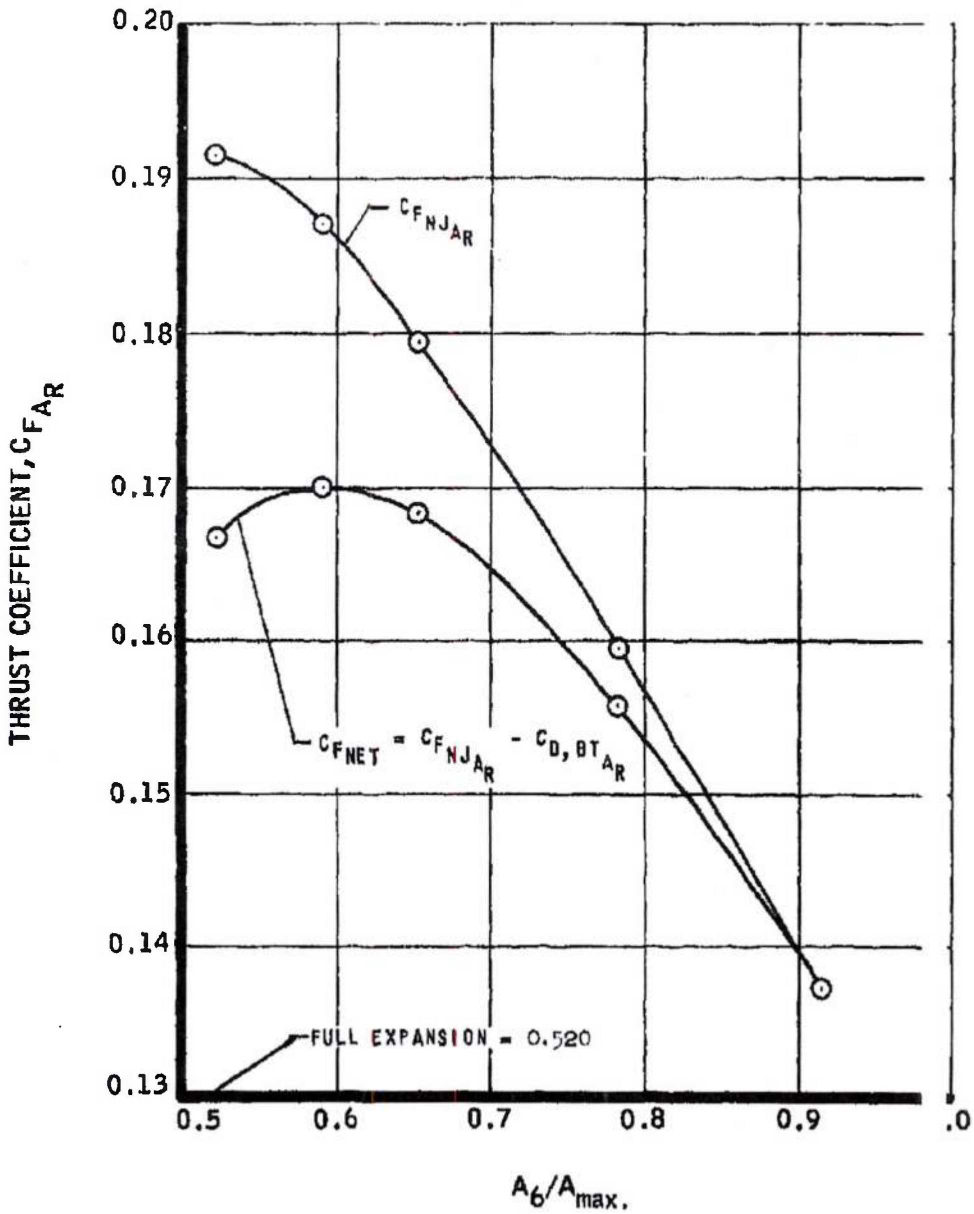

FIGURE 32

TABLE 4

FORCED CONVECTION CONFIGURATIONS

Configuration	Nozzle Area Ratio A_6/A_5	Length Ratio	Design Pressure Ratio Hot Condition	Design Pressure Ratio $\gamma = 1.4$	Comments
F.C. No. 1	3.567	1.00	2 2	28.0	Basic Clippinger Nozzle
F. C. No. 2	3.220	0.60	21.5	23.8	Intermediate Nozzle
F. C. No. 3	2.929	0.48	18.5	20.3	MA50-XCA Optimized Nozzle
F. C. No. 4	2.580	0.39	15.2	16.5	MA50-XCA Fully Expanded Nozzle

FORCED CONVECTION CONFIGURATION OF EXHAUST NOZZLE

X	Y
0.	27.56
14.46	27.56
25.73	21.53
32.44	17.61
41.44	15.20
41.94	15.20
43.78	15.29
45.58	15.57
46.79	15.84
49.80	16.58
52.81	17.32
55.83	18.08
58.83	18.85
61.84	19.61
64.85	20.40
67.86	21.14
70.87	21.84
73.88	22.48
76.89	23.04
79.90	23.56
82.91	24.07
85.92	24.54
88.93	25.00
91.94	25.40
94.94	25.81
96.60	26.02
97.95	26.18
100.96	26.51
103.97	26.84
109.99	27.33
116.01	27.75
122.03	28.10
128.05	28.37
134.07	28.59
140.09	28.72
146.11	28.79
153.03	28.83

CONFIGURATION	NOZZLE LENGTH X (INCHES)	AREA RATIO
F C NO. 1	153.03	3.60
F C NO. 2	109.99	3.24
F C NO. 3	96.60	2.93
F C NO. 4	85.29	2.59

REFERENCE:
MARQUARDT DWG. NO. X81289

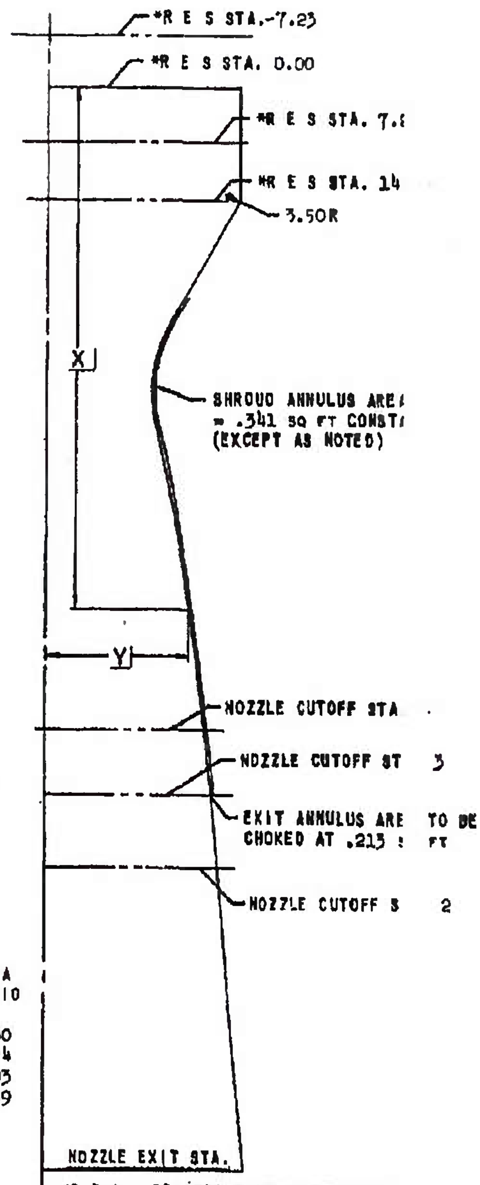

*R E S = REACTOR EXIT SIMULATION

EJECTOR CONFIGURATION OF EXHAUST NOZZLE

CONFIGURATION E 1
NOZZLE LENGTH [illegible] IN.
AREA RATIO [illegible]

X	Y	Y'
0	[illegible]	
[illegible]	[illegible]	
[illegible]	21.[illegible]	
[illegible]	17.61	
41.44	15.20	15.62
41.94	15.20	15.62
[illegible]	15.29	15.87
[illegible]	15.57	16.08
[illegible]		16.16
[illegible]		16.95
[illegible]		17.70
[illegible]		18.49
[illegible]		19.27
61.3[illegible]		20.08
[illegible]		20.39
67.8[illegible]		21.66
70.[illegible]		22.38
73.[illegible]		23.0[illegible]
76.8[illegible]		23.63
[illegible].90		24.17
[illegible].91		24.69
[illegible]		25.18
[illegible].93		25.66
91.9[illegible]		26.07
94.9[illegible]		26.49
96.60		26.70

REFERENCE:
MARQUARDT DWG. NO. X81290

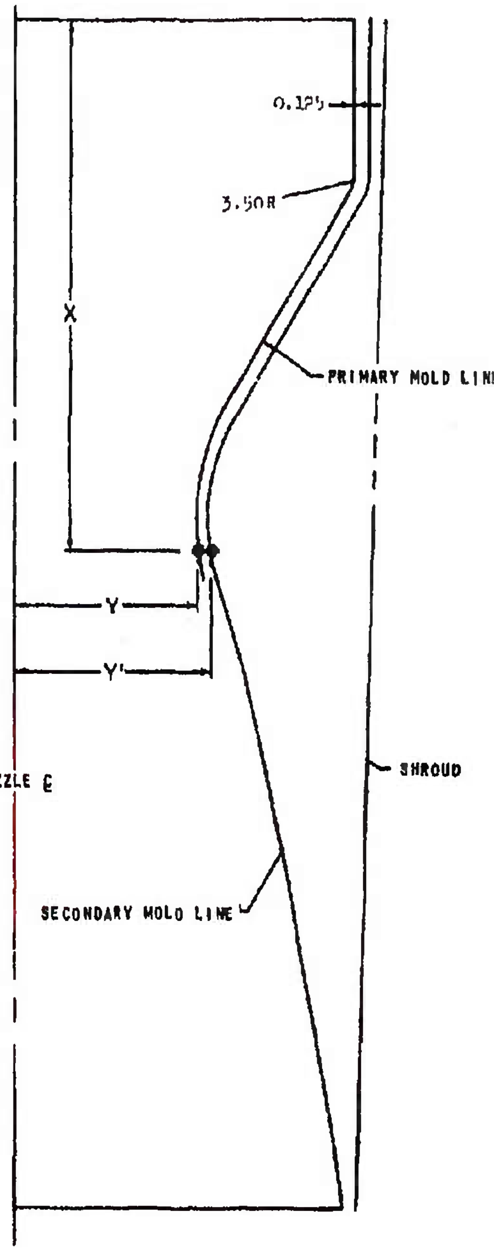

configurations have been conducted at the FluiDyne Engineering Cor ration Facilities at Elk River, Minnesota. Ninety-eight percent nozzle vel ity co-efficients have been recorded on all configurations tested. Results e further discussed in Section 3.8.2.

Aerothermodynamics of Nozzle Coolant Tubes

To analyze properly the installed characteristics of the coo nt-tube forced convection nozzle of Figure 31D, it is necessary to determine he aero-therm-dyr-amics of the cooling tubes. A computer program, Rita, v s written to solve the aerothermodynamics of the curved coolant tube by the m thod of finite differences. This program solves the heat transfer, friction, nd Mach number rise equations for a heated, curved tube of variable cross-s tional shapes and variable areas. This program was described in Referen 7.

Typical results of this program are as follows: A 3/4-inch nternal diameter tube was fitted to the nozzle contour of Figure 33. For tl s tube diameter, there is a total of 240 tubes forming the nozzle. For a to l coolant airflow of 113 lb/sec, each tube passes 0.47 lb/sec. The Mach num er into the tubes was 0.25. For these conditions the total pressure loss in the be was about 22 percent, the gas temperature rise was 183°F, and the maxi um tube wall temperature was 1500°F, occurring at the tube exit.

Program Rita has also been used to predict the pressure dr ps in the annular forced convection configuration. These relations are used t aid in the establishment of the optimum nozzle installation as discussed in a la r section of this report.

Nozzle Off-Design Performance

During the initial boost phase the ramjet exhaust nozzle mu operate as an unchoked (subsonic) nozzle. Similarly, at other points inside the ngine op-erating envelope the nozzle, although choked, may operate at pressu ratios sufficiently low to permit nozzle separation. Both of these condition invalidate the one-dimensional choked flow relationships assumed in the origin machine programs.

In Reference 7, a computer program was described wher a ramjet performance criteria during the initial boost phase could be determi d. This program, Nina, has been successfully run for the boost trajectory s own in Reference 10. The latest boost trajectory of the aerothermodynami contractor presented in Reference 11 has not been analyzed because the boost trajector has not been finalized for a missile sized to perform the ADO No. 11 mission.

Also presented in Reference 7 was the method of incorporating the experimental nozzle results into the computer program for more realistic t ust prediction at off-design conditions. These changes will be incorporated in a performance predictions next year.

Nozzle Configuration Studies

The aerodynamic analysis of the exhaust nozzle for the Model MA5 XCA engine has been handled at design point (Mach 2.8; ANA 421 Hot Day; altitud 1,000 feet) in two general categories. The more obvious was the investigat n of the primary propulsion nozzle, while the other was the performance evaluat n of the various cooling flows. The design criteria and techniques used to deriv the basic optimized primary nozzle contour were presented in Reference 9 and lis-cussed briefly above. The performance analysis of the primary flow will be pre-sented in the configuration study results to follow.

During the year, five techniques of nozzle cooling have been consid red as shown in Figure 31. Performance studies of the four more promising co ig-urations have been completed. These studies include the effect on net engin thrust of the primary nozzle flow, the engine cooling flow, the airframe coo ng flow, and the afterbody drag. The four configurations evaluated as installec sys-tems were:

(1) The annular, forced convection nozzle
(2) The tubular, forced convection nozzle
(3) The ejector nozzle
(4) The radiation cooled nozzle

With the first two configurations, the reactor side support cooling ow was maintained completely separated from the nozzle primary flow, while v h the third configuration, this cooling flow was introduced into the primary st am in the divergent section of the nozzle (just downstream of the primary nozzl throat). With the fourth configuration, the cooling flow was mixed with the i-mary flow upstream of the nozzle.

In the first two configurations listed above, the cooling flow drag w s minimized by expanding the secondary exhaust flow to equal the primary no le exhaust pressure with a convergent-divergent nozzle arrangement. The an ysis of each configuration was directed toward the definition of a nozzle [illegible] rust coefficient for each flow that was then used to establish the installed engi[illegible] net thrust coefficient including the nozzle afterbody and base drag.

The engine net thrust coefficient was expressed as:

$$C_{T_N} = C_{T_P} + C_{T_S} + C_{T_A} + C_{T_{BT}} + C_{T_b}$$

The net thrust coefficient of the primary nozzle flow is given by:*

$$C_{T_P} = 2\left[\frac{A_{oP}}{A_R}\left(C_{VP}\frac{V_{eP}}{V_o} - 1\right) + \frac{1}{\gamma_o M_o^2}\left(\frac{A_{eP}}{A_R}\right)\left(\frac{P_{eP}}{P_o} - 1\right)\right]$$

The net thrust equation for the secondary (engine cooling) f[illegible] w is:

$$C_{T_S} = 2\left[\frac{A_{oS}}{A_R}\left(C_{vS}\frac{V_{eS}}{V_o} - 1\right) + \frac{1}{\gamma_o M_o^2}\left(\frac{A_{eS}}{A_o}\right)\left(\frac{P_{eS}}{P_o} - 1\right)\right]$$

The net thrust equation for the airframe cooling flow is:

$$C_{T_A} = 2\left[\frac{A_{oA}}{A_R}\left(C_{VA}\frac{V_{eA}}{V_o} - 1\right) + \frac{1}{\gamma_o M_o^2}\left(\frac{A_{eA}}{A_o}\right)\left(\frac{P_{eA}}{P_o} - 1\right)\right]$$

The exhaust velocities, V_e, of each of the flows were the i[illegible] al velocities computed from the local properties at the beginning of each fin[illegible] expansion. The exhaust areas were the actual areas of each exhaust flow, and [illegible] thrust coefficients were referenced to the basic Model MA50-XCA 57-inch di[illegible] meter reference area. The exhaust pressure, P_e, was the nozzle exit press[illegible] e established in earlier studies of boattail-nozzle optimization (see Section [illegible].2.3).

The boattail and base drag coefficients are equivalent to th[illegible] expression:

$$C_D = \frac{A_{max}}{A_R}\int_{A_{min}}^{A_{max}} c_p \, dA$$

Values of boattail pressure coefficients were taken from Reference [illegible], while base pressure coefficients were taken from Reference 13.

*Symbol definitions at end of section.

Annular, Forced Convection Nozzle

The configuration of this nozzle is shown in Figure 35. Thi sys-tem used the basic optimized primary nozzle contour. The secondary cool ıg flow was passed through a constant flow area annular passage formed by th pri-mary nozzle wall and an outer shell. The airframe cooling flow was allow l to flow between the secondary outer wall and the airframe boattail. To reduc drag, pressures in both passages were maintained high by choking these fl vs near the exit of the exhaust with the dual-annular exhaust nozzle, which al permitted supersonic expansion to the primary nozzle exit pressure. Furt er, this arrangement eliminated the base drag consideration.

The ideal thrust of the primary nozzle was obtained by assu ing a one-dimensional isentropic expansion of the actual nozzle flow from the -stream total to the exhaust pressure, or simply:

$$F_{P_i} = \frac{W_P}{g} V_{epr}$$

The actual nozzle trust was computed from the expression:

$$F_P = \frac{W_P}{g} C_{VP} V_{eP}$$

where C_{VP} = 0.983, the experimentally determined coefficient presented i Section 3.8.2 of this report.

The secondary exhaust nozzle thrust coefficient was evaluat i by determining the pressure drop in the secondary annulus and computing the ctual thrusts of the secondary exhaust nozzle. The pressure drop was compute ısing the computer program Rlta described earlier in this section. A velocity c effi-cient of 96 percent was assumed for the secondary exhaust nozzle, and the exhaust velocity of both the actual and ideal cases was computed from the tual exhaust total temperature. The secondary nozzle exhaust flow was axial t minimize the divergence loss of this flow.

Tubular, Forced Convection Nozzle

The exhaust system of the tubular walled nozzle is shown in Figure 36. The primary nozzle thrust coefficient was assumed to be equ to that of the full annular nozzle, because any additional loss would be the re ılt of increased wall friction. Evaluation of the phenomena of boundary layer gr wth

DIAGRAM OF ANNULAR, FORCED CONVECTION NOZZLE EXHAUST S STEM

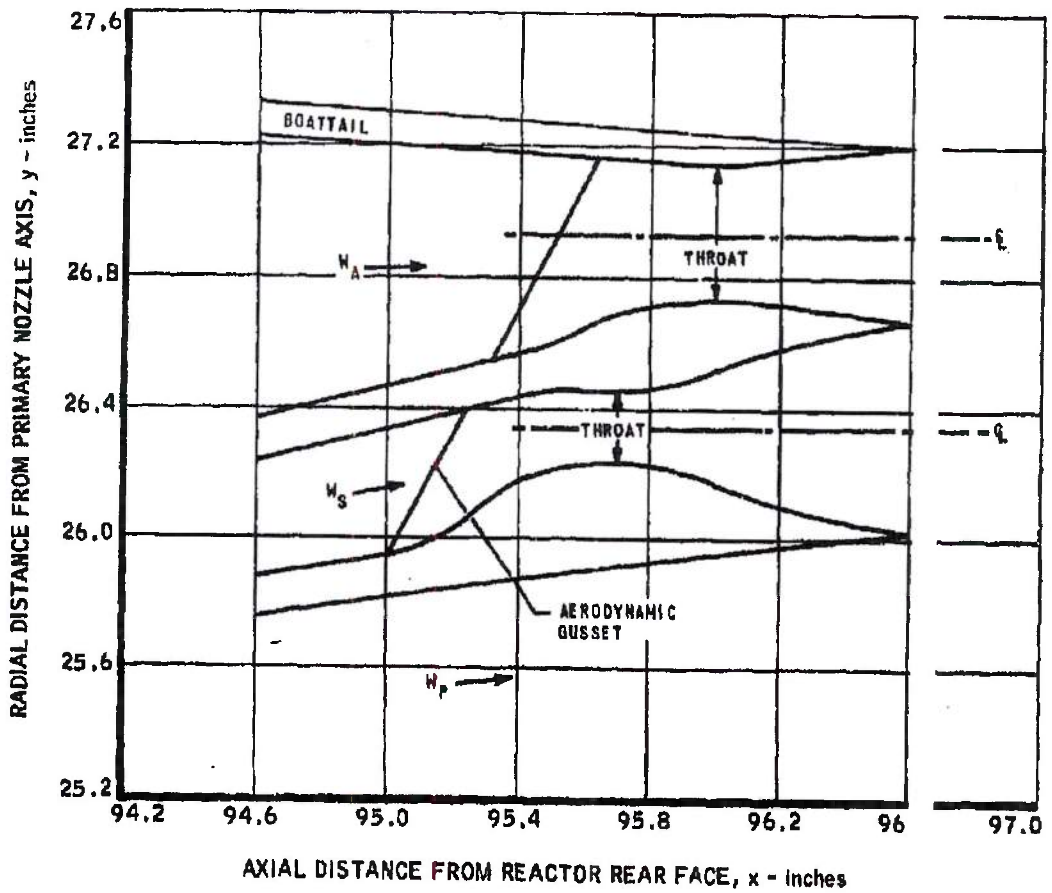

DIAGRAM OF TUBULAR, FORCED CONVECTION NOZZLE EXHAUST SYSTEM

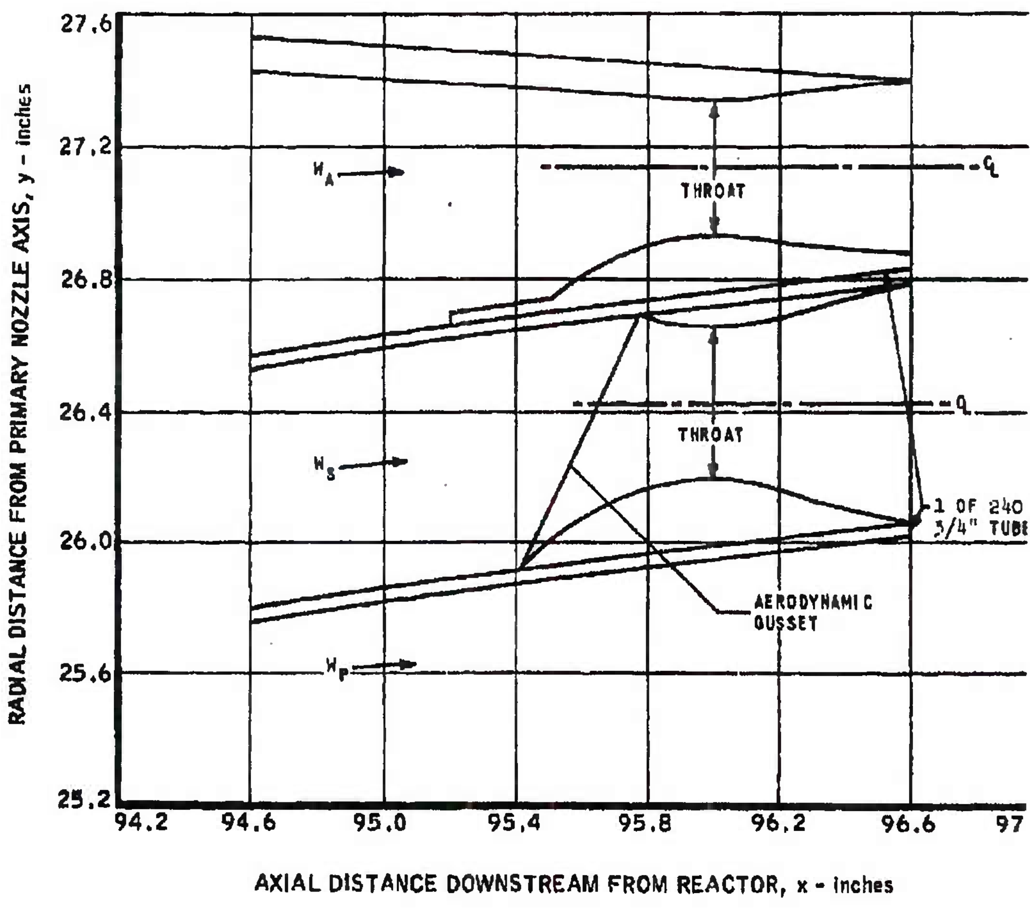

over the tubular wall to define a momentum loss that could be weigh . against the boundary layer momentum loss of the full annular nozzle would b excessively ambitious at this time. The analysis of the secondary flow was v y similar to the full annular case, the major differences being that there was . increased pressure drop through the tubes and that each of the 240 tubes incor rated a convergent-divergent nozzle at the exit.

Ejector Nozzle

The exhaust details of the ejector nozzle are shown i Figure 37. The analysis of the ejector nozzle was complicated by the supersoni mixing of the primary and secondary flows. This situation was handled by as ming each flow remained isolated from the other, but both were penalized by f ction with each other. Because the primary stream properties under the abov assumption (isolation) were identical with the full annular nozzle primary flow, was assumed that the friction loss between primary and cooling flows was function of the maximum velocity difference between the primary stream and th control volume causing the friction. A theoretical solution of the boundary yer loss of the primary flow in the annular nozzle provided a suitable reference Here the maximum velocity difference (stream to wall) was equal to the veloc y of the edge of the boundary layer at the nozzle exit. With the ejector nozz , the maximum velocity difference occurred where the secondary passage end d, because, with friction, the individual stream velocities would tend to converg Because the primary stream was assumed to slide within the sheath of the se ondary stream, the maximum velocity difference was merely the difference n velocity of the two streams at the above location. With these assumptions it as possible to write:

$$\Delta F_{ejector} = \Delta F_{forced\ convection} \frac{\text{maximum}\ \Delta V_{ejector}}{\text{maximum}\ \Delta V_{forced\ convecti}}$$

where ΔF was the momentum loss resulting from friction between t primary and secondary streams.

The actual thrust of the secondary flow was computed y using the total pressure at the secondary passage exit and the nozzle exit pre ure, and by subtracting one half of the $\Delta F_{ejector}$ term above. The pressure rop of the secondary passage upstream of the secondary unit was computed us g the program Rita. Because the total pressure of the secondary flow was e luated through the sonic region to the secondary flow passage exit, the noz e velocity coefficient was assumed to be unity. However, this secondary exha t flow was

DIAGRAM OF EJECTOR NOZZLE EXHAUST SYSTEM

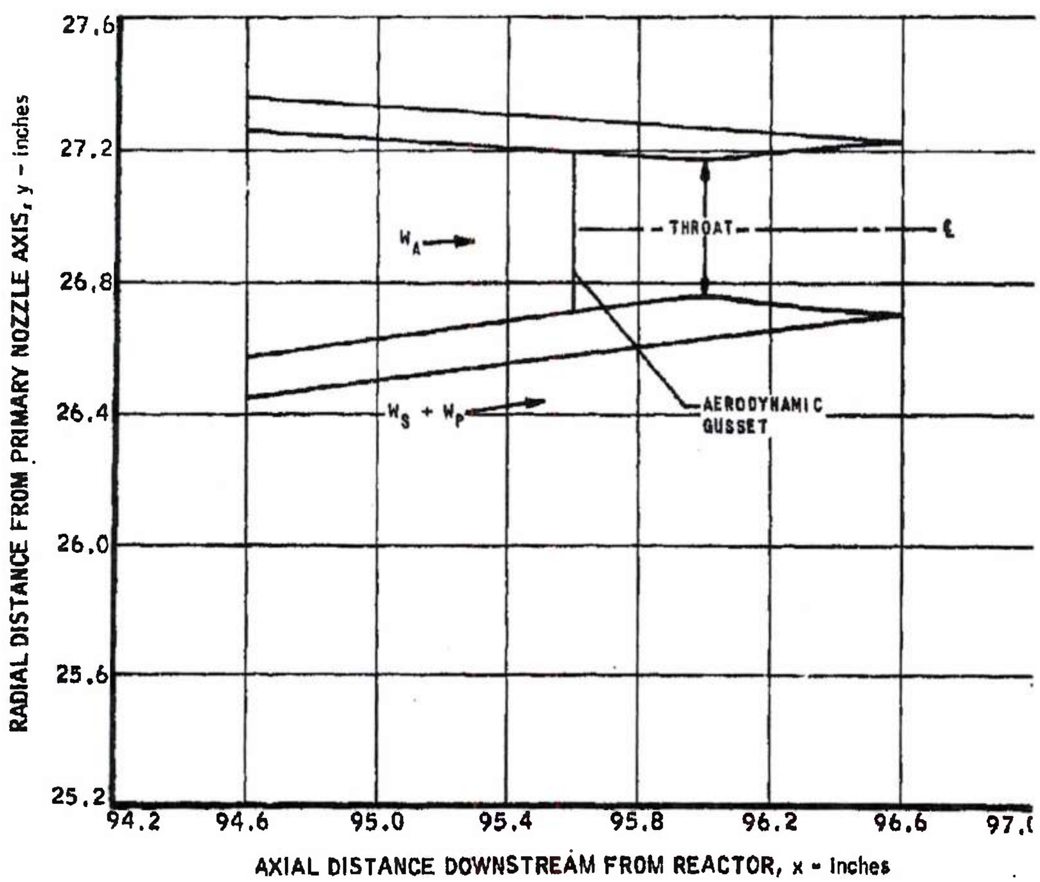

penalized for divergence loss at the exhaust nozzle exit. Both the a tual and ideal exhaust velocities were evaluated at the actual total temperatu e at the exit of the secondary passage.

To compute the actual thrust of the primary flow, th above analysis of the secondary flow was used in conjunction with reliable exp rimental data from a model of the specific configuration under analysis. Th two quantities were related by:

$$C_{VPS} = \frac{W_P C_{VP} V_{ePi} + W_S C_{VS} V_{eSi}}{W_P V_{ePi} + W_S V_{eSi}}$$

The combined coefficient, C_{VPS}, was presented in Section 3.8.2 of his report and obtained experimentally. The coefficient, C_{VS}, was the ratio c actual to ideal thrust of the secondary flow. With these coefficients, it was ssible to solve for the nozzle thrust coefficient, C_{VP}, of the primary flow, v ich would include friction, divergence, and interaction losses.

Radiation Cooled Nozzle

The exhaust configuration of this nozzle is shown in gure 38 . With this configuration, the secondary cooling flow was mixed with e primary flow at the reactor exhaust. Complete mixing was assumed upstrea from the nozzle, and both the primary and secondary flows were expanded th ough the single (somewhat larger) "primary" nozzle. Divergence and frictic losses were considered as in the case of the annular nozzle.

Nozzle Flow Conditions

Primary Flow

The primary flow rate for all configurations analyze was 1577 lbs/sec. The total pressure at the nozzle inlet was 31,000 psfa, ar the total temperature was 2060°F. Both were assumed constant throughout e expansion of the isentropic core to the optimized nozzle exhaust pressure of 1 10 psfa.

Secondary Flow

The secondary flow rate for all configurations consic red was 100 lbs/sec. The total pressure at the reactor side support exhaust wa taken to be 36,700 psfa for all cases except for the radiation cooled nozzle. T total temperature at this axial station was 1060°F. Total pressure drop and otal

DIAGRAM OF RADIATION COOLED NOZZLE EXHAUST SYSTEM

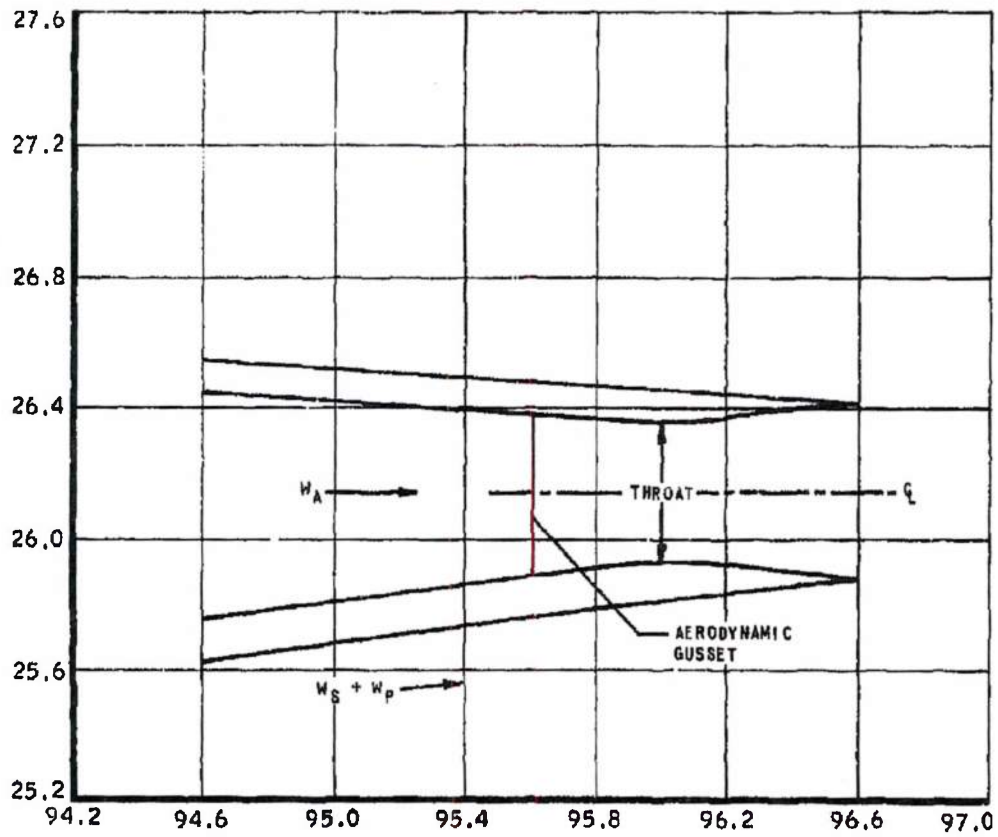

temperature rise resulted from friction and heat transfer to the se ndary flow. The secondary flow of all configurations evaluated was expanded to 680 psfa.

Airframe Cooling Flow

The aerothermodynamics contractor furnished the d a for this flow. The weight flow was 42.3 lbs/sec, and total pressure at the actor exit station was 7200 psfa. The flow exhaust was choked with 70.0 squa e inches of flow area. Solution of the continuity equation defined the total temp rature as 1280°F. To avoid the inconsistency of omitting one of the afterbod flows in the exhaust system analysis, the thrust coefficient of the airframe coo g flow was computed. For this computation, total temperature was assumed c nstant, and a 2 percent total pressure drop within the boattail was assumed. T is flow was also expanded to 1680 psfa.

Results

The primary nozzle thrust coefficient, C_{V_P}, was assume dentical for the annular and the tubular configurations and was established 0.983. The thrust coefficient of the primary flow with the ejector configuration was determined to be 0.9825. This reflected an interaction loss of approxim tely 0.05 percent from the basic forced convection configuration.

The thrust coefficients, total pressure drop, and total ten erature rise of the secondary flow expansion, where appropriate, were as llows:

	C_{V_S}	P_T (%)	T_T (°F)
Annular Nozzle	0.929	-14.1	+ 98
Tubular Nozzle	0.929	-21.8	+180
Ejector Nozzle	0.953	-11.4	+ 63

The decrease in thrust coefficient resulting from an increase in pr sure drop was compensated, to a degree, by an increase in total temperature

The primary and secondary flows of the radiation cooled n zzle were mixed prior to entering the nozzle. This condition resulted in a to l temperature of the mixture of 1990°F, or a change of 70°F, which would h e little effect on friction losses and divergent losses of the basic primary zzle. Thus the nozzle thrust coefficient for the combined primary and seconda flows of this configuration was also 0.983.

The boattail drag coefficient, $C_{D_{BT}}$, was determined to be -0.018 or the optimized nozzle-boattail configuration. Small variations in boattail ex area between configurations were assumed insignificant. The tubular nozz inherently had a section of base area and a resulting base drag coefficient, C_{D_b}, of -0.0056.

The net thrust coefficient of the various flows was as follows:

	C_{T_P}	C_{T_S}	C_{T_A}
Annular Nozzle	0.1983	-0.0007	-0.0028
Tubular Nozzle	0.1983	-0.0020	-0.0028
Ejector Nozzle	0.1977	-0.0004	-0.0028
Radiation Cooled Nozzle	0.1957	- -	-0.0028

The net thrust coefficients of the various installed exhaust system evaluated were as follows:

	C_{T_N}
Annular Nozzle	0.1768
Tubular Nozzle	0.1699
Ejector Nozzle	0.1765
Radiation Cooled Nozzle	0.1749

The above net thrust coefficients give an approximate comparison the four general configurations considered. The annular and the ejector con g-urations appear slightly favorable in the initial analysis. It is evident that ie tubular nozzle was penalized by higher pressure drop and base drag. The dia-tion cooled nozzle coefficient was slightly low as a result of the inefficient ix-ing upstream from the nozzle. While some optimization is evident in the a ive configurations, they still are only arbitrary configurations, analyzed for ge eral comparison. They cannot be considered sufficiently sophisticated to permi selection or elimination. Prior to final selection, the favored configuratio will be mechanically optimized to assure efficient fabrication.

The particular exhaust system selected for the Model MA50-XCA gine should be the one that yields superior performance and can be satisfactoril cooled. The superior performance should occur at design conditions, but t s cooling requirements must be fulfilled at the most extreme heating condition, which will be at off-design conditions. The performance of the pri ary nozzle has been optimized with regard to the boattail drag, and the cooling system is currently being optimized. To fairly evaluate each of the cooling s iemes under consideration, each should be optimized with respect to temperatu and mechanical design. The performance of each optimum cooling configura .on should then be evaluated for selection of one optimum configuration.

Generally, the nozzle cooling flow conveniently available l s been established by reactor and airframe cooling requirements. Furthe geometric variations can control, to a degree, the effectiveness of the cooling low. By increasing the local Mach number of the cooling flow, the nozzle w l temperature may be reduced, but the drag of the cooling flow will increase ecause of increased pressure drop. To minimize this drag, the geometric c figuration that will yield the maximum acceptable metal wall temperature wil be the one that will have the lowest pressure drop. When this configuration h been established, the cooling system analysis will continue with optimizati of nozzle performance by optimizing nozzle cooling flow.

Nomenclature

A = Area
C_D = Drag coefficient
C_T = Thrust coefficient
C_V = Velocity coefficient (also, nozzle thrust coefficie)
F = Thrust
M = Mach number
P = Pressure
T = Temperature
V = Velocity
W = Weight flow
g = Acceleration due to gravity
c_p = Local pressure coefficient
γ = Ratio of specific heats
θ = Angle with nozzle axis

Subscripts

A = Airframe cooling flow
BT = Afterbody boattail
N = Net (or installed)
P = Primary flow

Subscripts (Continued)

R	=	Reactor
S	=	Secondary flow
T	=	Stagnation conditions
b	=	Afterbody base
e	=	Exit (or exhaust)
i	=	Ideal
ic	=	Isentropic core
max	=	Maximum quantity of a considered interval
min	=	Minimum quantity of a considered interval
o	=	Free stream conditions
pr	=	Within limits of pressure ratio
w	=	Nozzle wall

3.3 ENGINE PERFORMANCE SUMMARY (PERFORMANCE BULLETIN NO. 4)*

3.3.1 Introduction

The purpose of the performance bulletin is to disperse quickly to interested parties The Marquardt Corporation's prediction of the performance of a nuclear ramjet propulsion system incorporating the Tory IIC type reactor. The first two performance bulletins presented performance of the Marquardt Model MA50-XCA propulsion system incorporating the basic Tory IIC reactor. Performance Bulletin No. 3, describing the Model MA50-XDA propulsion system, departed from the basic Tory IIC reactor design in that the reactor length was decreased and the diameter was increased.

This fourth performance bulletin represents Phase II of performance prediction, wherein reasonable advancements over present Tory IIC technology are studied. LRL has concurred in the basic feasibility of each of the items discussed herein.

*Dated 31 December 1961.

In general, these performance bulletins follow the format et forth in Reference 14. (See Item IV of the section entitled "Reports and D a Requirements.") Each bulletin supplements rather than replaces precedin bulletins.

3.3.2 Summary

With the publication of the first three performance bulleti , Phase I of the 1961 propulsion system performance prediction ended. This phase has been devoted to propulsion systems incorporating present Tory IIC echnology. Design point performance, off-design characteristics, and diamete scaling effects were presented along with inlet pressure recovery and reac or wall temperature influence coefficients. Performance Bulletins No. 1 nd No. 2 summarize Marquardt's prediction of performance of the Model M 50-XCA system using the basic Tory IIC reactor.

Using the engine size scaling information contained in the bulletins, the aerothermodynamic contractor established that the basic react diameter would have to increase from the nominal Tory IIC size of 57.0 to a out 63.0 inches to accomplish the ADO No. 11 mission. In order to improv aerothermodynamic performance as well as to reduce reactor weight, the f rward reflector thickness was decreased by 4 inches, the fueled length of th core was decreased by approximately 4 inches, and reactor diameter was in reased from 57.0 to 63.0 inches. This propulsion system, designated the MA50-XDA, provides the thrust necessary to perform the ADO No. 11 mission. This system was reported in Performance Bulletin No. 3.

Phase II of this year's effort, discussed in this fourth bul tin, deals with the Model MA50-XCA system performance effects associated ith realistic modifications to the Tory IIC reactor geometry and technology. G metric modifications include:

(1) Optimization of the reactor length-to-diameter ratio, L/D_e for constant D_e.

(2) An increase in the diameter of the base-block billet, hich allows a reduction in the number of tie rods.

(3) A change in fuel region void fraction by increasing th fuel element tube diameter.

Technological modifications include:

(1) Modifying the core power profile to maintain a consta elastic thermal stress of 15,000 psi and/or a maximum reac r wall temperature of 2500°F.

(2) Modifying the core power profile to maintain a constant elastic thermal stress of 18,000 psi and/or a maximum reactor wall ten perature of 2500°F. This higher stress limit study is prompted by the results achieved with the Tory IIA reactor, which operate successfully at power levels higher than design point.

(3) Reducing the amount of air flow to the tie rods, until a limiting temperature of 1650°F is achieved.

Finally, operating envelopes have been established for the basic Mod MA50-XCA propulsion system.

3.3.3 Scope

The goal of the Pluto performance studies conducted to date has been ıe incorporation of the Tory IIC type reactor in a reliable nuclear ramjet propul on system capable of performing Air Force mission requirements. Performanc Bulletin No. 4 differs from previous studies in that it is based on important e: en-sions of present Tory IIC technology. The performance gains achieved are be lieved realistic for a flight type propulsion system.

The design point for the Marquardt nuclear ramjet propulsion system s Mach 2.8, at a pressure altitude of 1,000 feet, under ANA Hot Day temperatur conditions. The maximum reactor wall temperature is 2500°F.

This performance bulletin includes the following:

Design

A brief description of the Model MA50-XCA engine is included w h drawings, weights and center of gravity, dimensional information for mountin points, and an over-all envelope including basic airframe dimensions. A maj modification of the reactor lateral support structure has been incorporated int the propulsion system design. The pressure vessel has been eliminated from ıe design, with the inner airframe skin assuming the function previously perform d by this component. The female track is now an integral part of the expansion shell and the male rail is still fastened to the airframe structure as previousl shown. The tangentially aligned Belleville spring stacks and the track and rai structure are integrated into a compact annulus. This system reduces the air frame outer mold line diameter by 4.375 inches.

Heat Rejection

Heat rejection rates for the Model MA50-XDA propul on system of Reference 4 are presented for design point conditions.

Performance

Model MA50-XCA propulsion system design point info mation (Reference 3) is presented in tabular form to be used as a basis fo compari- son with the following studies:

(1) The effects of reducing the front reflector 4 inches an the aft fueled core 4.1 inches.

(2) The effects of changing the core power profile to yiel a constant elastic thermal stress of 15,000 psi and/or a maximu wall tem- perature of 2500°F. For this study, the properties o thermal conductivity, modulus of elasticity, and the coefficien of expan- sion were considered to be temperature dependent.

(3) The effects of changing the core power profile to yiel a constant elastic thermal stress of 18,000 psi and/or a maximu wall tem- perature of 2500°F.

(4) The effects on performance when the basic base-block billet size is increased to 9 inches from the present 5 inches. F r this case the number of tie tubes has been reduced by the ratio :9, and the volume originally occupied is replaced with fueled co tubes.

(5) The effects of reducing the tie rod airflow until the ti rod reaches an equilibrium temperature of 1650°F.

(6) The effects of increasing the core void fraction by inc easing the fueled tube diameter from 0.227 to 0.230 inches.

Operating Envelopes

Operating envelopes for the basic Model MA50-XCA p opulsion system are described for the ANA Hot and Cold Days and the ICAO tandard Day temperatures. High speed operation is limited either by a ram air otal temper- ature of 1070°F or a diffuser duct pressure of 420 psia.

3.3.4 Definitions

Net Jet Thrust - Net jet thrust is defined as the sum of the change (momentum of the mass flow through the engine and the pressure differential acting upon the exit area, as shown in the following equation:

$$F_{nj} = \left(\frac{W_6 V_6 - W_o V_o}{g}\right) + \left(P_6 - P_o A_6\right)$$

The exit area (A_6) used in this equation corresponds to a fully expa l- ed nozzle at the design point. The momentum of the air used to cool both th side support system inside the pressure vessel and the exit nozzle is includ in the net jet thrust.

Net Jet Thrust Coefficient - Net jet thrust coefficient is defined as e net jet thrust divided by the incompressible dynamic pressure and by the re r- ence area of the reactor in square feet as shown in the following equation:

$$C_{F_{nj}} = \frac{F_{nj}}{1/2\ \rho_o V_o^2\ A_R}$$

The reference area used in this bulletin for the propulsion system, is 17.72 square feet.

Engine Installation Drag - Engine installation drag is defined as the sum of the inlet supersonic spillage drag, inlet bleed drag, and the engine b pass drag necessary for engine matching.

By agreement, the airframe contractor will take into account:

(1) The inlet installed drag other than the supersonic spillage tern such as the cowl drag, the diverter drag, and the inlet base dr

(2) The drag attributed to air bleed from inlet duct for power actu tion, air conditioning, or cooling of gamma-neutron shielding (airframe outside the pressure vessel

(3) Nozzle base and boattail drag

The drag of these items must be included to obtain the actual instal d thrust.

Engine Installation Drag Coefficient - Engine installation ag coefficient is defined as the engine installation drag of the previous paragr h divided by the incompressible dynamic pressure and the reference area of e reactor.

Installed Net Thrust - The installed net thrust is equal to e net jet thrust minus the engine installation drag. As pointed out in a prev us paragraph, only a portion of the engine installation drag is included her n.

Installed Net Thrust Coefficient - Engine installed net thr t coefficient is defined as the engine installed thrust divided by the incompre sible dynamic pressure and the reference area of the reactor.

Symbols - The following symbols and subscripts are used:

	Description	Unit
A	Cross-sectional area	sq ft
C	Coefficient	- -
F	Thrust	lb
M	Mach number	- -
P	Pressure	psf
T	Temperature	°Rankin
V	Velocity	fps
W	Weight flow rate	pps
g	Gravitational acceleration, 32.17	ft/sec^2

Subscripts - Subscripts shall be employed in accordance v h the following station identification sketch and tabulation:

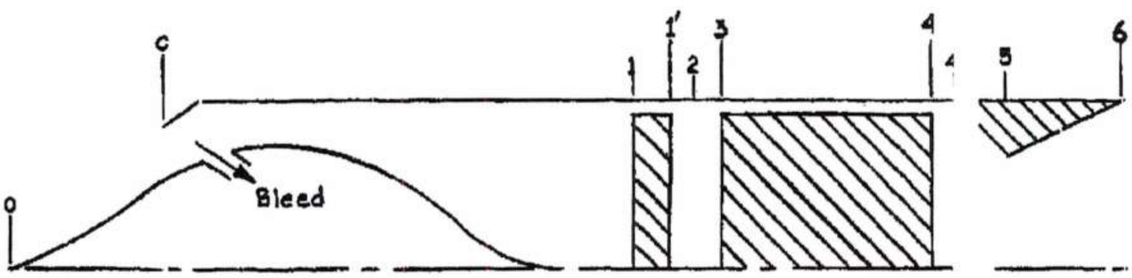

	Description
0	Free stream conditions
1	Forward face of reactor support grid
1'	Exit of reactor support grid
2	Plenum upstream from reactor face
3	Forward face of reactor
4	Exit of reactor
4'	Plenum downstream from reactor
5	Nozzle throat
6	Nozzle exit
c	Cowl lip
D	Drag
F	Thrust
j	Jet
n	Net
R	Reactor
s	Static
t	Total
w	Wall

3.3.5 Limitations

The performance of the basic Model MA50-XCA propulsion syste is based on the component nuclear heat generation data of Reference 1. W minor exceptions, which are generally discussed in the respective areas, nu- clear heat generation values for this performance bulletin were also take from Reference 1. However, the reactor power profiles for the 15,000-psi a 18,000-psi elastic thermal stress studies were generated by Marquardt.

The following revisions were made to the basic Model MA50-XC pro- pulsion system:

(1) Four inches of the reactor forward reflector have been rem ed and the nuclear heat generation in the remaining 6 inches ha not been changed from that shown in Reference 1.

(2) Four and one-tenth inches of material have been removed fr n the reactor aft core region, and the core power profile (as pres nted in Reference 1) has been terminated at this point.

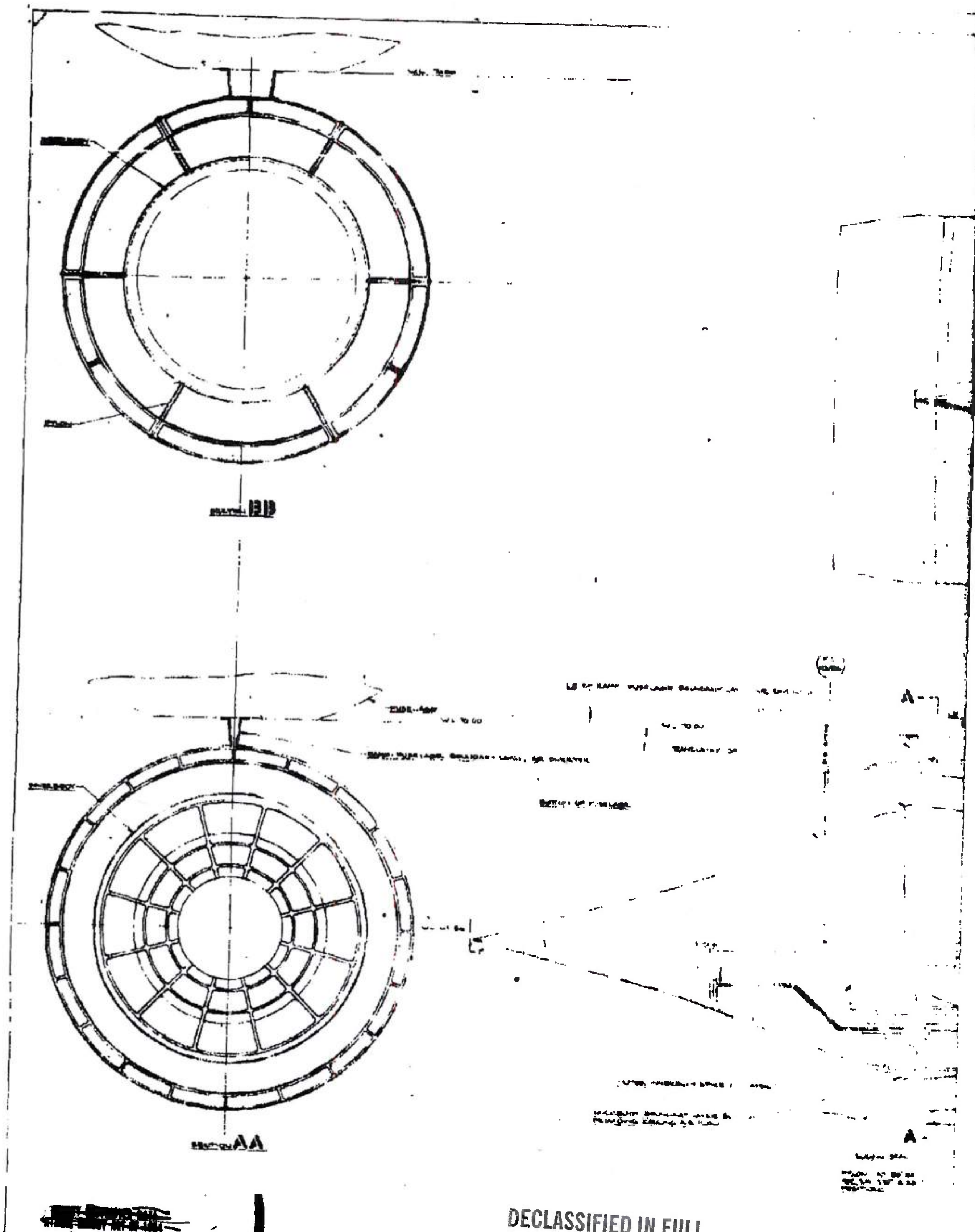

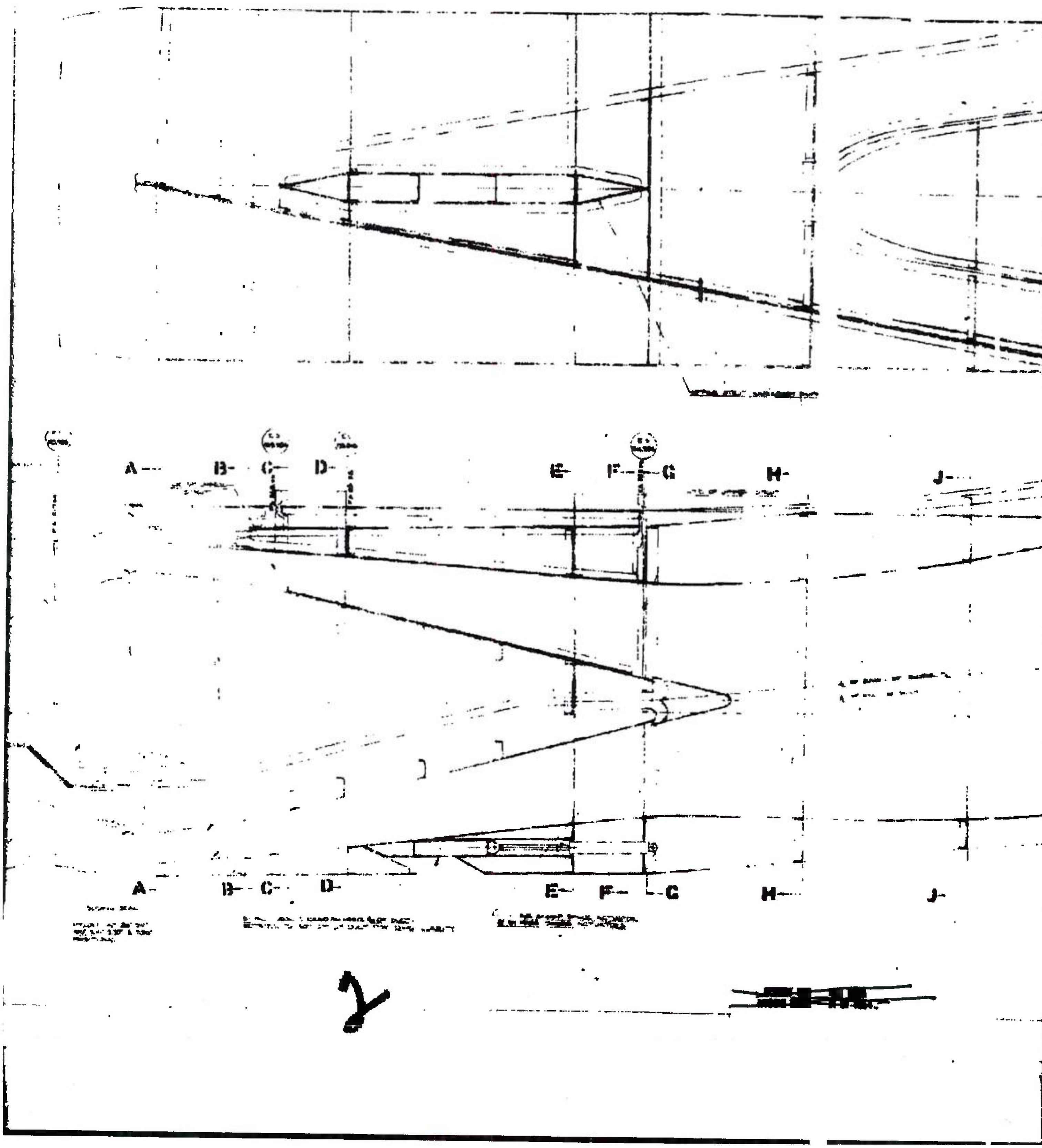
A
B
C
D
E
F
G
H
J

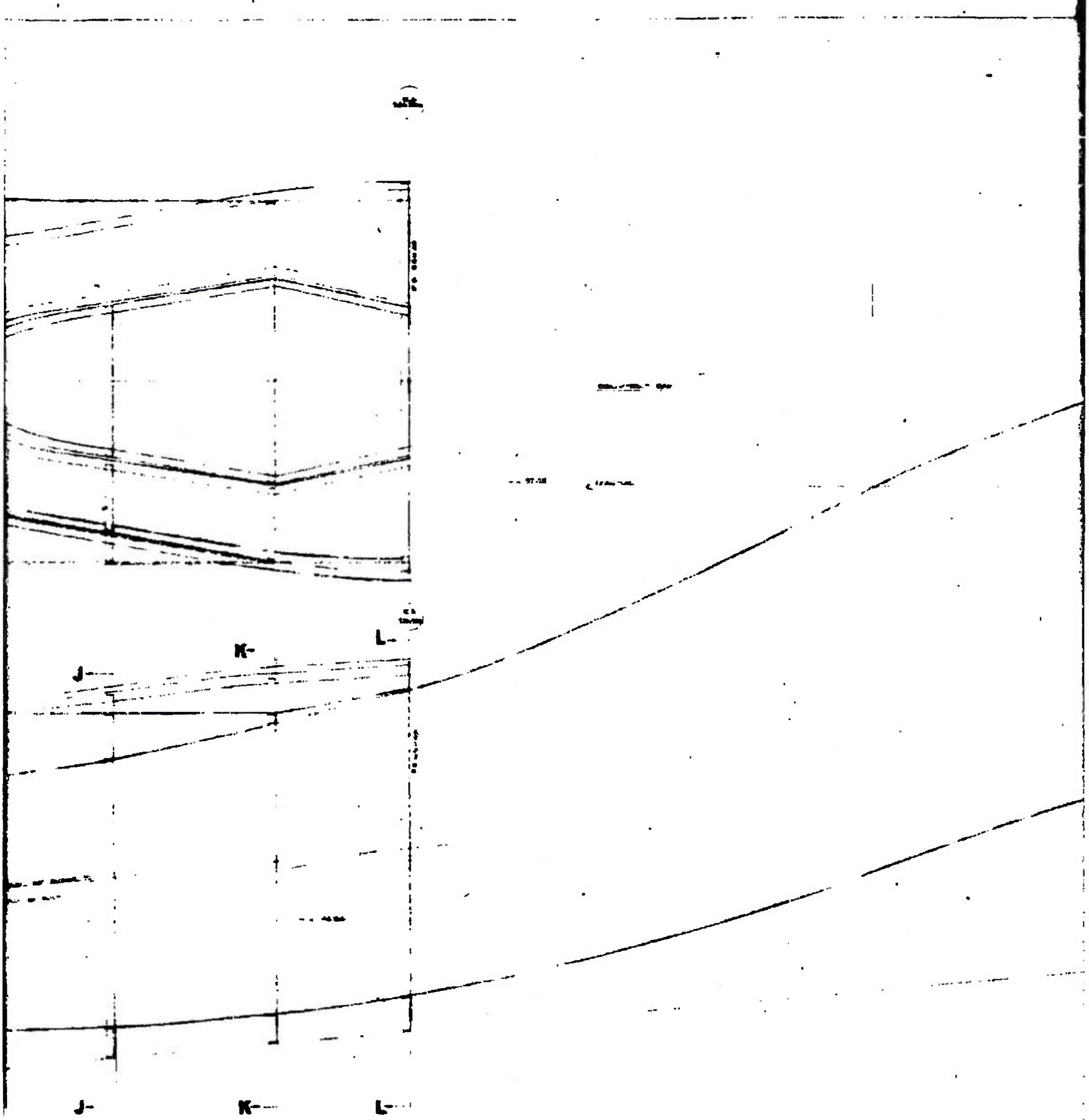

3

~~SECRET RESTRICTED DATA~~
~~ATOMIC ENERGY ACT OF 1954~~

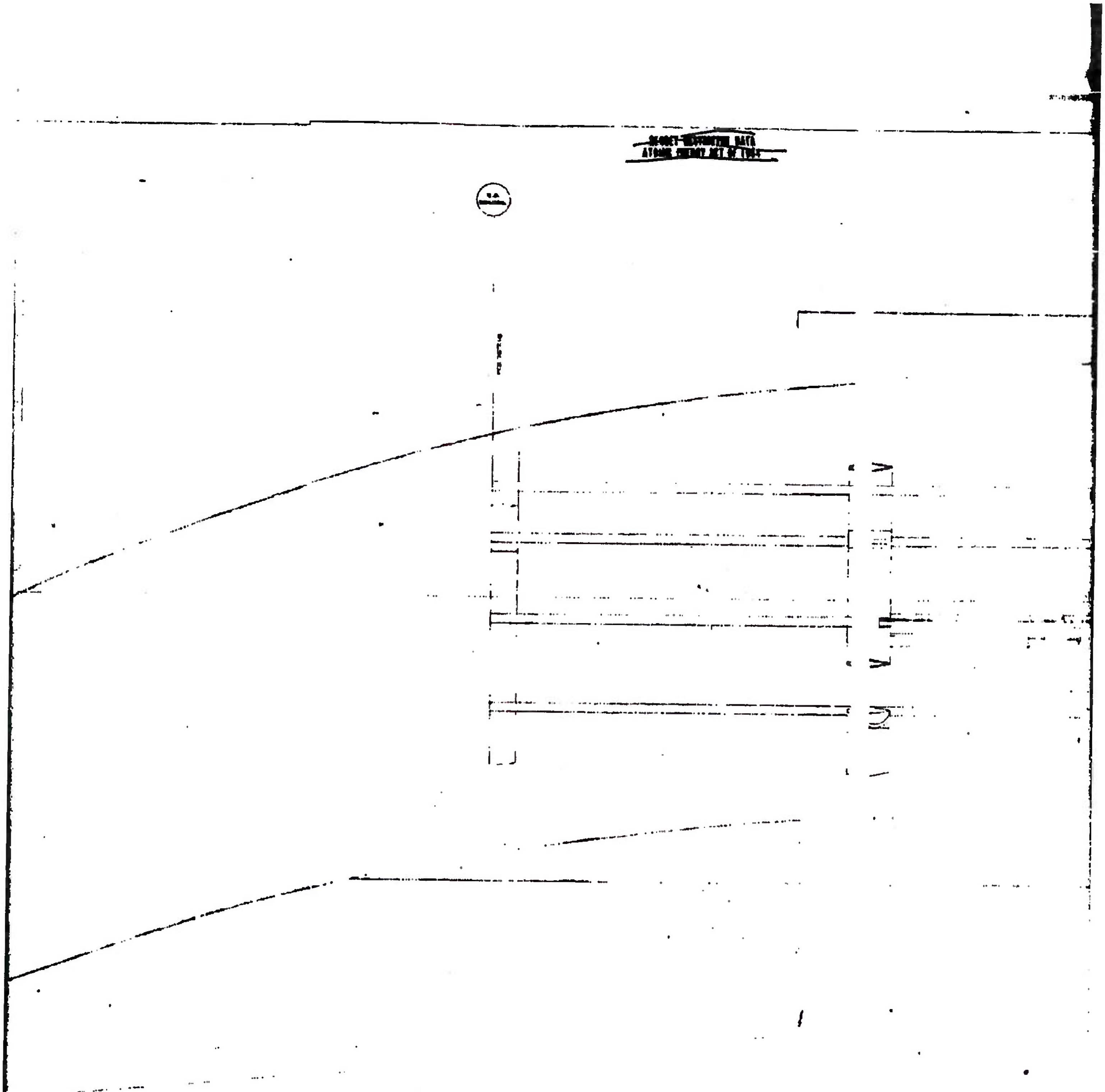

DECLASSIFIED IN FULL
Authority: EO 13526
Chief, Records & Declass Div, WHS
Date: MAY 2 9 2015

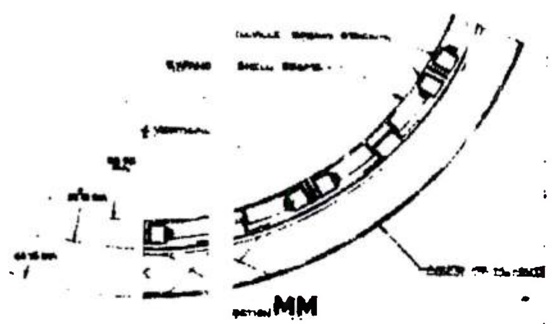

SECTION MM

~~SECRET RESTRICTED DATA~~
~~ATOMIC ENERGY ACT OF 1954~~

4

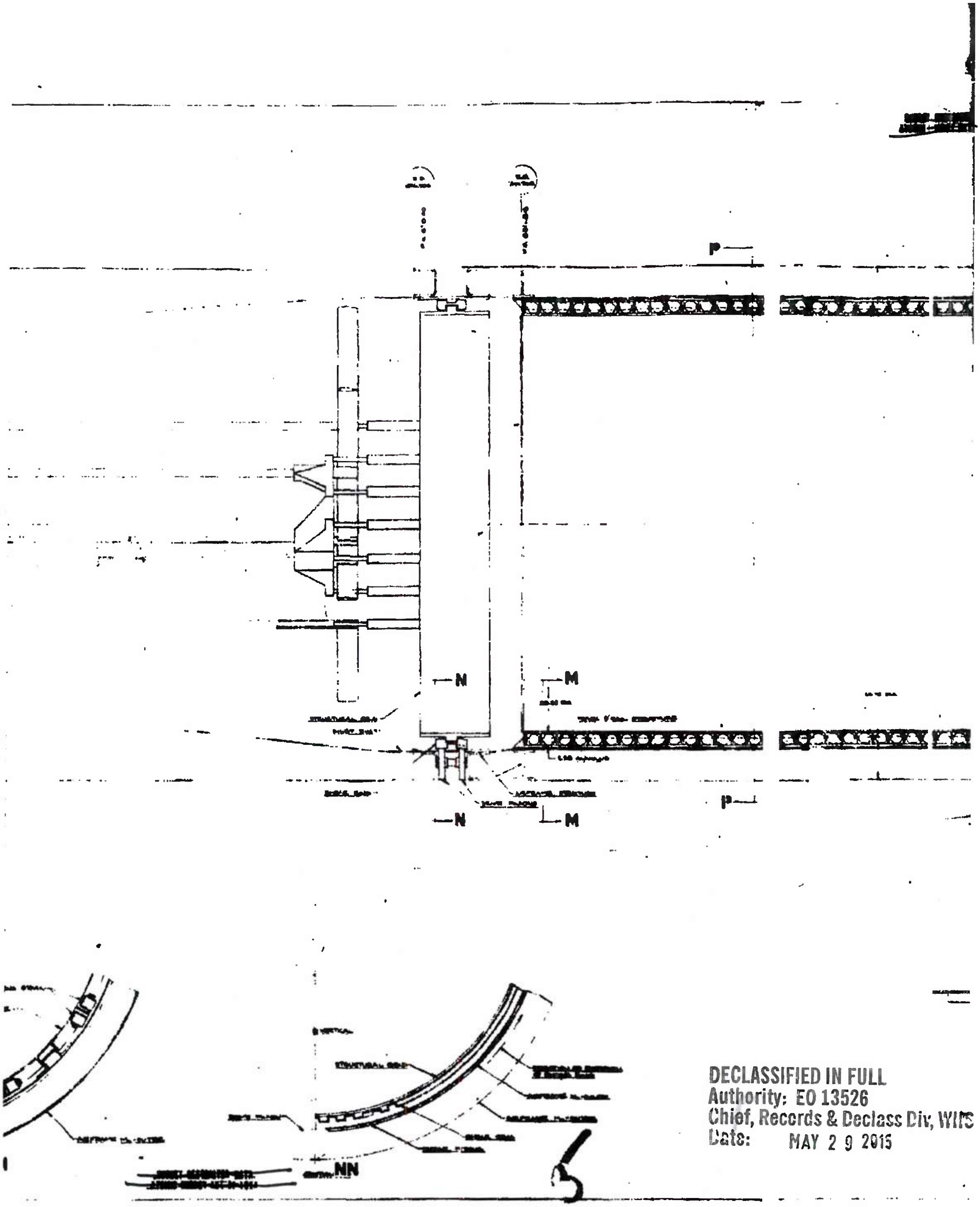
P
N
M
P
N
M
NN

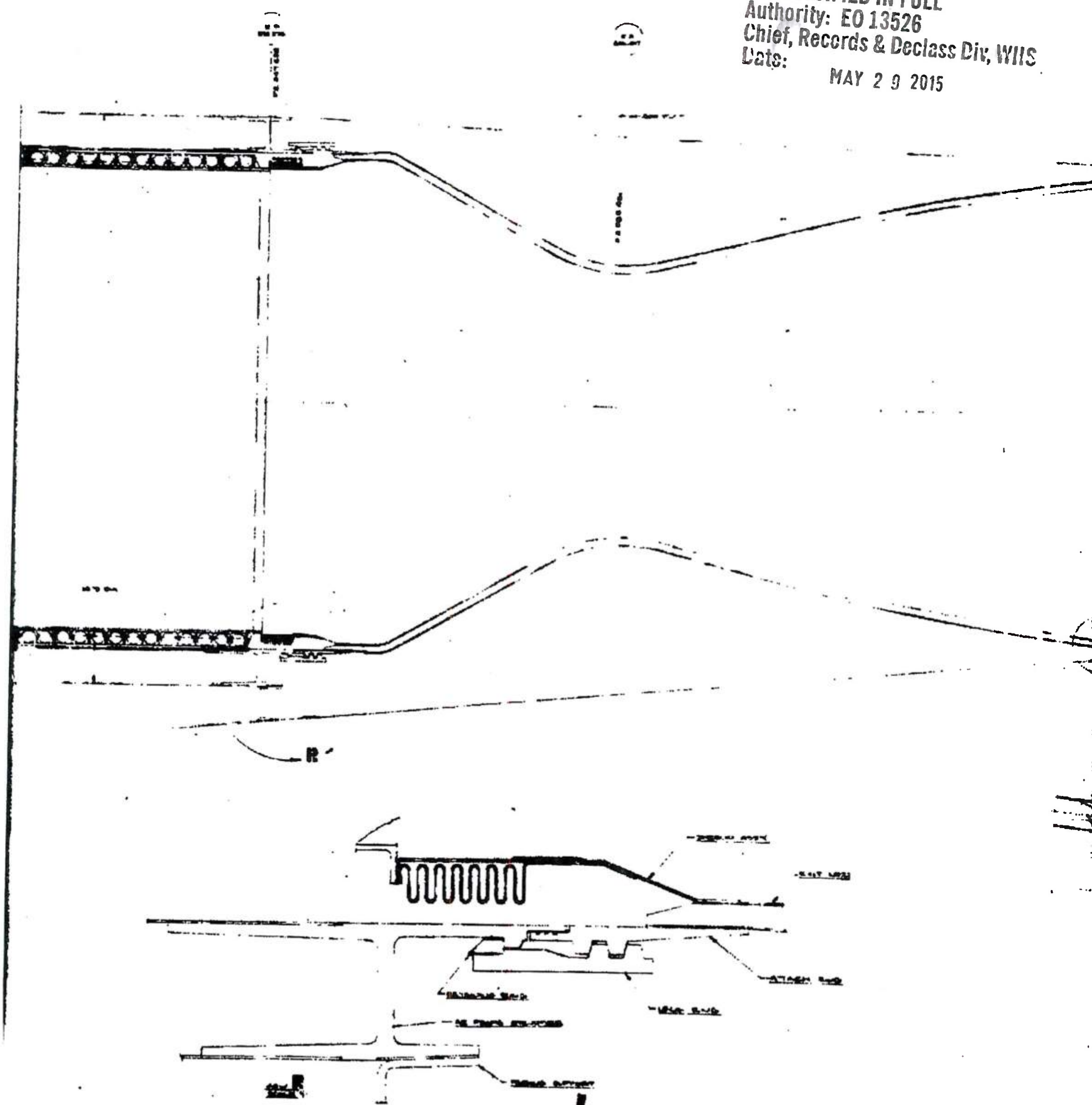

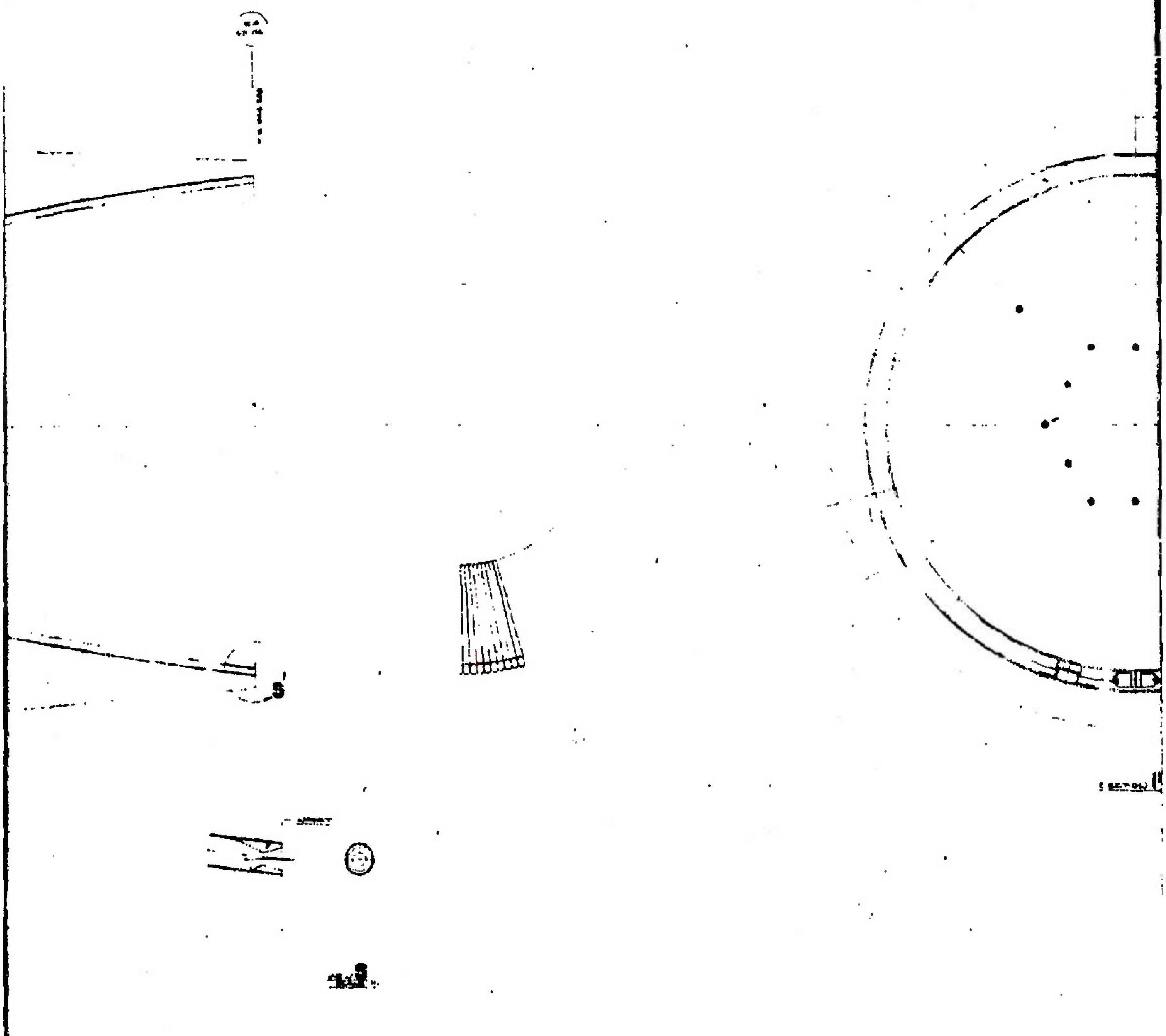

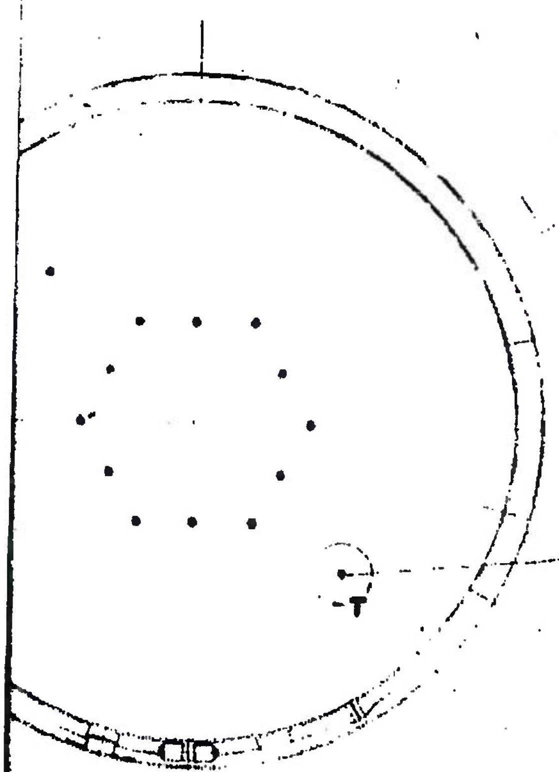

PP

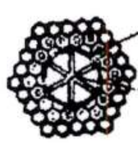

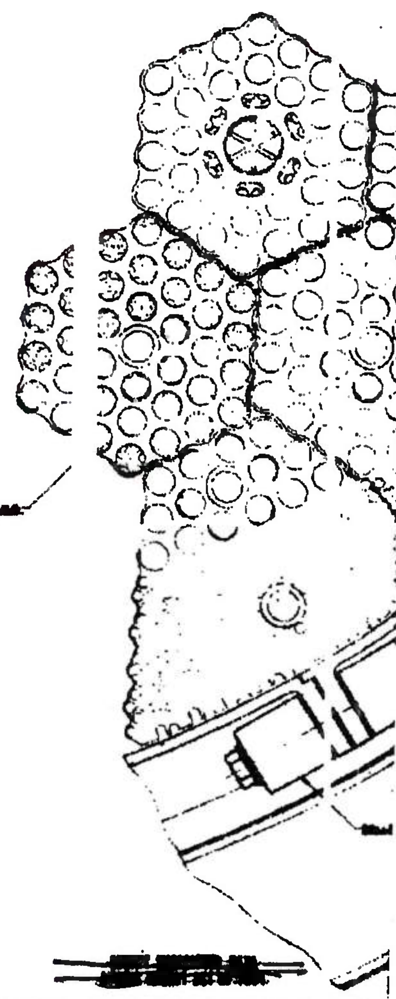

4

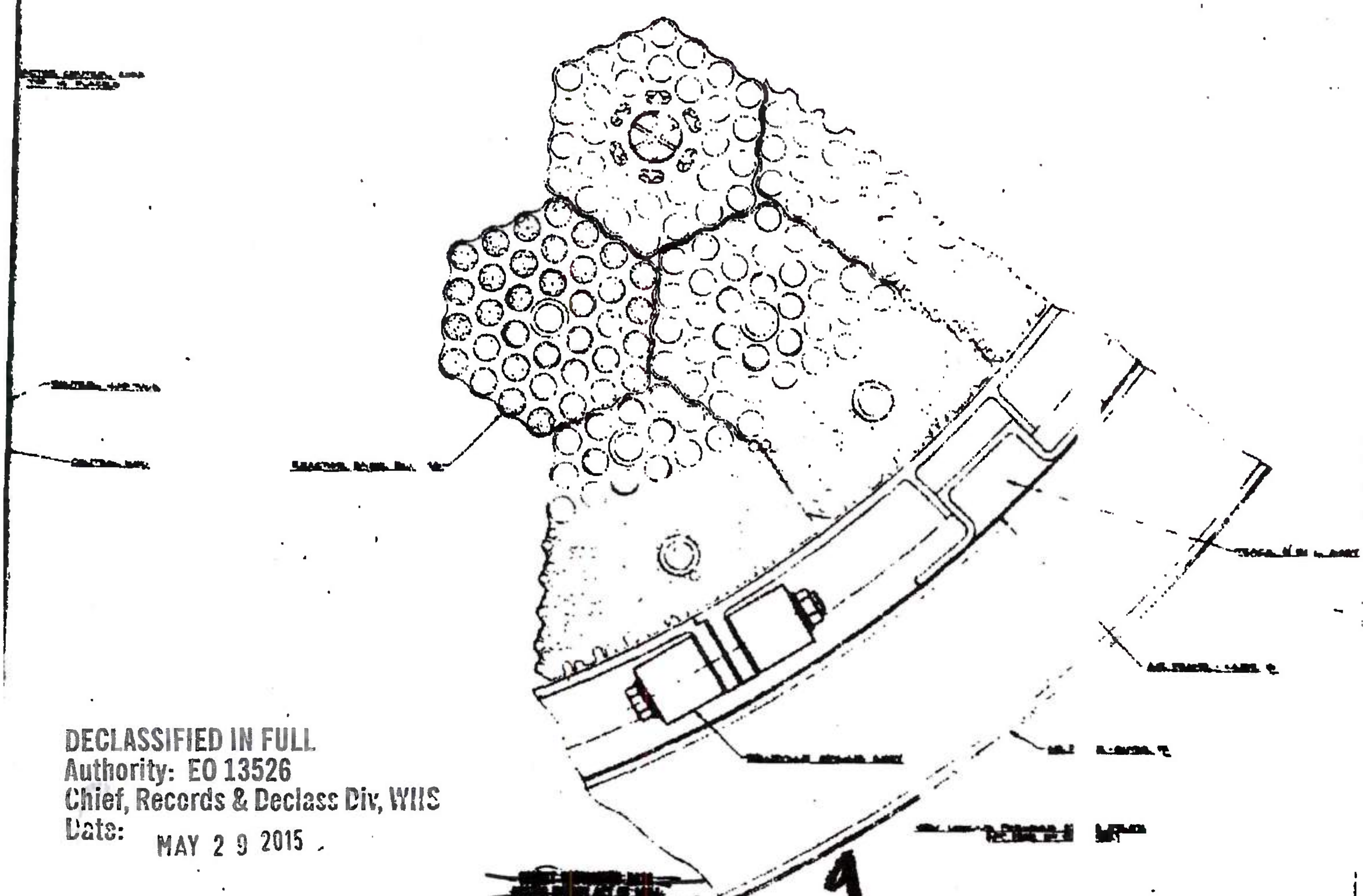

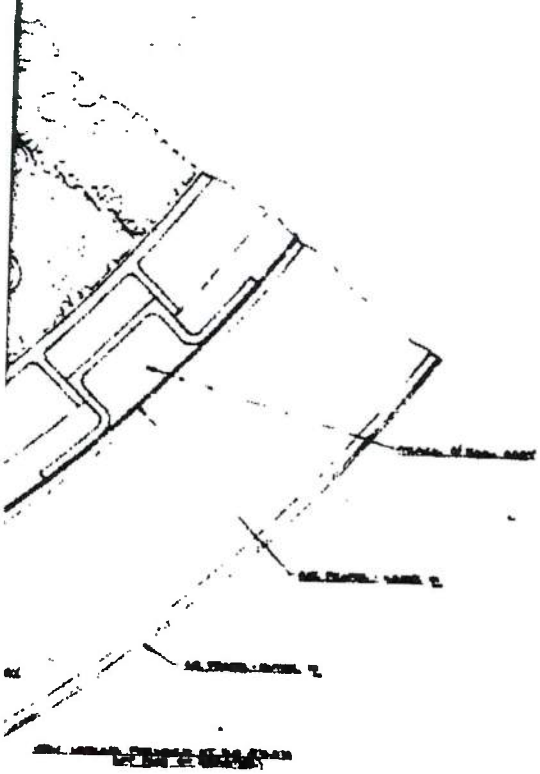

10

X81368

FIGURE

The front grid void fraction andequivalent flow hydraulic di: ieter for all cases considered were generated by Marquardt as were the basic he : transfer and friction correlations.

3.3.6 Description of Nuclear Ramjet Propulsion System

General Description

The Model MA50-XCA nuclear ramjet propulsion system c(sists of a vari.ble geometry supersonic inlet with a modified isentropic spike, ı subsonic diffuser incorporating a variable area bypass, a nuclear reactor sir lar in construction to the Tory IIC reactor with integrated control system, an a convergent-divergent exit nozzle.

Engine Geometry

Basic details of this integr::ted propulsion system design a: shown in Figure 39, (Marquardt Drawing Number X-81388). A brief descri; .on of the major components of the propulsion system follows:

The inlet, which is an underslung, axisymmetric, external nternal compression type, has a translating centerbody spike with a maximum s .ke travel capability of 7 inches. The spike actuation mechanism is housed wi in the centerbody structure and is air operated. Air is supplied to the actuator t rough a slot located on the centerbody structure.

The subsonic diffuser duct structure, from aft of the super mic inlet to the face of the reactor, is an integral part of the missile airframe s 'ucture. It will provide suitable fittings at the forward end for attachment of th(ınlet cowl and centerbody structure, and at the aft end for attachment to the in ır airframe shell.

The nuclear reactor is composed of a series of individual e ıments that make up the core, the front, rear, and radial reflectors. The reac r is maintained in the form of a right circular cylinder by a spring-loaded ex ınsion shell composed of 12 segments held together by a series of tangentially al ;ned stacks of Belleville springs. A series of axial tie tubes, which pass throu; the reactor, react and collect all aft directed loads through rear bearing plates a d transfer them to a front support structure.

A track and rail system supports the reactor within the mis le airframe and is designed for ease of installation. The pressure vessel has be ı eliminated from the design, the inner airframe shell assuming the function pre\ ›usly performed by this component. The female track is now an integral part f the expansion shell and the male rail is fastened to the airframe inner she: as previously shown. The tangentially aligned Belleville spring stacks and the t ıck and rail structure are thus integrated. This system (shown in Figure 39) w: permit ground handling equipment to lift and transfer the reactor assembly ' the missile airframe. This design also compensates for differential thermal ex; nsion between the reactor and airframe structure and will also transfer high adial inertia and vibration loads by tangential shear to the supporting airframe st· .cture.

All axial loads imposed on the reactor are transferred to th airframe through a shear ring structure located at the station of the reactor fı nt support structure.

The reactor control rod mechanisms are contained in an int ;rated package, which is mounted forward of the front support structure and ho\ ed within the inlet duct. Control rod actuators are mounted in the annulus bet· ıen the diffuser duct and the missile airframe.

The convergent-divergent exit nozzle is an integrally braze· unit formed from a series of longitudinal tubes shaped to the nozzle contour and · :apped with a spiral-wound wire. Nozzle cooling is provided by routing air thro· h the side support structure and then through the longitudinal tubes. The exit r zzle is cantilevered from the inner airframe shell near the rear face of the rea .or and is attached by a threaded lock ring.

Weight and Center of Gravity for Engine Components

A preliminary weight breakdown for the flight type reactor Iodel MA50-XCA) has been estimated, and the results are presented in Table 5 .

Based upon the reactor weights of Table 5, calculations in· cate that the propulsion system components have approximate weights and center ' gravity (CG) locations as shown below. Station locations (Engine Station, E! are used to indicate CG locations with respect to the over-all propulsion system

DECLASSIFIED IN FULL
Authority: EO 13526
Chief, Records & Declass Div, WHS
Date: MAY 2 9 2015

	Weight (lbs)	Center of Gravity Location (Engine Stati[illegible])
Inlet and spike	2,197	ES 182.6
Inlet duct	1,270	ES 405.6
Reactor controls	350	ES 445.9
Reactor assembly	12,830	ES 542.5
Exit nozzle	1,160	ES 604.8
TOTAL	17,806	ES 490.5

The center of gravity and station locations are also shown in [illegible]igure 39.

3.3.7 Heat Rejection

Heat rejection of the basic Model MA50-XCA propulsion sys[illegible]m was reported in Reference 3. A similar analysis has been performed for t[illegible] larger Model MA50-XDA propulsion system at design point conditions. With [illegible]n airflow rate of 120 lb/sec in the side support compartment, the springs reac[illegible]d a maximum temperature of about 1360°F. The total cooling airflow rate in[illegible]ie the airframe structure was kept at 50 lb/sec. At this flow rate, the pressu[illegible] shell reached a maximum temperature of 1280°F, the internal support me[illegible]ber in the airframe reached a temperature of 1510°F, and the vehicle skin temp[illegible]rature was 1000°F. The total heat rejected by this system is about 3.8 Mw. A [illegible]eakdown of this heat rejection is presented in Table 6. Heat generation rates i[illegible]he side support system for this analysis were calculated by Marquardt.

3.3.8 Control System Characteristics and Requirements

These data are unchanged from Reference 4.

3.3.9 Engine Performance

A tabulation of aerothermodynamic values at design point co[illegible]itions is presented in Table 7 to show the effects of each of the factors consi[illegible]red in this analysis. These effects can be compared with the basic Model MA50[illegible]CA propulsion system. The various changes and the results are discussed i[illegible] the order presented in the table.

	Weight (lbs)	Center of Gravity Location (Engine Stati))
Inlet and spike	2, 197	ES 182.6
Inlet duct	1, 270	ES 405.6
Reactor controls	350	ES 445.9
Reactor assembly	12, 830	ES 542.5
Exit nozzle	1, 160	ES 604.8
TOTAL	17, 806	ES 490.5

The center of gravity and station locations are also shown i Figure 39.

3.3.7 Heat Rejection

Heat rejection of the basic Model MA50-XCA propulsion sys m was reported in Reference 3 . A similar analysis has been performed for e larger Model MA50-XDA propulsion system at design point conditions. Wit an airflow rate of 120 lb/sec in the side support compartment, the springs reac d a maximum temperature of about 1360°F. The total cooling airflow rate in de the airframe structure was kept at 50 lb/sec. At this flow rate, the pressu shell reached a maximum temperature of 1280°F, the internal support me ber in the airframe reached a temperature of 1510°F, and the vehicle skin tem rature was 1000°F. The total heat rejected by this system is about 3.8 Mw. A reakdown of this heat rejection is presented in Table 6. Heat generation rates i the side support system for this analysis were calculated by Marquardt.

3.3.8 Control System Characteristics and Requirements

These data are unchanged from Reference 4.

3.3.9 Engine Performance

A tabulation of aerothermodynamic values at design point co litions is presented in Table 7 to show the effects of each of the factors consi red in this analysis. These effects can be compared with the basic Model MA50 XCA propulsion system. The various changes and the results are discussed the order presented in the table.

TABLE 6

HEAT REJECTION OF MA50-XDA PROPULSION SYSTEM
(Mach 2.8; ANA Hot Day; Altitude, 1,000 feet)

Item	Air Flow	Heat Rejection		
	(lb/sec)	(Btu/sec)	(Mw)	)
Spring Compartment	120	2479	2.62	6 .3
From Side Reflector	--	619	0.65	1 3
From Support Springs	--	1336	1.42	3 3
From Pressure Shell	--	524	0.55	1 7
Airframe	50	369	0.39	1 3
From Pressure Shell	--	78	0.08	2
From Airframe Support	--	284	0.30	9
From Vehicle Skin	--	7	0.01	2
To Ambient From Vehicle Skin	--	728	0.77	2 4
TOTAL	--	3576	3.78	1C .0

MAC A623

TABLE 7

COMPARISON OF AEROTHERMODYNAMIC PARAMETERS FOR VARIOUS MODIFICATIONS TO BASIC MODEL MA50-XCA PROPULSION SYSTEM AT DESIGN POINT (MACH 2.8; ALTITUDE, 1,000 FT; ANA HOT DAY)

Parameter	(1) Basic Model MA50-XCA System (Ref. 3)	(2) Length-Optimized Model MA50-XCA System (Ref. 4)	(3) Temperature Dependent Thermal Stress Properties for 15,000 psi	(4) Temperature Dependent Thermal Stress Properties for 18,000 psi	(5) Increase of Base Block Billet Size	(6) Reduced Air Flow Per Tie Rod	(7) Increase of Reactor Void Fraction
Reactor Air Flow, W_a, lb/sec	1580	1650	1580	1580	1580	1450	1580
Side Support Cooling Airflow, W_{a_c}, lb/sec	113	100	100	100	100	100	100
Core Tube Diameter, inches	0.227	0.227	0.227	0.227	0.227	0.227	0.230
Total Reactor Power, Q, Mw	518	535	534	552	536	514	518
Reactor Exit (mixed) Total Temperature, T_{t_4}, °R	2520	2510	2560	2600	2560	2580	2520
Reactor Pressure Recovery, P_{t_4}/P_{t_1}	0.678	0.689	0.679	0.660	0.670	0.680	0.705
Reactor Length, L_R, in.	627	54.6	62.7	62.7	62.7	62.7	62.7
Nozzle Throat Area, A_5, ft^2	4.94	5.08	--	--	--	--	--
Nozzle Exit Area, A_6, ft^2	12.7	13.2	--	--	--	--	--
Cowl Area, A_c, ft^2	7.97	8.25	--	--	--	--	--
Thrust Coefficient, C_F	0.200	0.206	0.205	0.210	0.205	0.201	0.202
Thrust, F, (Full Expansion), lb	39,700	40,900	40,700	41,700	40,700	39,900	40,100

~~SECRET RESTRICTED DATA~~
~~ATOMIC ENERGY ACT OF 1954~~

TABLE 7 (Continued)

Parameter	(1) Basic Model MA50-XCA System (Ref. 3)	(2) Length-Optimized Model MA50-XCA System (Ref. 4)	(3) Temperature Dependent Thermal Stress Properties for 15,000 psi	(4) Temperature Dependent Thermal Stress Properties for 18,000 psi	(5) Increase of Base Block Billet Size	(6) Reduced Air Flow Per Tie Rod	(7) Increase of Reactor Void Fraction
Thrust Coefficient Differential from Basic MA50-XCA, $\Delta C_{F_{A_R}}$	--	0.006	0.005	0.010	0.005	0.001	0.002
Percent Increase in Thrust Coefficient from Basic MA50-XCA, %	--	+3	+2.5	+5	+2.5	+0.5	+1

Constants: Inlet total pressure, P_{t_o} 393 psig
Inlet total temperature, T_{t_o} 1400°R
Inlet pressure recovery, P_{t_1}/P_{t_o} 0.807
Maximum core wall temp., T_w 2960°R
Reactor diameter, D_R 57 in. max.
Reactor area, A_R 17.70 ft^2

(1) The basic Model MA50-XCA propulsion system perfor ance is presented to provide a basis for comparison of the following items. A stailed discussion of the basic Model MA50-XCA propulsion system was prese :ed in Performance Bulletin No. 2 (Reference 3).

(2) The length-optimized Model MA50-XCA propulsion sy: em is characterized by the removal of four inches of forward reflector and 4. inches of the aft core. This version of the Model MA50-XCA was discussed in P :formance Bulletin No. 3 (Reference 4).

(3) The basic Tory IIC reactor power profile presented in he Tory IIC Data Book (Reference 1) is determined by a maximum allowable el stic thermal stress of 15,000 psi and a maximum wall temperature of 2500°F. ie stress calculation assumes that thermal conductivity, modulus of elasticity, d coefficient of expansion for beryllia are invariant with temperature and are ev uated at the 2500°F wall temperature. However, when the temperature depende ce of these same properties is accounted for, an improved power profile is obt ned which yields a constant 15,000 psi elastic thermal stress over the front p tion of the core and a maximum allowable wall temperature of 2500°F over the :ear portion. The resultant performance increase (thrust) is shown as 2.5 percer over the basic Model MA50-XCA. This increase is somewhat conservative : that airflow re-optimization would yield a slightly higher thrust.

(4) As an extension of the effort to improve the basic Tor IIC power distribution, a second computation was made using an elastic therm l stress limit of 18,000 psi in combination with a maximum wall temperature of 2)0°F. For the same airflow rate as the basic Model MA50-XCA, a 5 percent g n in thrust was achieved. Power profiles for items (3) and (4) are compared t the basic Tory IIC profile in Figure 40.

(5) The basic design of the Tory IIC reactor is dependent on the baseplate billet diameter. State-of-the-art in Niobium fabrication has i licated that this size might be increased from the present diameter of 5 inches about 9 inches. This would allow a reduction in the total number of tie rod since the temperature of the tie rods is currently around 1250°F, providing ligh margin of safety for allowable stress.

Reducing the number of tie rods in the core also reduces t volume occupied by unfueled cooling passages. By going to a 9-inch diame r billet, sufficient fueled region is added to the core to obtain a 2.5 percent crease in thrust over the basic Model MA50-XCA for the same airflow rate.

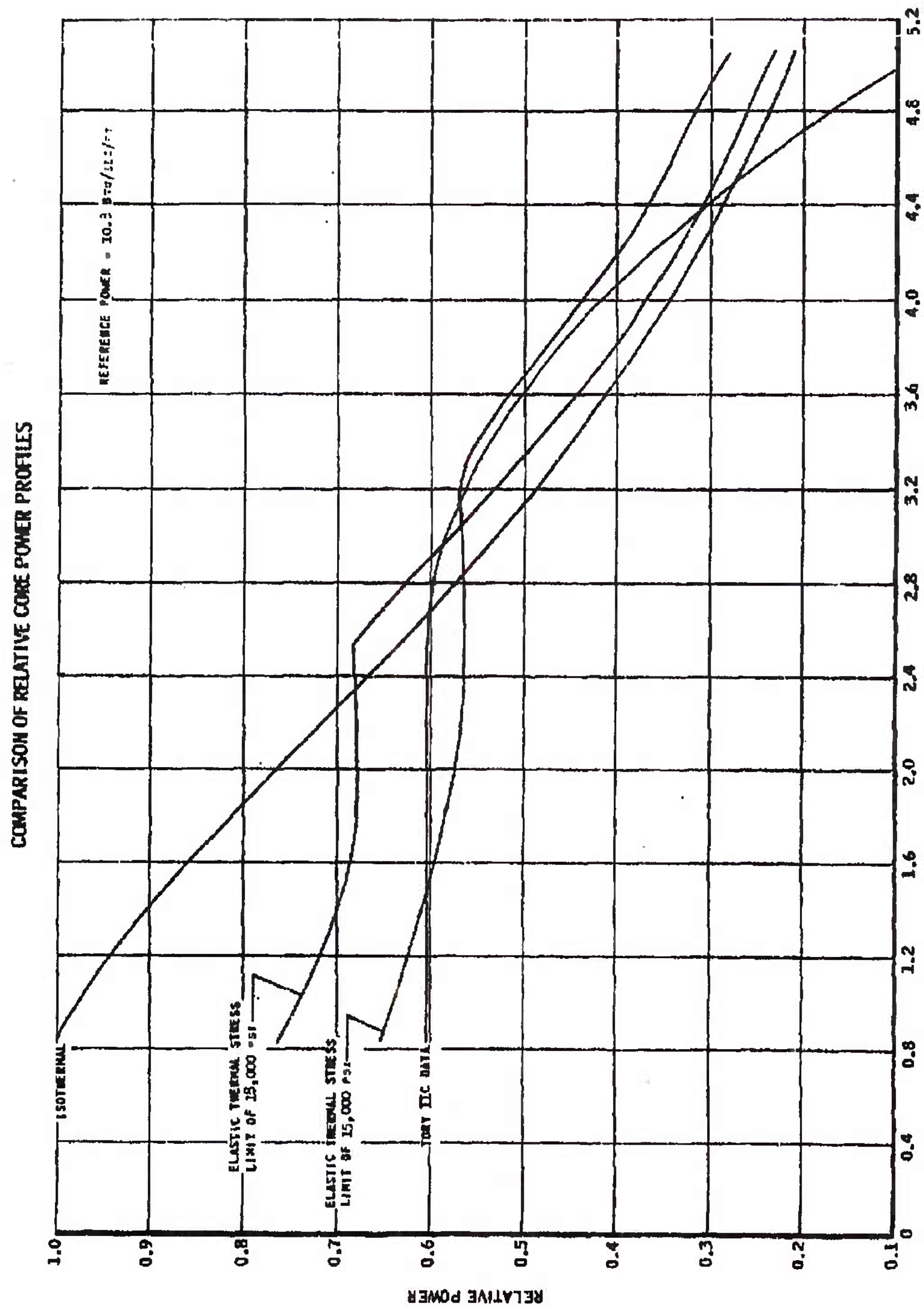
COMPARISON OF RELATIVE CORE POWER PROFILES
REFERENCE POWER = 10.3 BTU/...
ISOTHERMAL
ELASTIC THERMAL STRESS LIMIT OF 18,000 PSI
ELASTIC THERMAL STRESS LIMIT OF 15,000 PSI
TORY IIC DATA
RELATIVE POWER
1.0
0.9
0.8
0.7
0.6
0.5
0.4
0.3
0.2
0.1
0
0.4
0.8
1.2
1.6
2.0
2.4
2.8
3.2
3.6
4.0
4.4
4.8
5.2

(6) As a further step in the investigation of possible perfor .ance gains, a study was made of the effect of increasing tie rod temperature. Si :e a considerable margin of safety exists at the temperature (1250°F) predicted or the Model MA50-XCA engine, an increase in tie rod operating temperatu e appears quite feasible. Accordingly, the diameter of the tie rod cooling char el was reduced until a tie rod temperature of 1650°F was attained. The engin was then optimized for air flow. A relatively modest 0.5 percent increase in irust was achieved over the basic Model MA50-XCA engine.

(7) The internal diameter of the current Tory IIC fuel elem nt is 0.227 inches. To determine the effect on thrust of a small change in react r void fraction, performance calculations were made using a tube internal diam ter of 0.230 inches. This dimension was selected as representative of a minor c ange of geometry that would not greatly affect the fuel loading allowable limit. gain for the same total airflow rate as the basic Model MA50-XCA, a 1 percent g in in thrust is achievable.

Although these parametric studies are based on the diamete of the Tory IIC reactor, the performance gains noted are applicable to the large diameter Model MA50-XDA propulsion system.

3.3.10 Neutronics

Neutronic studies of the Model MA50-XCA and the Model M 50-XDA propulsion systems have been reported in previous performance bulleti (References 3 and 4), respectively). Neutronic analyses of the concepts presen d in this fourth bulletin have not been made during this period, but will be dis ussed in succeeding reports.

3.3.11 Operating Envelopes

Preliminary propulsion system operating envelopes have be n established for the Model MA50-XCA nuclear ramjet for the ANA Hot and Cold I y and for the ICAO Standard Day temperatures, and are presented in Figures 41, :, and 43, respectively. Limits for these envelopes have been established as f lows:

The Mach 2.0 lower limit was established arbitrarily. Hov ver, some basis for this selection arises from a requirement for a pressure ra o of 8 to 1 across certain pneumatic components. The upper altitude limit is e ablished as a line of constant diffuser exit pressure of 45 psia (which assures th aforementioned 8 to 1 pressure ratio) up to 50,000 feet, the maximum altitude of interest.

ESTIMATED ANA HOT DAY OPERATING ENVELOPE FOR THE MARQUARDT MODEL MA50-XCA RAMJET

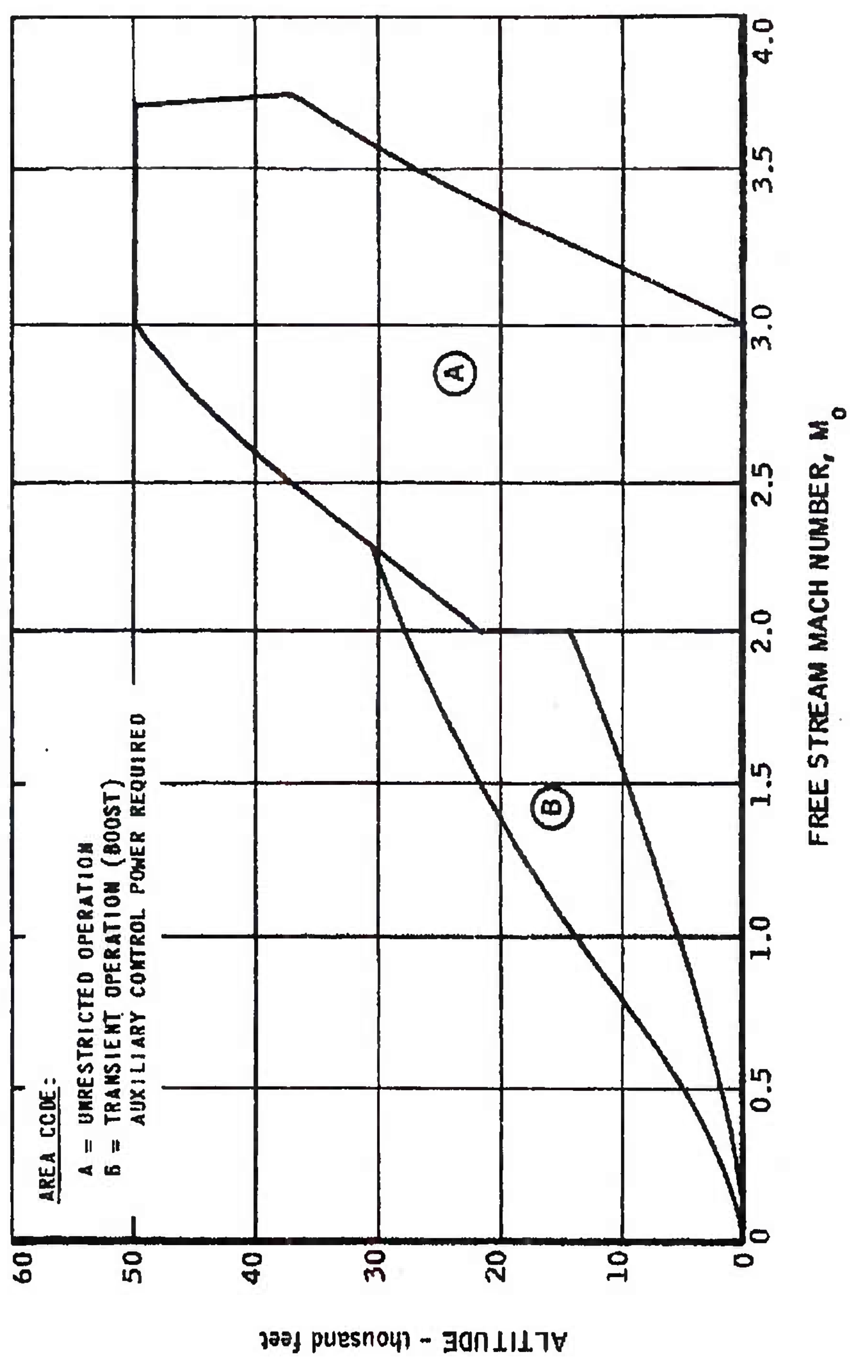

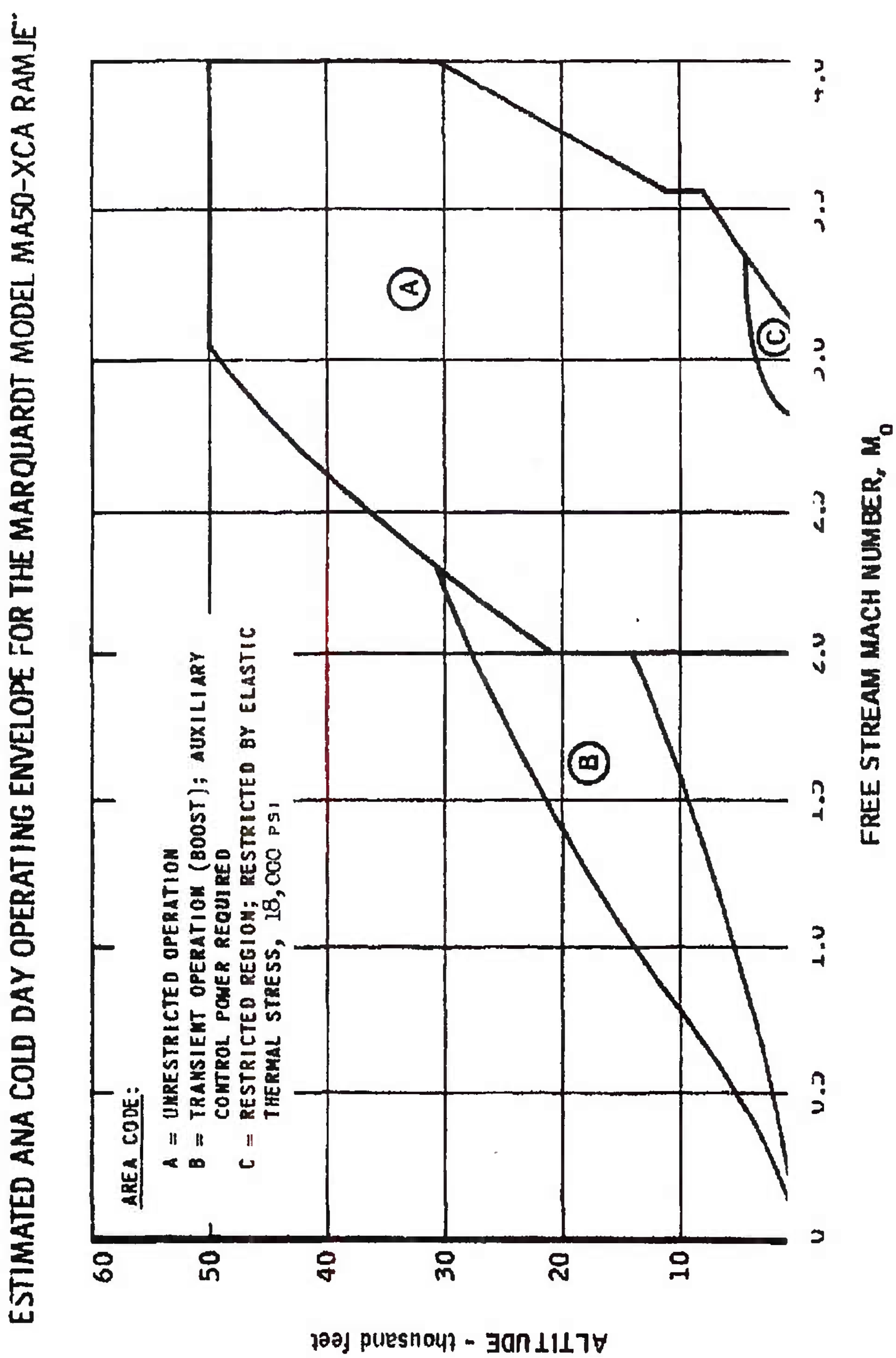
ESTIMATED ANA COLD DAY OPERATING ENVELOPE FOR THE MARQUARDT MODEL MA50-XCA RAMJET
AREA CODE:
A = UNRESTRICTED OPERATION
B = TRANSIENT OPERATION (BOOST); AUXILIARY CONTROL POWER REQUIRED
C = RESTRICTED REGION; RESTRICTED BY ELASTIC THERMAL STRESS, 18,000 PSI
A
B
C
60
50
40
30
20
10
ALTITUDE - thousand feet
0
1.0
FREE STREAM MACH NUMBER, M_0

ESTIMATED ICAO STANDARD DAY OPERATING ENVELOPE FOR THE MARQUARDT MODEL MA50-XCA RAMJET

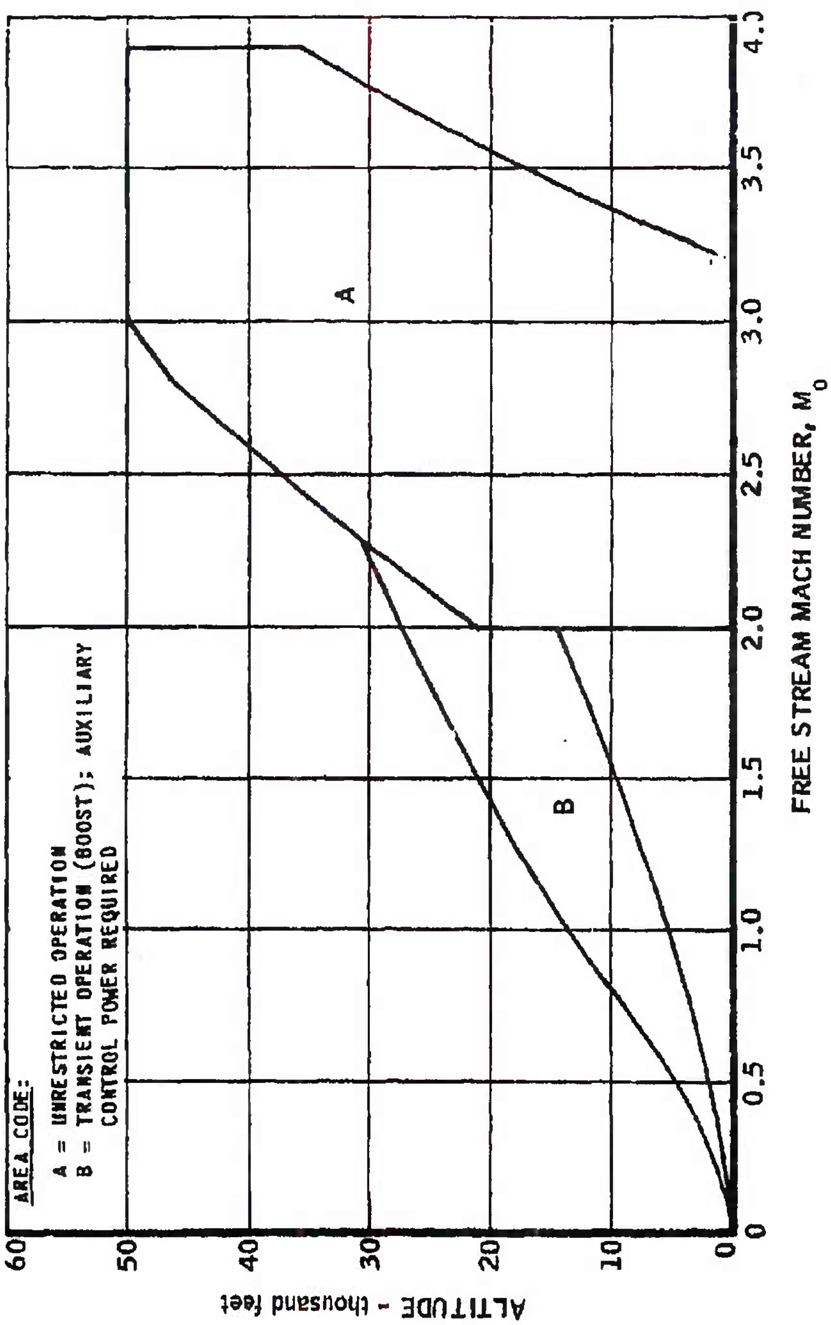

Limitation of the flight envelope at high speeds and altitude corresponds either to a ram air total temperature of 1070°F or a diffuser duct t al pressure of 420 psia. At sea level, these conditions limit the maximum fligh speed to Mach 3.0 at the ANA Hot Day temperature, to Mach 3.1 at ANA Col Day temperature, and to 3.2 at ICAO Standard Day temperature.

Note is made of the restricted operating region in the fligh envelope for the ANA Cold Day condition. The Tory IIC reactor power profile is lefined by an elastic thermal stress limit of 15,000 psi and a maximum wall temp rature of 2500°F at the design point. It is possible, under Cold Day conditio at high speed and low altitude, to attain a flow rate - core temperature con tion wherein the 15,000-psi allowable stress limit will be exceeded. Based on s cessful operation of the Tory IIA reactor at powers above the design value, a in concurrence with LRL, the limiting elastic thermal stress for off-design eration has been increased to 18,000 psi. Raising the stress limit has the effe of reducing the restricted operating region to the small area shown in Figure 4 . To operate in the restricted region, air flow and core temperature must be djusted in such a manner that the 18,000-psi stress limit will not be exceeded

The missile must be boosted into the propulsion system op ating envelope. Typical boost envelopes are shown in Figures 41, 42, and 3.

3.4 HEAT TRANSFER AND THERMAL STRESS ANALYSIS

3.4.1 Mechanical and Structural Design Support Studies

Inlet

The heat transfer effort directed toward the design of the propulsion system inlet assembly has been of a preliminary nature. Estimates of some steady state temperatures have been made for the following conditions: Mach 2 , ANA Hot Day, an altitude of 1,000 feet, and Mach 3.0, ANA Hot Day, an altitud of 1,000 feet. The underslung axisymmetric variable-geometry inlet analyzed shown in Figure 44 .

At the Mach 3.0 condition, calculations indicated that a temperature of about 1300°F may be expected with the airflow distribution shown in Figure 44 It was assumed that the inlet bleed airflow that enters the boundary layer bleed slot was used for cooling purposes. Half of this flow is directed forward in the centerbody while the other half is directed aft. At the time of the study, the forward-directed flow was channeled aft before it had a chance to cool the forw d-most section of the translating mechanism; consequently, this section reached temperature of approximately 1300°F. At the Mach 2.8 condition, the tempera ture of this section is 1130°F. The steady state temperatures calculated for p -tions of the inlet at the Mach 3.0 and Mach 2.8 conditions are presented in Fig e 44 . Later design configurations provide for passing a portion of the cooling a through this forward section, thereby lowering the temperatures shown in Figu 44 .

The inlet actuating mechanism presents the greatest potential heat tra fer problem in the entire inlet assembly. This mechanism, which has recently been defined, will be analyzed to determine cooling requirements. The cowl assembly, which has not been fully analyzed, is not expected to reach tempera-tures higher than those of Figure 44 .

Side Support Structure

The results and a discussion of the heat transfer studies of the Models MA50-XCA and MA50-XDA side support systems are presented in Section 3.4.

Reactor Tie Tubes

The steady state temperatures in a Tory IIC reactor tie tube (R-235 material) have been determined for design point conditions. The tie tube

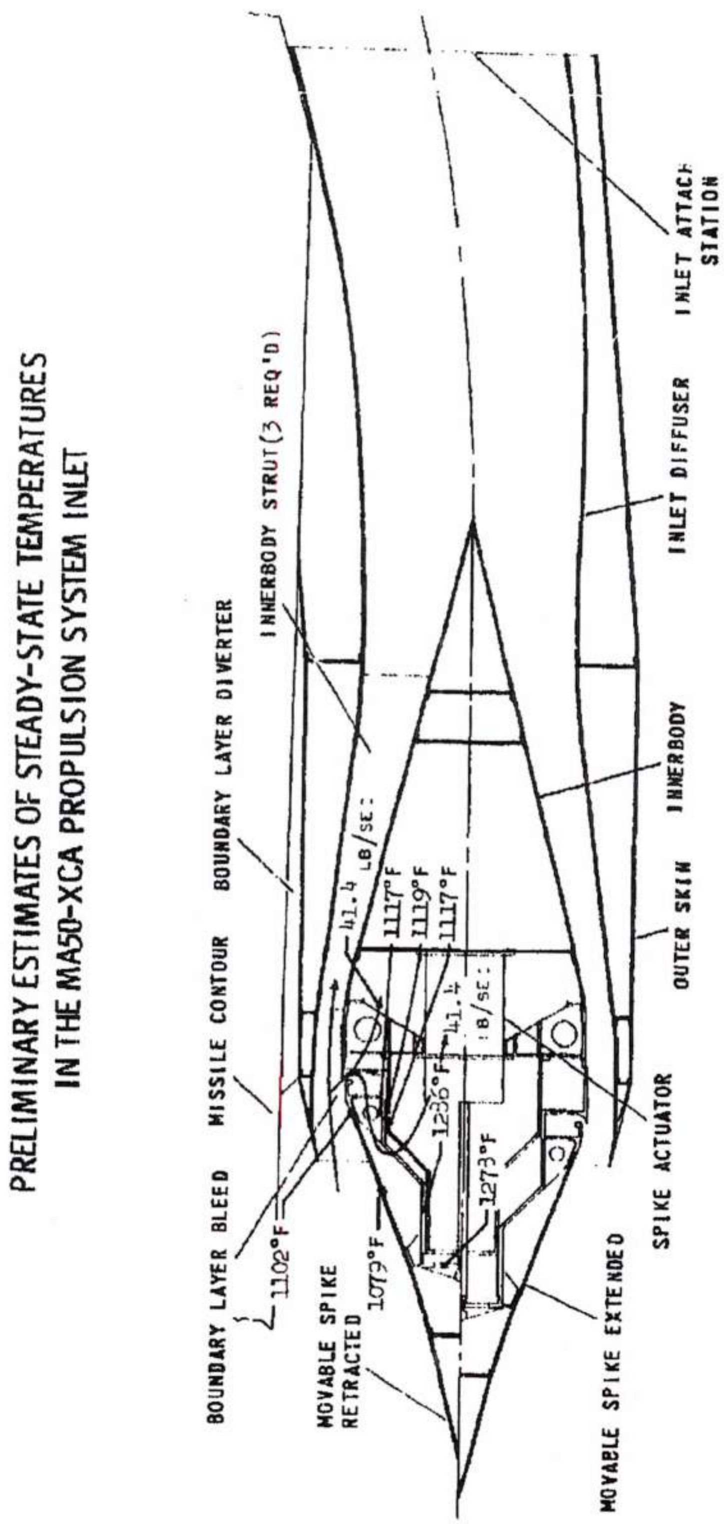

PRELIMINARY ESTIMATES OF STEADY-STATE TEMPERATURES IN THE MA50-XCA PROPULSION SYSTEM INLET

FIGURE 44

considered was located near the reactor centerline. The temperatures of the n-fueled beryllia surrounding the tie tube and the temperature rise of all coolin air streams were determined. The following values were obtained:

	Temperature (°F)
Maximum temperature of unfueled beryllia	2570
Air temperature rise in unfueled beryllia	1250
Maximum temperature of tie tube	1250
Air temperature rise in tie tube	110

Complete temperature distributions in the tie tube and surrounding unfueled beryllia are presented in Figure 45 . Some specific conditions used in the st ly are presented in Table 8.

More recent studies of a similar nature were conducted at the follow g conditions: Mach 3.0, ANA 421 Hot Day, sea level; and Mach 3.6, ANA 421 H t Day, an altitude of 30,000 feet. The studies produced maximum tie tube temp ra-tures of 1360° F and 1385° F, respectively. Additional off-design operation studies will be conducted in the future.

The tie tube configuration and the analytical models used are shown i Figure 46 . The reactor length model was simulated by an IBM 704 thermal a-lyzer program, which may be used for a variety of conditions and tie tube ma r-ials.

Exhaust Nozzle

At the beginning of the contract year, several exhaust nozzle types w re being considered for Pluto application. These nozzle types included the tubul forced convection, annular forced convection, baffle forced convection, film-cooled (or ejector), and radiation cooled configurations.

The baffled and the radiation cooled designs were eventually dropped or the reasons discussed in Section 3.2.2.

During the contract period, a considerable amount of detailed heat tr as-fer analysis effort was devoted to the tubular, forced convection configuration A preliminary analysis of the film-cooled (or ejector type) nozzle was also mad

The exit nozzle contour for the flight engine was established as a con er-gent-divergent, bell-shaped, fixed area type.

STEADY-STATE TEMPERATURES IN A TORY IIC TIE TUBE AN
SURROUNDING BERYLLIA AT DESIGN POINT CONDITION

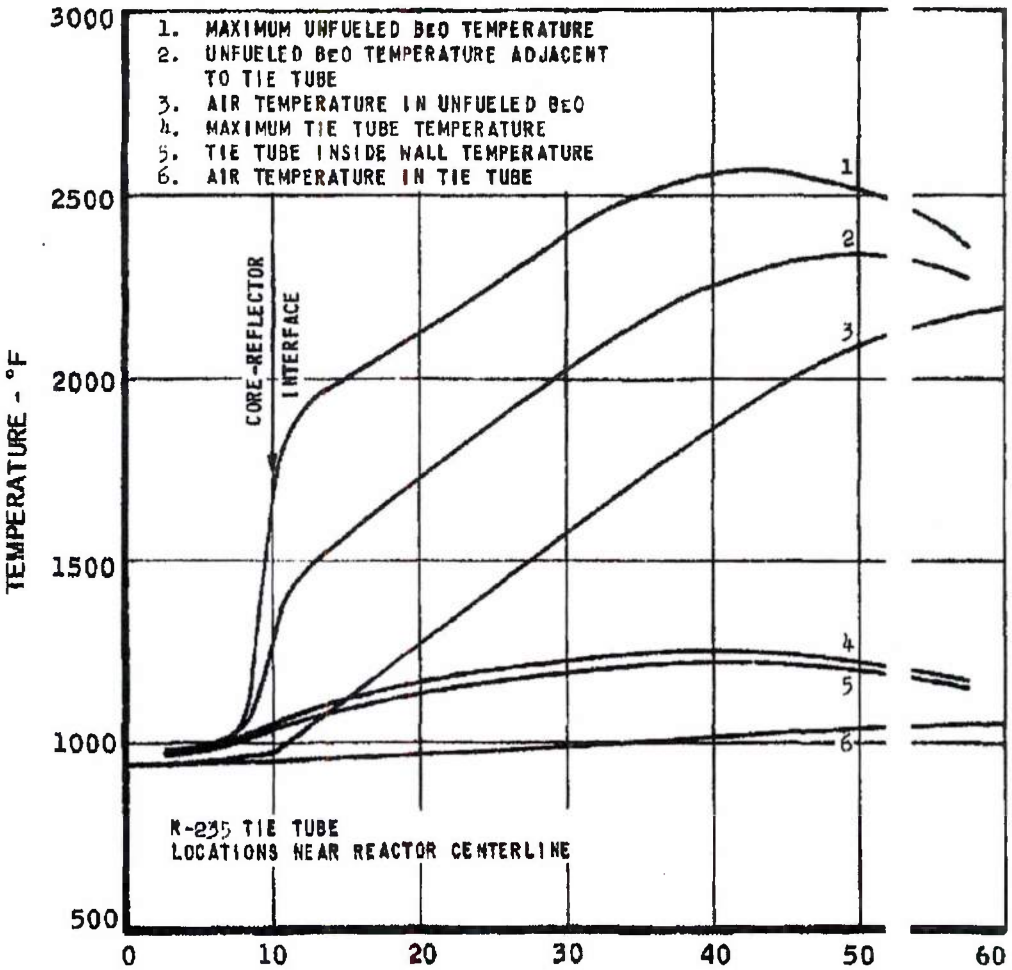

FIGURE 45

TABLE 8

CONDITIONS USED IN
TORY IIC TIE-TUBE HEAT TRANSFER STUDY

Item	Value
Tie Tube Material	R-235
Tie Tube Internal Diameter, in.	0.58
Tie Tube Outside Diameter, in.	0.66
Tie Tube Flow Area, sq. in.	0.264
Reactor Length, in.	60
Nuclear Heating in Tie Tube	Axial Profile
Nuclear Heating in Unfueled Beryllia	Axial Profile
Air Weight Flow Rate in Tie Tube, lb/sec	0.73
Air Weight Flow Rate in Unfueled Beryllia Tube, lb/sec	0.017
Unfueled Beryllia Void Fraction	0.148
Diameter of Hole in Unfueled Beryllia Tube, in.	0.12
Unfueled Beryllia Tube Flow Area, sq. in.	0.0113
Unfueled Beryllia Tube Solid Area, sq. in.	0.0649
Temperature of Fueled Beryllia, °F	Axial Profile
Thermal Conductivity of Unfueled Beryllia Btu/hr/ft/°F	9.0
Thermal Conductivity of Tie Tube, Btu/hr/ft/°F	13.0
Heat Transfer Coefficient in Tie Tube, Btu/hr/ft^2/°F	713.0
Heat Transfer Coefficient in Unfueled Beryllia Tube, Btu/hr/ft^2/°F	615.0

TORY IIC TIE TUBE CONFIGURATION AND ANALYTICAL MODELS

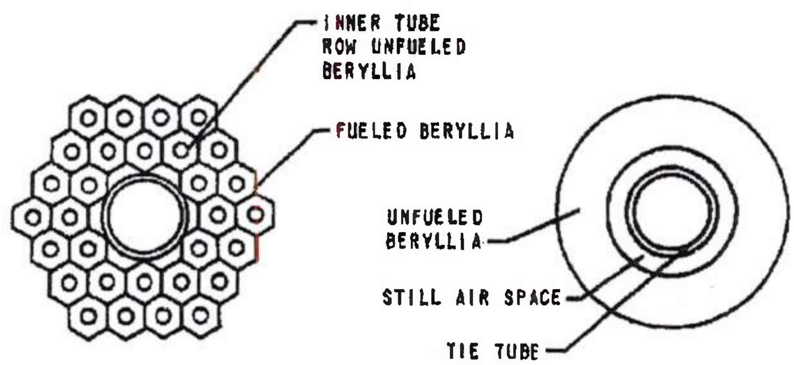

(A) TORY IIC TIE TUBE CONFIGURATION

(B) ANALYTICAL MODEL OF TIE TUBE CONFIGURATION

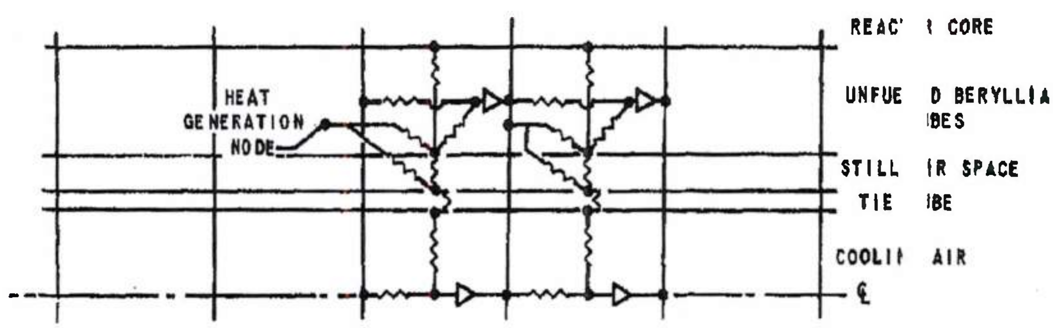

(C) NETWORK REPRESENTATION OF REACTOR TIE TUBE MODEL FOR THERMAL ANALYZER

Tubular, Forced Convection Nozzle

Two tube shapes were considered for the typical wire-wrappe nozzle of Figure 47. The first type analyzed had 402 tubes of rectangular cr s section, as shown in Figure 48. Each tube was assumed to have a constant fl w area of 0.1105 square inches along the length of the nozzle. The assumed co ing air available to the nozzle at this time was 50 lb/sec at 1200° F. It was assu ed that heat is exchanged between the outer surface of the cooling tubes and the a o-dynamic nozzle shroud by thermal radiation only. Maximum steady state tub temperatures were calculated to be 1488° F at Mach 3.0, sea level, ANA Hot ay, and 1456° F at Mach 3.0, sea level, ANA Cold Day.

Structural analysis indicated that round tubes would offer muc greater strength; consequently, the analysis of the square tube was dropped.

In the round tube configuration the tubes (0.375-inch ID x 0.01 -inch wall) were held at a constant perimeter rather than a constant flow area. The first analysis of a round tube yielded a maximum tube temperature of 155 F at Mach 3.0, sea level, and ANA Hot Day conditions. This study was repeat once omitting internal heat generation and again omitting both internal heat g -eration and reactor thermal radiation. The maximum tube temperatures obt ned from these studies were 1555° F and 1548° F, respectively.

Next, a preliminary optimization study was made to determin maximum tube temperatures as a function of tube size. The results of this dy are presented in Figure 49 where maximum nozzle-tube temperature and tota nozzle-tube weight are plotted against the inside diameter of the tube. In thi study, the tube wall thickness (0.010 inches) and cooling airflow (50 lb/sec) re held constant. The temperatures along the length of the nozzle are shown in Figure 50.

All of the nozzle heat transfer studies discussed above were based on a coolant airflow rate of 50 lb/sec at 1200° F. Later informati from LRL specified the coolant airflow rate to be 113 lb/sec and at a lower temperature. The temperature of this cooling air, which passes through th side support structure spring compartment, is about 1000° F. A tube size o approximately 13/16-inch outside diameter with a wall thickness of 0.020 inc s is necessary for this flow. The nozzle design utilized 240 of these tubes. A study was made to evaluate the heat transfer characteristics of this system a two design operating conditions: Mach 2.8, ANA Hot Day, an altitude of 100 feet; and Mach 2.8, ANA Cold Day, an altitude of 1000 feet. Pertinent

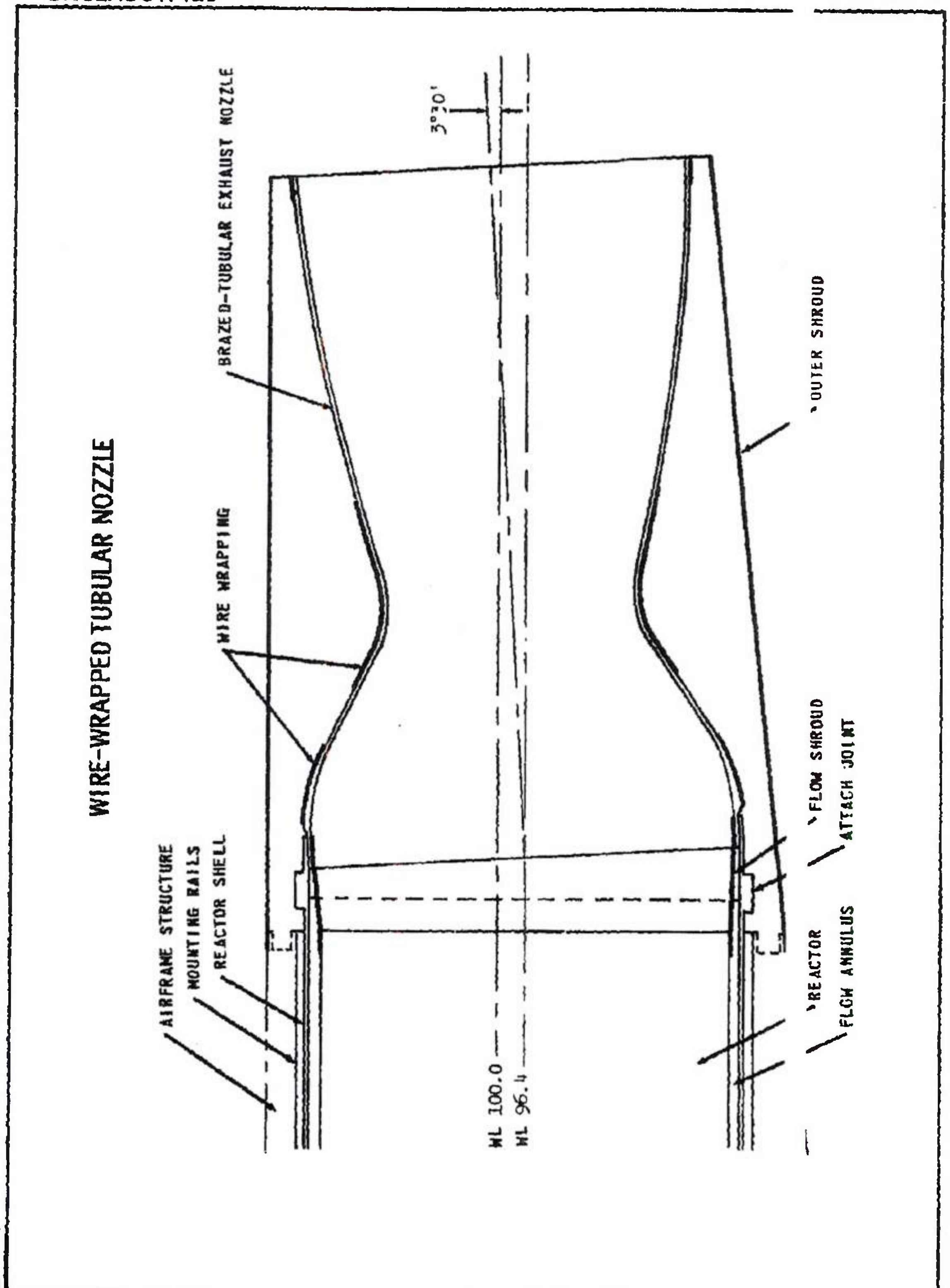

WIRE-WRAPPED TUBULAR NOZZLE

FIGURE 47

TUBULAR WIRE-WRAPPED CONFIGURATIONS FOR PLUTO ENGINE EXHAUST NOZZLE

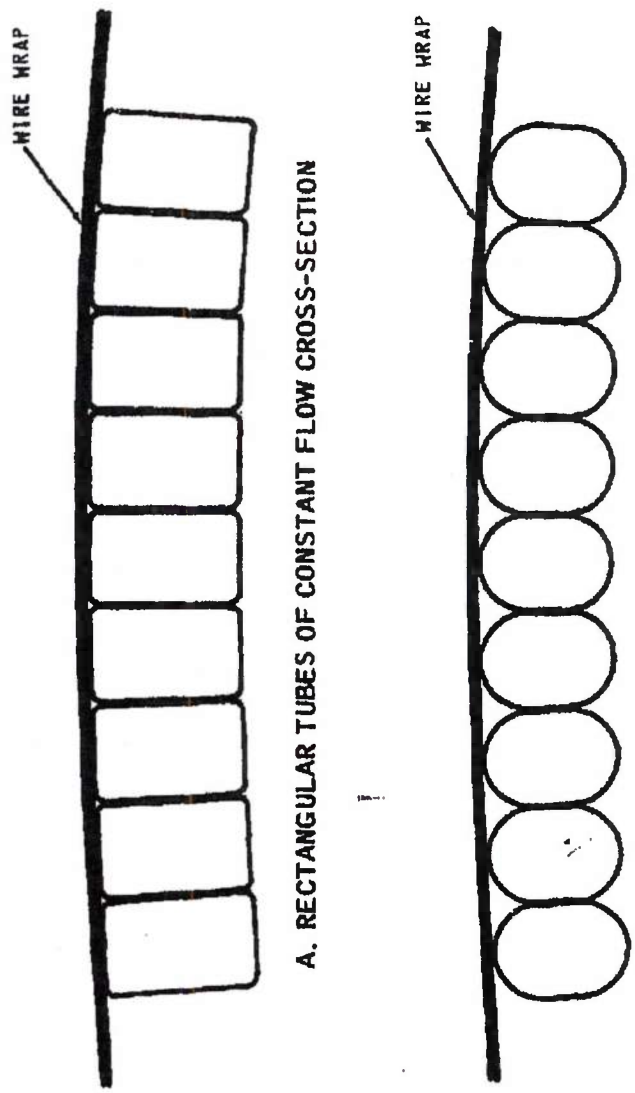

A. RECTANGULAR TUBES OF CONSTANT FLOW CROSS-SECTION

B. ROUND TUBES OF VARIABLE FLOW CROSS-SECTION

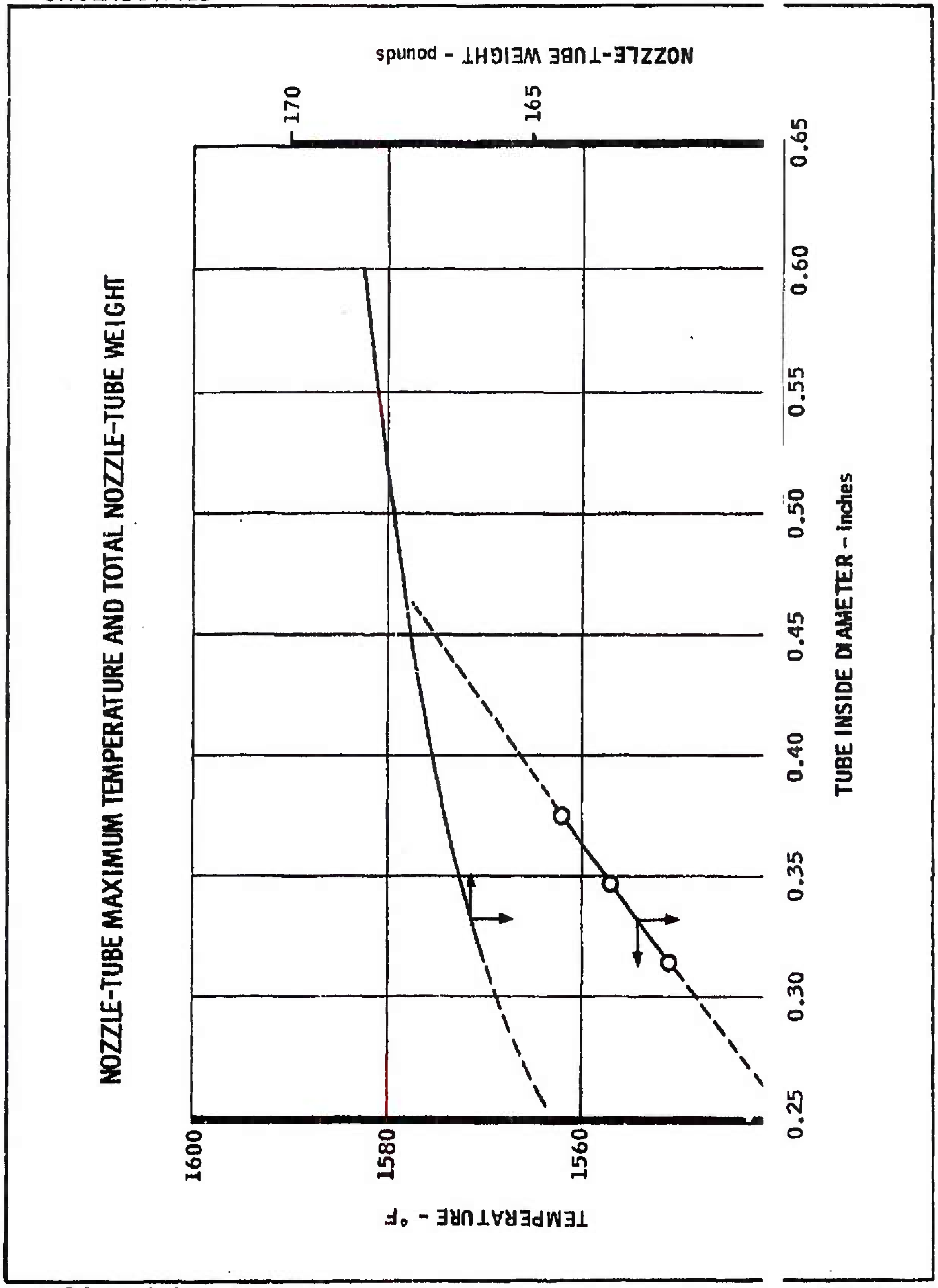

MAC A633

FIGURE 49

STEADY-STATE TEMPERATURES IN A PLUTO ENGINE EXHAUST NOZZLE

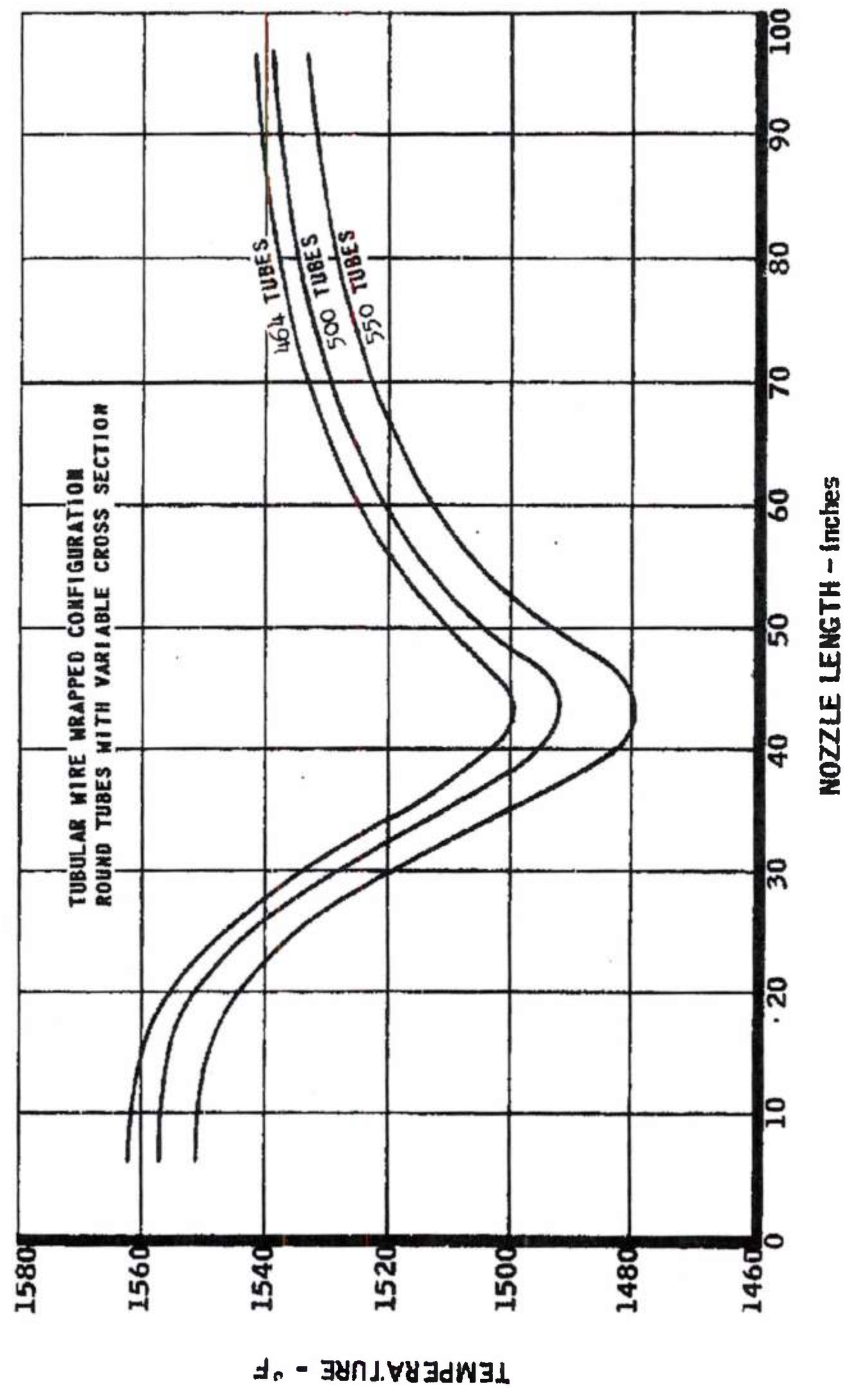

information for these two conditions is presented in Table 9. The re lts of the study are presented in Figures 51 and 52. The maximum tube temp ature at the design point condition is about 1500° F and occurs at the exit end. or the off-design condition (Cold Day), the maximum temperature, about 123(F, also occurs at the exit end.

The present nozzle design reflects a slightly changed in rnal contour. In addition, the flow was reduced to 100 lb/sec at a temperature of 1050° F. The 240 R-235 alloy cooling tubes (0.75-inch ID x 0.028-inch wall) are ound at the entrance end. In order to conform to the nozzle contour, these tut s are compressed or flattened, and the cross section takes on a wedge shape is shown in Figure 53. At design point conditions, the maximum tube tempera re for this configuration is 1475° F and occurs at the nozzle exit. The tempe ture distribution in the nozzle is presented in Figure 54. Off-design operatic studies are presently being conducted.

Annular, Forced Convection Nozzle

The nozzle cooled by an annular, concentric cooling cha nber is similar to the tubular nozzle in terms of simulation on the IBM 704 the mal analyzer program. Only minor modifications of the existing computer pr ram were necessary to produce a program for this nozzle. It is planned to evalı te steady state temperatures for this nozzle design.

Ejector or Film Cooled Nozzle

A study was made to obtain a preliminary estimate of tl steady state metal temperatures in an ejector type, or film-cooled, exhaust r zzle for the Model MA50-XCA propulsion system at design point conditions. It vas assumed that the convergent portion of the nozzle consisted of wire-wrap ed tubes, as previously described for the tubular nozzle. The cooling tubes (0.7 -inch ID x 0.028-inch wall) passed cooling air at 113 lb/sec with an inlet tempe ture of approximately 1000° F. The divergent portion of the nozzle was consi red to be a simple single shell extending from the outer surface of the wire-wra ed tubes. This divergent portion of the nozzle was film-cooled by the air issuing rom the cooling tubes slightly aft of the throat position. The temperature of th discharge air was calculated to be at 1100° F.

The film cooling achieved in the divergent portion of th nozzle is quite effective. A nozzle metal temperature of 1240° F was calculated t the exit end of the divergent portion, which represents a reduction of about 26(F from

TABLE 9

CONDITIONS OF HEAT TRANSFER STUDY OF MA50-XCA EXHAUST NOZZ E

Item	Design Point	Off-Desig Point
Mach Number	2.8	2.8
Altitude, ft	1000	1000
ANA Day	Hot	Cold
Reactor Power, Mw	516	626
Reactor Exhaust Air Total Temperature, °F	2060	2034
Reactor Exhaust Airflow, lb/sec	1577	1624
Coolant Air Inlet Temperature, °F	1008	670
Coolant Airflow Rate, lb/sec	113	129

STEADY-STATE TEMPERATURES OF WIRE-WRAPPED TUBULAR EXHAUST NOZZLE AT MACH 2.8, 1,000 FEET, ANA COLD DAY, 626-MW REACTOR POWER LEVEL

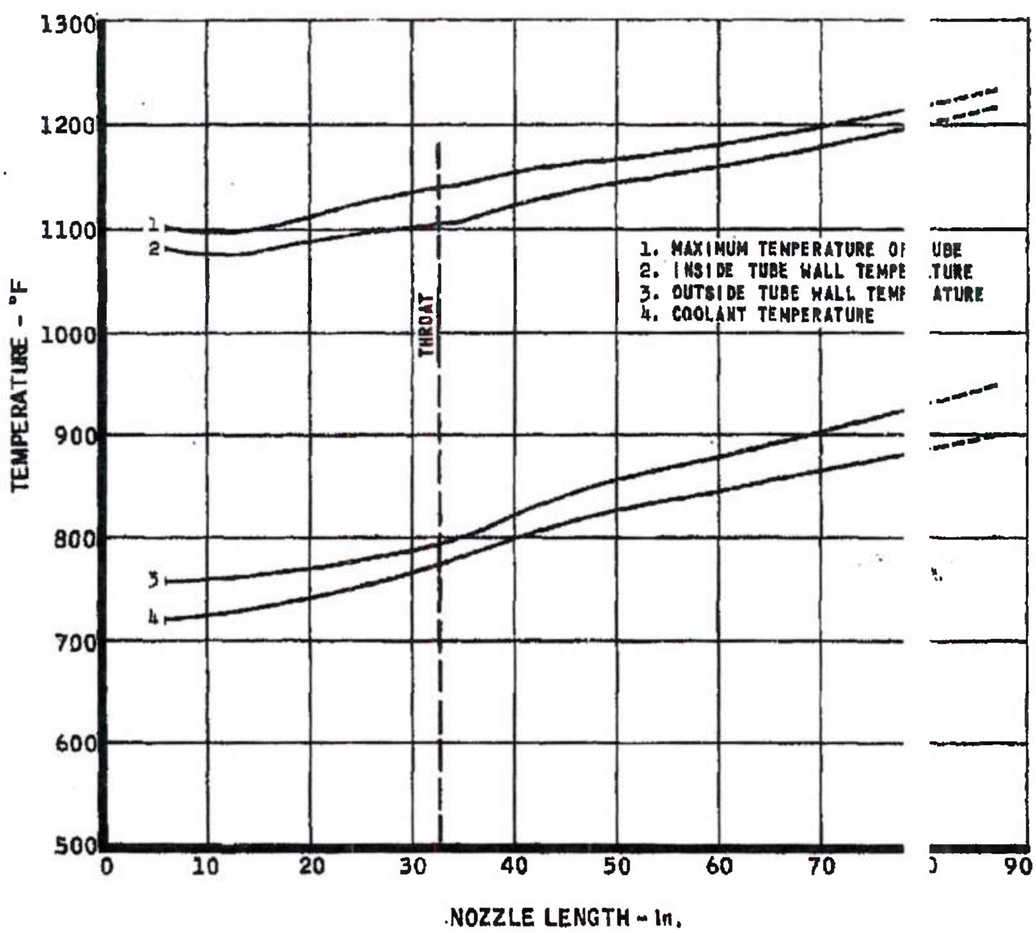

STEADY-STATE TEMPERATURES OF WIRE-WRAPPED TUBULAR EXHAUST NOZZLE AT MACH 2.8, 1,000 FEET, ANA HOT DAY, 516-MW REACTOR POWER LEVEL

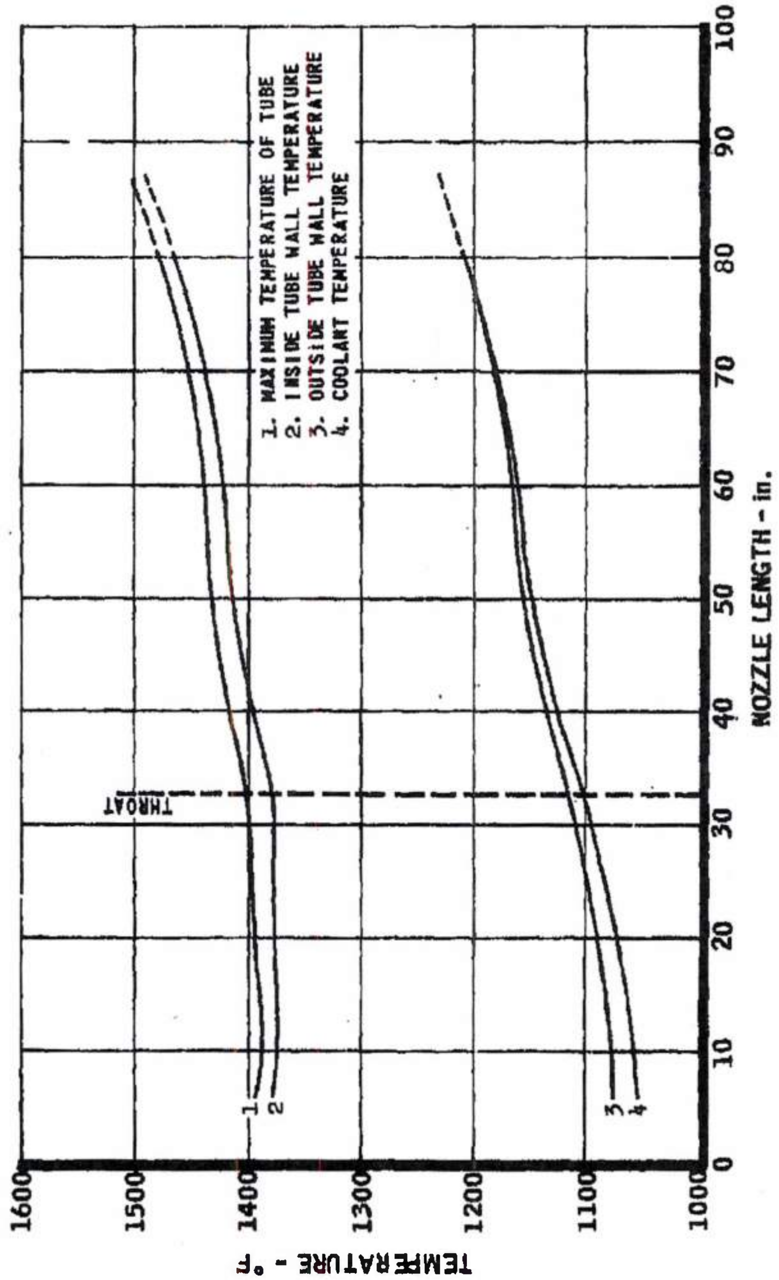

PHYSICAL DIMENSIONS OF EXHAUST NOZZLE COOLING TUBE

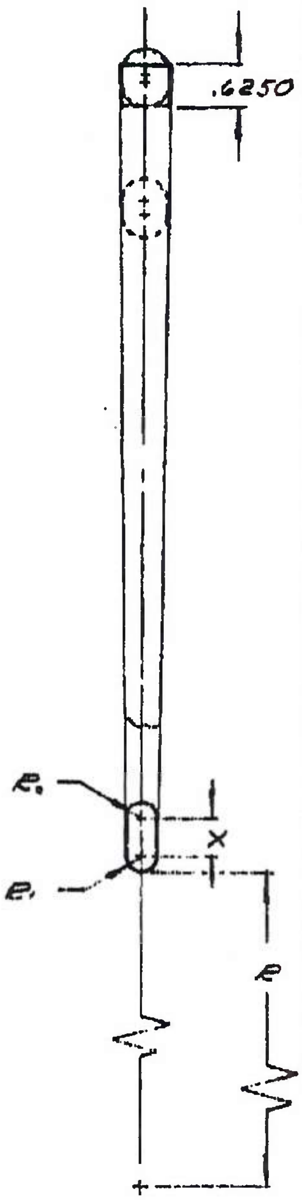

STA. (in.)	R (in.)	R_1 (in.)	R_0 (in.)	X (in.)	INTER ARE (sq i	
0.000	0.62"x1	1/2" Tra	pasoidal	Shape	.4	}*
3.000	0.62"x1	1/2" Tra	pasoidal	Shape	.4	
6.000	27.64	.366	.368	.122	.41	
7.871	27.385	.363	.365	.133	.44	
11.912	26.303	.349	.351	.177	.44	
15.703	24.534	.325	.329	.249	.4	
16.750	23.924	.317	.321	.274	.42	
18.750	22.769	.302	.306	.321	.41	
20.750	21.614	.287	.292	.369	.4	
22.750	20.460	.271	.277	.416	.3	
24.750	19.305	.256	.262	.463	.3	
26.750	18.150	.240	.247	.510	.3	
28.646	17.266	.229	.236	.546	.3	
30.666	16.724	.221	.229	.568	.3	
32.750	16.542	.219	.227	.576	.3	Throat
33.750	16.550	.219	.227	.575	.3	
33.868	16.570	.220	.228	.575	.3	
35.75	16.950	.225	.232	.559	.3	
37.75	17.455	.231	.238	.539	.3	
39.75	17.960	.238	.245	.518	.3	
41.75	18.465	.245	.251	.497	.3	
43.75	18.970	.251	.258	.477	.3	
45.75	19.475	.258	.264	.456	.3	
47.75	19.980	.265	.271	.435	.3	
49.75	20.470	.271	.277	.415	.3	
51.75	20.940	.278	.283	.396	.4	
53.75	21.380	.283	.288	.378	.4	
55.75	21.800	.289	.294	.361	.4	
57.75	22.220	.294	.299	.344	.4	
59.75	22.590	.299	.304	.328	.4	
61.75	22.950	.304	.308	.314	.4	
63.75	23.270	.308	.313	.301	.4	
65.75	23.580	.312	.316	.288	.4	
67.75	23.880	.316	.320	.276	.4	
69.75	24.160	.320	.324	.264	.4	
71.75	24.420	.323	.327	.254	.4	
73.75	24.660	.327	.330	.244	.4	
75.75	24.880	.330	.333	.235	.4	
77.75	25.080	.333	.335	.227	.4	
79.75	25.280	.335	.338	.219	.4	
81.75	25.450	.338	.340	.212	.4	
83.75	25.620	.340	.342	.205	.4	
85.75	25.760	.342	.344	.199	.4	
87.85	25.865	.343	.345	.195	.4	Exit

*Transition Section Between Station 3.000 & 6 00

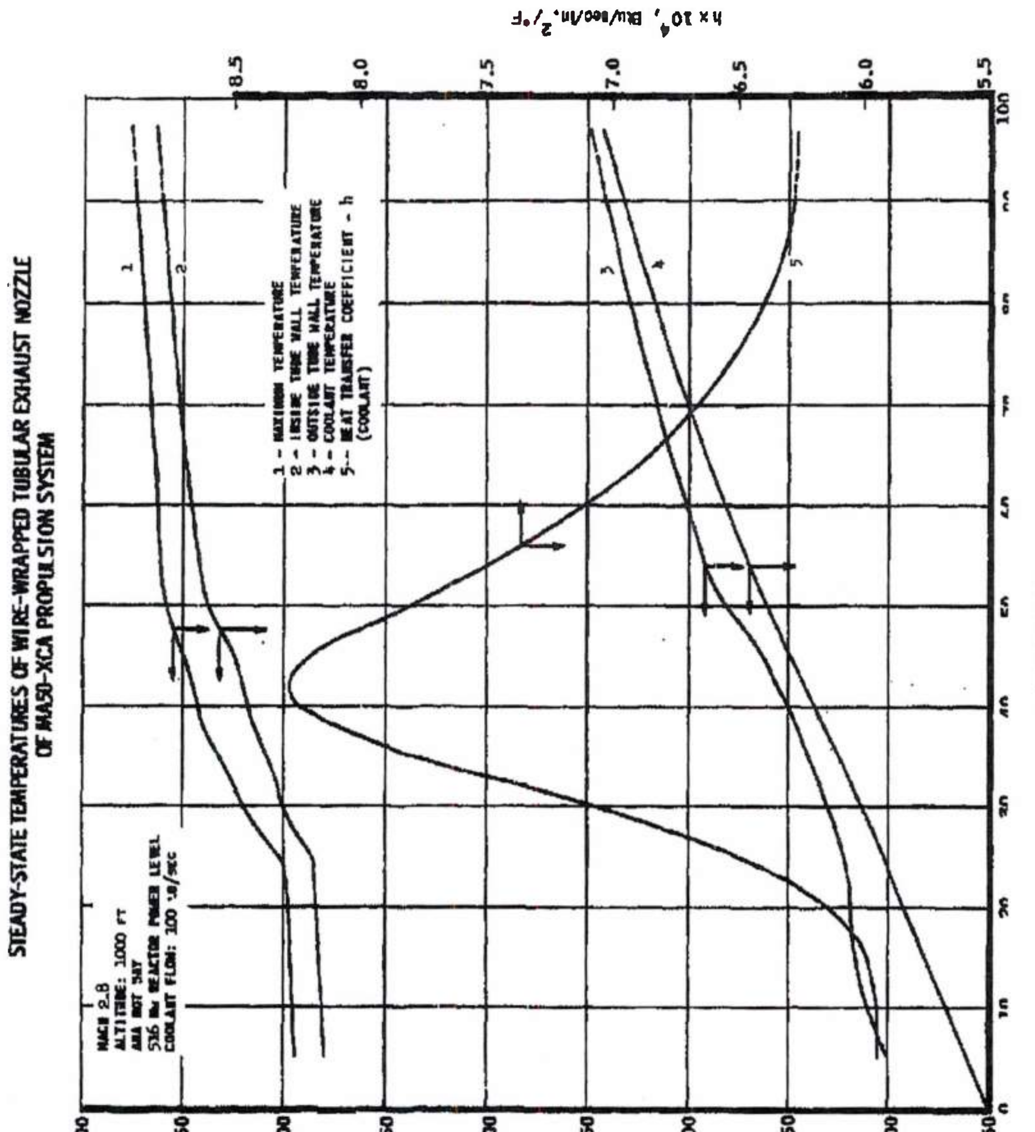
STEADY-STATE TEMPERATURES OF WIRE-WRAPPED TUBULAR EXHAUST NOZZLE
OF MA50-XCA PROPULSION SYSTEM
MACH 2.8
ALTITUDE: 1000 FT
ARA HOT DAY
516 Mw REACTOR POWER LEVEL
COOLANT FLOW: 100 lb/SEC
1 - MAXIMUM TEMPERATURE
2 - INSIDE TUBE WALL TEMPERATURE
3 - OUTSIDE TUBE WALL TEMPERATURE
4 - COOLANT TEMPERATURE
5 - HEAT TRANSFER COEFFICIENT - h (COOLANT)
1
2
3
4
5
TEMPERATURE - °F
1500
1450
1400
1350
1300
1250
1200
1150
1100
1050
NOZZLE LENGTH - inches
0
10
20
30
40
50
60
70
80
90
100
h x 10^4, Btu/sec/in.^2/°F
8.5
8.0
7.5
7.0
6.5
6.0
5.5

that reported earlier for an all-tubular nozzle. However, the maxi um metal temperature of the nozzle is about 1400° F and occurs in the conver :nt tubular portion at the throat position. A reduction in this value might be po sible by using smaller tubes in the convergent portion; however, the pressu drop in the tubes and the balancing of the static pressures inside the nozzle anc .t the exit of the cooling tubes will be limiting factors. Figure 55 is a plot of th tempera-tures in the film-cooled nozzle.

An excellent correlation for the evaluation of film-cc .ing systems is presented in Reference 15. This method was used in the above a .lysis and has been successfully put in a form suitable for simulation by the II 1 704 ther-mal analyzer program. A thermal analyzer program is now being nstructed for future studies of ejector or film-cooled nozzles.

Nozzle Attachment Fitting

The flight engine nozzle attachment fitting shown in Figure 6 has been analyzed using the thermal analyzer to determine steady state temp atures at both Hot and Cold Day conditions (Mach 3.0, sea level). Maximum :mperatures obtained for the Hot and Cold Day conditions are 1440° F and 1060° respec-tively. Temperature distributions are shown in Figure 57.

To determine the effect of heat generation in the fitting, ar .nalysis was made under the same conditions with nuclear heating omitted. The aximum temperature for this case was 1202° F under Hot Day conditions ind ating that nuclear heat generation accounted for 238° F of the nozzle attachme tempera-ture.

At the present time, it is assumed that the nozzle attachm t fitting of Figure 56 may be used on all air-cooled configurations of the exha .t nozzle.

3.4.2 Performance Support Studies

Heat Rejection Rates

Studies have been made to determine steady state tempera res and heat rejection rates in the Model MA50-XCA propulsion system side sup rt struc-ture. The primary objective of these studies was to estimate the h t rejection rates in the side support system for evaluation of propulsion systen performance. For this reason, the analytical model chosen did not treat in detail ich com-ponents as support springs. The analytical model used is shown in igure 58.

MAXIMUM STEADY-STATE METAL TEMPERATURES IN AN EJECTOR OR FILM-COOLED NOZZLE FOR THE MA50-XCA PROPULSION SYSTEM

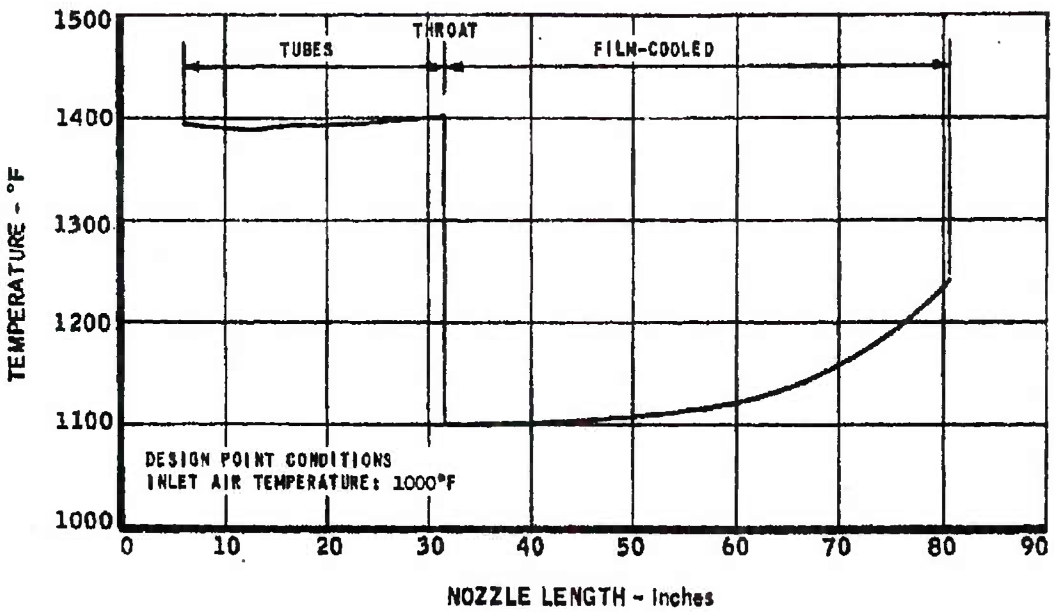

EXHAUST-NOZZLE-TO-REACTOR-SHELL ATTACHMENT

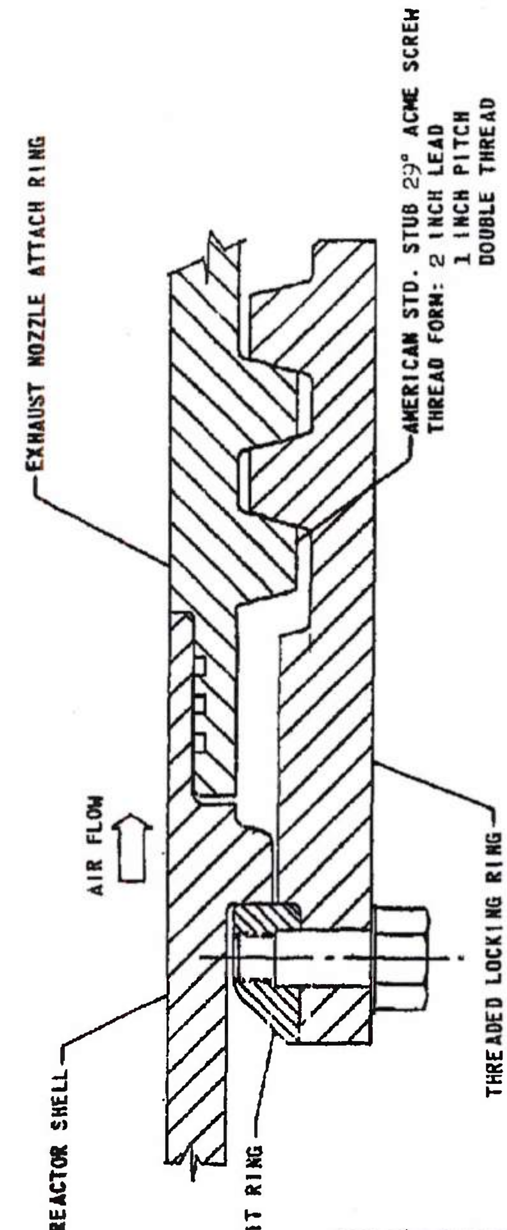

STEADY-STATE TEMPERATURE PROFILE FOR NOZZLE ATTACHMENT FITTING

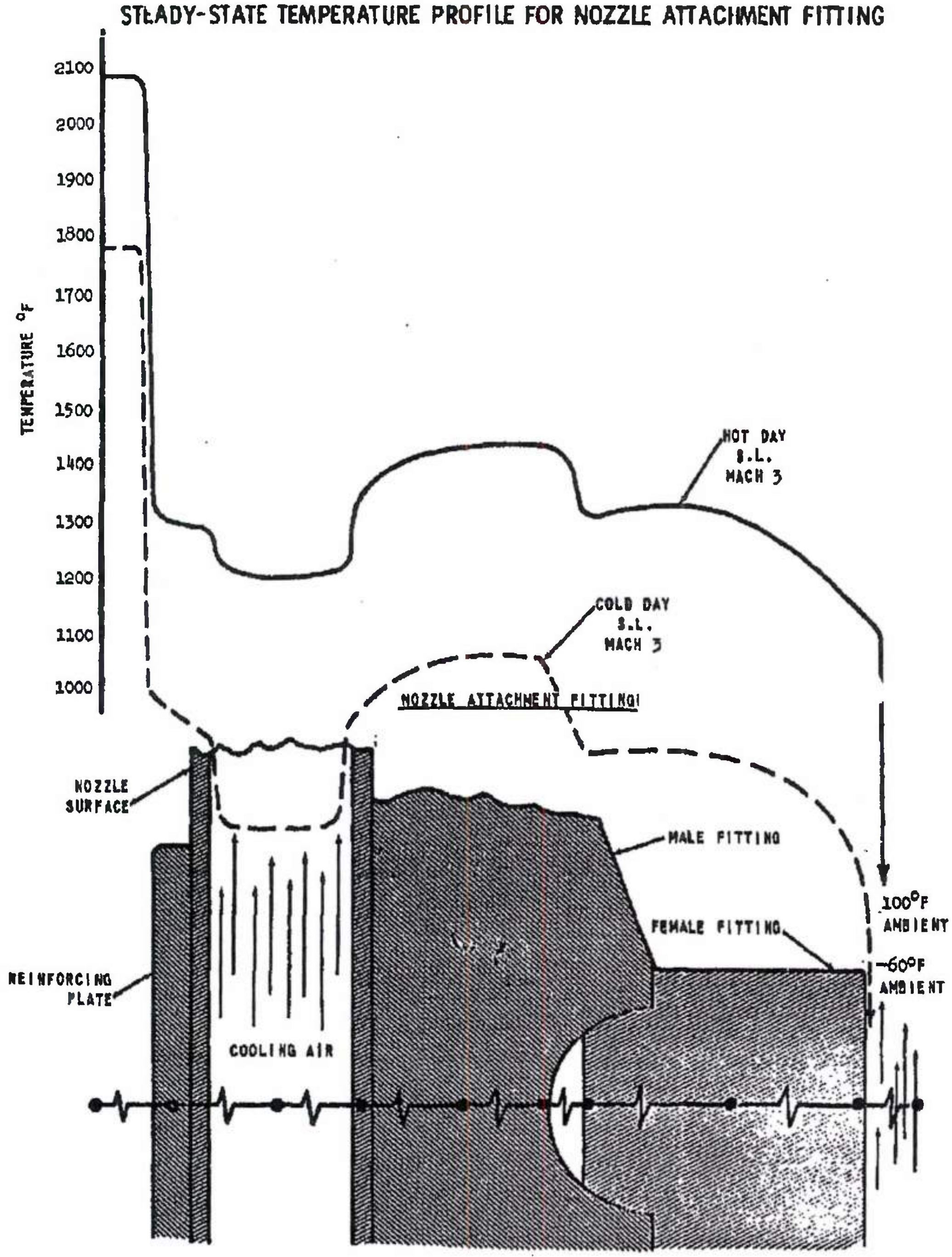

ANALYTICAL MODEL FOR DETERMINATION OF PROPULSION SYSTEM HEAT REJECTION

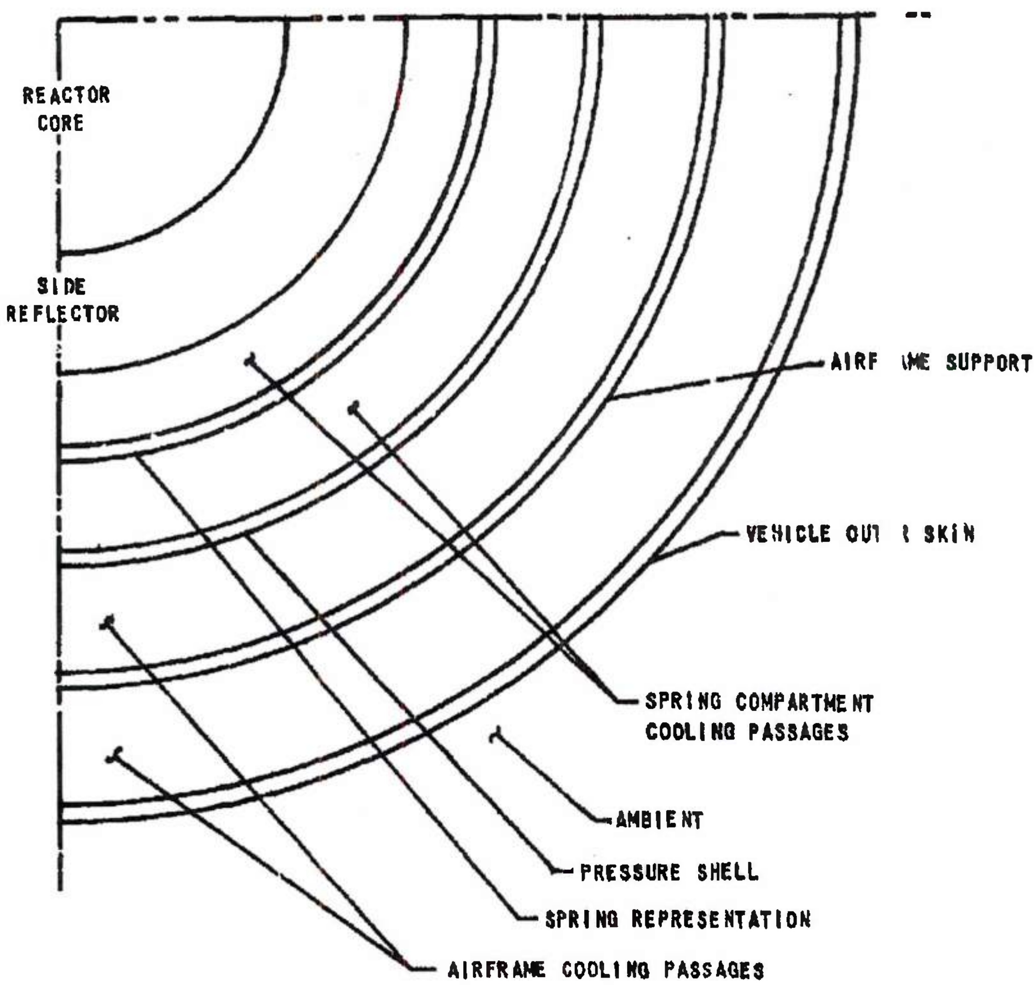

A reactor length simulation of this model on the IBM 704 thermal analyzer p o-gram was used for computation of the temperatures that were used to deterr ne the heat rejection rates.

Calculations, based on the best estimates of nuclear heat generatio in the support system and airframe, were made for design point conditions (M: h 2.8, ANA 421 Hot Day, and an altitude of 1000 feet). With an airflow rate o 113 lb/sec in the support spring compartment, bounded by the reflector and ie pressure shell, the support springs reached a maximum temperature of abo 1120° F. The total cooling airflow rate inside the airframe structure was a sumed to be 50 lb/sec. At this flow, the pressure shell reached a maximun temperature of 1180° F, the internal support member in the airframe reach a temperature of 1480° F, and the vehicle skin maximum temperature was 10C ° F. A complete temperature distribution is presented in Figure 59 . The total l at rejected by the system, i.e., the heat absorbed by the coolant streams, is out 3.0 Mw. A complete breakdown of the heat rejection is presented in Table . This information was presented in Performance Bulletin No. 2. (Reference 3)

Recent studies of the Model MA50-XDA propulsion system (larger lam-eter, shorter length reactor) at design point conditions were also conducted determine the steady state temperatures and heat rejection rates. Nuclear eat generation rates were calculated at Marquardt. With an airflow rate of 120 /sec in the support spring compartment, the support springs reached a maximum em-perature of approximately 1360° F. The total cooling airflow rate inside the ir-frame structure was kept at 50 lb/sec. At this flow the pressure shell reac d a maximum temperature of 1280° F, while the internal support member in the ir-frame reached a temperature of 1510° F. The vehicle skin temperature in t s case was about 1000° F. The total heat rejected by this system is about 3.8 Mw. A complete temperature distribution is presented in Figure 60 , and a breal own of the heat rejection is presented in Table 6 . This information is present l in Performance Bulletin No. 4, which is an integral part of this report (Sectio 3.3).

Fuel Element Thermal Stress Analysis

The reactor fuel elements are the energy source that produces the thrust of the propulsion system. The transient behavior of these fuel eleme s and the preservation of their structural integrity have a direct bearing on th performance of the propulsion system. To insure the highest performance s-sible, studies have been made to adjust reactor power profiles to give the m xi-mum thrust without exceeding a safe beryllia thermal stress limit. In addit n, an IBM thermal analyzer program was devised to calculate the transient beh vior of a fueled tube.

STEADY-STATE TEMPERATURES IN MA50-XCA PROPULSION SYSTEM AND AIRFRAME

DESIGN POINT CONDITIONS: MACH 2.8; 1000 FT; ANA HOT DAY; REACTOR POWER LEVEL = 516 MW
AIR FLOW THROUGH SUPPORT STRUCTURE = 113 LB/SEC
AIR FLOW THROUGH AIRFRAME = 50 LB/SEC
INLET AIR TEMPERATURE = 942°F

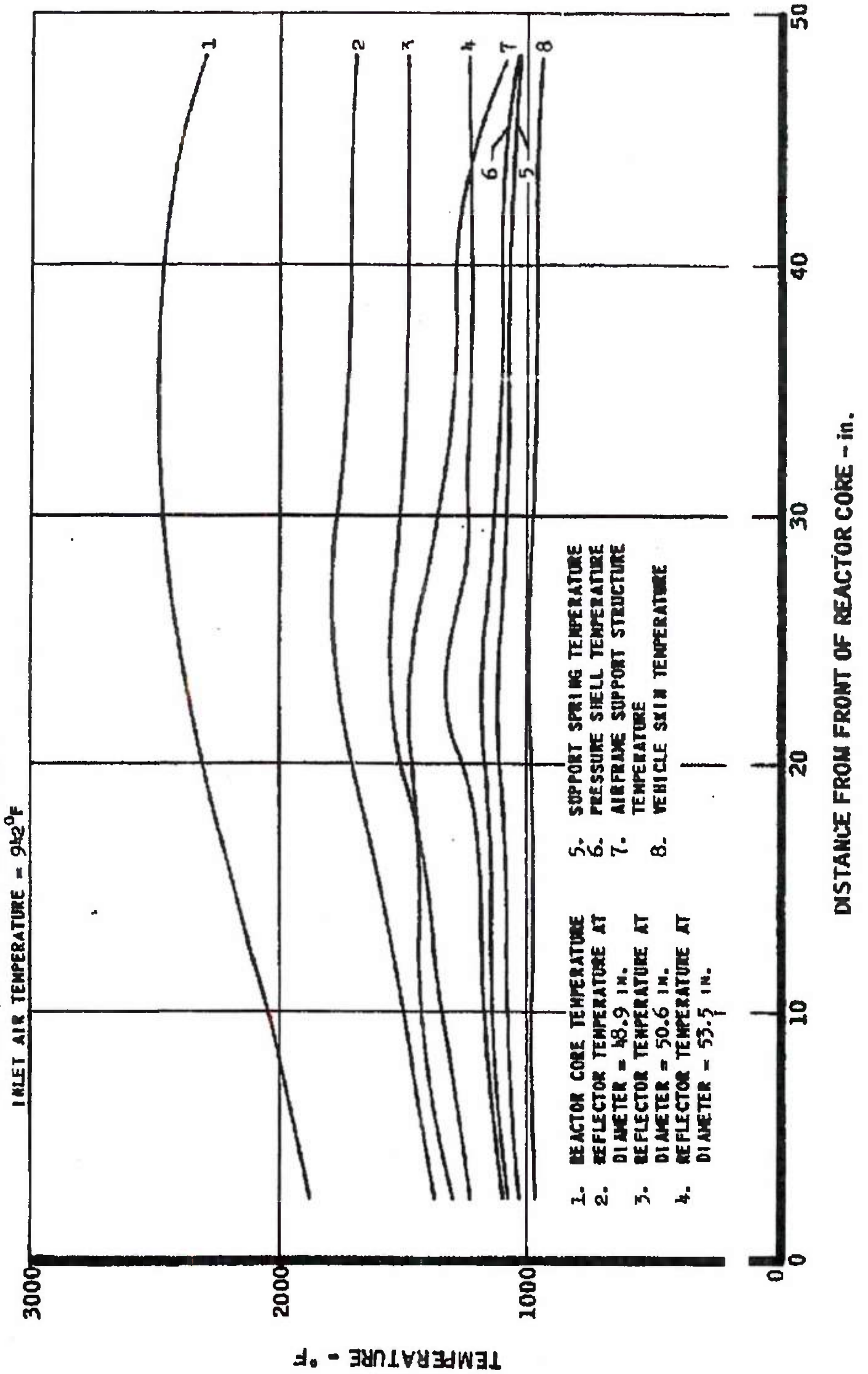

FIGURE 59

TABLE 10

HEAT REJECTION OF MA50-XCA PROPULSION SYSTEM
(Mach 2.8; ANA Hot Day; Altitude, 1,000 feet)

ITEM	Air Flow (lb/sec)	HEAT REJECT[illegible]N (Btu/sec)	(Mw)	[illegible])
Spring Compartment	113	1845	1.95	[illegible]4.2
From Side Reflector	--	729	0.77	[illegible].4
From Support Springs	--	628	0.66	[illegible].8
From Pressure Shell	--	488	0.52	[illegible].0
Airframe	50	349	0.37	[illegible].1
From Pressure Shell	--	56	0.06	[illegible].0
From Airframe Support	--	286	0.30	[illegible].9
From Vehicle Skin	--	7	0.01	[illegible].2
To Ambient From Vehicle Skin	--	684	0.72	[illegible].7
TOTAL	--	2878	3.04	1[illegible].0

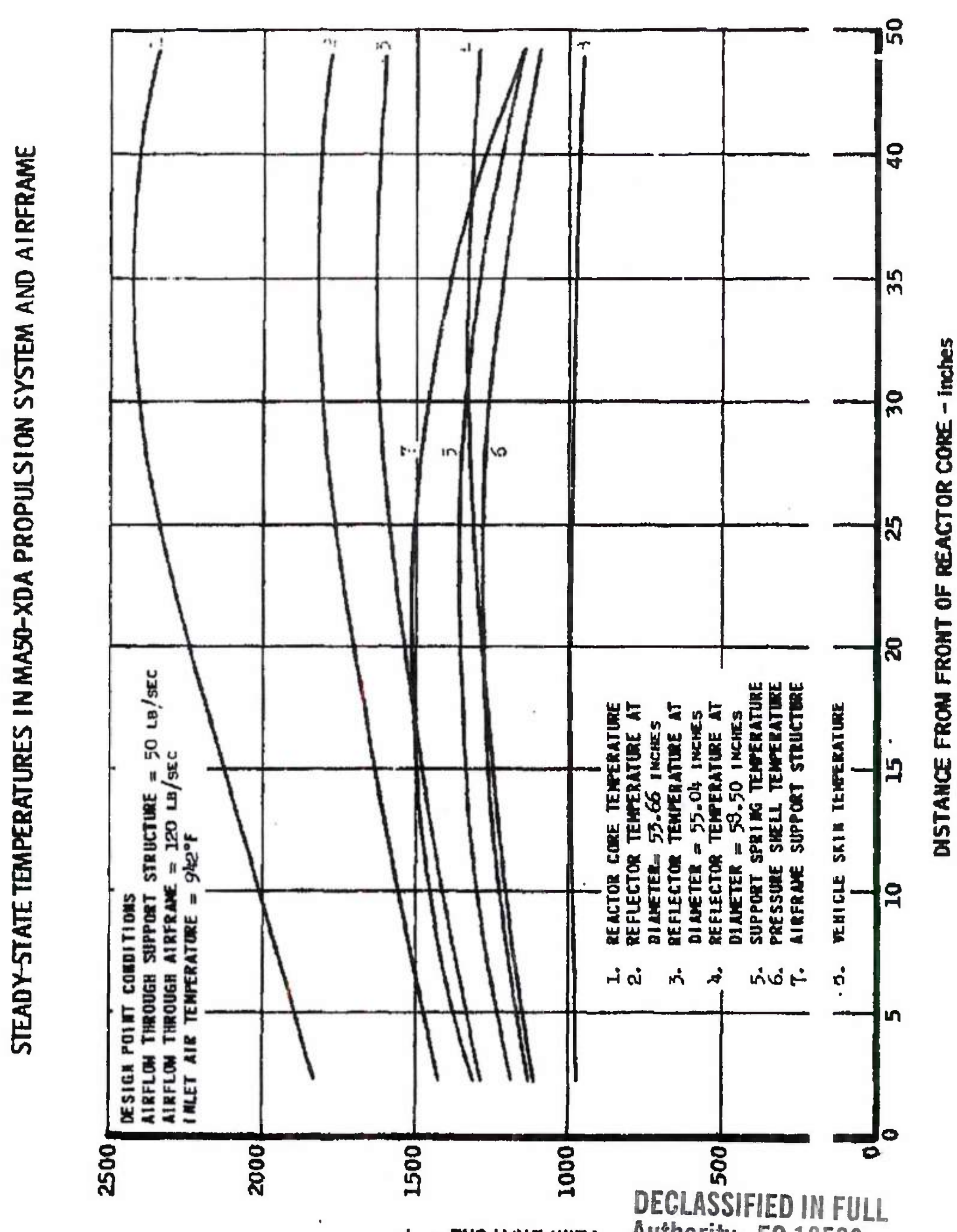
STEADY-STATE TEMPERATURES IN MA50-XDA PROPULSION SYSTEM AND AIRFRAME
DESIGN POINT CONDITIONS
AIRFLOW THROUGH SUPPORT STRUCTURE = 50 LB/SEC
AIRFLOW THROUGH AIRFRAME = 120 LB/SEC
INLET AIR TEMPERATURE = 942°F
1. REACTOR CORE TEMPERATURE
2. REFLECTOR TEMPERATURE AT DIAMETER = 53.66 INCHES
3. REFLECTOR TEMPERATURE AT DIAMETER = 55.04 INCHES
4. REFLECTOR TEMPERATURE AT DIAMETER = 58.50 INCHES
5. SUPPORT SPRING TEMPERATURE
6. PRESSURE SHELL TEMPERATURE
7. AIRFRAME SUPPORT STRUCTURE
8. VEHICLE SKIN TEMPERATURE
TEMPERATURE - °F
2500
2000
1500
1000
500
0
DISTANCE FROM FRONT OF REACTOR CORE - Inches
0
5
10
15
20
25
30
35
40
45
50

Reactor Fueled Tube Thermal Stress

The steady state elastic thermal stress in a fueled beryllia tube in t : Tory IIC reactor has been determined for various power generation and tem era- ture levels. In addition, the temperature difference across the wall of a fue d tube has been determined at the same conditions. Generalized charts of thes results are presented in Figures 61 and 62 .

These charts were used at Marquardt to revise the Tory IIC reactor axial power curve to produce more thrust. These power curves are based u| n a limiting fueled tube thermal stress of 15,000 psi and 18,000 psi, and/or a r ıxi- mum wall temperature of 2500° F. Figure 40 is a plot of the new power cur es along with that for Tory IIC and for a fueled tube with an isothermal wall tem era- ture of 2500° F. From the 15,000-psi thermal stress axial power curve and e- sultant air and tube wall temperatures obtained from Figures 61 and 62 , th maximum elastic thermal stress (tensile) and the maximum temperature in t : tube were computed. These results are presented in Figure 63.

Reactor Fueled Tube Transient Temperatures

An analysis of the effect upon propulsion system performance of suc en changes in reactor airflow, inlet air temperature, and reactor power has be made possible by the construction of a thermal analyzer program simulating Tory IIC core-length fuel element.

The program will yield the maximum fuel element temperature, wal temperature, outlet air temperature, heat transfer coefficient (based on film temperature), and film temperature for varying air flow rates, inlet air tem peratures, and reactor power level. The thermal resistance and capacity of ne beryllia fuel element are functions of the fuel element temperature.

This program will be used to assist in the evaluation of transient p: - pulsion system performance at various flight conditions.

3.4.3 Control System Support Studies

Control Rod Actuator

Preliminary estimates of the steady state temperatures in a flight t· e control rod actuator were made, for the following flight conditions: Mach 3. ANA Hot Day, an altitude of 1000 feet. In the stationary or nonoperating con - tion (the most pessimistic condition in the heat transfer sense) with a total

MAXIMUM ELASTIC THERMAL STRESS (TENSILE) IN A TORY IIC FUEL TUBE

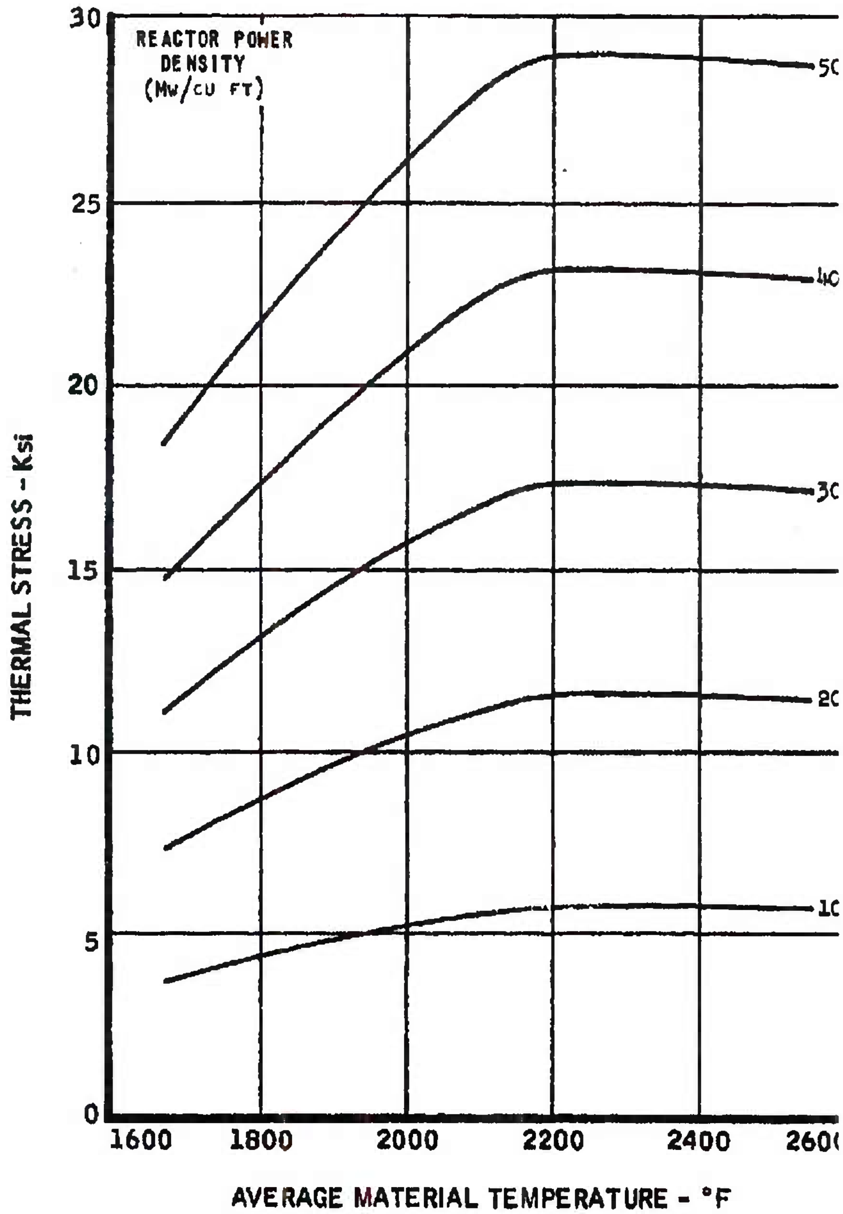

MAC A603

FIGURE 61

MATERIAL TEMPERATURE DIFFERENCE IN TORY IIC FUELED TUBE

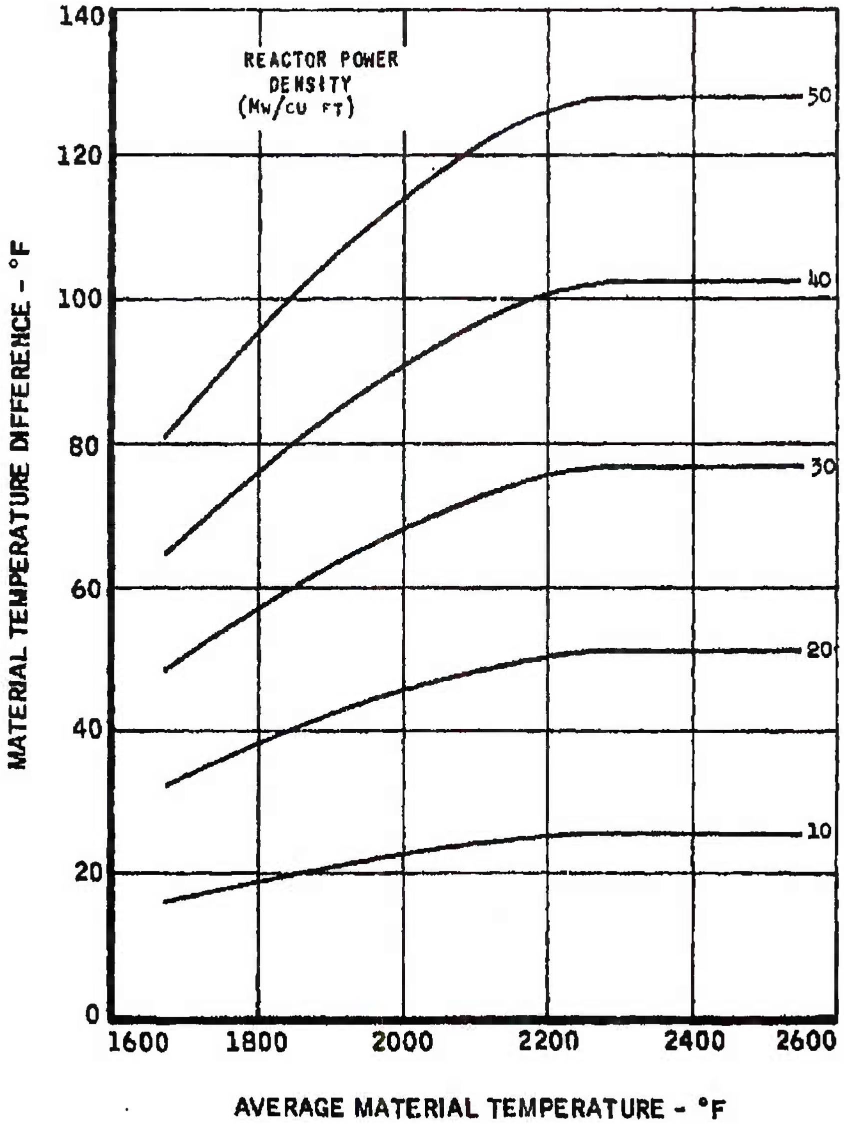

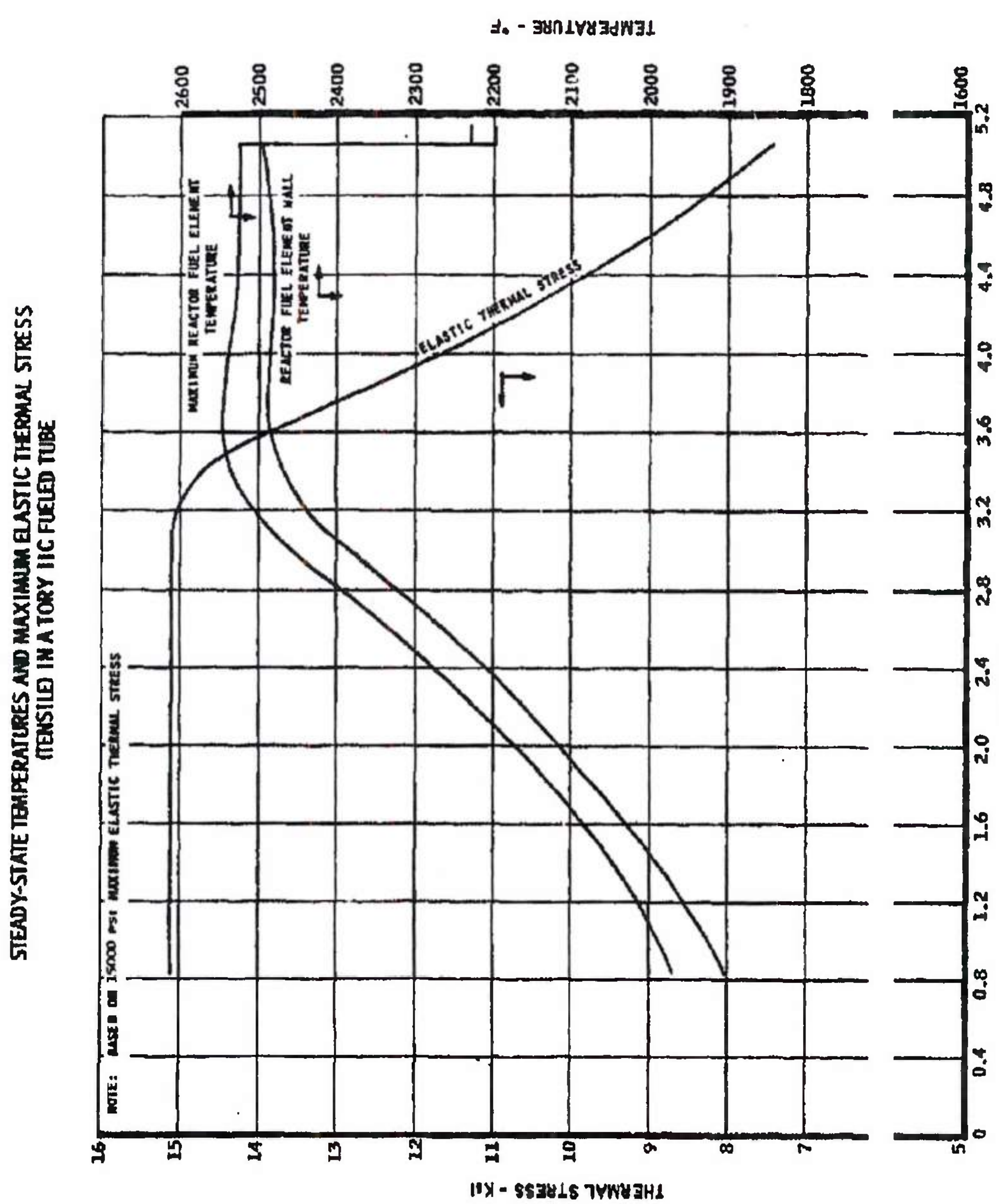
STEADY-STATE TEMPERATURES AND MAXIMUM ELASTIC THERMAL STRESS
(TENSILE) IN A TORY IIC FUELED TUBE
TEMPERATURE - °F
THERMAL STRESS - Ksi
REACTOR LENGTH, feet
MAXIMUM REACTOR FUEL ELEMENT TEMPERATURE
REACTOR FUEL ELEMENT WALL TEMPERATURE
ELASTIC THERMAL STRESS
NOTE: BASED ON 15000 PSI MAXIMUM ELASTIC THERMAL STRESS
2600
2500
2400
2300
2200
2100
2000
1900
1800
1600
16
15
14
13
12
11
10
9
8
7
5
0
0.4
0.8
1.2
1.6
2.0
2.4
2.8
3.2
3.6
4.0
4.4
4.8
5.2

FIGURE 63

leakage airflow of 0.04 lb/sec (at 1060° F) through the actuator, the maximu m steady state temperature was estimated to be about 1087° F. A complete te: - perature map is presented in Figures 64 and 65. The temperature limit f : the actuator was 1600° F.

The actuator, constructed almost entirely of Stellite 3 and 6B, was .s- sumed to be located in the inlet duct, 60 inches from the reactor front face. The nuclear internal heating of the actuator, due to the attenuation of gamma ra(i- tion, is presented in Figure 66. The actuator, one of five, was oriented w h its axis perpendicular to the airflow in the inlet duct. The airflow in the 56 nch internal diameter duct is about 1800 lb/sec at 1060° F. All bearings in the . tu- ator were assumed to have an effective void fraction of 0.35.

The IBM 704 thermal analyzer program was used to make the calcu i- tions. A program was constructed that may be used for future temperature evaluations. With some modifications, this program may be used for calcu tion of transient temperatures, consideration of varying thermal properties, etc

3.5 MECHANICAL AND STRUCTURAL DESIGN

The mechanical design effort during 1961 was directed toward the (- sign of an integrated flight type propulsion system incorporating the Tory II reactor. Design layouts of the Model MA50-XCA engine were completed, a ng with layouts of major engine components.

3.5.1 Engine-AirFrame Integration

Lateral Support Structure

In the interests of optimizing the reactor support structure from a er- formance standpoint - i.e., adequately supporting the Tory IIC reactor insid a minimum diameter airframe - several design concepts have been under inve i- gation. To fulfill its function the reactor lateral support system must prope ly constrain the reactor core elements, transfer all flight loads to the airfram accommodate differential thermal expansion between reactor and airframe, nd provide the structural support necessary for reactor installation and ground handling.

Spring Design

Of the methods studied to date, a pre-loaded spring system offers e most effective solution to the reactor support problem. To meet the above

STEADY-STATE TEMPERATURES FOR NUTATING DISK MOT R OF CONTROL ROD ACTUATOR

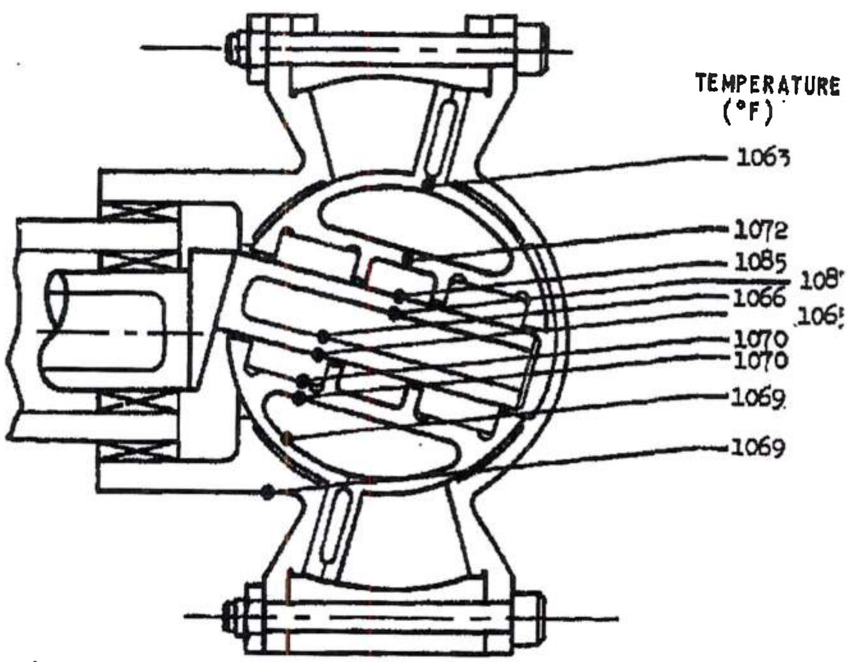

FIGURE 64

STEADY-STATE TEMPERATURES FOR GEAR TRAIN OF CONTROL ROD ACTUATOR

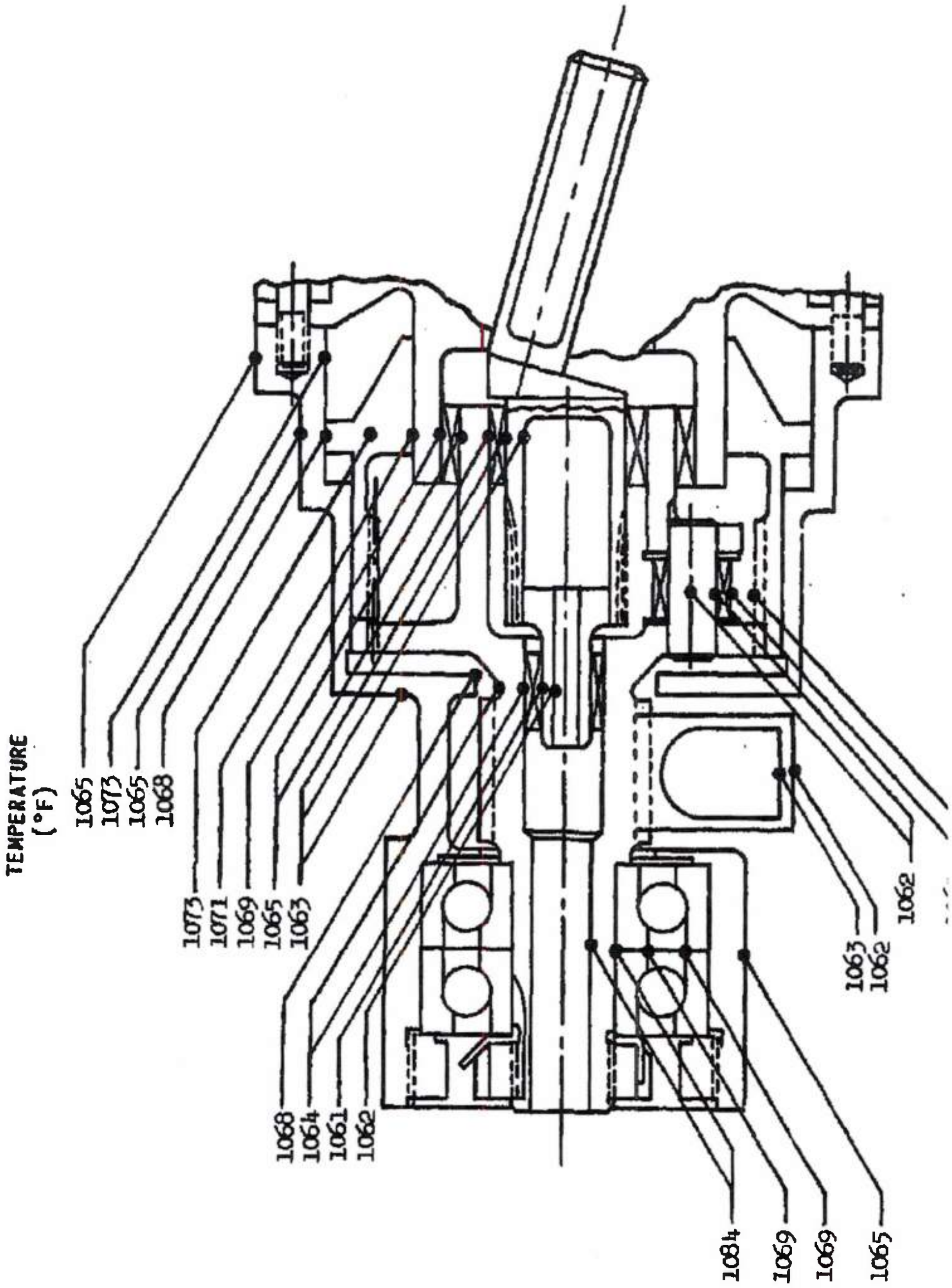

NUCLEAR HEATING IN CONTROL ROD ACTUATOR

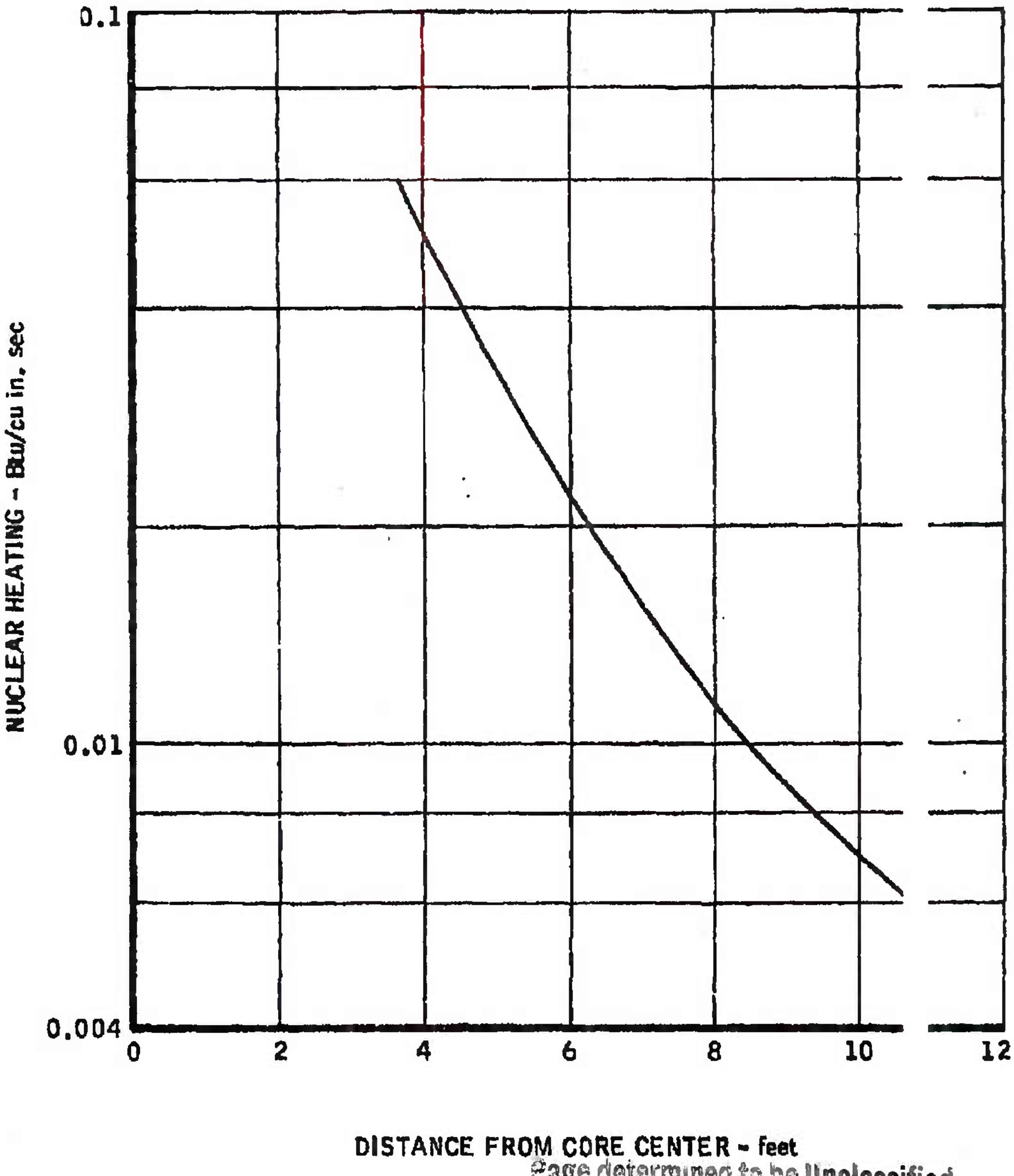

requirements a spring system is needed that has a low load-to-deflection rat for thermal expansion and a high load-to-deflection ratio when subjected to inertia loads.

The optimum spring should exhibit a nonlinear load deflection as sho n below:

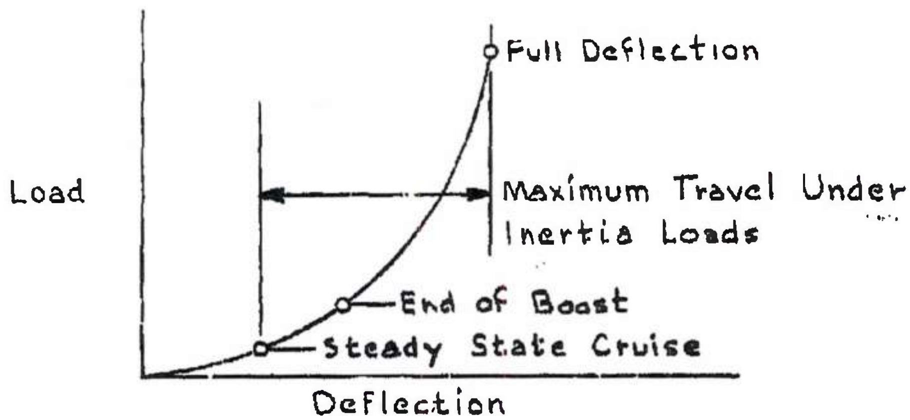

Types of springs analyzed include tubular, corrugated, Belleville, a d "buggy" configurations (Reference 9). The tubular and corrugated springs exhibited either low load-high deflection or high load-low deflection characteristics that were incompatible with the required nonlinear relationship. Th Belleville spring was the only geometry studied that approximated the desirec load-deflection characteristics. Figure 67 shows the physical arrangement o the Belleville design; however, final recommendations as to the spring config uration best suited for the ground test engine awaits the outcome of the full sc le lateral attachment tests to be performed in 1962.

Vibration Studies

Vibration analyses have been performed in an effort to define the dynamic response characteristics of the reactor and associated components. T complexity of the structure precludes a rigorous analysis, but useful design information can be obtained from analyses of idealized models.

BELLEVILLE SPRINGS IN REACTOR LATERAL SUPPORT STRUCTURE

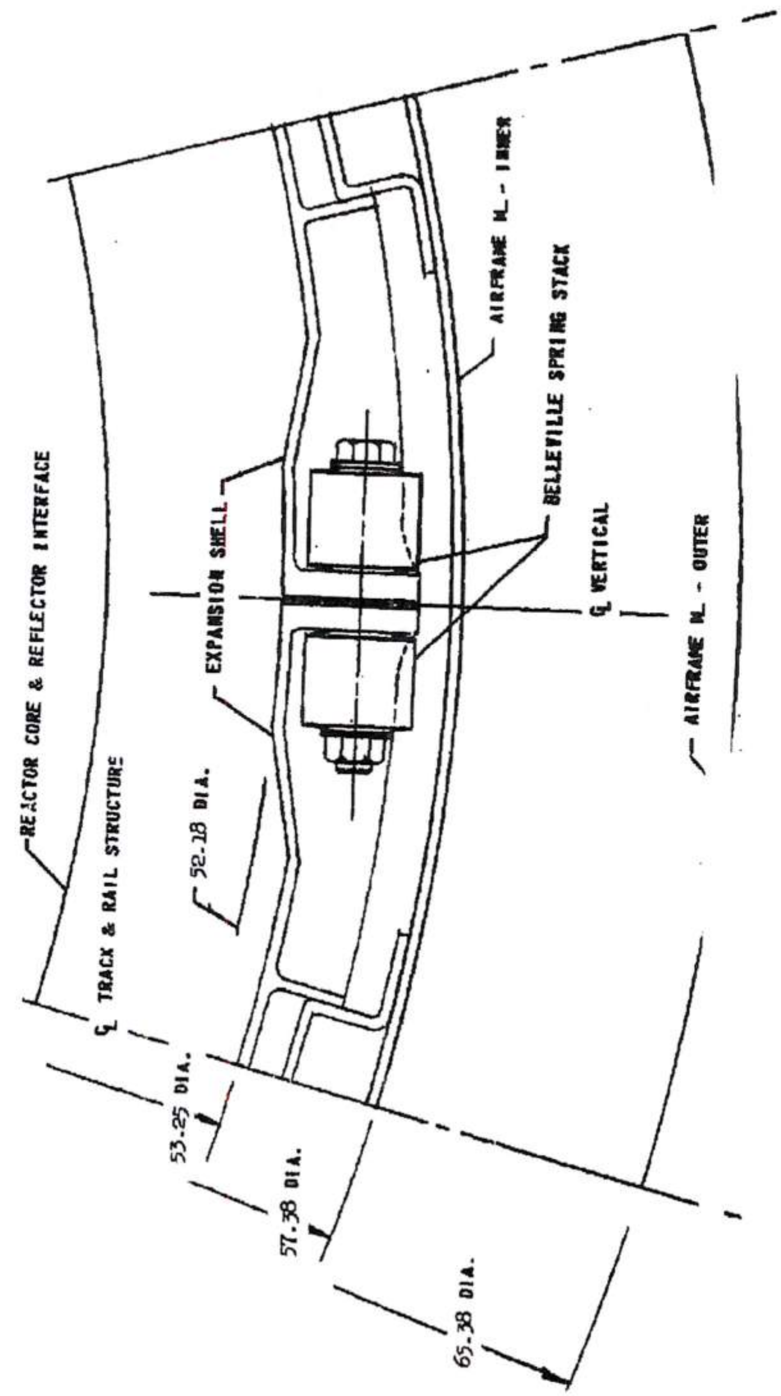

FIGURE 67

One such model assumed an inelastic fluid cylinder vibrating in a ho o-geneous elastic medium. Results of this study as described in References 16 and 8 indicate that appreciable excitation of distortional modes is unlikely in he frequency range of interest (5-30 cps). However, a low frequency resonance could exist corresponding to the rigid body translation mode.

These results suggest another dynamic model that may be used to in ude the effect of damping on the system. For this model the tangential (Bellevill spring reactor support (Figure 67) is idealized into a single-degree-of-free m, slip-damped system. The analysis of this system is pointed toward deriving n equivalent static load, which is reacted by the springs. The tangential sprin system and its idealized model are illustrated in Figure 68.

Although the model is for tangential springs, it applies equally well a radial spring support system, requiring only minor modifications in the equa ons.

The equivalent static load is given as:

$$V = AW\alpha$$

where

A = Amplification factor
W = Body weight
α = Input inertia load factor

Since W and α have known values, the amplification factor remains t be determined.

The assumptions used are:

(1) The airframe surrounding the reactor remains circular.
(2) The core behaves as a rigid cylinder.
(3) Only the translational mode is of interest.
(4) The only damping present results from friction on the periphery of the core.

Assumptions (2) and (3) permit the use of standard derivations (Reference 17) that give the amplification factor as:

TANGENTIAL SPRING SYSTEM AND IDEALIZED MODEL

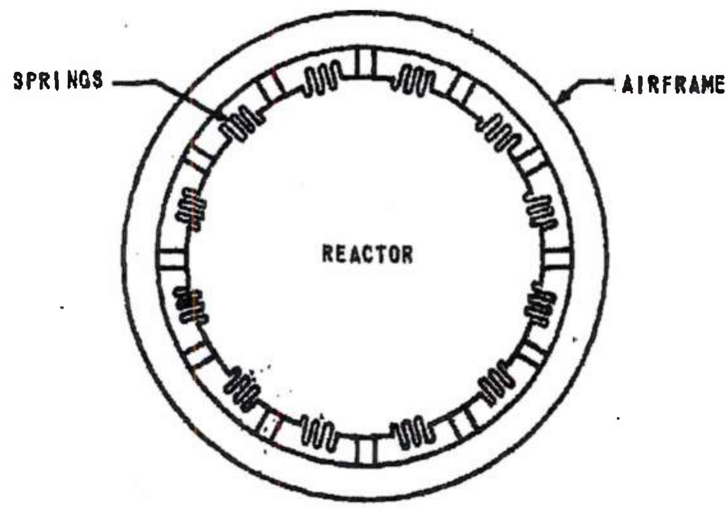

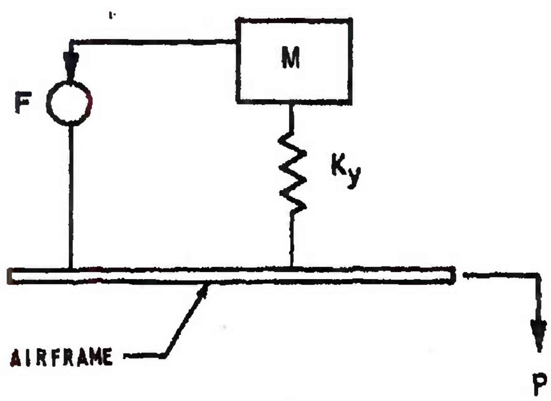

FIGURE 68

$$A \cong \frac{\sqrt{1 - \left(\frac{4}{\pi}\,\frac{F}{P}\right)^2}}{1 - \frac{f^2}{f_n^{\,2}}}$$

where

f = Driving frequency
f_n = Resonant frequency of system

$$\left(f_n = \frac{1}{2}\sqrt{\frac{K_y}{M}}\right)$$

P = Driving force
F = Resisting friction force

The above equation represents an approximate solution of the dry friction damping case.

The driving force is given as:

$$P = W[illegible]$$

From a static analysis of the load distribution of the system, the equations shown below are found to apply.

The friction force is given as:

$$F = 4\mu Rp$$

where

μ = Coefficient of friction
p = Clamping pressure
R = Radius at which the pressure is applied

Transverse spring constant:

$$K_y = \frac{2\pi^2}{N} \cdot K_c$$

K_c = Spring constant of individual spring
N = Number of springs

Maximum clamping shell tension and body pressure due to inertia is:

$$T_I = \frac{V}{\pi}$$

$$P_I = \frac{T_I}{R} = \frac{V}{\pi R}$$

With the above dynamic and static equation, coupled with the proper input loads, it is theoretically possible, by adjusting the static pressure and spring constant, to limit the body movements to tolerable amounts. At the same time, the vibrating system can be made relatively independent of frequency by increasing the friction force of the system. Conversely, it may be made independent of friction by keeping the ratio f/f_n below a critical value. The optimum design represents a compromise between a stiff system, which limits inertial deflections, and a soft spring to accommodate thermal expansions.

There are, in general, three other factors that may give some help. One is, that any excitation of core distortional modes will increase the damping factor. Another is the possibility of reducing the amplification factor at resonance by introducing nonlinearity into the spring design. The third is that the driving vibration is actually highly damped rather than steady state as assumed. The investigation of these parameters will be continued in the future.

Engine Weight and Balance

Engine weight and center of gravity (CG) locations have been calculated for the Model MA50-XCA propulsion system using the basic Tory II reactor. The weights of the major engine components and the CG locations are as follows:

	Weight (lbs)	Center of Gravity Locations (Engine Station)
Propulsion System	17,806.5	490.47
Inlet	2,197.0	182.59
Diffuser Duct	1,270.0	405.64
Reactor	12,829.4	542.47
Reactor Controls	350.0	445.94
Exhaust Nozzle	1,160.1	604.77

The respective center of gravity locations are shown in Figure 69.

Because there is a possibility that a reactor of larger diameter than the present Tory IIC will be required to provide desired thrust, weight and CG calculations were performed for reactor configurations having diameters 5 inches and 10 inches larger. Performance optimization studies have also indicated that it may be desirable to reduce the reactor core length. Weight and CG location calculations were made for a variety of reduced reactor lengths. For every one inch reduction in reactor length, there is a weight reduction of 246 pounds. The results of the diameter and length studies are presented in Reference 9.

3.5.2 Engine Inlet and Diffuser

Designs have been completed for the basic inlet (Figure 70) as well as the alternate inlet (Figure 71). Both inlets are underslung, variable geometry, axisymmetric types with S-shaped diffuser duct. Material selections have been made for structural items on the basis of the latest thermodynamic studies that define maximum operating temperatures for various portions of the translating spike and its supporting structure. These temperatures range from 1079°F to 1286°F. The following materials have been selected:

Cowling lip and large structural castings — Haynes Stellite Alloy 31
Sheet metal structure — N-155 CRES
Less severely stressed castings in centerbody — Type 347 CRES

Spike Translation

Four methods of inlet spike translation were studied using the following design criteria:

[redacted]

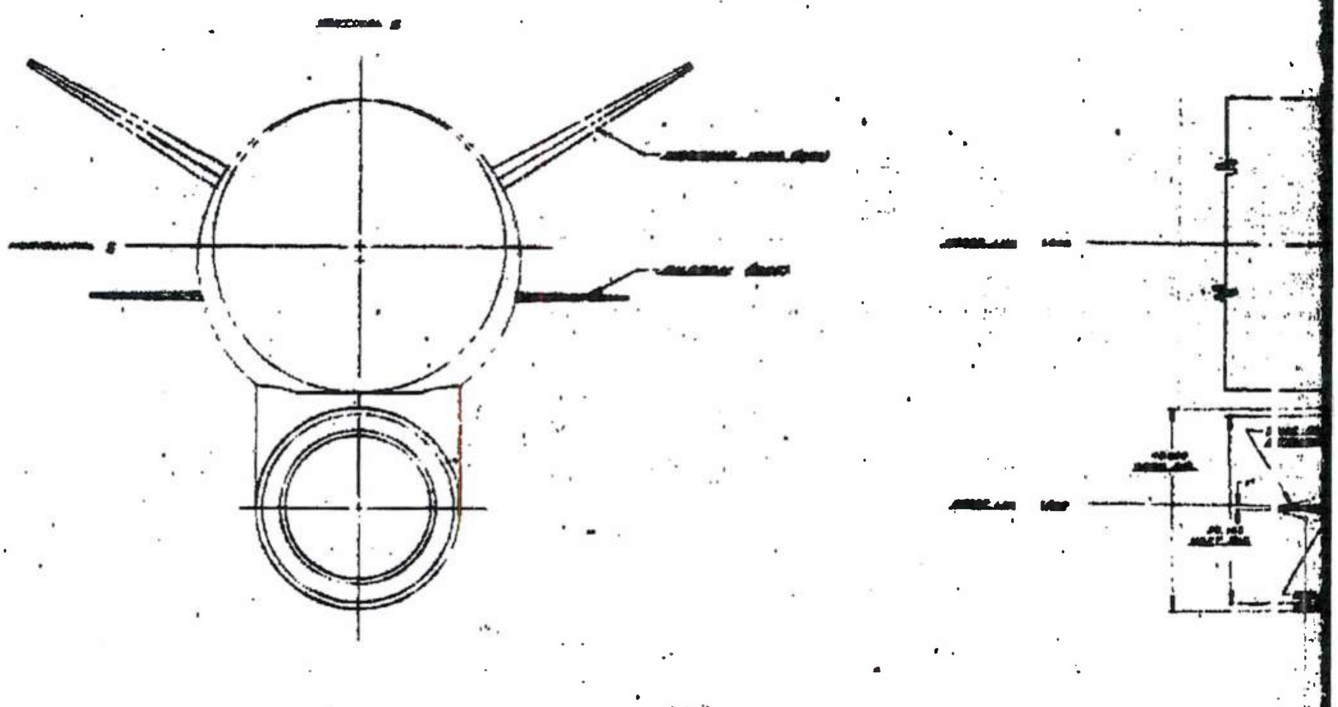

VIEW LOOKING AFT

[redacted]

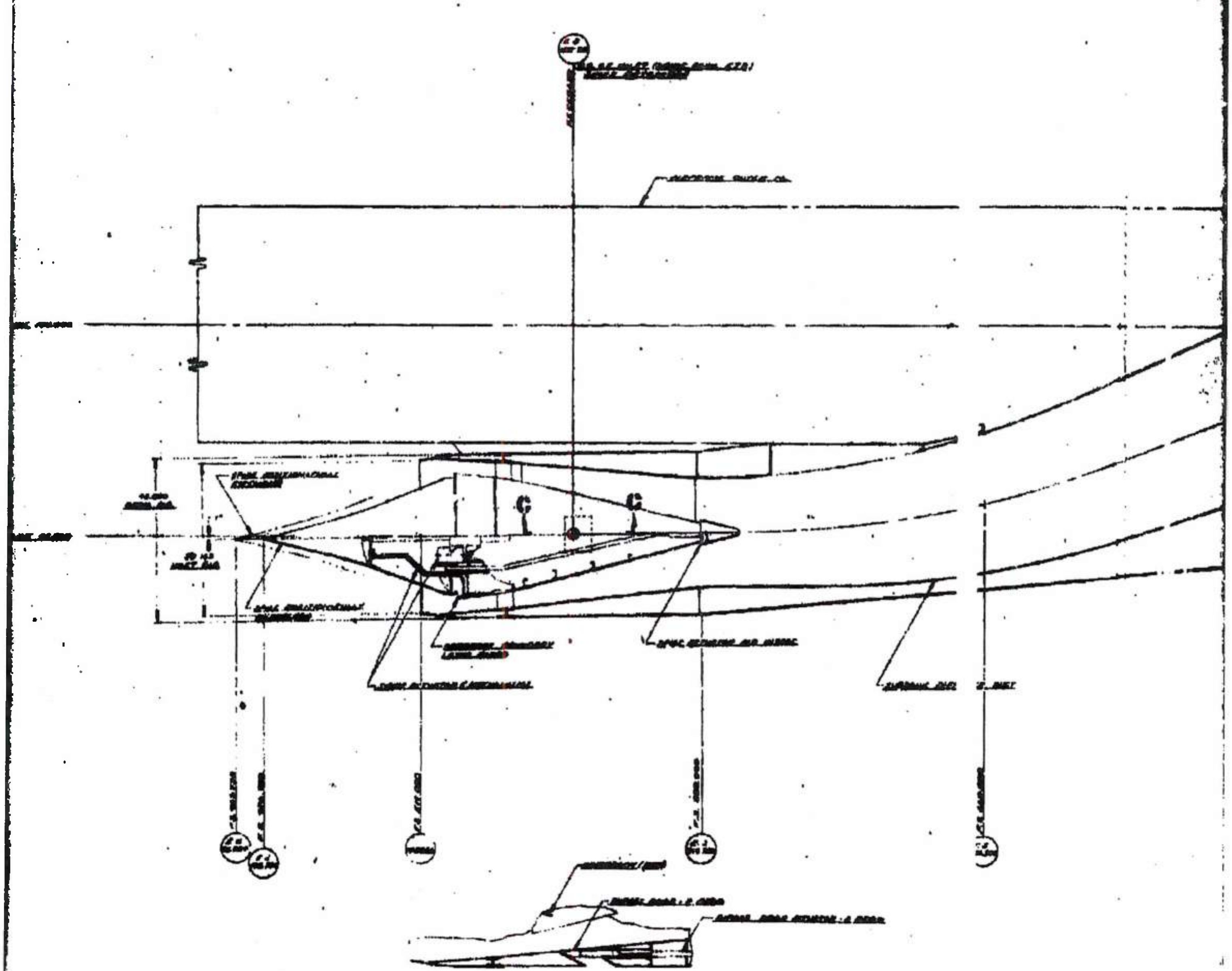

SECTION C-C

2

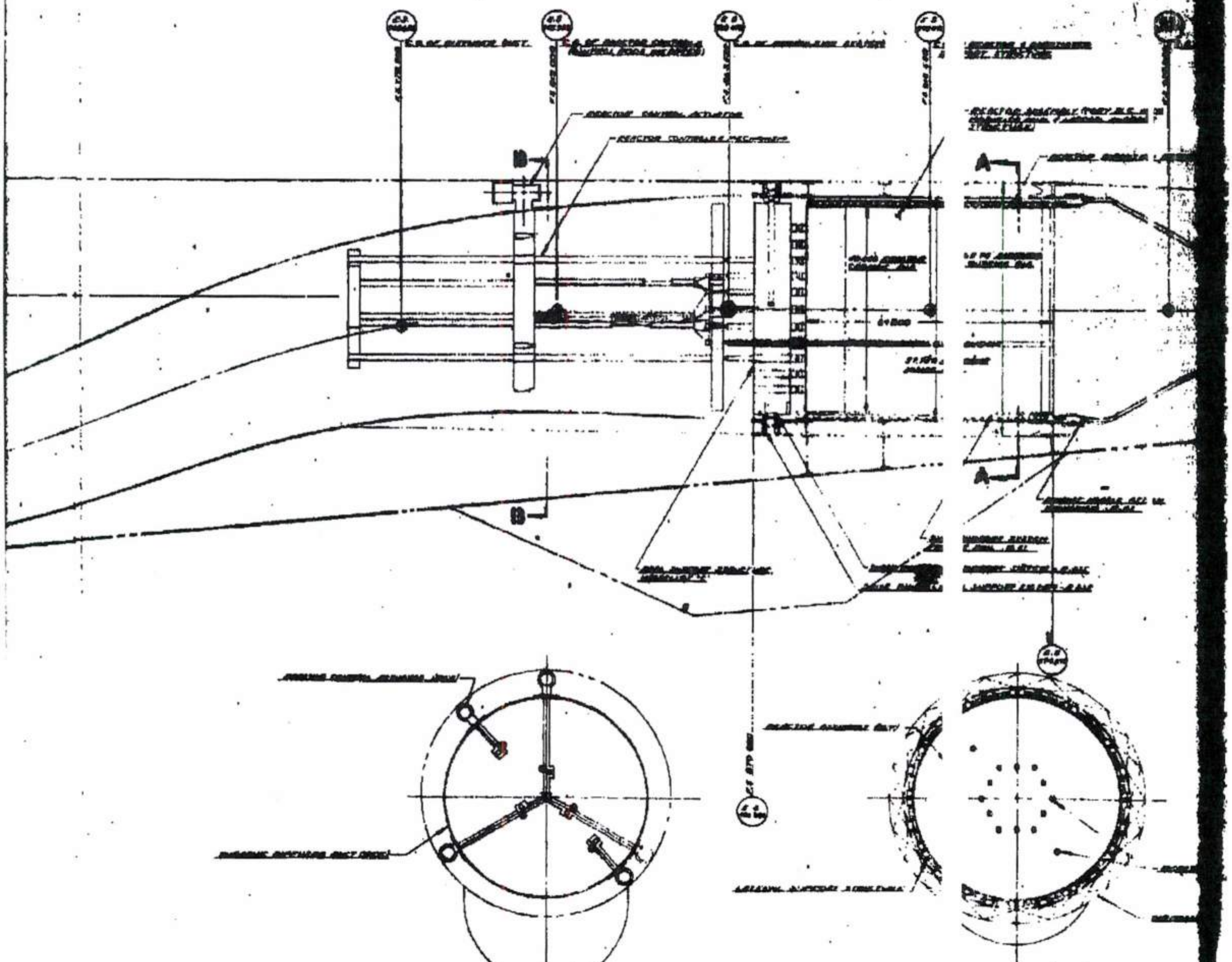

SECTION A-A

SECTION B-B

3

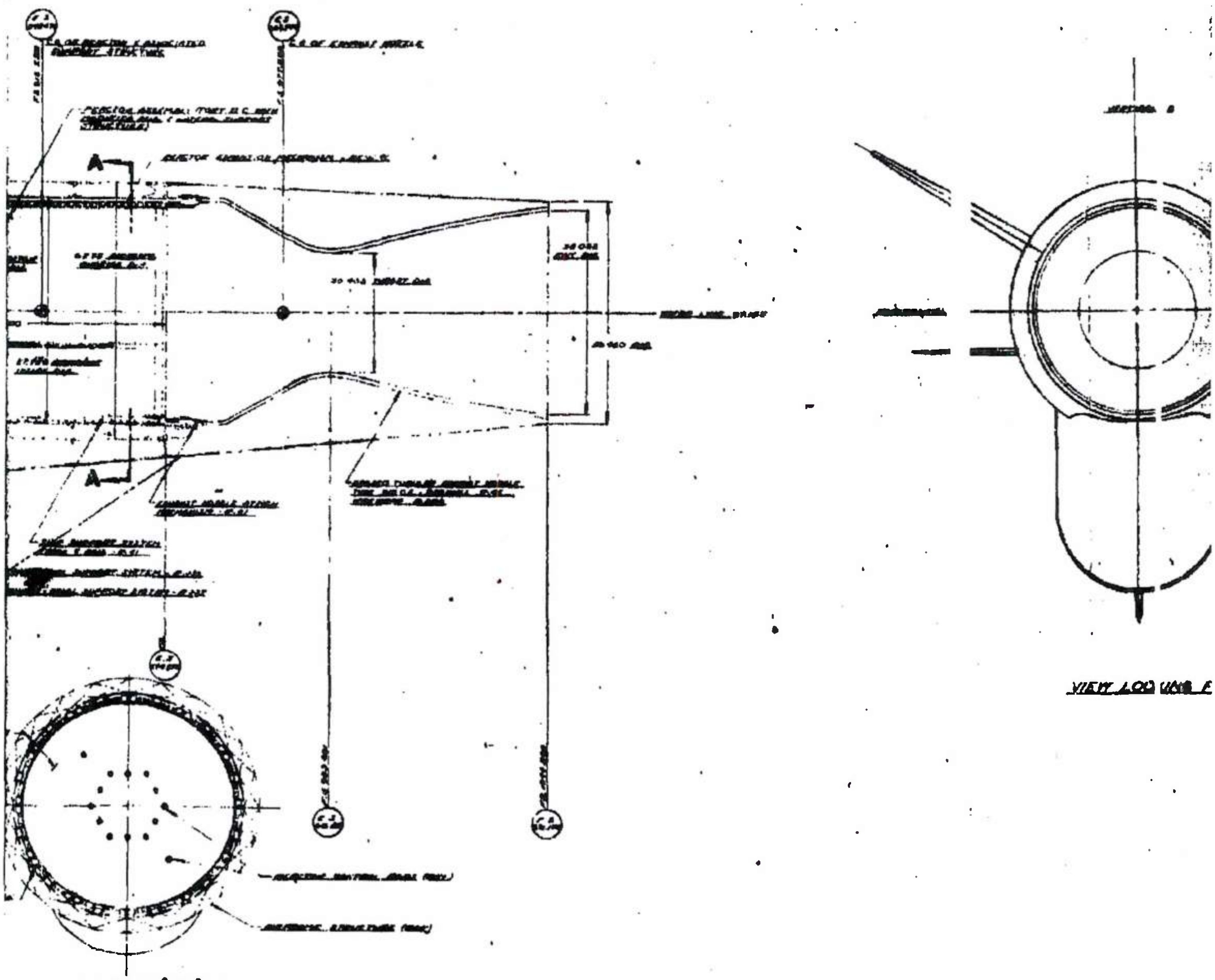

SECTION A-A

U

[redacted]

REPORT [illegible]76

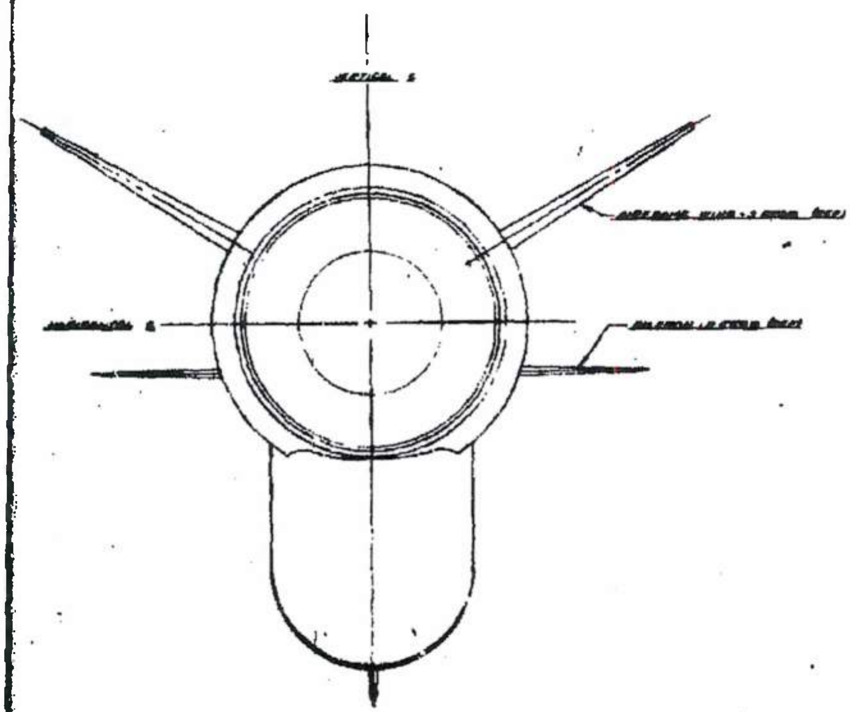

VIEW LOOKING FWD.

MARQUARDT AIRCRAFT CO.

22329

PROPULSION SYSTEM MA50XCA

X 81381

FIGURE 69

SECRET

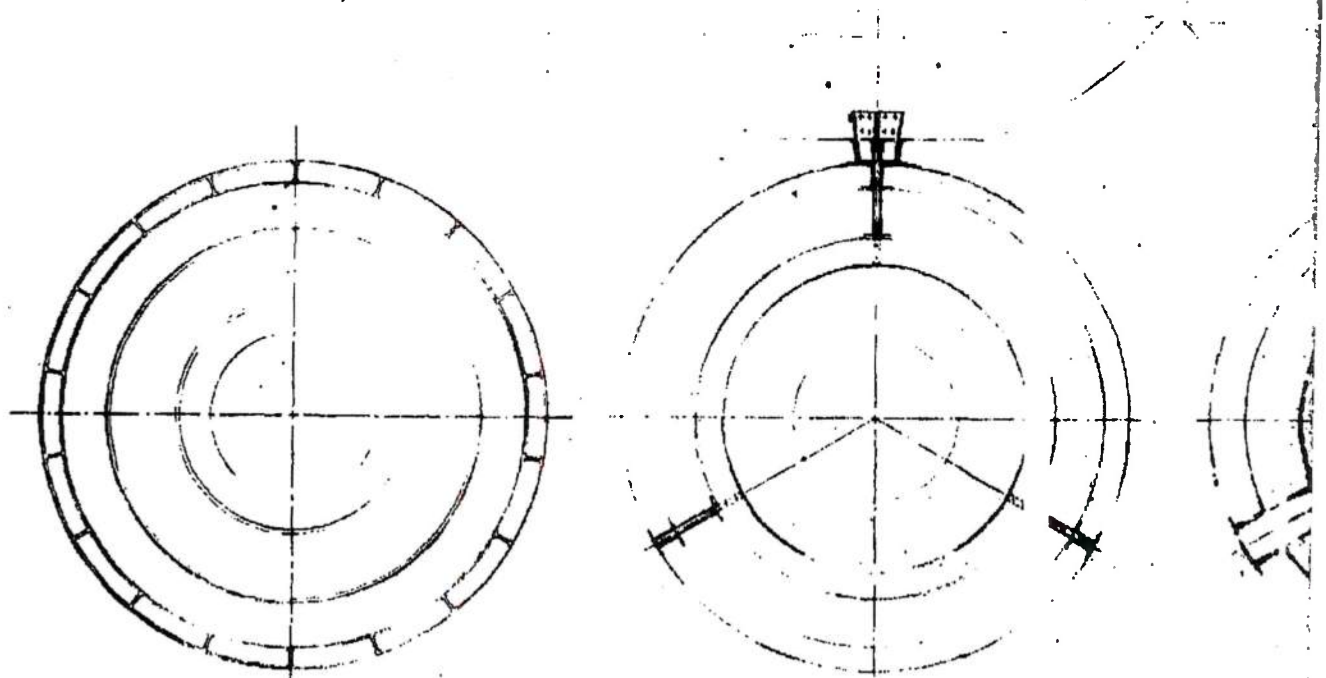

H - H

A - A

SECRET

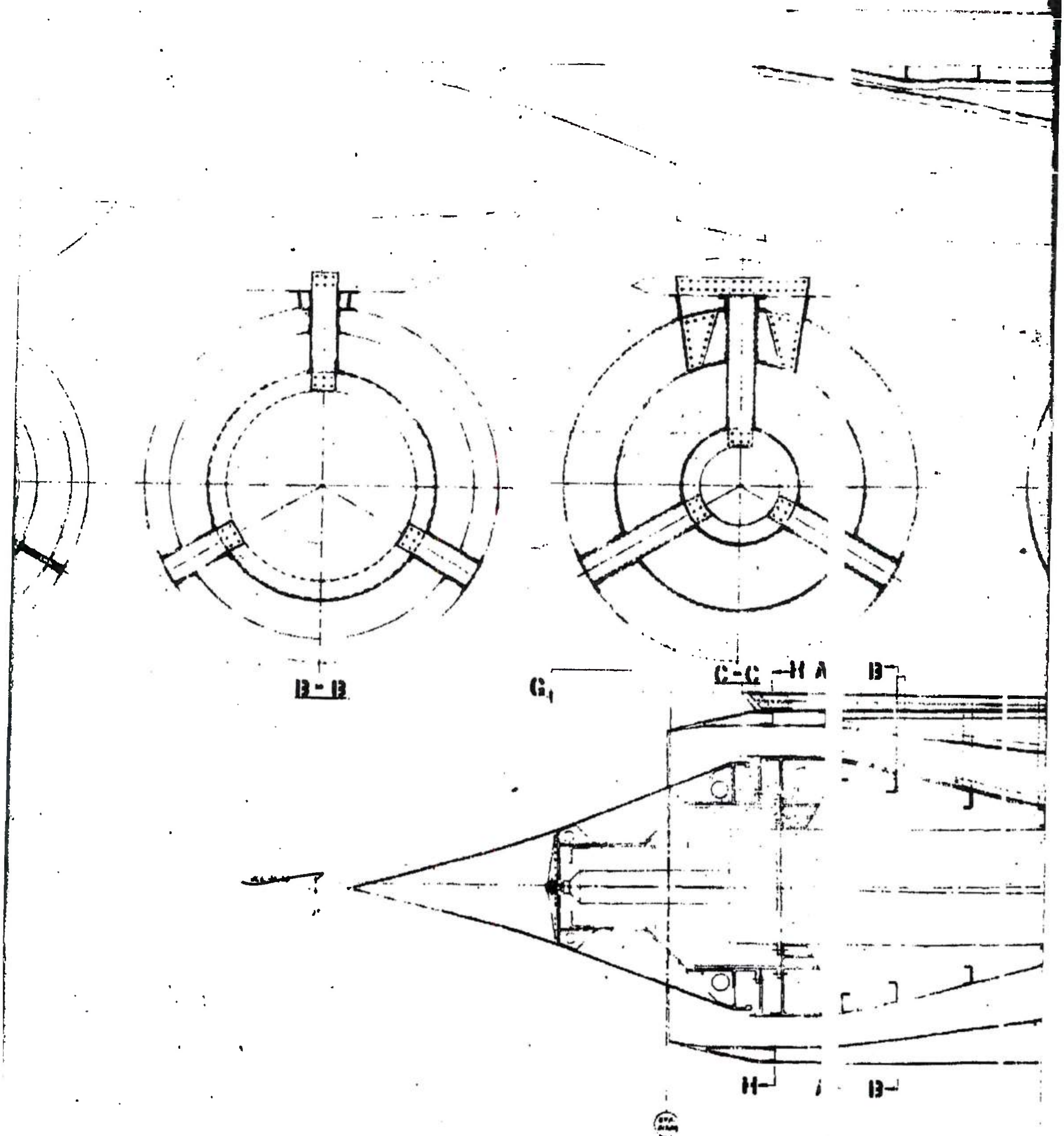

2

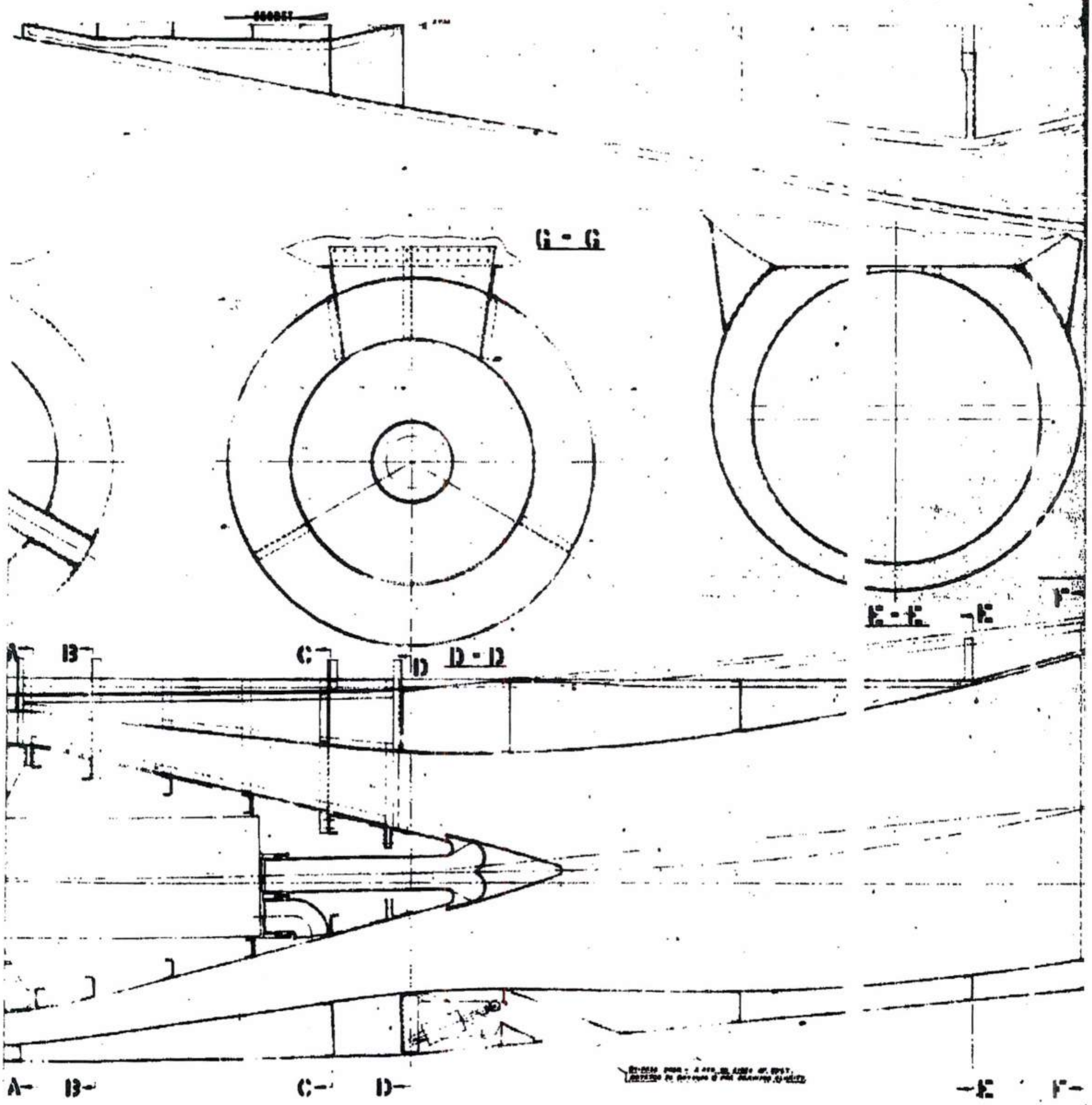

3

[redacted]

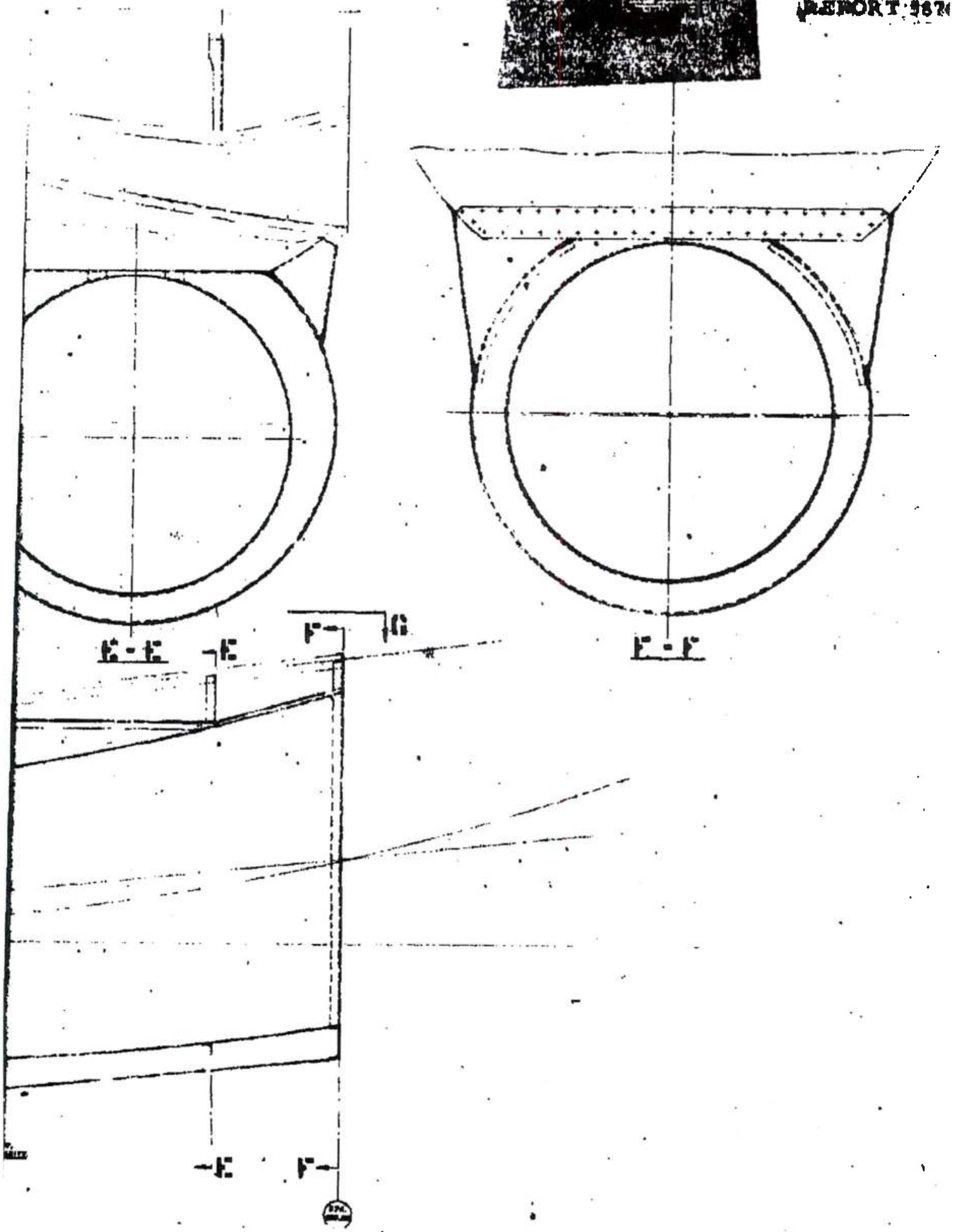

~~SECRET~~

AXISYMMETRIC INLET

6132-. FIGURE 0.

X 81242
LAYOUT - INL

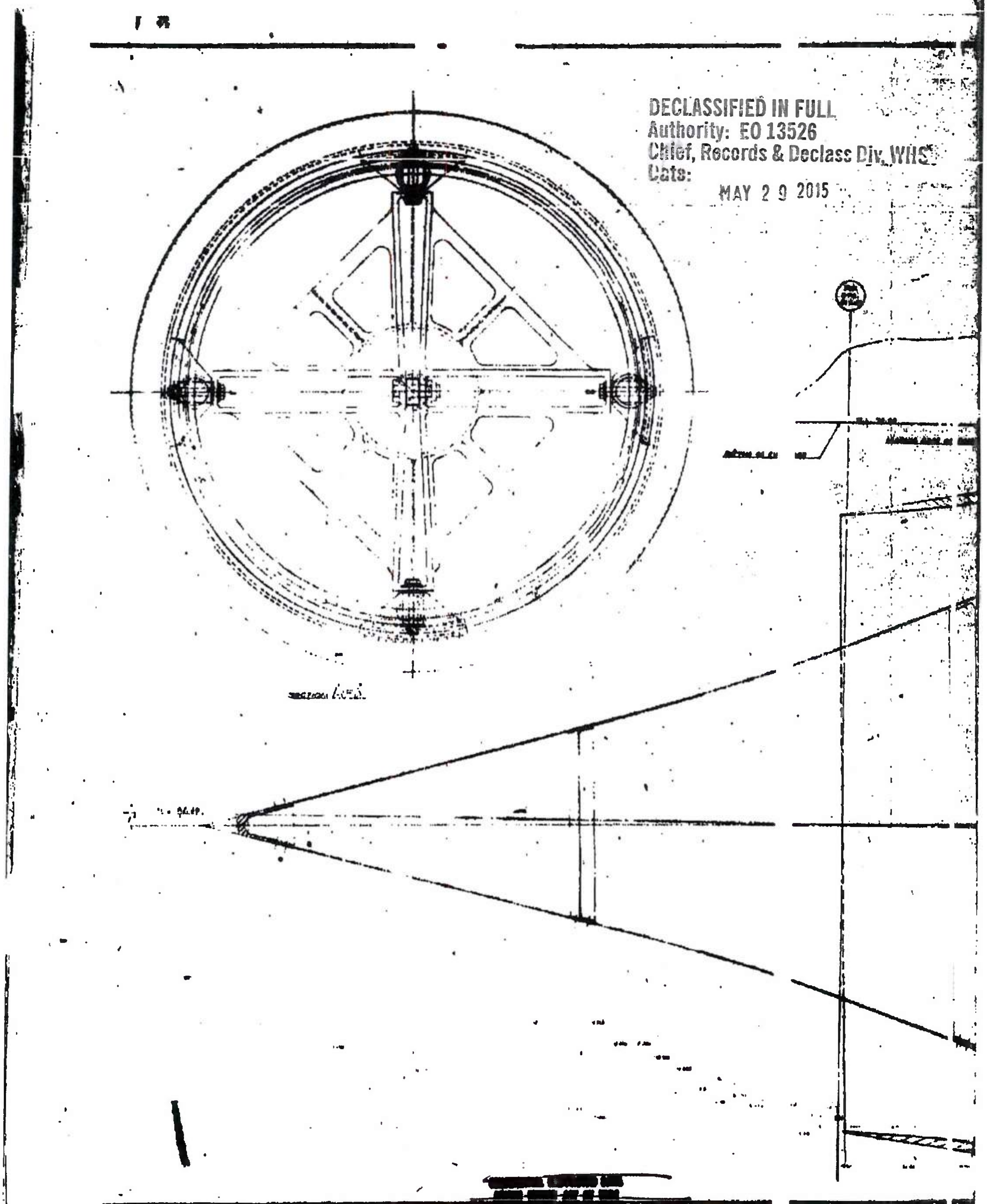

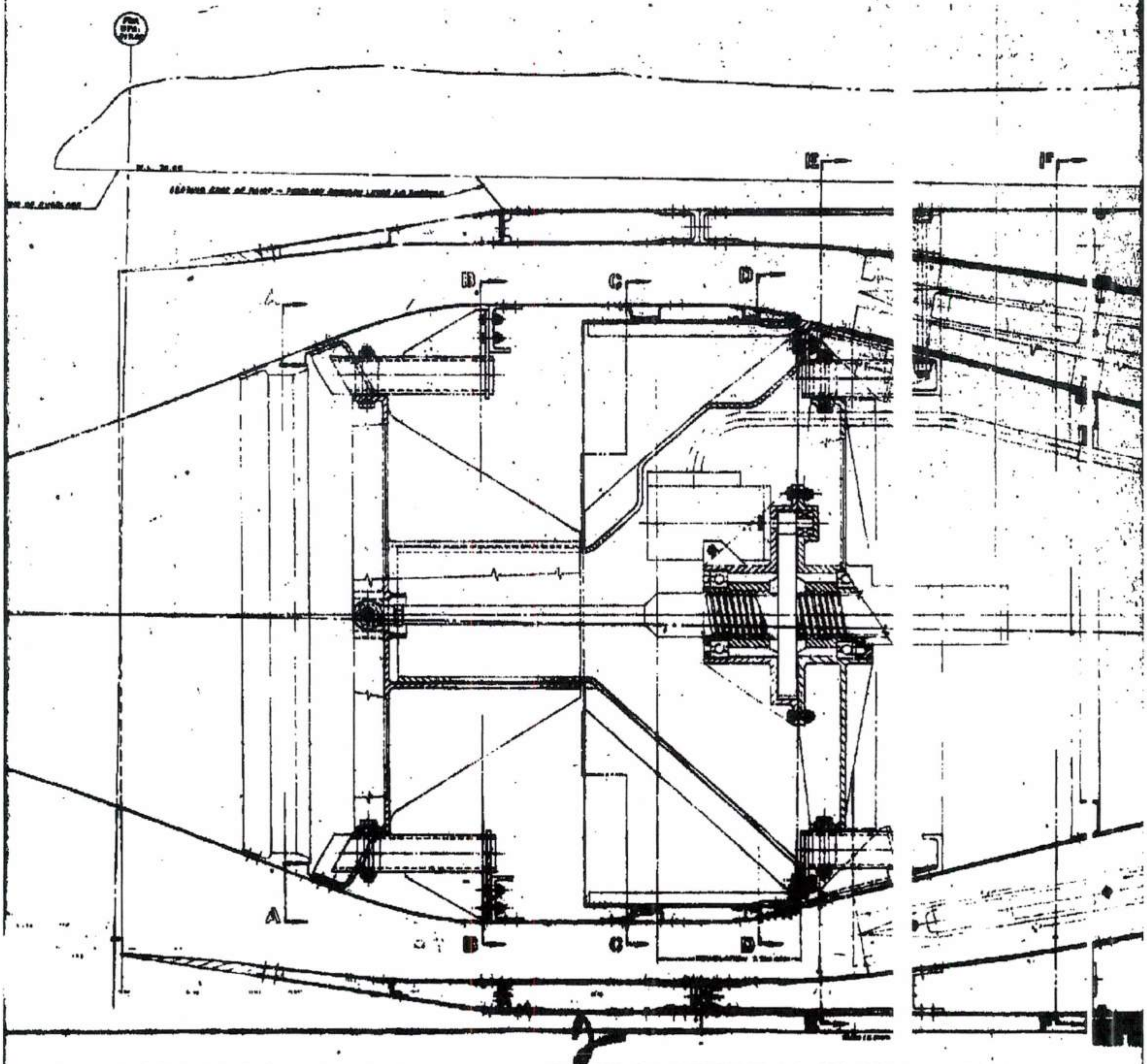
E
F
B
C
D
A
B
C
D

[redacted]

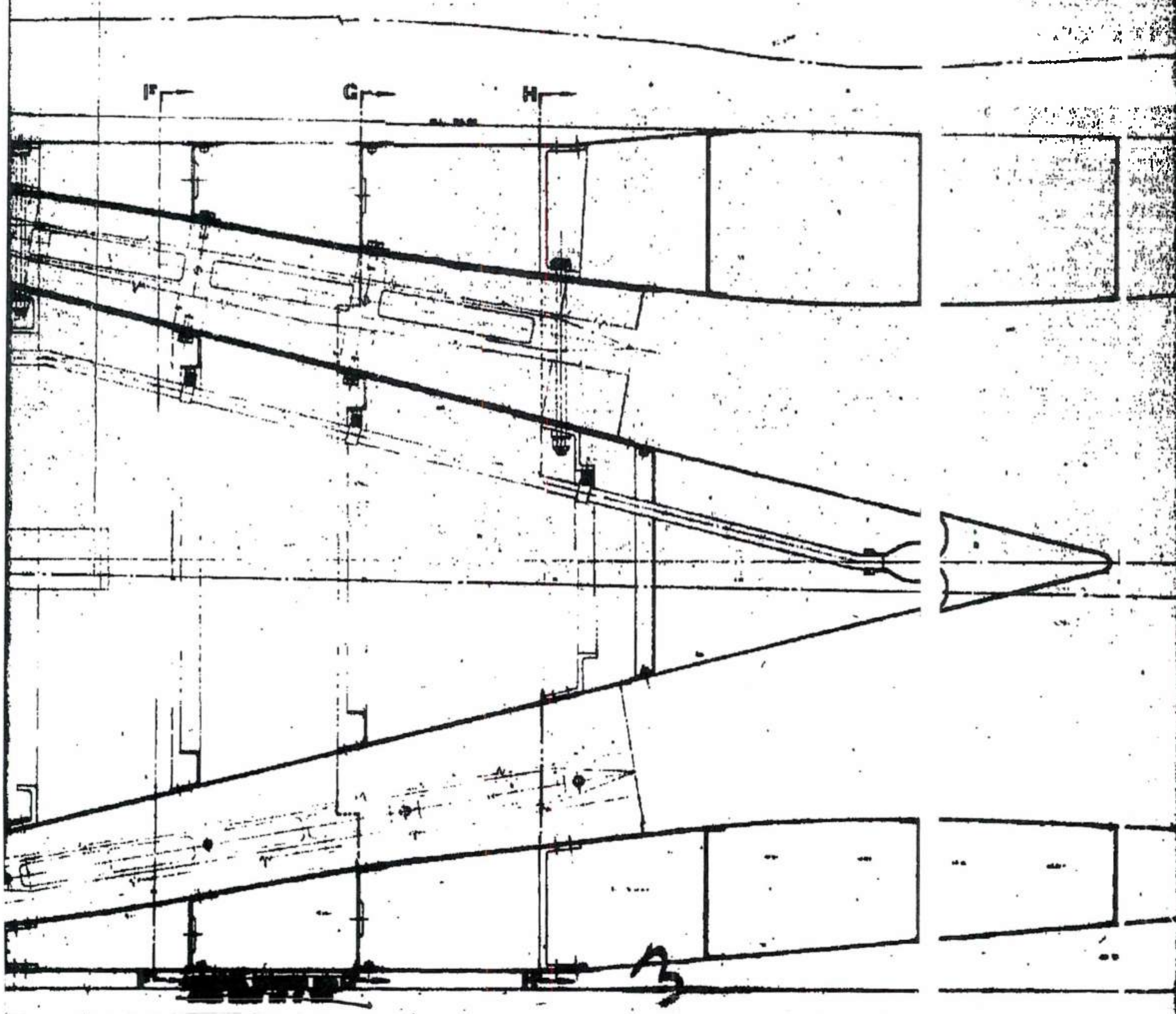

[redacted]

[redacted]

[redacted]

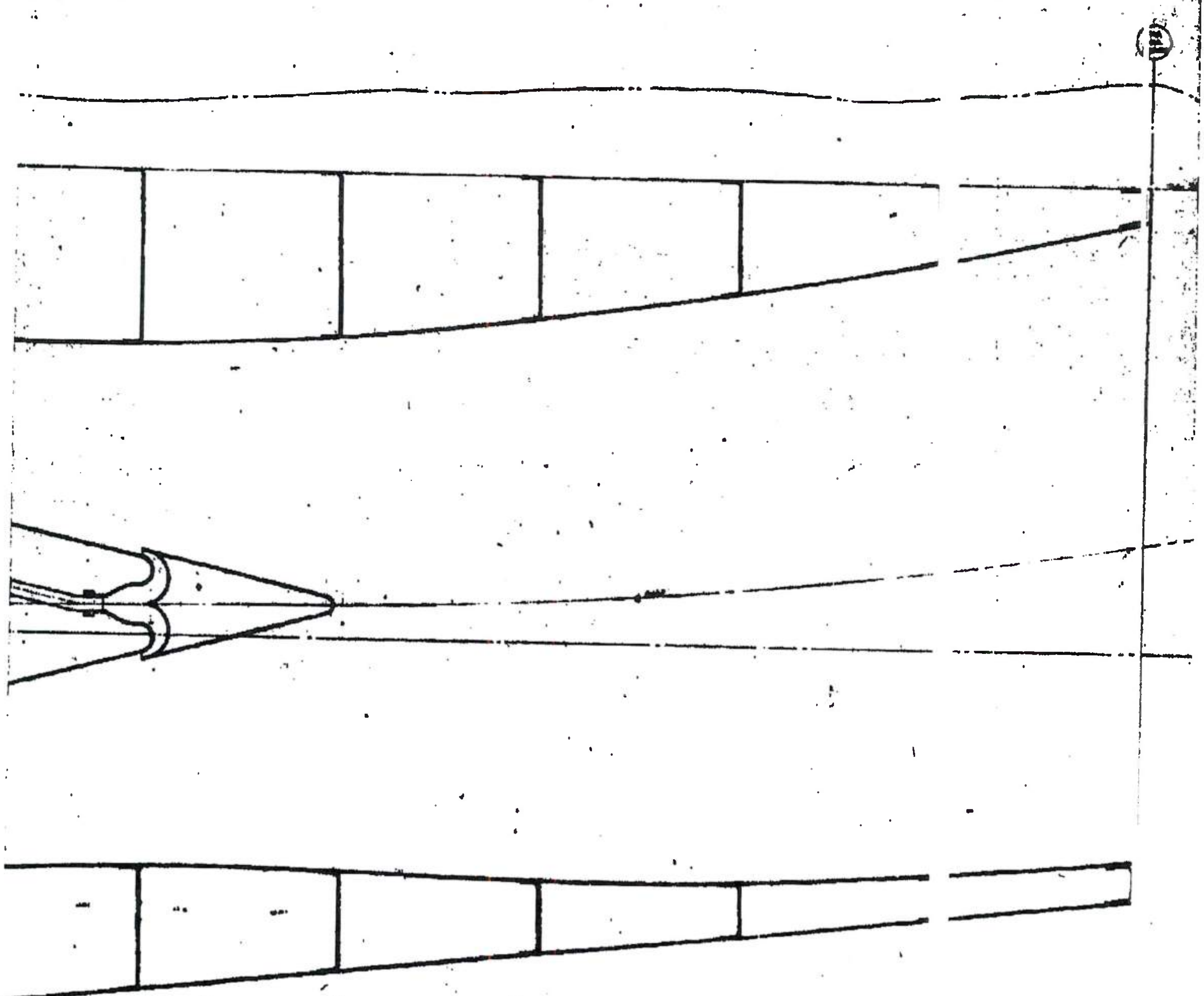

14

[redacted]

[redacted]

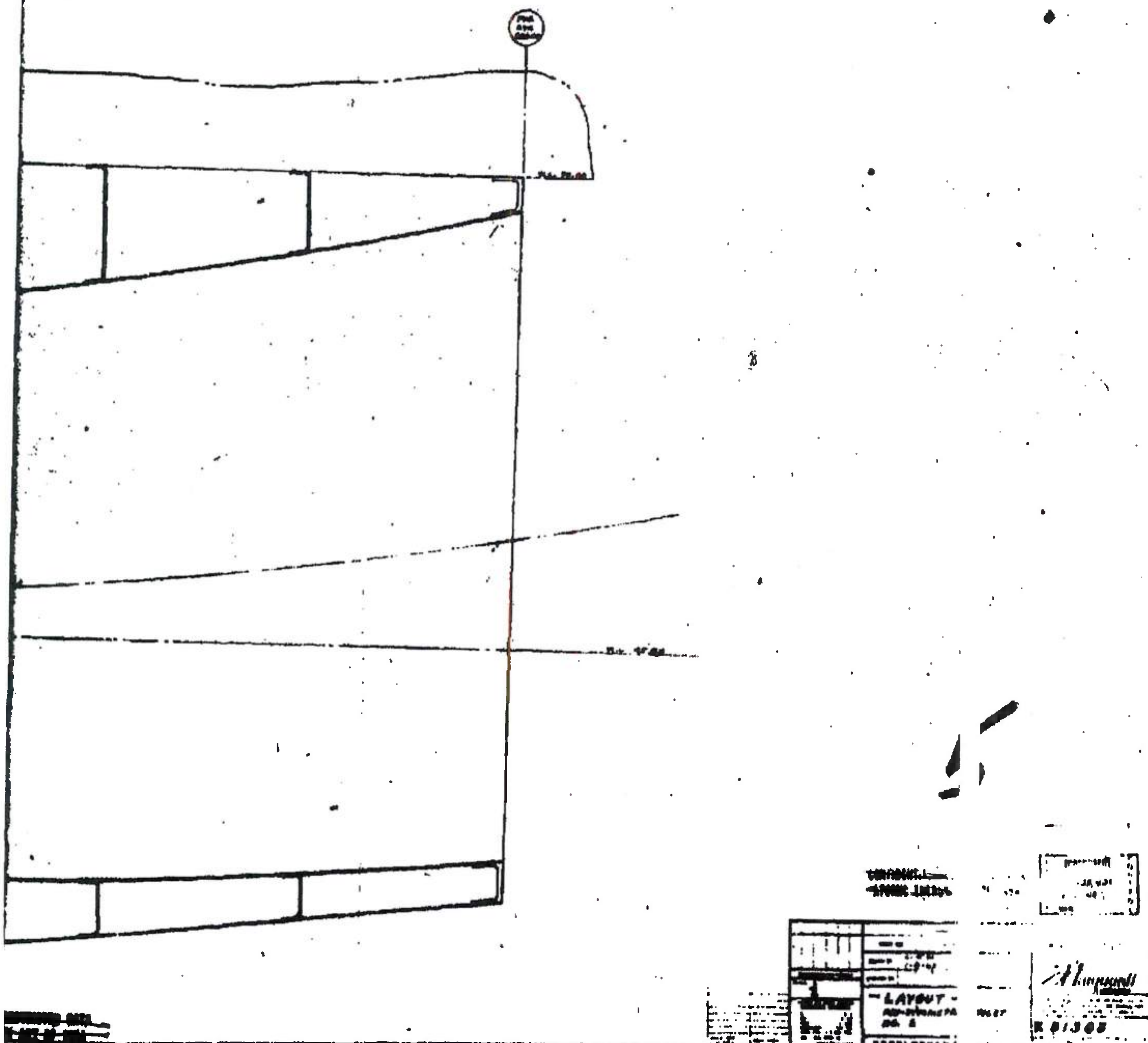

FIGURE 7?

Spike load	16,000 pounds
Spike travel	7 inches
Translation rate	7 inches in 6 seconds
Maximum temperature	1200°F

The methods investigated included a rotating nose cone coupled to a ...m having a high lead angle, a simple rack and pinion arrangement, an air-boost... d rack and pinion system, and a ball screw actuator. In each case, power is su... plied by a pneumatic motor. Because of the more evenly distributed masses, ...naller wall thicknesses, lighter overall weight, and lower power requirements, ...he ball screw actuating system has been tentatively selected as the best method of ...pike actuation. A proposed design is shown in Figure 72.

3.5.3 Exhaust Nozzle Design

The exhaust nozzle contour for the flight engine has been es...tablished to be a convergent-divergent type, fixed area nozzle. Two configurati...s have been evaluated for mechanical and structural integrity.

Wire-Wrapped Tubular Nozzle

The design for the wire-wrapped tubular nozzle employs a ...nstant perimeter longitudinal tube, die-formed in a convergent-divergent shap... Forming varies the cross section area in respect to the inner nozzle radius. ...he tubes are brazed together to form the shell of the nozzle and are then circ...nferentially wrapped with wire. The wire wrapping is required when the hoop te...ion loads exceed the allowable tension of the brazed joint between the tubes. ...rly design studies were based on a coolant airflow rate of 50 lb/sec at 1200°F ...here tubes of 7/16 to 9/16 inches in diameter were required. The latest inform...tion from LRL specifies the coolant airflow rate at 100 lb/sec. This rate dict...es a tube size of 13/16-inch outside diameter with a wall thickness of 0.020 in...hes. A total of 240 tubes of this dimension is required. Each tube is forme... into a convergent-divergent shape and flattened into a 1.5° arc. The forwar... nd of each tube makes a transition to a trapezoidal cross section for brazing to ...he attach ring. This simplifies the machining operation required to mate the ...bes to the attach ring.

Maximum gap between parts should not be greater than 0.0(inches if structural reliability of the brazed joints is to be insured.

Studies are being conducted to determine optimum material and possible fabrication problems inherent with this design.

PROPOSED BALLSCREW ACTUATOR

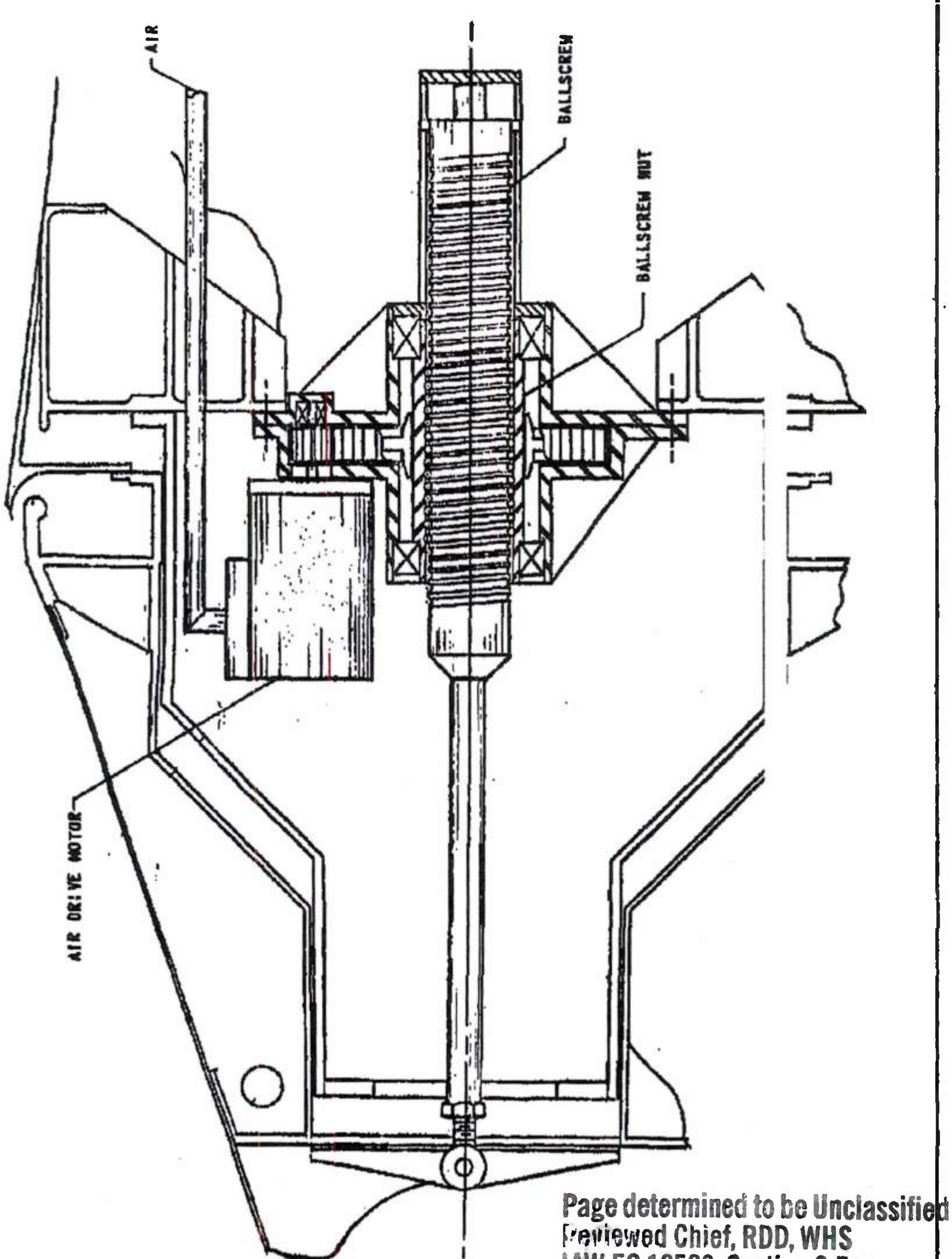

A preliminary selection of materials is as follows:

Attach Ring -- Hastelloy C
Tubes -- R-235 or Rene' 41
Wire -- A286

Ejector Nozzle

Preliminary design studies have been completed for the ejector typ exhaust nozzle shown in Figure 73.

This design employs a convergent-divergent outer shell with an in r shell in the convergent area only. The annulus between the inner and outer iell is sized such that the engine cooling air will pass through and cool the conve gent portion by forced convection. The divergent portion is then film-cooled by e air issuing from the annular passage just aft of the throat.

Preliminary design studies have been based on 0.125-inch thick Re e' 41 material for the two shells.

3.6 NEUTRONICS

The threefold objective of the neutronics program has been:

(1) To increase the performance potential of the basic Tory IIC reactor through parametric studies
(2) To delineate the mission performance capabilities of the Tor IIC reactor in terms of time effects
(3) To develop improved analytical techniques and calculation mc els

Attempts to extract additional performance from the Tory IIC reac r have involved studies of the effects of increasing the reactor diameter, redu ing the reactor length, and modifying the longitudinal reactor power profile.

Time effects studies have been initiated to account for fuel burnup, poison buildup, power profile deviations, and fuel loss, but there is still mu a work to be done in these areas. The analysis of time effects will be a majo item in the neutronics program for 1962.

3.6.1 Tory IIC Reactor Analysis

Seven complete, two-dimensional studies of the Tory IIC r ctor configuration have been completed during the year. The two-dimension . diffusion theory code Angie, developed by the LRL, was used for the analysis It was of particular interest to investigate design performance, to match desi a power requirements, and to determine leakage and internal fluxes.

The different studies have assumed a variety of operating t nperature levels throughout various regions of the core. Initial studies used t ee temperature regions of 1800, 2100, and 2500° F within the core, with a 1450 F front reflector, an 1800° F radial reflector, and a 2100° F rear reflector. Later studies, for simplicity, represented the core at a constant temperature : 2500° F. Radial power was assumed to be flat in all calculations with the axia power distribution taken from Reference 1. The one-dimensional, 18-group neutronic code Zoom was used to match radial and axial power independently. Predicted fuel distributions were used to obtain initial loadings for the 180 fue d regions for the Angie two-dimensional calculations.

The assumed reactor model has R-235 tie rods as opposed the LRL design incorporating both R235 and Rene' tie rod materials. The R2 design will require a smaller fuel investment for criticality. The final mo l studied indicated an effective multiplication factor, k_{eff}, of 1.03 for a fuel vestment of 69 pounds, significantly below the investment required in the Tor IIC design where Rene' tie rods are included.

The geometry and physical data for the final Angie neutron s model of the Tory IIC reactor are shown in Figure 74. Relative power and el distributions for the 180 core regions considered are shown in Figure 75. he maximum absolute leakage fluxes for each group at the front, side, and ear of the reactor are noted in Figure 76. The energy limits of the 18 group sed in the analysis are shown in Table 11.

Additional studies of the Tory IIC configuration are planned or 1962. A reactor model exactly matching the LRL Tory IIC model will be stu ed to establish a firm basis for all future comparison studies.

3.6.2 Isothermal Wall Version of Tory IIC

The neutronic feasibility of an isothermal wall version of th Tory IIC reactor was investigated as one possible means of increasing the pe ormance

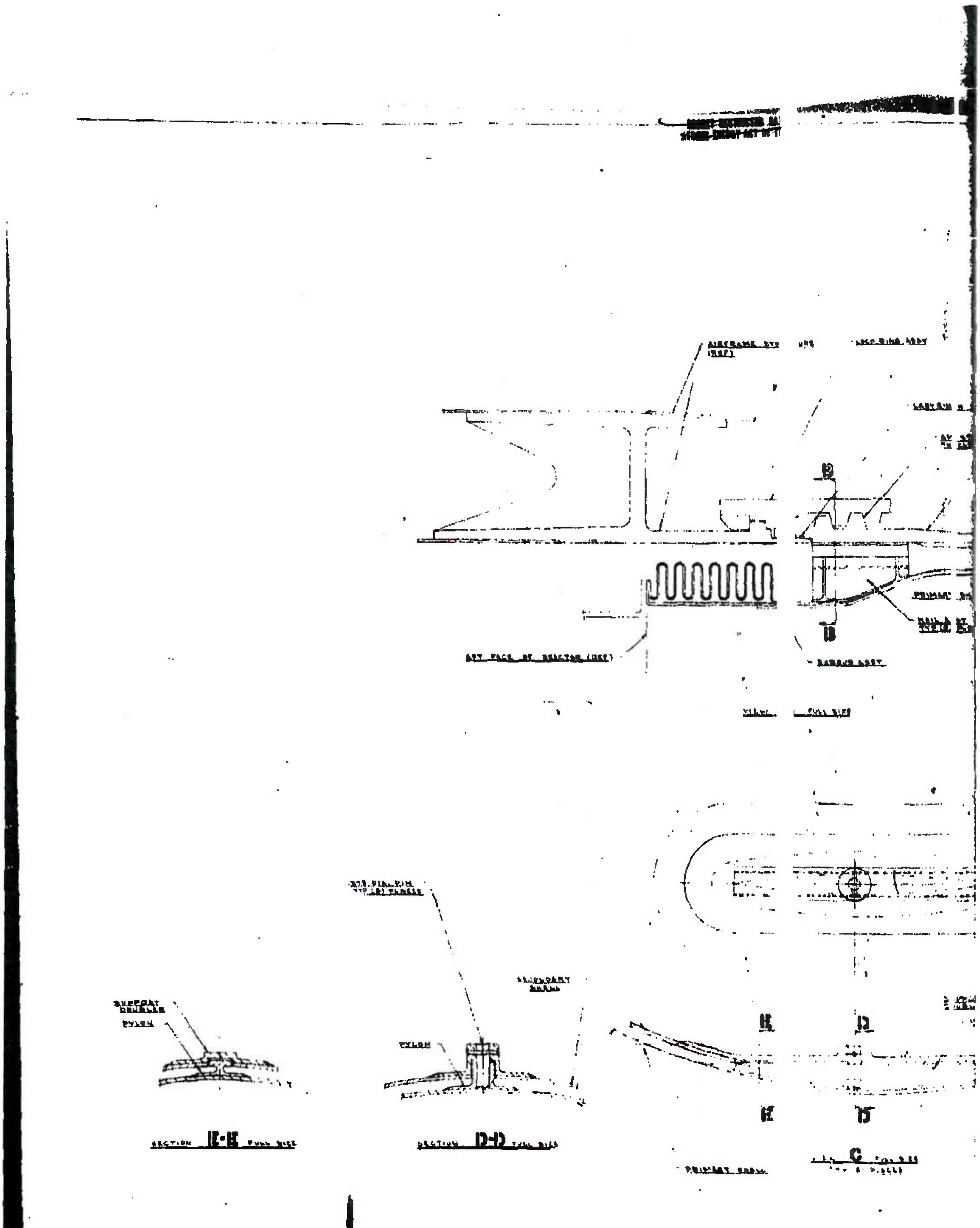
PYLON

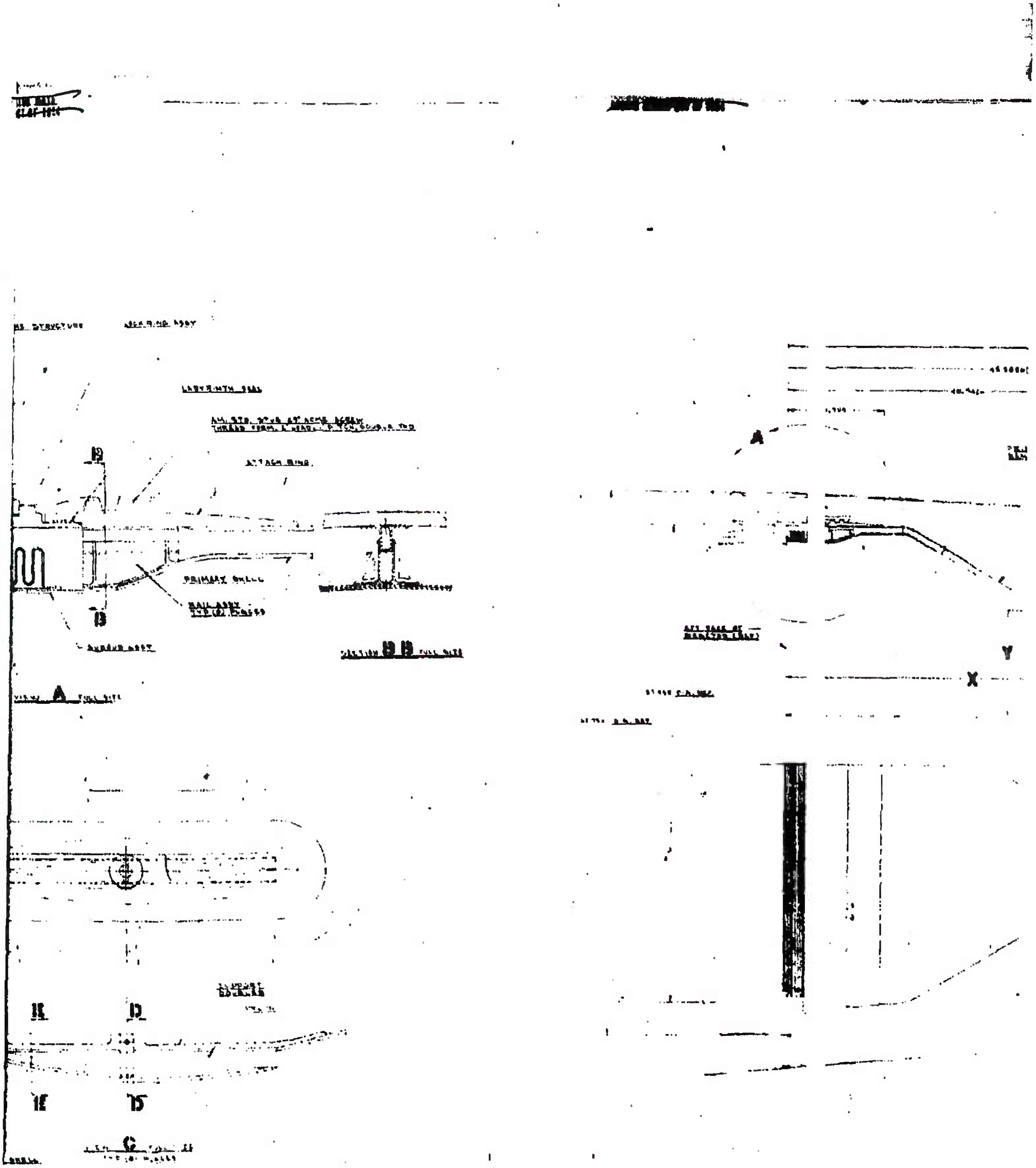

2

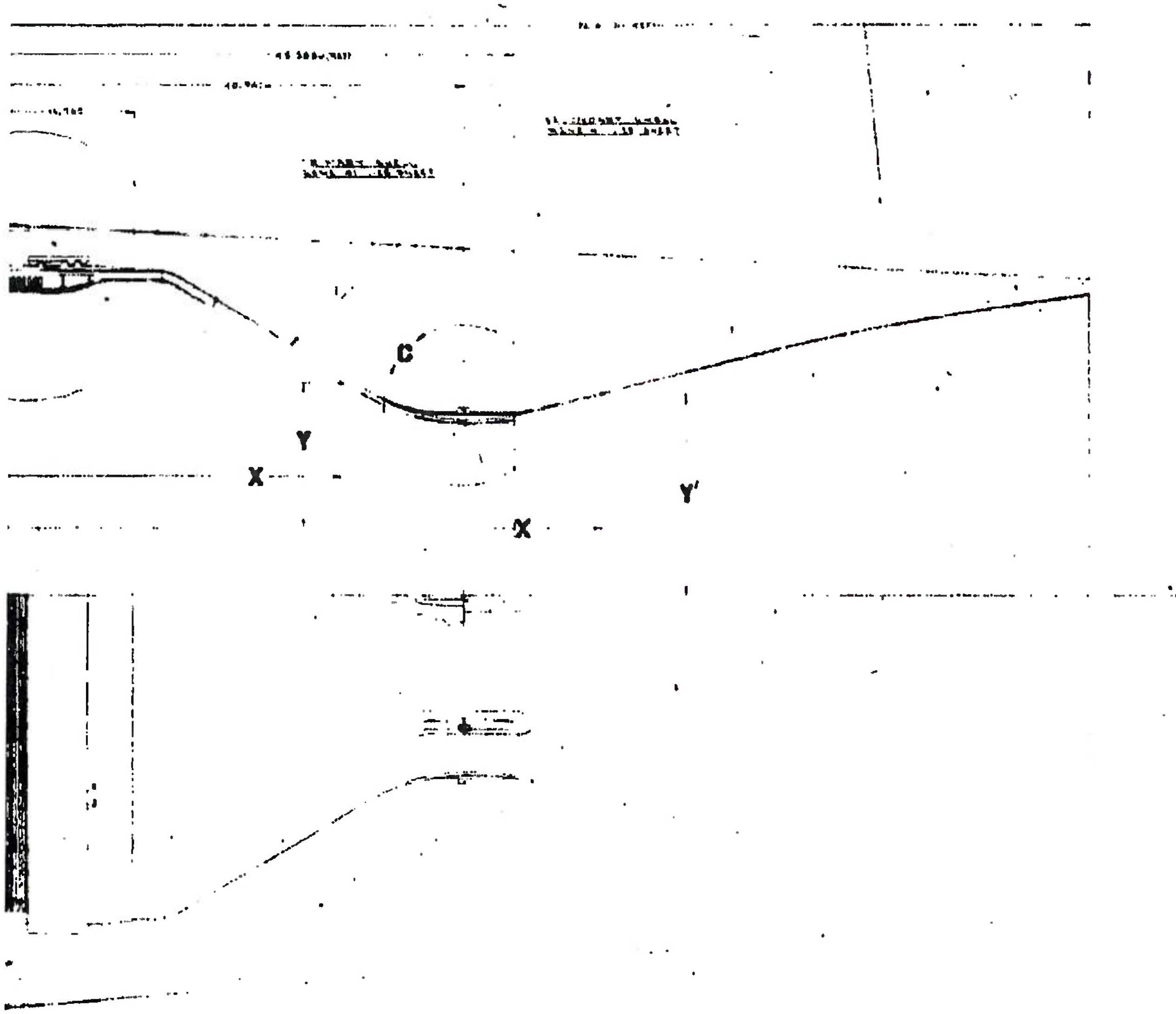

X	Y		
0	[illegible]		
[illegible]	[illegible]		
[illegible]	[illegible]		
13.8305			
[illegible]	[illegible]		
32.6559			
[illegible]	[illegible]		
41.9446	[illegible]		
[illegible]	[illegible]		
45.6086	[illegible]		
47.8336			
[illegible]			
[illegible]			
[illegible]			
[illegible]			
[illegible]			
[illegible]			
[illegible]			
[illegible]			
[illegible]			
[illegible]			

3

~~RESTRICTED DATA~~
~~ATOMIC ENERGY ACT OF 1954~~

DECLASSIFIED IN FULL
Authority: EO 13526
Chief, Records & Declass Div, WHS
Date: MAY 2 9 2015

STRAIGHT LINE [illegible]
STRAIGHT LINE (CONSTANT [illegible])
[illegible]
[illegible]
STRAIGHT LINE [illegible]
STRAIGHT LINE [illegible]
[illegible]
[illegible]
STRAIGHT LINE

X	Y	Y'
[illegible]	[illegible]	[illegible]
[illegible]	[illegible]	[illegible]
[illegible]	[illegible]	
[illegible]		[illegible]
[illegible]	[illegible]	
[illegible]		[illegible]
[illegible]	[illegible]	[illegible]
[illegible]	[illegible]	[illegible]
[illegible]	[illegible]	[illegible]
[illegible]	[illegible]	[illegible]
[illegible]		[illegible]
[illegible]		[illegible]
[illegible]		[illegible]
[illegible]		[illegible]
[illegible]		[illegible]
[illegible]		[illegible]
[illegible]		[illegible]
[illegible]		[illegible]
[illegible]		[illegible]
[illegible]		[illegible]
[illegible]		[illegible]
[illegible]		[illegible]

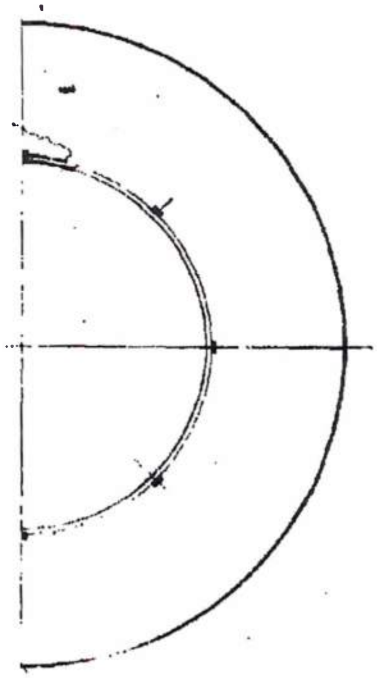

4

MARQUARDT AIRCRAFT CO.
SECRET RESTRICTED
22402

Marquardt
NOZZLE ASSY
EJECTOR
X01390

FIGURE 7?

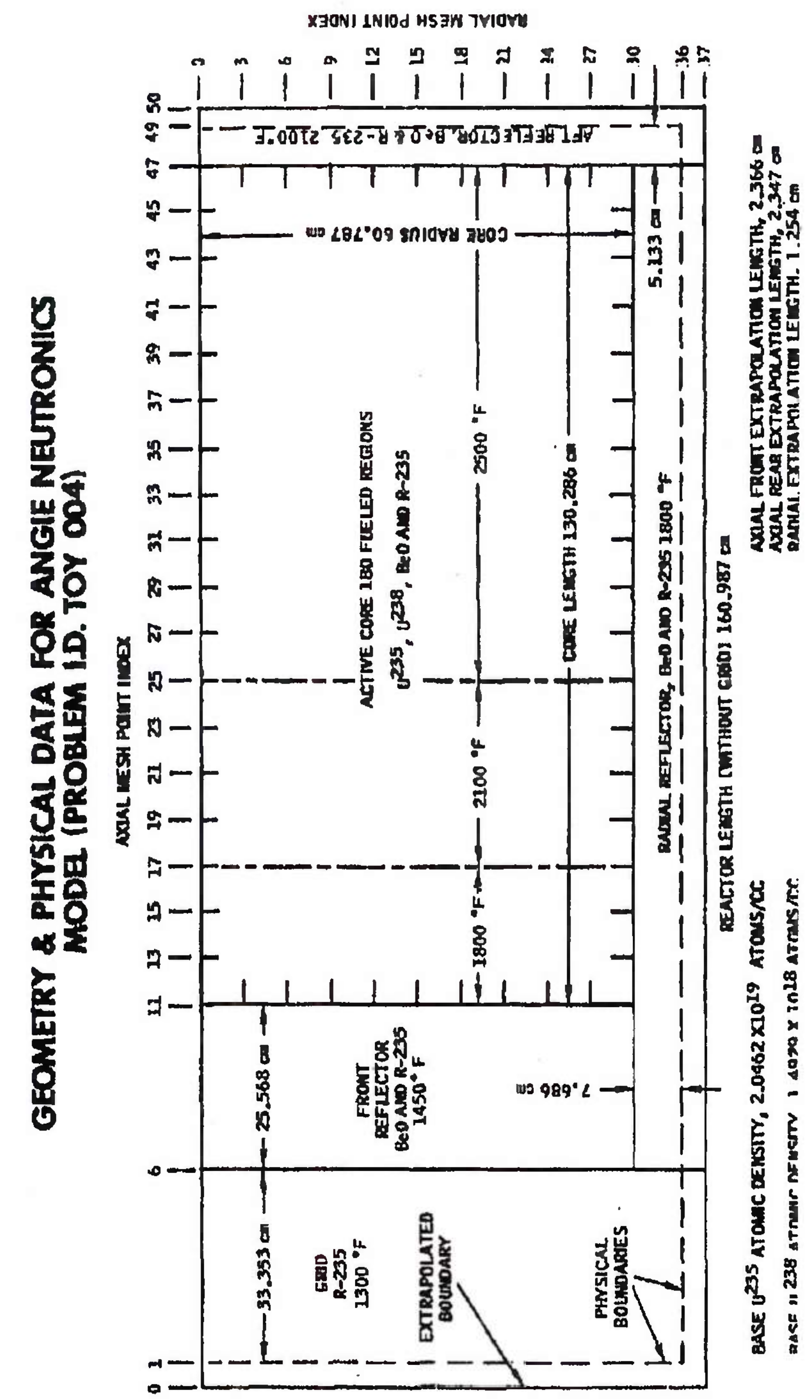
GEOMETRY & PHYSICAL DATA FOR ANGIE NEUTRONICS MODEL (PROBLEM I.D. TOY 004)
RADIAL MESH POINT INDEX
AXIAL MESH POINT INDEX
AFT REFLECTOR, BeO & R-235 2100°F
CORE RADIUS 60.787 cm
5.133 cm
ACTIVE CORE 180 FUELED REGIONS
U^{235}, U^{238}, BeO AND R-235
2500 °F
2100 °F
1800 °F
CORE LENGTH 130.286 cm
RADIAL REFLECTOR, BeO AND R-235 1800 °F
REACTOR LENGTH (WITHOUT GRID) 160.987 cm
FRONT REFLECTOR BeO AND R-235 1450° F
25.568 cm
7.686 cm
33.353 cm
GRID R-235 1300 °F
EXTRAPOLATED BOUNDARY
PHYSICAL BOUNDARIES
AXIAL FRONT EXTRAPOLATION LENGTH, 2.366 cm
AXIAL REAR EXTRAPOLATION LENGTH, 2.347 cm
RADIAL EXTRAPOLATION LENGTH, 1.254 cm
BASE U^{235} ATOMIC DENSITY, 2.0462 X10^{19} ATOMS/CC

POWER & FUEL DISTRIBUTION FOR FINAL ANGIE NEUTRONICS MODEL PROBLEM I.D. TOY 004

CORE CENTER - AXIAL REGIONS

CORE FRONT - RADIAL REGIONS

	1 (1.000)	2 (1.000)	3 (1.000)	4 (1.000)	5 (1.000)	6 (1.000)	7 (1.000)	8 (1.000)	9 (.997)	10 (.977)	11 (.940)	12 (.883)	13 (.809)	14 (.712)	15 (.602)	16 (.484)	17 (.354)	18 (.227)
1	1.051 +5.1 1.491	1.034 +3.4 1.455	1.025 +2.5 1.331	1.014 +1.4 1.210	1.018 +1.8 1.106	1.029 +2.9 1.022	1.024 +2.4 1.000	1.027 +2.7 1.042	1.023 +2.6 1.075	1.005 +2.9 1.099	0.984 +4.7 1.106	0.910 +3.1 1.130	0.834 +3.1 1.143	0.733 +2.9 1.147	0.621 +3.1 1.143	0.499 +3.1 1.143	0.371 +4.8 1.116	0.239 +5.3 1.099
2	1.056 +5.6 1.540	1.045 +4.5 1.491	1.025 +2.5 1.371	1.021 +2.1 1.254	1.016 +1.6 1.143	1.020 +2.0 1.060	1.022 +2.2 1.033	1.027 +2.7 1.075	1.014 +1.7 1.116	1.004 +2.8 1.130	0.985 +4.8 1.143	0.911 +3.1 1.160	0.836 +3.3 1.181	0.735 +3.2 1.181	0.619 +2.8 1.181	0.497 +2.7 1.181	0.369 +4.2 1.160	0.240 +5.7 1.130
3	1.055 +5.5 1.641	1.036 +3.6 1.615	1.028 +2.8 1.470	1.015 +1.5 1.343	1.007 +0.7 1.222	1.023 +2.3 1.130	1.018 +1.8 1.099	1.021 +2.1 1.147	1.019 +2.2 1.181	0.995 +1.8 1.210	0.984 +4.7 1.222	0.910 +3.1 1.235	0.832 +2.8 1.254	0.731 +2.7 1.264	0.620 +3.0 1.254	0.493 +1.9 1.264	0.369 +4.2 1.235	0.239 +5.3 1.210
4	1.065 +6.5 1.804	1.031 +3.1 1.804	1.025 +2.5 1.641	1.043 +4.3 1.470	1.008 +0.8 1.360	1.023 +2.3 1.254	1.008 +0.8 1.222	1.016 +1.6 1.264	1.020 +2.3 1.303	0.982 +0.5 1.331	0.978 +4.0 1.343	0.904 +2.4 1.371	0.826 +2.1 1.395	0.725 +1.8 1.395	0.614 +2.0 1.395	0.489 +1.0 1.395	0.366 +3.4 1.360	0.237 +4.4 1.343
5	1.038 +3.8 2.113	1.035 +3.5 2.113	1.020 +2.0 1.923	1.013 +1.3 1.727	1.000 0.0 1.565	1.009 +0.9 1.443	1.039 +3.9 1.395	1.032 +3.2 1.443	1.034 +3.7 1.491	1.030 +5.4 1.515	0.973 +3.5 1.540	0.900 +1.9 1.565	0.836 +3.3 1.593	0.735 +3.2 1.593	0.622 +3.3 1.593	0.499 +3.1 1.593	0.371 +4.8 1.565	0.240 +5.7 1.540
6	1.050 +5.0 2.529	1.027 +2.7 2.596	1.020 +2.0 2.364	1.021 +2.1 2.093	1.010 +1.0 1.876	1.017 +1.7 1.727	1.019 +1.9 1.669	1.038 +3.8 1.727	1.007 +1.9 1.777	1.020 +4.4 1.804	0.964 +2.6 1.841	0.891 +0.9 1.876	0.827 +2.2 1.905	0.726 +2.0 1.905	0.613 +1.8 1.905	0.497 +2.7 1.905	0.365 +3.1 1.876	0.240 +5.7 1.841
7	1.037 +3.7 3.193	1.030 +3.0 3.352	1.015 +1.5 3.031	1.010 +1.0 2.682	1.002 +0.2 2.381	0.990 -1.0 2.172	1.027 +2.7 2.093	1.040 +4.0 2.149	1.011 +1.4 2.210	0.975 -0.2 2.250	0.962 +2.3 2.291	0.889 +0.7 2.327	0.826 +2.1 2.364	0.724 +1.7 2.381	0.611 +1.5 2.381	0.491 +1.4 2.407	0.364 +2.8 2.364	0.237 +4.4 2.327
8	1.026 +2.6 4.215	1.023 +2.3 4.555	1.010 +1.0 4.094	0.998 -0.2 3.581	0.993 -0.7 3.130	0.996 -0.4 2.858	3.995 -0.5 2.728	1.004 +0.4 2.801	1.014 +1.7 2.858	0.976 -0.1 2.922	0.953 +1.4 2.981	0.879 -0.5 3.031	0.813 +0.5 3.096	0.712 0.0 3.096	0.601 -0.2 3.130	0.490 +1.2 3.130	0.362 +2.3 3.096	0.237 +4.4 3.031
9	1.003 +0.3 5.772	1.008 +0.8 6.312	0.836 -16.4 5.772	0.981 -1.9 4.894	0.976 -2.4 4.249	0.980 -2.0 3.822	0.981 -1.9 3.648	0.987 -1.3 3.731	0.997 0.0 3.822	0.959 -1.8 3.890	0.936 -0.4 3.973	0.836 -2.3 4.055	0.800 -1.1 4.143	0.700 -1.7 4.143	0.590 -2.0 4.173	0.483 -0.2 4.215	0.355 0.3 4.173	0.235 +3.5 4.094
10	0.945 -5.5 7.584	0.945 -5.5 8.311	0.936 -6.4 7.331	0.925 -7.5 6.312	0.903 -9.7 5.442	0.931 -6.9 4.894	0.936 -6.4 4.659	0.940 -6.0 4.728	0.941 -5.6 4.812	0.992 -5.6 4.894	0.891 -5.2 5.007	0.822 -6.9 5.110	0.758 -6.3 5.226	0.663 -6.9 5.226	0.565 -6.1 5.276	0.458 -5.4 5.357	0.341 -3.7 5.357	0.225 -0.9 5.442

CORE AFT

CORE OUTER EDGE

NOTE:
RELATIVE POWER SHOWN ON UPPER OPRTION OF REGION
MEAN PERCENTAGE DEVIATION FROM IDEAL POWER SHOWN ON CENTER OF REGION

RELATIVE FUEL LOADING SHOWN ON LOWER PORTION OF REGION
IDEAL POWERS ARE SHOWN IN PARENTHESIS AND ARE CONSTANT FOR EACH RADIAL REGION
REGIONS ARE NOT TO SCALE

MAXIMUM NEUTRON LEAKAGE CURRENT SPECTRA
(PROBLEM I.D. TOY 004)

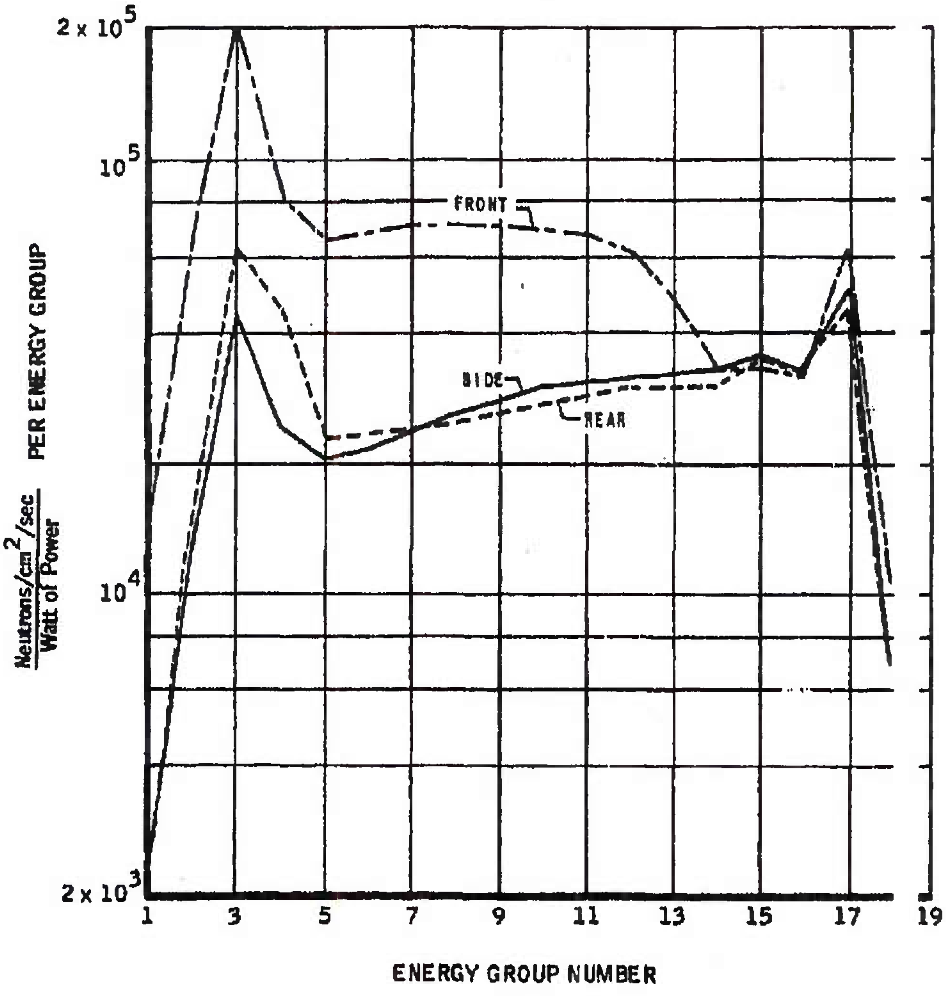

FIGURE 76

TABLE 11

ANGIE ENERGY GROUP LIMITS

Energy Group	Energy Boundaries (ev)
1	$0 - 3.162 \times 10^{-2}$
2	$3.162 \times 10^{-2} - 1.0 \times 10^{-1}$
3	$1.0 \times 10^{-1} - 3.162 \times 10^{-1}$
4	$3.162 \times 10^{-1} - 1.0$
5	$1.0 - 3.162$
6	$3.162 - 1.0 \times 10^{1}$
7	$1.0 \times 10^{1} - 3.162 \times 10^{1}$
8	$3.162 \times 10^{1} - 1.0 \times 10^{2}$
9	$1.0 \times 10^{2} - 3.162 \times 10^{2}$
10	$3.162 \times 10^{2} - 1.0 \times 10^{3}$
11	$1.0 \times 10^{3} - 3.162 \times 10^{3}$
12	$3.162 \times 10^{3} - 1.0 \times 10^{4}$
13	$1.0 \times 10^{4} - 3.162 \times 10^{4}$
14	$3.162 \times 10^{4} - 1.0 \times 10^{5}$
15	$1.0 \times 10^{5} - 3.162 \times 10^{5}$
16	$3.162 \times 10^{5} - 1.0 \times 10^{6}$
17	$1.0 \times 10^{6} - 3.162 \times 10^{6}$
18	$3.162 \times 10^{6} - 1.0 \times 10^{7}$

of the Model MA50-XCA system. The most significant change was th increased power generation in the forward regions of the core with a correspon .ng increase in fuel concentration. The neutronic feasibility of the isothermal wa depends on the maximum fuel concentration required in any particular region (a) percent (by weight) limit has been established by LRL as a reasonable maxir m allowable fuel concentration).

The two-dimensional diffusion theory code, Angle, was use with 18 energy groups as in the basic Tory IIC model. Geometry and physic data for the model are identical to the data noted in Figure 74. The "ideal" cial power requirements for an isothermal wall system are shown in Figure 77 Radial power generation is assumed to be flat. Three 18-group Angle probl as were required to match the desired profiles. The volumetrically weighted, verage axial power profiles for each of the three cases are also shown in Figure ' .

The relative fuel distribution and relative power distributio for each of the 180 fueled regions of the reactor core are shown in Figure 78 . he final fuel loading requirement imposed a maximum fuel concentration of 1 06 weight percent of uranium oxide 'n uranium oxide and beryllia. The resulti g effective multiplication factor, k_{eff} is 1.038 for a U-235 mass of 84.88 poun i. This value is compared with the 69.0 pounds required in the basic Tory II model for a k_{eff} of 1.033. It should be noted that both cases assume all R-235 e rods in the reactor design. The maximum leakage flux profiles for the isoth rmal reactor are shown in Figure 79 .

The isothermal wall version of the Tory IIC appears feasibl from purely neutronic considerations although critical mass requirements ave increased. Additional study of the configuration will be completed if tl rmal stress limitations are eased and if the enhanced performance is required in ie system.

3.6.3 Reactor Sizing Studies

In addition to the isothermal wall system, the neutronic cha cteristics of three other possible reactor designs have been investigated during he year. Two designs were based on ceramic diameters of 59 inches and 64 ir hes. No changes in length or power distribution from the basic Tory IIC were ncorporated in these two models. The third model used a ceramic diameter of 5 5 inches, with a 4.1-inch reduction in active core length and a 4-inch reductio in front reflector thickness to make the model 8.1 inches shorter than the ba c Tory IIC design. The nuclear ramjet engine based on this reactor design is d signated the Model MA50-XDA propulsion system.

SECRET ~~RESTRICTED DATA~~
~~ATOMIC ENERGY ACT OF 1954~~

AXIAL POWER CORRELATION FOR ANGIE NEUTRONICS MODELS OF THE TORY IIC REACTO
ISOTHERMAL WALL - 2500° F

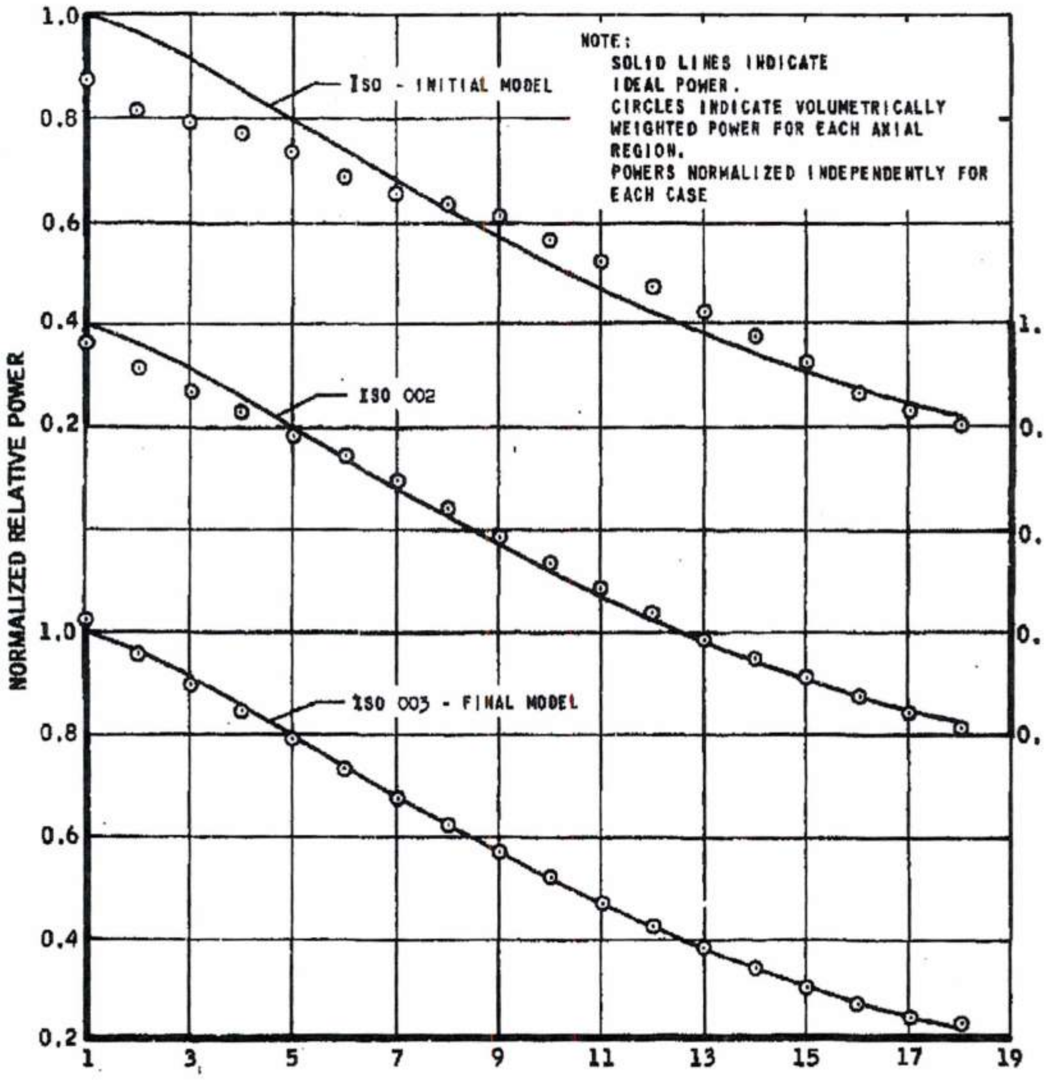

SECRET ~~RESTRICTED DATA~~

POWER & FUEL DISTRIBUTION FOR FINAL ANGIE NEUTRONICS MODEL, ISOTHERMAL CORE (PROBLEM I.D. ISO 003)

CORE CENTER - AXIAL REGIONS

CORE FRONT - RADIAL REGIONS

	1 (1.000)	2 (.961)	3 (.912)	4 (.858)	5 (.797)	6 (.737)	7 (.679)	8 (.623)	9 (.570)	10 (.517)	11 (.468)	12 (.422)	13 (.382)	14 (.344)	15 (.310)	16 (.278)	17 (.248)	18 (.222)
1	1.050 +5.0 3.512	.959 -0.2 3.561	.902 -1.1 2.998	.841 -2.0 2.461	.784 -1.6 1.997	.720 -2.3 1.663	.650 -4.3 1.453	.609 -2.2 1.266	.562 -1.4 1.152	.504 -2.5 1.069	.495 -1.9 1.015	.411 -2.6 1.000	.372 -2.6 1.012	.334 -2.9 1.069	.303 -2.3 1.170	.275 -1.1 1.365	.234 -5.6 1.772	.237 +6.8 2.371
2	1.047 +4.7 3.659	.956 -0.5 3.720	.897 -1.6 3.114	.843 -1.7 2.549	.781 -2.0 2.062	.721 -2.2 1.723	.650 -4.3 1.486	.612 -1.8 1.304	.559 -1.9 1.192	.508 -1.7 1.099	.459 -1.9 1.042	.411 -2.6 1.024	.372 -2.6 1.039	.336 -2.3 1.086	.302 -2.6 1.192	.272 -2.2 1.405	.247 -0.4 1.772	.234 +5.4 2.461
3	1.050 +5.0 3.887	.965 +0.4 3.983	.896 -1.8 3.361	.850 -0.9 2.716	.784 -1.6 2.187	.720 -2.3 1.807	.668 -1.6 1.568	.610 -2.1 1.365	.557 -2.3 1.247	.508 -1.7 1.152	.459 -1.9 1.099	.410 -2.8 1.086	.372 -2.6 1.086	.335 -2.6 1.152	.296 -4.5 1.281	.272 -2.2 1.486	.245 -1.2 1.894	.237 +6.8 2.617
4	1.036 +3.8 4.316	.963 -0.2 4.423	.901 -1.2 3.720	.817 -4.8 3.067	.791 -0.8 2.399	.710 -3.7 1.997	.647 -4.7 1.723	.602 -3.4 1.509	.557 -2.3 1.365	.503 -2.7 1.266	.456 -2.6 1.192	.413 -2.1 1.170	.376 -1.6 1.170	.335 -2.6 1.247	.300 -3.2 1.383	.272 -2.2 1.611	.244 -1.6 2.026	.234 +5.4 2.891
5	1.039 +3.9 5.029	.963 -0.2 5.177	.901 -1.2 4.316	.843 -1.7 3.412	.783 -1.8 2.716	.730 -0.9 2.229	.675 -0.6 1.894	.615 -1.3 1.663	.562 -1.4 1.509	.516 -0.2 1.383	.465 -0.6 1.304	.415 -1.7 1.281	.376 -1.6 1.304	.339 -1.5 1.365	.303 -2.3 1.509	.274 -1.4 1.807	.246 -0.8 2.341	.233 +5.0 3.361
6	1.036 +3.6 6.105	.963 +0.2 6.364	.894 -2.0 5.289	.837 -2.4 4.165	.788 -1.1 3.260	.730 -0.9 2.653	.673 -0.9 2.229	.615 -1.3 1.933	.568 -0.4 1.753	.513 -0.8 1.611	.464 -0.9 1.509	.423 +0.2 1.486	.377 -1.3 1.509	.338 -1.7 1.568	.307 -1.0 1.753	.247 -0.4 2.758	.232 +4.5 3.983	.274 -1.4 2.112
7	1.034 +3.4 7.756	.955 -0.6 8.291	.898 -1.5 6.825	.843 -1.7 5.289	.787 -1.3 4.089	.726 -1.5 3.260	.677 -0.3 2.716	.620 -0.5 2.341	.569 -0.2 2.112	.527 +1.9 1.933	.472 +0.9 1.807	.420 -0.5 1.772	.381 -0.3 1.807	.341 -0.9 1.894	.308 -0.6 2.112	.275 -1.1 2.549	.250 +0.8 3.361	.231 +4.1 5.029
8	1.029 +2.9 10.[illegible]03	.952 -0.4 11.350	.892 -2.2 2.617	.840 -2.1 9.244	.791 -0.8 7.016	.728 -1.2 5.289	.686 +1.0 4.211	.629 +1.0 3.478	.577 +1.2 2.988	.521 +0.8 2.399	.475 +1.5 2.258	.424 +0.5 2.187	.383 +0.3 2.229	.344 0.0 2.371	.311 +0.3 2.653	.276 -0.7 3.260	.248 0.0 4.423	.232 +4.5 6.647
9	1.023 -2.3 13.914	.949 -1.2 15.693	.893 -2.1 12.632	.842 -1.9 9.399	.790 -0.9 7.016	.741 +0.5 5.462	.689 +1.5 4.478	.632 +1.4 3.808	.578 +1.4 3.361	.528 +2.1 3.067	.474 +1.3 2.850	.433 +2.6 2.758	.385 +0.8 2.850	.347 +0.9 2.988	.310 0.[illegible] 3.4[illegible]	.280 +0.7 4.211	.248 0.0 5.840	.234 +5.4 9.077
10	1.004 +0.4 17.274	.955 -0.6 19.134	.900 -1.3 15.301	.850 -0.9 11.350	.798 +0.1 8.507	.741 +0.5 6.647	.688 +1.3 5.462	.638 +2.4 4.638	.587 +3.0 4.089	.534 +3.3 3.720	.481 +2.8 3.478	.432 +2.4 3.412	.390 +2.1 3.478	.349 +1.5 3.659	.313 +1.0 4.165	.282 +1.4 5.177	.251 +1.2 7.263	.232 +4.5 11.796

CORE AFT

CORE OUTER EDGE

NOTE:
RELATIVE POWER SHOWN ON UPPER PORTION OF REGION
IDEAL POWERS ARE SHOWN IN PARENTHESIS AND ARE CONSTANT FOR EACH RADIAL REGION
PERCENTAGE DEVIATION OF POWER FROM IDEAL POWER SHOWN IN CENTER PORTION OF REGION
RELATIVE FUEL LOADING SHOWN ON LOWER PORTION OF REGION
REGIONS ARE NOT TO SCALE

MAXIMUM NEUTRON LEAKAGE CURRENT SPECTRA
(PROBLEM I.D. ISO 003)

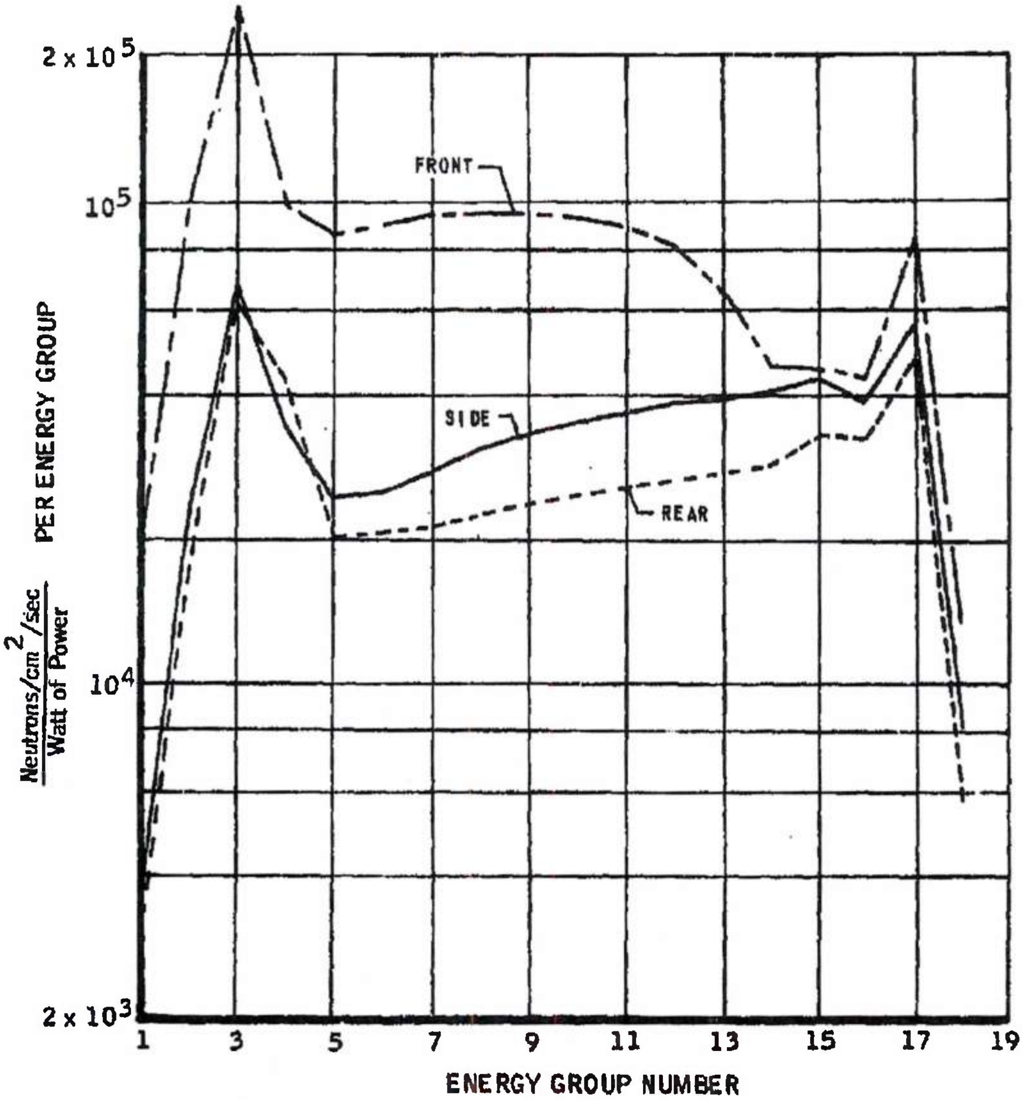

The geometry and physical data for the 59-inch diameter v sion of the Tory IIC reactor are shown in Figure 80 . An initial fuel loading o 34.88 pounds was assumed giving a k_{eff} of 1.11. Critical mass iterations to red e the k_{eff} were not completed due to computer time limitations. Three compl :e Angie problems were required to obtain proper convergence to the basic T ry IIC power distribution. The Angie-predicted power and fuel distributions are iown in Figure 81 . Significant fuel reductions can be achieved with the de gn. Future iterations on fuel requirements will be completed if interest is expr sed in the larger systems.

The geometry and physical data for the 64-inch diameter v sion of the Tory IIC reactor are shown in Figure 82 with the corresponding A ie-predicted power and fuel distributions noted in Figure 83 . A k_{eff} of 1.12 is redicted for a fuel loading of 85 pounds. No iterations on fuel requirements for critical system were completed.

The design of particular interest was the shortened length, ncreased diameter version of Tory IIC designated as the reactor for the Mod MA50-XDA propulsion system. The required core power distribution is identic to the basic Tory IIC without the aft 4.1 inches of core length. Satisfactory mat ing of the required power was accomplished with three Angie models. The fi l Angie neutronics model had a k_{eff} of 1.031 with a critical mass of 81.32 pou s. A maximum fuel concentration of 5.14 percent of uranium oxide in uraniu oxide and beryllia was predicted in the calculation. This is well within allow le limits. The mean fission energy decreased slightly from 0.228 ev for the b ic Tory IIC to 0.223 ev for the Model MA50-XDA system.

Geometrical data for the model are indicated in Figure 84 required fuel distributions in Figure 85 , and corresponding maximum leaka currents for each energy group in Figure 86 . The reactor appears feasible nd may approach the flight type reactor for the nuclear ramjet system if th st increases over the basic Tory IIC system are required.

3.6.4 Reactor Lifetime Studies and Time Effects

A limited analysis of the lifetime characteristics of Pluto t e reactors has been performed to facilitate engine ground test planning. Addit nal extensive study will be required to assess adequately the time effects.

The much simplified initial analysis assessed the effects o fuel burnup, neutronic poison buildup, and loss of core material by erosion. A nstant

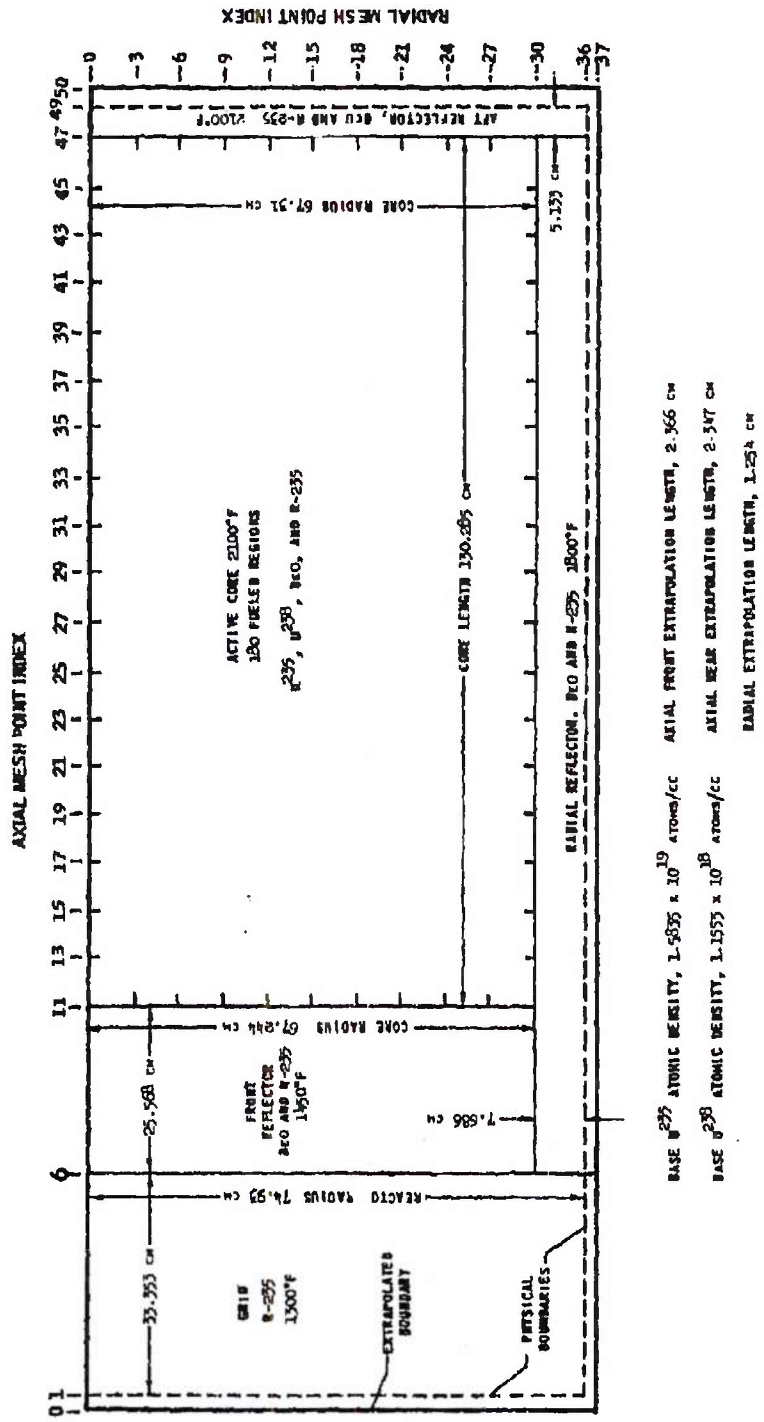

GEOMETRY AND PHYSICAL DATA FOR ANGIE NEUTRONICS MODEL (PROBLEM I.D. BIG 002)

DECLASSIFIED IN FULL
Authority: EO 13526
Chief, Records & Declass Div, WHS
Date: MAY 2 9 2015

~~SECRET RESTRICTED DATA~~
~~ATOMIC ENERGY ACT OF 1954~~

The Marquardt Corporation
VAN NUYS, CALIFORNIA

Report 5876

POWER AND FUEL DISTRIBUTION FOR FINAL ANGIE NEUTRONICS MODEL (PROBLEM I.D. BIG 002)

CORE CENTER - AXIAL REGIONS

CORE FRONT - RADIAL REGIONS

CORE AFT

	1		3	4	5	6	7	8	9	10	11	12	13	14	15	16	17	18
1	1.007 ([illegible]) 1.57[illegible]	1.006 ([illegible]) 1.539	[illegible] ([illegible]) 1.358	1.043 ([illegible]) 1.220	1.012 ([illegible]) 1.148	1.025 (1.000) 1.087	1.032 (1.000) 1.016	[illegible] (1.000) 1.006	1.031 (0.997) 1.016	1.017 (0.977) 1.031	[illegible] (0.940) 1.054	0.922 (0.883) 1.054	[illegible] (0.503) 1.067	[illegible] (0.712) 1.050	[illegible] (0.602) 1.054	[illegible] ([illegible]) 1.042	[illegible] ([illegible]) [illegible]	[illegible] (0.22[illegible]) [illegible]
2	1.005 1.636	1.010 1.577	1.004 1.458	1.055 1.272	1.009 1.180	1.055 1.085	1.019 1.054	1.036 1.031	1.034 1.042	1.019 1.054	0.985 1.085	0.925 1.085	0.846 1.102	0.754 1.122	0.618 1.085	0.490 1.067	0.352 1.031	[illegible] 1.03[illegible]
3	1.027 1.737	[illegible] 1.688	1.008 1.539	1.058 1.349	1.012 1.252	1.026 1.164	1.028 1.113	1.026 1.102	1.032 1.113	1.019 1.126	0.974 1.148	0.913 1.164	0.843 1.164	0.739 1.164	0.617 1.148	0.492 1.128	0.352 1.102	0.21[illegible] 1.10[illegible]
4	0.994 1.908	1.005 1.877	1.004 1.711	1.017 1.504	1.013 1.377	1.025 1.272	1.032 1.220	1.039 1.203	1.031 1.220	1.019 1.295	0.973 1.272	0.924 1.272	0.859 1.287	0.735 1.287	0.617 1.222	0.491 1.252	0.351 1.220	0.21[illegible] 1.20[illegible]
5	1.009 2.171	0.999 2.174	1.030 1.362	1.011 1.757	1.005 1.591	1.015 1.482	1.024 1.415	1.027 1.358	1.036 1.415	1.019 1.458	0.979 1.463	0.924 1.482	0.845 1.504	0.743 1.482	0.626 1.463	0.455 1.438	0.361 1.377	0.226 1.321
6	1.002 2.580	0.998 2.527	0.998 2.394	1.004 2.109	1.003 1.906	1.007 1.757	1.015 1.688	1.028 1.663	1.032 1.688	1.012 1.711	0.975 1.737	0.921 1.774	0.895 1.790	0.739 1.774	0.622 1.757	0.491 1.711	0.360 1.636	0.227 1.579
7	[illegible] 3.222	0.993 3.357	0.986 3.055	0.994 2.700	0.993 2.594	1.005 2.203	1.008 2.109	1.022 2.076	1.027 2.109	1.012 2.144	0.969 2.174	0.912 2.286	0.834 2.245	0.732 2.226	0.617 2.203	0.492 2.144	0.358 2.092	0.226 1.962
8	0.992 4.224	0.981 4.538	0.987 4.117	0.985 3.562	0.990 3.176	1.000 2.913	1.004 2.757	1.019 2.700	1.016 2.757	0.998 2.816	0.965 2.881	0.907 2.913	0.828 2.947	0.727 2.947	0.613 2.881	0.490 2.816	0.357 2.700	0.225 2.547
9	[illegible] 5.731	0.976 6.321	0.983 5.707	0.974 4.912	0.979 4.313	0.995 3.933	1.007 3.707	1.008 3.651	1.007 3.707	0.996 3.781	0.956 3.892	0.895 3.933	0.819 3.986	0.725 3.986	0.615 3.892	0.487 3.828	0.397 3.651	0.285 3.453
10	[illegible] [illegible]	0.973 8.123	0.969 7.252	0.972 6.253	0.983 5.465	0.990 4.789	0.998 4.706	1.013 4.513	1.011 4.706	0.977 4.805	0.959 4.912	0.900 4.989	0.822 5.068	0.721 5.068	0.608 4.989	0.486 4.912	0.394 4.706	0.224 4.613

CORE OUTER EDGE

NOTE: RELATIVE POWER SHOWN IN UPPER PORTION OF REGION
RELATIVE FUEL LOADING SHOWN ON LOWER PORTION OF REGION
REGIONS ARE NOT TO SCALE
IDEAL POWERS ARE SHOWN IN PARENTHESIS AND ARE CONSTANT FOR EACH RADIAL REGION

MAC A433

~~SECRET RESTRICTED DATA~~

N22C50 ~~ATOMIC ENERGY ACT OF 1954~~

FIGURE 81

GEOMETRY AND PHYSICAL DATA FOR ANGIE NEUTRONICS MODEL (PROBLEM I.D. BST 005)

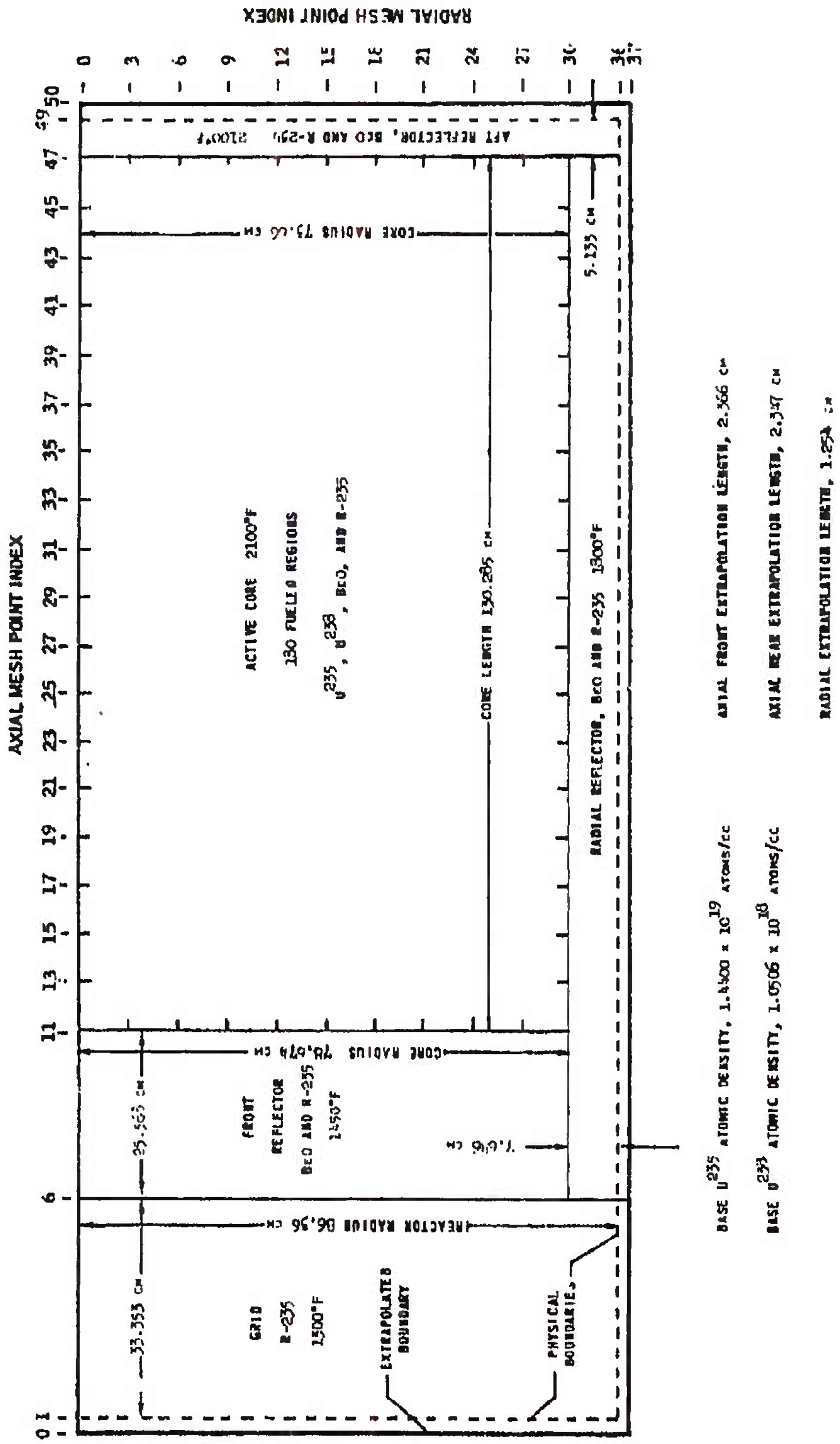

POWER AND FUEL DISTRIBUTION FOR FINAL ANGIE NEUTRONICS MODEL (PROBLEM I.D. BST 005)

CORE CENTER - AXIAL REGIONS

CORE FRONT - RADIAL REGIONS

Radial region	1	2	3	4	5	6	7	8	9	10	11	12	13	14	15	16	17	18
1	1.021	1.003	0.99[illegible]	0.993	0.994	1.008	1.008	0.991	0.950	0.373	[illegible]	0.882	0.822	[illegible]	[illegible]	[illegible]	[illegible]	[illegible]
	(1.000)	(1.000)	(1.000)	(1.000)	(1.000)	(1.000)	(1.000)	(1.000)	(0.997)	(0.977)	(0.940)	(0.865)	(0.809)	(0.712)	(0.602)	[illegible]	[illegible]	[illegible]
	1.561	[illegible]	1.354	1.233	1.134	1.058	1.020	1.021	1.032	1.048	1.056	1.087	[illegible]	[illegible]	[illegible]	[illegible]	[illegible]	1.00[illegible]
2	1.007	0.976	0.999	0.986	0.955	0.981	1.014	0.991	0.993	0.971	0.955	0.855	0.824	0.719	[illegible]	[illegible]	0.35[illegible]	0.23[illegible]
	1.612	1.561	1.405	1.275	1.161	1.096	1.048	1.048	1.058	1.077	1.087	1.112	1.124	1.124	1.12[illegible]	1.112	[illegible]	[illegible]
3	1.012	0.988	0.994	0.992	0.992	0.999	1.005	0.991	0.990	0.975	0.955	0.886	0.814	0.717	0.598	0.465	0.352	[illegible]
	1.700	1.657	1.499	1.351	1.233	1.152	1.112	1.112	1.124	1.134	1.152	1.176	1.193	1.193	1.193	1.17[illegible]	1.152	[illegible]
4	1.007	0.998	0.993	0.966	0.988	0.996	1.001	0.979	0.984	0.959	0.948	0.875	0.806	0.710	0.592	0.461	0.35[illegible]	0.251
	1.663	1.817	1.657	1.510	1.351	1.254	1.219	1.219	1.219	1.247	1.264	1.292	1.308	1.308	1.308	1.292	1.248	1.17[illegible]
5	0.995	0.996	0.999	1.005	0.995	1.000	1.000	1.011	1.011	0.989	0.952	0.895	0.824	0.725	0.617	0.495	0.363	0.23[illegible]
	2.119	2.087	1.886	1.679	1.536	1.434	1.379	1.564	1.579	1.405	1.434	1.456	1.477	1.477	1.476	1.45[illegible]	1.405	1.36[illegible]
6	0.997	1.00[illegible]	1.001	0.996	0.985	0.995	0.991	0.995	1.000	0.977	0.959	0.885	0.812	0.718	0.607	0.492	0.36[illegible]	0.23[illegible]
	2.520	2.520	2.277	2.031	1.835	1.700	1.635	1.612	1.635	1.657	1.700	1.727	1.752	1.752	1.752	1.727	1.679	1.61[illegible]
7	1.000	0.998	0.993	0.991	0.987	0.992	0.952	0.993	0.992	0.972	0.941	0.881	0.795	0.711	0.604	0.450	0.35[illegible]	0.25[illegible]
	3.155	3.225	2.921	2.578	2.511	2.134	2.031	2.005	2.031	2.066	2.119	2.156	2.189	2.189	2.189	2.156	2.087	2.00[illegible]
8	1.001	1.036	0.995	0.988	0.985	0.987	0.985	0.990	0.989	0.967	0.930	0.874	0.805	0.706	0.604	0.486	0.35[illegible]	0.25[illegible]
	4.211	4.389	3.994	3.483	3.085	2.830	2.675	2.637	2.673	2.715	2.771	2.830	2.890	2.890	2.890	2.860	2.771	2.63[illegible]
9	1.005	1.001	0.995	0.991	0.983	0.985	0.984	0.988	0.988	0.965	0.927	0.868	0.801	0.702	0.600	0.489	0.353	0.233
	[illegible]	3.646	5.708	4.909	4.294	3.897	3.678	3.610	3.650	3.720	3.818	3.897	3.972	3.994	3.972	3.972	3.813	3.65[illegible]
	1.012	1.011	1.002	0.954	0.990	0.990	0.988	0.994	0.995	0.967	0.951	0.873	0.805	0.705	0.602	0.488	0.363	0.231
	[illegible]	[illegible]	[illegible]	[illegible]	[illegible]	[illegible]	[illegible]	[illegible]	[illegible]	[illegible]	[illegible]	[illegible]	[illegible]	[illegible]	[illegible]	[illegible]	[illegible]	[illegible]

CORE AFT

CORE OUTER EDGE

NOTE: RELATIVE POWER SHOWN ON UPPER PORTION OF REGION
RELATIVE FUEL LOADING SHOWN ON LOWER PORTION OF REGION
REGIONS ARE NOT TO SCALE
IDEAL POWERS ARE SHOWN IN PARENTHESIS AND ARE CONSTANT FOR EACH RADIAL REGION

GEOMETRY AND PHYSICAL DATA FOR FINAL ANGLE NEUTRONICS MODEL
MA50 XDA (PROBLEM I.D. FIN 003)

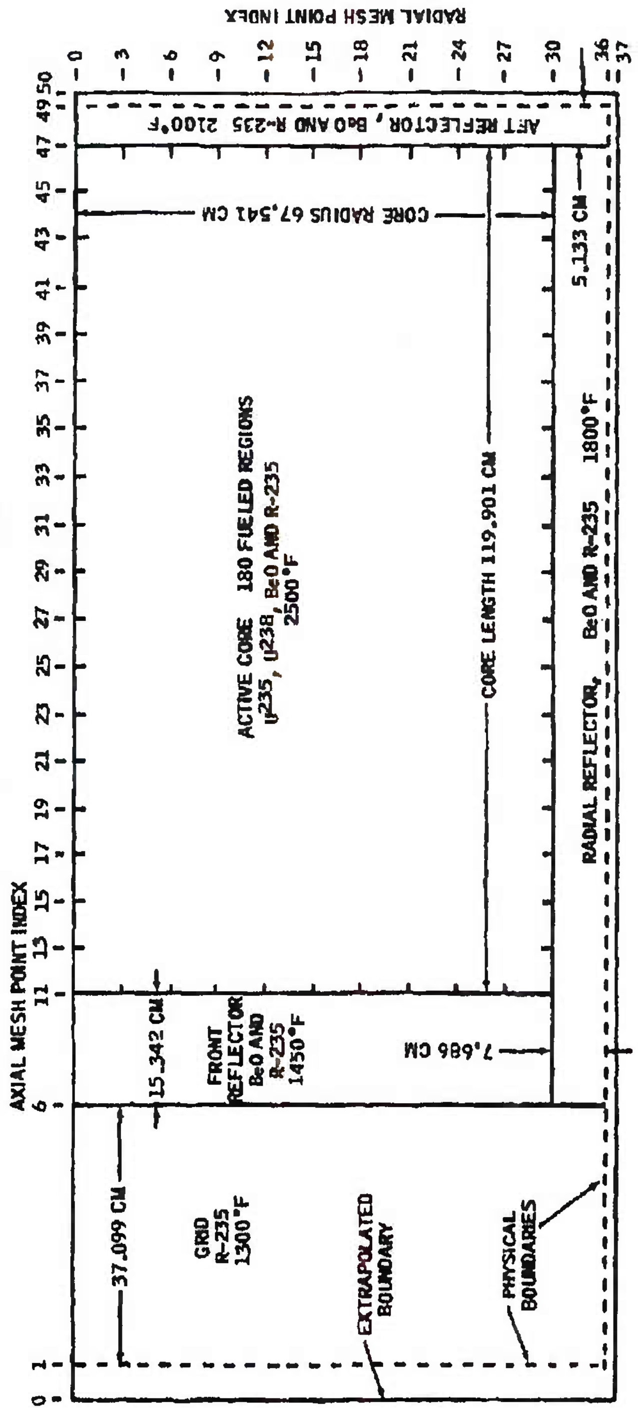

AXIAL FRONT EXTRAPOLATION LENGTH, 5.065 CM
AXIAL AFT EXTRAPOLATION LENGTH, 1.989 CM
RADIAL EXTRAPOLATION LENGTH, 1.224 CM

BASE U^{235} ATOMIC DENSITY, 1.64174×10^{19} ATOMS/CC
BASE U^{238} ATOMIC DENSITY, 1.19783×10^{18} ATOMS/CC
REACTOR PHYSICAL LENGTH (WITHOUT GRID), 140.376 CM
REACTOR PHYSICAL RADIUS, 75.227 CM

MAC A&R

POWER AND FUEL DISTRIBUTION FOR FINAL ANGIE NEUTRONICS MODEL MA50 XDA PROBLEM I.D. FN 003

CORE CENTER - AXIAL REGIONS

CORE FRONT - RADIAL REGIONS

	1 (1.000)	2 (1.000)	3 (1.000)	4 (1.000)	5 (1.000)	6 (1.000)	7 (1.000)	8 (1.000)	9 (.996)
1	0.991 -0.56 1.968	0.996 -0.38 1.770	1.000 -0.05 1.519	0.995 -0.54 1.332	1.005 +0.55 1.183	1.007 +0.69 1.087	1.000 +0.04 1.034	1.002 +0.24 1.004	1.000 +0.35 1.000
2	0.988 -1.22 2.032	0.993 -0.69 1.818	1.006 +0.56 1.571	0.993 -0.73 1.358	0.993 -0.73 1.219	0.997 -0.33 1.119	1.003 +0.32 1.057	1.005 +0.46 1.034	1.000 +0.36 1.027
3	0.993 -0.70 2.140	0.998 -0.25 1.935	1.003 +0.28 1.655	0.994 -0.57 1.457	1.002 +0.20 1.290	1.003 +0.33 1.183	0.994 -0.57 1.119	1.003 +0.29 1.087	1.003 +0.67 1.087
4	0.991 -0.87 2.355	0.991 -0.85 2.140	0.999 -0.11 1.842	0.993 -0.70 1.571	1.002 +0.19 1.414	0.998 -0.19 1.290	1.003 +0.29 1.219	0.998 -0.24 1.192	0.998 +0.16 1.183
5	0.993 -0.68 2.693	0.991 -0.93 2.456	0.989 -1.11 2.104	1.001 +0.07 1.818	0.996 -0.44 1.606	0.998 -0.24 1.456	1.004 +0.35 1.377	1.006 +0.58 1.332	1.006 +1.03 1.332
6	0.986 -1.35 3.200	0.993 -0.74 2.968	0.999 -0.10 2.527	0.992 -0.76 2.156	0.994 -0.62 1.904	1.001 +0.08 1.731	1.004 +0.38 1.616	1.000 +0.02 1.571	1.001 +0.51 1.571
7	0.986 -1.40 4.02[illegible]	0.992 -0.85 3.744	0.992 -0.77 3.200	0.989 -1.14 2.693	0.991 -0.93 2.355	0.999 -0.14 2.140	0.998 -0.22 2.001	1.003 +0.35 1.935	1.005 +0.91 1.904
8	0.977 -2.26 5.315	0.988 -1.23 4.997	0.986 -1.42 4.232	0.994 -0.65 3.535	0.991 -0.94 3.049	0.998 -0.18 2.753	0.998 0.21 2.560	1.004 +0.40 2.456	1.006 +1.01 2.456
9	0.982 -1.80 7.242	0.984 -1.59 6.934	0.985 -1.53 5.776	0.983 -1.70 4.783	0.994 -0.63 4.072	0.998 -0.22 3.624	1.001 +0.08 3.353	1.003 +0.27 3.251	1.005 +0.93 3.200
10	0.982 -1.83 9.254	0.984 -1.57 8.770	0.984 -1.55 7.242	0.989 -1.13 5.989	0.992 -0.80 5.078	0.997 -0.32 4.527	1.003 +0.28 4.187	1.009 +0.85 4.028	0.998 +0.16 4.028

	10 (.981)	11 (.952)	12 (.908)	13 (.851)	14 (.784)	15 (.704)	16 (.616)	17 (.509)	18 (.393)
1	0.985 +0.43 1.009	0.959 +0.68 1.027	0.912 +0.39 1.057	0.862 +1.29 1.087	0.785 +0.15 1.160	0.704 +0.04 1.248	0.619 +0.57 1.377	0.50[illegible] -0.52 1.571	0.388 -1.27 1.726
2	0.980 -0.12 1.034	0.955 +0.36 1.057	0.913 +0.58 1.087	0.852 +0.06 1.130	0.791 +0.92 1.183	0.708 +0.56 1.271	0.613 -0.[illegible] 1.414	0.506 -0.63 1.606	0.386 -1.53 1.834
3	0.978 -0.31 1.100	0.962 +1.04 1.119	0.917 +0.99 1.146	0.857 +0.72 1.192	0.785 +0.18 1.271	0.707 +0.37 1.358	0.620 +0.71 1.501	0.507 -0.48 1.704	0.387 -1.50 1.937
4	0.988 +0.72 1.192	0.956 +0.39 1.219	0.916 +0.89 1.248	0.855 +0.47 1.304	0.785 +0.07 1.377	0.705 +0.18 1.482	0.621 +0.81 1.655	0.510 +0.20 1.855	0.339 -1.04 2.035
5	0.981 +0.03 1.358	0.957 +0.54 1.377	0.918 +1.14 1.414	0.859 +0.93 1.482	0.786 +0.20 1.571	0.704 +0.01 1.704	0.613 -0.49 1.885	0.506 -0.57 2.156	0.389 -1.03 2.560
6	0.987 +0.65 1.571	0.958 +0.64 1.616	0.908 +0.05 1.669	0.858 +0.85 1.731	0.793 +1.19 1.842	0.710 +0.78 2.001	0.619 +0.41 2.252	0.509 +0.05 2.560	0.395 +0.52 3.049
7	0.979 -0.16 1.935	0.960 +0.85 1.968	0.919 +1.17 2.032	0.855 +0.53 2.140	0.791 +0.90 2.294	0.713 +1.26 2.486	0.618 +0.35 2.830	0.508 -0.16 3.251	0.395 +0.57 3.857
8	0.980 -0.10 2.486	0.954 +0.2[illegible] 2.527	0.915 +0.80 2.627	0.856 +0.61 2.753	0.791 +0.93 2.968	0.706 +0.22 3.283	0.613 +0.39 3.744	0.512 +0.56 4.345	0.395 +0.63 5.181
9	0.990 +0.44 3.251	0.957 +0.52 3.353	0.913 +0.52 3.476	0.856 +0.57 3.674	0.793 +1.19 3.966	0.707 +0.47 4.409	0.622 +1.02 5.078	0.509 +0.06 5.989	0.394 +0.30 7.260
10	0.984 +0.29 4.072	0.958 +0.61 4.187	0.913 +0.50 4.345	0.861 +1.22 4.585	0.790 +0.81 4.997	0.708 +0.64 5.524	0.619 +0.50 6.394	0.510 +0.27 7.650	0.395 +0.42 9.621

CORE AFT

CORE OUTER EDGE

NOTE:
IDEAL POWERS ARE SHOWN IN PARENTHESIS AND ARE CONSTANT FOR EACH RADIAL REGION.
RELATIVE POWER SHOWN ON UPPER PORTION OF REGION.

PERCENTAGE DEVIATION OF POWER FROM IDEAL POWER SHOWN IN CENTER PORTION OF REGION.
RELATIVE FUEL LOADING SHOWN ON LOWER PORTION OF REGION.
REGIONS ARE NOT TO SCALE.

N22C27

FIGURE 85

MAXIMUM NEUTRON LEAKAGE FLUX SPECTRA
PROBLEM I. D. FIN 003

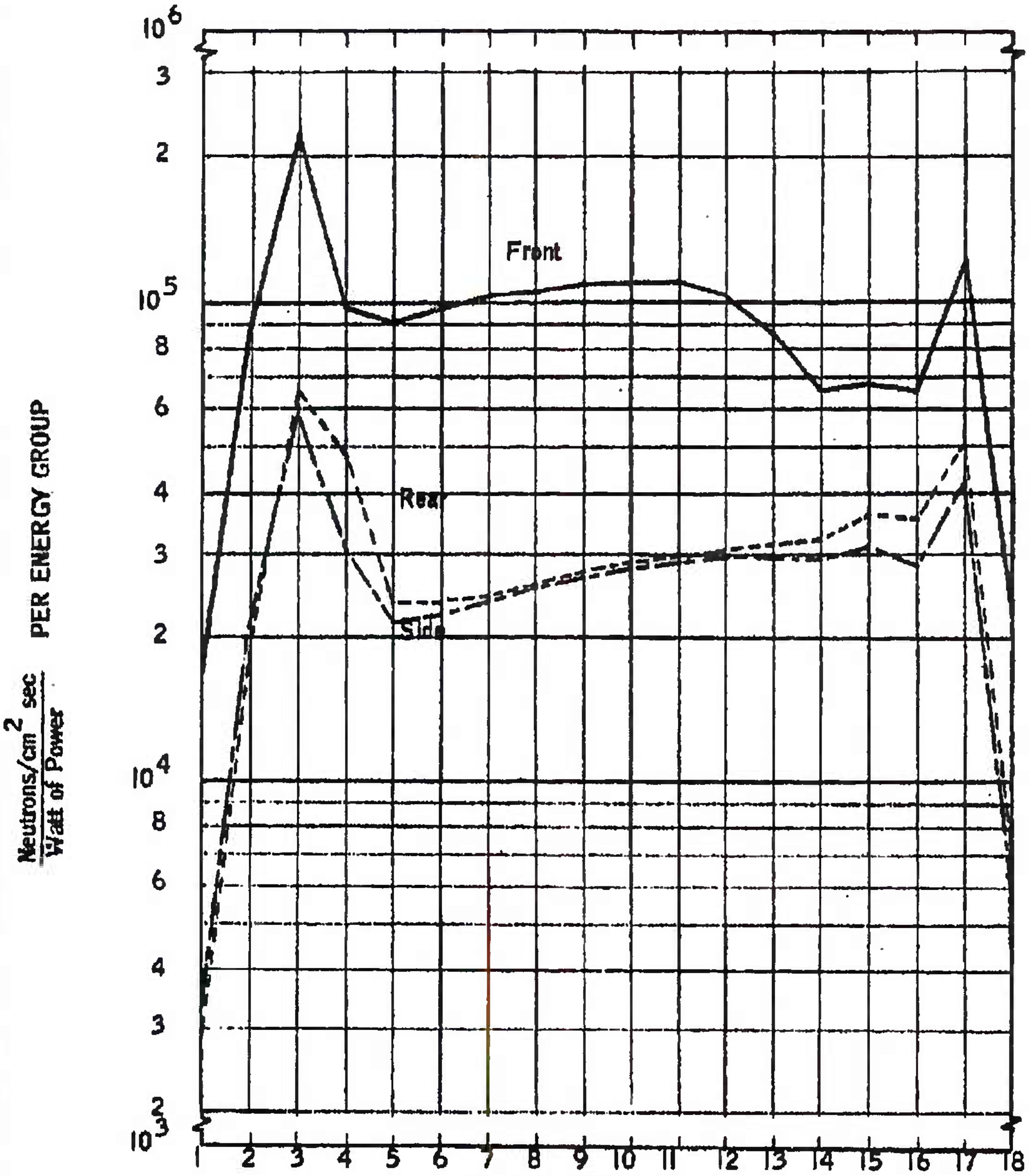

erosion rate of 0.2 percent of core material per hour of operating t ie was assumed for the period of operation. Such a rate would result in a ch ge in k_{eff} of 0.005 per hour. The results of a one-group homogeneous burnup alculation were compared with calculations of the Marquardt two-dimensional ultigroup burnup code Firedragon over a typical Pluto flight history. The sin lified model was found to give conservative answers and was accepted for the pr iminary analysis noted here. The required initial multiplication factor at op rating temperature is shown in Figure 87 as a function of reactor lifetime fo wo total power conditions.

The effects of operating time on the system can be divided to two parts. First, the effect of the accumulation of fission products, which incl e xenon-135 and samarium-149 as well as those that emit gamma rays with ener r above the $Be^9(\gamma, n)Be^8$ threshold. Second, the effects of control rod motion n the power distribution.

The poison effect in Δk, is readily obtained by solving the onventional fission product production equations for each region of the reactor. The effect of the $Be^9(\gamma, n)Be^8$ reaction on k_{eff} can be estimated in terms of β $_{eff}$ and the effective delayed neutron fraction.

The changes in k_{eff} and in power distribution resulting fro control rod motion are more difficult to calculate. Knowing the reactivity comp nsation required for poison buildup, the corresponding control rod positions c 1 be computed with the Angie program using the method of Wachspress (Refe ence 18) to represent a thin, cylindrical poison ring.

A method is being developed for the synthesis of three-dim nsional power shapes in the reactor with the control rods inserted. This sy thesis is necessitated by the fact that the physical arrangement of the control ods is inconsistent with the mathematical model used to calculate control ro worth.

3.6.5 Neutronics Methods Development

Calculation methods development has been required to allo a faster and more reliable evaluation of Pluto type reactors. Additional work in his area is anticipated.

The IBM-704 program Angelita was developed to prepare i ut for the Angie program. Angelita uses flux-weighted average fission micro opic cross sections as a function of the density of the fissionable material to de ermine the

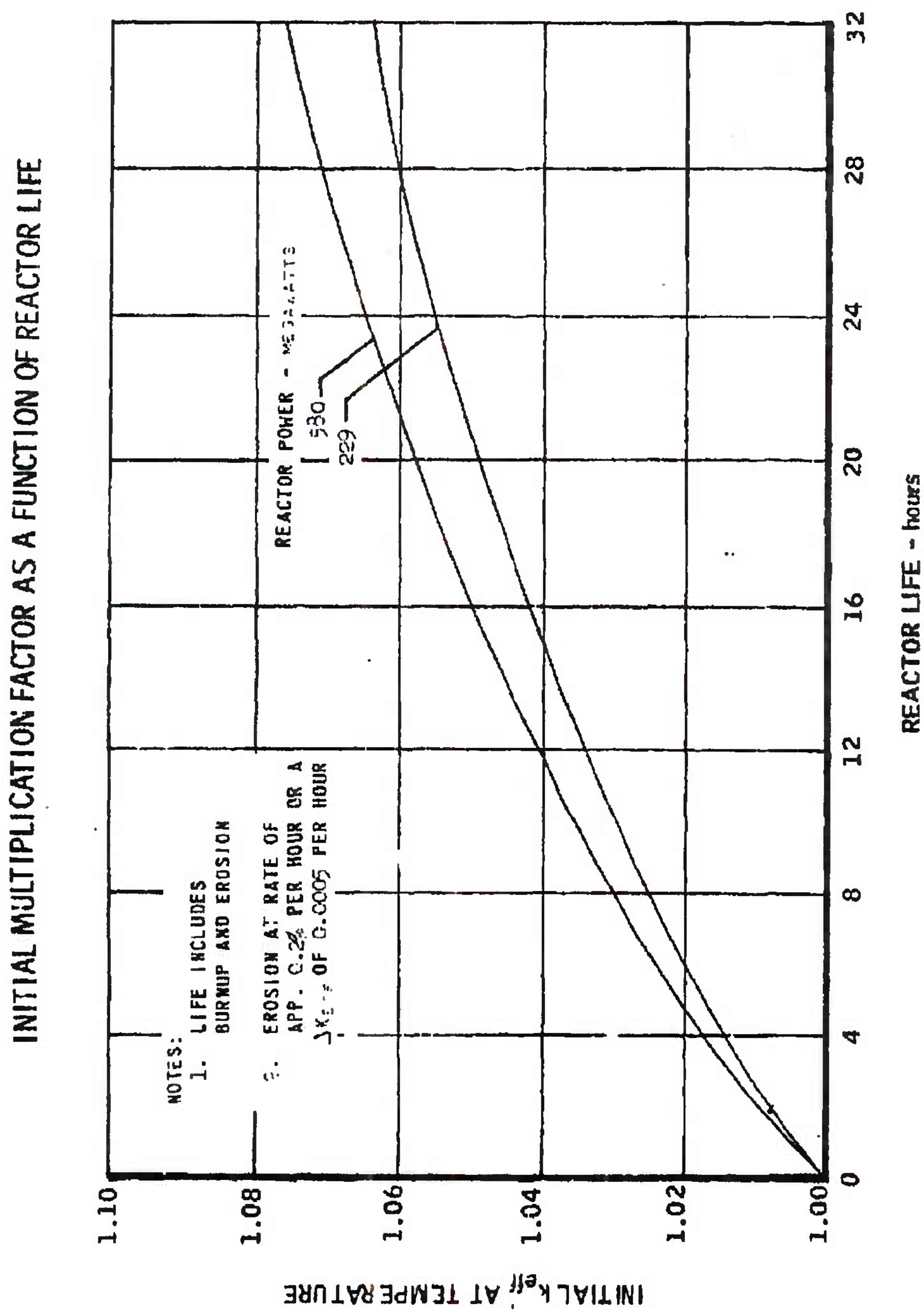
INITIAL MULTIPLICATION FACTOR AS A FUNCTION OF REACTOR LIFE
REACTOR POWER - MEGAWATTS
530
229
NOTES:
1. LIFE INCLUDES BURNUP AND EROSION
2. EROSION AT RATE OF APP. 0.2% PER HOUR OR A Δk_{eff} OF 0.0005 PER HOUR
REACTOR LIFE - hours
INITIAL k_{eff} AT TEMPERATURE
1.10
1.08
1.06
1.04
1.02
1.00
0
4
8
12
16
20
24
28
32

new fuel distribution from the previous power profiles and fuel distr utions. The program also punches cards in Angle input format to give the r ative distributions of all materials in the reactor.

The IBM-704 program Flexita reads the relative neutron fl es from Angle output tapes, averages the mesh point fluxes for each region, nd obtains the volume weighted average flux over the entire core for each ener group. The program also averages the powers for each region, normalizes em, and renormalizes them to any desired position.

The IBM-704 FORTRAN code Pronto was developed for the reparation of cross section input to the reactor code PDQ. The program calcu tes macroscopic diffusion, absorption, removal, and fission cross sections f each group and each region from microscopic cross sections and atomic densiti s.

A st dy of the validity of diffusion theory for analysis of Pl o type reactors has been initiated. In using diffusion codes for reactor co utations, it is necessary to represent the reactor by many regions of sufficie size to make diffusion theory applicable. The requirement of small region or adequate representation of spatial variation is incompatible with the re irement of large regions demanded by diffusion theory. It is conceivable that i some cases there is no "mesh size" that satisfies both requirements adequately. Initial investigations of the question will be made using a one-dimensional, o -velocity transport equation. Studies will be extended to verify the validity o ower distributions derived from application of diffusion theory.

3.7 Radiation Analysis and Shielding

The radiation analysis and shielding effort is concerned wit specifying the Pluto in-flight radiation environment, description of radiation e ironment and hazards during launch, delineation of shielding and nuclear heat g problems, and integration of overall system shielding requirements.

Work performed during 1961 has resulted in the specificati of the Pluto radiation environment comprising dose rate information, neut n and gamma spectrum data, and reactor leakage flux. Nuclear heating s dies of many engine components have been completed, but additional study ll be required during the 1962 contract period. System shielding requirem ts, not studied in great detail during the contract year, will be pursued furt er during 1962.

3.7.1 Computation of Radiation Levels for the Tory IIC Reactor

Radiation levels for the Tory IIC reactor have been calculated and re presented in the form of neutron and gamma isodose curves and doses forw :d of the reactor in Figures 88 and 89. The radiation levels are consisten with the information published by LRL in the Tory IIC Data Book. These result will be reviewed and updated as the Tory IIC reactor design becomes more firm r established.

The General Electric Shielding Program 04-2 was used to obtain b :h the neutron and gamma dose rates at various positions outside the reactor.

The radial power distribution within the core was taken to be flat, hile the axial power distribution was obtained by fitting curves to the data in Re r-ence 19. The core was longitudinally divided into four regions with each re on being represented by an appropriate power distribution function. The funct ns used to fit the data were as follows:

Function	Range*, (cm)
$P(Z) = 1$	5 to 64.4
$P(Z) = \cos 0.027\,(Z-5)$	-5 to 5
$P(Z) = \cos 0.0183(Z-9.8)$	-5 to -35
$P(Z) = \cos 0.0202(Z-5.625)$	-35 to -64.4

3.7.2 Gamma Spectra for Tory IIC

The General Dynamic Shielding Program D-53 was used for deterr n-ing the energy spectrum of the gamma radiation from the Tory IIC reactor. The code employs moments method data (Reference 20) to specify the transfer photons between energy levels. The reactor core is divided into 254 volum elements, and the power within each volume element is calculated. The co : assumes that the power comes from a point source located in the center of ich volume element.

The geometric configuration and the composition of the reactor mu t be specified in order to calculate the number of mean free paths, μr, of m -terial encountered in traversing the distance from each source point to the :-tector point in question. Use of the value of μr for different materials in t : equation for I_o, $(E, E_o, \mu r)$ effectively assumes that the scattering effect the material is equivalent to that of an equal number of mean free paths of beryllia.

*Referenced to core geometrical center

GAMMA AND NEUTRON ISODOSE CURVES

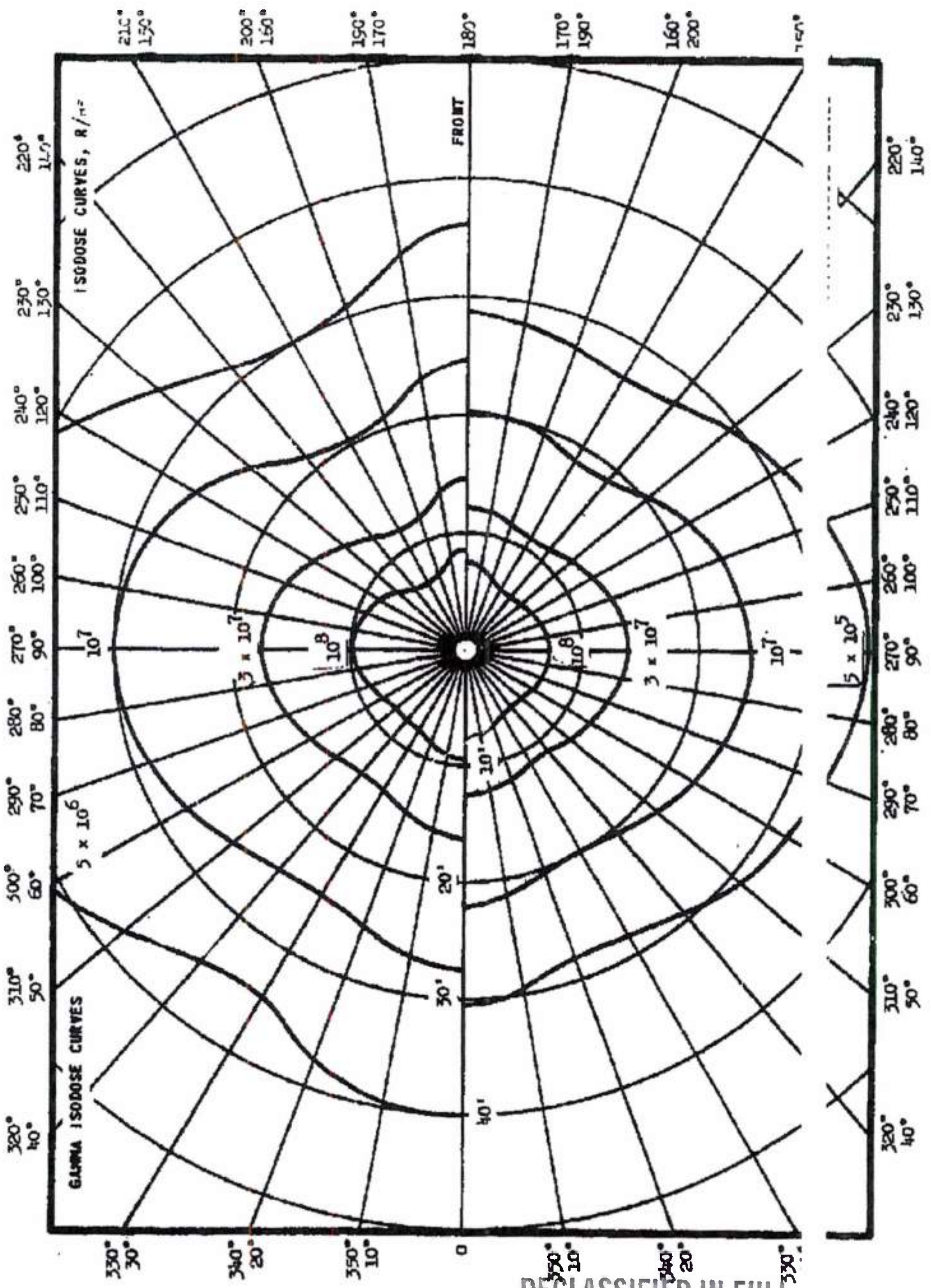

NEUTRON AND GAMMA DOSE RATES
AS A FUNCTION OF DISTANCE FORWARD OF REACTOR CENTER

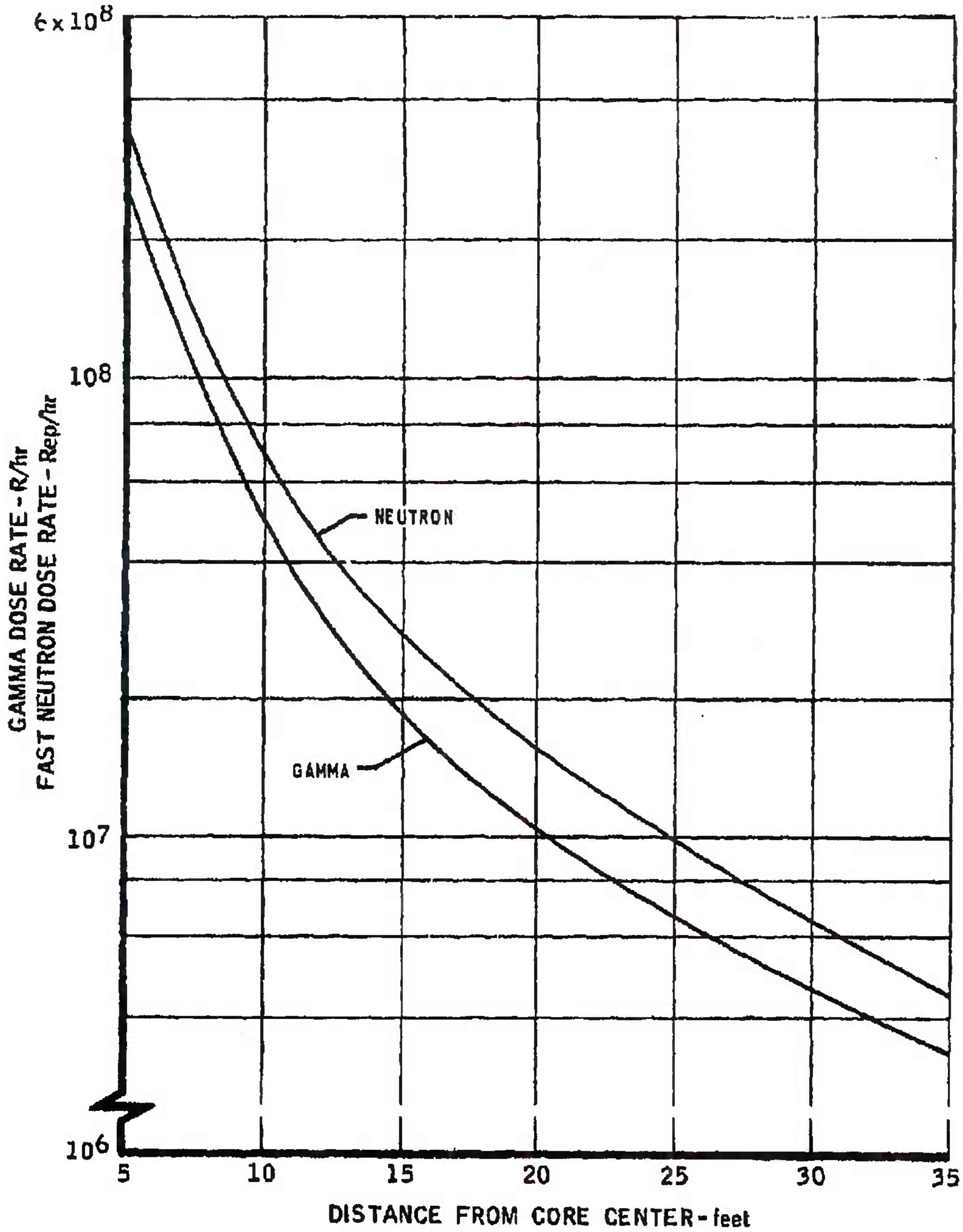

FIGUI ; 89

The output of the Program D-53 gives flux values for seve energy levels as well as the total dose. The total dose is calculated by (1) tilizing flux-to-dose conversion factors for the seven energy levels and (2) imerically integrating over the energy interval.

The Program 04-2 was run for each of the receiver points n order to obtain total doses that could be compared with the Program D-53 d es. The results are compared in Table 12.

3.7.3 Neutron Spectra for Tory IIC

The Program 04-2 was used to calculate the neutron spect of the Tory IIC reactor utilizing moments method data for beryllia. The ta furnish a differential number flux per Mev, $N_0(r,E)$, as a function of ener and penetration distance for a unit point isotropic fission source in berylli The neutron flux per Mev, ϕ (r,E), outside the reactor can be calculated l performing the three Program 04-2 integrations over the Albert-Welton ke el (see Reference 21 for appropriate values of Albert-Welton constants).

The neutron flux per Mev, ϕ (r,E), was calculated for si energy levels: E = 0.33, 1.096, 2.44, 3.64, 5.43, and 8.10 Mev. The ne ron spectra were established at eight receiver points, and the results are tabul ed in Table 13. The results are for a power level of 1 watt. Flux densities at ny other power level can be obtained by multiplying the tabulated values by t power level of interest. The main contribution to error is expected to be e infinite medium assumption inherent in the moments method data. The hig r energy fluxes are more accurately predicted than those of lower energy.

3.7.4 Nuclear Heating Analysis of Nickel Shell

A peripheral shim to reduce structural nuclear heating ha been proposed by LRL to replace part of the radial beryllia reflector of the ory IIC reactor. The reduction of nuclear heating in the side support struc re has been analyzed in a preliminary manner. More detailed calculation will be performed to obtain the accuracy required.

The idealized configuration of the reactor with and without eripheral shims is shown on Figure 90. The non continuous distribution of r terials in the side support structure is homogenized for calculation purposes.

The gamma rays that contribute to heating within the side pport structure are those produced in the core and those produced in the s ims and side support structure from neutron capture. Gamma production fr m neutron inelastic scattering has been ignored as a minor component.

TABLE 12

GAMMA FLUX DENSITIES OUTSIDE TORY IIC REACTOR CORE

Position		Energy Groups (Photons/cm²/sec/Mev)*						
Radial r (cm)	Axial z (cm)	E1	E2	E3	E4	E5	E6	E7
124.2	894	3.12/12	7.20/11	2.22/11	8.96/10	3.65/10	9.03/9	1.29/
152	89	1.13/14	2.51/13	7.73/12	3.07/12	1.24/12	3.04/11	4.27/
89	254	3.61/13	8.42/12	2.61/12	1.06/12	4.33/11	1.08/11	1.54/
89	102	8.90/13	2.03/13	6.39/12	2.68/12	1.14/12	2.98/11	4.50/
89	0	5.37/14	1.19/14	3.67/13	1.44/13	5.80/12	1.40/12	1.94/
77.5	0	6.69/14	1.49/14	4.63/13	1.83/13	7.36/12	1.79/12	2.51/
82.5	20	6.27/14	1.40/14	4.30/13	1.70/13	6.81/12	1.65/12	2.29/
82.5	40	5.67/14	1.26/14	3.89/13	1.53/13	6.12/12	1.49/12	2.07/
82.5	60	3.98/14	8.93/13	2.76/13	1.10/13	4.42/12	1.08/12	1.52/
82.5	-40	3.82/14	8.57/13	2.66/13	1.06/13	4.28/12	1.05/12	1.48/
82.5	-60	2.18/14	4.99/13	1.56/13	6.27/12	2.59/12	6.44/11	9.26/
112	163	4.23/13	1.04/13	3.32/12	1.39/12	5.84/11	1.51/11	2.25/
107	123	6.30/13	1.47/13	4.67/12	1.95/12	8.28/11	2.15/11	3.21/
76.2	228	4.79/13	1.12/13	3.47/12	1.41/12	5.75/11	1.42/11	2.03/
127	305	2.07/13	4.88/12	1.52/12	6.22/11	2.55/11	6.40/10	9.22/
190	152	4.40/13	9.9/12	3.07/12	1.24/12	5.06/11	1.27/11	1.82/
86.4	412	1.54/13	3.55/12	1.10/12	4.43/11	1.80/11	4.46/10	6.34/
152	762	4.10/12	9.46/11	2.93/11	1.18/11	4.83/10	1.19/10	1.71/
152	889	3.06/12	7.05/11	2.18/11	8.79/10	3.58/10	8.87/9	1.27/
152	1020	2.34/12	5.40/11	1.67/11	6.72/10	2.74/10	6.80/9	9.70/
152	1140	1.88/12	4.34/11	1.34/11	5.42/10	2.20/10	5.47/9	7.78/

* $N/n = N \times 10^{n}$

TABLE 13

NEUTRON SPECTRA FOR ONE WATT OF POWER

Position		Flux, $\phi(r,E)$ $(n/cm^2$ sec Mev $)$					
Radial r (cm)	Axial z (cm)	E = 0.330	E = 1.096	E = 2.44	E = 3.64	E = 5.43	= 8.10
89.0	254	1.74/4	4.23/3	1.98/3	2.21/2	1.18/2	.73/1
25.4	472	6.84/3	1.65/3	7.71/2	8.84/1	4.61/1	.57/0
7.63	513	5.75/3	1.39/3	6.48/2	7.41/1	3.88/1	.46/0
152	1140	9.21/2	2.25/2	1.04/2	1.19/1	6.30/0	.67/-1
77.5	0	3.84/5	9.30/4	4.29/4	5.23/3	2.63/3	.71/2
82.5	20	3.59/5	8.68/4	3.98/4	4.91/3	2.45/3	.43/2
82.5	-60	1.13/5	2.75/4	1.27/4	1.50/3	7.71/2	.12/2
82.5	60	2.23/5	5.39/4	2.48/4	3.05/3	1.52/3	.16/2

IDEALIZED CONFIGURATION OF TORY IIC REACTOR WITH AND WITHOUT PERIPHERAL SHIMS

(DIMENSIONS IN CM)

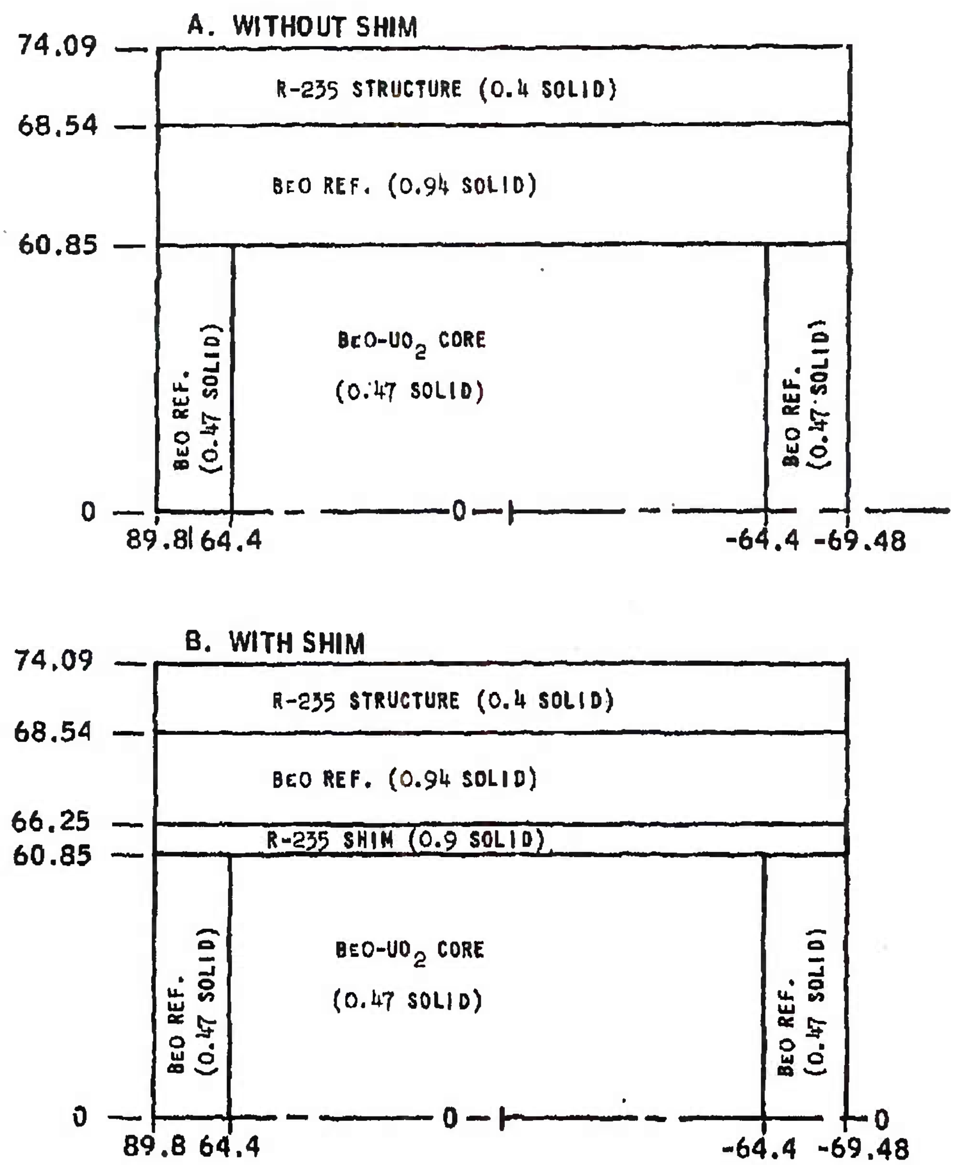

The heating due to core gammas was calculated with the P gram 04-2. The buildup factor option applied was the semi empirical technique f Kalos (Reference 22) for water followed by iron to represent beryllia fol wed by R-235.

Neutron fluxes, required for the determination of capture mma source strengths, were calculated with Zoom, the one-dimensional multi-group, diffusion theory code developed by LRL. Future calculatior will be based on leakage values generated by the Angie program. The cap re gamma source strengths, the cumulative sum of the product of group flux a d group cross sections, are shown in Figure 91 as a function of position r the two design cases.

The evaluation of the heating distribution resulting from th capture gamma source was completed using the Grace II code of Atomics Ir rnational (Reference 23). Several approximations are involved in the meth . The shim and side support structure are represented as infinite slabs, e source strength distributions are represented as exponentials, and Taylor expo-nential expression for buildup is used. Use of these approximation allows the relationships predicting the heating due to capture gammas to be ex ressed in a closed form in terms of exponential integrals.

The radial distribution of heating from each gamma compo ent at the maximum heating location is shown in Figure 92. The total gamm heating is shown in Figure 93. While the gamma heating within the side s pport structure has been appreciably reduced, the total gamma ray heat neration in the shim and support structure is greater than in the correspond g design without shims. More detailed calculations including a Monte Carlo tudy of the heat generation will be required to assess accurately the value the shim arrangement.

3.7.5 Tory IIC Reflector Nuclear Heating Analysis

The Program 04-2 was used for determining gamma ray f x levels within the side and end reflectors of the Tory IIC reactor. The po r distri-butions, reactor configuration, and reactor composition were taker rom Reference 1. Gamma ray heating in the reflectors is calculated d ectly from the Program 04-2 group fluxes by employing the 10-group energy a sorption coefficients of the material at each receiver point examined. Neut n heating, a relatively small fraction of the total nuclear heating contribution, was esti-mated on the basis of the detailed reflector neutron heating calcula ons made for the Model MA50 reactor design (Reference 24).

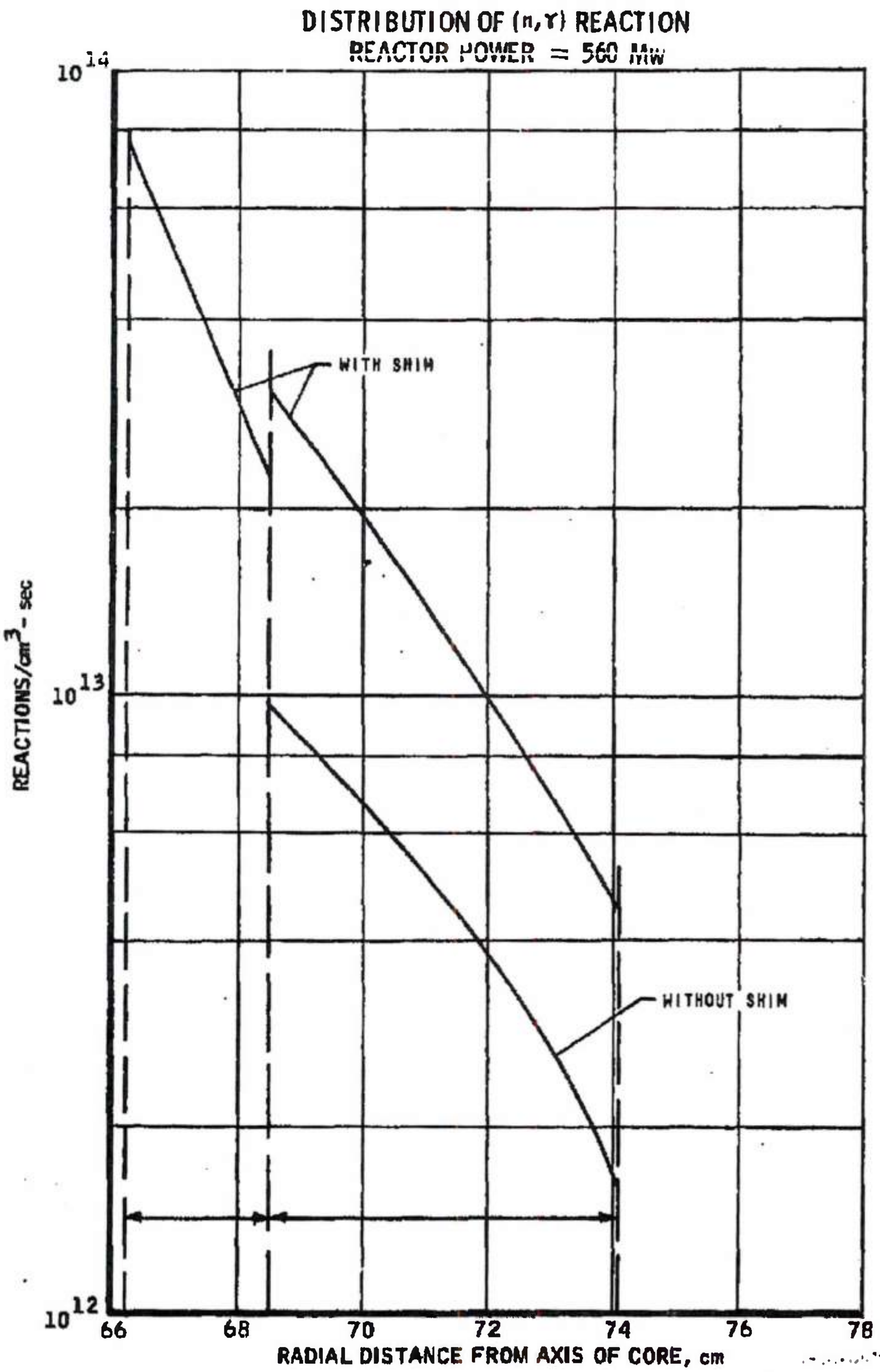
DISTRIBUTION OF (n,γ) REACTION
REACTOR POWER = 560 Mw
10^{14}
10^{13}
10^{12}
REACTIONS/cm^3-sec
WITH SHIM
WITHOUT SHIM
66
68
70
72
74
76
78
RADIAL DISTANCE FROM AXIS OF CORE, cm

RADIAL DISTRIBUTION OF HEATING FROM EACH GAMMA COMPONENT
REACTOR POWER = 560 Mw

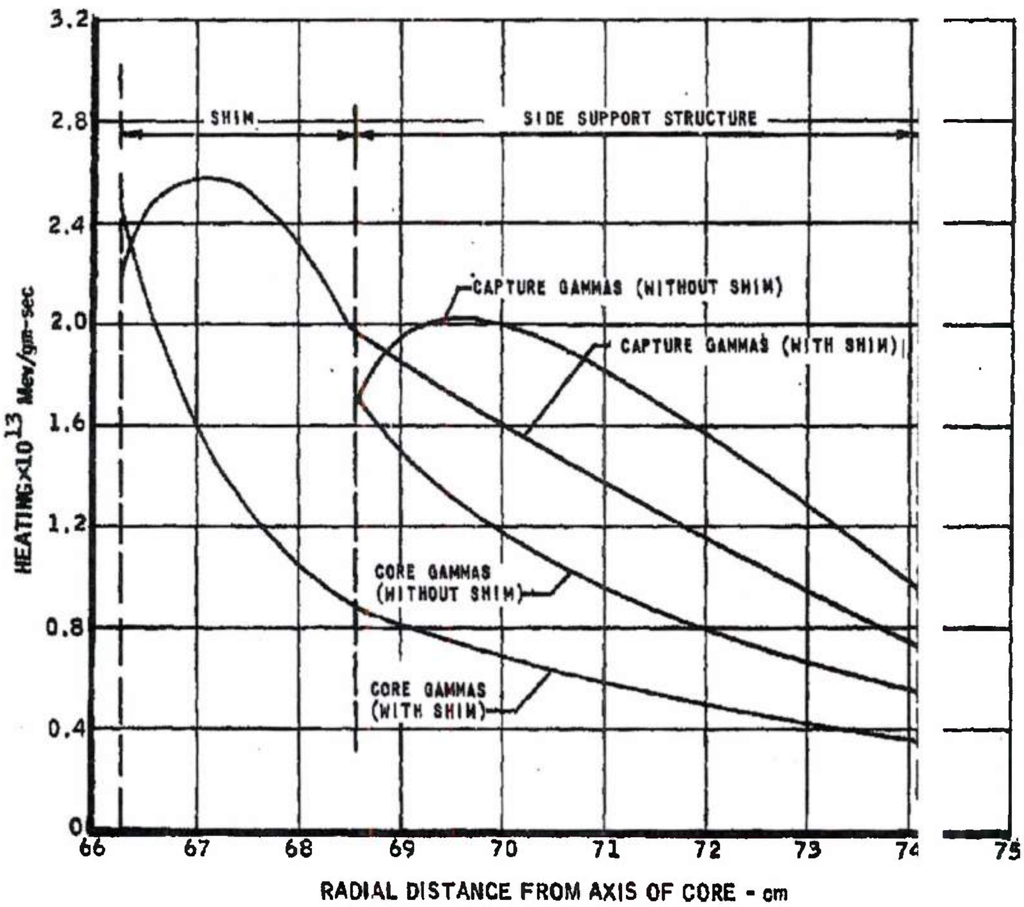

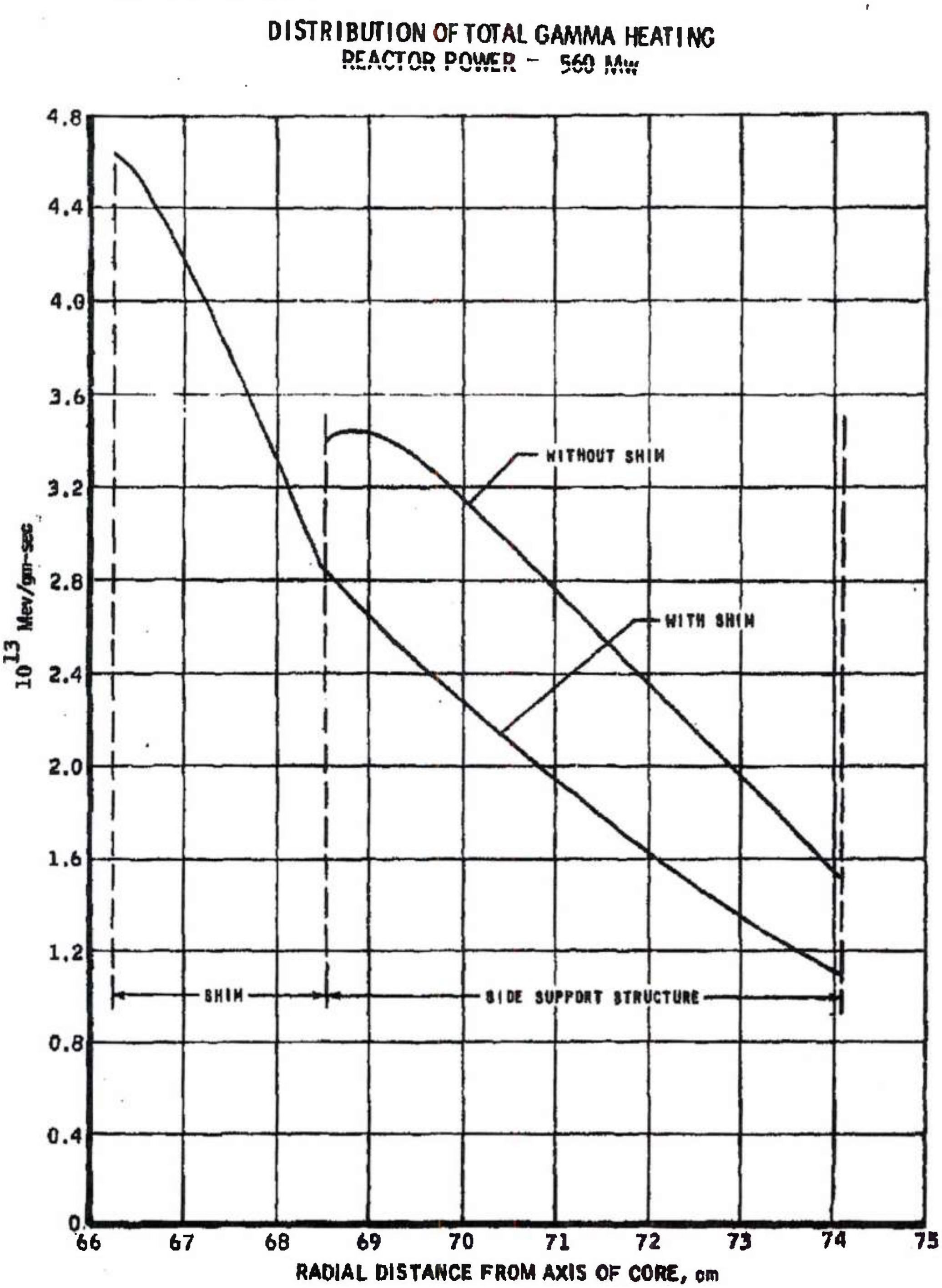
DISTRIBUTION OF TOTAL GAMMA HEATING
REACTOR POWER – 560 Mw
10^{13} Mev/gm-sec
4.8
4.4
4.0
3.6
3.2
2.8
2.4
2.0
1.6
1.2
0.8
0.4
0
66
67
68
69
70
71
72
73
74
75
RADIAL DISTANCE FROM AXIS OF CORE, cm
WITHOUT SHIM
WITH SHIM
SHIM
SIDE SUPPORT STRUCTURE

The axial heating distribution in the end reflectors is sho\ in Figure 94. The nuclear heating for the side reflector along one radial pc ition is shown in Figure 95. Radial factors for front and rear reflectors ere obtained to allow the use of the centerline heating values to estimate :ating at any radial and axial position. However, the assumption is made th the radial and axial heating distributions are mutually independent. Because iis is not strictly valid, some error will be introduced in the extrapolations. Any points of particular interest can be calculated directly using the Program 4-2 code.

NUCLEAR HEATING FOR END REFLECTORS

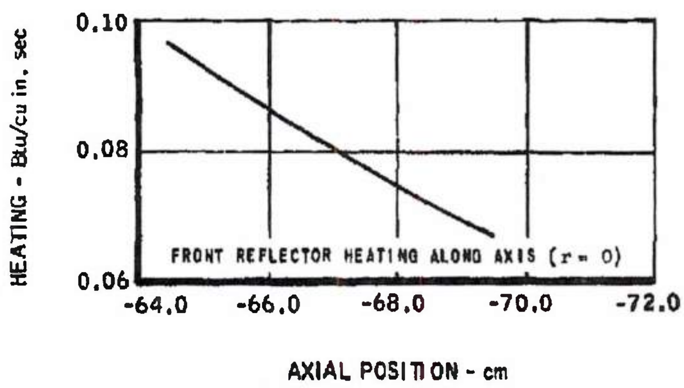

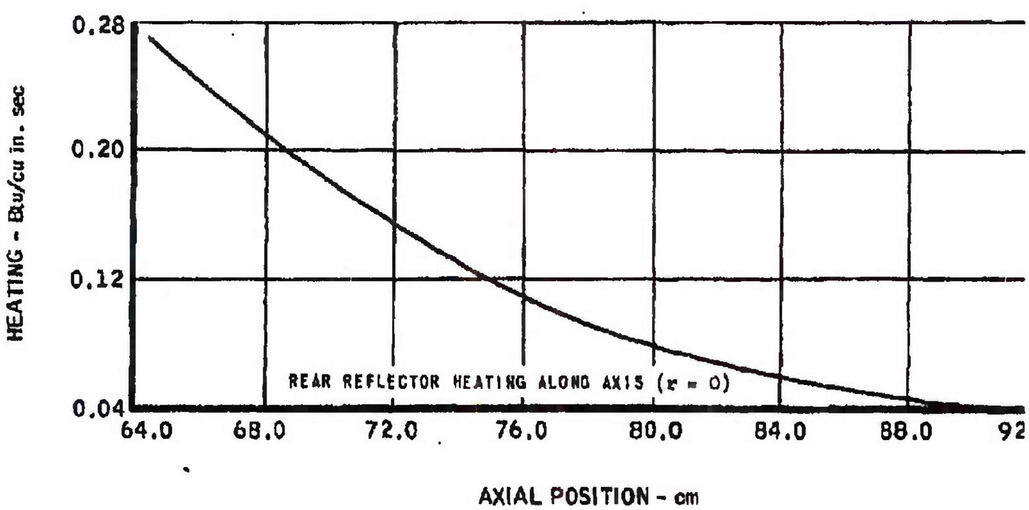

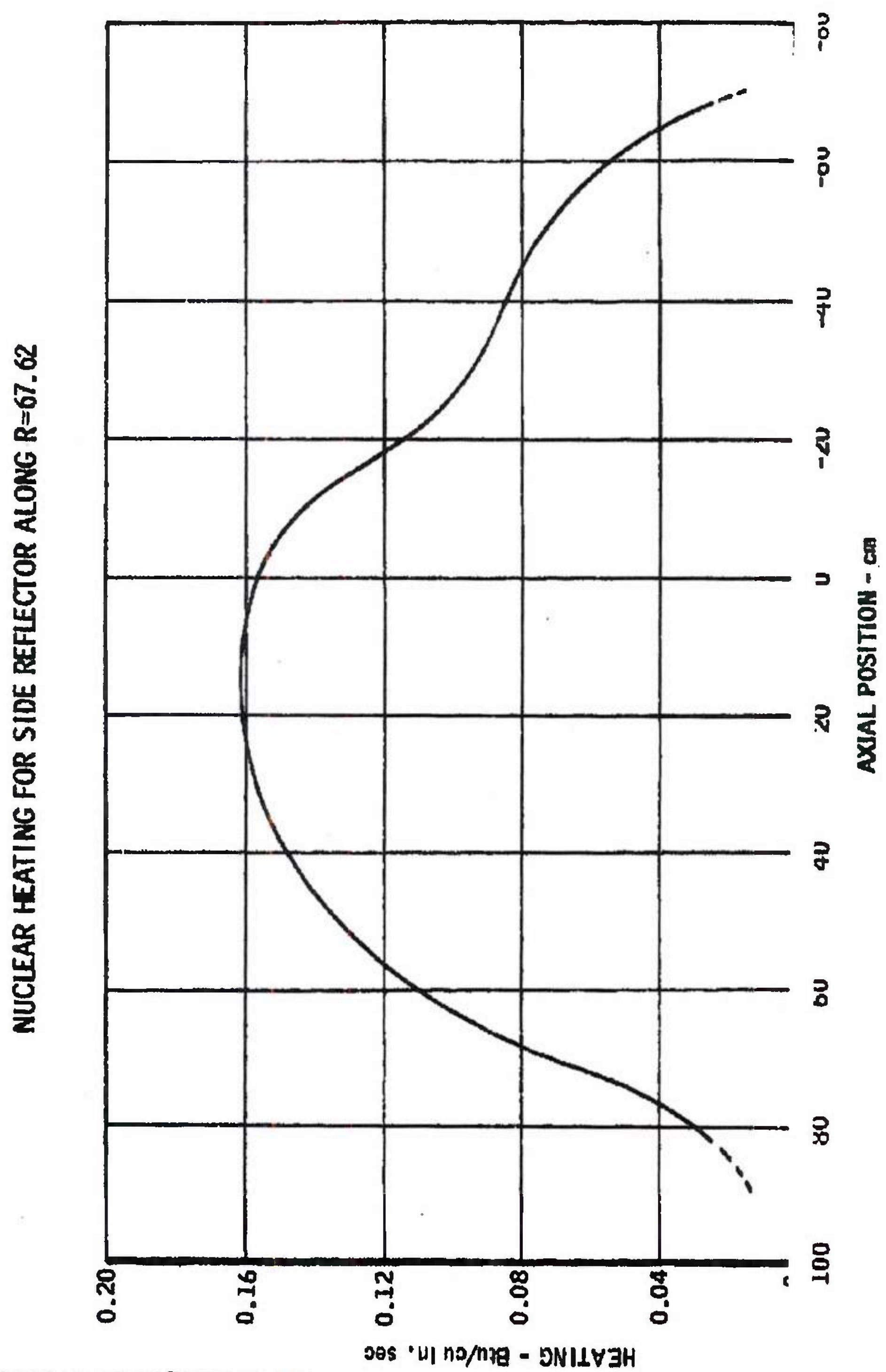
NUCLEAR HEATING FOR SIDE REFLECTOR ALONG R=67.62
HEATING - Btu/cu in, sec
0.20
0.16
0.12
0.08
0.04
AXIAL POSITION - cm
-80
-60
-40
-20
0
20
40
60
80
100

3.8 AERODYNAMIC EXPERIMENTS

Design and performance predictions for the nuclear-powered ramj propulsion system are based upon iterative considerations of material temp a- ture limitations, relationships between allowable reactor temperature and a temperature rise across the reactor, heat addition per unit frontal area of at source, and exhaust nozzle performance. In addition, the thrust-to-drag m rgin is inherently small and is particularly sensitive to inlet installed drag, inle pres- sure recovery, and drag penalties associated with inlet bleed and boundary yer diverter systems, as well as nozzle efficiency. The iteration of all these p a- meters to an accurate prediction of performance is not amenable to analytic methods without certain critical experimental inputs. Consequently, consic r- able effort was expended in 1961 toward the acquisition of experimental data o aid in the resolution of key aerodynamic problems.

3.8.1 Inlet Model Tests

Negotiations for the inlet test facility were begun in March 1961. sits were made to the two most promising facilities, Tunnel A of AEDC, Tullah a, Tennessee, and the Unitary Plan Tunnel at NASA Langley Field, Virginia. os- sessing test sections measuring 4 by 4 feet, both facilities are capable of M ch number variation from high transonic to Mach 4.0. The NASA facility was lect- ed over the AEDC facility on the basis of less work load, slightly larger mc el size, and available tunnel calibrations at desired Mach numbers.

The original program objective was to test the underslung axisymr tric inlet mounted beneath the missile forebody selected by the aerothermodynar cs contractor. The test objective was to establish the installed performance o such a system. The configuration performance, such as inlet pressure recovery bleed requirements, airflow characteristics, and installed drag as a functic of angle of attack, yaw, inlet variable geometry condition, and throttle plug pc ition, were desired over the Mach number range from 1.5 to 4.0.

The inlet test program was defined by the Air Force as a joint effo be- tween Marquardt and the aerothermodynamics contractor. In May 1961, a int meeting was held at Marquardt with representatives of the aerothermodynar cs contractor and the Propulsion Laboratory (Aeronautical Systems Division) i attendance. As a result of this meeting it was agreed to expand the test prc ram as follows:

(1) An alternate axisymmetric inlet mutually agreeable tc he aerothermodynamics contractor and Marquardt would be fabricated and test l along with the basic inlet. The alternate inlet configuration would be chosen c the basis that it was less sensitive to angle-of-attack and yaw.

(2) Simulation of various longitudinal inlet locations bene h the fuselage would be made. This simulation was accomplished in the mod by the addition or removal of inserts in the body ahead of the inlet. An inlet f w field survey was desired by the aerothermodynamic contractor for each sim lated inlet position.

(3) Body boundary layer effects upon inlet operation were o be studied in two ways: first, the fuselage boundary layer thickness at the inl . station would be changed by boundary layer trips on the body nose, and/or y the variations in the forebody length as described in the preceding paragrap second, the body nose ahead of the inlet would be lowered with respect to the in t. The purpose of this step is to establish the effect of ingestion of fuselage b ndary layer upon inlet performance.

Following the finalization of program objectives and scope a second visit was made to the Unitary Plan Tunnel (NASA) in May, and arra gements were made for 3 to 4 weeks of tunnel time beginning about 1 November 1 1.

Details of the alternate inlet were established by represen tives of the aerothermodynamics contractor and Marquardt in July 1961. The ternate inlet differs from the basic inlet in that the compression fan from the in t spike is not focused on the lip but rather is spread out and reflected from the c vl inner surface as shown in Figure 30. The alternate inlet (including a revis l centerbody) is interchangeable with the basic inlet on the model. It is longer b has a somewhat smaller external cowl angle, and has distributed bleed rather ian a localized bleed slot as has the basic inlet.

A detailed test outline was prepared for the revised progr n and was presented to NASA on 23 August 1961. By this time it was apparer that the 1 November test date could not be met with the existing model fabric ion schedule, and it was requested that the test date be moved to about 1 Decemb 1961. NASA consented to the test date change, but objected to the length of the p ogram as affecting test cell occupancy requirements and recommended elimi tion of all flow field survey runs. A revised test outline was prepared and di ussed 17 October 1961 with representatives of the Air Force and the aerothe nodynamics contractor in attendance. It was agreed that limited flow survey ru s near the design point would be obtained. The drag model would be tested wi out inlet bleed to determine the effect of bleed flow on the external pressure listributions around the inlet fairings.

Figures 96 and 97 show the inlet model during assembly. The m lel was shipped from Van Nuys 7 November and all checkout procedures and ca bra- tions were accomplished pending installation on 4 December 1961.

Installation was delayed by NASA until 15 December. A checkout n on 18 December indicated excessive vibration in the tunnel drive motor. NAS. sus- pended the test program in order to correct the discrepancy.

Testing is scheduled to continue in early January 1962.

3.8.2 Exhaust Nozzle Model Tests

The exhaust nozzle model tests conducted during November at the FluiDyne Elk River Aerodynamics Laboratory were performed to verify de. gn and performance prediction assumptions. Experimental data obtained inclu e primary nozzle thrust coefficients, nozzle discharge coefficients, the effec of nozzle secondary (cooling) flow upon the nozzle thrust coefficient, and the nozzle wall pressure distribution to provide nozzle drag load data.

The specific nozzle configurations tested are shown in Figure 98. Addi- tional detailed nozzle contouring information is shown in Figure 99 for the ri- mary nozzles, and in Figure 100 for the forced convection and ejector confi ura- tions. As indicated in Figure 99, four of the primary nozzle models consi : of truncations of a single contour. In addition to providing thrust, flow, and p es- sure data on the present optimized primary nozzle configuration (Model FC), the testing of additional nozzle lengths of the same basic contour will provi additional verification of the optimized nozzle data and will supply useful da for future installation optimization studies.

The nozzle configurations shown in Figure 100 provided the mecha cal geometry to supply secondary (cooling) flow in a manner similar to two of t cooling methods under current consideration. Forced convection cooling o he full length of the nozzle is provided with the Model FC-3 configuration, whi in the ejector nozzle the divergent section is film-cooled. The effect of these vo methods of cooling on the overall nozzle performance was evaluated experi en- tally.

The particular static thrust stand upon which these nozzle models ere tested is shown in Figure 101. The data recording equipment used in the te : is also shown. Pressures were recorded photographically from mercury colu n manometer panels and Heise gages. Valve-metered, high-pressure, prim y and secondary airflows were measured by using calibrated smooth-approac choked orifices that conformed to the ASME code. Pressure data were rec ded

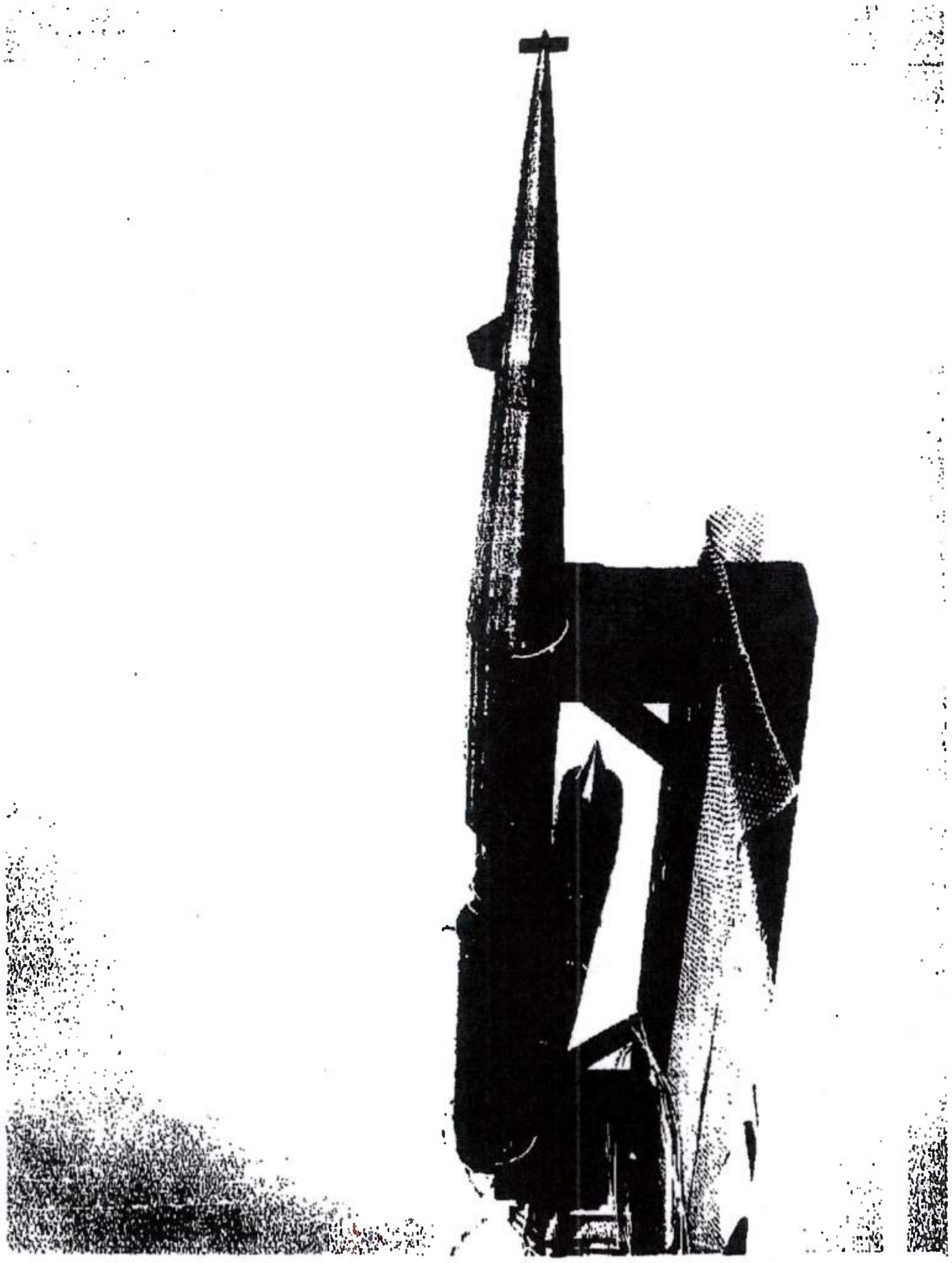

4018-2

FIGURE 96 - Inlet Model During Assembly

4018-1

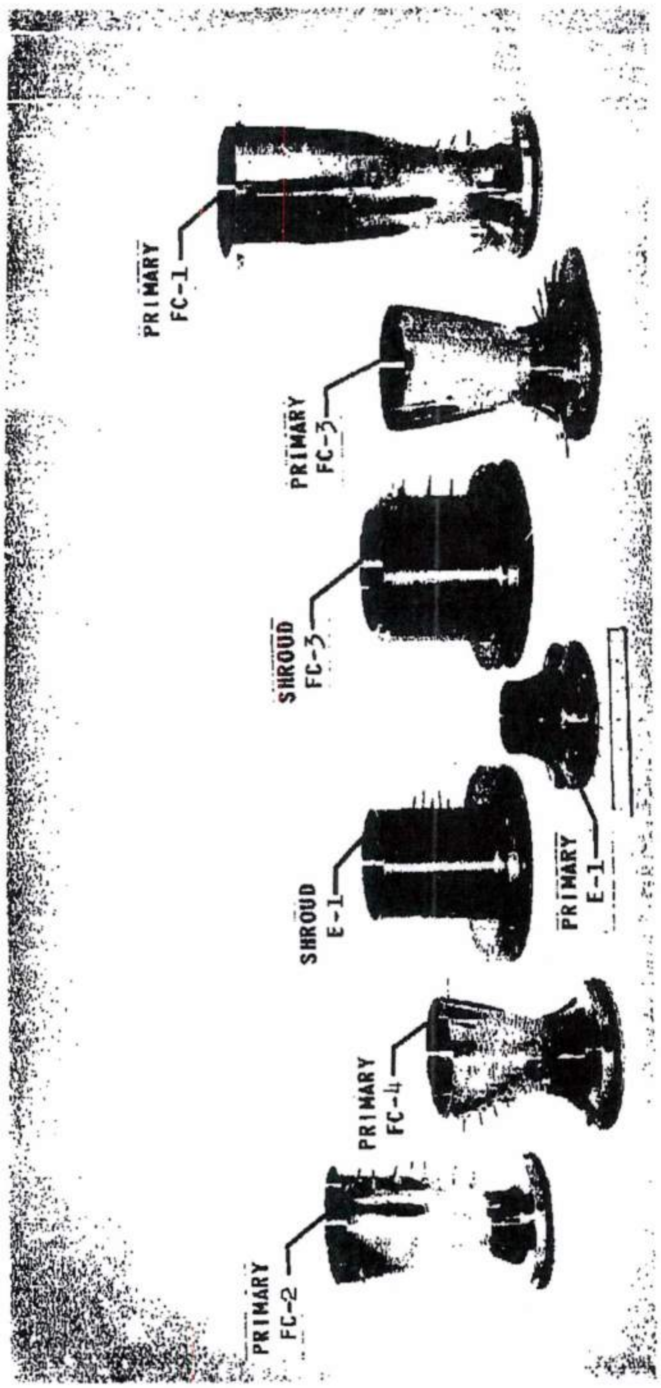

4084-2

MAC A623

CONTOURS OF PRIMARY NOZZLES

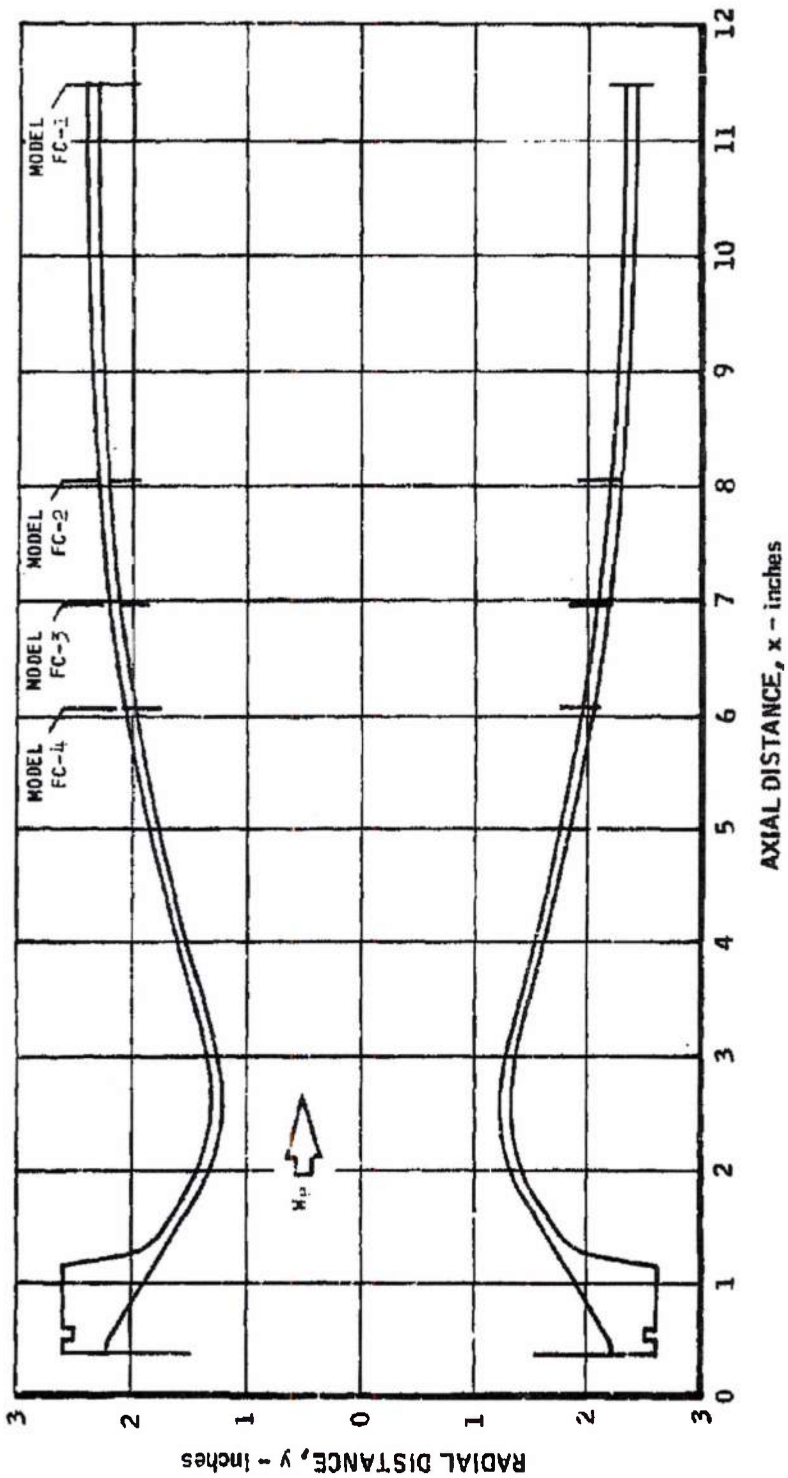

CONTOURS OF FORCED CONVECTION AND EJECTOR NOZZLES

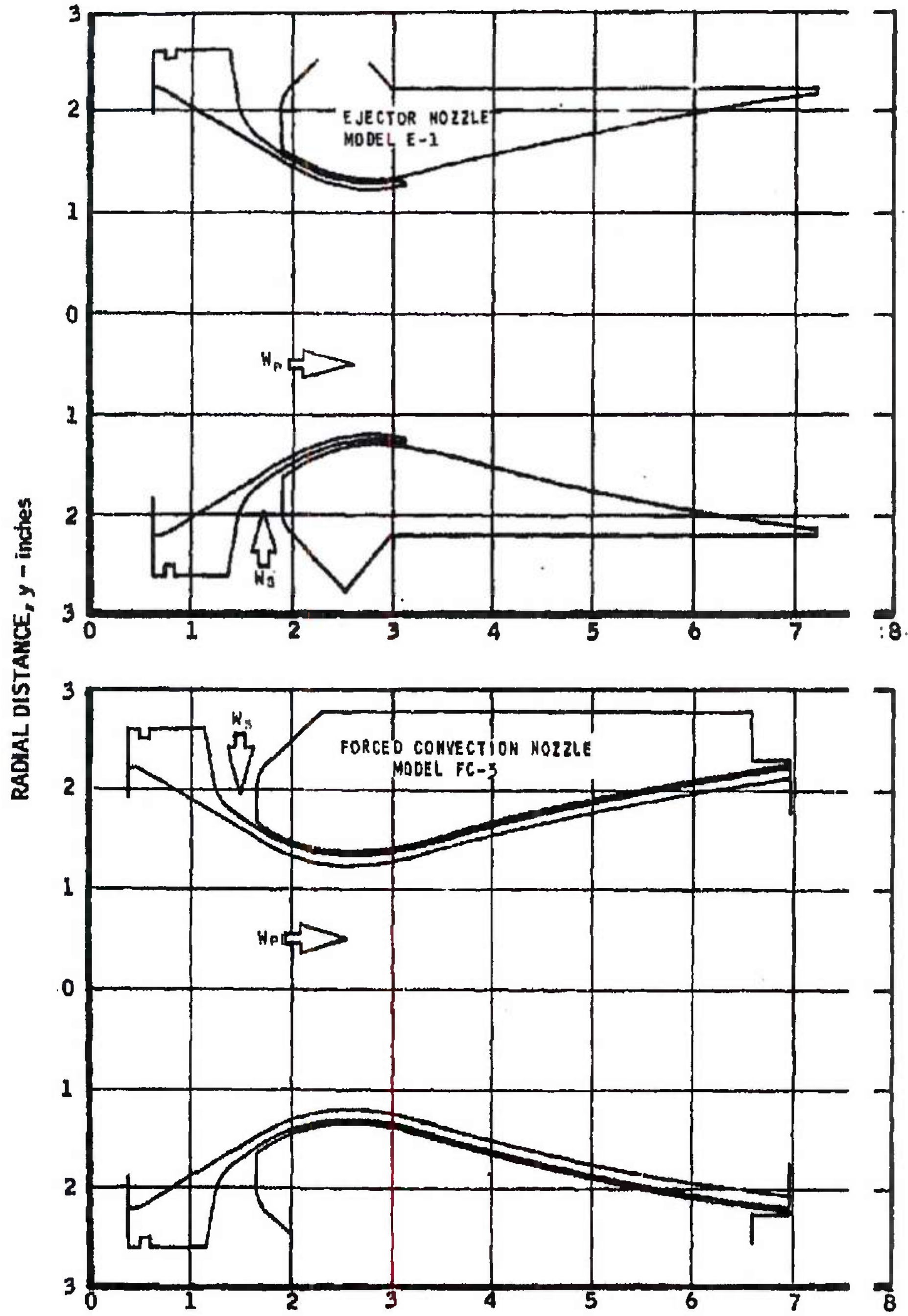

FIGURE 100

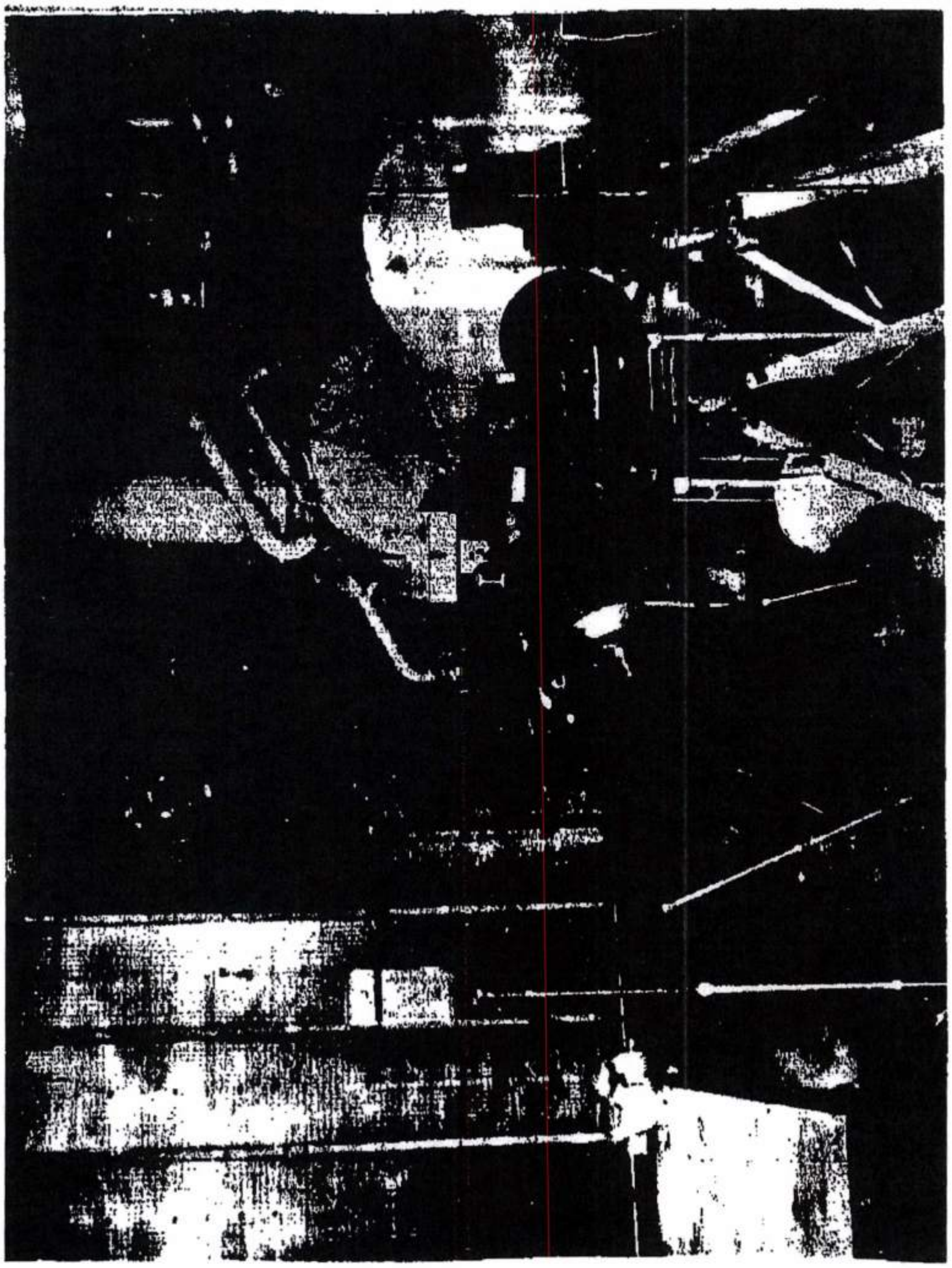

FIGURE 101 - Static Thrust Facility at FluiDyne Elk River Aerodynamics Laboratory

from various significant locations, such as in the supply piping upst eam from the nozzle, along the nozzle walls, and in the exhaust plenum.

The actual thrust of each nozzle was determined by subtrac ng a measured nozzle drag force from the computed free stream thrust upstr am from the nozzle. Each nozzle was secured to the inlet tube by a beam bal ice assembly and a flexible seal.

The seal prevented leakage of primary flow, and the balanc provided the nozzle positioning structure. When flow was introduced through ie nozzle, the downstream drag force of the nozzle was measured with a strain age in the balance and an electronic indicator. Because of the flexible seal, f ce readings were slightly pressure sensitive; therefore, balance calibrations in ided this variable. Thrust coefficient data from the system were believed to ave an absolute accuracy of ± 0.2 percent.

Tests of the nozzle models were conducted over a pressure atio (P_t/P_a) range of 2 to 30. The secondary flow models were also test i with secondary flows, W_S, equal to 0, 3.5, and 7.0 percent of primary flow W_P. The primary inlet total pressure (and primary flow) were retained nomi lly constant for all runs. The nozzle pressure ratio was varied by controlling tl exhaust plenum pressure with a steampowered ejector system.

The thrust coefficient term used in this section is the ratio f the actual thrust to the ideal thrust of the actual nozzle weight flow expanded to the operating exhaust ambient pressure. The coefficient for primary flow alone i equivalent to:

$$C_T = \frac{\text{Actual thrust of primary flow}}{\frac{W_P}{g} V_{P,i}}$$

and with both primary and secondary flows:

$$C_T = \frac{\text{Actual thrust of the combined flows}}{\frac{W_P}{g} V_{P,i} + \frac{W_S}{g} V_{S,i}}$$

where the primary and secondary ideal exhaust velocities were eval ated at the operating total-to-ambient exhaust pressure ratios of each individua flow.

The thrust coefficients from tests of the four primary nozzles are s own in Figure 102. Coefficients at design pressure ratio exceeded 0.98 for all fc r primary nozzles. Model FC-2 demonstrated the highest coefficient that was o- tained from the tradeoff of divergence loss and friction as the nozzle length v s varied. However, this nozzle would be longer than the current installation e velope permits. The Model FC-3 yielded a thrust coefficient of 0.983 at the o- timized, cold flow, design pressure ratio of 20.3. In the separated regime, s area ratio increased, the expected decrease in thrust coefficient occurred.

With secondary flow, the overall thrust coefficient (as defined in the second equation above) decreased because of the pressure drop in the second y flow passage and the momentum loss resulting from the convergent secondar exhaust passage. The overall thrust coefficient of Model FC-3 decreased fr n 0.983 to 0.977 when secondary flow was introduced, as shown in Figure 103. Further, the thrust coefficient was independent of secondary flow variation e ept when the nozzle was highly separated. In this condition, flow separation was n- hibited by increasing secondary flow, and a decrease in thrust coefficient resulted.

Without secondary airflow, the design-point thrust coefficient of the ejector configuration was 0.981, as shown in Figure 104. This value is sligl y less than that achieved for the Model FC-3 configuration, and is the result of he wall discontinuity in the primary flow of the ejector configuration. When eje or secondary flow was introduced, the thrust of the primary flow increased as t discontinuity was smoothed out, and the thrust of the secondary flow increase above that of the Model FC-3 because of the additional momentum rise with supersonic expansion. These two small increases appeared to equal the sec d- ary flow pressure drop, and mixing losses for the overall thrust coefficient - mained unchanged at 0.981.

In the separated regime with the ejector nozzle, the secondary flow - duced separation and improved the thrust coefficient. When the secondary fl v was 3.5 percent of primary flow, the thrust improvement was greater than th flow at 7.0 percent of primary, indicating that an optimum secondary flow e st- ed and was bracketed by test data. However, the cooling requirement of sec d- ary flow is much more important than the performance advantage at greatly er- expanded operating pressure ratio conditions.

The thrust coefficients defined by force measurement were verified using the nozzle wall pressure distribution to define the nozzle drag. The wa pressure distribution resulting from the primary nozzle flows is shown plotte

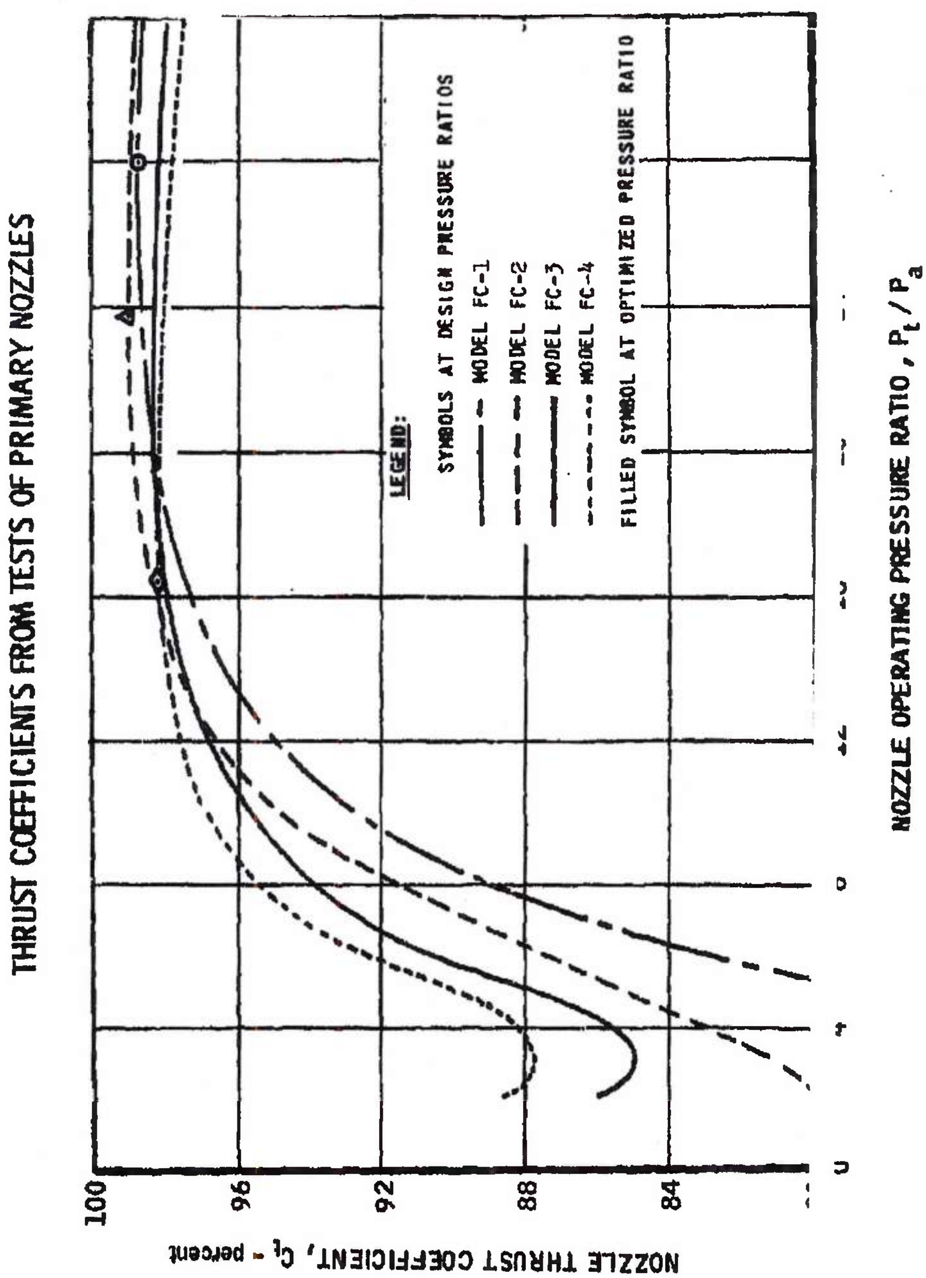
THRUST COEFFICIENTS FROM TESTS OF PRIMARY NOZZLES
LEGEND:
SYMBOLS AT DESIGN PRESSURE RATIOS
MODEL FC-1
MODEL FC-2
MODEL FC-3
MODEL FC-4
FILLED SYMBOL AT OPTIMIZED PRESSURE RATIO
100
96
92
88
84
NOZZLE THRUST COEFFICIENT, C_f - percent
NOZZLE OPERATING PRESSURE RATIO, P_t / P_a

THRUST COEFFICIENT OF FORCED CONVECTION NOZZLE (MODEL FC-3)

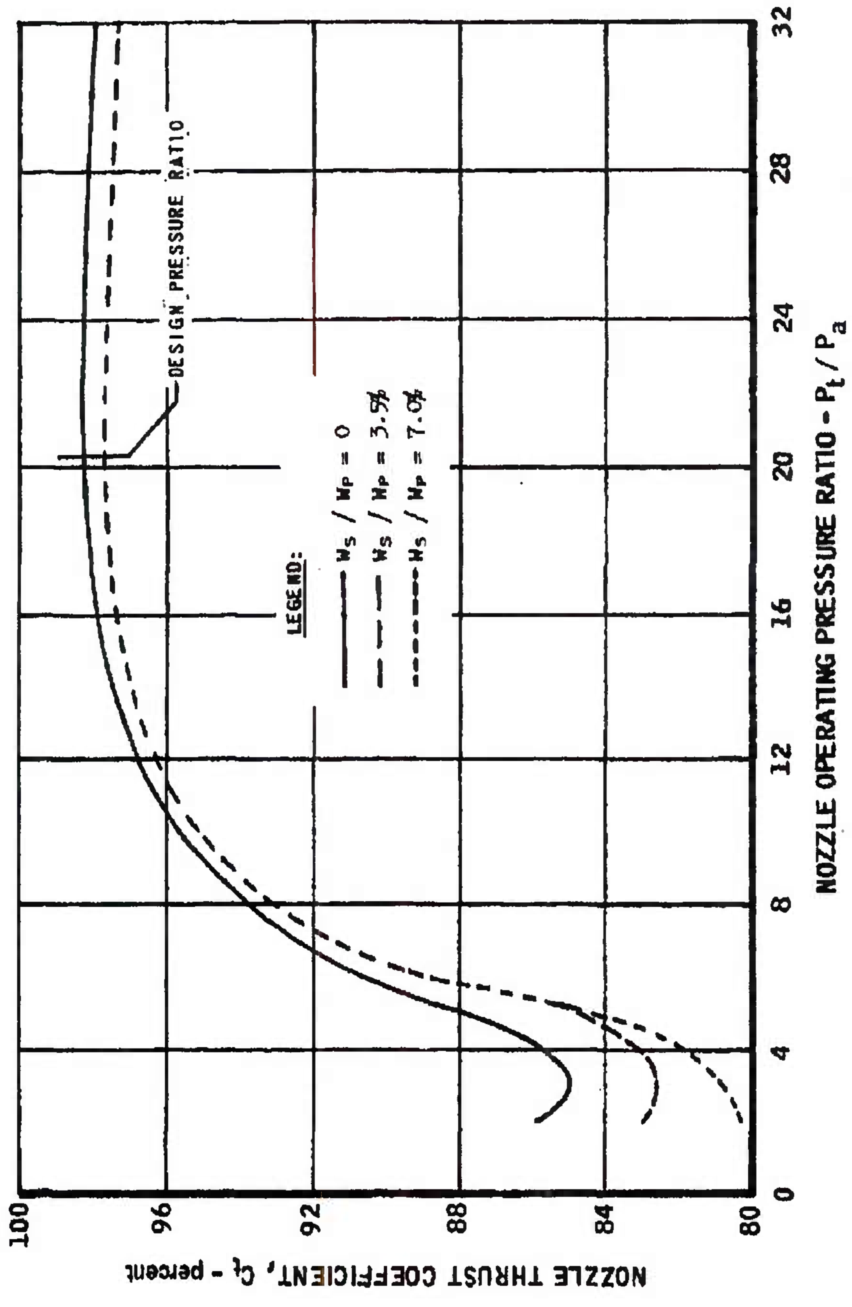

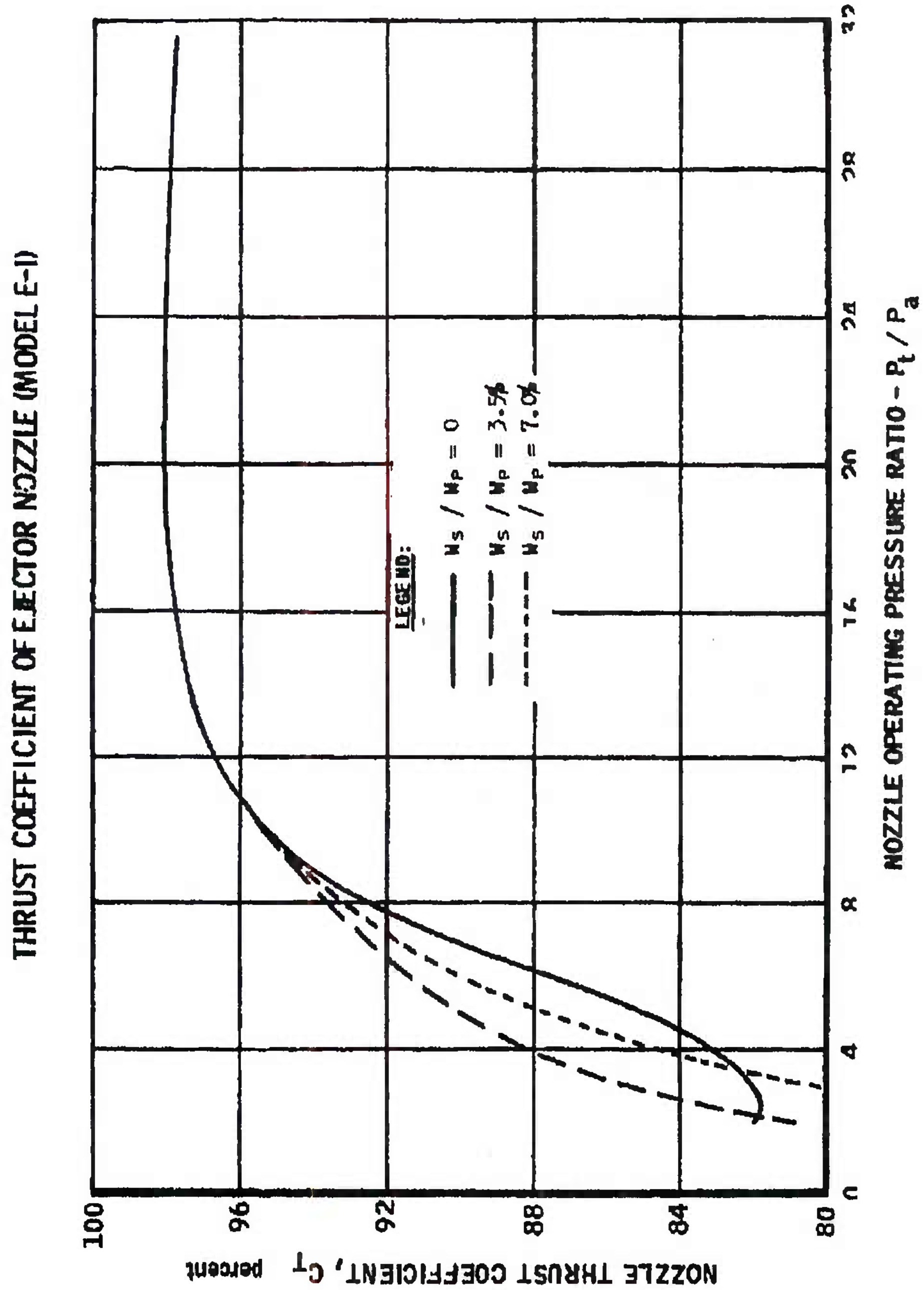
THRUST COEFFICIENT OF EJECTOR NOZZLE (MODEL E-I)
LEGEND:
$W_S / W_P = 0$
$W_S / W_P = 3.5\%$
$W_S / W_P = 7.0\%$
NOZZLE THRUST COEFFICIENT, C_T percent
100
96
92
88
84
80
NOZZLE OPERATING PRESSURE RATIO - P_t / P_a
0
4
8
12
16
20
24
28
32

against expansion ratio in Figure 105. The composite data shown are the a er-age of data taken from each of the four primary models. Very little variat n in local wall pressure ratio existed between models. The deviations from ie-dimensional flow that are shown were consistent with expected trends in ax lly symmetric flow.

Figure 106 is a shadowgraph of the exhaust flow from Model FC-3 t design pressure ratio. The weak shocks visible in the exit were generated n the nozzle wall from a slight reduction in local expansion rate along the wa that coalesced into the weak shocks visible at the exit. This condition indi ted that the wall curvature approximately 3 inches downstream from the throat 'as slightly excessive. The wall pressure distribution contained no apparent l al variation, which tends to indicate that the shocks did not retain their single lis-continuity identity completely upstream to the wall. Very weak shocks in t divergent section of a propulsion nozzle have no significant effect on the th ıst efficiency of the nozzle. The high thrust coefficient of the subject nozzle v 'ifies this.

The low nozzle contour curvature through the throat region result in a discharge coefficient of 0.991. Values of discharge coefficient computed rom data taken from all five primary nozzle configurations were essentially ide ical, because all convergent contours were identical. No particular trend of var ıtion with pressure ratio was apparent, indicating that the discharge coefficient as constant over the complete operating range.

Results of the experimental program are thus quite encouraging. ozzle thrust coefficients of 98 percent or better have been achieved for both force con-vection and ejector configurations. Further, it is anticipated that full scal nozzles will yield even better thrust coefficients, because the performance 'ill improve with Reynolds number. Also, improved performance can be expe ed for the ejector configuration, because the primary nozzle liner thickness i the model was greatly out of proportion to the nozzle throat diameter and creat d a relatively large disturbance in the nozzle flow field. These results will l further studied to indicate the desirability of nozzle contour changes, pres re losses in the secondary cooling systems, and nozzle installation optimizati ı.

3.8.3 Aerodynamic Coupling Tests

General

The purpose of the aerodynamic coupling test was to investigate su -pected problem areas that were revealed by analytical studies.

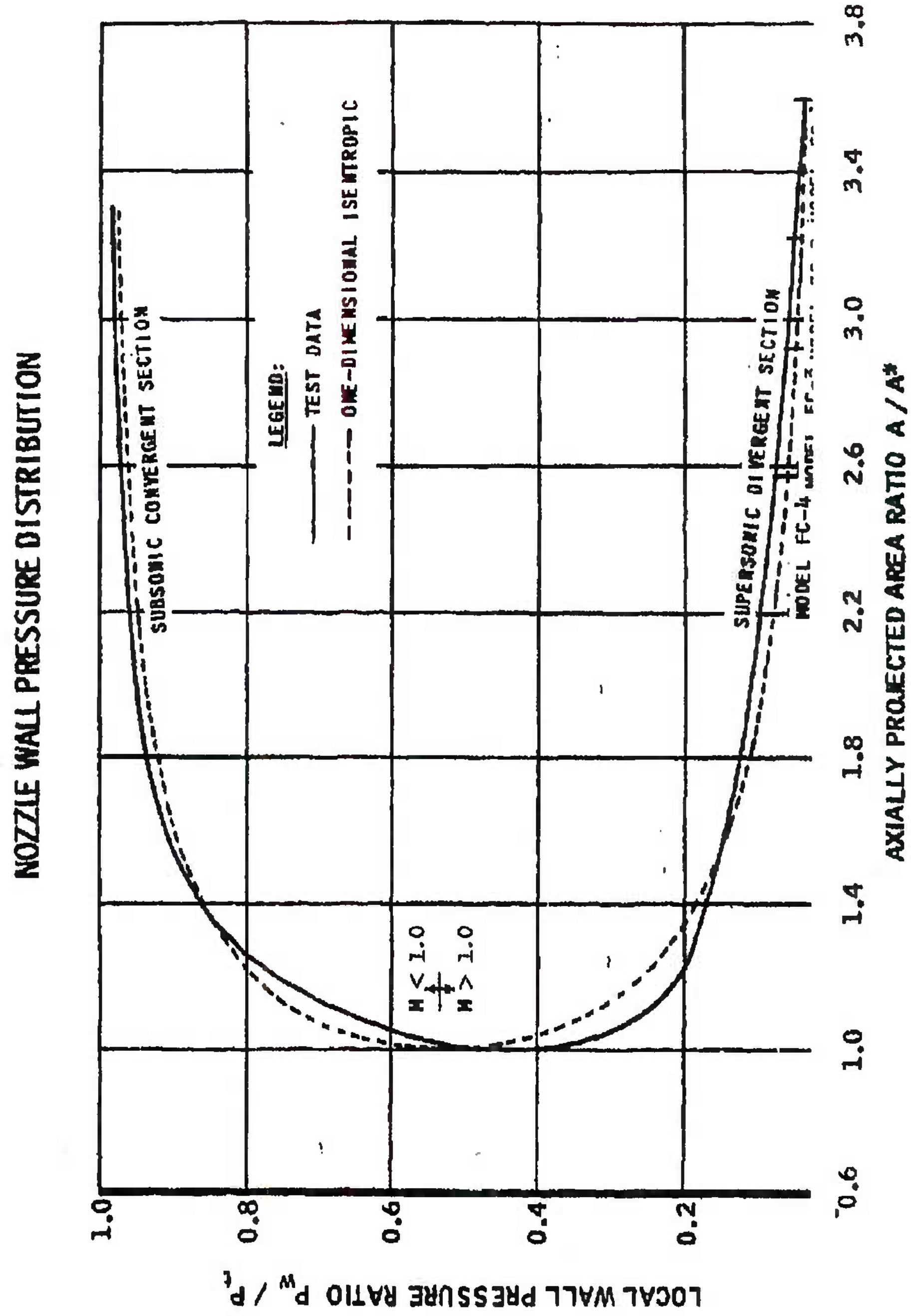
NOZZLE WALL PRESSURE DISTRIBUTION
LEGEND:
TEST DATA
ONE-DIMENSIONAL ISENTROPIC
SUBSONIC CONVERGENT SECTION
SUPERSONIC DIVERGENT SECTION
MODEL FC-4
M < 1.0
M > 1.0
1.0
0.8
0.6
0.4
0.2
LOCAL WALL PRESSURE RATIO P_w / P_t
0.6
1.0
1.4
1.8
2.2
2.6
3.0
3.4
3.8
AXIALLY PROJECTED AREA RATIO A / A*

FIGURE 105

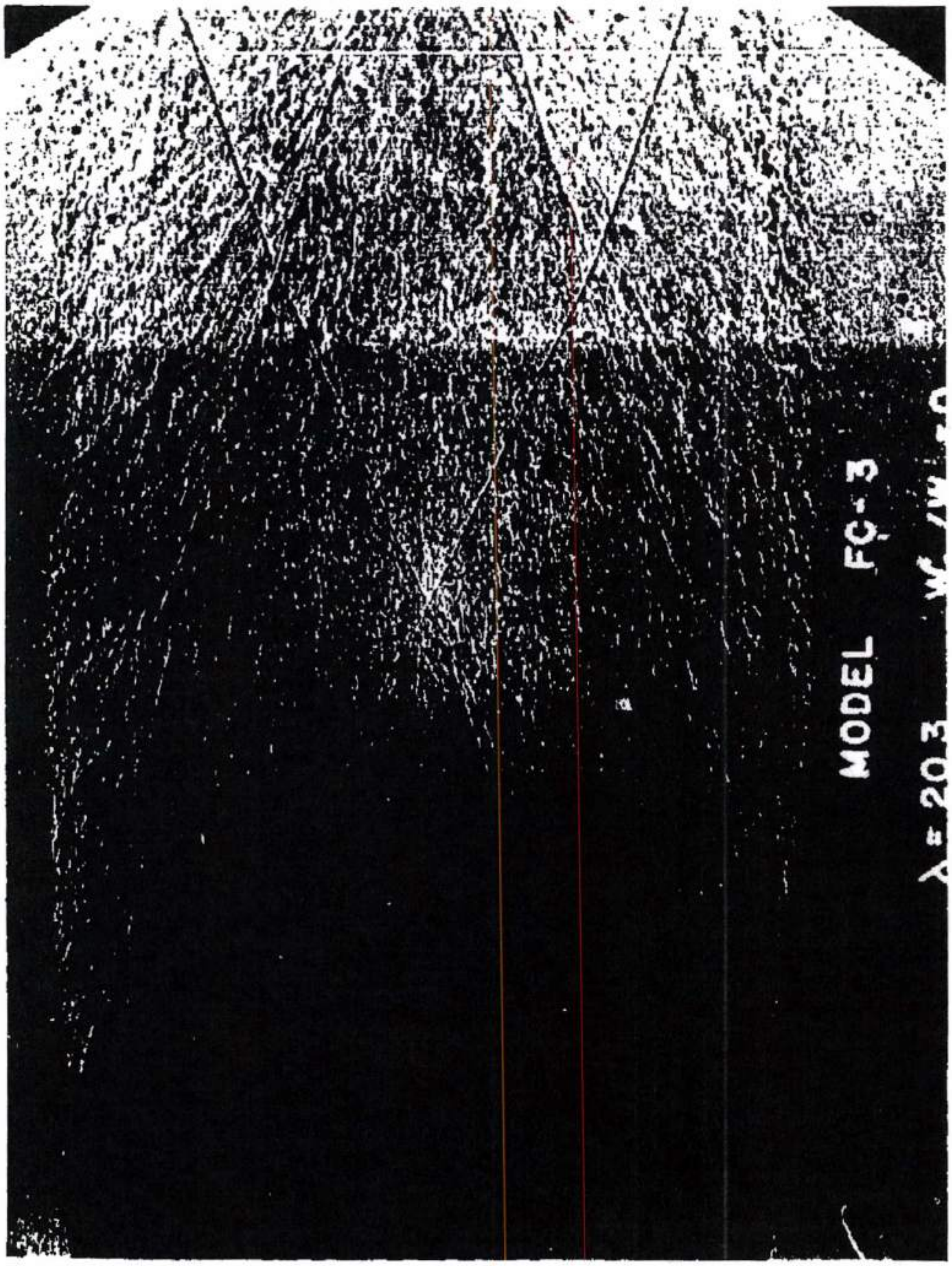

C4074-2

FIGURE 106 - Shadowgraph of Exhaust Flow from Forced Convection Nozzle at Design Pressure Ratio

The primary areas of investigation are discussed below:

(1) The results of rather tedious hand calculations to dete nine the effect of typical diffuser exit profiles on the performance of the nuc ar ramjet engine were presented in Reference 25. For this study, the methoc of approach involved satisfying mass and momentum relationships while maintai ng the reactor exit static pressure at the undisturbed or uniform flow value. From early single tube analyses, it was concluded that the reactor overall pres ıre drop probably would be a controlling factor in determining the flow-strai; tening ability of the reactor. A simplified method of analysis, which cons ved neither mass nor momentum, was then made to determine qualitatively the fect of pressure drop and flow straightening. The results of the simplified stuc (reported in Reference 7), in conjunction with the previous analysis of Refere ce 25, lead to the comparison of profile straightening parameters presented in gure 107.

The analyses indicate that the reactor is an effective flow raightener; i.e., the tube weight flow perturbations due to an imposed total pre ure profile are reduced. In particular, these studies indicate that local reacto wall temperature increases due to tube weight flow reduction with imposed p ofile are small and tolerable. The primary purpose of the aerodynamic coup ng test was, therefore, to provide an experimental verification of the analytical edictions.

(2) At the reactor rear face, pressure distortions, and he ce, tube weight flow perturbations may result from the multiple flow passag lischarge, structural blockage, and flow mixing. In addition, the convergent p rtion of the exit nozzle may impose a further static pressure distortion if physi al coupling is too close. Attempts to evaluate these items by literature survey and analytical predictions were not satisfactory. Thus, the second purpose o the aerodynamic coupling test was to provide experimental data on pressure d tortions at the rear face of the reactor.

(3) A third area, later considered, was the determination f reactor noise generation levels. It was anticipated that noise measurement obtained for a representative reactor configuration would give some insight i to problems of this nature that might exist in the full scale reactor.

Thus, this type of test and associated hardware could prod ce data that would aid directly in nuclear propulsion system analysis and would a valuable tool in verifying analytical models and concepts.

COMPARISON OF PROFILE STRAIGHTENING CHARACTERISTICS
MA50XA-1 AT DESIGN POINT

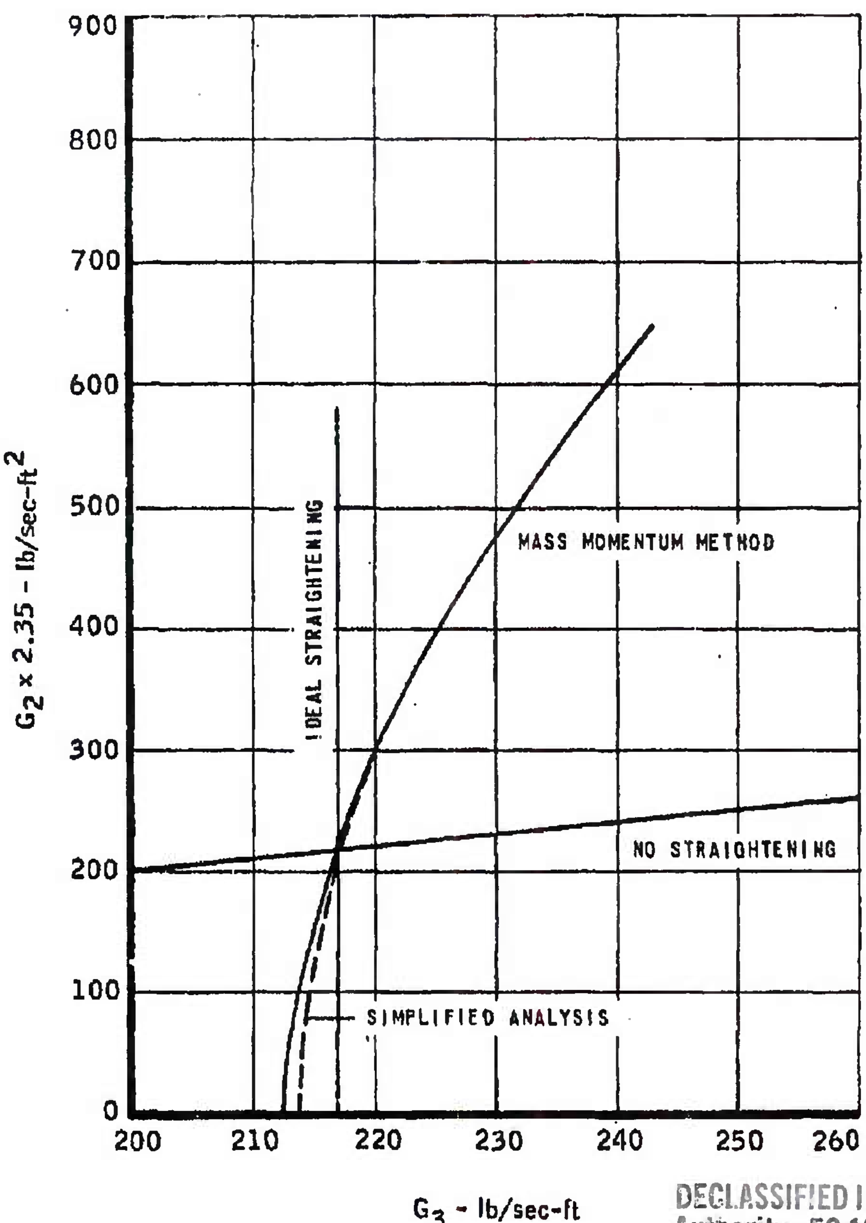

Aerodynamic Coupling Test Hardware

The use of a simulated full-length reactor section was pre cated on the belief that only with a full-length section could a realistic react : pressure drop be obtained. A test section diameter was established at 18 in es for the following reasons:

(1) A test section of this size would provide a centrally lo ated Tory IIC standard unit cell free from any duct wall airflow effects.

(2) A test section of this size would provide a simulated c ntrol rod and tie rod unit cell that at some later date could be evaluated with the tached up-stream control rod drive rod and actuator mechanisms. It was felt hat the air-flow blockage of the actuator mechanisms, which were not fixed in ometry at the time of coupling hardware design, could not be simulated in a d t diameter smaller than 18 inches.

(3) Airflow requirements for a test item of a larger diam er would compromise desired operating times.

The aerodynamic flow lines of the Tory IIC reactor were s nulated as closely as possible; however, some modifications in construction a l assembly methods were required to facilitate instrumentation and to reduce h rdware costs.

The simulated Tory IIC reactor section or module, which referred to as the "tube bundle," is constructed of aluminum hexagonal tube of the size and arrangement similar to the Tory IIC. These tubes are held lon tudinally by two end retainer plates secured by rods that pass through the ra al segment blocks. The radial segment blocks, which restrain the tube bundle aterally, are further secured by steel strapping around the circumference. Figu e108 is a photograph of the test item partially assembled. Figure 109 is an : view of the assembled tube bundle showing the steel strapping. The large t be is the control rod tie tube. The aft retaining plate and an instrumentation late had not yet been installed. Figure 110 is a photograph of the aft plate s owing the general arrangement of instrumentation and the size of tubes used. Figure 111 shows the completed tube bundle assembly installed in the 18-inch ct. This view shows the front face instrumentation and the simulated control rod inserted into the control rod tie tube.

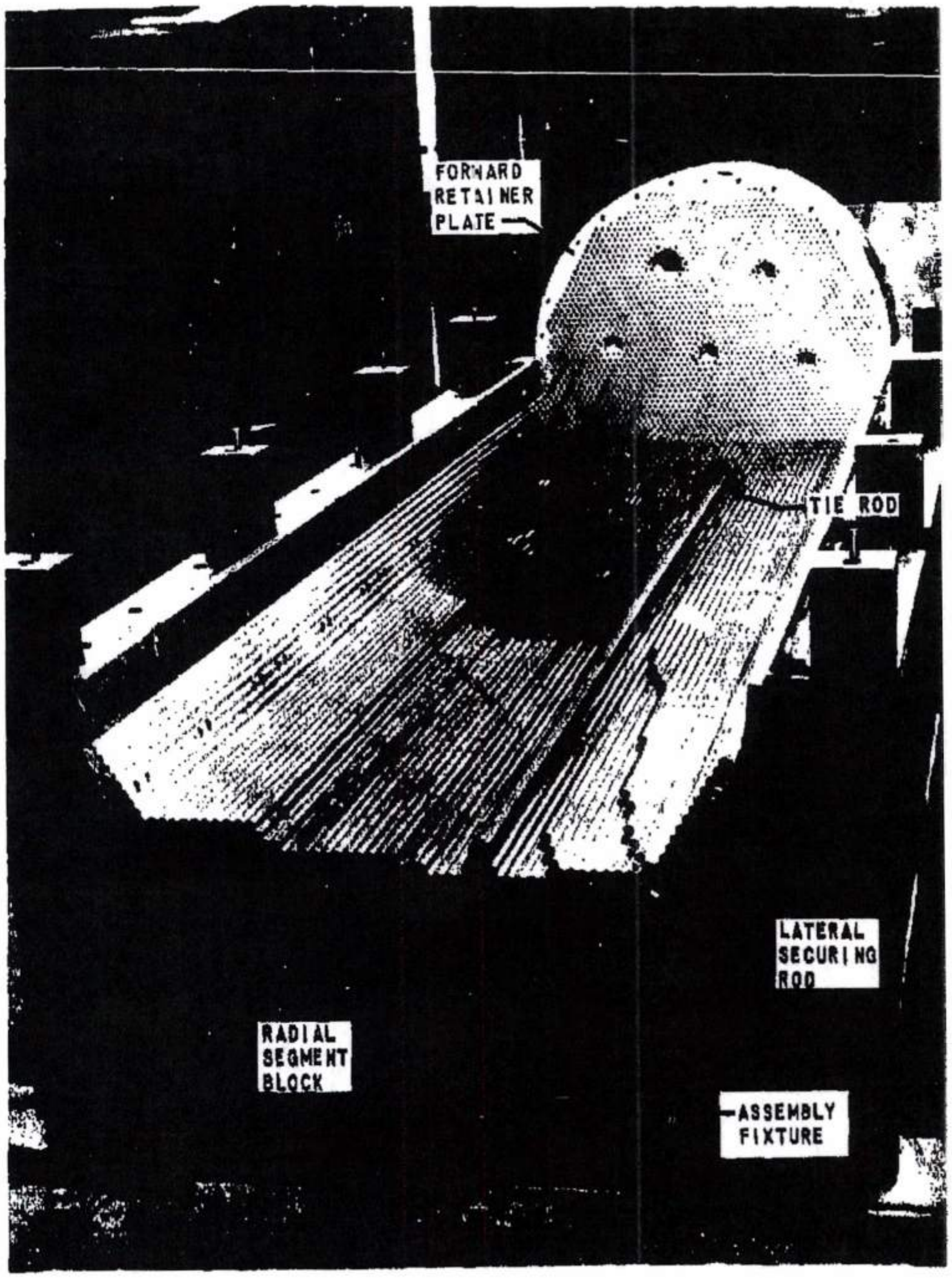

3946-2

FIGURE 108 - Buildup of Simulated Reactor Segment for Aerodynamic Coupling Test

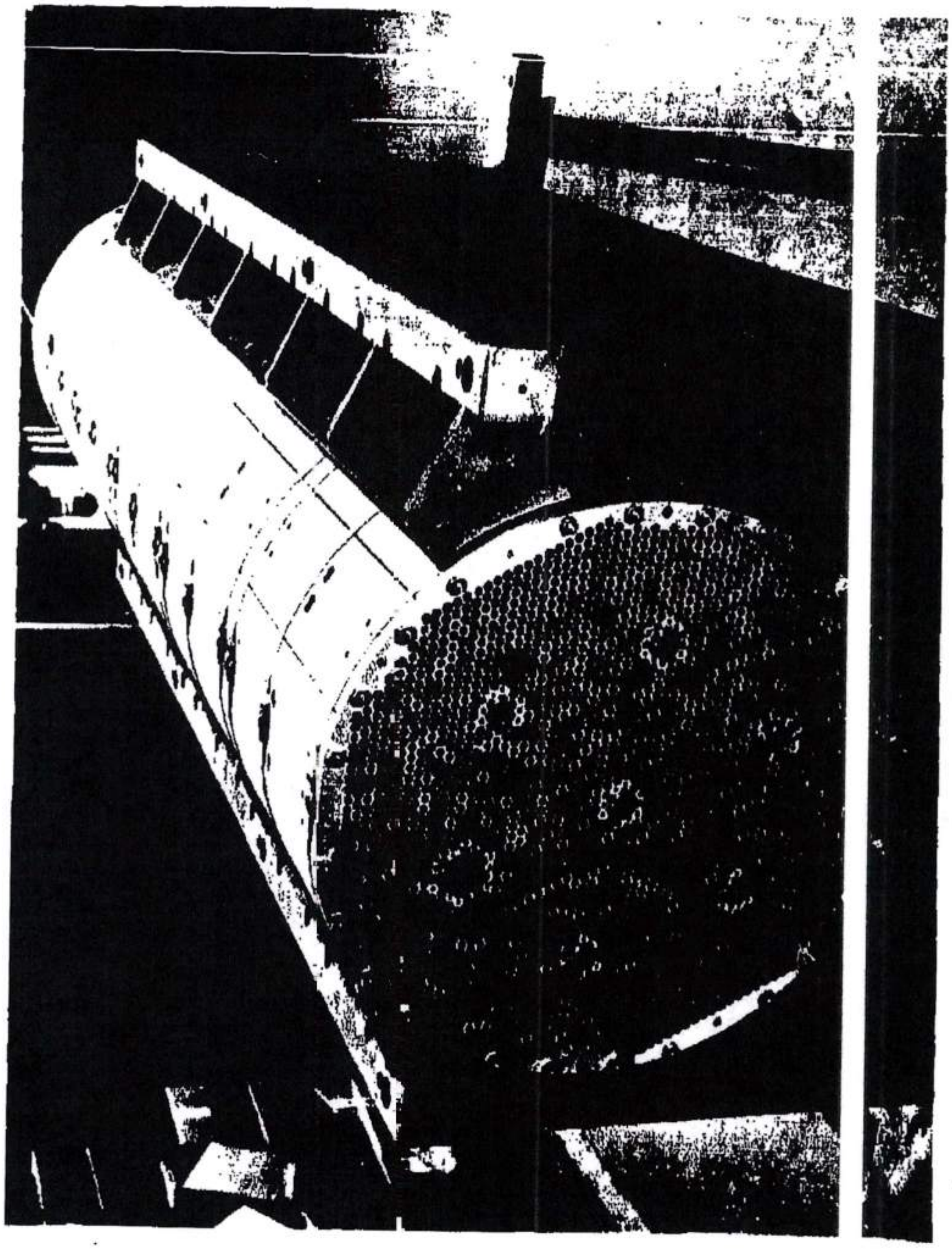

3946-5

FIGURE 109 - Completion of Buildup of Tubes in Simulated Reactor Segment

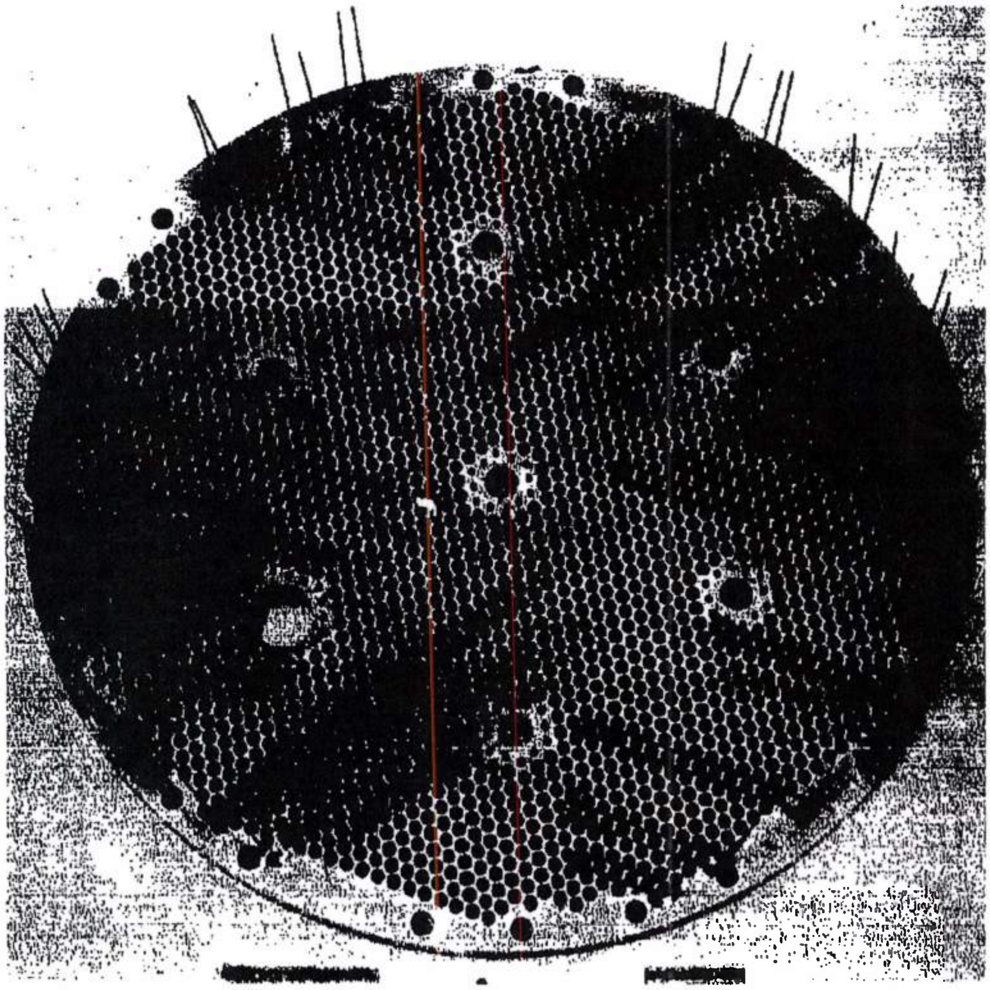

3946-4

FIGURE 110 - Aft Plate with Instrumentation and Tubes Used to Build Up Simulated Reactor Segment

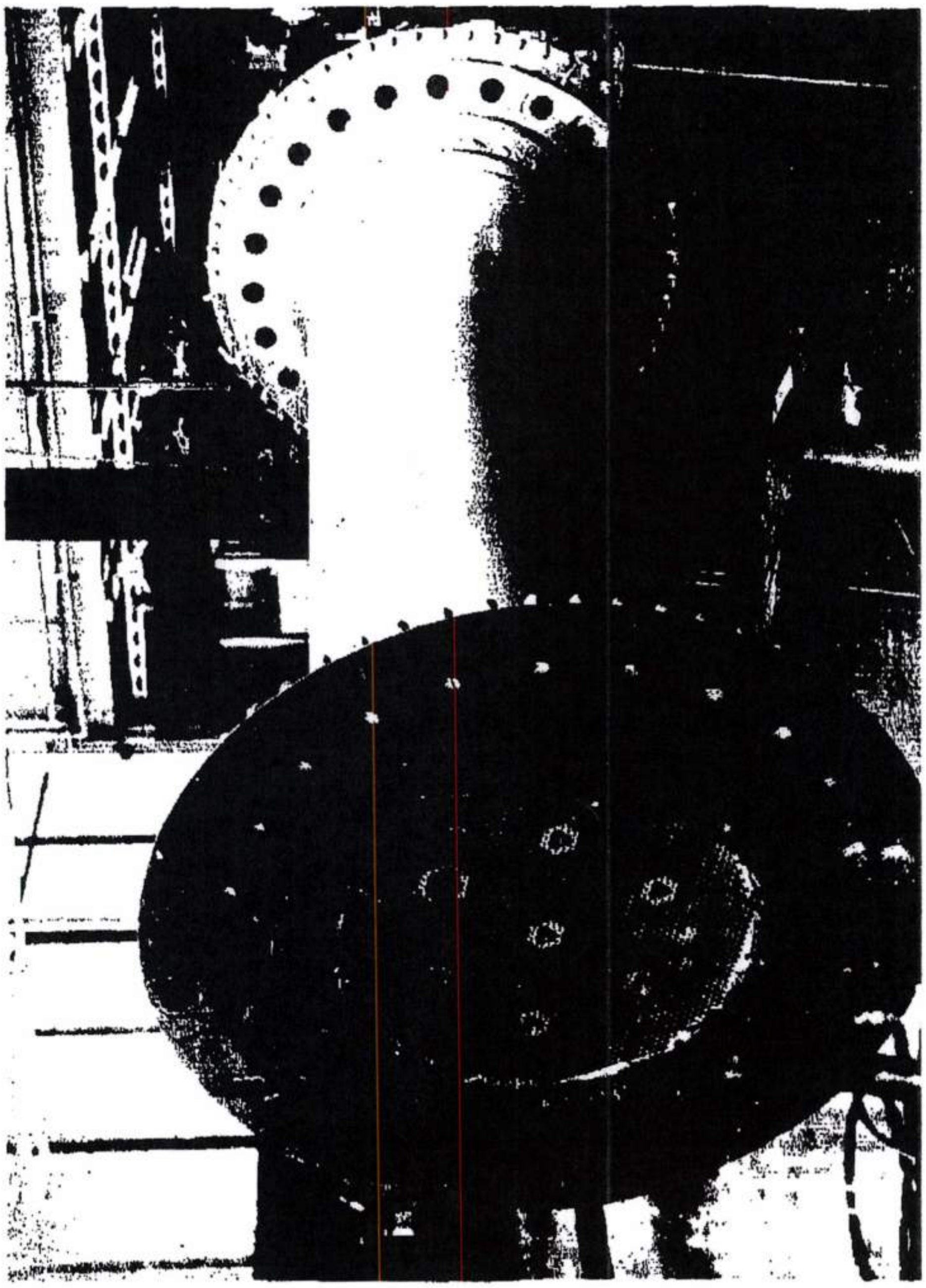

3946-9

FIGURE 111 - Simulated Reactor Segment Installed in 18-inch Duct

Test Plan

The test plan was formulated on the basis of four test phases. In th first phase, the plan was to generate a pressure profile and to determine thi profile at the face position of the reactor test section without the test section being installed.

In the second phase, the basic test section, with instrumentation, w ld be installed and tested with the same profiles. (The basic test section consi of the bundle of aluminum hexagonal tubes and the end retainer plates.) Test results from the first phase would be used to evaluate the validity of the anal i-cally predicted pressure profile effects discussed earlier.

In the third test phase, the simulated fore and aft reactor support structures were to be added to the basic test section. However, between con ceptual design and actual testing, it became evident that this configuration wc ld be of secondary importance because of the changing Tory IIC fore and aft su ort design and the design of a flight type reactor. This phase was therefore dro ed as an immediate test objective.

The final test phase was devoted to the investigation of reactor-nozz coupling length. Three nozzle positions were evaluated with a flat pressure o-file upstream of the test section.

All test runs were accomplished with a constant airflow of 70 pps at ambient temperature for full Reynolds number simulation at the tube exit and at a tube exit Mach number closely simulating actual reactor conditions.

The pressure instrumentation for the complete test item including m a-surement of total airflow, individual tube airflows, and duct pressure profile totaled about 150 individual pickups. Figure 112 shows schematically how so e of this instrumentation was used to obtain tube Mach number, airflows, and pressure drops. Figure 113 shows the test item installed in the cell.

Test Results

Only a gross analysis of the test data has been accomplished at this me to establish overall results and to determine the presence of any outstanding unexpected trends. A detailed discussion of the results, which will be compa ed to analytical predictions where possible, will be presented in the next progre report.

SCHEMATIC OF COUPLING TEST INSTRUMENTATION

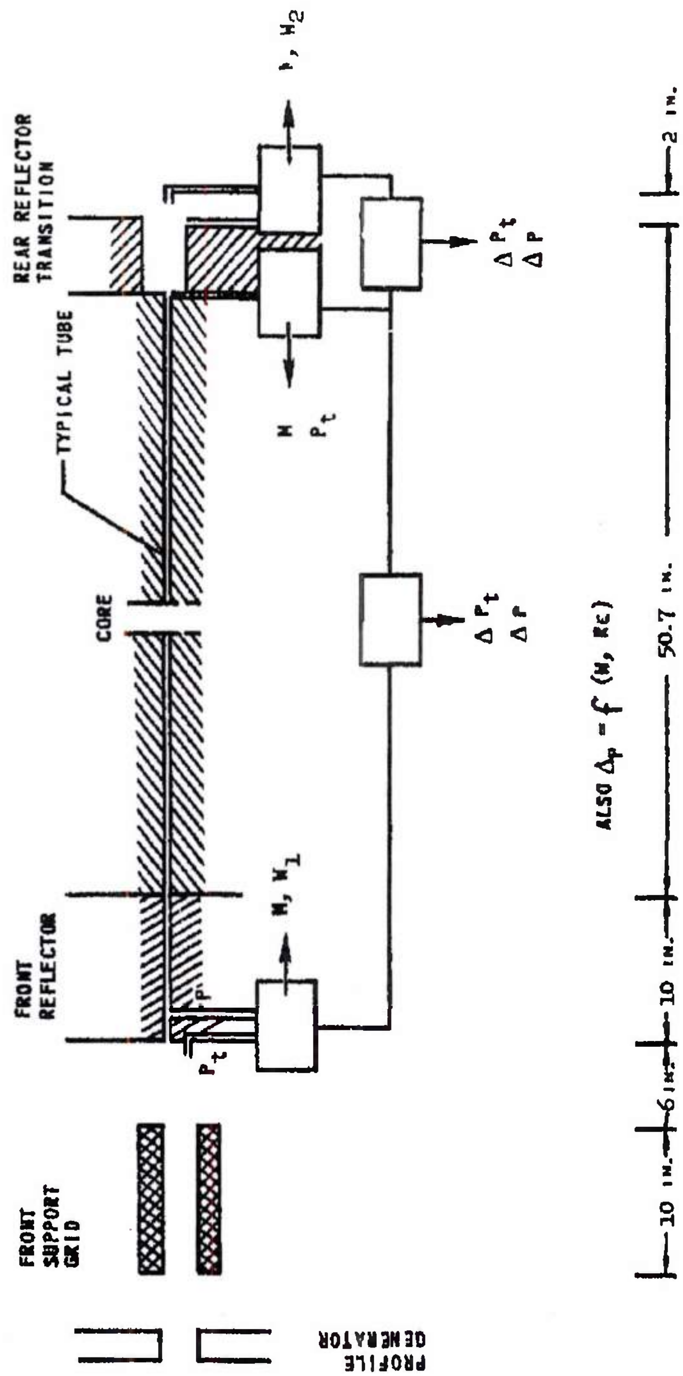

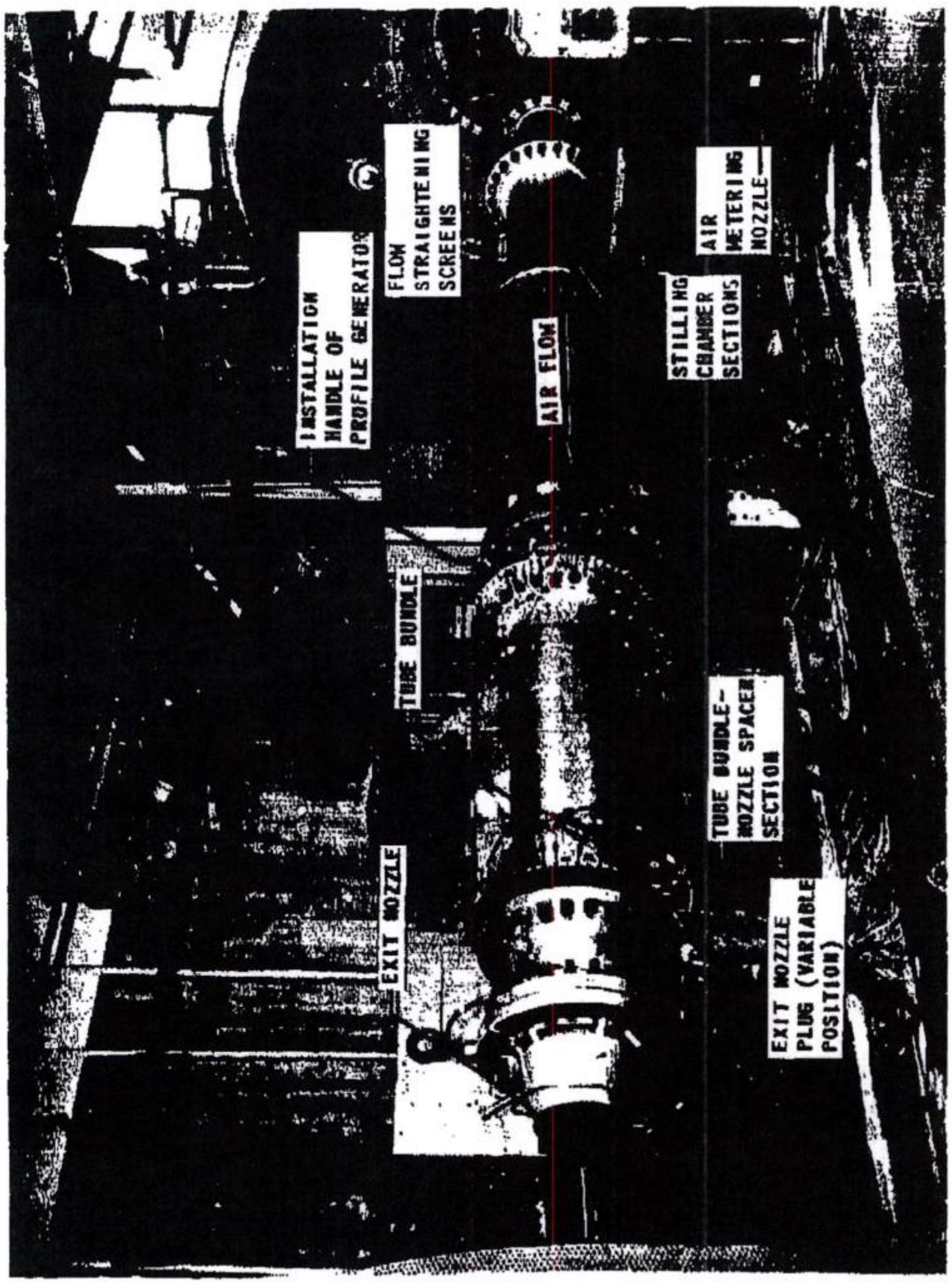
INSTALLATION HANDLE OF PROFILE GENERATOR
FLOW STRAIGHTENING SCREENS
AIR FLOW
STILLING CHAMBER SECTIONS
AIR METERING NOZZLE
TUBE BUNDLE
EXIT NOZZLE
TUBE BUNDLE-NOZZLE SPACER SECTION
EXIT NOZZLE PLUG (VARIABLE POSITION)

T2972-3

Airflow distribution results, for imposed profiles and exit ozzle coupling length variation, are discussed below for the simulated fue d core tubes (D_e = 0.229 inches), which pass about 90 to 95 percent of th total airflow.

<u>Imposed Profiles</u>

Two types of total pressure profiles (in addition to the lat profile) were imposed at a distance of 14 inches (L/D_R of 0.8) upstream of .e tube bundle face by inserting unchoked concentric or eccentric orifices i the 18-inch ducting. Duct pressure distortions were measured about 2 inches c wnstream of the orifice (12 inches upstream of the tube bundle). The total press re was again measured on the fore and aft faces of the tube bundle for a dis rete number of tubes. The static pressure for the same tubes was measured jus downstream of the tube entrance and again at the tube exit.

Two test points, Figures 114 and 115, are presented f : the case of essentially flat profiles to be used later for comparing profiles a l the effects of exit nozzle coupling length. Total pressure distortion in percent s indicated and is computed as:

$$\left(\frac{P_{T_{max}} - P_{T_{min}}}{P_{T_{avg}}} \right) \times 100$$

Using this method of computing distortion, the sign of the answer w l always be positive.

For the detailed analysis to be presented in the next p gress report, the following distortion parameters will be used:

$$\frac{P_{T_{max}} - P_{T_{avg}}}{P_{T_{avg}}}, \quad \frac{P_{T_{min}} - P_{T_{avg}}}{P_{T_{avg}}}$$

However, this type of analysis requires manually computed, zone-v ighted, pressure- and airflow-averaged numbers. Time was not available accomplish this work.

AERODYNAMIC COUPLING TEST
DUCT STATIC AND TOTAL PRESSURE PROFILES
MEASURED UPSTREAM FROM TUBE BUNDLE ENTRANCE

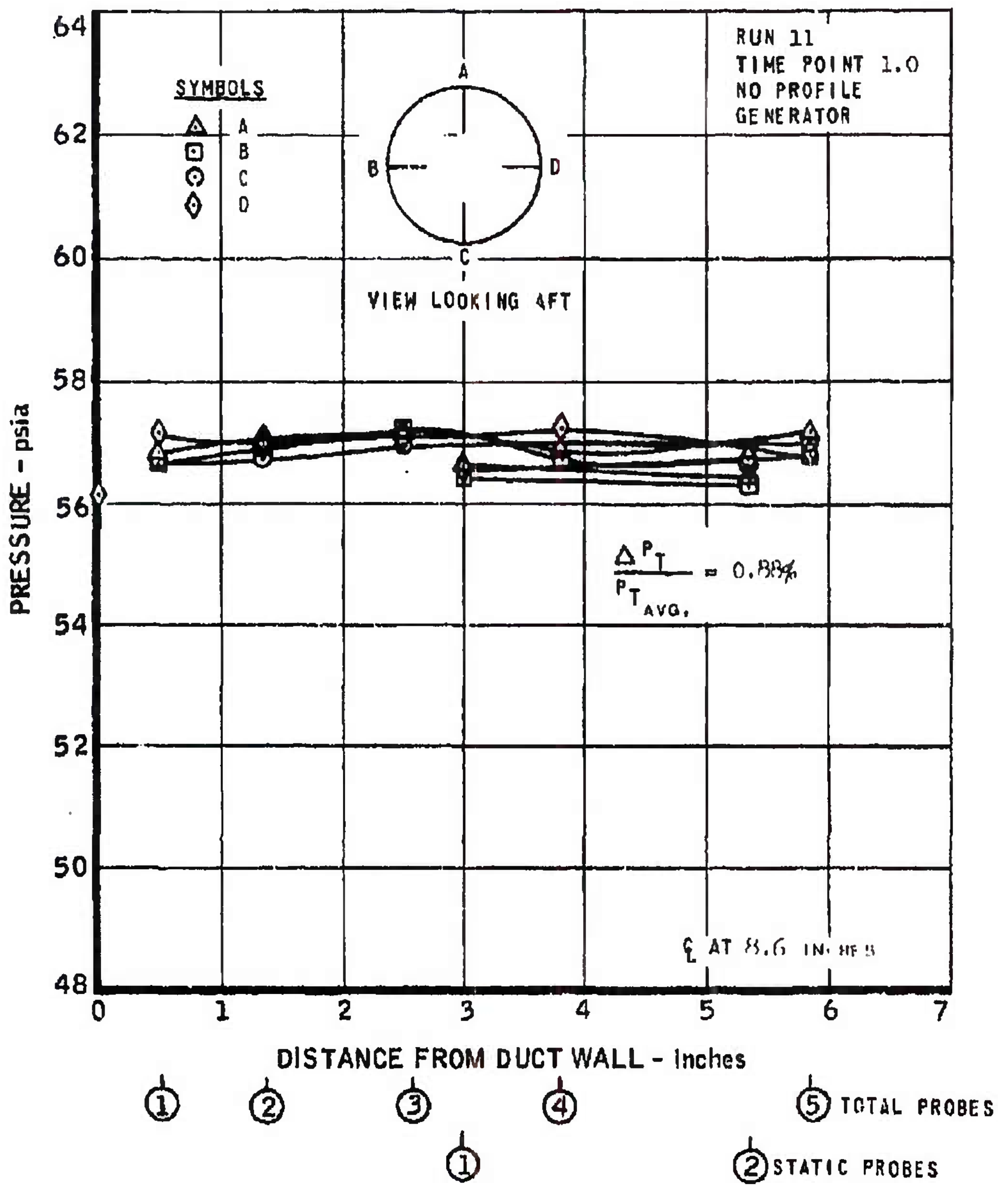

RADIAL STATION FROM DUCT WALL

AERODYNAMIC COUPLING TEST
DUCT STATIC AND TOTAL PRESSURE PROFILES
MEASURED UPSTREAM FROM TUBE BUNDLE ENTRANCE

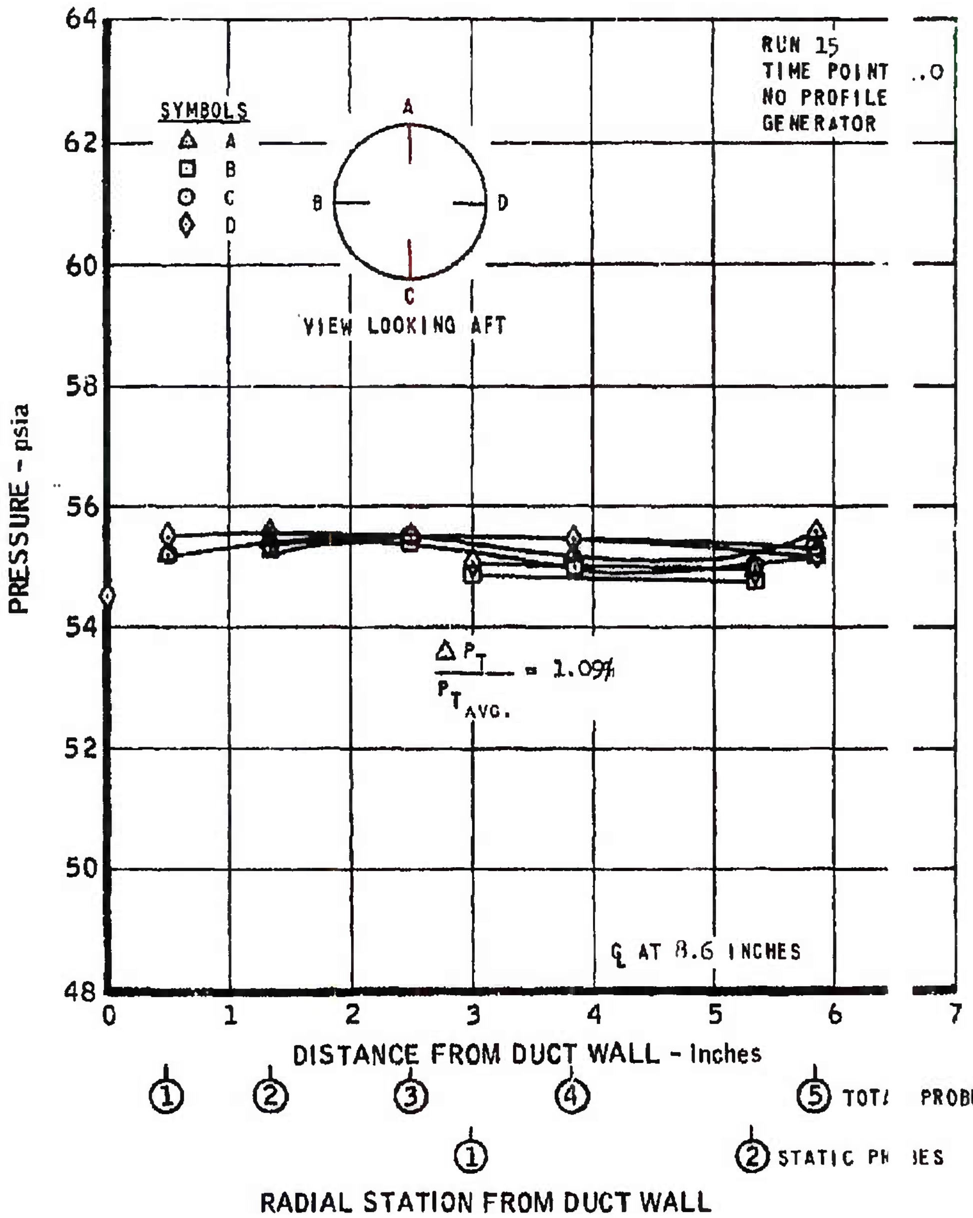

Figures 116 and 117 show the total and static pressure distorti ns at the module exit for Figures 114 and 115. Primary tube airflow rate is al) shown. Tube airflow distortion is presented and has been computed as:

$$\frac{W_{a_{max}} - W_{a_{min}}}{W_{a_{avg}}} \times 100$$

Figures 118 and 119 present the duct pressure profiles for con n- tric and eccentric profile generator orifices of the same size measured just downstream of the orifice plates. Although the same size, the eccentric pr ile generator (Figure 118) produces a higher distortion than does the concentric generator. Figures 120 and 121 present tube airflow and exit static distorti data, again measured at the tube bundle exit. Figure 122 presents the impo d duct profile generated by an orifice slightly smaller (but still unchoked) thar hat used for the previously discussed profiles. Figure 123 presents the corres nd- ing tube bundle exit data. Figure 124 presents gross airflow distribution an aft face static pressure distortion data. The data indicate a variation of exi face static pressure profile with imposed total pressure profile. The variat m of gross tube weight flow with imposed total pressure profile, while not com pletely analyzed at this time, is within 5 percent of the predicted value.

Exit Nozzle Coupling Length

Three exit nozzle coupling lengths were tested to determine whether the length of the nozzle coupling would impose a static pressure dis r- tion on the aft face of the module exit. Length is defined as the distance bet een the aft face of the module and the start of the converging portion of the exit nozzle. Nozzle couplings of the following three lengths were tested:

(1) A length thought sufficient to isolate any possible effects i - posed by the nozzle. This was a length, L/D_R, of 1.34, ere D_R = 17.25 inches (the internal diameter of the module du).

(2) A length described as "design," which originated from the Mach 2.7 design point concept of the Model MA50-XA-1 fu scale propulsion system. The "design" scaled length for t e coupling test hardware was L/D_R = 0.335.

AIR FLOW AND PRESSURE DISTORTIONS MEASURED AT TUBE BU DLE EXIT
RUN 11

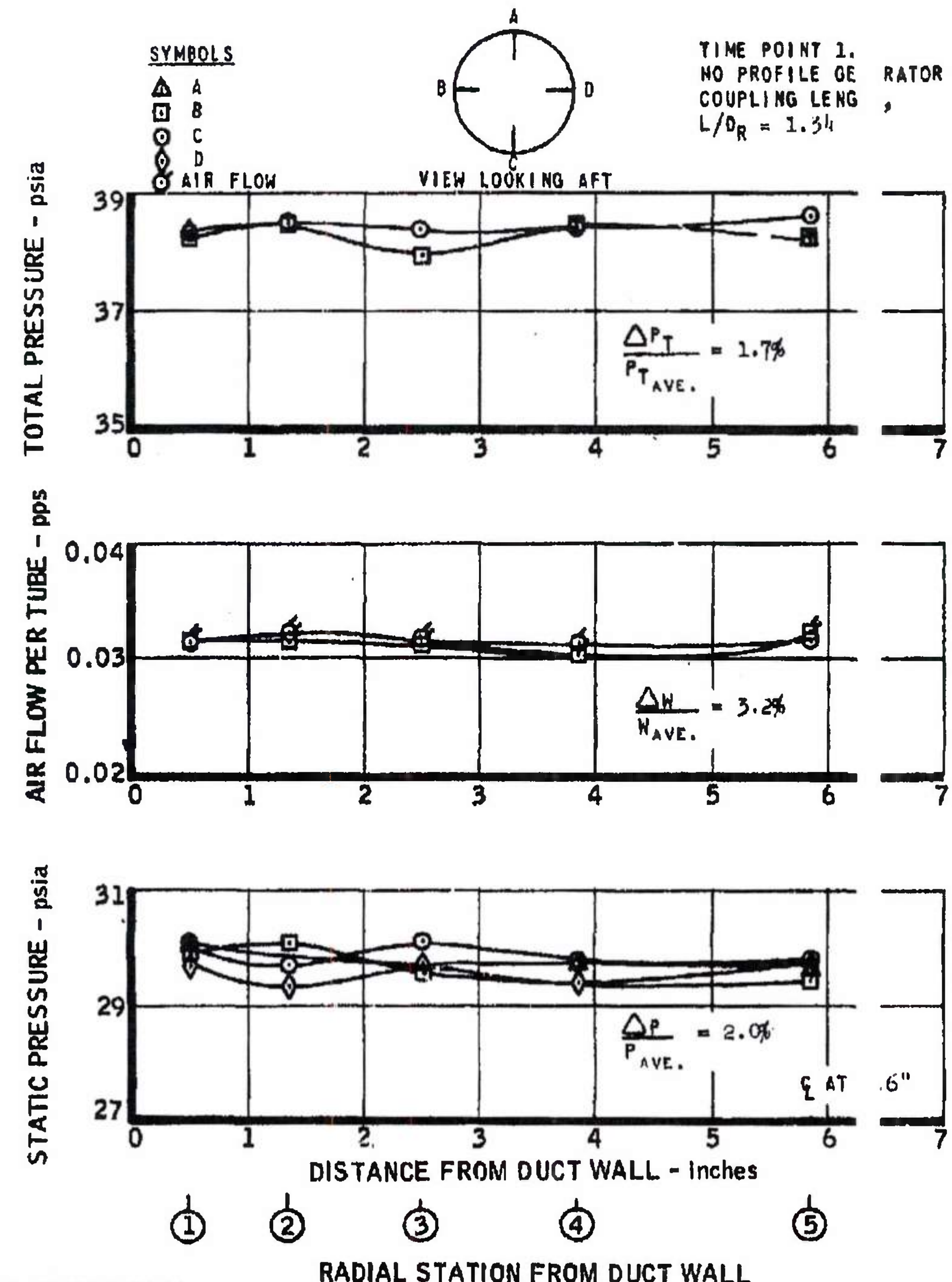

FIGURE 116

AIR FLOW AND PRESSURE DISTORTIONS MEASURED AT TUBE BUNDLE EXIT
RUN 15

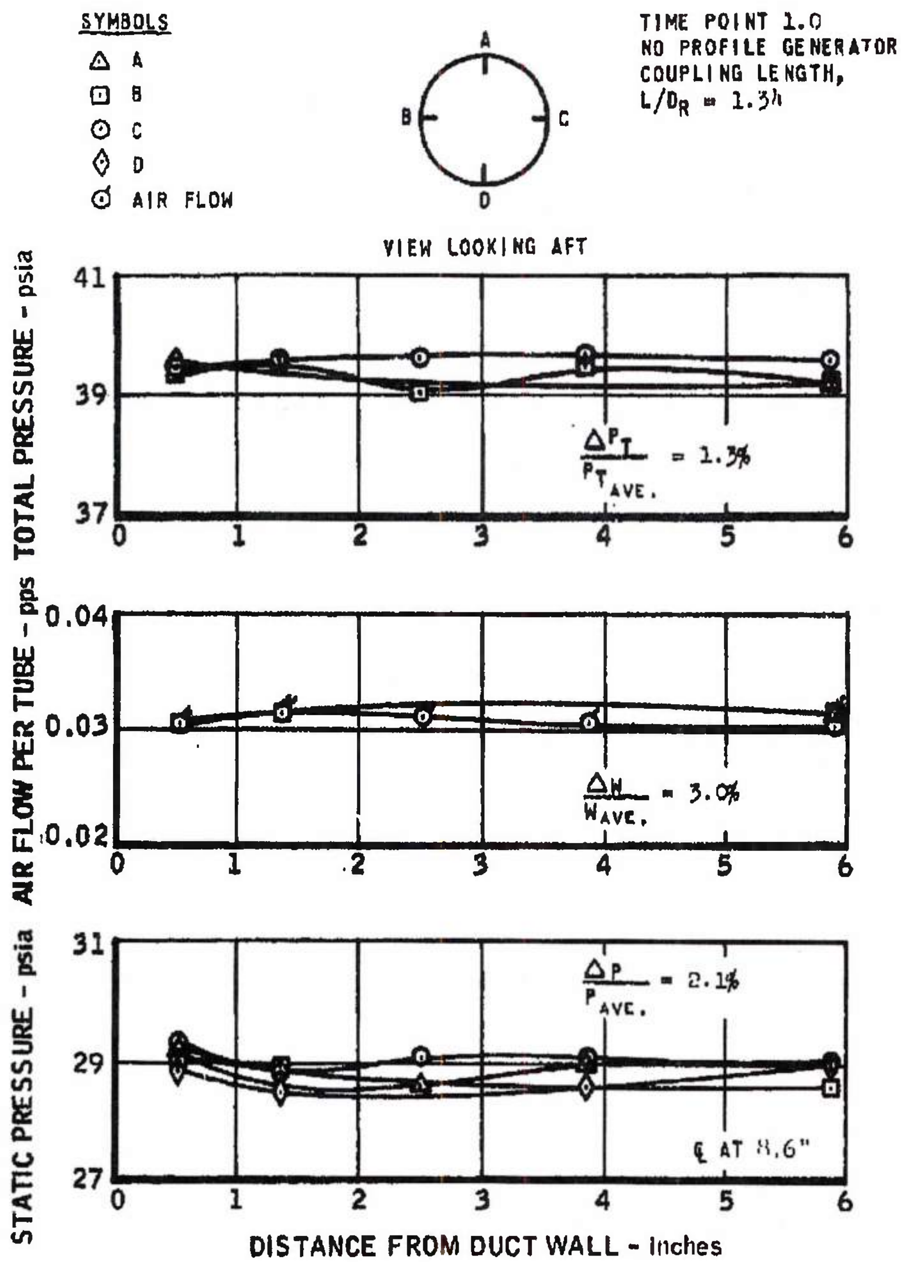

AERODYNAMIC COUPLING TEST
DUCT STATIC AND TOTAL PRESSURE PROFILES
MEASURED UPSTREAM FROM TUBE BUNDLE ENTRANCE

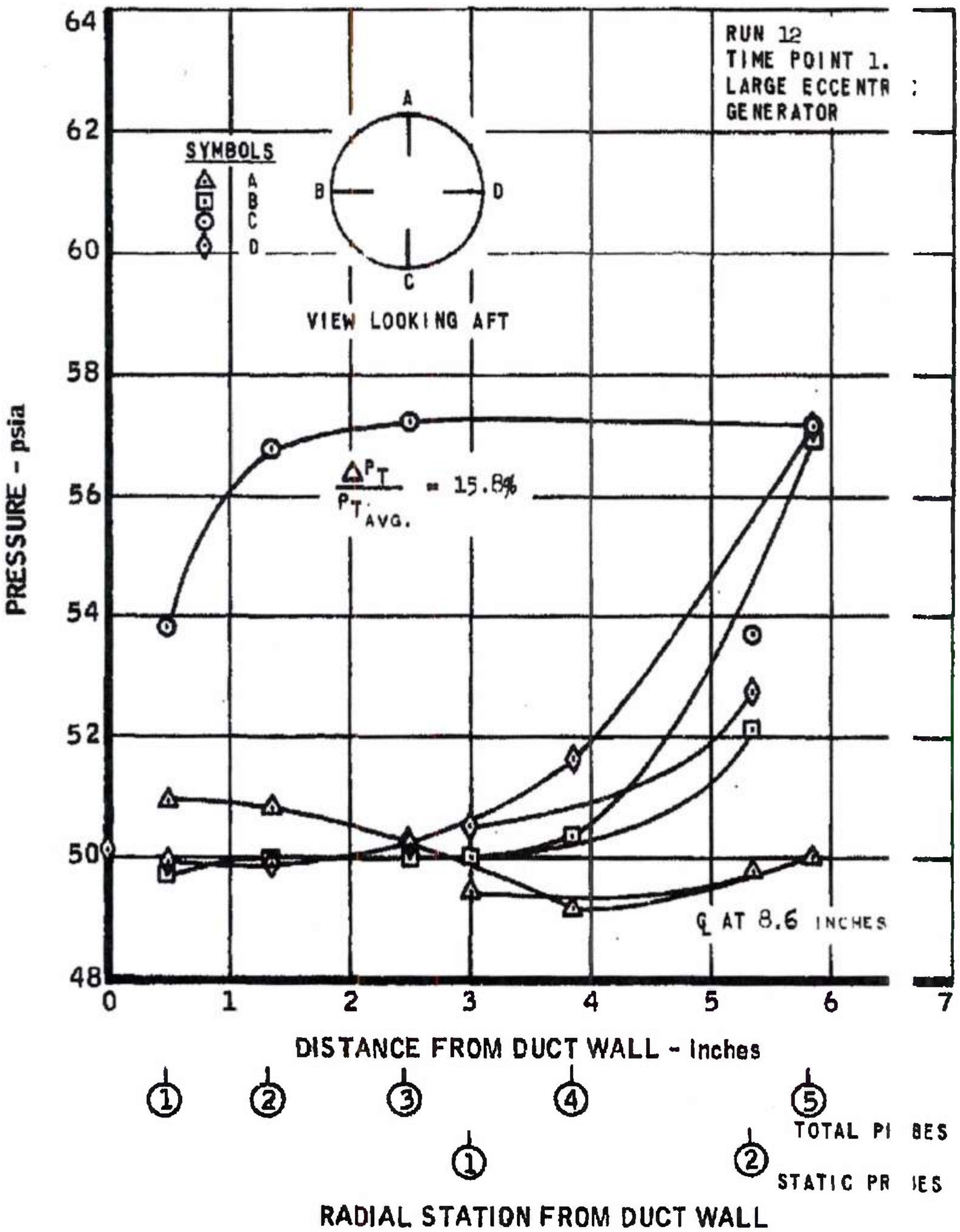

AERODYNAMIC COUPLING TEST
DUCT STATIC AND TOTAL PRESSURE PROFILES
MEASURED UPSTREAM FROM TUBE BUNDLE ENTRANCE

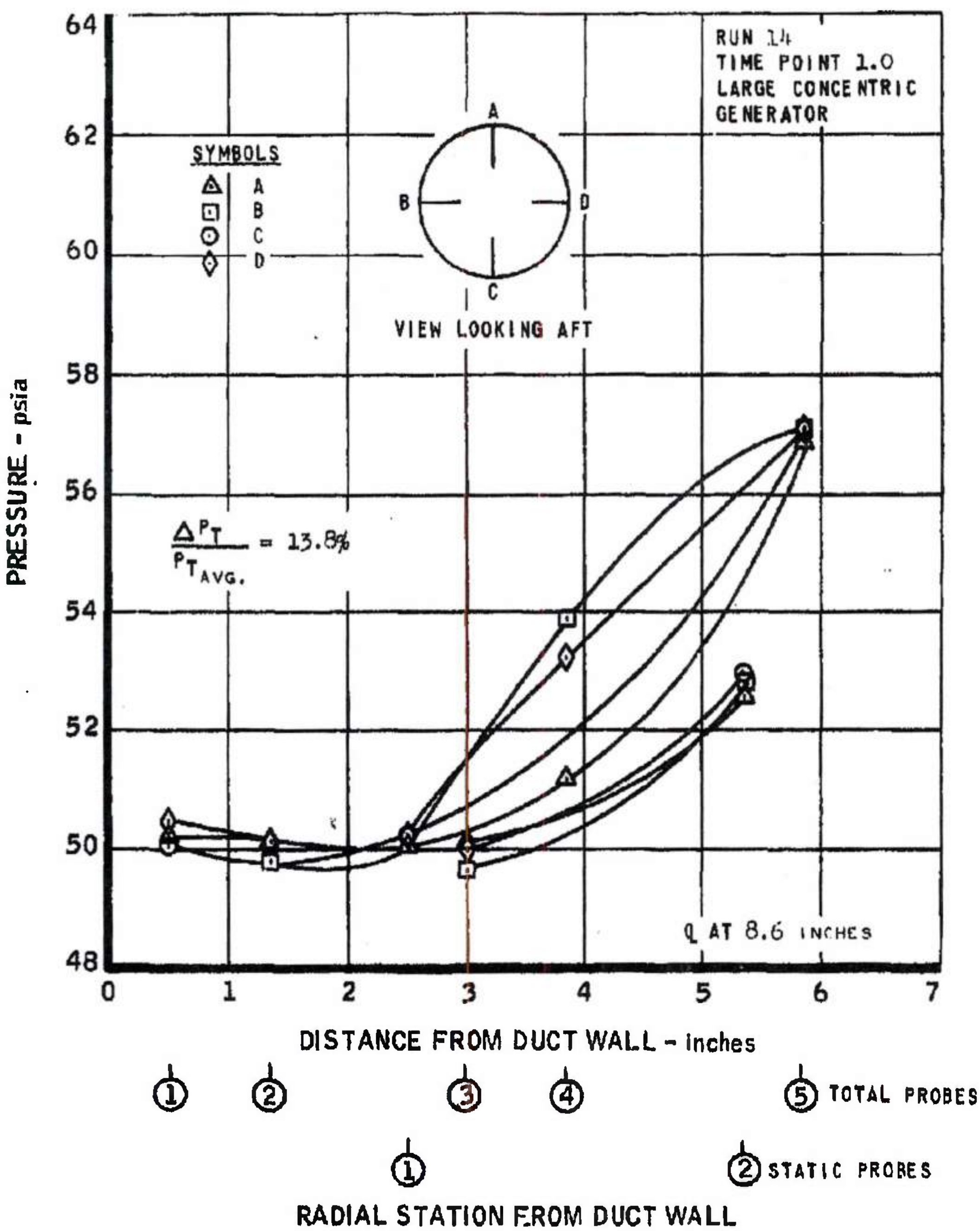

AIR FLOW AND PRESSURE DISTORTIONS MEASURED AT TUBE BU[illegible]DLE EXIT
RUN 12

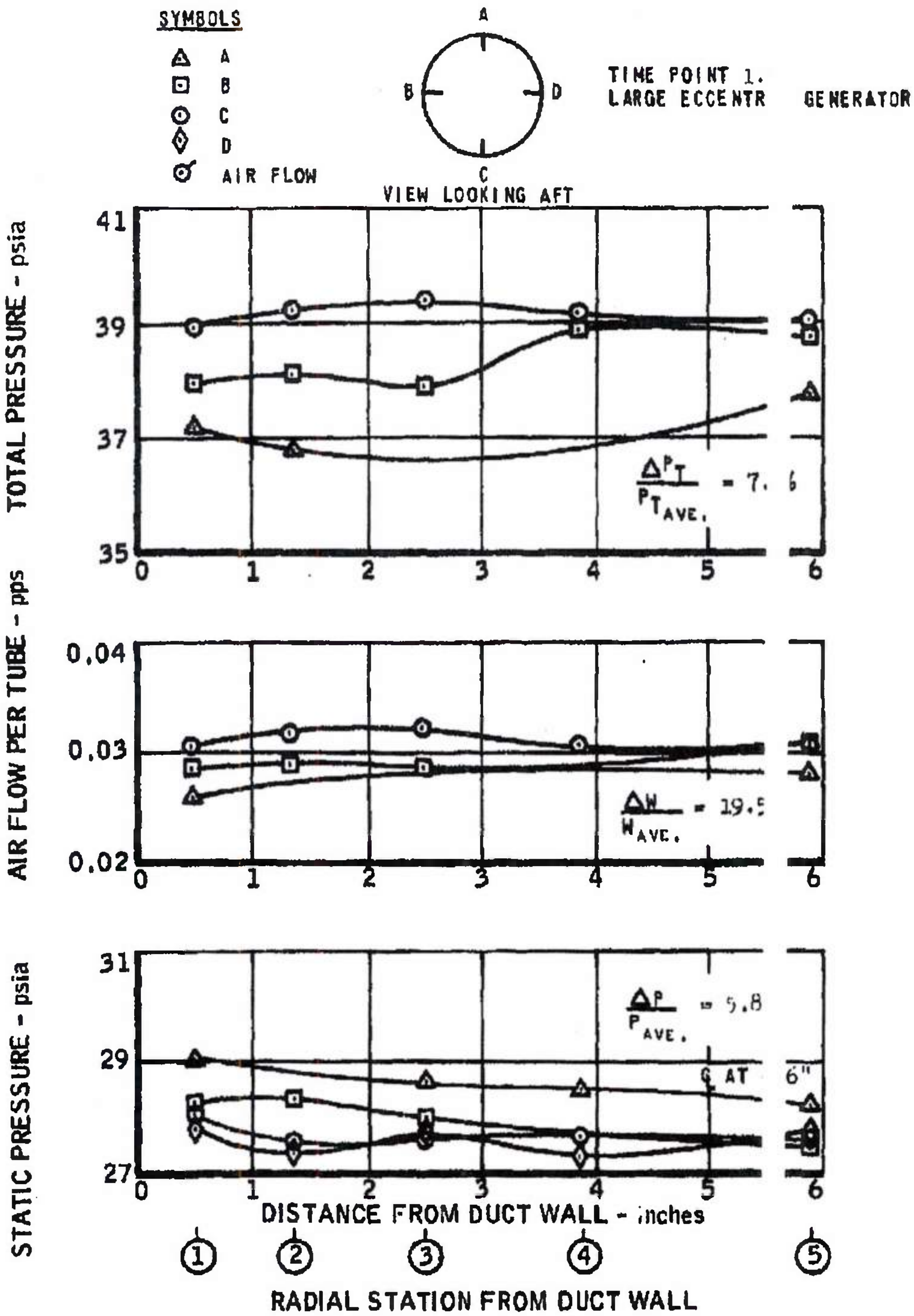

AIR FLOW AND PRESSURE DISTORTIONS MEASURED AT TUBE BUNDLE EXIT
RUN 14

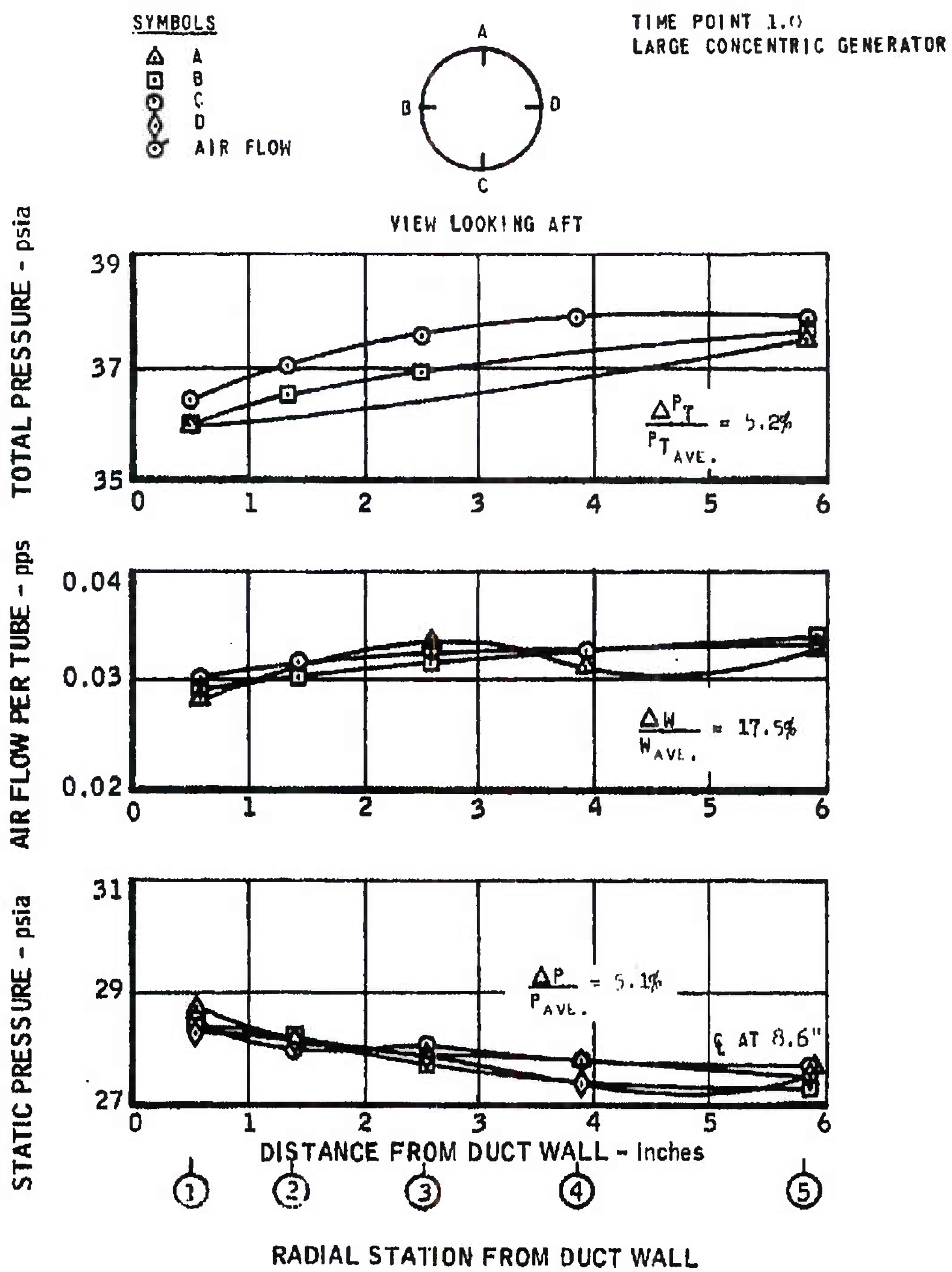

AERODYNAMIC COUPLING TEST
DUCT STATIC AND TOTAL PRESSURE PROFILES
MEASURED UPSTREAM FROM TUBE BUNDLE ENTRANCE

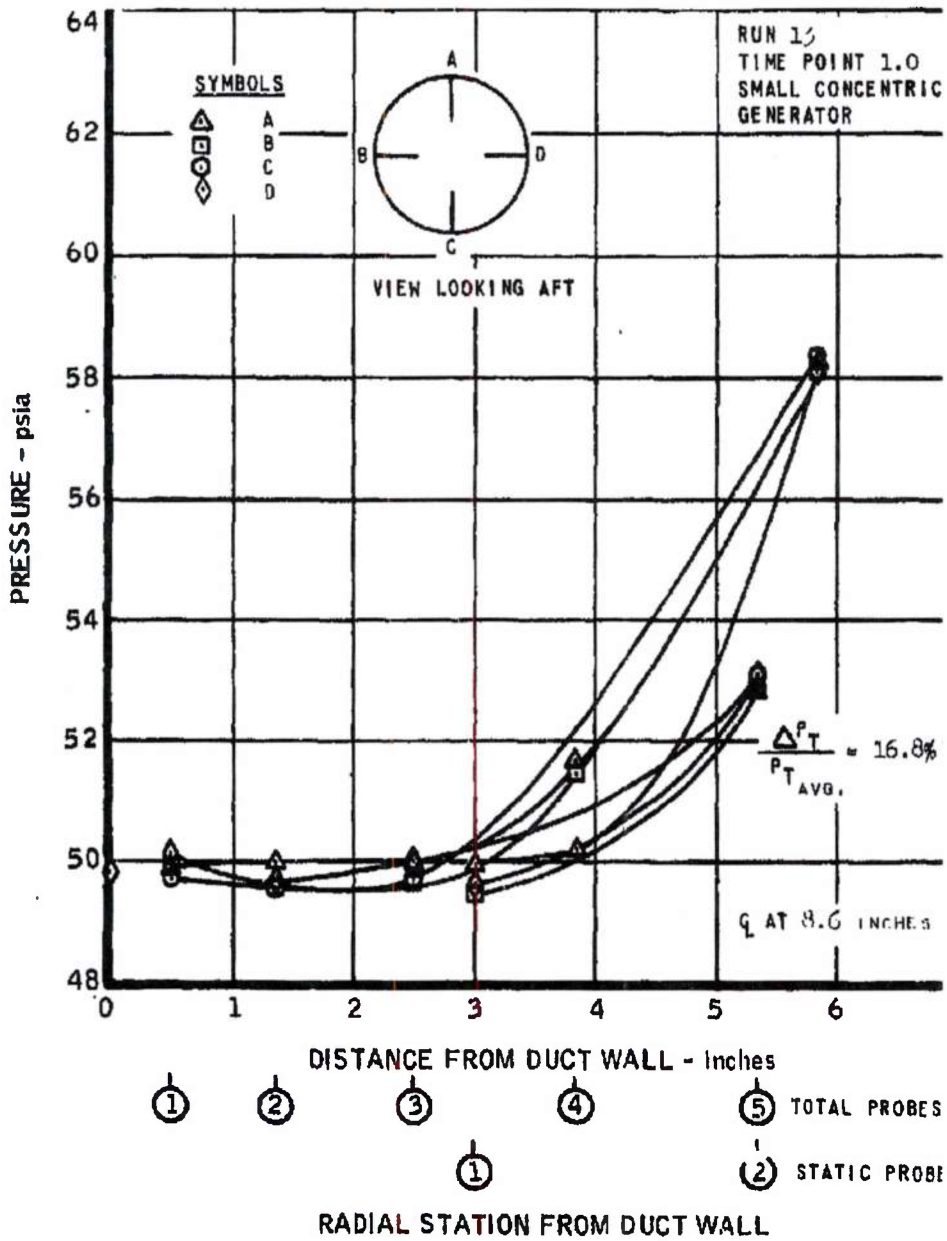

AIR FLOW AND PRESSURE DISTORTIONS MEASURED AT TUBE BUNDLE EXIT
RUN 13

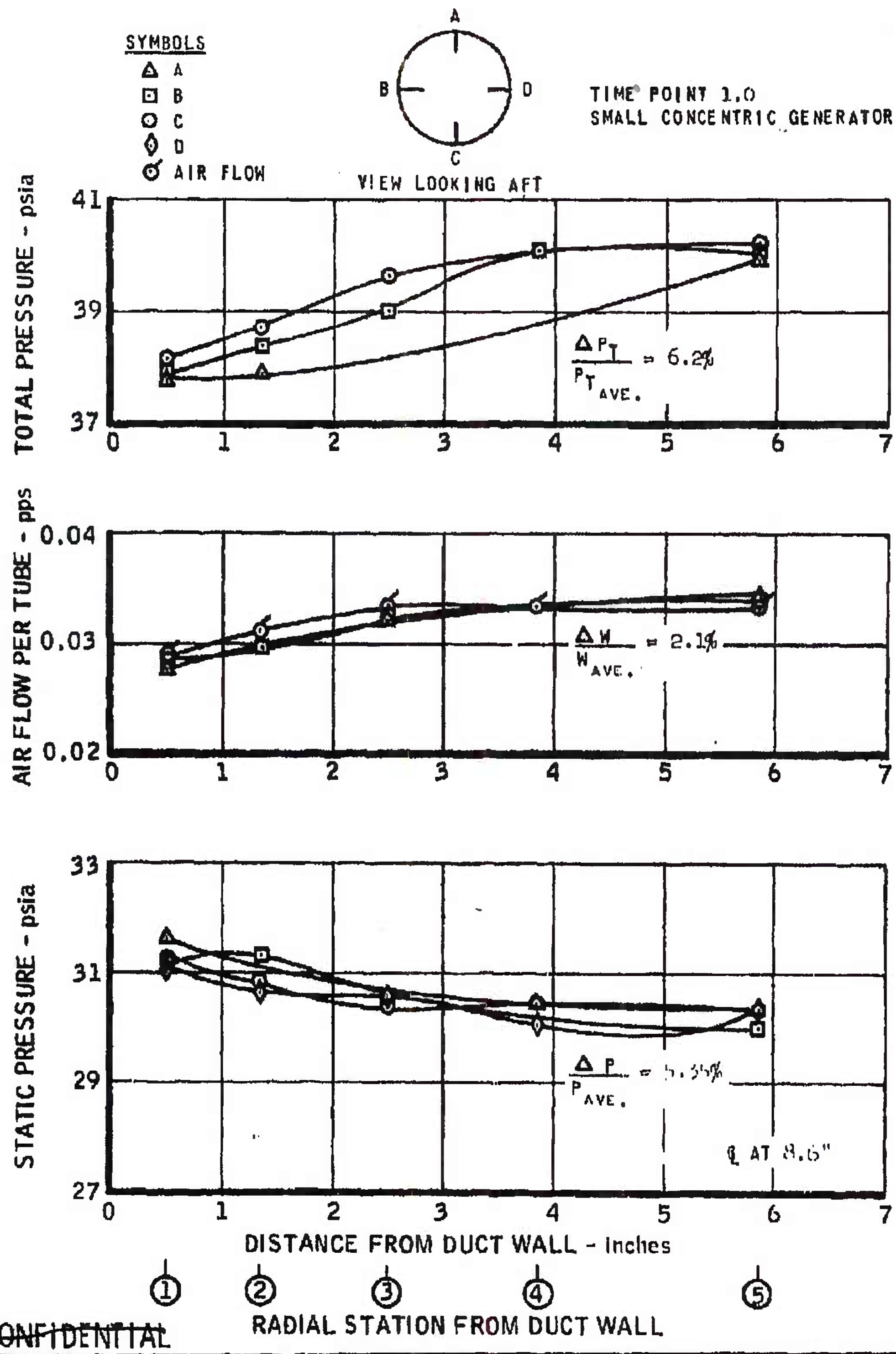

IMPOSED PRESSURE PROFILE DISTORTION ANALYSIS

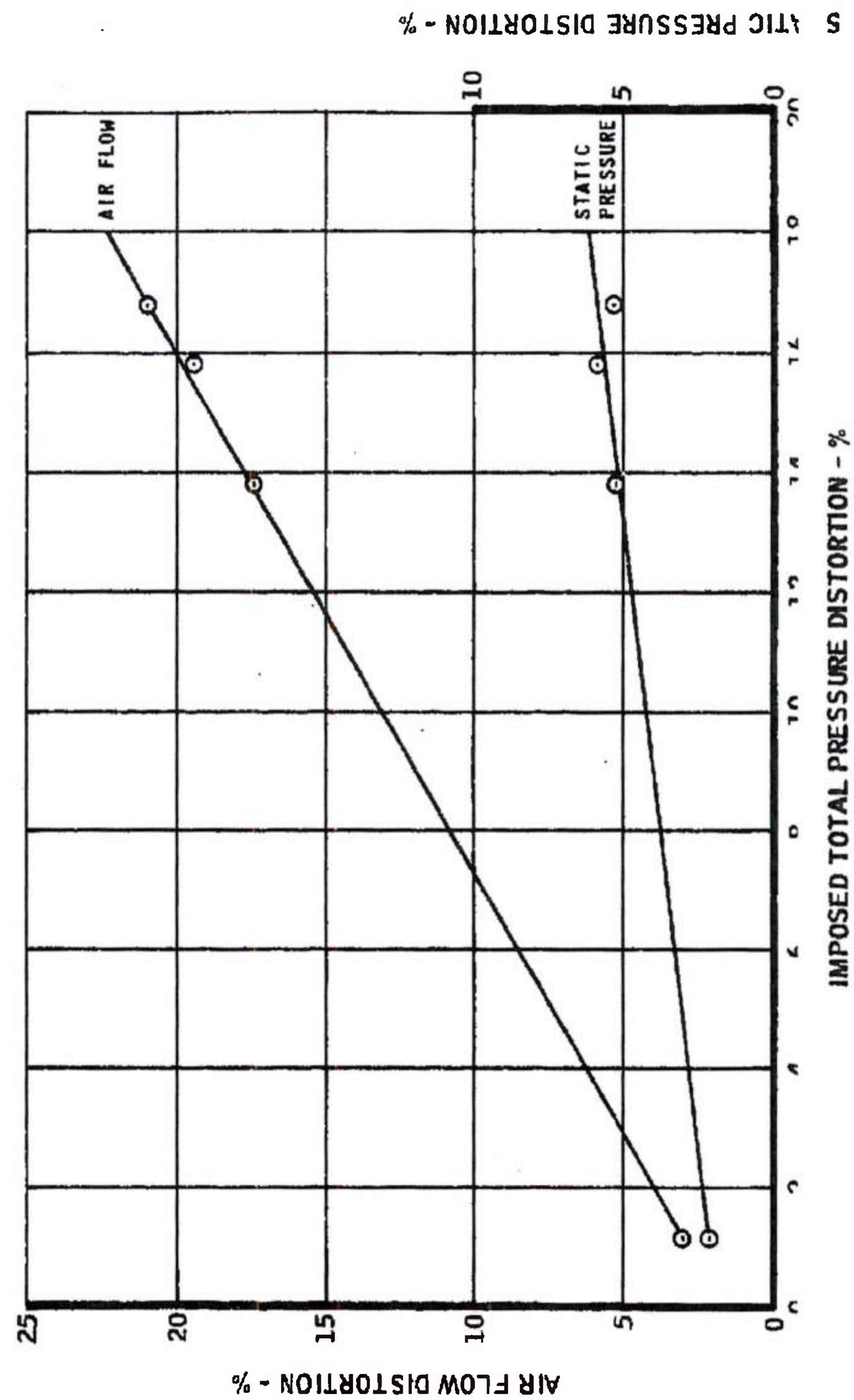

(3) A minimum length consistent with instrumentation leado and physical attachment of the nozzle to the module exit station. This length was $L/D_R = 0.25$.

All test runs to evaluate length effects were made without imposing module inlet pressure profiles. Inlet total pressure distortion for all runs as about 1.1 percent.

Figures 125 and 126 present the airflow and pressure distort n data for the "design" and minimum length, while Figures 116 and 117 prese the data for the long length ($L/D_R = 1.34$). Using the static pressure and ai - flow distortion data for the three coupling lengths, inspection of Figure 127 indicates that the "design" coupling length would have to be increased from $L/D_R = 0.335$ to approximately $L/D_R = 0.41$ to reduce the distortion level t the "base" case of the long length. The actual distortion data for the "base' ase are used here only in a qualitative manner, because the data presented is su ject to more detailed analysis. However, applying this qualitative data to the fu scale Model MA50-XCA propulsion system indicates that the upstream plen a chamber for the full scale nozzle will have to be increased in length by 5 to inches.

Noise and Vibration Analysis

Noise (pressure level) and vibration data were recorded for l of the test runs. In addition, data were recorded during several test runs f : conditions with the exit nozzle plug-in, which results in a lower tube exit M ch number. Data recorded in this manner should aid in defining the effect of t e exit velocity on sound level. It is anticipated that noise and vibration data c - tained from the aerodynamic coupling test will give insight into the noise le ls of a full scale propulsion system employing this type of nuclear reactor as e heat source.

The recorded noise and vibration data have not been analyzec at this time. However, Figure 128 presents a sample of the raw data. These ata indicate that no discrete frequencies occur and that only random noise level are present.

3.8.4 Nozzle Attachment Test

A study has been made to investigate airflow leakage results of the nozzle attachment test to determine what the effect would be on overall prop l- sion system thrust.

AIR FLOW AND PRESSURE DISTORTION DATA FOR DESIGN COUPLING LENGTH
RUN 17

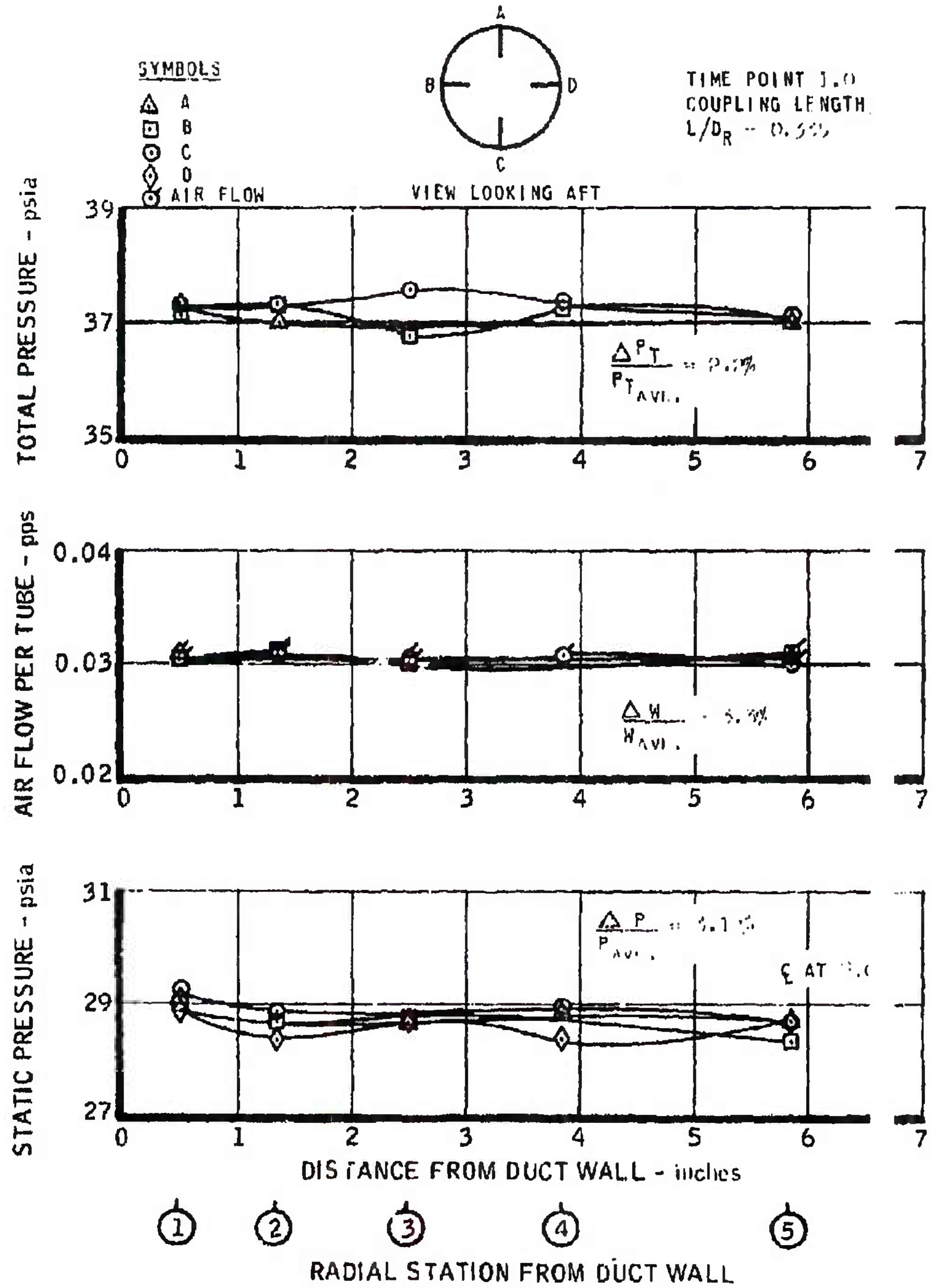

AIR FLOW AND PRESSURE DISTORTION DATA FOR MINIMUM COUPLING LENGTH
RUN 16

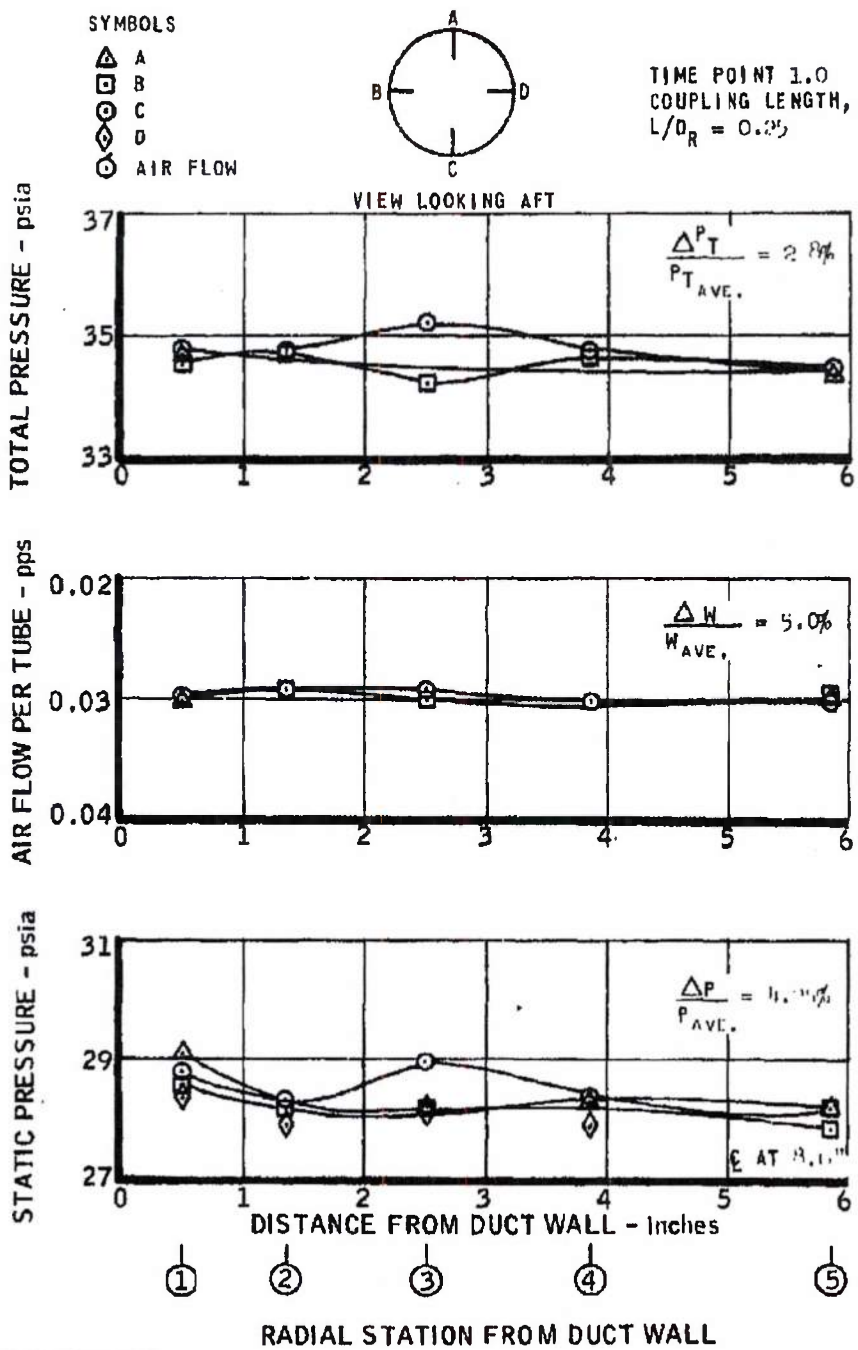

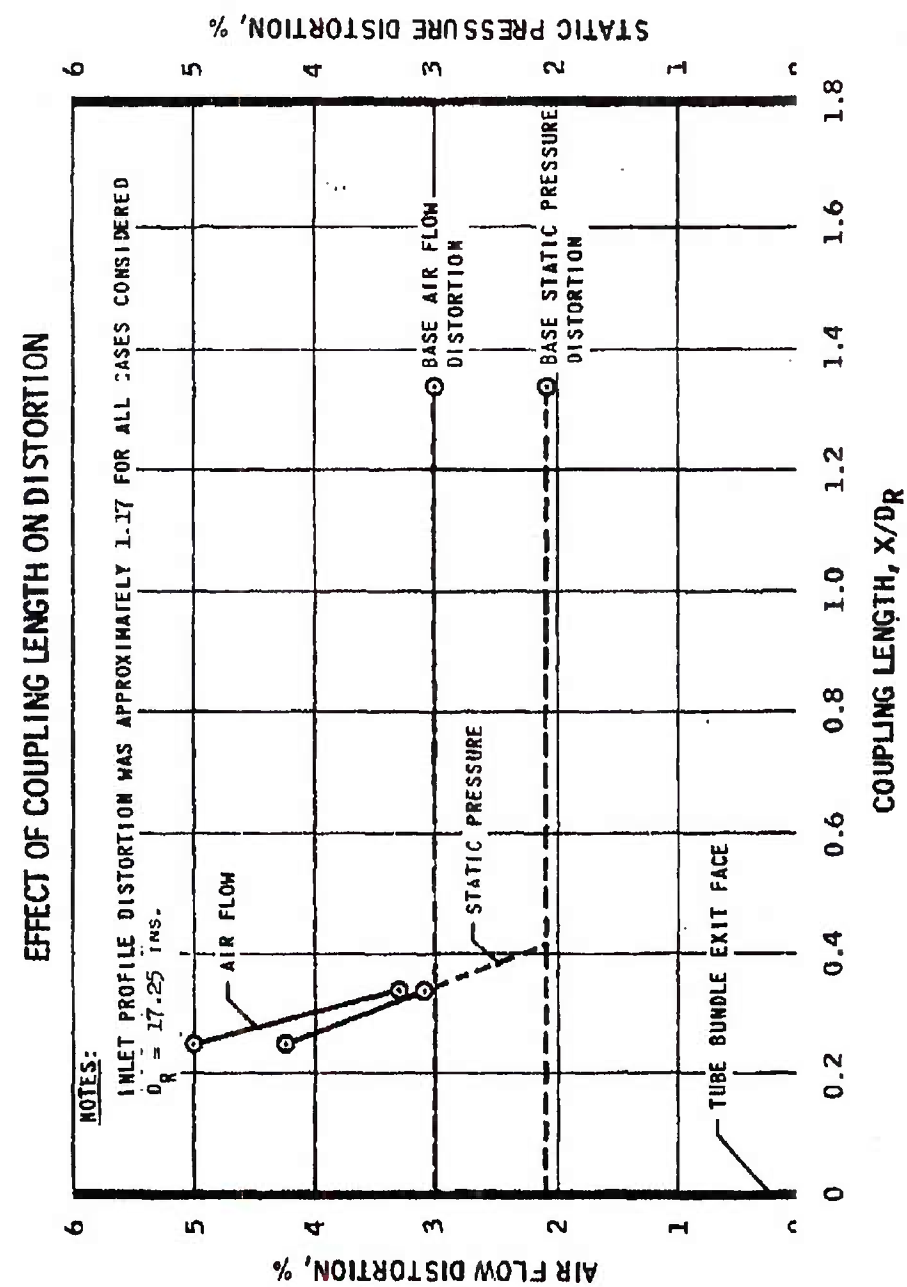
EFFECT OF COUPLING LENGTH ON DISTORTION
STATIC PRESSURE DISTORTION, %
6
5
4
3
2
1
0
NOTES:
INLET PROFILE DISTORTION WAS APPROXIMATELY 1.17 FOR ALL CASES CONSIDERED
D_R = 17.25 INS.
AIR FLOW
STATIC PRESSURE
BASE AIR FLOW DISTORTION
BASE STATIC PRESSURE DISTORTION
TUBE BUNDLE EXIT FACE
0
0.2
0.4
0.6
0.8
1.0
1.2
1.4
1.6
1.8
COUPLING LENGTH, X/D_R
AIR FLOW DISTORTION, %

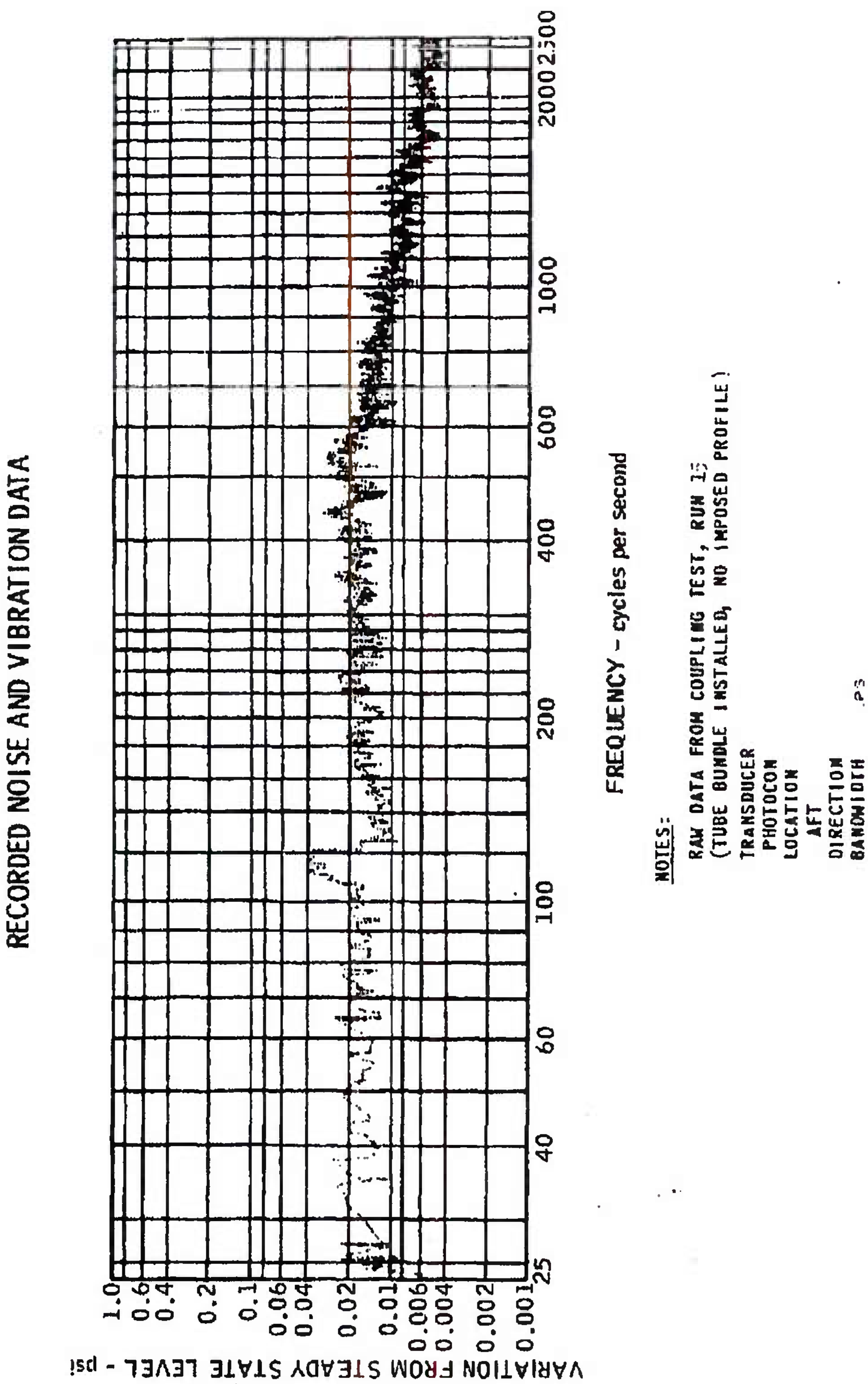
RECORDED NOISE AND VIBRATION DATA
VARIATION FROM STEADY STATE LEVEL - psi
1.0
0.6
0.4
0.2
0.1
0.06
0.04
0.02
0.01
0.006
0.004
0.002
0.001
25
40
60
100
200
400
600
1000
2000
2300
FREQUENCY - cycles per second
NOTES:
RAW DATA FROM COUPLING TEST, RUN 15
(TUBE BUNDLE INSTALLED, NO IMPOSED PROFILE)
TRANSDUCER
PHOTOCON
LOCATION
AFT
DIRECTION
BANDWIDTH

Taking the leakage rate reported at the ambient temperat ·e conditions from Section 3.9.6, an effective choked flow area can be compute Assuming this flow area, a change in air temperature and a constant pressu , a curve of airflow rate versus temperature can be computed. Figure 129 pr ents such a curve with the additional data point obtained from the test at high t mperatures. While the latter data point indicates that the effective leakage area lecreases with temperature, the following analyses will assume the conserv .ve computed curve results.

At the Model MA50-XCA engine design point condition (M :h 2.8, an altitude of 1000 feet, ANA Hot Day), the temperature of the Model 1A50-XCA side support-exit nozzle cooling air in the vicinity of the nozzle at ch ring is about 1050°F. The static pressure will be approximately 250 psig Assuming that the attach ring is at this air temperature (conservative result will be obtained because the temperature of the ring will be slightly highe than the cooling air temperature), a leakage rate of 0.41 pps is indicated f m the curve. The reactor total airflow rate at design point is 1577 pps. Thus, e leakage rate is about 0.03 percent. The Model MA50-XA-1 thrust influen coefficients that were reported in previous quarterly reports are applicable to ıe Model MA50-XCA engine to the first order. From these coefficients, th leakage rate represents a thrust decrement of 0.1 percent, which is considere ıegligible.

3.9 STRUCTURAL EXPERIMENTS

3.9.1 Exhaust Nozzle Attachment Test

The purpose of the exhaust nozzle attachment test was to valuate the operational reliability and structural integrity of a full scale nozzl attachment assembly under simulated load and temperature conditions. The a achment method chosen for investigation was a threaded coupling arrangem ıt in which an internally threaded locking ring engaged external threads on th mating nozzle section. A labyrinth-type seal was used to close off the joi :. Details of the attachment are shown in Figure 56. All components were fab .cated from A-286 material.

The mated rings were fitted to a specially designed bello fixture, which closed off the ends of the test item, allowing it to be interna y pressurized. This arrangement can be seen in Figure 130.

Because of the potential hazard associated with the use o .ir as a pressurizing medium, special safety precautions were exercised. Refrasil was

AIR FLOW LEAKAGE RESULTS OF NOZZLE ATTACHMENT TEST

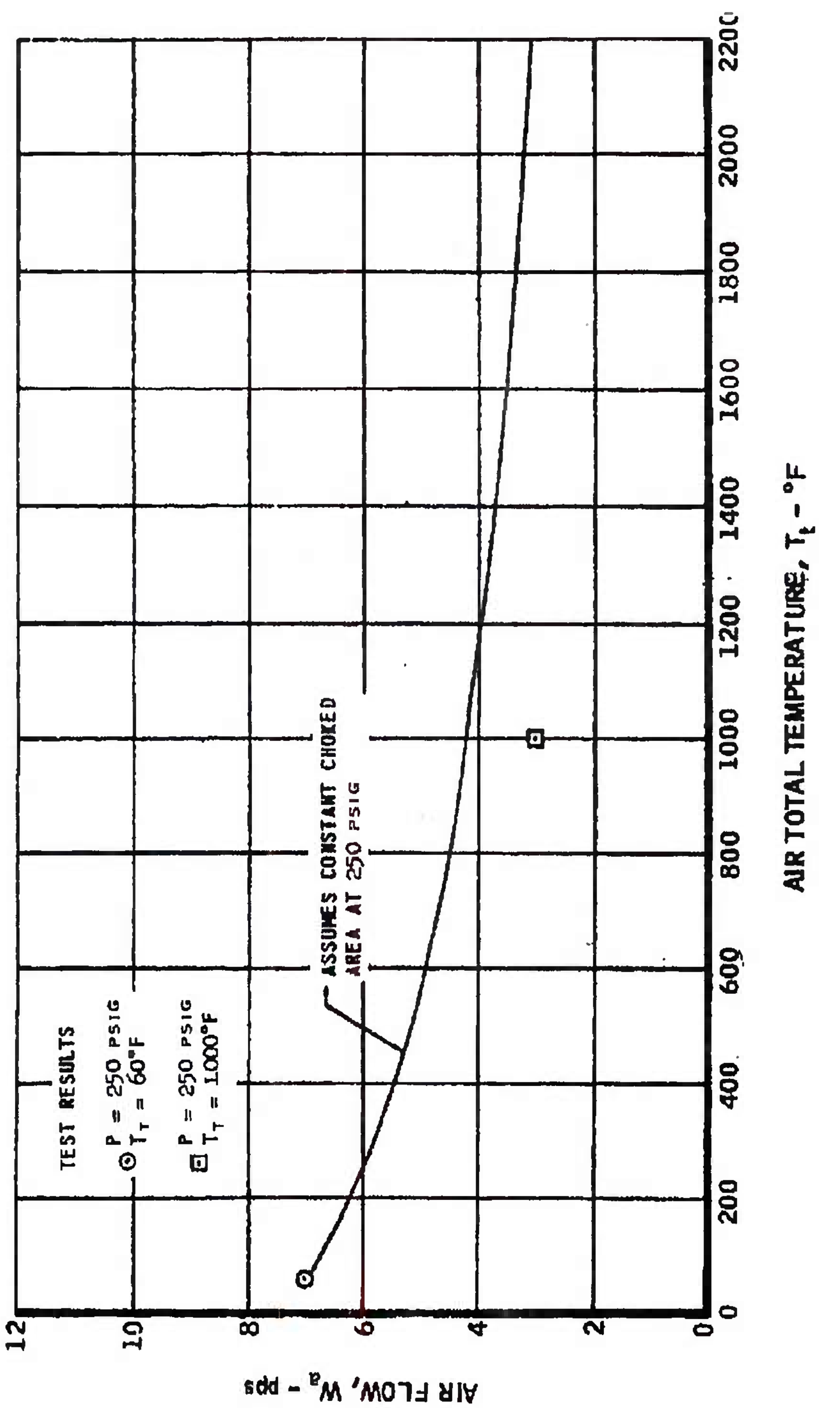

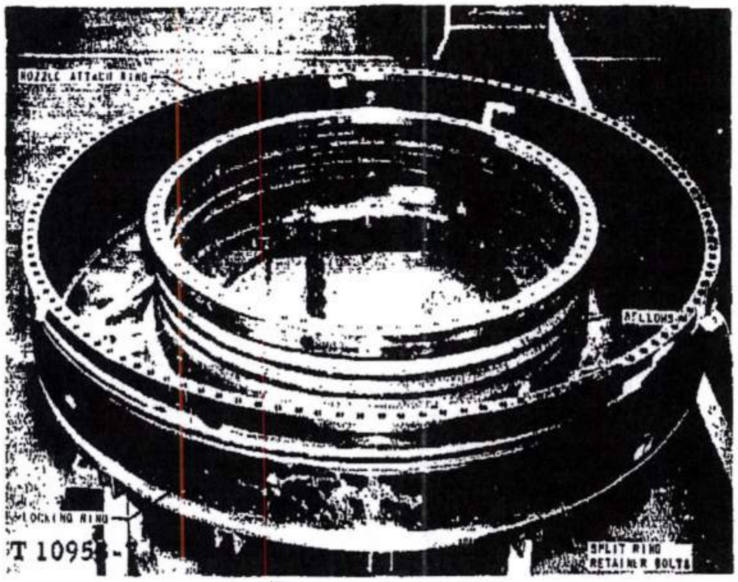

A. Partial Assembly

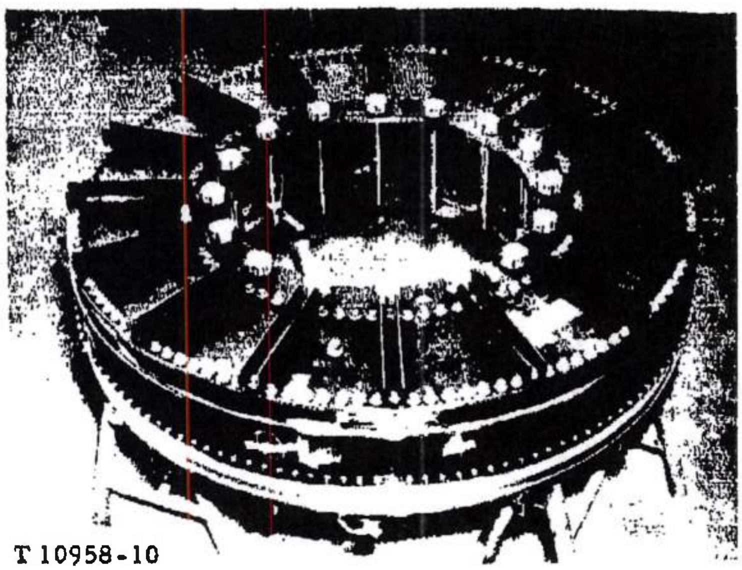

B. Final Assembly

FIGURE 130 - Test Item for Exit Nozzle Attachment Test

packed into the annular chamber to reduce the volume of air, and a ring c large snubber bolts was installed to contain the hardware in the event of a struc ıral failure.

Instrumentation included strain gages, thermocouples, and stati ›res-sure pickups. Figure 131 shows the test item being installed in a special pre-pared pit. Hot air was introduced into the pit from a SUE burner, provid g temperatures up to 1400°F, and high-pressure air was used to impose an ıter-nal design load of 350,000 pounds.

Initial tests consisted of pressure checks at ambient temperatur :o record stresses and to measure air leakage through the aerodynamic seal The test item was then disassembled and inspected. Ambient temperature tes were followed by a series of high-temperature, high-pressure tests. After ea run, the test item was disassembled and checked for proper operation and dim ısion-al change. In the final test run, the joint was held at design pressure anc em-perature (250° psig and 1400°F) for 3 1/2 hours, at which time the bellow fix-ture failed. Upon disassembly and inspection it was found that no dimens nal change had occurred, and the locking ring still functioned properly. Res :s of the test can be summarized as follows:

(1) Air leakage rates through the aerodynamic seal at ambient a d 1100°F temperature were 0.69 pps and 0.29 pps, respective , at 250 psig.

(2) Adequate structural integrity of the joint was demonstrated.

(3) Quick disconnect capability of the threaded lock ring was su tan-tiated by the ease of ring operation after each test run.

3.9.2 Engine-Airframe Lateral Attachment Test

Late in the year an experiment was initiated to evaluate propose engine airframe lateral attachment systems under simulated flight conditions of mper-ature and vibration. The test item will consist of a 10-inch thick full sca ra-dial section of the reactor core and suspension system.

Primary test objectives include (1) the evaluation of assembly st .c-tural integrity, and (2) the determination of deformation modes, spring re ıxa-tion, and response to random and programmed vibrations.

Page determined to be Unclassified
Reviewed Chief, RDD, WHS
IAW EO 13526, Section 3.5
Date: MAY 2 9 2015

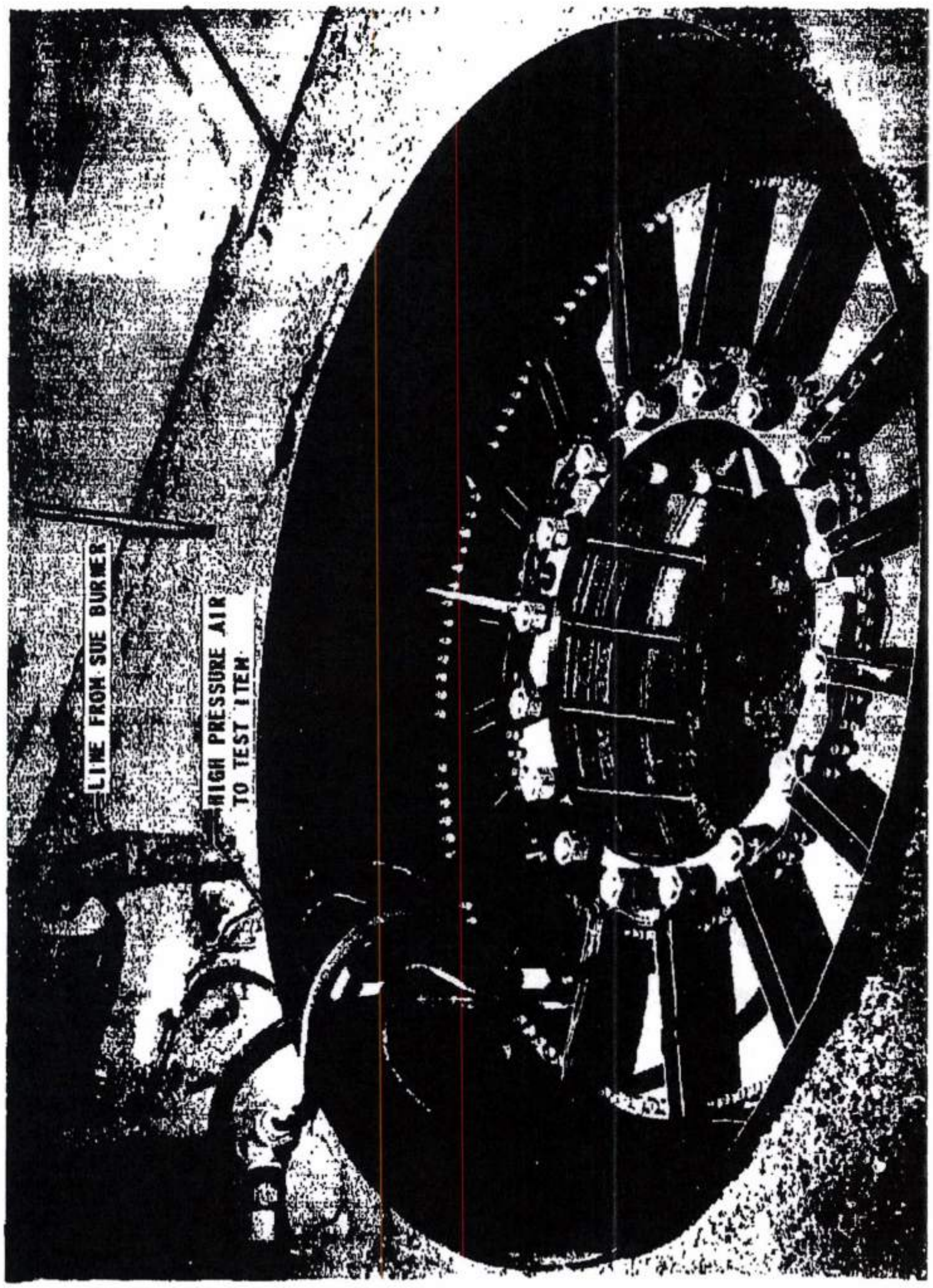

FIGURE 131 - Exit Nozzle Attachment Test Item in Ground Pit

T 10958-11

The first test, scheduled in February 1962, will involve a reactor up- port system utilizing corrugated springs, as shown in Figure 132 . The s nu- lated reactor core section will be built up of hexagonal stainless steel tube This section will allow simulation of mass and slip plane effects.

The test item will be mounted in a shaker table capable of imposin a 5-g sinusoidal vibration over a range of 5 to 2000 cps. Planned test condit ns are listed in Table 14.

Calibration and checkout of facility control equipment and recordi apparatus are complete; instrumentation for measuring acceleration, defle ion, and strain have been installed on the test item; and the corrugated springs ve been calibrated. Load-deflection characteristics of the springs are neede n order to impose the correct amount of preload on the core section, and to ter- mine post-test spring relaxation.

A SUE burner will provide heated air for bringing the test item to e 1300° F design point temperature. The various components of the test har are are shown in Figure .33.

3.10 MATERIALS INVESTIGATIONS

3.10.1 High-Temperature Materials Data

During the past year investigations have been conducted to obtain eded design information not presently available on alloys that have been chosen candidate structural materials for the Pluto engine. The short time and/o creep rupture properties of base and welded material in tension have been studied for Hastelloy R-235 and Rene' 41 alloys, and, to a more limited ext t, AISI type 321 stainless steel. Similar properties of base material for the co 713C and Hastelloy C alloys were studied. The tests performed on Hastell C are part of a program to study the comparative properties of base and wel d air- and vacuum-melted material.

The tensile properties were studied in a temperature range from to 1800° F as applicable to each alloy. The creep deformations of interest we e between 0.1 and 1.0 percent, and the times for creep and rupture were bet een 0 minutes and 10 hours. The alloys were in the form of sheet, plate, or c t rod; welds were performed by the TIG (tungsten electrode, inert gas) proc s. The data summarized here (Tables 15 through 27 and Figures 134 throu 138) give the results obtained, in a comparative manner, for the base and weld materials of Hastelloy R-235 alloy and Rene' 41 alloy sheet and plate, AISI ype 321 stainless steel sheet, and the base material of Hastelloy C air-melted loy plate and Inco 713C alloy cast rods.

CORRUGATED SPRINGS IN REACTOR LATERAL SUPPORT STRUCTURE

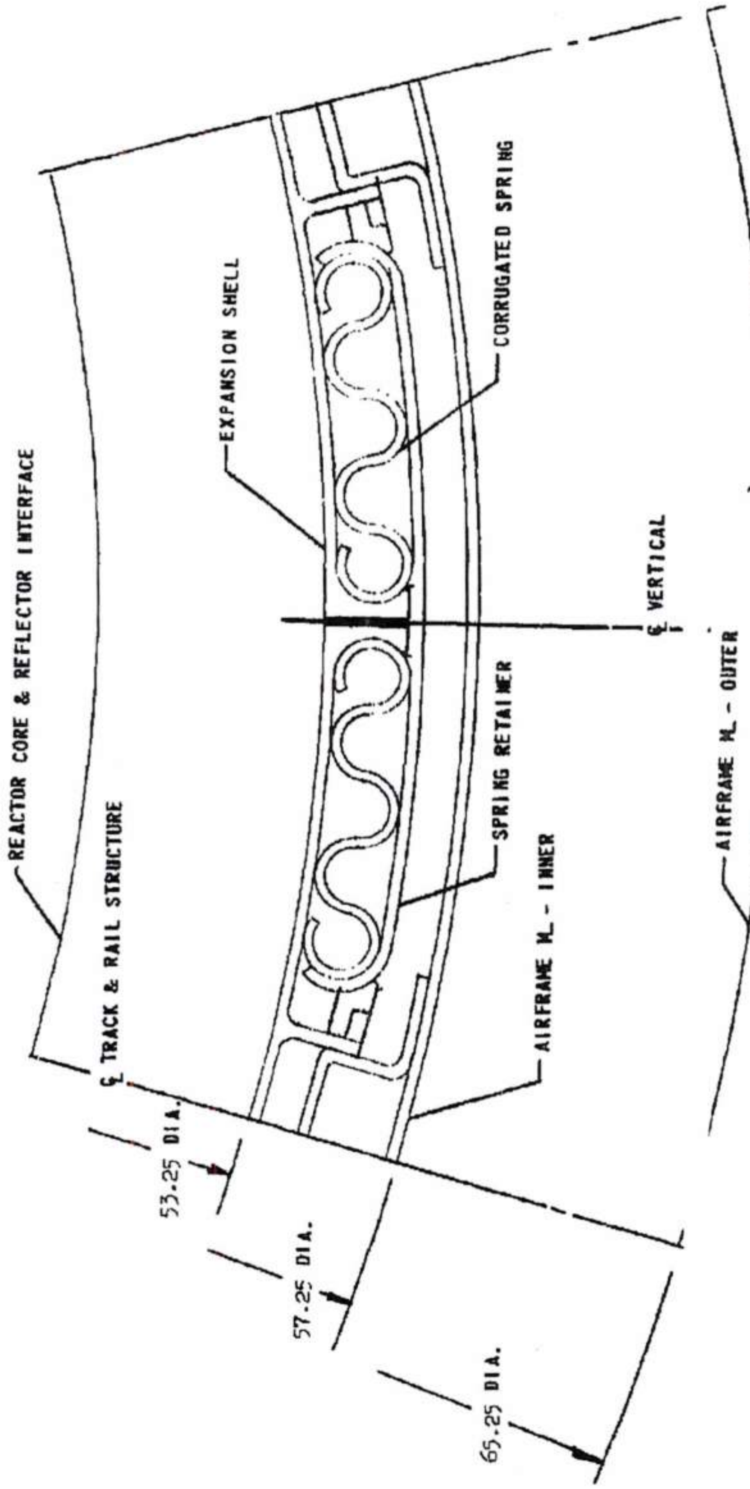

TABLE 14

TEST CONDITIONS FOR VIBRATION
OF SIMULATED REACTOR CORE SECTION

	Cond. No.	Temp. (°F)	Frequency (cps)	Input	Input	Duration (min)	Number of Tests
Assembly	1	Room	NA	--	--	--	--
Static*	2	Room	NA	--	-	--	--
Frequency Scans	3	Room	5 - 1000	0.5	NA	15	2
	4	Room	5 - 1000	1.0	NA	15	2
	5	Room	5 - 1000	1.5	NA	15	2
Static	6	Room	NA	--	--	--	--
Flat Random	7	Room	5 - 2000	1.95 rms	0.002	15	1
	8	Room	5 - 2000	1.95 rms	0.002	15	1
	9	Room	5 - 2000	3.2 rms	0.005	15	1
Static	10	Room	NA	--	--	--	--
Flat Random	11	1300	5 - 2000	1.95 rms	0.002	15	1
	12	1300	5 - 2000	1.95 rms	0.002	15	1
	13	1300	5 - 2000	3.2 rms	0.005	15	1
Static	14	Room	NA	--	--	--	--
Programmed Random	15	1300	5 - 2000	(To be prescribed)		15	1
	16	1300	5 - 2000			10 hours	1
Static	17	Room	NA	--	--	--	1
Frequency Scan	18	Room	5 - 1000	0.5	NA	15	1

* Static tests include core pressure measurement, spring preload measurement, and gaps between outer spring, shells and outer ring and between rails and mating tracks.

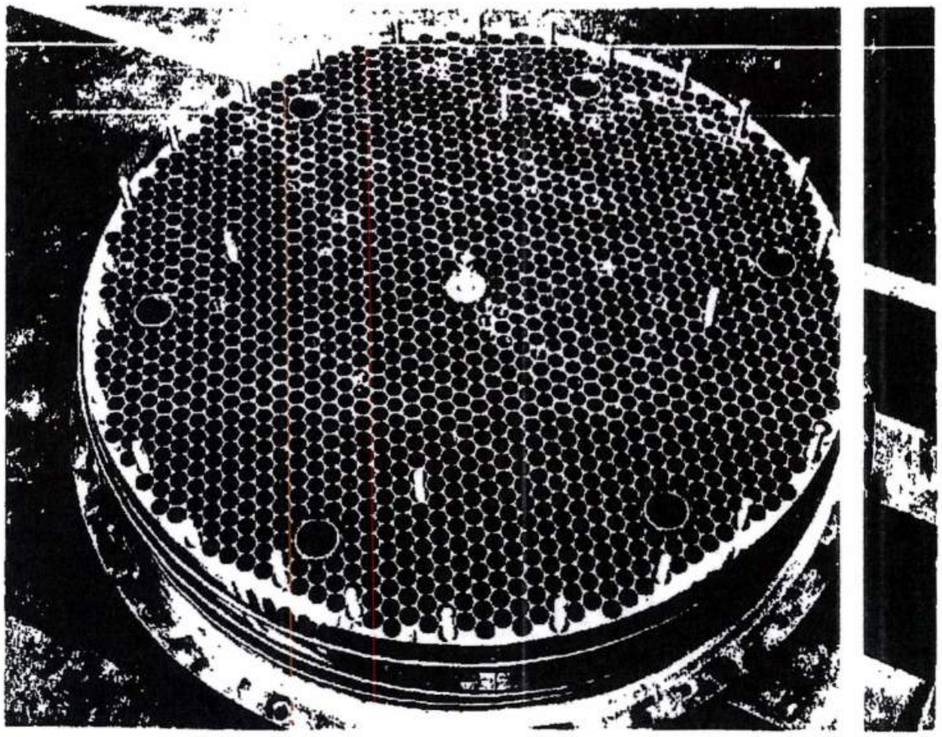

4142-7

A. Core Matrix

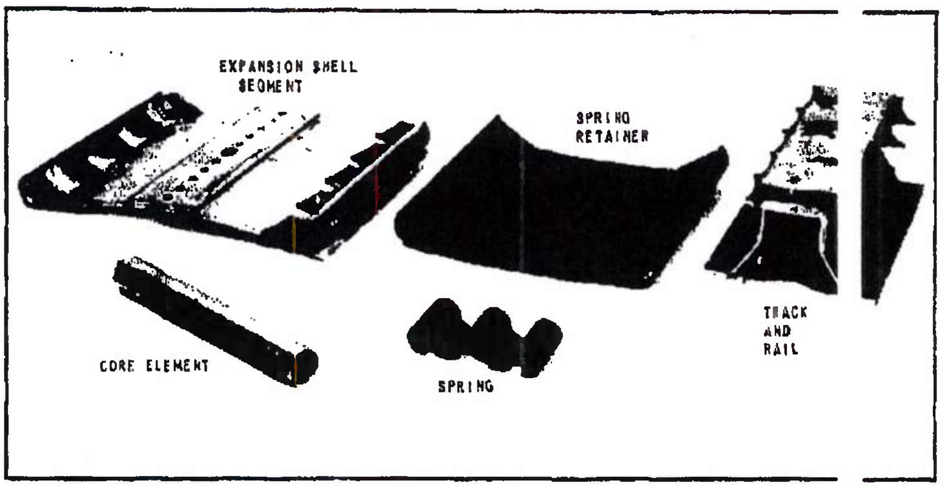

4142-8

B. Side Support Components

FIGURE 133 - Lateral Attachment Test Items

TABLE 15

COMPARATIVE SHORT TIME TENSILE PROPERTIES OF HASTELLOY R-235 ALLOY SHEET BASE AND WELDED MATERIAL

Test Temperature (°F)	Specimen Type*	Proportional Limit (Ksi)	0.2% Yield Strength (Ksi)	Ultimate Tensile Strength (Ksi)	Elongation in 2 in. (%)
78	B	89.0	103.0	167.0	27.5
	W	94.0	111.0	149.0	10.0
	WF	88.0	117.5	171.0	22.0
1200	B	88.0	97.0	140.0	30.0
	W	60.0	99.5	140.0	12.0
	WF	74.0	100.0	136.0	16.0
1400	B	94.0	107.0	133.0	7.5
	W	76.0	105.0	128.0	5.0
	WF	80.0	100.0	124.0	6.5
1600	B	63.0	88.0	98.0	2.5
	W	53.0	76.0	87.5	2.0
	WF	68.0	78.0	90.0	1.0
1800	B	26.0	30.0	40.7	15.0
	W	14.0	21.5	34.3	14.0
	WF	16.0	22.0	32.2	13.0

* B = Base material: sheet 0.072 in. thick; aged at 1600° F for 30 minutes

W = Welded without filler by fusion; sheet 0.063 in. thick

WF = Welded with filler R-235 wire by fusion; sheet 0.063 in. thick

All welds transverse; aged at 1600° F for 30 minutes

TABLE 16

COMPARATIVE CREEP AND RUPTURE PROPERTIES OF
HASTELLOY R-235 ALLOY SHEET BASE AND WELDED MATE[illegible]AL

Test Temperature (°F)	Creep %	Creep Time (hours)	Rupture Time (hours)	Stress (Ksi)	Mate[illegible]al Tes[illegible]d*
1200	0.1	0.5 min	48 min	110	[illegible]
	0.1	1.13	1.73	105	[illegible]
	0.1	2.7	2.7	95	[illegible]
	0.5	44 min	--	110	[illegible]
	0.5	--	--	105	[illegible]
	0.5	--	--	95	[illegible]F
1400	0.1	18.4	18.4	50	[illegible]
	0.1	1.2	1.2	50	[illegible]
	0.1	0.27	0.27	50	[illegible]
1600	0.1	16 min	20.5	25	[illegible]
	0.1	3.6min	7.03	25	[illegible]
	0.1	26 min	39.5	25	[illegible]F
	0.5	10.33	--	25	[illegible]
	0.5	2.83	--	25	[illegible]
	0.5	13.7	--	25	[illegible]F
	1.0	15.83	--	25	[illegible]
	1.0	5.3	--	25	[illegible]
	1.0	27.5	--	25	[illegible]F
1800	0.1	40 min	Test Discont. 4.83	10	[illegible]
	0.1	1.25	9.9	9	[illegible]
	0.1	2.2	15.5	7	[illegible]F
	0.5	2.8	--	10	[illegible]
	0.5	4.16	--	9	[illegible]
	0.5	9.6	--	7	[illegible]F
	1.0	3.62	--	10	[illegible]
	1.0	5.8	--	9	[illegible]
	1.0	11.5	--	7	[illegible]F

* B = Base metal: sheet 0.072 in. thick; aged at 1600°F for 30 minutes
W = Welded without filler; sheet 0.063 in. thick
WF = Welded with Hastelloy R-235 alloy filler wire; sheet 0.063 in. thick
All welds transverse; aged at 1600°F for 30 minutes

TABLE 17

COMPARATIVE SHORT TIME TENSILE PROPERTIES OF HASTELLOY R-235 ALLOY PLATE BASE AND WELDED MATERIAL

Test Temperature (°F)	Specimen Type*	Proportional Limit (Ksi)	0.2% Yield Strength (Ksi)	Ultimate Tensile Strength (Ksi)	Young's Modulus (psi x 10^6)	Elongation in 2 in. (%)
78	B	70	94.2	156.3	31.5	33
	WF	--	--	---	--	--
1200	B	60	84.3	106.0	26.0	24.5
	WF	59.0	82.0	121.0	23.4	18
1400	B	62	82.0	104.7	24.0	10
	WF	69.0	86.1	112.0	24.1	8
1600	B	54	72.9	83.0	21.0	9.5
	WF	60.4	75.2	93.0	19.3	6
1800	B	14	14.8	25.1	13.0	34.5
	WF	15.0	23.0	27.9	15.8	33

* B = Base material: plate 0.250 in. thick; annealed at 2200°F for 15 minutes, water quenched; aged at 2050°F for 30 minutes, air cooled

WF = Welded with Hastelloy R-235 alloy filler wire; plate 0.250 in. thick

All welds transverse; annealed at 2200°F for 30 minutes, water quenched: aged 2050°F for 30 minutes, air cooled

TABLE 16

COMPARATIVE CREEP AND RUPTURE PROPERTIES OI
HASTELLOY R-235 ALLOY PLATE BASE AND WELDED MATI :IAL

Test Temperature (°F)	Creep %	Creep Time (hours)	Rupture Time (hours)	Stress (Ksi)	Mate al Tes d*
1200	0.1	7.13	7.2	85	B
	0.1	12.3	12.3	83	W
1400	0.1	17.0	Test discontinued	50	B
	0.1	4.65	4.67	50	W
1600	0.1	1.25	14.3	30	B
	0.1	0.33	5.07	30	W
	0.5	5.75	--	30	B
	0.5	2.15	--	30	W
	1.0	8.83	--	30	B
	1.0	3.33	--	30	W
1800	0.1	1.75	16.7	5	B
	0.1	1.6	32.0	5	W
	0.5	7.3	--	5	B
	0.5	10.7	--	5	W
	1.0	8.86	--	5	B
	1.0	32.0	--	5	W

* B = Base metal: plate 0.250 in. thick; annealed at 2200° F for 15 min es, water quenched; aged at 2050° F for 30 minutes, air cooled
WF = Welded with Hastelloy R-235 filler wire; plate 0.250 in. thick

All welds transverse; annealed at 2200° F for 15 minutes, water quenched; aged at 2050° F for 30 minutes, air cooled

TABLE 19

COMPARATIVE SHORT TIME TENSILE PROPERTIES OF RENE' 41 ALLOY SHEET BASE AND WELDED MATERIAL

Test Temperature (°F)	Specimen Type*	Proportional Limit (Ksi)	0.2% Yield Strength (Ksi)	Ultimate Tensile Strength (Ksi)	Elongation in 2 in. (%)
78	B	75	102.2	148.4	13
	W	64.6	93.6	148.0	27
	WF	81.0	104.0	136.0	6.5
1200	B	58.4	89.8	134.2	23
	W	44.0	80.0	119.5	27
	WF	70.0	88.5	122.0	29
1400	B	56.4	90.9	139.6	17
	W	70.0	88.0	109.0	8
	WF	74.5	93.0	114.0	4
1600	B	52.8	81.9	97.2	9.5
	W	51.0	78.0	97.2	7.5
	WF	67.5	80.0	93.0	3.0
1800	B	30.7	38.6	44.8	15
	W	26.0	32.8	43.9	16
	WF	24.5	36.0	43.4	12

* B = Base material: sheet 0.064 in. thick; annealed at 2150°F for 2 hrs, air cooled; aged at 1650°F for 2 hrs, air cooled

W = Welded without filler; sheet 0.053 in. thick

WF = Welded with Rene' 41 alloy wire

All welds transverse; annealed at 2150°F for 2 hrs, air cooled; aged at 1650°F for 4 hrs, air cooled

TABLE 20

COMPARATIVE CREEP AND RUPTURE PROPERTIES OF RENE' 41 ALLOY SHEET BASE AND WELDED MATERIAL

Test Temperature (°F)	Creep %	Creep Time (hours)	Rupture Time (hours)	Stress (Ksi)	Material Tested*
1200	0.1	0.26	43.1	100	B
	0.05	21	86.8	100	W
1400	0.1	20.3	65	60	B
	0.2	8.8	22.2	65	W
	0.5	14.5	--	65	W
	0.6	48.9	--	60	B
	1.0	60	--	60	B
	1.0	20	--	65	W
1600	0.1	28.7	12.6	35	B
	0.05	3.5	26.3	32	W
	0.5	8.1	--	35	B
	0.5	15.9	--	32	W
	1.0	9.8	--	35	B
	1.0	22	--	32	W
1800	0.1	4.1	28.6	10	B
	0.05	0.33	50.7	11	W
	0.5	12.7	--	10	B
	0.5	4.2	--	11	W
	1.0	18.3	--	10	B
	1.0	49	--	11	W

* B = Base material: sheet 0.064 in. thick; annealed at 2150°F for 2 hrs, air cooled; aged at 1650°F for 4 hrs, air cooled

W = Welded without filler; sheet 0.050 in. thick

All welds transverse; annealed at 2150°F for 2 hrs, air cooled; aged at 1650°F for 4 hrs, air cooled

TABLE 21

COMPARATIVE SHORT TIME TENSILE PROPERTIES OF RENE' 41 ALLOY PLATE BASE AND WELDED MATERIAL

Test Temperature (° F)	Specimen Type*	Proportional Limit (Ksi)	0.2% Yield Strength (Ksi)	Ultimate Tensile Strength (Ksi)	Young's Modulus (psi x 10^6)	Elongation in 2 in. (%)
78	B	94	110	138	30	4.5
	WF	84.9	113	168	28.9	13.5
1200	B	73	96	+	24+	+
	WF	72	97.5	138	24.2	8.0
1400	B	76	102	151	21	10.5
	WF	68	87.9	142	21.9	8.0
1600	B	65	88	100	19	14.5
	WF	75	94.2	108	20.7	8.5
1800	B	27	29	39	17.5	22
	WF	29.5	38.7	47.9	16.9	5.0

* B = Base material: 5/16 in. plate; annealed at 2150° F for 2 hrs, air cooled; aged at 1650° F for 4 hrs, air cooled

W = Welded with filler Rene' 41 wire; 0.250 in. plate

All welds transverse; annealed at 2150° F for 2 hrs, air cooled; aged at 1650° F for 4 hrs, air cooled

\+ = Grips failed prior to ultimate loading

TABLE 22

COMPARATIVE CREEP AND RUPTURE PROPERTIES O:
RENE' 41 ALLOY PLATE BASE AND WELDED MATERIA

Test Temperature (°F)	Creep %	Creep Time (hours)	Rupture Time (hours)	Stress (Ksi)	Mat ial Te ed*
1200	0.1	1.0 min	Test discontinued	120	[illegible]
	0.1	32.5	Test discontinued	95	F
	0.5	3.23	--	120	[illegible]
	0.5	113.0	--	95	F
	1.0	12.75	--	120	[illegible]
	1.0	--	--	95	F
1400	0.1	3.0	17.5	75	[illegible]
	0.1	1.0	10.6	76	F
	0.5	8.86	--	75	[illegible]
	0.5	3.67	--	76	F
	1.0	11.9	--	75	[illegible]
	1.0	5.55	--	76	F
1600	0.1	3.6	16.2	35	[illegible]
	0.1	1.5	7.5	34	F
	0.5	10.9	--	35	[illegible]
	0.5	4.1	--	34	F
	1.0	12.7	--	35	[illegible]
	1.0	5.13	--	34	F
1800	0.1	2.75	7.95	10	[illegible]
	0.1	1.0	6.1	12	F
	0.5	5.2	--	10	[illegible]
	0.5	2.57	--	12	F
	1.0	5.95	--	10	[illegible]
	1.0	3.5	--	12	F

* B = Base material: plate 0.3125 in. thick; annealed at 2150° F for 2 :s, air cooled; aged at 1650° F for 4 hrs, air cooled

WF = Welded with filler Rene' 41 wire; 0.250 in. plate
All welds transverse; annealed at 2150° F for 2 hrs, air cooled; aged at 1650° F for 4 hrs, air cooled

TABLE 23

COMPARATIVE SHORT TIME TENSILE PROPERTIES OF
AISI TYPE 321 STAINLESS STEEL SHEET, BASE, AND WELDED MATERIAL

Test Temperature (°F)	Specimen Type*	Proportional Limit (Ksi)	0.2% Yield Strength (Ksi)	Ultimate Tensile Strength (Ksi)	Young's Modulus (psi x 10^6)	Elongatic in 2 in. (%)
72	B	26	43	83	25	55
	W	30	43	84	.25	47
300	B	23	37	66	22	37
	W	28	38	66	20	37
600	B	26	34	60	17	33
	W	29	34	60	19	29
800	B	26	36	59	21	31
	W	23	32	57	24	27

* B = Base material: sheet 0.125 in. thick

W = Welded material without filler; sheet 0.125 in. thick

All welds transverse; roll planished after welding

TABLE 24

SHORT TIME TENSILE PROPERTIES OF INCO 713 AL OY

Test Temperature (°F)	Proportional Limit (Ksi)	0.2% Yield Strength (Ksi)	Ultimate Tensile Strength (Ksi)	Young's Modulus (psi x 10^6)	I ongation 1 2 in. (%)
78	86	115	132	27.2	5.5
1200	80	104	128	26	4
1400	89	108	128	25	2
1600	84	110.5	119	18	3
1800	34	51	74	14	6.5

Material: as cast rods 0.250 in. diameter

Heat treatment: as received

TABLE 25

CREEP AND RUPTURE PROPERTIES OF INCO 713C ALLOY

Test Temperature (°F)	Creep %	Creep Time (hours)	Rupture Time (hours)	Stress (Ksi)
1200	0.1	4.25	No rupture	110
	0.5	13.9	--	110
1400	0.1	0.28	21.2	80
	0.5	3.1	--	80
	1.0	7.5	--	80
1600	0.1	0.25	17.4	45
	0.5	3.5	--	45
	1.0	8	--	45
1800	0.1	0.5 min	3.46	30
	0.5	0.3	--	30
	1.0	2.03	--	30

Material: as cast rods 0.250 in. diameter

Heat Treatment: as received

TABLE 26

SHORT TIME TENSILE TEST PROPERTIES OF
HASTELLOY C ALLOY PLATE - AIR MELTED

Test Temperature (°F)	Proportional Limit (Ksi)	0.2% Yield Strength (Ksi)	Ultimate Tensile Strength (Ksi)	Elongat n in 2 i (%)
78	30.0	57.5	115.6	58
1000	27.5	37.3	92.3	53
1200	26.8	37.0	85.2	53
1400	27.0	33.3	67.9	44
1600	28.0	32.2	55.3	43

Material: plate 0.250 in. thick

Heat Treatment: as received from mill

TABLE 27

CREEP AND RUPTURE PROPERTIES OF
HASTELLOY C ALLOY PLATE - AIR MELTED

Test Temperature (° F)	Creep %	Creep Time (minutes)	Rupture Time (minutes)	Stress (Ksi)
1200	0.1	9.0	Not ruptured	40
	0.5	39.2	--	40
	1.0	46.9	--	40
1400	0.1	0.13	Not ruptured	30
	0.5	1.17	--	30
	1.0	1.82	--	30
1600	0.1	0.02	2.20	20
	0.5	0.10	--	20
	1.0	0.17	--	20

Material: plate 0.250 in. thick

Heat Treatment: as received from mill

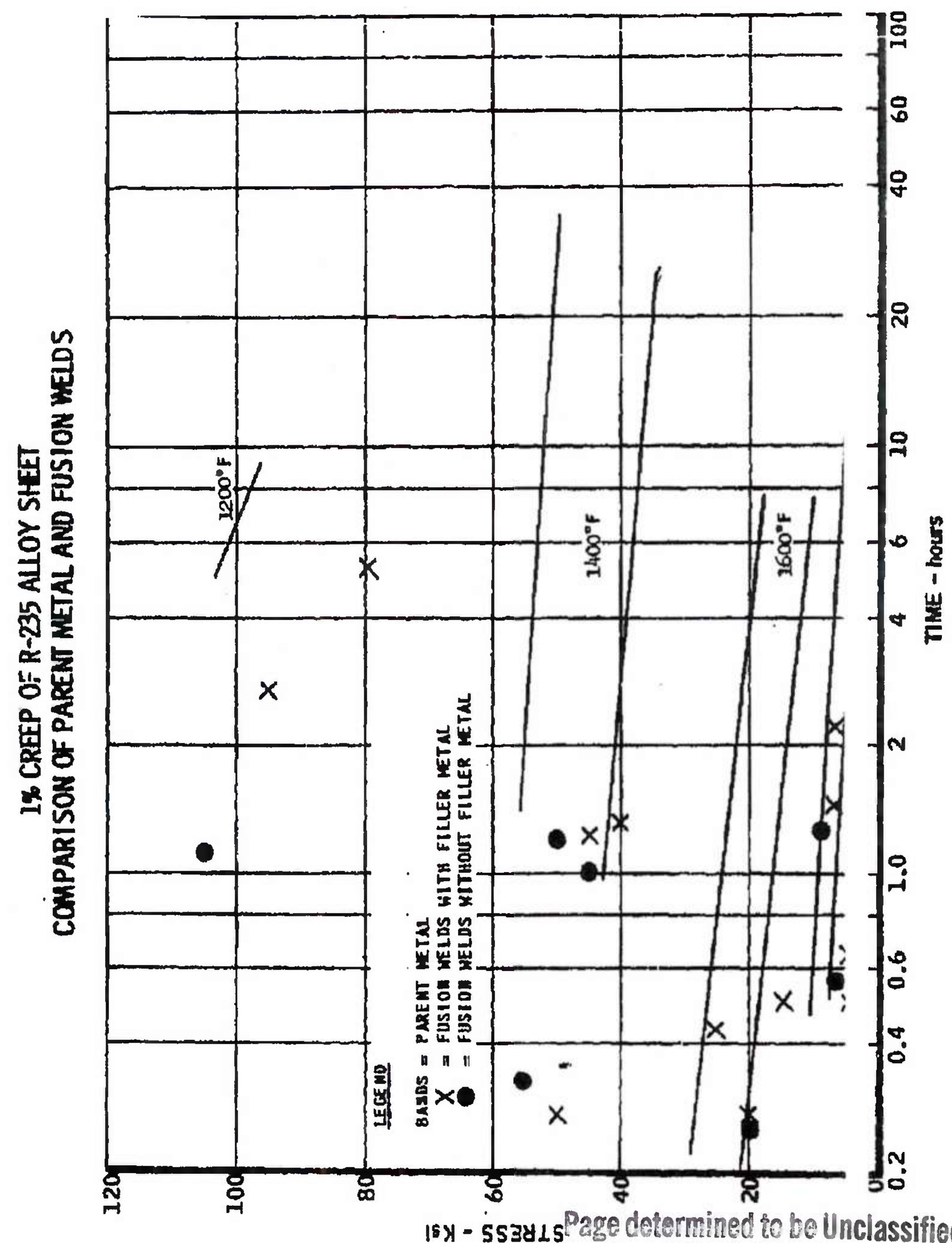
1% CREEP OF R-235 ALLOY SHEET
COMPARISON OF PARENT METAL AND FUSION WELDS
LEGEND
BASIS = PARENT METAL
X = FUSION WELDS WITH FILLER METAL
● = FUSION WELDS WITHOUT FILLER METAL
1200°F
1400°F
1600°F
STRESS - Ksi
TIME - hours
120
100
80
60
40
20
0
0.2
0.4
0.6
1.0
2
4
6
10
20
40
60
100

IGURE 134

1% CREEP OF R-235 ALLOY PLATE
COMPARISON OF PARENT METAL AND FUSION WELDS

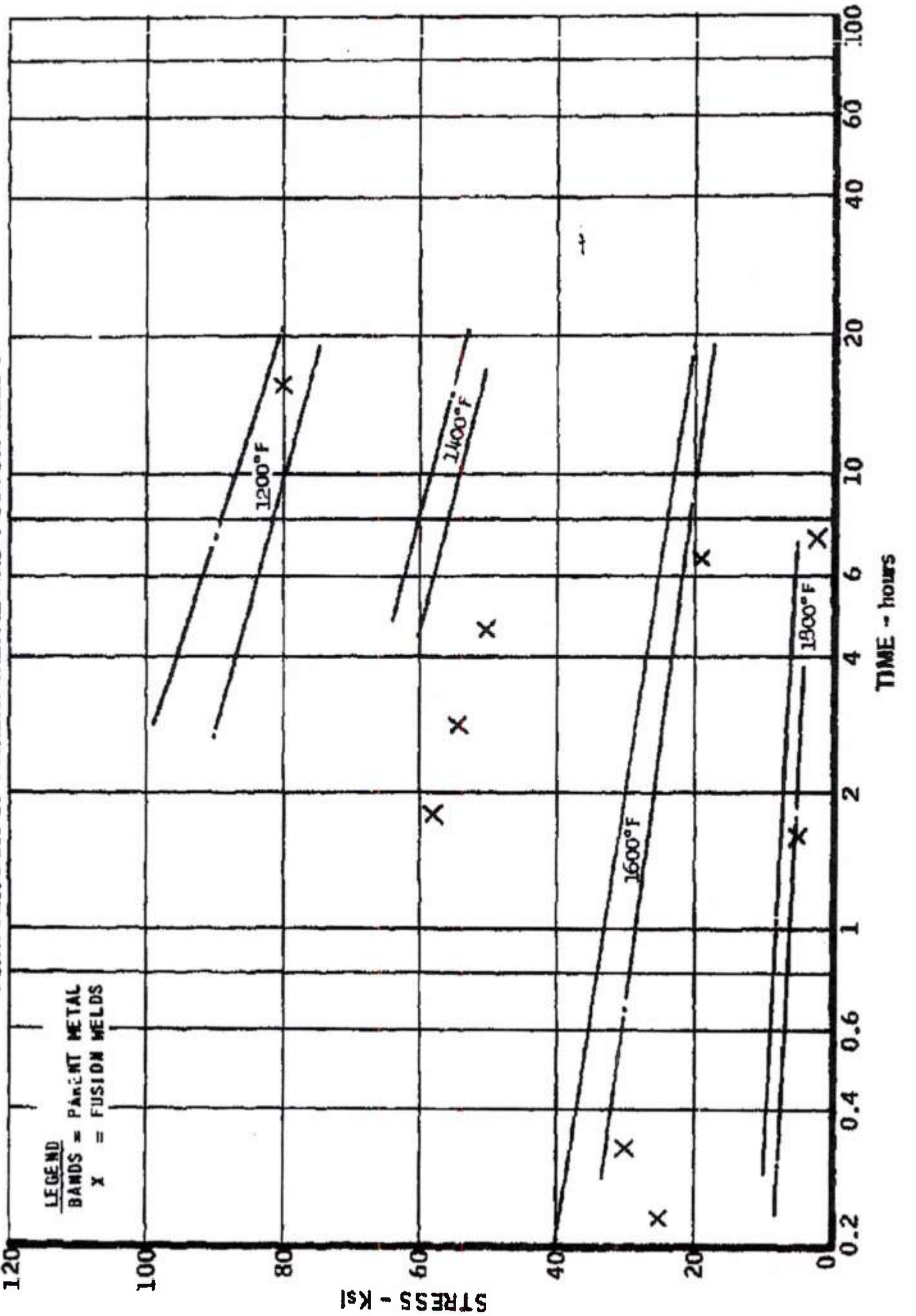

1% CREEP OF RENE' 41 ALLOY SHEET
COMPARISON OF PARENT METAL AND FUSION WELDS

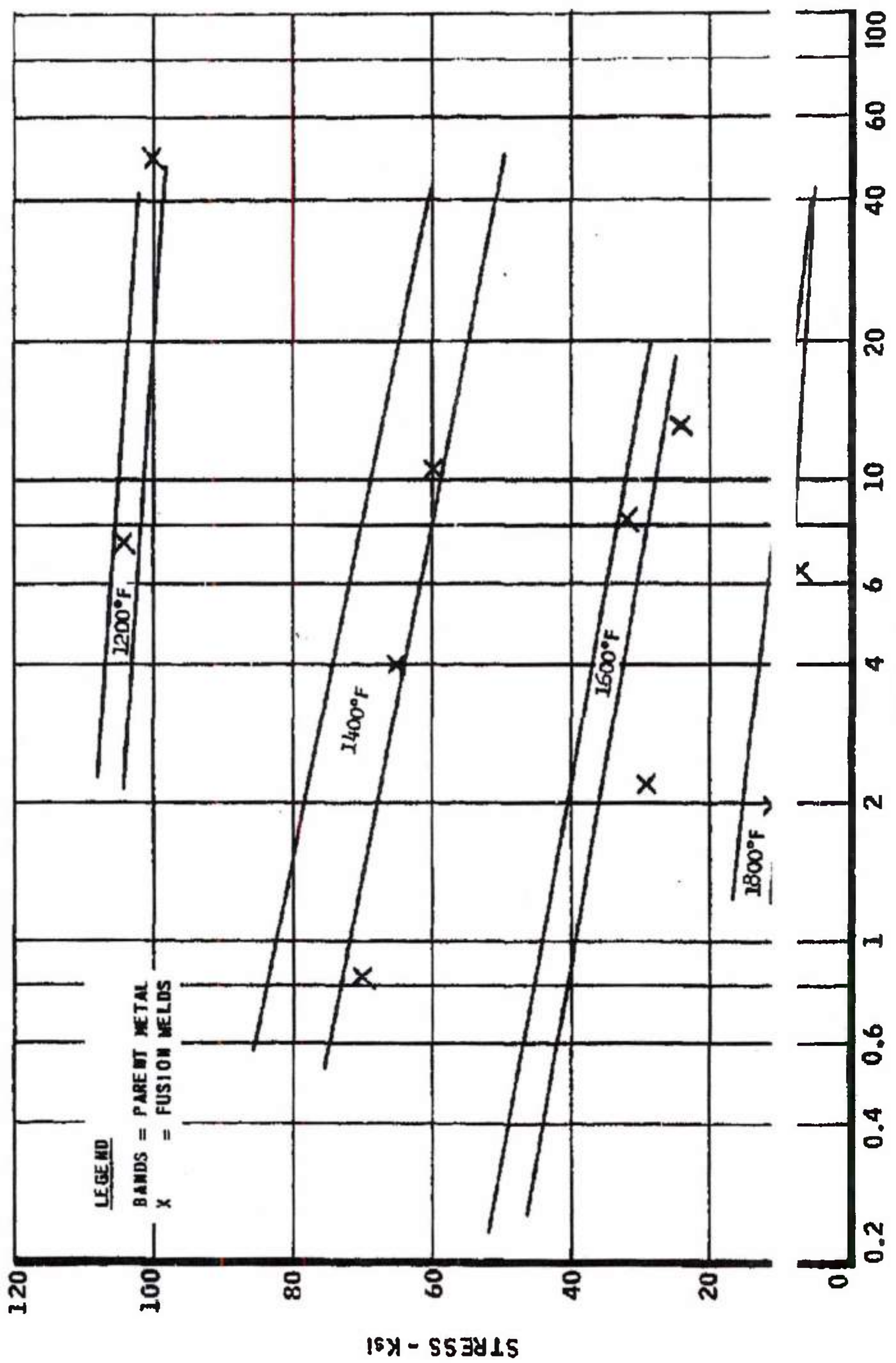

1% CREEP OF RENE' 41 ALLOY PLATE
COMPARISON OF PARENT METAL AND FUSION WELDS

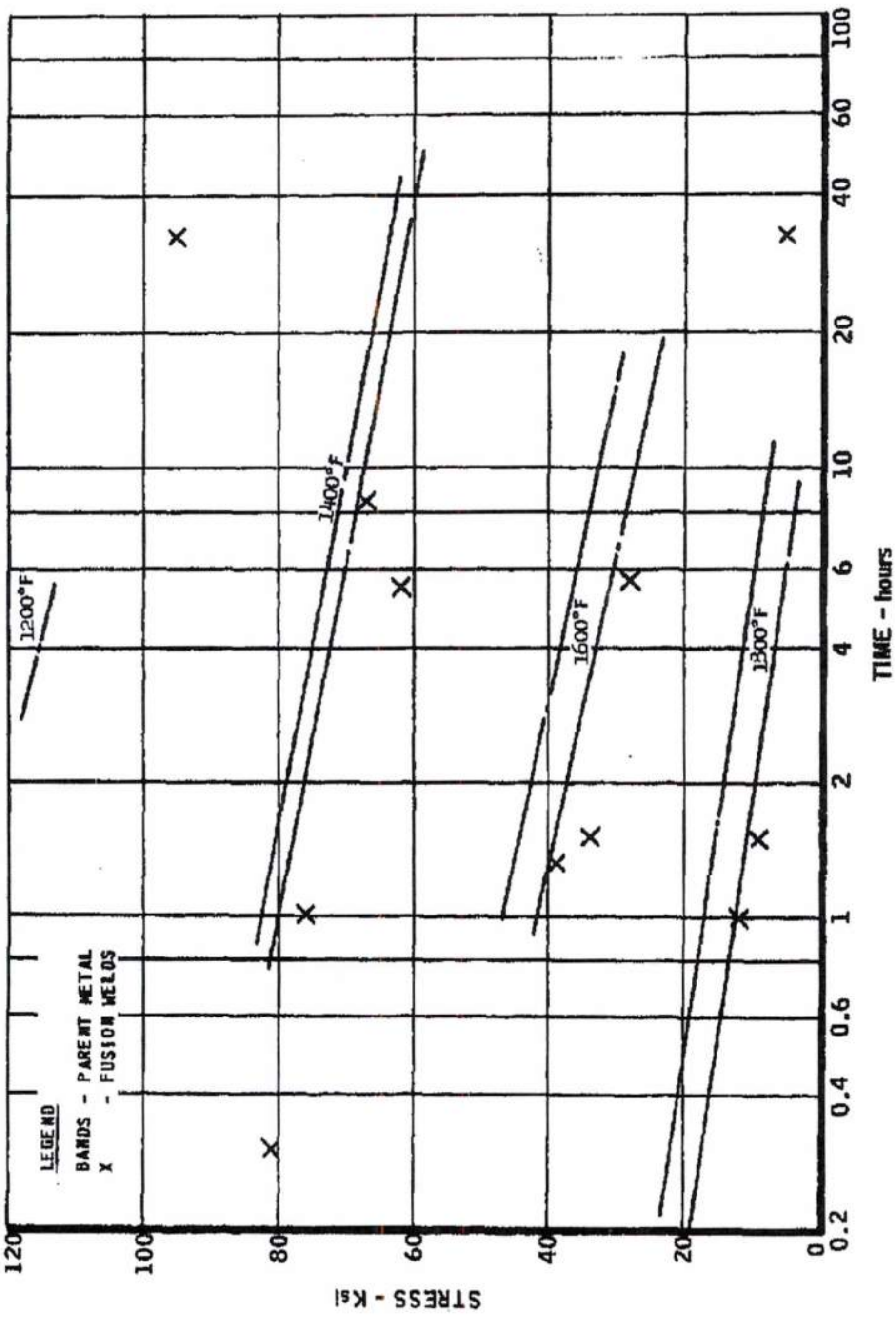

TENSILE PROPERTIES OF TYPE 321 STAINLESS STEEL SHEET

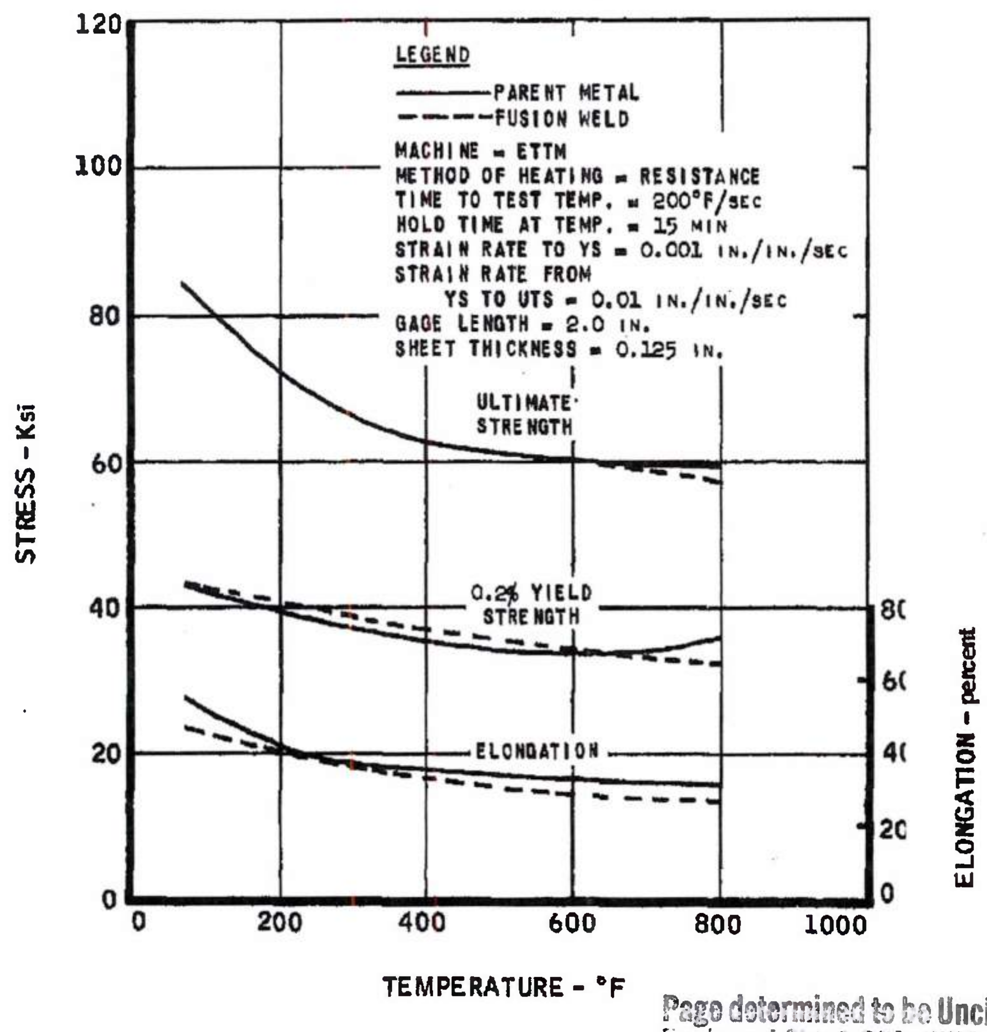

Three points should be noted from examination of the data presented

(1) The change in mechanical properties of an alloy depending on whether the material is in the form of sheet or plate. This behavior is, of course, expected. The program for next year includes the testing of other fc ms of the alloys that may be used as structural members in the Pluto engine, su as forgings, castings, tubing, and wire so that the spread in design values fo the alloys may be known.

(2) The allowances, if any, that must be made in design values to account for a welded structure and the welding procedure to be used. The M (metal alloy electrode, inert gas) process for welding is being developed for Hastelloy C alloy plate for further comparisons with the TIG process. Tests re planned for the coming year so that comparative results will be available.

(3) Inconsistencies within the same material due to alloy behavior o production history. In particular, the results of all tensile tests are based o one, or, at best, a few samples due to the large area to be covered for the y r. It is necessary to test a large number of samples to establish statistical tren and reliability bands. The effort for the following year will be directed towa more complete and statistical data based on the results presented here the be er to define design values.

3.10.2 Beryllia Testing

Durability Tests

A program was undertaken in 1961 to provide experimental informat n on the durability of beryllia when exposed to the combined operating and envi n-mental conditions expected during a typical mission profile for the nuclear ra 1-jet missile. Data describing the mechanisms of hydrolysis and erosion are r -quired to assess the effects of core deterioration on mission performance capabilities.

The beryllia specimens tested during 1961 were hot-pressed blocks ie inch in diameter and one inch in length. The blocks were pierced by seven fl v passages, each 0.20 inches in diameter. Two types of specimen materials w re tested, pure beryllia and beryllia plus one percent of magnesia. Properties the specimen materials tested were almost identical:

	Beryllia	Ber lia plu 1% Mag sia
Percent Theoretical Density	98 - 99	98 99
Grain Size (microns)	30 - 40	30 40
Modulus of Rupture (psi)		
Room Temperature	20 - 25,000	20 - 2 000
1500° F	15 - 18,000	-

A flow test rig was assembled that can supply one pound pe second of vitiated air at temperatures up to 2500° F for periods up to and incl ing ten hours. Fixed specific humidities of approximately 4 and 8 percent re imposed by using either hydrogen or propane for heat input. In a typic test run, four beryllia blocks were placed end to end in a specially designed a l instrumented pipe section.

A total of 24 specimens (12 pure beryllia; 12 beryllia and o percent magnesia) were used during an accumulated 26 hours of testing. Af r exposure to the high-temperature, high-humidity air all specimens took on a azed appearance, and almost all samples showed evidences of thermal cr king between adjacent holes. In a few cases these cracks were enlarged by rosion. This effect can be seen in Figure 139.

Not enough tests have been performed to allow statistical e luation of all the dependent variables associated with the hydrolysis phenomen . However sufficient experimental information has been obtained to establish tr ids and to serve as a preliminary basis for comparison with the results obtain . by other investigators. Test results can be summarized as follows:

(1) The hydrolysis mechanism is effectively nonexistent at empera- tures below 2000° F.

(2) In general, the samples with one percent magnesia exh ited 20 to 25 percent less total material loss than the pure ber lia under the same conditions.

(3) Increasing the specific humidity from approximately 4 approximately 8 percent had the apparent effect of increasing t e erosion rate by as much as a factor of 4.

(4) The average rate of material loss from the pure beryll samples was approximately 4.5%/hr (by weight).

FIGURE 139 - Beryllia Hydrolysis Specimen L-6 (After Exposure)

(5) The average rate of material loss from specimens wit[illegible] one percent magnesia was approximately 3.5%/hr (by weight).

The test conditions employed to date are considered rather [illegible]evere with regard to the moisture content of the air. In order to more accur[illegible]ely simulate flight engine conditions (maximum specific humidity up to 3 per[illegible]ent at temperatures up to 2800° F), two new air heaters have been installe[illegible] in the test facility. These heaters will permit testing at temperatures up to 3[illegible]0° F with controlled humidity levels from zero to above 3 percent.

Thermal Shock Tests

In cooperation with Atomics International, Marquardt has [illegible]rformed a total of three tests to evaluate the thermal shock resistance of hot-[illegible]essed beryllia. The first two of these tests were performed in December [illegible]960 and reported in the first period of 1961. The third test, conducted in mid [illegible]961, was reported in Reference 8.

The purpose of these tests was to determine the magnitude [illegible]f the thermal stresses induced in, and the structural damage suffered by [illegible]beryllia specimens air-quenched from a high temperature. The three tests [illegible]iffered only with respect to specimen size and method of fabrication. The elem[illegible]ts in the first test were one-inch thick hexagonal blocks, 3 1/4 inches acros[illegible] flats, with cored holes. The elements used in the second test were the same [illegible]e but had drilled holes. The blocks used in the third test had drilled holes bu[illegible] were 5 1/4 inches across flats.

Each test module consisted of nine blocks contained in a sp[illegible]cially designed holder. An assembled module is shown in Figure 140.

The beryllia blocks were extensively instrumented with the[illegible]mocouples in order to obtain temperature profiles. Under typical test conditi[illegible]s the module temperature was raised to 2400° F with vitiated air (19 pps [illegible] 250 psig) at a rate calculated to keep the thermal stress at a safe level. Wit[illegible] the module temperature stabilized at 2400° F, the air temperature was reduce[illegible] [illegible]nstantaneously to approximately 1600° F. The thermal shock associated w[illegible] this temperature change was manifested in the form of broken blocks an[illegible] random hairline cracks. Comparison of pre- and post-test specimen weigh[illegible] indicated no loss of material due to erosion.

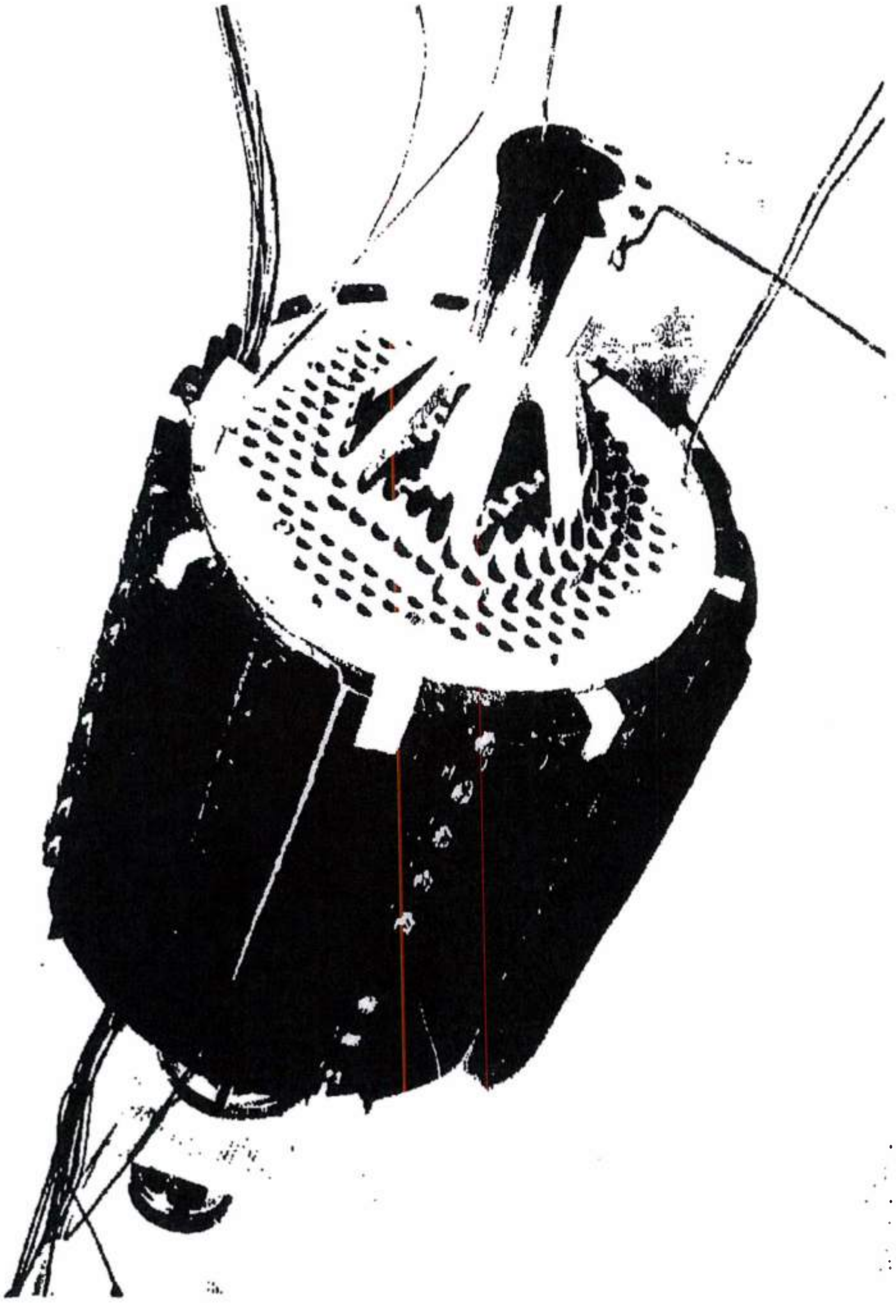

T2928-7

FIGURE 140 - Atomics International Hot Pressed Beryllia in Test Module

Significant conclusions drawn from the three tests are a: follows:

(1) The capacity of the beryllia plates to withstand shar; emperature changes is directly related to method of fabrication a d density uniformity.
(2) The modulus of elasticity and/or rupture of the bery .a plate must be based on local density rather than bulk density.
(3) The type of crazing and cracking encountered in the sts very probably would not adversely affect reactor operatic .

3.10.3 High-Temperature Springs

An area of major concern in the design of the Pluto syst a is the control of differential thermal expansion between various component in the reactor support structure. The expansion of components must be accom odated without relieving necessary restraining forces or imposing overloads at itical regions. One method of controlling this expansion is the use of springs.

An extensive spring evaluation program was initiated an partially carried out during 1961 utilizing spring designs that could be incc porated into the basic structural supports of the Pluto reactor. Three types c springs are under investigation: (1) Belleville, (2) corrugated, and (3) plate

In order to evaluate and verify the spring designs, expe nental tests were conducted to provide performance data for each spring confi uration. The tests were performed under simulated flight environmental condit ons of temperature and vibration. Compression and tension tests of the corrug ted springs and compression tests of the Belleville and plate-type springs we conducted to determine load-deflection performance and spring relaxation und conditions of normal dynamic cycling, rapid repetitive cycling, and vibration a both ambient and elevated temperatures to 1400° F for extended time periods.

Rene' 41 alloy material was selected for all springs as t best available high-temperature alloys for the anticipated operating conditi ns.

Belleville Springs

Figure 141 shows a typical 10-spring stack of Bellevill springs. A single spring is 0.10 inches thick, 2.00 inches in outside diamete , 0.875 inches in internal diameter, and 0.045 inches in coned height. Test con gurations consisted of individual Belleville springs, 10 springs stacked in a se es arrangement, and 6 springs stacked in parallel-series combination. The spring tester is shown in Figure 142 . Instrumentation included a load cell to ndicate loads up to 5000 pounds, a direct reading dial indicator for deflection d a, and temperature readout.

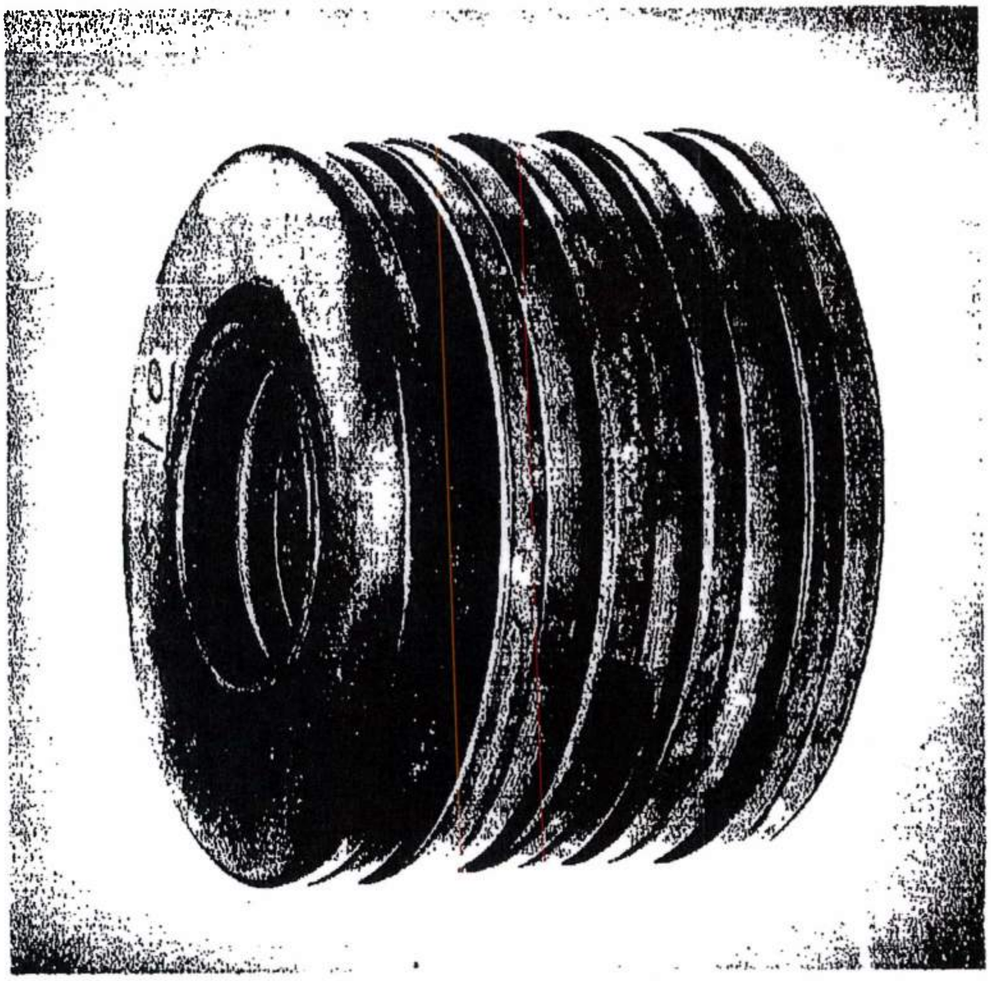

3879-3

FIGURE 141 - Ten - Spring Stack of Belleville Springs

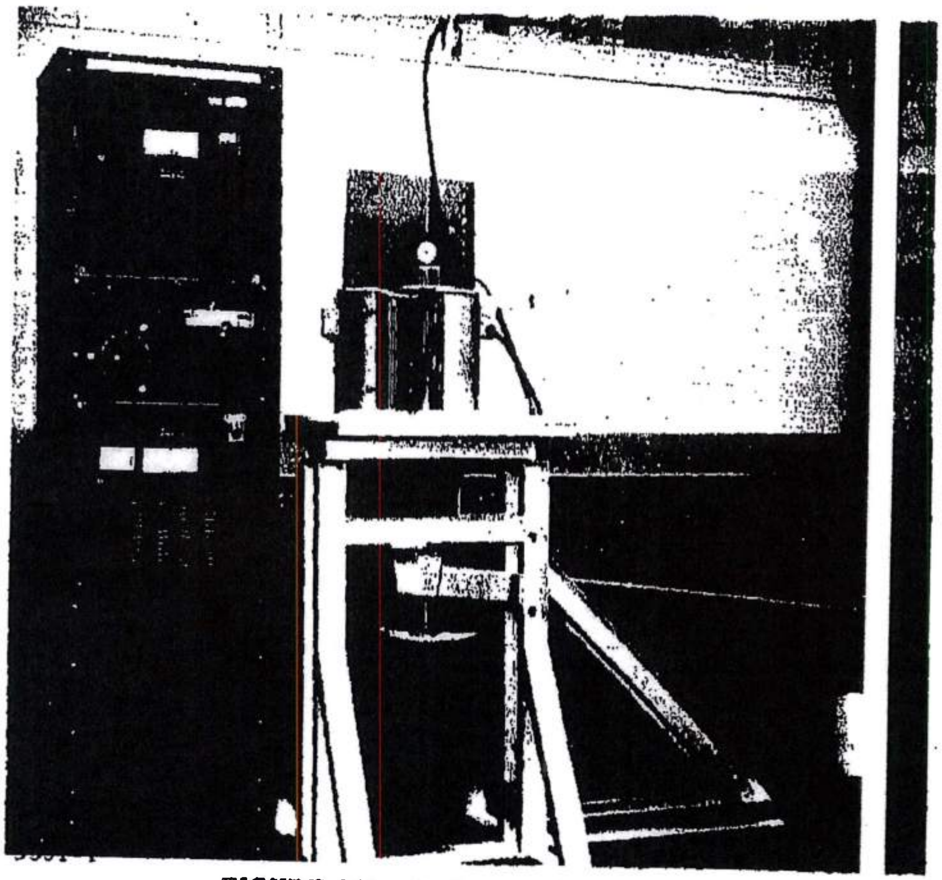

FIGURE 142 - Belleville Spring Tester

For the vibration tests, the spring tester was modified by replacing [the] load cell with a pneumatic piston vibrator linked through the spring tester as shown in Figure 143.

Results of the load-deflection and vibration tests for the Belleville springs can be summarized as follows:

(1) In general, during the first few load cycles, both single springs [a]nd stack configurations showed initial relaxations, very close to predicted value

(2) At ambient temperature and 1200° F, the springs demonstrated [ve]ry little additional relaxation with continued load cycling. However, at 1400° F [th]e springs indicated an increased rate of relaxation with additional load cycling.

(3) The constant deflection test for the extended period (10 hours) a[nd] load cycling for the extended time (accumulative 10 hours) resulted in small [lo]ss of load-carrying capability at ambient and 1200° F, whereas at 1400° F the lo[s]s was considerable.

(4) Evaluation of spring performance under vibration conditions at 1200° F and 1300° F was inconclusive due to test equipment difficulties.

Conclusions that may be drawn from these results are summarized [as] follows:

(1) Load-deflection performance of the springs verified the trend of design; i.e., the springs were designed with a load-deflection curve approac[hi]ng linearity.

(2) Belleville springs fabricated to the present design from Rene' 4[1] alloy are satisfactory for use at temperatures to 1200° F. In the 1300 to 140[0°] F temperature range, spring performance will be marginal.

(3) Spring performance above 1300° F is apparently affected by wor[k] hardening and material creep. Indications are that these detrimental characteristics can be circumvented by limiting deflections to less than 80 percent [of] the spring deflection capability.

(4) Because the springs undergo an initial relaxation, they should b[e] load-deflection cycled prior to final assembly.

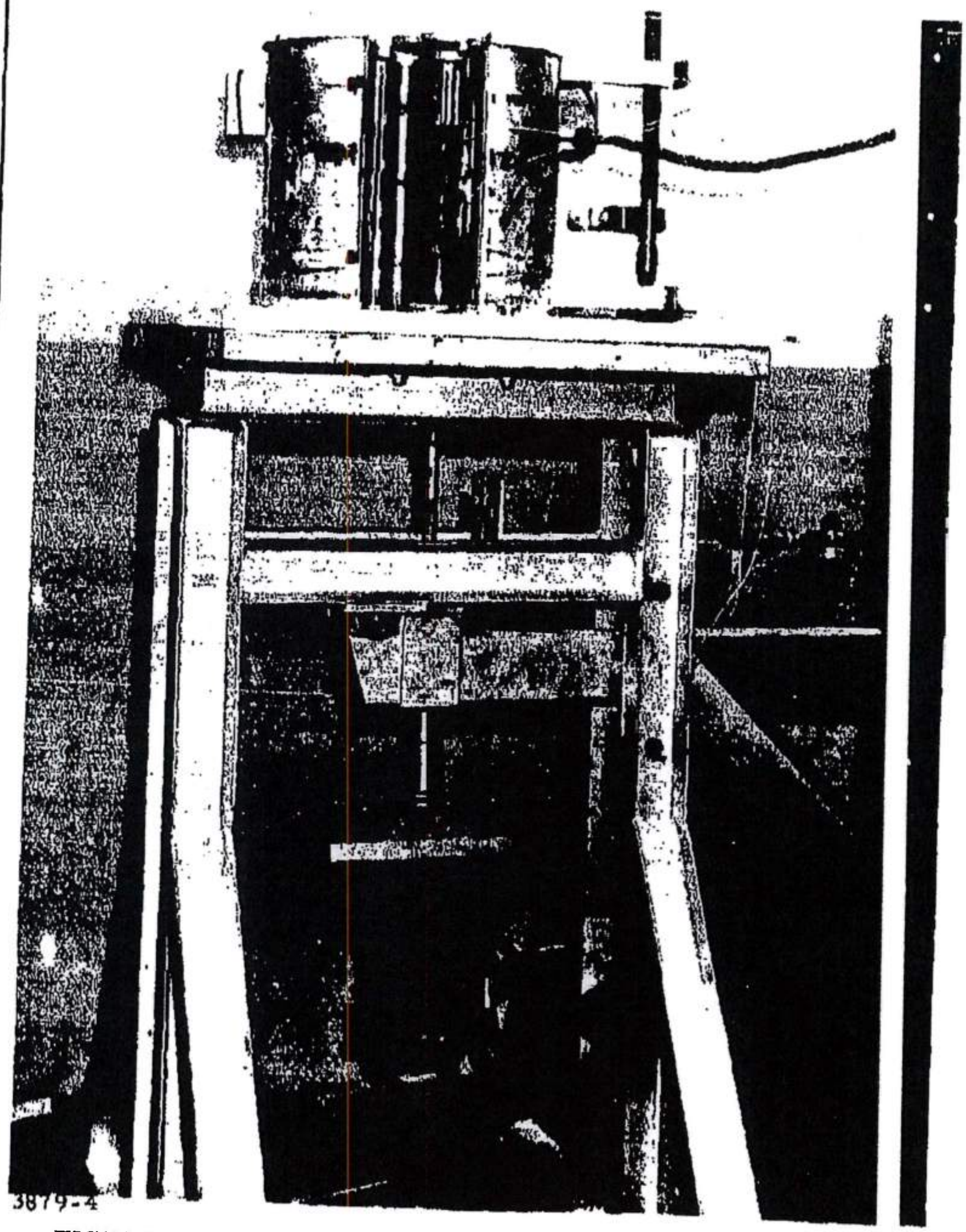

FIGURE 143 - Belleville Spring Tester with Vibrator Installed

Corrugated Springs

Figure 144 shows the configuration of the corrugated springs used ir the evaluation tests. In the figure, the longer spring is 11.3 inches long and ıs a nominal thickness of 0.100 inches. The shorter spring is 10.2 inches long lth a nominal thickness of 0.125 inches.

Ambient temperature tests of corrugated springs were performed on he Baldwin Universal Test Machine at the Marquardt Materials and Process Lab :a- tory. Figure 145 shows this setup. The springs were instrumented with stı in gages to obtain tensile and compressive strain data at the inner and outer con ›- lutions of the spring. Load, deflection, and strain values were recorded. T: elevated temperature test setup is shown in Figure 146.

Rapid cycling tests were performed on corrugated springs at ambien temperature and 1400° F to document spring fatigue characteristics. Figure ł7 shows a spring being cycled at 1400° F in the Elevated Temperature Test Mac ine. Load, deflection, temperature and cycling frequency were recorded. The fol lowing results were obtained:

(1) No relaxation (permanent set) occurred during normal tension cycling tests at maximum test conditions of 0.280-inch extensions, 482-pounc loads, and temperatures ranging from ambient to 1400° F.

(2) Load-deflection values, obtained from the normal tension tests, matched predicted performance for both ambient and elevated temperatures.

(3) Under rapid tension cycling tests at 1400° F, spring relaxation o curred and appeared to be linear and continuous for individual test runs of 1 1 hours, 4 1/2 hours, and 6 hours. This was true for both the 0.100- and 0.12 inch thick springs. Maximum deflection for these tests was 0.279 inches wit: a maximum load of 430 pounds. Cumulative relaxation values for a series of s: rt tests on a given spring exceeded the values obtained for a continuous test on ε similar spring over the same total time period. Also, the composite time-relaxation curve was nonlinear for the series of short tests.

(4) Rapid tension cycling of one 0.100-inch spring to 0.295-inch ext- -sion (332-pound load) at 1200° F temperature for two separate six-hour perio did not produce elongation.

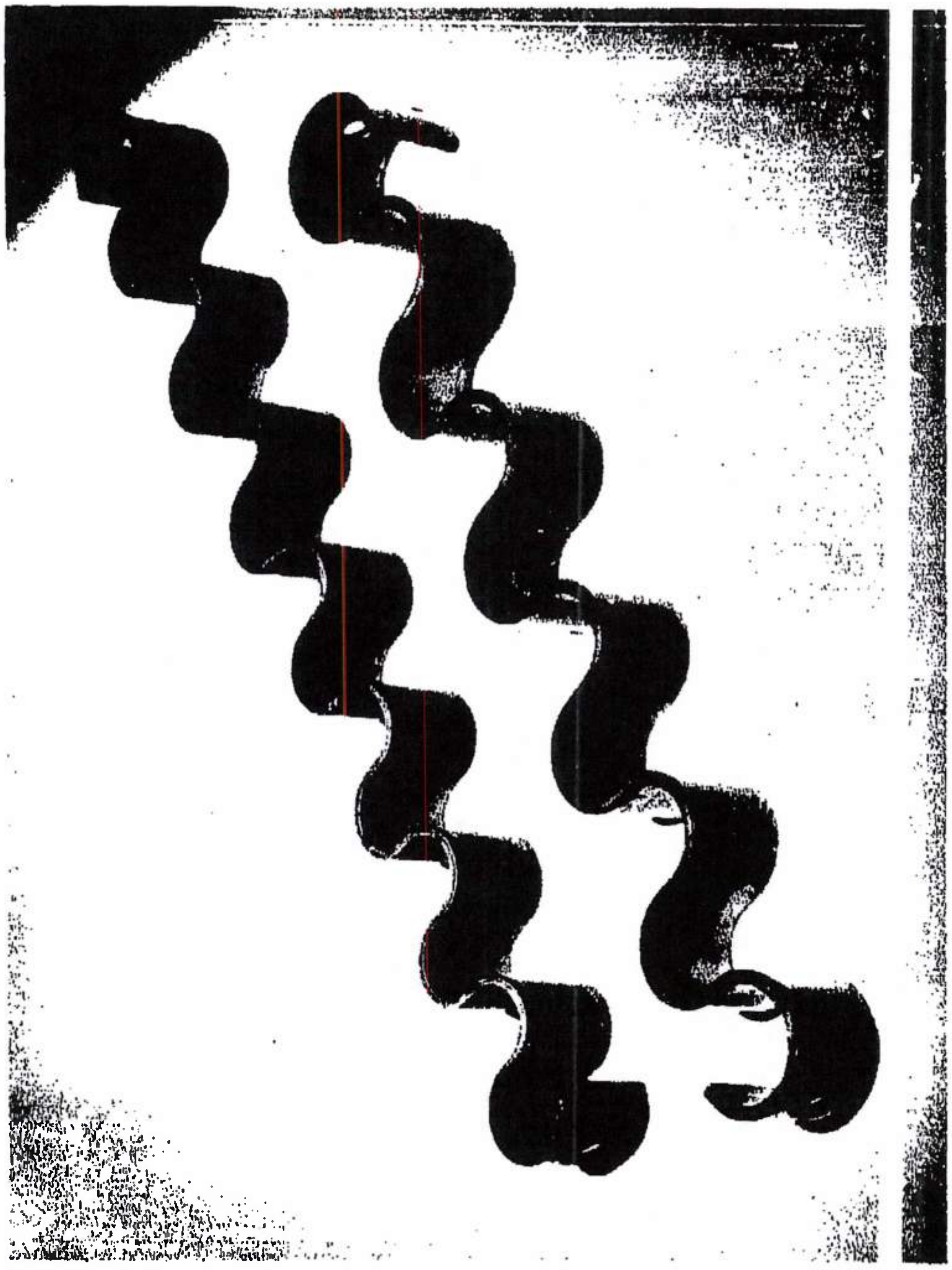

3566-1

FIGURE 144 - Corrugated Side Support Springs

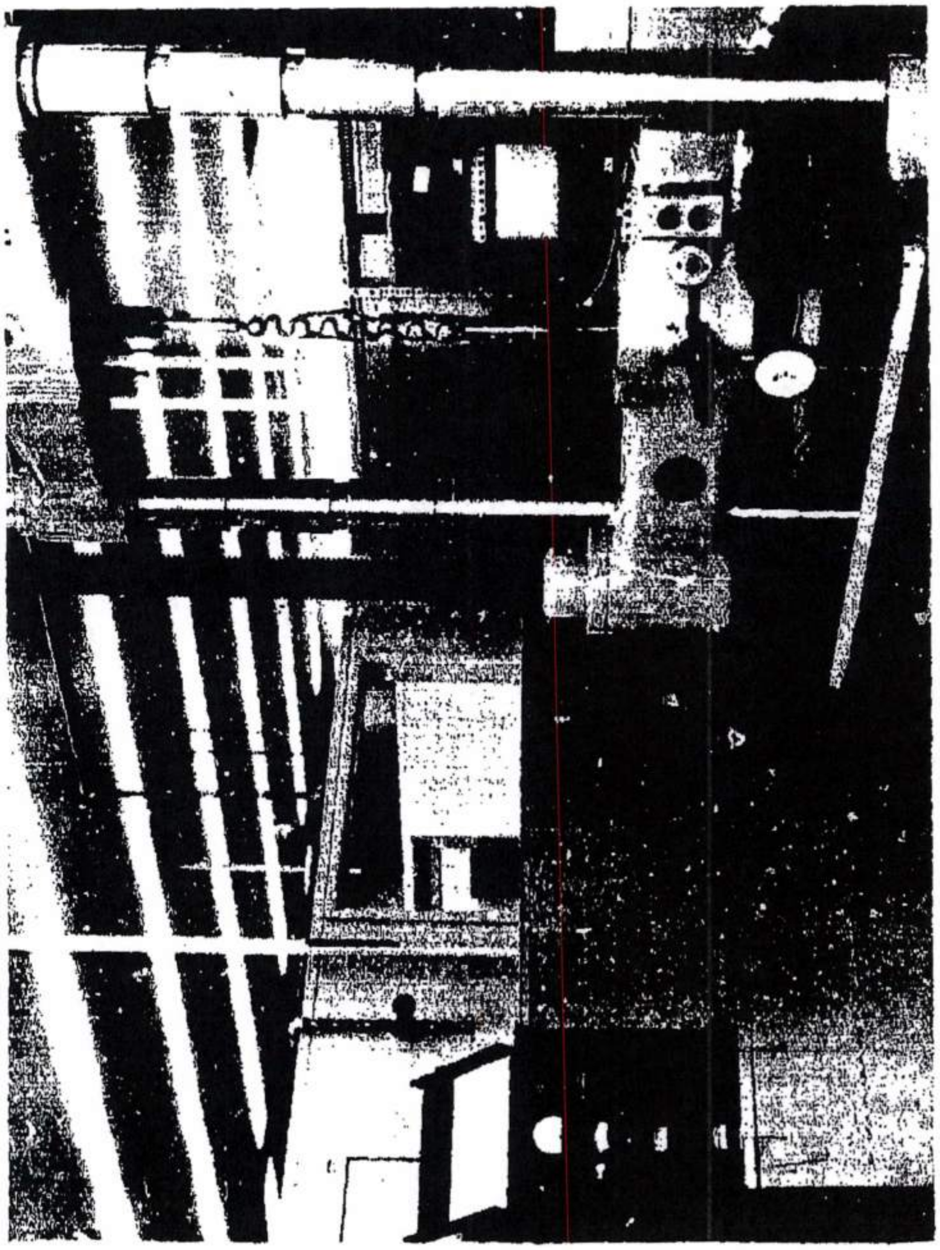

3566-5

FIGURE 145 - Corrugated Side Support Springs Installed in Baldwin

mentation

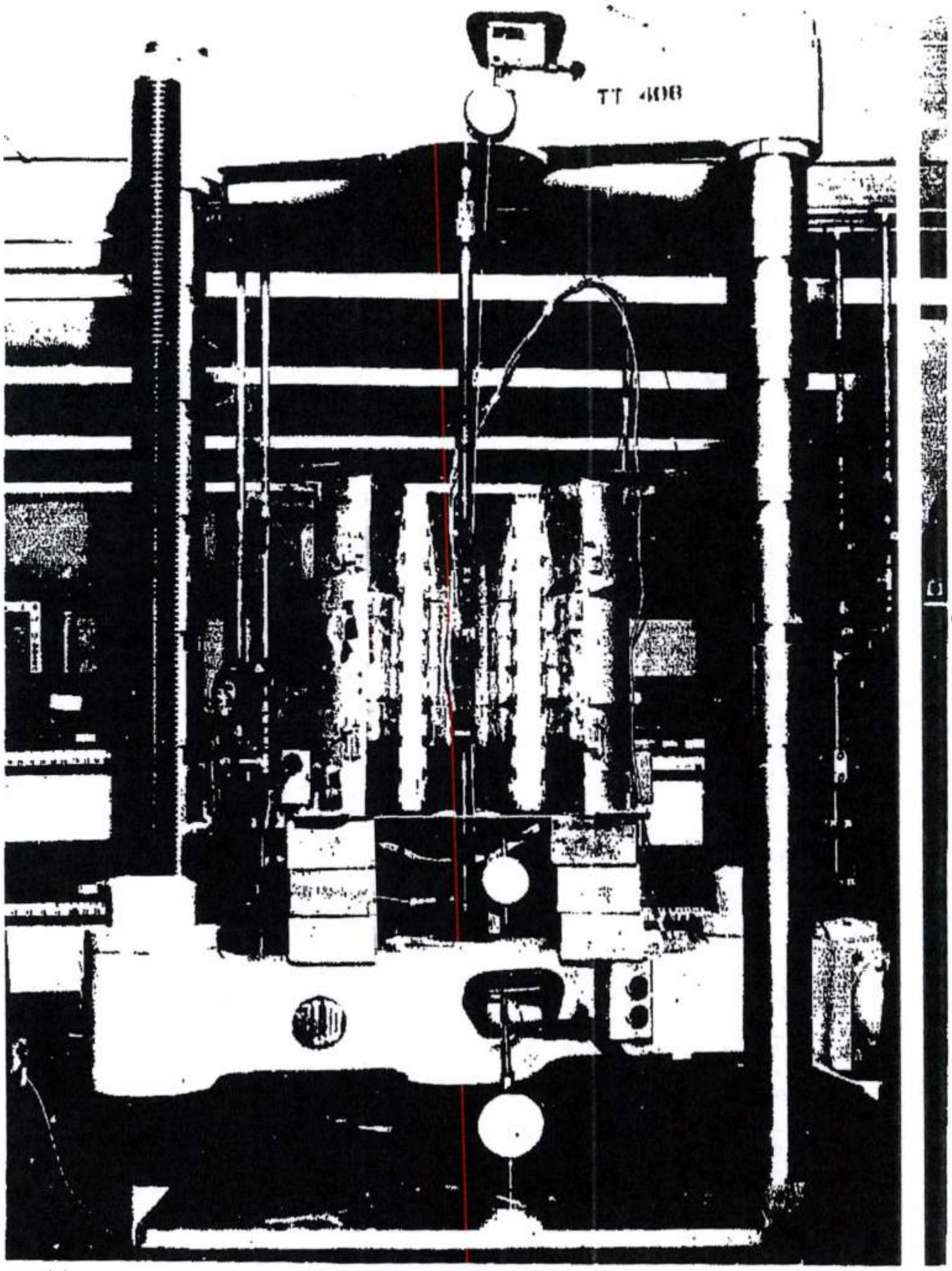

3566-7

FIGURE 146 - Elevated Temperature Test of Corrugated Side Support Spring

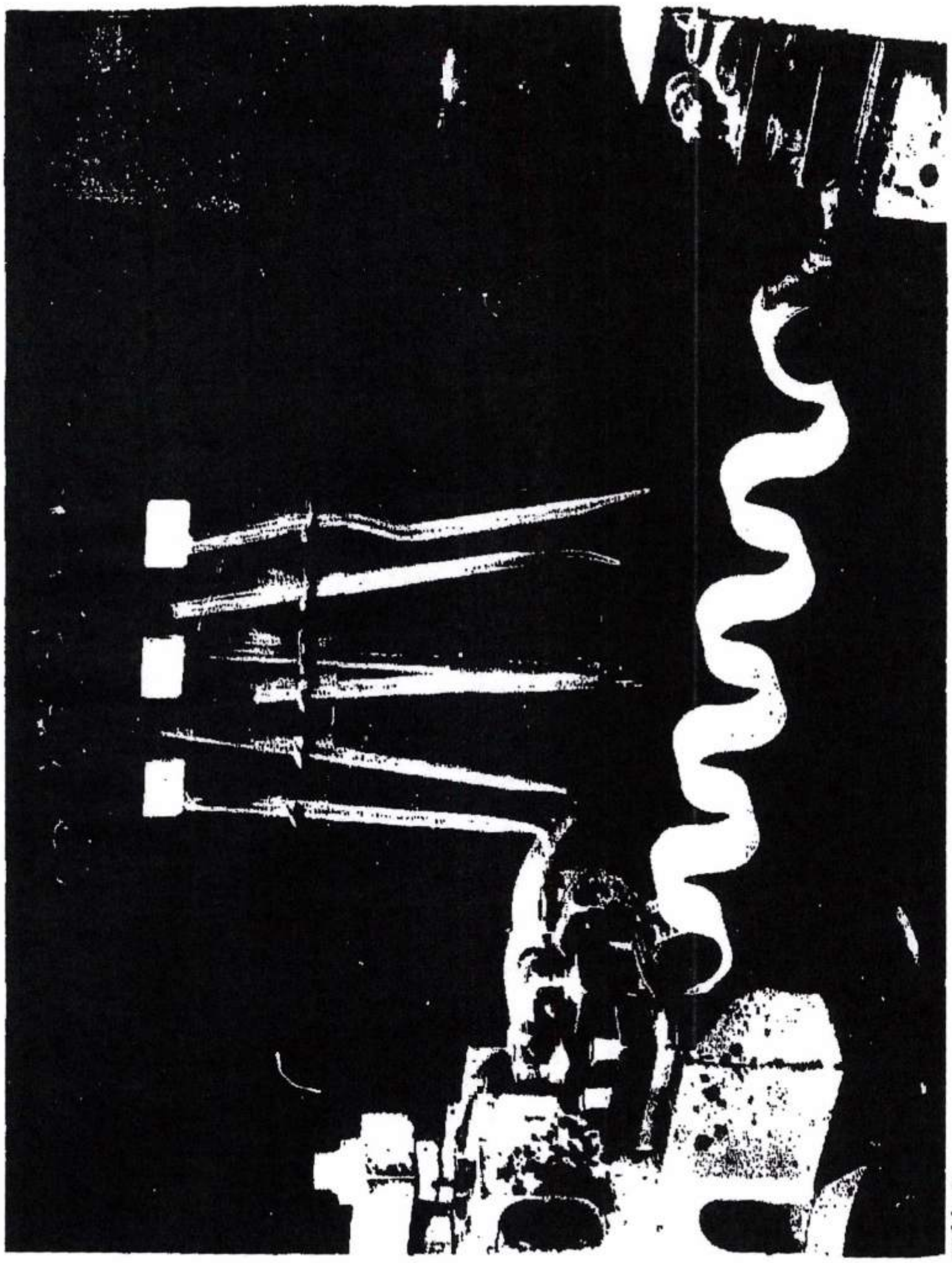

3566-9

FIGURE 147 1400°F Test of Corrugated Spring in Elevated Temperature Test Machine

MAC A633

From these results, the following conclusions were reache[d]

(1) Corrugated springs can be adequately designed by "cur[ve]d beam" formulae to meet requirements of a particular application.

(2) Corrugated springs are particularly sensitive to shape [an]d tolerance discrepancies. To assure acceptably uniform performance characte[r]istics, strict manufacturing quality control must be maintained.

(3) Material creep and work-hardening experienced in the [..]00° F rapid cycling tests can be eliminated if tension bending stresses do not ex[ce]ed approximately 75 percent of the allowable tensile stress for zero creep at [th]at temperature.

(4) The magnitude of corrugated spring relaxations resulti[ng] from rapid cycling generally have a negligible effect upon spring rate during su[bs]equent testing, provided the induced tension bending stresses do not exceed [a]pproximately 60 percent of the allowable tensile stress for zero creep.

Plate Springs

Figure 148 shows the plate springs as tested in this progr[am]. The plate springs were tested for load-deflection characteristics at roon[m] temperature and elevated temperature in the Baldwin Test Machine in a test [s]etup similar to that used for the corrugated springs. No rapid cycling testing [o]f these springs was performed. Problems arose during the testing that res[ul]ted in erratic and inconclusive test results. Further testing of plate sprin[gs] is planned for 1962.

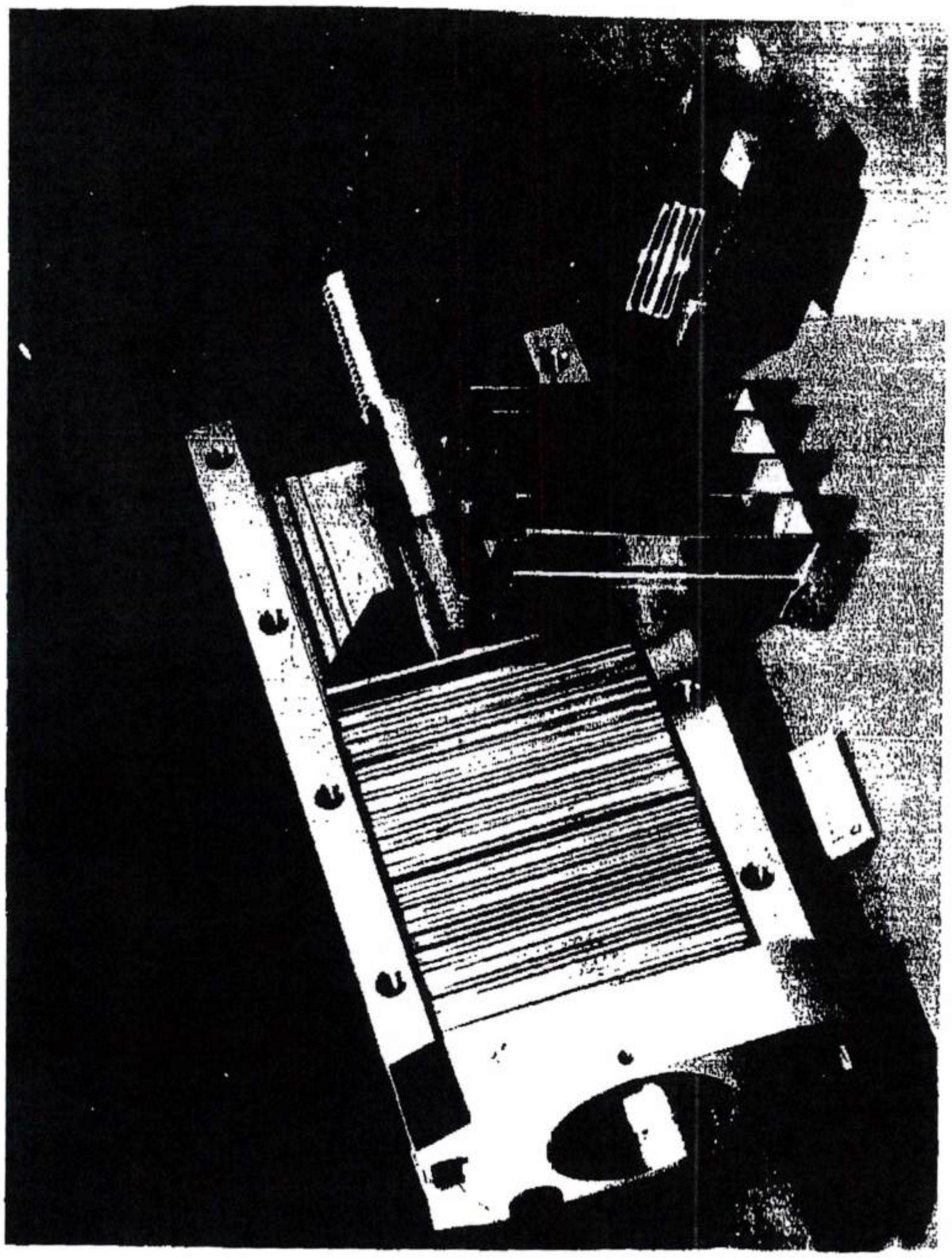

3718-5

[illegible]
and Compression Testing

4.0 PROPULSION SYSTEM CONTROLS

4.1 GENERAL STATUS

During the year 1961 a balanced program was planned for th development of Pluto propulsion system controls. The controls activities fell int three logically separated, although not independent, categories. The categori are generally described as (1) system analysis, pertaining to the generation o requirements and specifications for the control system and its components; (2) con ol system components, pertaining to the design, development, and testing of se sers, electronic computing devices, and pneumatic actuators; and (3) irradiati testing, pertaining to the investigation of materials, components, and design chniques to permit sustained operation of controls devices in a nuclear environm nt.

During the course of the year's activities it became obvious hat more rapid progress was being made in the development of electronic com ting devices and sensers than was being made in the development of high-tempera re pneumatic actuators. Thus, in order to maintain a balanced program leadi to coordinated completion schedules for system testing, portions of the electr c and senser development programs were curtailed to place increased bud t emphasis upon pneumatic actuator development. In particular, a two-phase p gram was initiated to evaluate, under controlled test conditions, the friction a wear characteristics of selected materials and the relative advantages of vari s lubrication systems for use at high temperatures.

The following sections describe the 1961 activities in the ab e-mentioned categories.

4.2 CONTROL SYSTEMS ANALYSIS

4.2.1 Minimum Startup Interval

One of the limitations that determines the minimum value o engine startup time is the dynamic response of the nuclear instrumentation used the ground control system, such as log count rate (LCR) and ln n circuits. The circuits operate with low pulse repetition rates and low current inputs.

A dynamic closed-loop analysis has been performed on the ternal ln n loop incorporating mathematical models of typical existing nuclear i trumentation. The limiting instrumentation characteristics are the smoothing filte dynamics in the LCR circuits that are dominant in the lower level channels. In t analysis the following assumptions and conditions were used:

(1) The primary control parameter is either ln n or inverse perio from source level to the power level at which the inflight control system is s tch-ed into control. The system is operated closed-loop, where continuous cont l of ln n or inverse pe iod is provided.

(2) Typical commercially available nuclear instrumentation is used n the ground nuclear control system.

(3) The automatic, programmed command (ln n or inverse period) vas assumed to be one-decade step inputs, for which instrumentation response ch r-acteristics were available. The reactor was restricted to periods longer tha 1 second for two reasons: (a) the outputs from the nuclear instrumentation rep sent maximum rate-of-change quantities that the instrumentation is capable of pr id-ing for input decade step commands, and (b) an inverse period override is au ion-eered (monitored for selection) so that the actual reactor period cannot be le than 1 second.

(4) The source level is taken at 1 milliwatt.

The internal ln n loop was analyzed for two reasons: this loop is co - mon to all outer control loops, and the dynamics of the internal ln n loop are ne limiting dynamics in the outer control loops using ln n or inverse period as primary control parameters. Reactor temperature during the interval from source level to about 1 percent design point power is near ambient. Thus, c e temperature is of no practical use as a control signal during rapid startups.

The analysis indicates that, with the nuclear instrumentation include , the ln n loop is stable when the coarse rod control subsystem and inflight con ol reactor compensator are removed. Because the coarse rod control subsyste is used only to compensate for large reactivity changes due to temperature coef ci-ent effects and long term poison effects, the coarse rod is not needed for cor rol during the interval from source insertion to the launch power level. In this i er-val, the reactor temperature remains near ambient and reactivity changes du to temperature changes are negligible. Use of the coarse rod control subsyster for scram is not excluded. The closed-loop response for the internal ln n loop (Reference 26) was studied using the basic engine control system configuratic with the addition of instrumentation dynamics derived from experimental data These data were furnished by General Dynamics/Electronics and appeared in he Twentieth Quarterly Progress Report.

During startup from source level to the power level at which control s transferred from the ground equipment to the inflight control system, the gro nd nuclear instrumentation and control equipment are part of the internal ln n lo) (the control equipment consists, in part, of counters, ion chambers, LCR circuits, and ln n amplifiers). The signal smoothing characteristic of the LCR and ln n circuits are a function of the flux level and contribute signi: :ant amounts of phase shift at low counting rates and low current inputs to the ln : amplifier. The effects of these dynamics in the control loop were considered b: insertion of appropriate dynamic equations for the blocks in the internal ln n loo that is shown here.

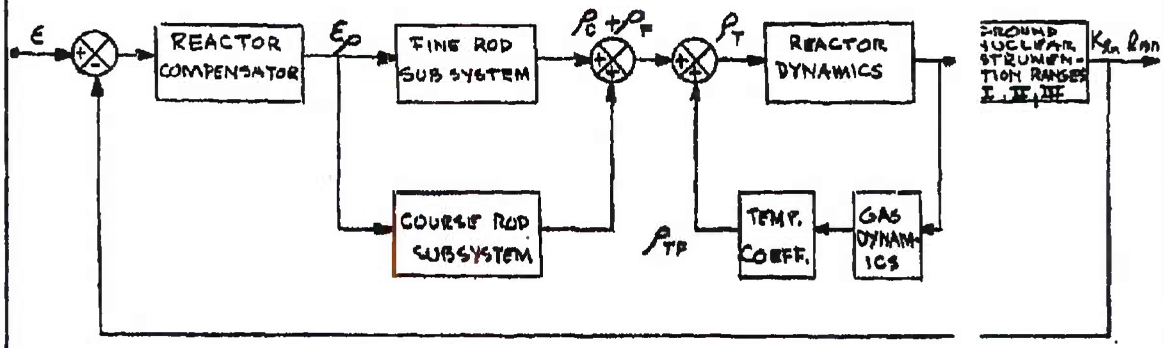

Detailed mathematics of these functional blocks, except the .nstrumentation, will not be included here as this information is fully discuss l in Reference 26. The following sketch of instrumentation channels an ranges indicates the values assumed with typical counter and ion chamber sens ivities and Pluto flux levels.

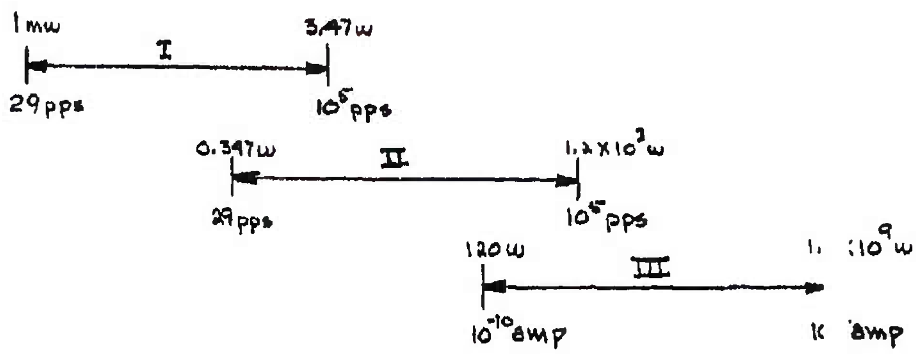

An overlap of one decade has been included between the ranges. Th switching points between ranges were taken at the lowest level of each range, because these are the points at which the time response of the instrumentatio is the slowest, and hence these points represent the worst conditions possible f fast automatic control. As the power level increases, the time response of t instrumentation also improves until it is no longer a limiting factor in the loc dynamics.

To determine a mathematical model of the instrumentation, a theore cal curve was fitted to the experimental data provided by the manufacturer. The he- oretical transfer function that describes this curve was then used to represe the instrumentation in the internal ln n loop.

At the very low power levels during startup there is no airflow throu h the reactor, and the core is at ambient temperature. This condition results reducing the transfer function of the core to the form of a simple integration ith a very low gain. When the effect of the temperature coefficient is added, the ain through the internal temperature feedback of the reactor is so low that the re ctor can be treated as an open loop. This means that the phase shift for the inter l ln n loop at this condition starts at -180° for zero frequency as compared to 0° at the higher temperature inflight conditions where the gas dynamics have an effect. If the instrumentation dynamics of Ranges I and II are added to this l p, an instability results. To overcome this condition it is necessary to remove e coarse rod subsystem and the reactor compensator from the loop. (It should e noted that the coarse rod subsystem has a free integration with second order dynamics and that the basic function of the coarse rod is to control the reacti ty effects of large temperature changes occurring during launch and long term i- soning. These destablizing dynamics are eliminated by holding the coarse r subsystem inoperative during initial fast startup at low power levels.)

As the power level increases, the instrumentation dynamics improv and are no longer the limiting factor in the closed-loop response. Since the sam LCR circuit is used for both Ranges I and II, the closed-loop dynamics for these t ranges are identical. The closed-loop rise times for these ranges using ste in- puts of one decade each were calculated for the entire range, and the fastest s- sible controlled power profile for Ranges I and II using these dynamics has b n plotted in Figure 149.

In Range III, the ln n amplifier is in the loop. The ln n amplifier ha no integration and a smaller time constant; hence, the instrumentation dynamic do not limit a power rise to a period slower than 1.0 second. The closed-loop se times for Range III were calculated for one-decade steps and were included i Figure 149.

REACTOR POWER - REAL TIME PROFILE

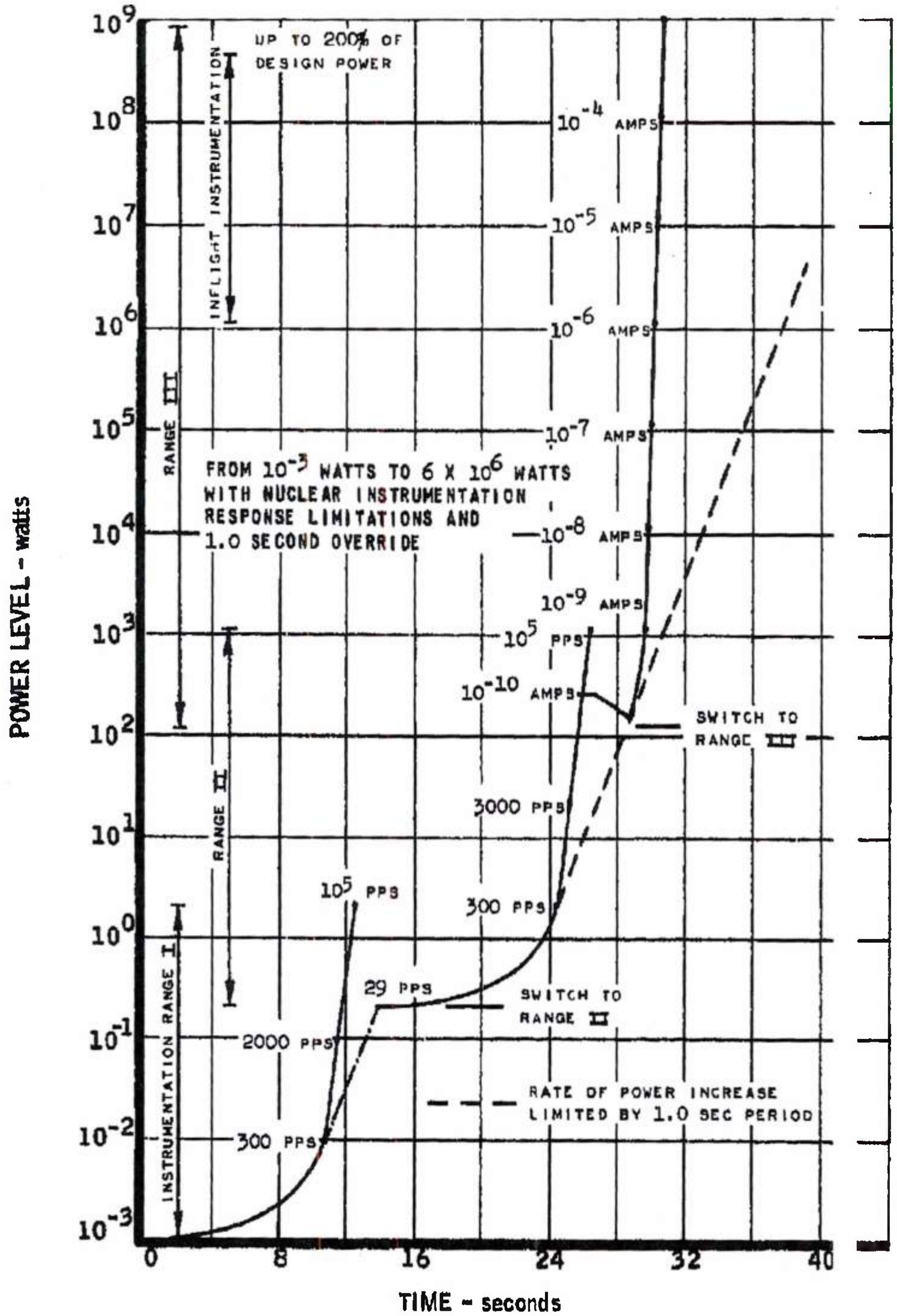

Figure 149 shows the minimum time in which the reactor could be a o-matically taken up to 1 percent of design power when the worst possible dyna ic ranges of available instrumentation are included with a switching overlap of e decade, and a 1.0-second period override. Source strength can be increase to reduce this time and improve system stability. To reduce the time further a smaller overlap between the ranges may be utilized, and much of the instrum n-tation limitation can be avoided. The minimum time required under the wor conditions to attain 1 percent of design power from source insertion is appro - mately 39.0 seconds.

4.2.2 Control Response For Inlet Restart at Low Altitude Condition

A simplified dynamic analysis has been completed to determine whe er it is feasible, from an airframe maneuvering point of view, to incorporate ir the Pluto inlet design the capability of restart during the low-altitude penetra on phase of the mission.

The main objective of the study was to determine the time available detect an unstarted inlet condition, to perform the necessary controls functic, and to restart the inlet with the following limitations:

(1) The inlet cannot be restarted at a Mach number less than 2.75
(2) The inlet cannot be restarted at an angle of attack greater than 7.0 degrees
(3) An appreciable loss of altitude from the 1,000-foot cruise condi on is prohibitive

It was determined that the optimum airframe maneuver during an ur started condition is to hold altitude and to allow the vehicle to increase the a le of attack as required. In this mode the forward velocity will decrease until - start is accomplished, or until speed drops below Mach 2.75. It is shown th , using this type of maneuver, the vehicle will slow down to Mach 2.75 in appr i-mately 3 seconds with very small changes in altitude or angle of attack, due t he action of the autopilot (Figure 150). This time interval was established assu ing that the thrust is equal to zero from the instant of unstart until the inlet is re started, and that the drag is increased during this period by approximately 7 per-cent (Figure 151). These values of thrust and drag represent the most pessi is-tic case.

There would be no advantage to a pitchup maneuver to increase altit le with an unstarted inlet unless the minimum Mach number at which restart ca be

AIRFRAME TRANSIENT RESPONSE
DURING PERIOD OF INLET UNSTART AND RESTART

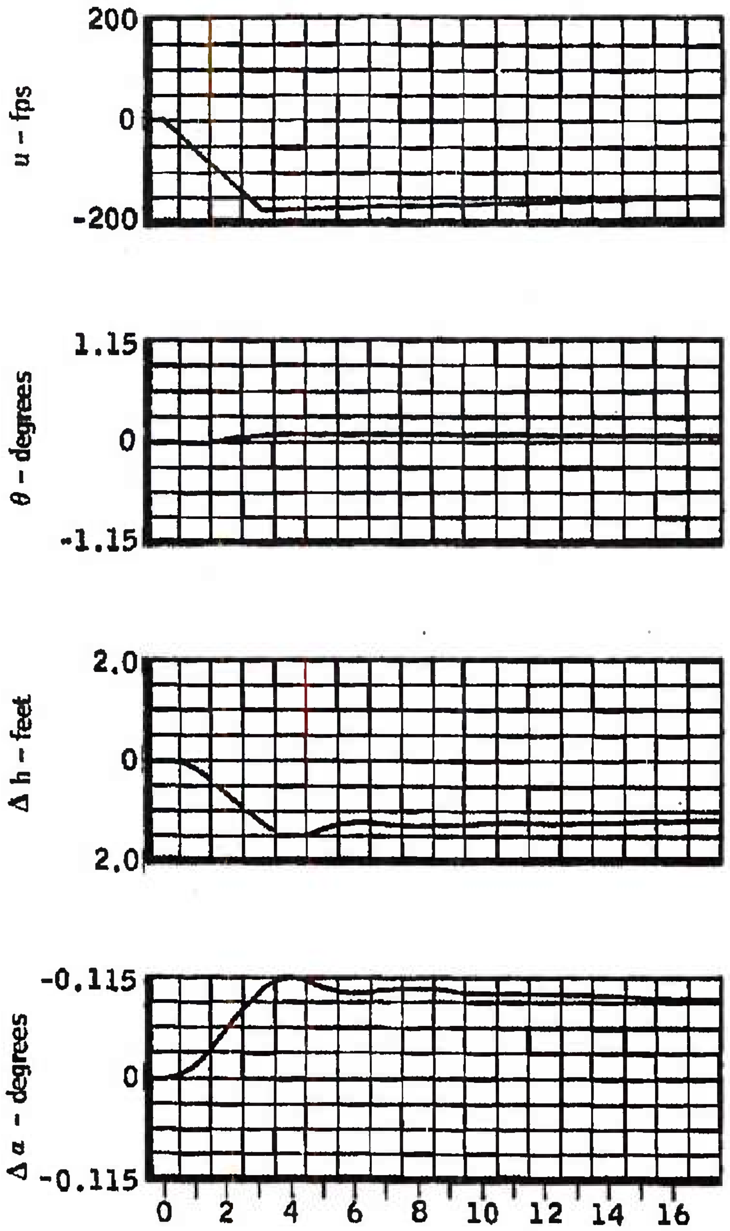

DECLASSIFIED IN FULL
Authority: EO 13526
Chief, Records & Declass Div, WHS
Date:
MAY 2 9 2015

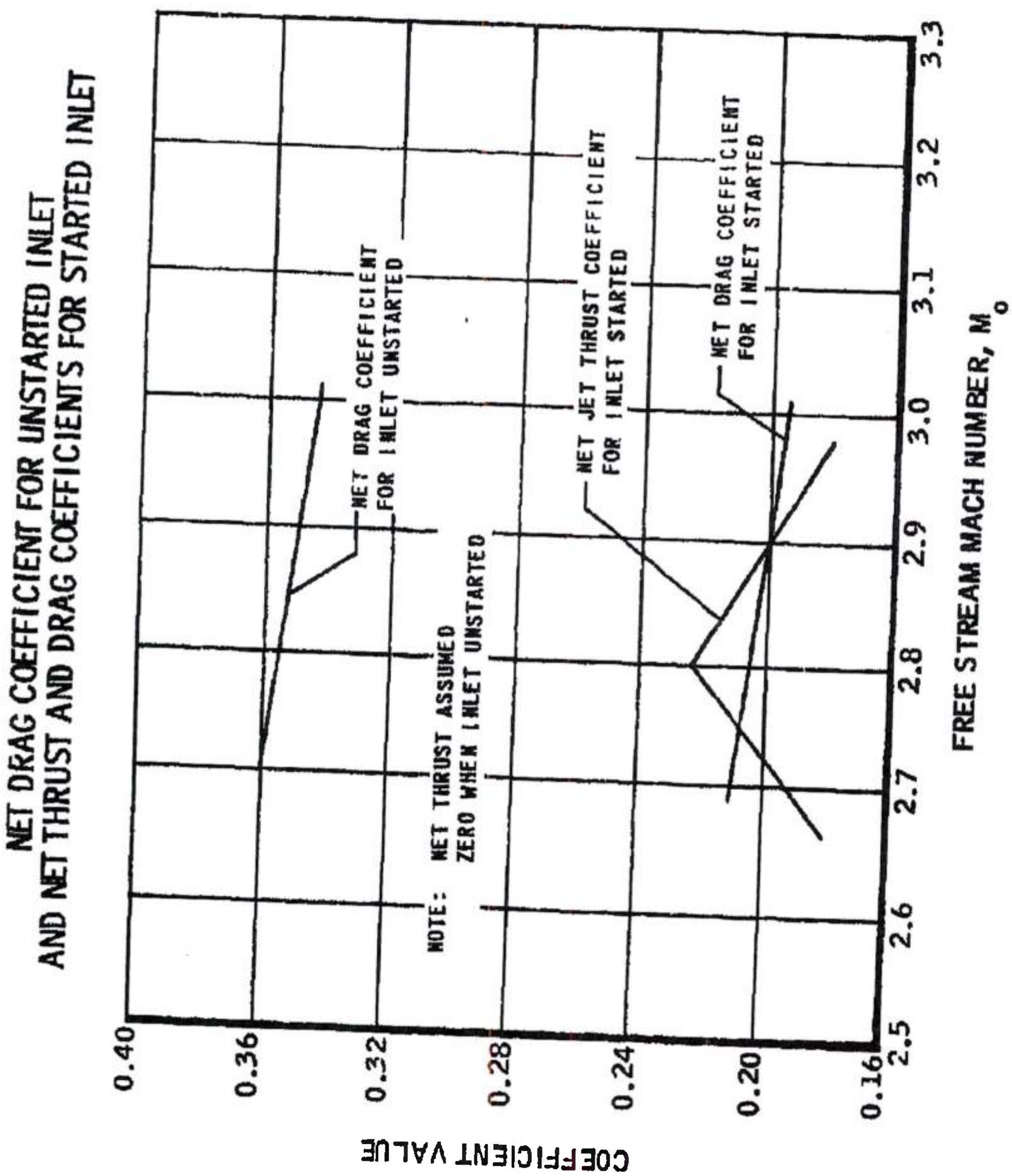

accomplished at the higher altitude is significantly lower than Mach . 75. It is still necessary, when the vehicle is climbing without power, to over- me the effects of the increased drag due to the higher angle of attack and the oss of kinetic energy used for climbing.

The analysis was performed using general linearized three- egrees-of-freedom equations of motion, which represent longitudinal missile m tions about the stability axis resulting from perturbations in selected flight cond ions (Reference 27). The pitch control and altitude control autopilot equa ons that were given in the Twent eth Quarterly Progress Report were used f r closed-loop control of the longitudinal airframe dynamics.

The complete set of closed-loop equations were simulated c the analog computer to obtain the transient response of the system.

The net thrust and drag were programmed using the curves 1 Figure 151. The solution, resulting in Figure 150, was obtained by the following equence: unstart was simulated by increasing the total drag and reducing thru to zero; just before the forward velocity reached the lower limit for restart, ne inlet was restarted and thrust and drag were taken from the curves for the sta ted condition at the new Mach number. It is seen that, even though the inlet is re arted, a long acceleration period is required to reach Mach 2.90 again as the hrust-drag margin is low. Should an unstarted condition arise again before the ehicle could accelerate close to normal speed, the subsequent time for restart w ild be very short. It is therefore important to establish the possibility of recur nce of the conditions that can initially cause unstart. For a repetitive restart pability, the allowable time for each restart would be approximately 3.0/N se onds where N is the desired number of restarts.

4.3 CONTROL SYSTEM COMPONENTS

4.3.1 Neutron Flux Senser

The 1959 and 1960 ion chamber irradiation test programs we e designed to investigate the operating characteristics of a high-temperature, u compensated ion chamber suitable for Pluto application. The first test prog am was designed to test the upper operating limits of the prototype design in hi n neutron and high gamma radiation fields. The second test program was desi ned to determine the temperature capabilities of the ion chamber. In both th e tests the ion chambers were operated in the General Electric Materials Testi Reactor (MTR). In the first test series, the ion chamber was operated direc y in the core in a thermal neutron flux of 10^{14} nv and a gamma dose of 10^9 R/hr. In the s :ond test series the ion chamber was operated inside a furnace capsule to simulat operating temperatures up to 1200°F.

In both of these test series the ion chambers were operated in high t er-mal neutron flux fields. The ion chamber signal current was primarily due t the (n, B^{10})→(α, Li) interaction with the filling gas. Previous study work of Pl o flux spectrum indicated that the ratio of chamber neutron current to gamma r-rent would be high enough that an uncompensated ion chamber could be used r measuring reactor power. However, this condition is true only when the cha i-ber is located directly in the core reflector where the thermal neutron flux i maximized. Any other location would require the use of a moderator to ther a-lize the neutron flux for detection, or the use of a compensated ion chamber. Either approach would complicate the overall system.

The purpose of the 1961 ion chamber irradiation test program was tc n-vestigate methods of improving the gamma current discrimination of the Plu uncompensated ion chamber. To conduct such an investigation, a reactor wa required that had high fast-neutron flux, gamma flux, and low thermal-neutr 1 flux. The reactor selected for this work was the General Dynamics test rea or located in the Nuclear Aerospace Research Facility at General Dynamics/ Fort Worth.

For this work, two Pluto-type uncompensated ion chambers were us d for the detectors. The first chamber was a standard B^{10}-coated, neutron io za-tion chamber. The second chamber was identical but was uncoated. The tw ion chambers were manifolded together to a common gas filling and venting syst n. Nitrogen, argon, xenon, helium, and hydrogen were alternately used as filli gases.

The experiment was so conducted that the saturation characteristics were taken for both the neutron and gamma ion chambers. Saturation curves were ob-tained for all filling gases at different pressures and at three temperature le els.

Figure 152 is a plot of the current collected in the gamma ion chamb r at different operating pressures. It should be noted that the gamma current in-creased as the density of the filling gas increased.

Figure 153 is a plot of the current collected in the neutron ion cham er. It should be noted that the current collected is actually the sum of the neutro and gamma current of the uncompensated ion chamber. As expected, the ionizat n current curves increase with pressure, leveling off when the range of the (α Li)

GAMMA ION CHAMBER CHARACTERISTICS

FILLING GAS TEMPERATURE = 780°F

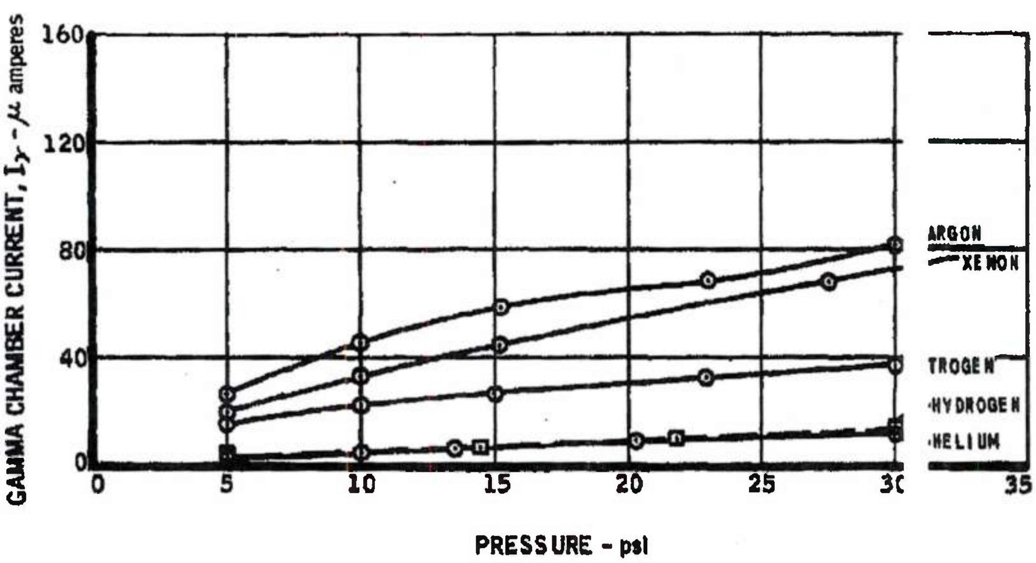

NEUTRON ION CHAMBER CHARACTERISTICS

FILLING GAS TEMPERATURE = 780°F

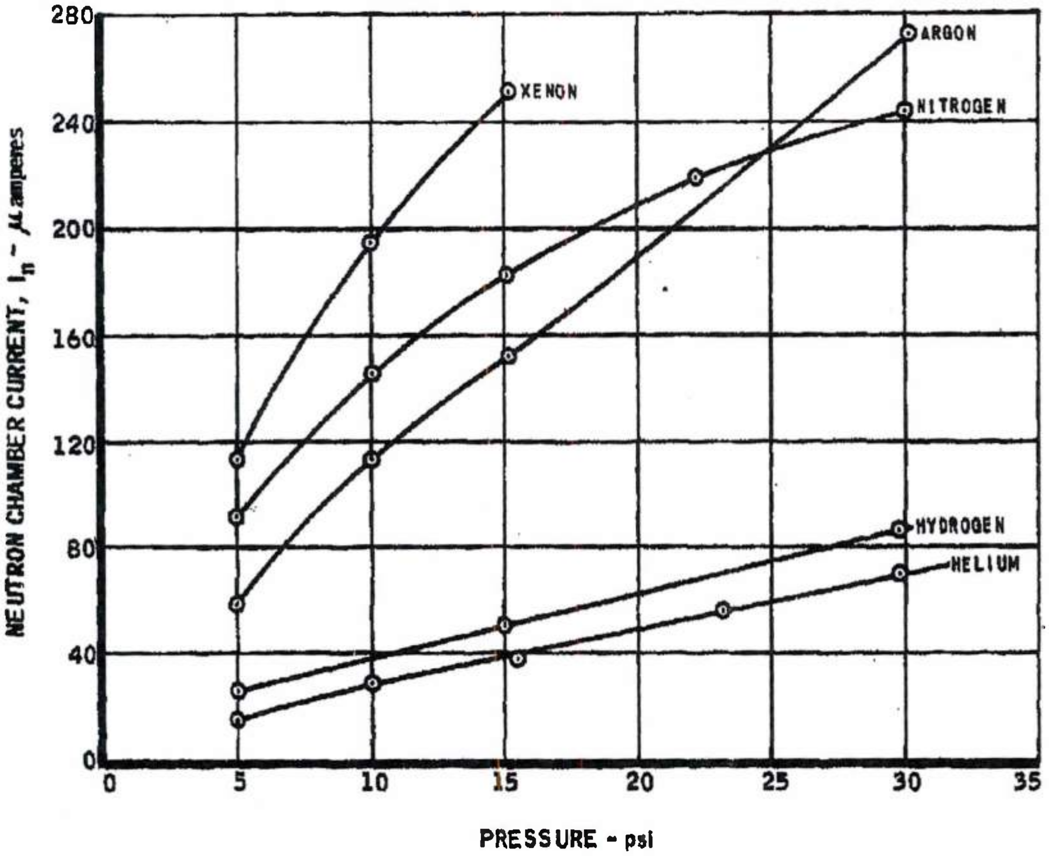

particles resulting from the (n, B^{10}) reaction equal the plate spacin of the ion chamber. Normally, the curves reach a saturation value; however, n this case the gamma current continued to add to the total ionization current a: :he gas pressure increased.

Figure 154 is a plot of the ratio of ionization current collec d from the neutron chamber to the ionization current collected from the gamma :hamber for different filling gases. Surprisingly, hydrogen gas proved to have t highest neutron/gamma ratio of all the gases used. This high ratio is appa ntly caused by the fast neutrons interacting with the hydrogen atoms, ionizing th hydrogen gas directly by collision rather than by the normal thermal neutron 10 reaction. This method of using hydrogen filling gas to decrease the gamma se itivity of an uncompensated ion chamber is a new idea. It may be very useful fo extending the range of uncompensated ion chambers when operating in fast neu on flux environments.

4.3.2 Temperature Sensers

Thermocouples

At the beginning of 1961, calibration data, drift, and aging aracteristics had been obtained on several metallic thermocouple systems in ding:

Platinum vs. platinum - 10 percent rhodium
Platinum vs. platinum - 5 percent rhodium
Platinum vs. platinum - 20 percent rhodium
Platinum - 5 percent rhodium vs. platinum - 20 percent rh ium
Platinum - 6 percent rhodium vs. platinum - 30 percent rh ium
Iridium vs. iridium - 40 percent rhodium

Also, there were two combinations of the platinum vs. platinum-rhc ium system doped with 1 and 2 percent palladium.

In general, the maximum drift was about 1 to 2 percent. T e independent linearity errors for the platinum vs. platinum - 10 percent rho um thermocouple was about $\pm$ 1 percent in the region of 1000 to 3000°F. All of he systems have larger nonlinear characteristics in the range of 0 to 1000°F.

An analytical study of thermocouple circuits was conducted and the effects of circuit resistance in the connecting system were predicte and experimentally verified. Series and parallel thermocouple operation was vestigated, and it was shown that the terminal voltage of a series network was r ltiplied by

NEUTRON CHAMBER - GAMMA CHAMBER CURRENT RATIO

FILLING GAS TEMPERATURE = 780°F

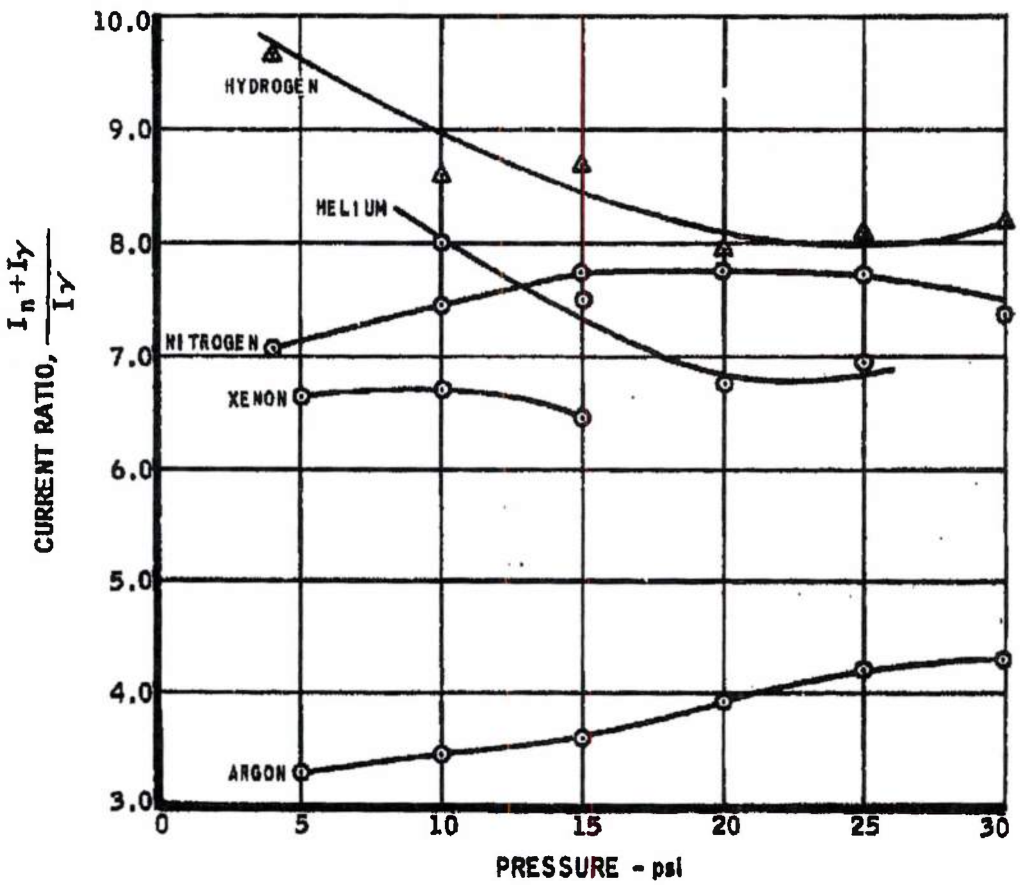

the number of series junctions but reduced by the effect of the seri and parallel resistance in the circuit. In parallel operation, the terminal vc age was the same as in the case of the single junction, reduced slightly by the e ect of circuit resistances. Tests were also conducted on some metallic ther iocouples (tungsten rod vs. a graphite sheath). The results indicated a large ut nonlinear voltage output with temperature, and a large number of thermocouj : failures after one 10-hour run of several thermocouples. It was concluded t at poor electrical reliability, relatively large size, and lack of mechanical urability made this type of thermocouple unsuitable for the required applicat ns of in-core temperature instrumentation.

Thermocouple insulators were experimentally investigated . part of the thermocouple tests and insulation resistance between two wires n the two-hole insulators was measured as a function of temperature up to 28)° F for alumina and magnesia. Insulation resistance of the alumina was sl htly higher than the magnesia at 2800° F, and was about 40,000 ohms at this te perature. Reference 28 contains the extensive temperature test results of the arious thermocouple systems, insulators, resistance-type temperature se sers, and bridge circuits.

In late 1960 and early 1961, a thermocouple irradiation expe ment was performed in which platinum vs. platinum - 10 percent rhodium the mocouples at 2500° F were irradiated to a total integrated fast neutron dose of .bout 6 x 10^{19} nvt and a total integrated thermal-neutron dose of about 1.6 x 1 ^{20} nvt. In addition, a platinum vs. platinum - 10 percent rhodium thermocoup : and a chromel-alumel thermocouple in an environment of about 1400° F w re irradiated in the same test capsule. The insulation resistance of a two-h le alumina thermocouple insulator was also measured. Reference 29 contains complete description of the pre-radiation, radiation, and post-radiation test conducted in 1961. In general, the results indicated that the maximum perma nt decalibration of the platinum vs. platinum - 10 percent rhodium thermoc ples was about 0.8 percent at an operating temperature of 2500° F and a ma mum integrated flux of 6 x 10^{19} nvt fast neutrons and 1.6 x 10^{20} nvt therma neutrons. The data also indicated essentially constant insulation resistance f the same operating temperature and values of integrated flux. In order to is late any thermal aging effects that may have occurred during the 500-hour i radiation test at 2500° F, a 500-hour aging test was performed using thermo uples fabricated from the same batch of wire as that used in the irradiation ests.

The results of this test indicated a thermal drift of 1°F at the end of 500 ho s of operation.

Resistance-Type Temperature Sensers

At the beginning of 1961, a survey of commercially available resista :e-type temperature sensers had indicated that no sensers of this type were co - mercially available for operation to 3000°F. In addition, an analytical stu had been completed to predict the extent of strain gage effects, and experin ntal work had been started on platinum wire resistance units. The analytical st ly showed that the magnitude of these strain gage effects was small and neglig le, and the preliminary experimental work indicated that the insulation resista e characteristic of the winding form was a significant factor in affecting the l ear-ity of these devices at temperatures above 2000°F.

During 1961, both platinum, iridium, and tungsten wire resistance e - ments were calibrated using various winding geometries and forms. The tu g-sten sensers were calibrated in inert and vacuum environments. The rep .t-ability with temperature cycling of the platinum wire sensers was significa .y better than that of the tungsten units.

A special winding form constructed to minimize the insulation resis nce shunting effect on the senser, in conjunction with a total platinum wire resi :-ance of about 27 ohms at 2800°F, produced the most successful results to te. Figure 155 is the calibration curve of this experimental platinum wire resi ance senser from ambient to 2800°F. This device has an independent linearity ror of about ±3 percent over the entire temperature range.

4.3.3 Pneumatic Control Components

At the beginning of the contract year, the 4-inch-stroke actuator sy em had been completely designed and fabricated, and the unit was ready for tes ng. The design of the 40-inch-stroke actuator was complete, and fabrication ha been initiated. Design of the test equipment for use in evaluating the actuat s had commenced.

During 1961, significant progress in perfecting high-temperature, p u-matic components was achieved. The 4-inch-stroke actuator system was c n-pletely evaluated and the evaluation provided data for design improvements future actuators. Fabrication of the 40-inch-stroke actuator was complete

CALIBRATION OF EXPERIMENTAL PLATINUM WIRE RESISTANCE SI ISER

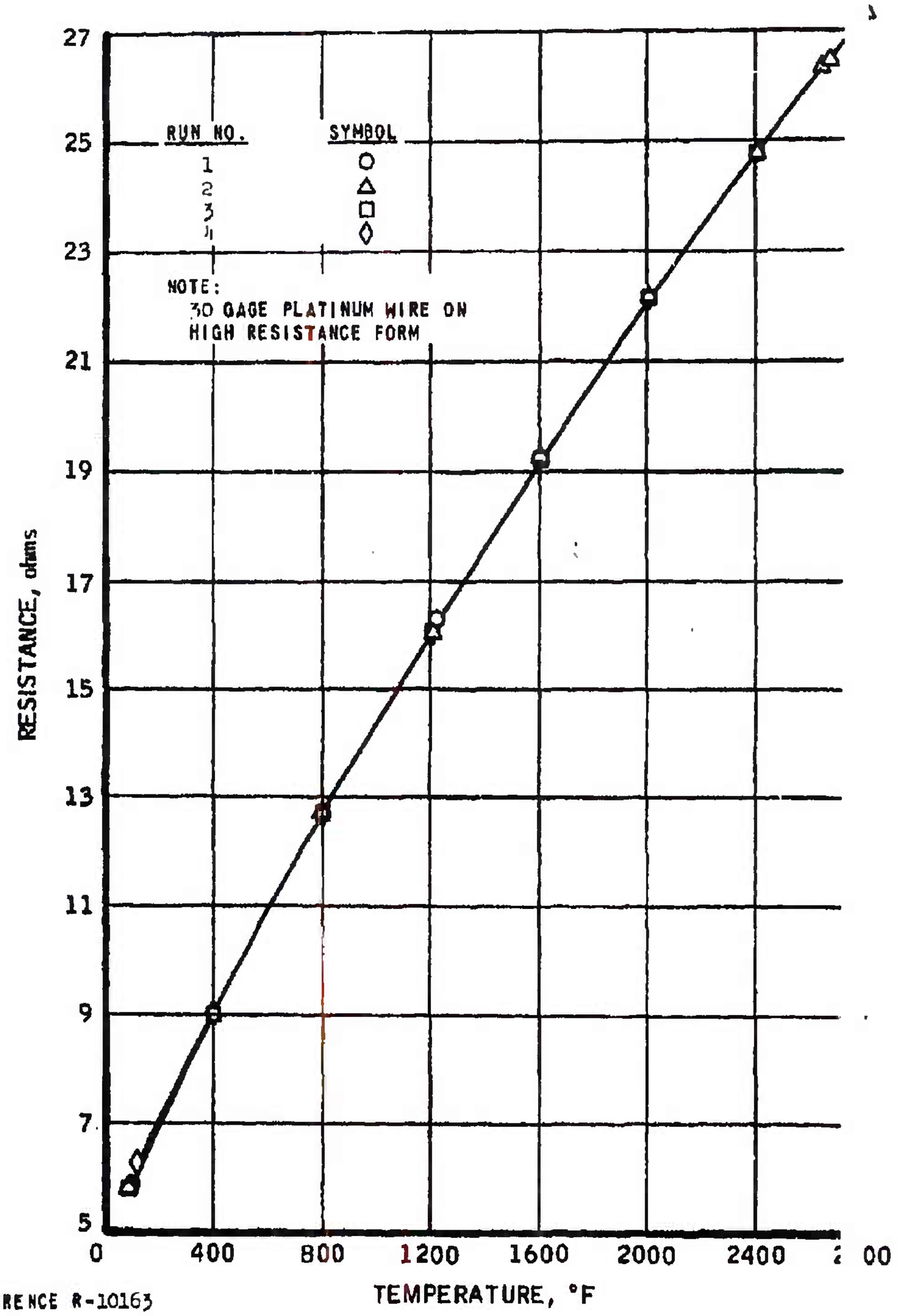

REFERENCE R-10163

and extensive testing at both room temperature and 1000° F resolved many problems and resulted in dynamic performance for short periods compatible with flight requirements. A research program covering high-temperature materials and lubrication was initiated under which a survey of the state-of-the-art of high-temperature lubricants was completed, screening of the mos promising lubricants and materials accomplished, and testing initiated.

Four-Inch-Stroke Actuator

Performance testing of the 4-inch-stroke actuator was completed, a i the program objective of optimizing system performance utilizing existing hardware was achieved. The actuator shown installed in its environmental oven (Figure 156) was operated at room temperature for 40 hours. Two suc ess-ful one-hour tests were conducted at 1000° F.

Frequency response, resolution, and transient response characteris cs of the actuator were evaluated during ambient and high-temperature phases the tests. The poor resolution obtained (3.5 percent at room temperature a i 4 percent at 1000° F) was the result of earlier extensive high-temperature te -ing of the motor. This testing resulted in larger dead band than specified i the design.

Transient response data showed that actuator performance was well within design specifications. Use of a lead-lag network reduced the oversh t and settling time during closed-loop testing without affecting cutoff during fr -quency response. The overshoot was 12 percent of the input as compared to the maximum specified value of 20 percent.

The frequency response data (Figures 157 and 158) show the 90° pha shift point for the room temperature test to be 4.3 cps, and for the 1000° F st, 3.8 cps. These test data correlate closely with the values specified by the a-lytical actuator studies.

The accumulated test data show good correlation with the predicated er-formance and provide information valuable to the prediction of future actuat performance.

Forty-Inch-Stroke Actuator

Fabrication of the 40-inch-stroke actuator shown in Figure 159 was m-pleted, and extensive room temperature and high-temperature testing of co -ponents and of the complete system was accomplished.

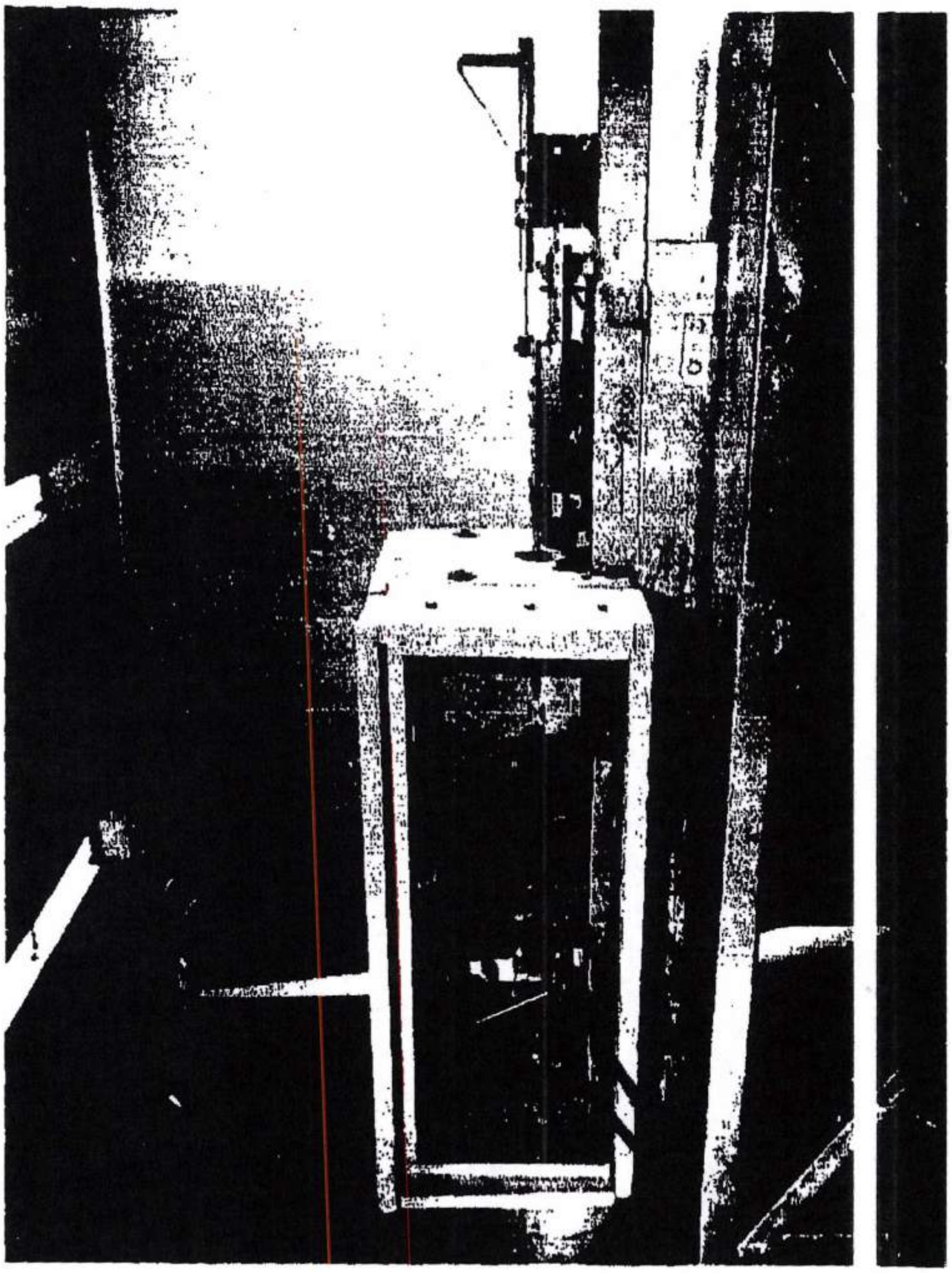

3772-3CN

FIGURE 156 - Four-Inch-Stroke Actuator Installed in Environmental Oven

CLOSED LOOP FREQUENCY RESPONSE OF ACTUATOR
WITH FORWARD LOOP GAIN INCREASED BY FACTOR OF FIVE
TEST DATA AT 1070° F

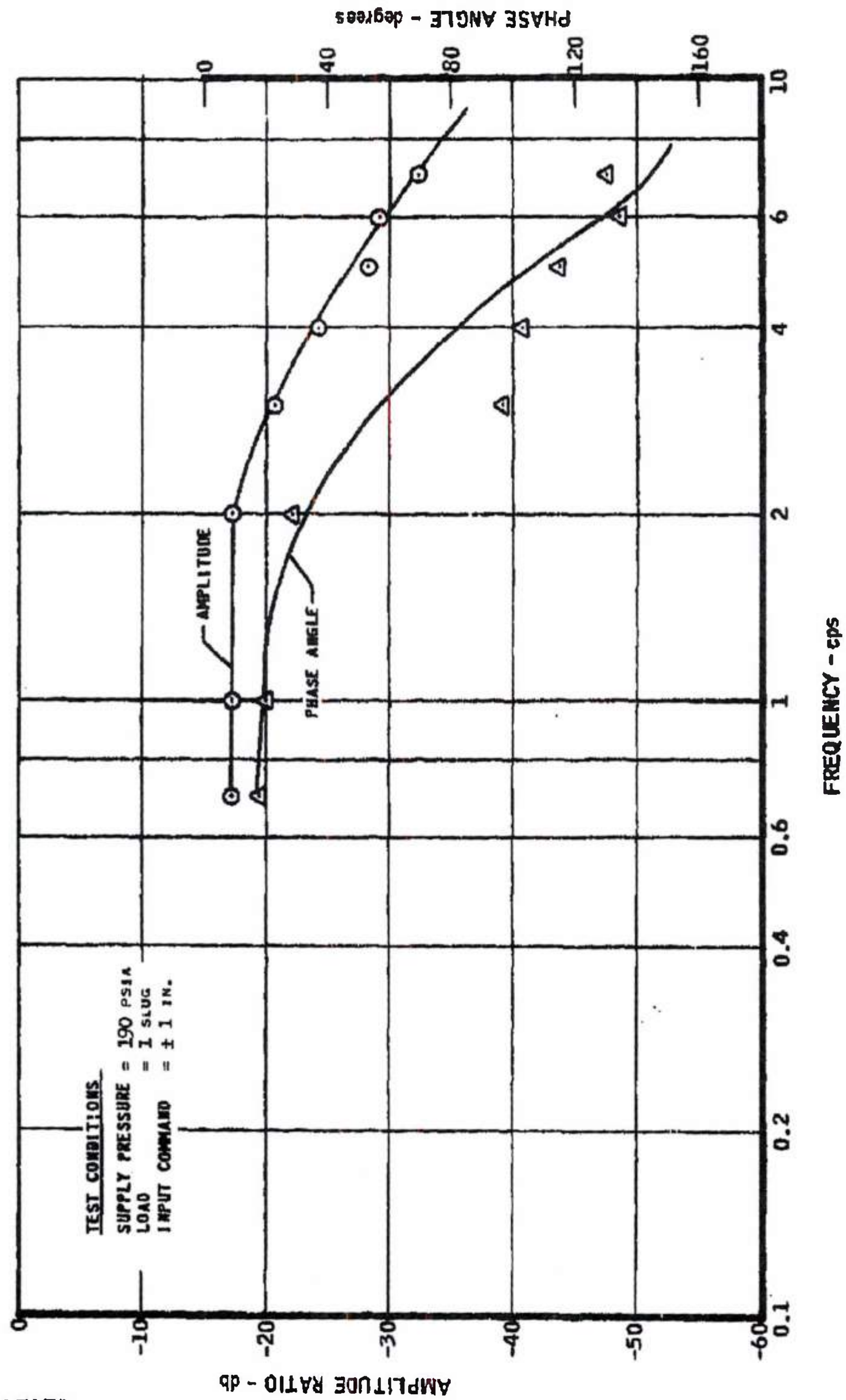

CLOSED LOOP FREQUENCY RESPONSE OF ACTUATOR
WITH FORWARD LOOP GAIN INCREASED BY FACTOR OF FIVE
TEST DATA AT AMBIENT TEMPERATURE

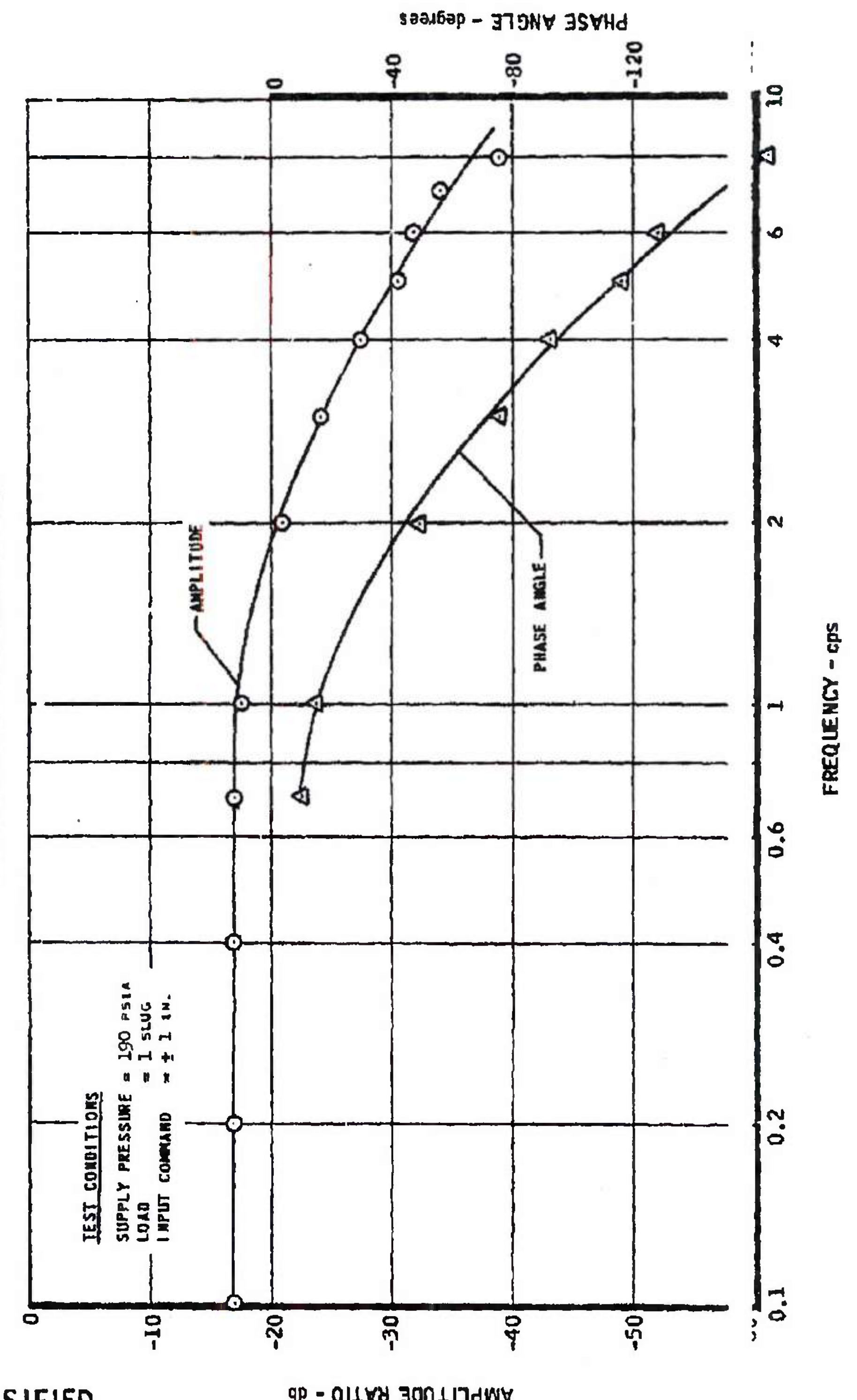

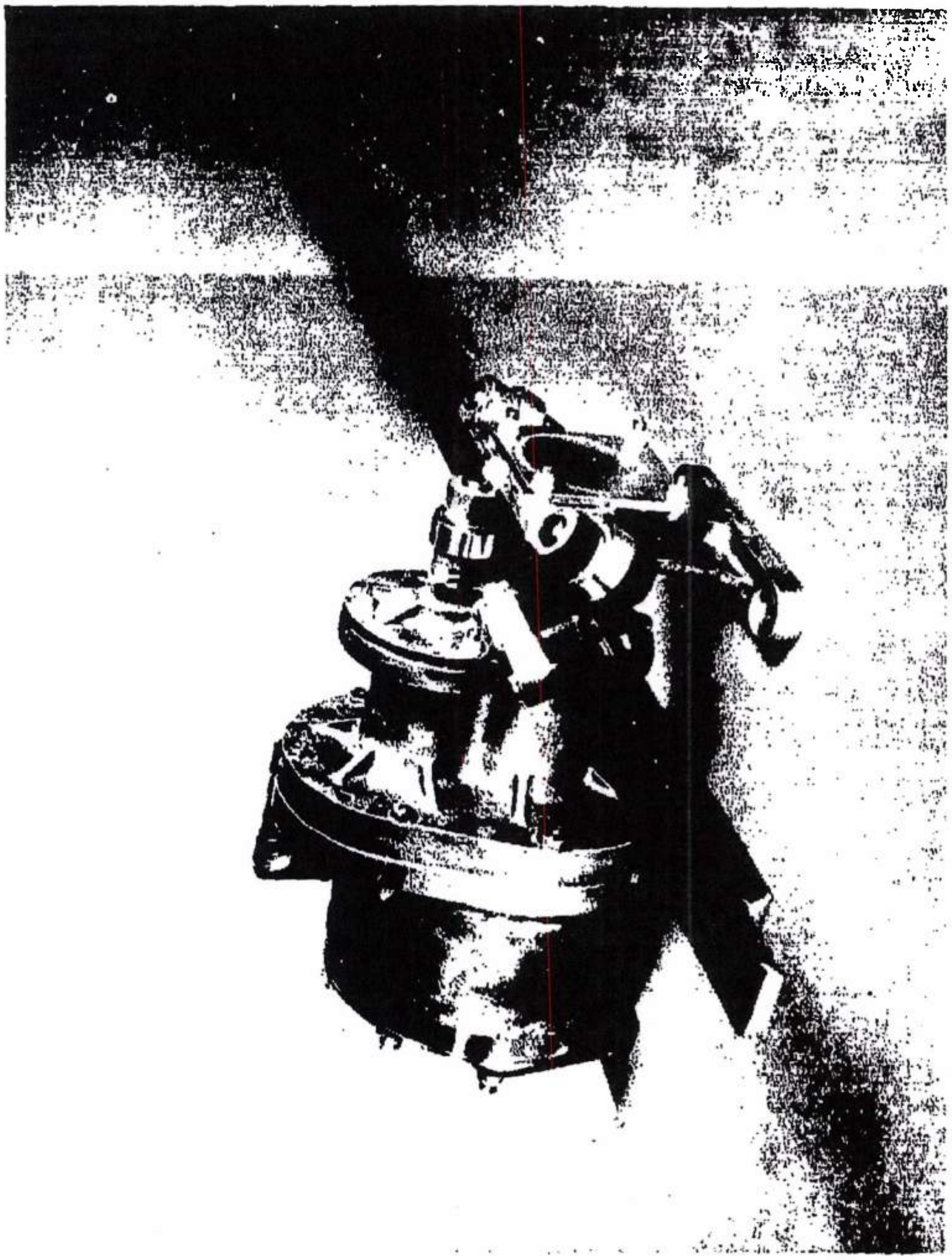

3751-4CN

FIGURE 157 - Forty-Inch-Stroke Actuator

Component testing consisted of evaluation of two types of li ear trans-ducers (a linear variable differential transformer and a variable r .uctance type), the first and second stage valves, and the nutating disk mot .

The transducer evaluation included testing of both types at oom temp-erature and at 1000° F to determine their linearity and repeatabilit character-istics. It was determined that the linear variable differential tran former in combination with its oscillator and demodulator exhibited poor lin rity and re-peatability at both room and 1000° F temperatures. The variable luctance transducer met the specified requirements for both linearity and r eatability at both temperature conditions and was used in subsequent system ests of the complete actuator assembly.

Bench testing of the motor indicated that leakage and fricti were with-in design limits; however, severe inertial knock occurred betwee the nutating disk and the splitter plate during operating. As a result the splitt plate was eliminated, and a pin and shoe arrangement was installed at the pe iphery of the disk to balance out the inertial forces arising from the nutatin notion.

Motor operation was much improved by this modification, it repeated failures of the pin pointed up the need for design refinements to re ce the stress concentration at the pin. Appropriate design changes have en made which will be incorporated in all future actuator motors.

Bench testing of the valve, which consisted of a torque mot and first and second stage spool valves, indicated a number of problems, w ch were resolved in the following manner. Static sensitivity of the valve w found to be poor, and the feed back gain of the second stage was modified t eliminate this problem. The first stage gain was found to be inadequate. H ever, to circumvent the delay associated with redesign and fabrication, the irst stage valve from the 4-inch-stroke actuator was substituted, because its erformance was found to be satisfactory. Repeated malfunctions of the second tage valve were encountered. When it was determined that malfunction was e to the spool binding in the sleeve, the clearance between the spool and th sleeve was increased. It was also found that valve performance was being se rely limited by excessive dead band in the torque motor. Because the only two orque motors available for the high-temperature operation had similar characte stics, it was necessary to minimize dead band effects through the use of electr ic compen-sation in the forward loop of the servo system.

Initial tests of the actuator were conducted at room temperature, a l resolution, transient response, and frequency response tests were perforr :d to determine the actuator's dynamic capabilities. Approximately 60 hours f operating time were accumulated during this testing. Frequency response 'as found to be 4 1/2 cycles without compensation and 8 to 10 cycles using prop - tional plus integral and lead-lag networks. Resolution was one tenth of 1 p - cent (Figure 160), and transient response (Figure 161) showed overshoot s a maximum of 20 percent. Actuator performance was limited due to low g n and dead band in the torque motor. However, operation of the actuator at w inlet pressures (40 psi) demonstrated its ability to operate at pressures cc - parable with those to be encountered in the inlet duct of the Pluto engine at high altitudes.

Checkout of the environmental oven used to conduct high-temperatu : testing was completed, and the actuator was installed. The initial high-te p- erature test of the actuator was of half-hour duration at 1000° F. Actuator per- ation was achieved at this temperature; however, problems were encounte ed in the clutch that is used to shift from the servo to the scram mode of oper tion. Clutch malfunction was due to the use of ambient air to operate the clutch while the actuator was at the 1000° F test temperature. This problem was elimi ted by installing coils in the environmental oven so that the clutch air is heate be- fore entering the actuator. This solution has proved satisfactory.

The second high-temperature run of the actuator assembly was of 1 hour duration at 1000° F. Operation of the actuator was satisfactory, and dynan : performance was comparable to that exhibited during the low-temperature est- ing. Reworking of the valve successfully eliminated mechanical binding pr o- lems that occurred during initial tests. Additional valve evaluation will be e- quired to eliminate dead band and improve dynamic performance.

High-Temperature Materials and Lubrication Research

In the course of the Marquardt effort to develop 1200° servo actuati g equipment, it became increasingly obvious that the lack of documented infc - mation on the friction and wear characteristics of materials at elevated te p- eratures was hindering development progress. During 1961, a two-phase p o - gram was initiated in the hope of alleviating this problem.

The first phase consisted of a literature survey involving intensive e- search study and abstracting to determine the state-of-the-art. In additio visits were made to all companies and research agencies prominent in the eld

RESOLUTION OF FORTY-INCH-STROKE ACTUATOR

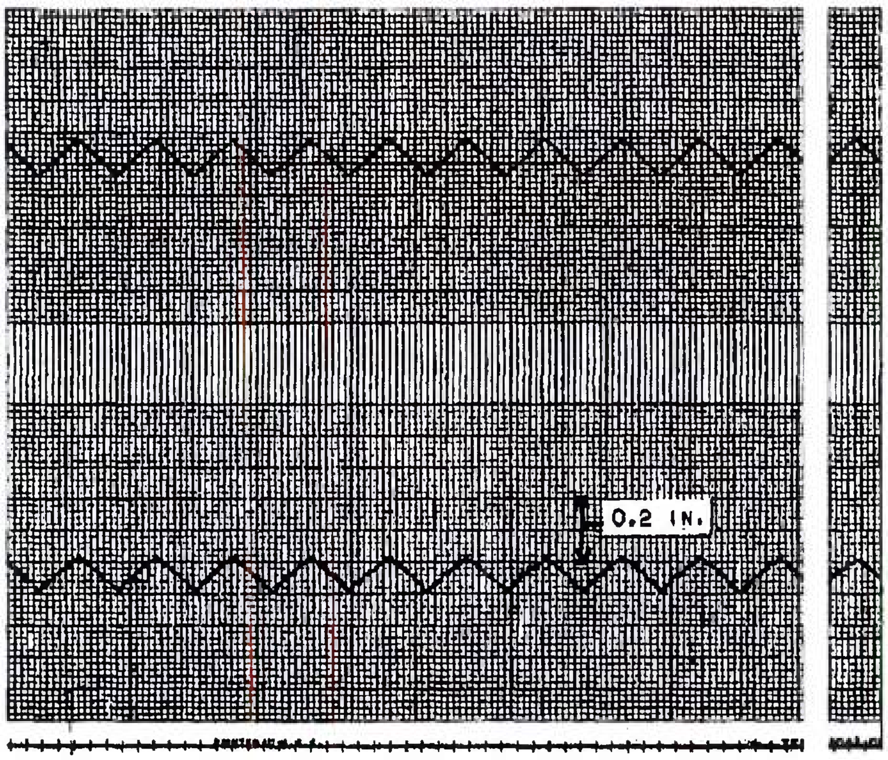

$P_s = 40$ psi

$T_s = T_A = 70°F$

FIGURE 160

TRANSIENT RESPONSE OF FORTY-INCH-STROKE ACTUATOR

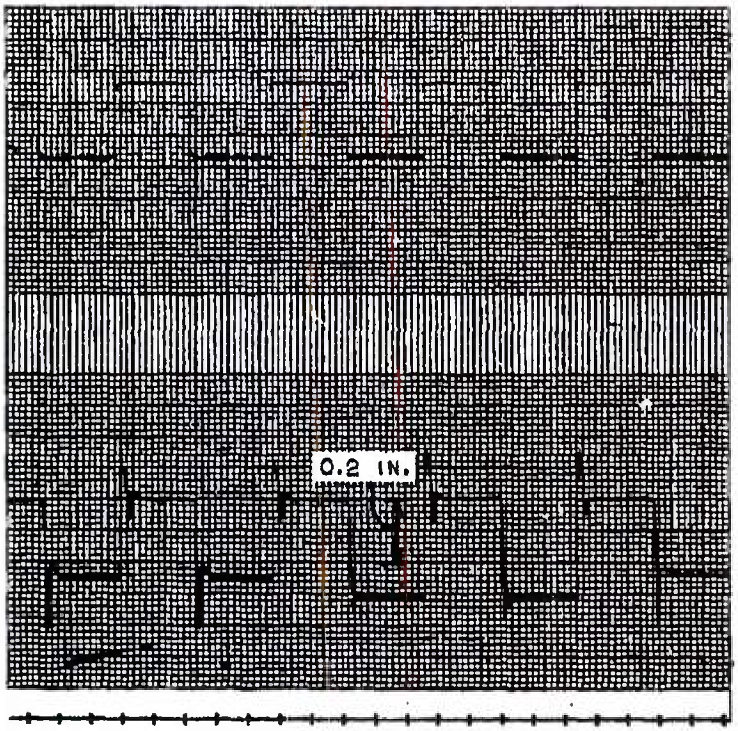

$P_s = 150$ psi

$T_s = T_A = 70°F$

of high-temperature materials and lubricant research. As a resul of these surveys, it was concluded that there are four basic approaches to t e high-temperature lubrication problem that are particularly applicable to ie Pluto system: a dry film lubricant, a solid lubricant compact, a continu is- or intermittent-flow dry lubricant system, and a pneumostatic bearin

A Dry Film Lubricant applied to the bearing surface is the implest from a hardware design standpoint. However, the three basic prol ems of securing adequate adhesion, long wear life, and good lubrication at iigh and low temperatues may not be amenable to timely solution.

The following list of candidate dry film lubricants and wear oatings came out of the survey:

(1) Lead with silica (NASA lubricant coating)
(2) Other low melting point glasses with or without additive (Midwest Research, Massachusetts Institute of Technol y, University of Illinois, and Aeronautical System Divisior a lubricant coating)
(3) Flame sprayed cermets and ceramincs (Linde-a wear c ating)
(4) Conversion coatings, such as oxides, silicones or chro es (wear coatings)
(5) Precious metal coatings (Southwest-a lubricant coating)
(6) Proprietary coatings (Columbia Broadcasting System R search Laboratories, Alpha Molykote, Electrofilm, General M gna Plate, Stratos, "Surf-Kote"-lubricant coatings)

In the case of a self-generating oxide coating (current Marq ardt approach) used for its anti-wear properties, some benefit might be gained by maintaining a more uniform oxide coating. The Boeing Company, ranklin Institute, and General Electric Corporation have accomplished con derable research engineering on pneumatic bearings applicable to this type f problem.

Solid Lubricant Compact applied against bearing wear surfa es is more complex from a mechanical standpoint, but provides "lubrication i depth" resulting in longer life. The "compact" can be applied by using inse s that rub against the bearing components or by using spacer balls or spacer ollers formed from a lubricant compact.

DECLASSIFIED IN FULL
Authority: EO 13526
Chief, Records & Declass Div, WHS
Date: MAY 2 9 2015

Graphites, self-oxidizing mixtures, laminar layer solid lubricants, and precious metals are being considered as the lubricating element. Boei[illegible], Clevite, National Carbon, NASA, NAMC, and others have been working on [illegible]is principle. In general, wear rates of the compact are high, in order to kee[illegible] a good lubricant supply available, so the compact itself cannot be dimensiona[illegible]y critical.

A Continuous- or Intermittent-Flow Dry Lubricant System using a [illegible]r-rier gas is the most mechanically complex, but holds the greatest potential for long life and heavy duty. The selection of lubricant materials should n[illegible] be critical because of the continuous replenishment feature.

Metering of the lubricants and their injection into the airflow would [illegible]e the primary problem. The advantages are that (1) molybdenum disulfide a[illegible] other excellent dry lubricants can be used, and (2) the continuous replacem[illegible]nt and greater uniformity of distribution should allow an extremely long wear [illegible]fe comparable to conventional hydrocarbons used at lower temperatures.

A Pneumostatic Bearing would be less complex than a solid lubrica[illegible] compact, but probably more so than a dry film. However, it could be use[illegible] only if a higher pressure gas source than ram-air were made available.

Within the present state-of-the-art, some type of lubricant is defin[illegible]ly required to reduce friction and wear. Low friction coefficients are desira[illegible]e to improve performance characteristics of the control system, and wear r[illegible]e must be minimized to keep operating tolerances within allowable limits.

Hydrostatic gas bearings are possible only if a flowing gas source i[illegible] available at pressure levels of about four times the maximum bearing pres[illegible]re load. Little or no hydrodynamic lift can be expected from the oscillating a[illegible]ion of the current Marquardt motors consisting of a ball and disk. This desig[illegible] does not lend itself to use of hydrodynamic lift principles because bearing conta[illegible] area would have to be sacrificed to obtain hydrostatic support area.

The choice of substrate materials presents a much reduced problem when lubricants are used, unless the lubricant is a conversion coating. In this case the substrate must be selected for the desired chemical reaction. Normally the substrate material must be chosen with consideration of the following properties:

DECLASSIFIED IN FULL
Authority: EO 13526
Chief, Records & Declass Div, WHS
Date: MAY 2 9 2015

(1) Maximum hot hardness for load carrying capacity
(2) Dimensional stability from solid state reactions and relaxation of internal stresses
(3) Good ductility and impact resistance
(4) Good thermal conductivity to minimize frictional hot s ots
(5) Good oxidation resistance to maintain surface finish a d dimensions
(6) A modulus of elasticity of 25,000,000 to 35,000,000 p . for optimum contact area
(7) Machineability

Some of the more promising substrate materials are (1) Haynes 2 (2) Hastelloy "C", (3) Hastelloy "X", (4) Rene' 41, (5) Nitrotung. In general, t e cermets possess superior hardness to the wrought super alloys but have i erior impact resistance, and are difficult to machine. The wrought super allo should be superior in overall performance for temperatures up to 1500° F. owever, as mentioned before, cermets show some promise as wear coat at th lower temperatures.

The second phase of the materials and lubricant research rogram consisted of further screening of candidate high-temperature substra materials and lubricants and correlating literature findings with Marquardt ata. This portion of the work was conducted on the Marquardt-designed pin d disk type friction and wear test machine, which is patterned after the succ sful NASA equipment. At present five test plates and fourteen pins of succe ful substrate materials are being tested. In addition, six selected lubricant co ings of a propriety nature are being obtained for evaluation.

The objective of this program is to find the best combinati of substrate material and lubricant coating for the flight prototype serv actuator for the Pluto control system.

4.3.4 <u>Electronics</u>

At the beginning of 1961, most of the magnetic amplifiers d computing devices suitable for use in the temperature and reactor compensa on loops had been fabricated, and limited test data had been obtained. Figure 2, which is a simplified block diagram of the temperature control and reacto compensation loops, is included for clarification. These components included igh gain temperature error amplifier, operational type amplifier, a three ecade diode-network-type log amplifier, buffer amplifiers suitable for summi and general amplification, and a driver amplifier designed to drive the high-t nperature torque motors used in the 40-inch linear actuator system. Metho s for providing the required integration in the common error path and met ds for mech-

EXPERIMENTAL TEMPERATURE CONTROL AND REACTOR COMPENSATION LOOPS

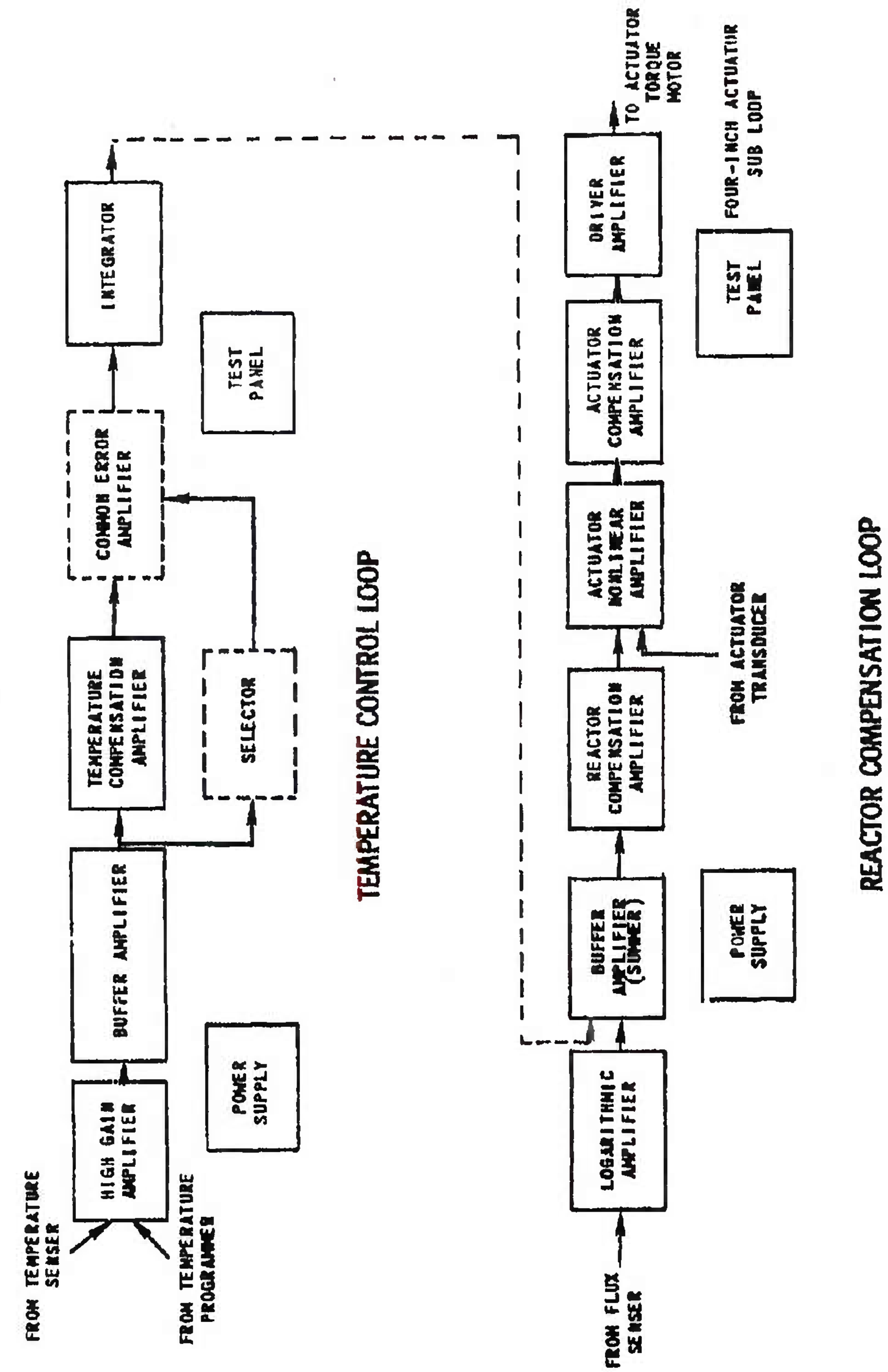

FIGURE 162

anization of the auctioneer or error selector were being considere

During the first half of 1961, development tests of the above nentioned components continued, the development of an electronic integrator ıcorpora-ting magnetic amplifiers was started, and the error selector was s bcontracted to an outside vendor for procurement. This contract was subsequ ntly termin-ated for nonperformance. Selected components and magentic ampl ier circuits were prepared for irradiation tests at General Dynamics/Fort Wo ı. The mag-netic amplifiers were designed to meet the requirements of the co rol system and were fabricated, tested, and shipped to Fort Worth. These ar lifiers in-cluded a 400-cps high-gain second harmonic type, and 400-cps and 4800-cps push-pull self-saturating type amplifiers. The second harmonic a plifier is suitable for the first stage of the temperature error amplifier and e integrator. The push-pull self-saturating type represents the buffer amplifier onfiguration. Components irradiated along with the amplifier included cores, apacitors, resistors, and diodes of the same type as used in the amplifiers. alf of the amplifiers used special, radiation-resistant ZJ225 General Electr diodes of thin base width construction. The remaining amplifiers used stan rd type silicon junction diodes.

A preliminary report (Reference 30), containing pertinent st results of the August irradiation tests was published in August 1961. In ge ral, the circuits containing the ZJ225 diodes withstood greater radiation ex osure for a given performance index than the circuits that contained the ordi ry diodes. One 4800-cps amplifier using ZJ225 diodes remained satisfactory an integra-ted fast neutron dose of 2 x 10^{15} nvt. This radiation dose is greate than the dose expected for the electronic system during a typical Pluto mis on. One of the ZJ225 diodes performed satisfactorily to 10^{16} nvt, and five dio s were good to about 10^{15}nvt; however, about 70 percent of the ZJ225 diod exhibited excessive reverse leakage currents as high as 400 microamperes 200 volts, which significantly exceeded the anticipated 50 microamperes. Pr iminary discussions with the supplier indicated that variations in manufact e occurred and that the excessive leakage was probably a surface leakage phe menon. All of the components tested except the semiconductors exhibited s all or neg-ligible changes in their characteristics to 10^{16} nvt.

During the second half of 1961, the amplifiers and computin components, including the log amplifier and an electronic integrator using magn ic ampli-fiers, were satisfactorily tested at temperatures from ambient to 5°F. The driver amplifier was exhaustively tested and used in the 40-inch-s oke actua-tor development tests. Preliminary tests have been started on the ascaded units in the temperature and reactor compensation loops, and an e or selector feasibility design has been completed.

Second generation 400-cps high-gain and 4800-cps buffer type amplifiers have been designed, fabricated, and preirradiation tested using the information acquired from the August tests.

The development tests of these second generation circuits included comprehensive simulated diode degradation tests in which the forward volta drop and the reverse leakage current of the diodes was increased beyond the expected values at 10^{15} nvt. A circuit description, performance characteris cs, and effects of simulated diode radiation damage on these second generation r-cuits are presented here.

Circuit Description

(1) Second Harmonic Modulator Rectifier Amplifier

A DC magnetic amplifier possessing very high gain and excellent stability has been developed. The amplifier consists of a typical magnetic modulator followed by a rectifier filter. The magnitude and polarity of the output is controlled by the DC input.

For comparison purposes, two methods of rectification are being us l. In one case, a dual anode zener is used for rectification; in the other, a dic e bridge with an RC network inside the bridge is used. Figure 163 is a schematic of the second harmonic modulator with alternate methods of demodula on shown.

Several design features are incorporated to make the amplifier radia tion resistant. A tabulation of amplifier characteristics is given in Table 2

Stamped ring cores of Hy Mu 80 material were selected to provide high gain and good stability. To take into account the increased forward dro through the rectifiers with radiation, a higher gate voltage is used.

Null shift, and gain change are caused principally from change of dic e characteristics. Selection of the diodes minimizes this effect. In addition careful selection of the diodes a design objective was to obtain the highest p - sible open loop gain with the resultant advantages of increased negative feed back.

DIAGRAM OF 400 cps SECOND HARMONIC, d-c MAGNETIC AMPLIFIE

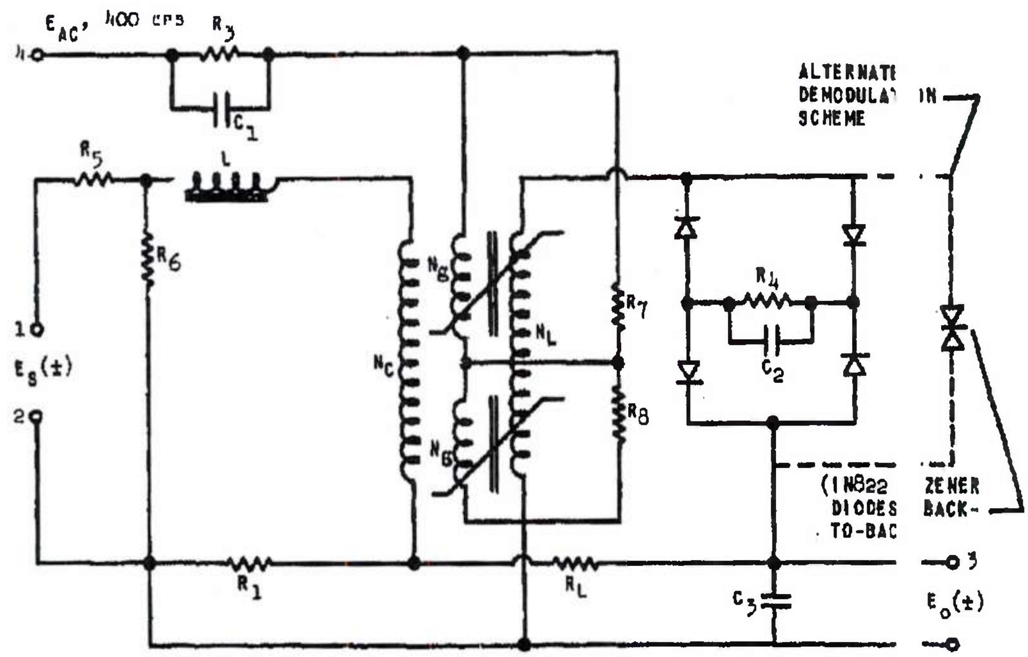

TABLE 28

AMPLIFIER CHARACTERISTICS

Characteristics	400-cps Magnetic Amplifier	4800-cps Magnetic Amplifier
Voltage Gain (Closed Loop)	490	20
Load Impedance, ohms	10,000	10,000
Linear Output Range, volts	±2	±40
Linearity, percent	Better than 1	Better than 1
Null Shift with +10% Supply Voltage Variation, millivolts	3 (Output)	7 (Output)
Null Shift with +10% Supply Frequency Variation	3 (Output)	3 (Output)
Null Shift with Temperature Variation, 75° F to 180° F	2 (Output)	5 (Output)
Frequency Response (-45° phase shift), cps	5.5	100

(2) Self-Saturating Magnetic Amplifier

A self-saturating push-pull DC amplifier having a good freq ency response and stability has been developed. To provide the desired g n bandwidth figure, a supply frequency of 4800 cps is used. Cores were lected of 1 mil Hy Mu 80 material to provide high ampere turn gain. A larg amount of negative voltage feed back provides good null stability. To comper ate for increased forward drop in the diodes with radiation, a higher gate vc age is used. The use of a bridge circuit serves to reduce diode leakage. Figure 164 is a schematic of the push-pull amplifier. Characteristics of the a plifier are given in Table 28.

Degradation Tests

Tests simulating diode degradation were conducted on all a plifier types. Degradation in the form of increased forward drop was sir lated by inserting a battery in series with the diodes. Reverse leakage was simulated by placing a resistor across the diode.

The 4800-cps DC amplifier uses eight diodes per assembly however, only four of the eight are in sensitive circuit positions that may be ffected by degradation. Diode degradation information taken from the earlier rradiation tests (August, 1961) indicate an increase in forward drop of from 2 3 volts, and a reverse leakage of 20 to 100 microamperes in the ZJ 225 diod , depending upon the diode selection. A case where the forward drop does t occur uniformly in all diodes (nontracking) is simulated by placing a batt y in series with only one diode, or a maximum condition of unbalance when a b ttery is in series with 2 diodes (same amplifier). This case represents a mo severe condition under radiation.

The modulator-bridge rectifier amplifier uses four diodes, ll of which are in positions sensitive to degradation. Radiation data previousl taken indicate a forward drop increase of from 1.0 to 1.5 volts, and a peak eakage current of 10 to 20 microamperes for the currents and voltages that ex st in this circuit. Maximum null shift occurs when the forward drop increas is not uniform in all diodes. Such a condition is simulated by inserting a ba ery in series with only one diode.

DIAGRAM OF 4800 cps PUSH-PULL, d-c MAGNETIC AMPLIFIER

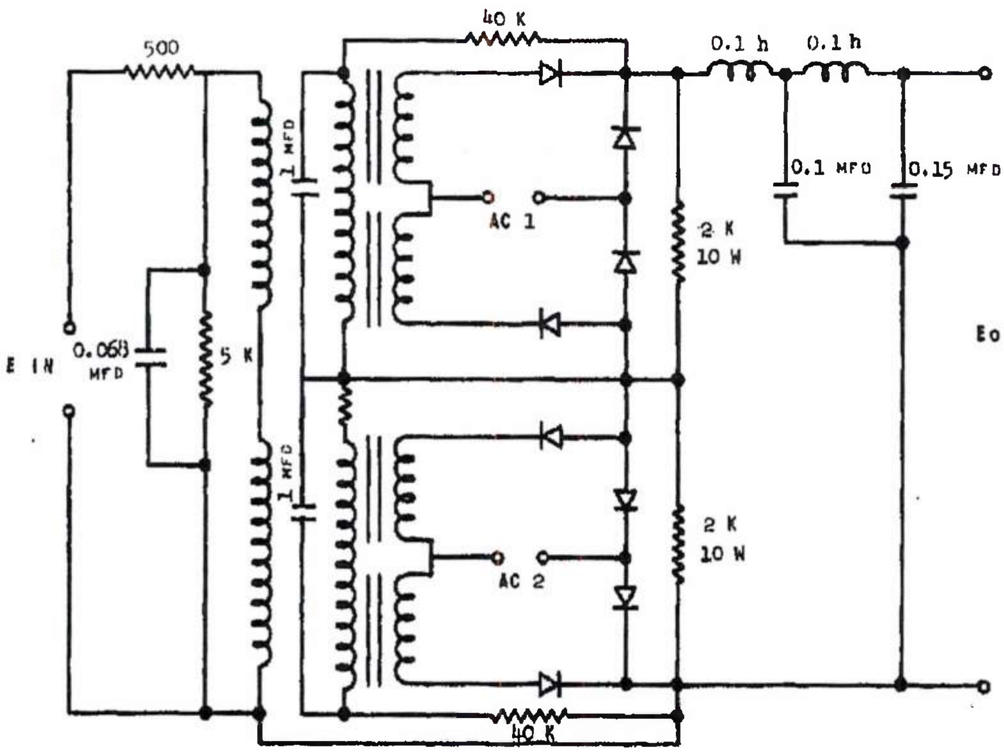

COILS = TMC 169A

The modulator-zener rectifier amplifier is somewhat sensiti e to degradation of the zener diode. The August radiation tests on dual anod zener diodes indicated some changes in the zener voltage; however, the cha ;e was quite symmetrical. But a marked increase in reverse leakage did oc ır during these tests. Zener diodes permanently degraded in radiation test to a level of 10^{16}nvt were tested in these amplifiers, and show a negligibl null shift, but a gain reduction of about 15 percent. The August radiation data o these zeners indicated that about 50 percent of the damage occurred betwee 10^{15} nvt and 10^{16} nvt; therefore, it is suspected that less than 10 percent gain eduction will occur in these amplifiers to 10^{15} nvt.

4.4 RADIATION EFFECTS TESTING

4.4.1 General Status

The detailed results of the irradiation test conducted at Gene al Dynamics/Fort Worth in August 1961 showed that further investigatio was necessary in order to isolate and ascertain the effects of gamma irradiat on on diode performance. Subsequent testing carried out at the Hughes Aircraft g mma facility showed that certain diodes were more affected by gamma radiat on than others. These differences in behavior were finally traced to variatio in the manufacturing process.

There followed a detailed screening program to select diodes suitable for use in a set of second generation magnetic amplifiers being prepa :d for irradiation in the General Dynamics/Fort Worth reactor facility in Ja uary 1962.

A total of 160 General Electric ZJ225 thin-based diffused-sil on diodes were obtained. The diodes were divided into three groups, represent g three different methods of manufacture. Each group was then subjected to series of tests designed to eliminate those diodes least suited for use in a hi radiation environment.

Each group first underwent elevated temperature tests (125° F and 165° F). The groups were then irradiated with a cobalt-60 source in the Marquardt Radiation Effects Laboratory, at about 2×10^5 R/hr of gammas. Finally, each batch received $\sim 10^{12}$ nvt (fast) at the Atomics International KEWB facility.

The diodes chosen for use in the test amplifiers were selected on th following basis:

Among Groups

Those groups that exhibited least absolute leakage current,
Those groups that exhibited least inverse current spread within a group.

Within a Group

Those diodes that exhibited least tracking spread, (current vs. voltage).

In general, none of the diodes subjected to gamma radiation alone or gamma and neutron radiation (in the KEWB facility) displayed the large inverse leakage currents typical of the original set of diodes used in the August irradiation tests. It is estimated that the second generation amplifi -s, using carefully selected components, will suffer a gain reduction of less th: 10 percent from the fast neutron dose of 10^{15} nvt that they will receive in January 1962.

4.4.2 General Dynamics Test

Preparations for the General Dynamics tests began in May 1961, in close cooperation with the Fort Worth reactor facility staff. The following items were included in the irradiation program:

(1) Zener diodes
(2) ZJ225 General Electric diodes
(3) Diodes, Inc. thin-based silicon diodes
(4) Motorola thin-based silicon diodes
(5) Mylar capacitors
(6) Silver mica capacitors

(7) Magnetic cores (Delta max, 2-mil diam. winding; H[illegible] Mu 80-1 2-mil diam. winding)
(8) Resistors (wire wound)
(9) 4800-cps magnetic amplifiers
(10) 400-cps magnetic amplifiers
(11) High-gain magnetic amplifiers
(12) Magnetic voltage reference

The components and circuits were assembled on special [illegible]uminum grids supplied by General Dynamics. These grids were than ins[illegible]lled in an environmental chamber, which was maintained at a constant tem[illegible]erature of 100° F throughout the irradiation. Figure 165 shows the data han[illegible]ing equipment used to check the circuits for proper operation after instal[illegible]tion in the chamber.

The test components were exposed to an integrated neutr[illegible] flux of $\sim 10^{16}$ nvt over a period of 49 hours.

The reactor power was programmed as follows:

Time (hours)	Reactor Power (KW)	Flux (E>0.33 me
0 - 4	5.3	3.5×10^8n
4 - 34	140	9.2×10^9n
34 - 49	2500	1.7×10^{11}

Preirradiation and post-irradiation data, as well as data accum[illegible]ated during the irradiation period, have been analyzed and are summarized [illegible] Section 4.3.4 of this report.

4.4.3 Gamma Irradiations of Magnetic Amplifier Components

On 13 September 1961 a group of 20 General Electric ZJ2[illegible] thin-based silicon diodes, which were left over from General Dynamics irr[illegible]liations in August, were irradiated in the 500-curie, cobalt-60 gamma sou[illegible]e at Hughes Aircraft Company. The purpose of the test was to determine wh[illegible]her the reverse characteristics of the diodes were affected by gamma fl[illegible]ds of 10^5 to 10^6R/hr at ambient temperatures. The results showed that cert[illegible]n diodes failed rapidly in the reverse direction as a result of gamma radi[illegible]tion only.

DECLASSIFIED IN FULL
Authority: EO 13526
Chief, Records & Declass Div, WHS
Date: MAY 2 9 2015

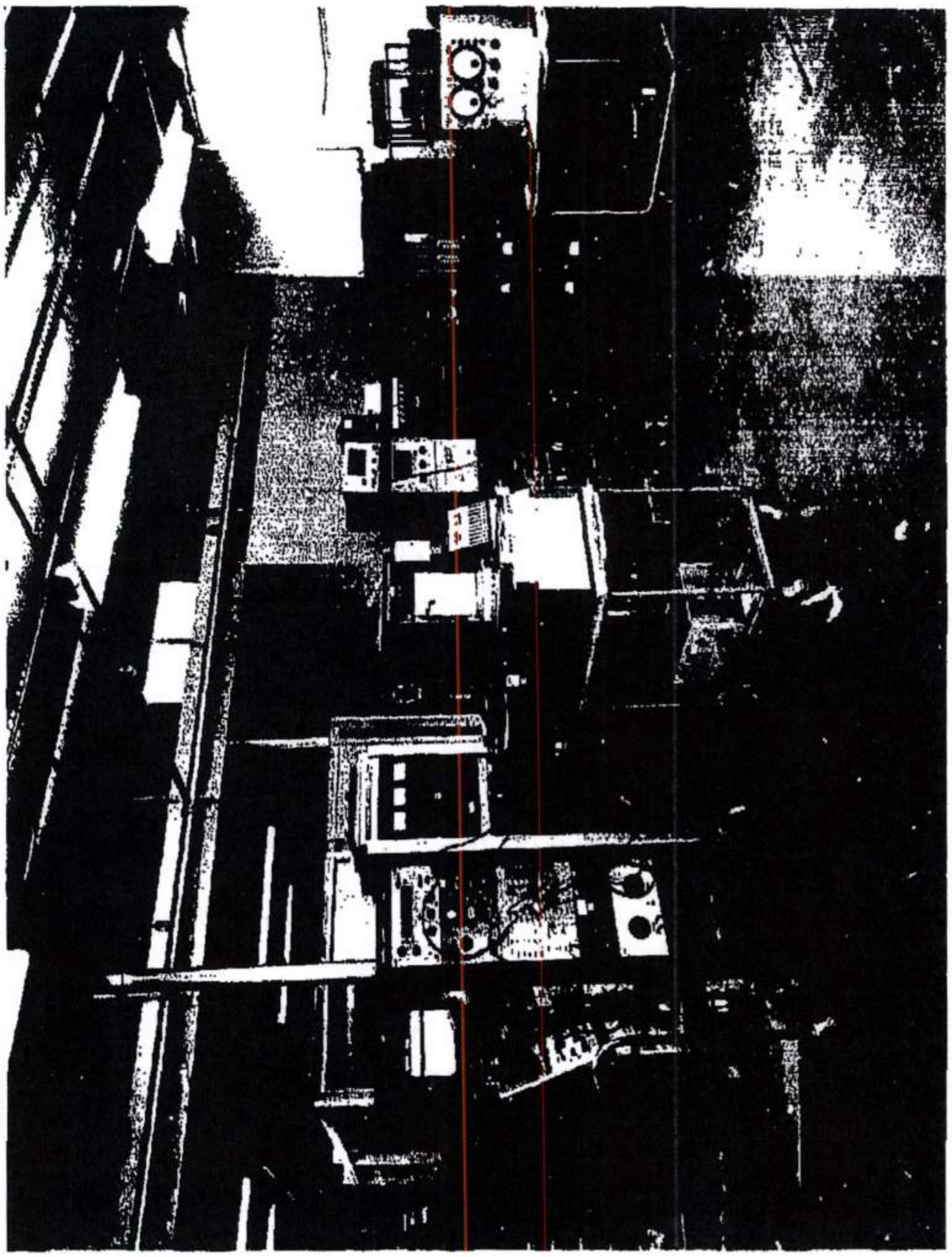

FIGURE 165 - Data Handling Equipment Used to Check Circuits

Following these tests, a 105-curie, cobalt-60 gamma sour e was purchased and installed in the Marquardt Radiation Effects Labor ory for the purpose of screening magnetic amplifier components suspecte of being sensitive to gammas. During the period from 15 November to 22 ovember 1961, a total of 158 diodes and 7 capacitors scheduled for the Janu y 1962 General Dynamics irradiations were tested in gamma fields up to .7 x 10^5 R/ hr.

4.4.4 Low Level Neutron Irradiations of Magnetic Amplifier Co ponents

As further check on the radiation resistance of magnetic a plifier components, arrangements were made with the Atomic Energy C mmission and Atomics International for the use of the KEWB reactor for th purpose of irradiating diodes in a combined neutron and gamma field. Th fast neutron dose (E>2.9 Mev) was specified to be approximately 10^{12} nvt A dosimeter run using sulphur and gold foils was made at the KEWB on November 1961 using the same setup that would be used for the tests. In add ion, several diod s were included to check their induced activity.

The preliminary test showed sufficient induced activity in e diodes to require special handling although the entire assembly was shie ed with cadmium. The sulphur dosimeters yielded an average neutron fl (E>2.9 Mev) .7 x 10^5 neutrons/cm^2/watt. On 7 December 1961, 126 G neral Electric diodes were irradiated for a period of 3 hours and 26 mi tes at a power level of 480 watts. In addition to sulphur and gold foils, g mma dosimeters were included to determine the integrated gamma dose. st runs were made on individual reverse characteristics before, during, nd after the run. In addition forward curves were taken on every fifth dio during the run. Dosimetry results from the sulphur foils showed an ave ge integrated neutron flux (E>2.9 Mev) of 1.33 x 10^{12} nvt.

4.4.5 1962 Irradiation Program

This company, in conjunction with the Chance Vought Cor ration, is making preparation for testing second generation magnetic am ifier circuits at the General Dynamics/Fort Worth reactor facility. Thes preparations include the mounting of test amplifiers and experimental Ge ral Electric ZJ225 diodes on General Dynamics-furnished expanded alum um sheets, preparation of cables, and data handling equipment. The integra d neutron flux is expected to be a minimum of 10^{16} nvt (E>0.33 Mev). Thes circuits and components will be irradiated at ambient temperature. This ork is proceeding according to schedule.

5.0 FLIGHT ENGINE FACILITY AND TEST PLANNING

Test facility planning during FY 1961 has included site location stuc es, economic studies of air heater and air supply system alternates, design crite ia revisions, refined facility cost estimates, and operations and maintenance st i- ies. In addition, the Underground Air Storage (UAS) Experiment achieved im portant milestones, such as core drilling program completion, final pilot cha n- ber site selection, chamber design completion, fabrication and construction specifications preparation, and complete instrumentation and data reduction s- tem design.

5.1 FACILITY DESIGN STUDIES

5.1.1 Flight Engine Ground Test Facility Site Location

A review of potential facility sites was conducted to assure that the underground exploration program for the UAS Experiment would cover suffic nt area to be applicable to any feasible Flight Engine Ground Test Facility site selection. As the cost of the air supply line between the UAS chamber and th test point is relatively high, it is very desirable to locate the UAS chamber c se to the Facility test point. The review of potential sites was concluded, with ur sites being selected for study. The area investigated and the four locations n- sidered are shown in Figure 166.

Site P-1, which is 8,500 feet from Tory II test point, was conside d because it permits unrestricted deployment of personnel around the test poin with no effect from Tory IIC operations. Dr. J. C. Manning, consulting geo - gist, indicated that there is a strong possibility that suitable rock exists at t s point.

Site P-2, in the amphitheater, was recommended by the United Sta es Geological Survey (USGS) as a desirable site for a full-scale UAS chamber. Shadow shielding afforded by the high terrain surrounding this location provi s an additional advantage. The location of site P-2 permit operations without n- terference from Tory IIC. However, an additional expense for the extension f services is necessitated.

SITE SELECTION STUDY

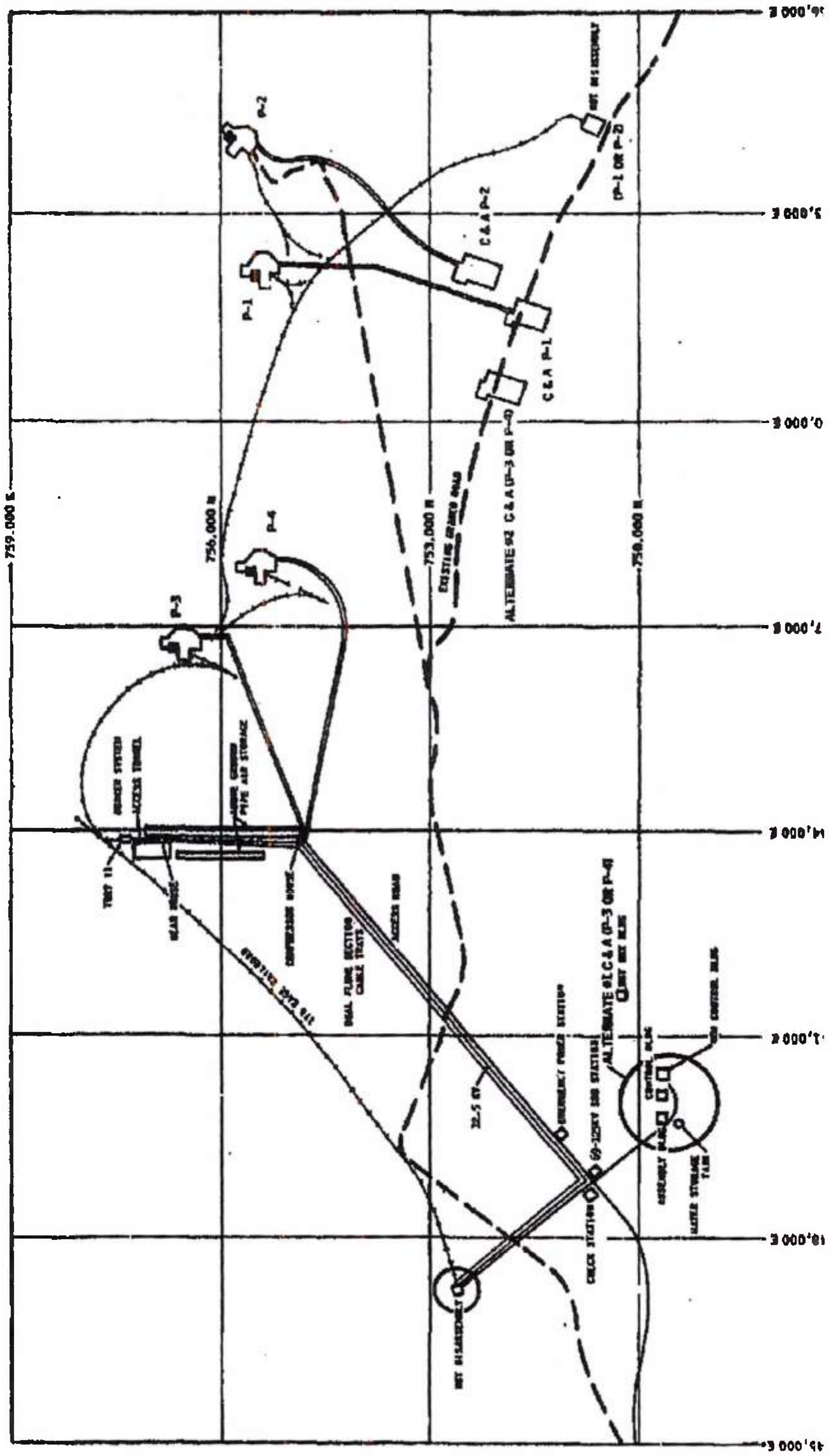

FIGURE 166

Site P-3, located 3,000 feet from Tory IIC, provides the very minimum practical separation from the Tory IIC test point. Such close proximity offers the advantage of possible sharing of support facilities. However, there the disadvantage of interference from Tory IIC operation, as well as the under tainty of site suitability for underground air storage due to visible faulting of t rock structure in this area.

Site P-4 was evaluated in the interest of eliminating some of the operational interference between Site P-3 and Tory IIC. Suitability for underground air storage was also very questionable.

Facilities at sites P-3 and P-4 could be operated from control and administration centers already existing at the general Tory IIC support facilit area.

Core drilling operations for the UAS Experiment, discussed in a lat section of this report, confirmed that the rock structure in the P-3 and P-4 areas was unsuitable for an underground air storage installation. A test core hole in this area disclosed soft altered rock and suggested this might be a maj shear zone.

5.1.2 Facility Performance Criteria

Revisions have been made to the facility performance criteria to reflect new engine test planning, and to obtain a minimal cost test facility. Instrumentation and controls design criteria have been updated in accordance wi these performance criteria revisions. The revisions take into account:

(1) Latest engine test planning, including new engine development schedules and facility utilization

(2) Analysis of exhaust fission product data from experimental reports

(3) Use of a standard mission trajectory as the basis for facility testing capability

(4) Testing of flight type engines only, rather than both boilerplate and flight type

(5) Change from stored energy heating to continuous heating of test air

(6) Changes in required run time from 25 to 93 minutes

(7) Change from one to two UAS chambers (for the 90-m ute facility)

(8) Sharing of the Tory hot disassembly building and rail oad by the flight engine ground test program

(9) Sharing of certain service buildings with Tory and m imization of test point exhaust handling equipment

5.1.3 Air Supply System

Underground Air Storage and Tory IIC Tie Line Study

To determine the cost of sharing the full scale UAS cham er between the Tory IIC facility and the proposed Flight Engine Ground Test F ility, a cost and feasibility study has been made of the required physical pipe cc nections, based upon an assumed location of the UAS chamber midway betwee the two facilities.

Sizing of pipe connections for the Tory IIC facility and th flight engine facility was based upon the following needs:

	Tory IIC	F ght Engine Facility
Type of Test	Direct connect	F ee jet
Weight Flow	2160 pps	3)0 pps
Mach Number	3.0	3)
Inlet Total Pressure, P_{t_o}	382 psia	5 : psia
Terminal Pressure P_t Tank	772 psia	1 :0 psia
Run Time	23.1 minutes	1 9 minutes
Altitude	Sea Level	S Level
Angle of Attack	Zero	Z ro
Type of Day	ANA Cold Day	A A Cold Day

DECLASSIFIED IN FULL
Authority: EO 13526
Chief, Records & Declass Div, WHS
Date: MAY 29 2015

To meet the Tory IIC requirements, the tie-line from the UAS c .mber would require eight parallel runs of 12-inch diameter N-80 steel casing at cost of $ 2,000,000; the tie-line to the Flight Engine Ground Test Facility would e-quire seven parallel runs of the same size and type at a cost of $ 1,750,00(The combined cost of connecting the two facilities together will be $ 3,750,000. For the case of using a single pipe rather than multiple pipes, the Tory IIC fac .ty would require a pipe 27 1/2 inches in diameter at a cost of $ 5,150,000, ar the Flight Engine Ground Test Facility would require a pipe 25 1/2 inches in d me-ter at a cost of $ 4,500,000 or a combined cost of $ 9,650,000. The storag capacity of the pipes or casing would reduce the UAS chamber cost by appr ci-mately 7 percent.

On a comparative basis, the cost of sharing a single full scale \ AS chamber would be $ 8,750,000 as against $ 6,000,000 for an independent ch mber to serve each facility. In view of the increased flexibility and service avai .ble with independent facilities, the most desirable and most economical arran; ment consists of a chamber located as close as possible to each test point.

Cross-Country Deployment of Tory IIC Addition

A separate study was made in an effort to increase the utilizatio of both the UAS chamber in the Flight Engine Ground Test Facility and the ai: storage addition planned for Tory IIC. Prior to construction, the intent w to realign the planned air storage addition for Tory IIC from a north-south to n east-west direction and interconnect it with the UAS chamber. The Tory I air storage addition, specified at that time, utilized 27 legs of 10 3/4-inch pip casing approximately 2100 feet long.

This cross-country extension of pipe casing was investigated as storage supply for Tory IIC, as well as a connecting line from the UAS cha ber to Tory IIC air supply system. The feasibility of aboveground installation pipe over long stretches of undulating terrain has been included as part of e study. The cross-country piping was anchored at both ends and laid in a s ies of shallow horizontal sine waves and supported by roller and pillow block p e supports to take up the thermal and pressure expansion.

The number of legs for this cross-country extension is :pendent upon the location of the Flight Engine Ground Test Facility. Therefore pipe casing arrays were studied for sites P-2 (10,000 feet from Tory) and P- (4,000 feet from Tory). A summary of results of this study is presented in T ble 29 . The number of legs of 10 3/4-inch OD pipe casing required to provide Tory IIC operating duration equal to that of the current addition was also de :rmined for each facility separation distance. Figure 167 shows the total pres ıre drop for 6- and 14-leg arrangements and their corresponding lengths meas ·ed from the Tory IIC manifold. The study indicates that it would be feasible t extend the Tory IIC air storage addition cross-country to connect the UAS ch nber of the Flight Engine Ground Test Facility with realization of the followin objectives:

(1) Economical use of common air storage and compre or systems for the Tory IIC and Pluto facilities

(2) Adequate separation distances between the two facil ies to avoid interference in construction, maintenance, and ope .tions

A comparatively small increment of additional casing (ε ove that planned for Tory IIC) compensates for the airflow pressure drop ε d would provide the same required run time.

Air Heater System

Changes made in the performance criteria are reflecte .n air supply heater run time and cost. In addition to including both of these fa ors in the performance criteria change, added emphasis has been placed on :ater reliability.

The maximum required continuous heater output, occur .ng during free jet flow of 3025 lbs/sec at a total pressure of 543 psia and a tal temperature of 1060°F, is 720,000 Btu/sec. A heater system comprised f four vitiated air heater units, each with its own separate control system, :fers the following advantages:

(1) Increased operational reliability, because malfunct n of one heater will have a much reduced effect upon deliver l air temperature

TABLE 29

CHARACTERISTICS OF CROSS-COUNTRY DEPLOYMENT OF TORY IIC AIR STORAGE ADDITION

Characteristic	Currently Planned Tory IIC Air Storage Addition	Extension to Flight Engine Ground Test Facility Site P-4	Extension to Flight Engine Ground Test Facility, Site P-2
Number of Legs (10 3/4 in. OD by .400 in. Wall Casing)	27	14	6
Length of Legs (ft)	2050	4000	10,000
Air Flow Rate Required from Addition Only (pps)	1122	1122	1122
Air Flow Rate Required from UAS Chamber - Maximum Tory IIC Flow Rate (pps)	2000	2000	2000
Additional Casing Needed to Equal Current Addition (ft)	0	650	4650
Total Casing Length (ft)	55,350	56,000	60,000
Available Tory IIC Run Time from Casing* Only at 1122 pps (min)	5	5	5
Pressure Drop at 1122 pps - Flow from Casing Only (psi)	--	8	128
Pressure Drop at 2000 pps - Flow from UAS Chamber through Casing (psi)	--	170	890
Available Tory IIC Run Time* with UAS Connected (min)	--	27.3	17

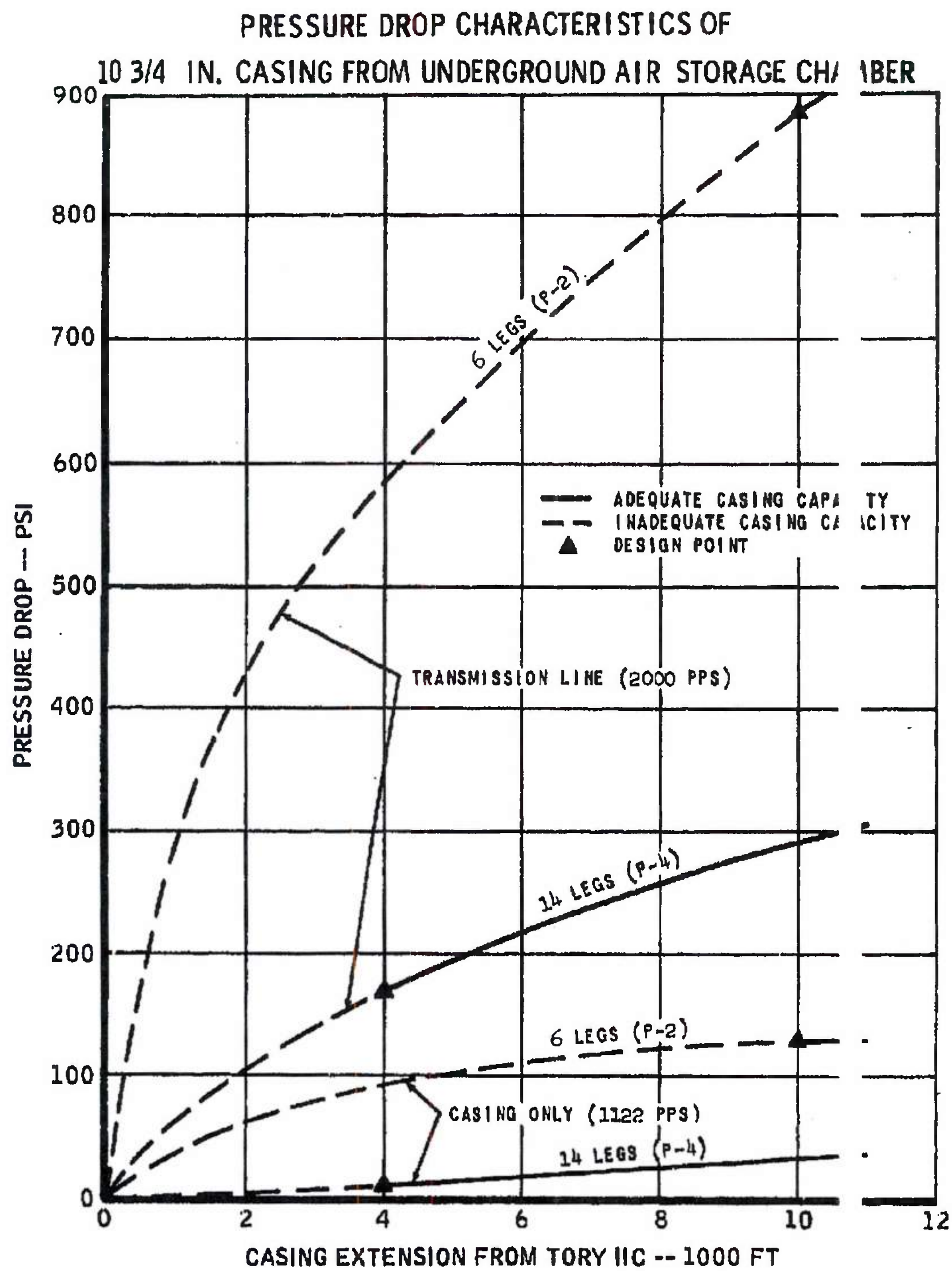
PRESSURE DROP CHARACTERISTICS OF
10 3/4 IN. CASING FROM UNDERGROUND AIR STORAGE CHAMBER
PRESSURE DROP -- PSI
CASING EXTENSION FROM TORY IIC -- 1000 FT
0
100
200
300
400
500
600
700
800
900
0
2
4
6
8
10
12
ADEQUATE CASING CAPACITY
INADEQUATE CASING CAPACITY
DESIGN POINT
6 LEGS (P-2)
TRANSMISSION LINE (2000 PPS)
14 LEGS (P-4)
6 LEGS (P-2)
CASING ONLY (1122 PPS)
14 LEGS (P-4)
MAC A673

(2) More reliable scaling, because the size of each of the four uni more closely approximates the heater successfully tested in th vitiated air heater experiment

(3) Less severe design stress problems due to reduction of diame r of each high-pressure, high-temperature unit

The preliminary design of the fuel system has been completed. Tl s design provides for the unlikely event of a heater unit flameout by means of c m-ponent paralleling. One heater unit flameout could produce a momentary air temperature drop of approximately 195°F. It appears that currently conside ed reactor core materials could cope with a sudden air temperature drop of 200 250°F.

Figure 168 shows the preliminary design of the skid-mounted vitiat l heater assembly.

Liquid Air Supply System Alternate

Liquid air supply systems have been investigated to determine whe ıer the missile-stimulated increase in this country's liquid air generating capabi - ties has had an appreciable effect on their cost. Large masses of air can be stored at low pressure in liquid form and then pumped, vaporized, and heate to the pressure and temperature required.

There were three approaches taken in this study:

(1) Purchase of liquid air from existing Government and private sources with on-site storage and vaporization

(2) Manufacture of liquid air at a privately owned and operated on-site plant (captive plant)

(3) Manufacture of liquid air at a Government owned and operated on-site plant

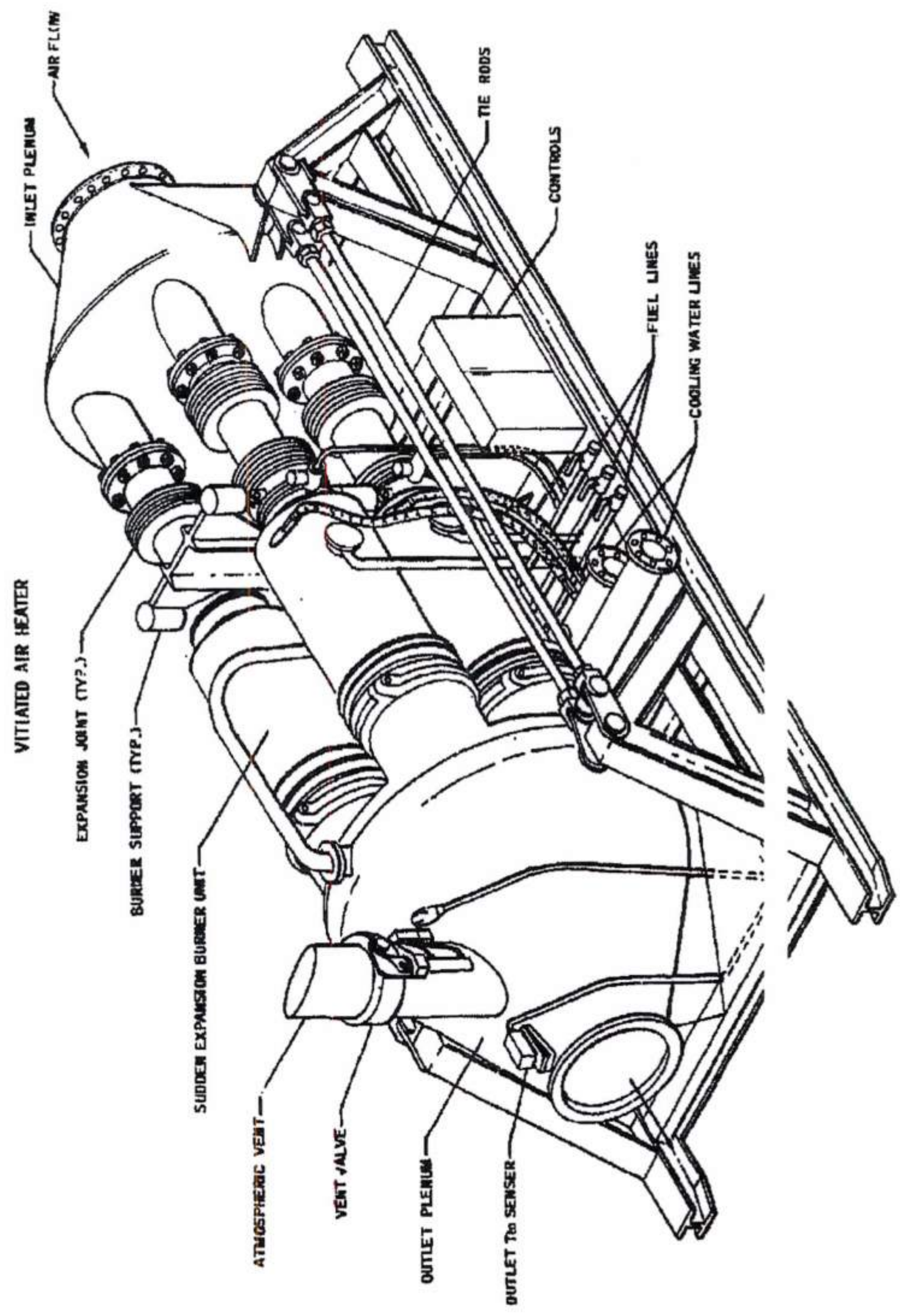

VITIATED AIR HEATER

Estimated costs were made on 4-million, 11-million, and 27-mi ion-pound storage capacities, representing 25-minute, 90-minute, and full tra ctory continuous run test capabilities. The 4-and 27-million-pound supply estim es were based on a 5-year life; the 11-million-pound supply on a 2-year life. 'hese systems were compared with the corresponding size of the UAS system. T tal costs for the systems are compared in Figures 169, 170, and 171. The r-formance criteria and estimated costs are listed as follows:

Design Requirements

Total Storage	4 million pounds	27 million pou ds
Production Rate	1.5×10^6 lbs/day	1.5×10^6 lbs/ ay
Maximum Airflow	3600 pps	3600 pps
Test Air Pressure (P_{t_o})	630 psig	630 psig
Air Temperature to Heater	460°R	460°R
Runs per Year	50	25
Life Expectancy	5 years	5 years

Estimated Cost
(Millions of Dollars)

	4-Million-Pound Storage		27-Million Pou Storage	
	Initial Fixed Cost	Annual Operating Cost	Initial Fixed Cost	Ann ıl Oper ing Cc t
Purchased Liquid Air*	5.54	14.73	10.54	30 9
Captive Plant**	5.54	7.30	10.54	15 1
Government Plant	19.07	2.99	24.02	5 8
Underground Air Storage	6.52	.30	20.24	3

- - - - - - - - - - - - - -

* Total existing U.S. production is committed for the next 5 years; opera ng costs must include amortization of new capacity for the contract.

** Based on guaranteed production for the life of the contract.

COMPARISON OF COST OF FOUR-MILLION-pound LIQUID AIR SYSTEM WITH COST OF UNDERGROUND AIR STORAGE

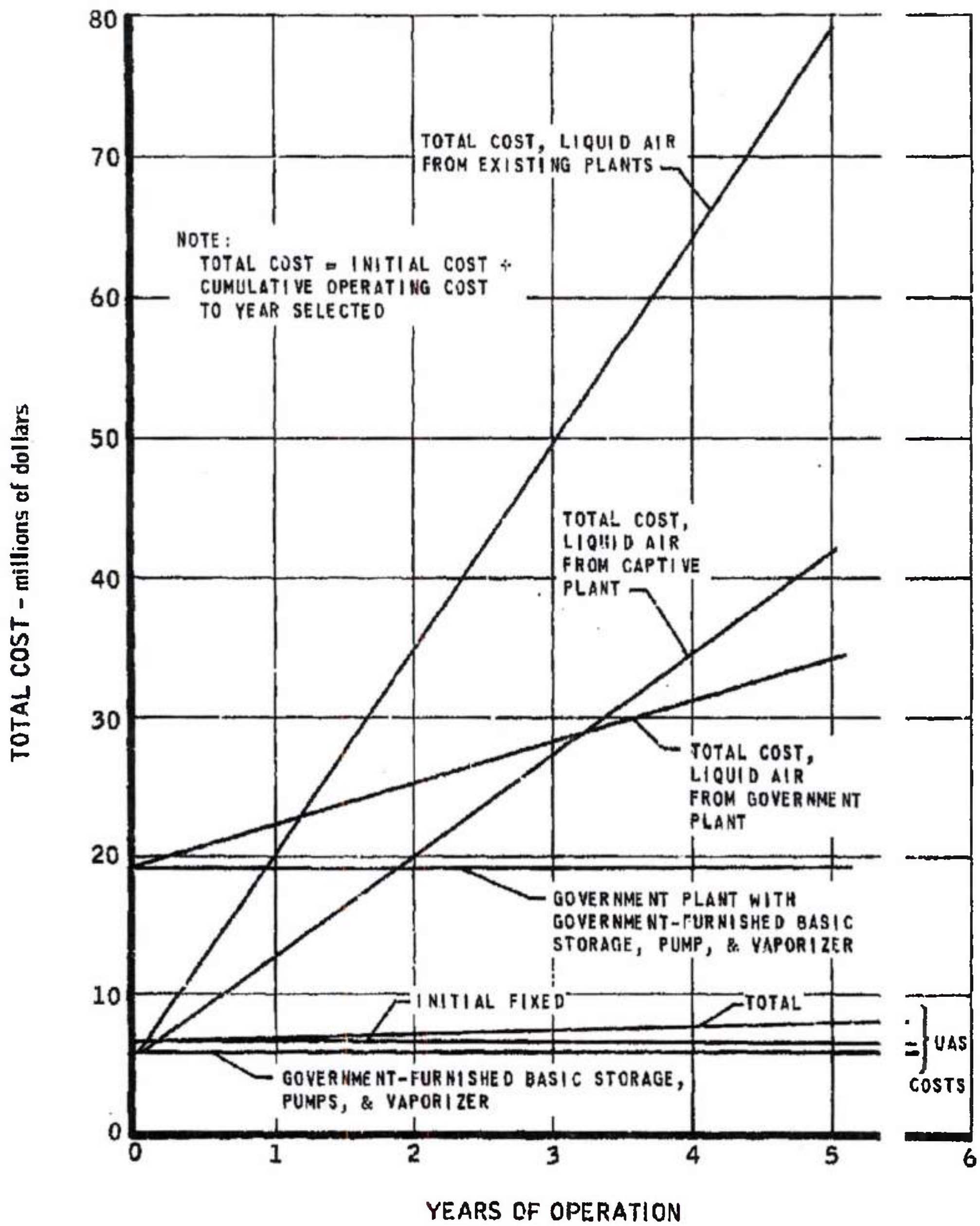

MAC A673

COMPARISON OF COST OF ELEVEN-MILLION-pound LIQUID AIR SYSTEM WITH COST OF UNDERGROUND AIR STORAGE

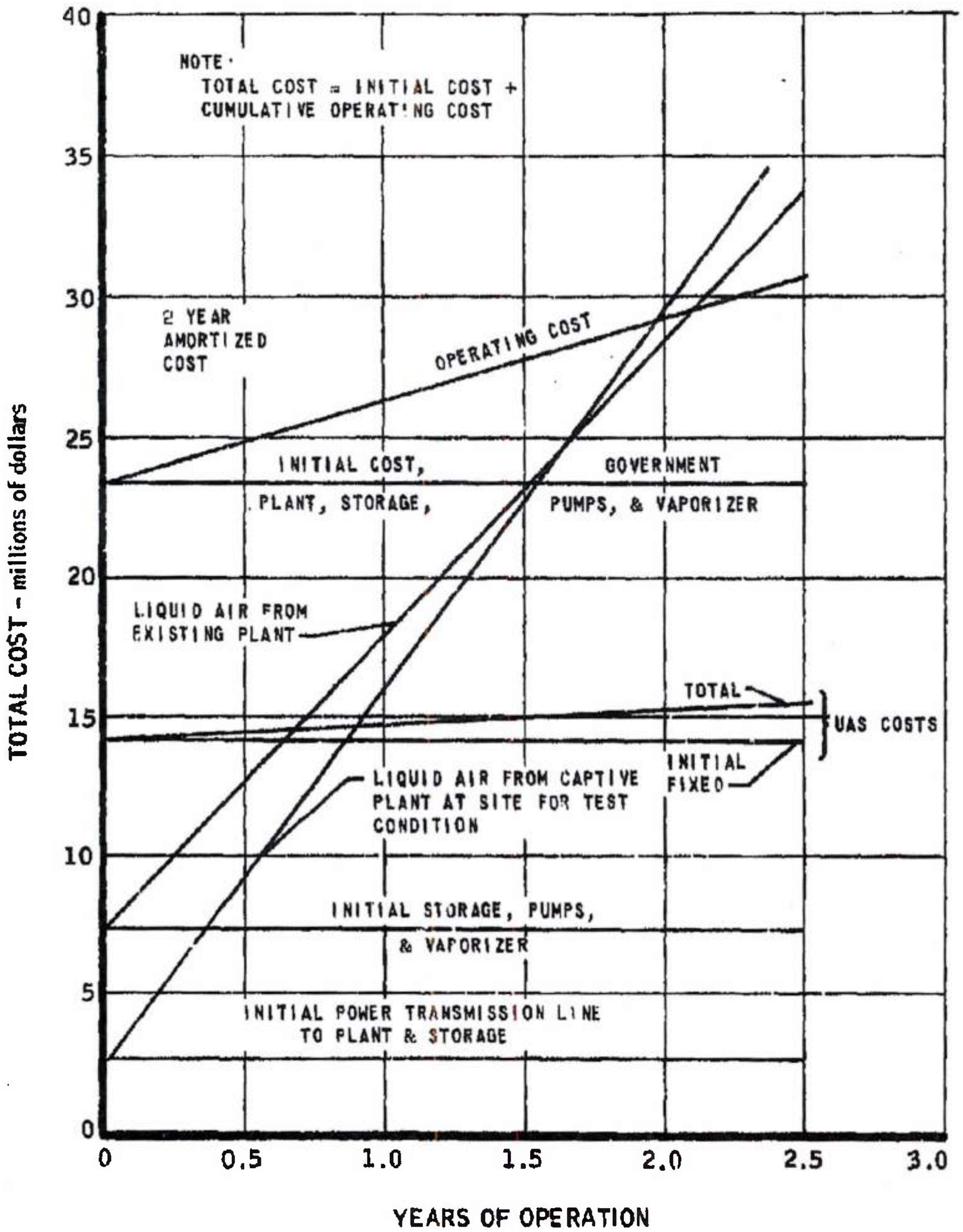

COMPARISON OF COST OF TWENTY-SEVEN-MILLION-pound LIQUID AIR SYSTEM
WITH COST OF UNDERGROUND AIR STORAGE

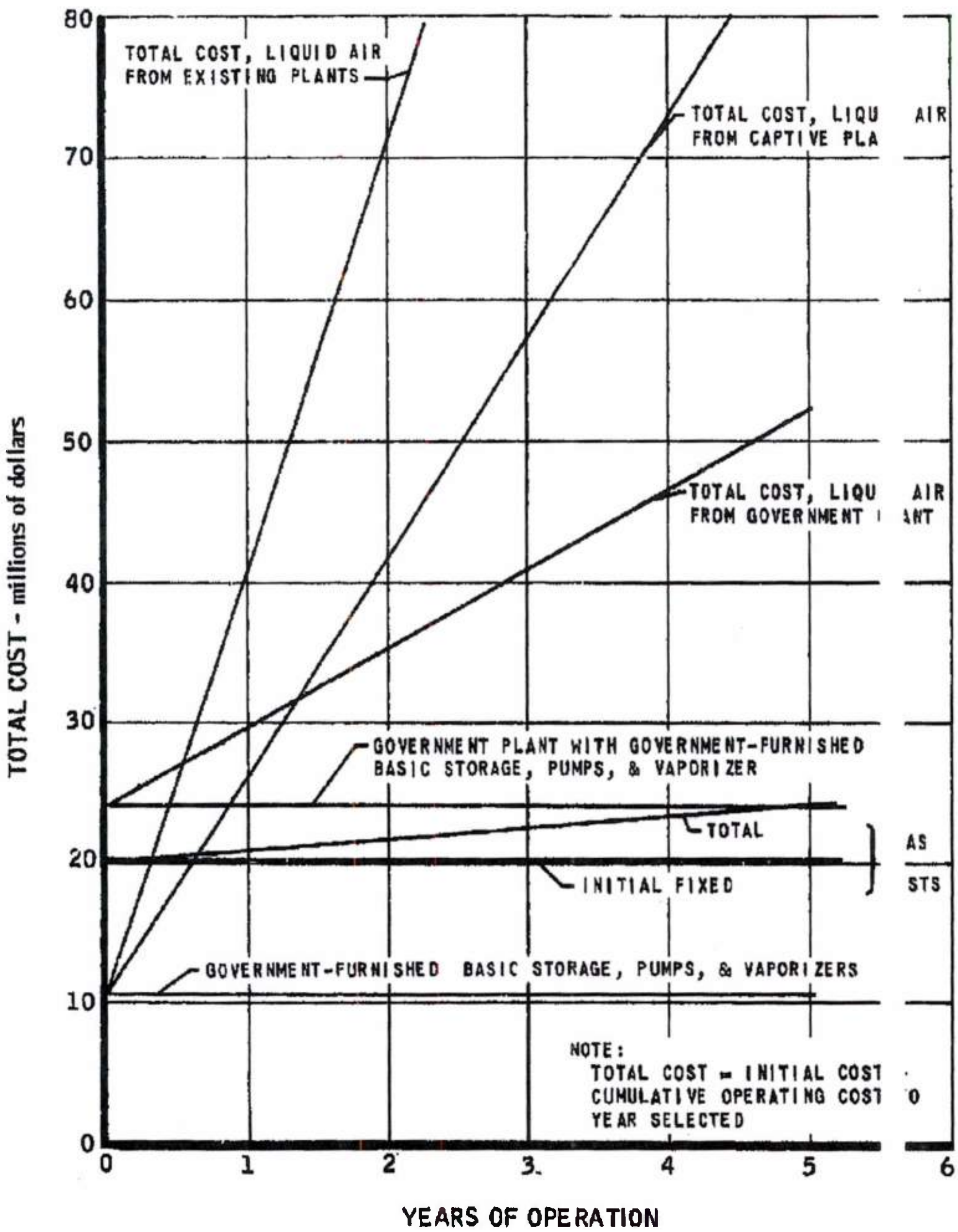

Design Requirements

Total Storage	11 million pounds
Production Rate	1.836×10^6 lbs/day
Maximum Airflow	2,000 pps
Test Air Pressure	630 psig
Air Temperature to Heater	460°R
Runs per Year	17.5
Life Expectancy	2 years

Estimated Cost
(Millions of Dollars)

	Initial Fixed Cost	Annual Operating Cost
Purchased Liquid Air*	7.425	10.50
Captive Plant**	2.6	13.55
Government Plant	23.4	2.95
Underground Air Storage	14.09	.50

In addition to the unfavorable economics, other undesirable charac teristics of liquid air storage systems include:

(1) Transient lag and control difficulties during vaporization, incl ing surging and overpressurization

(2) Unusually large heat release capacity required for vaporizatio

(3) Vaporizer tube burnout and leakage is a definite possibility, wi catastrophic failure very probable

(4) Unusually large amounts of electrical power are required, in e cess of currently available power at the Nevada Test Site

- - - - - - - - - - - - - -

* Total existing U.S. production is committed for the next 5 years; operatir costs must include amortization of new capacity for the contract.

** Based on guaranteed production for the life of the contract.

Cost comparisons of the liquid air system and UAS cham r systems, (Table 30) show the UAS system to be the least costly. Its reliabil y, due to inherent simplicity and maintainability, further recommend it for t Flight Engine Ground Test Facility.

Continuous Air Compressing System

A continuous air supply system with the following perfor ance criteria has been studied:

Test airflow maximum	3,600 pps
Test air pressure, P_{t_o}	630 psia
Air temperature to heater	990°R (530°F) temperat re out of compressor without after ooler

To meet the above design criteria, the compressing syst n will require approximately 1,269,000 horsepower. Because of the remot ocation of the facility, several types of drives were considered, including ele ric motor (with and without generating plant), diesel engine, gasoline engine, nd gas turbine. Both initial and operating costs for each system are shown i Figure 172. Centrifugal compressors with electric drive proved the most econo ical, with purchased electric power. Comparison of continuous compressing ant costs with UAS chamber system costs is shown in Table 30.

Aboveground Air Storage System

A cost analysis was performed for an aboveground Tory A-type air storage system, based on the use of threaded oil-well casing to sto 15 million pounds of air at a pressure of 3600 psia. This corresponds to a 90 ninute run time. A desirable feature of such a system is that large masses of teel are utilized. These masses provide a comparatively large heat sink, v ich minimizes the air temperature drop during a blowdown test run and red es the required capacity of an air heating system.

Undesirable features of the system include (1) the systen ressure drop during a run because of the great lengths of relatively small-s e flow paths, and (2) the high degree of skill and quality control required during i stallation. Probably the greatest objection to this system is the high cost. Th estimated cost of the above-specified aboveground air storage, based on Tory IA and IIC facility costs, totals $49,535,000. This cost must be compared wi the approximate $9,000,000 cost estimated for a comparable UAS system.

MAC A673

TABLE 30

SUMMARY OF FACILITY COSTS

Type of Cell	Single Closed	Single Closed	Single Closed	Single Closed	Single Closed	Single Closed
Type of Air Supply	Underground	Underground	Underground	Liquid Air Site Mfg.	Liquid Air Site Mfg.	Continuous Compressors
Usable Air Supply, lbs	3,000,000	11,000,000	20,000,000	3,000,000	20,000,000	Unlimited
Total Air Stored, lbs	4,120,000	15,100,000	27,500,000	4,120,000	27,500,000	Unlimited
Recharge Time, days	3	6	20	3	20	--
Recharge Rate, lbs/day	1,000,000	1,833,333	1,000,000	1,000,000	1,000,000	--
Average Available Run Time (at 1960 pps) mins.	25.5	90	Complete Trajectory	25	170	Unlimited
Exhaust Handling System	Minimal	Minimal	Minimal	Minimal	Minimal	Minimal
Free Jet Angle of Attack Capability, degrees	±10	±10	±10	±10	±10	±10
New Hot Component Service Building	No	No	No	No	No	No
Air Heater System	Vitiated	Vitiated	Vitiated	Vitiated	Vitiated	Vitiated
Service Buildings	Share with Tory IIC	Share with Tory IIC	Share with Tory IIC	Share with Tory IIC	Share with Tory IIC	Share with Tory IIC
Number of Runs to Complete Trajectory	7	2	1	7	1	1
Air Supply System	$ 8,853,000	$16,000,000	$18,173,500	$21,400,000	$26,350,000	$85,780,000
Test Cell Installation and Support Serv.	2,027,200	2,030,000	3,355,000	2,030,000	2,030,000	2,030,000
Exhaust Handling System	238,500	240,000	245,000	240,000	240,000	240,000
Instrumentation and Controls	1,222,600	1,230,000	1,252,700	1,230,000	1,230,000	1,230,000
Hot Component Service Building	--	--	--	--	--	--
Service Buildings	583,300	587,000	599,200	587,000	587,000	587,000
Site Development and Utilities	1,811,000	1,813,000	1,856,900	1,813,000	1,813,000	1,813,000
Required Facility Funding	$14,735,600	$21,900,000	$25,482,300	$27,300,000	$32,250,000	$91,680,000

CONTINUOUS AIR COMPRESSING SYSTEM COSTS

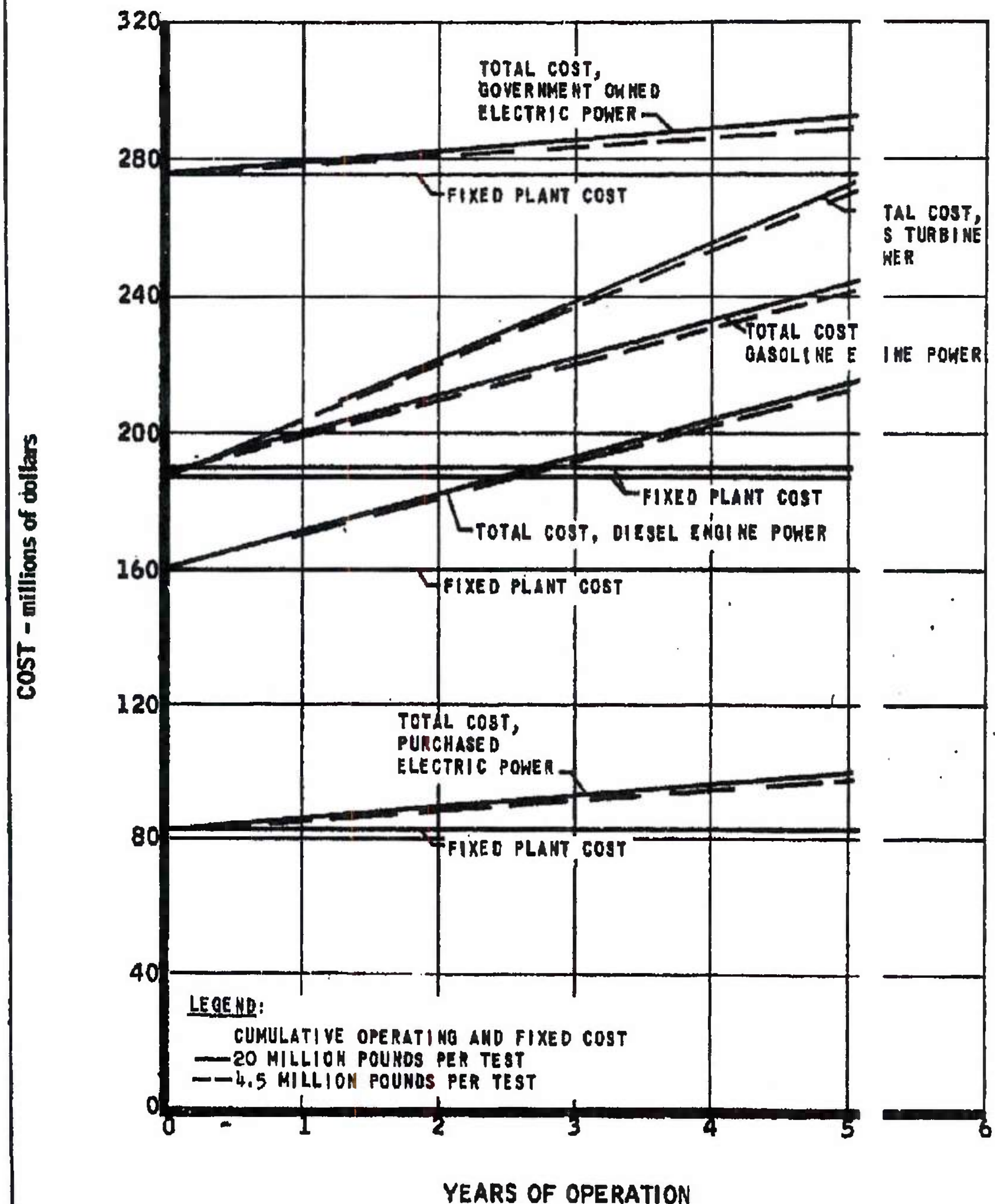

FIGURE 172

Underground Air Storage Chamber Arrangement

An investigation has been made of one-chamber vs. two-chamber u ier- ground air storage of test air for the Flight Engine Ground Test Facility. Co :s of the two concepts were compared, as well as the advantages and disadvanta ·s of each. The two-chamber concept provides much greater operational flexibi ty, reliability, and maintainability. Valve manipulation will permit charging of c e chamber while the other is blowing down during a test, or both may be used s nul- taneously for long run testing. Figure 173 shows the arrangement and sizing f : a 15-million-pound (90-minute run duration) two-chamber air storage system. 'he separation distance of 835 feet is required to allow full storage pressure in o chamber while the other chamber is at atmospheric pressure.

5.1.4 Instrumentation and Controls

The performance criteria for the Flight Engine Ground Test Facili in the area of data acquisition and facility controls has been revised and upda d. Facility instrumentation and controls may be divided into the following systen :

(1) Air pressure control system

(2) Air temperature control system

(3) Data acquisition and handling systems

Air Pressure Control System

The preliminary design of the air pressure control system was upc :ed and revised in the following areas:

(1) Pressure reducing valves (P_{t_o} control)

(2) Low pressure air supply (reactor aftercooling)

(3) Startup, run, and shutdown control per latest test item plannin

(4) Safety interlocks, based on latest test point operational analysi , use of the vitiated air heater system, and Pluto engine ground on- trol system definition.

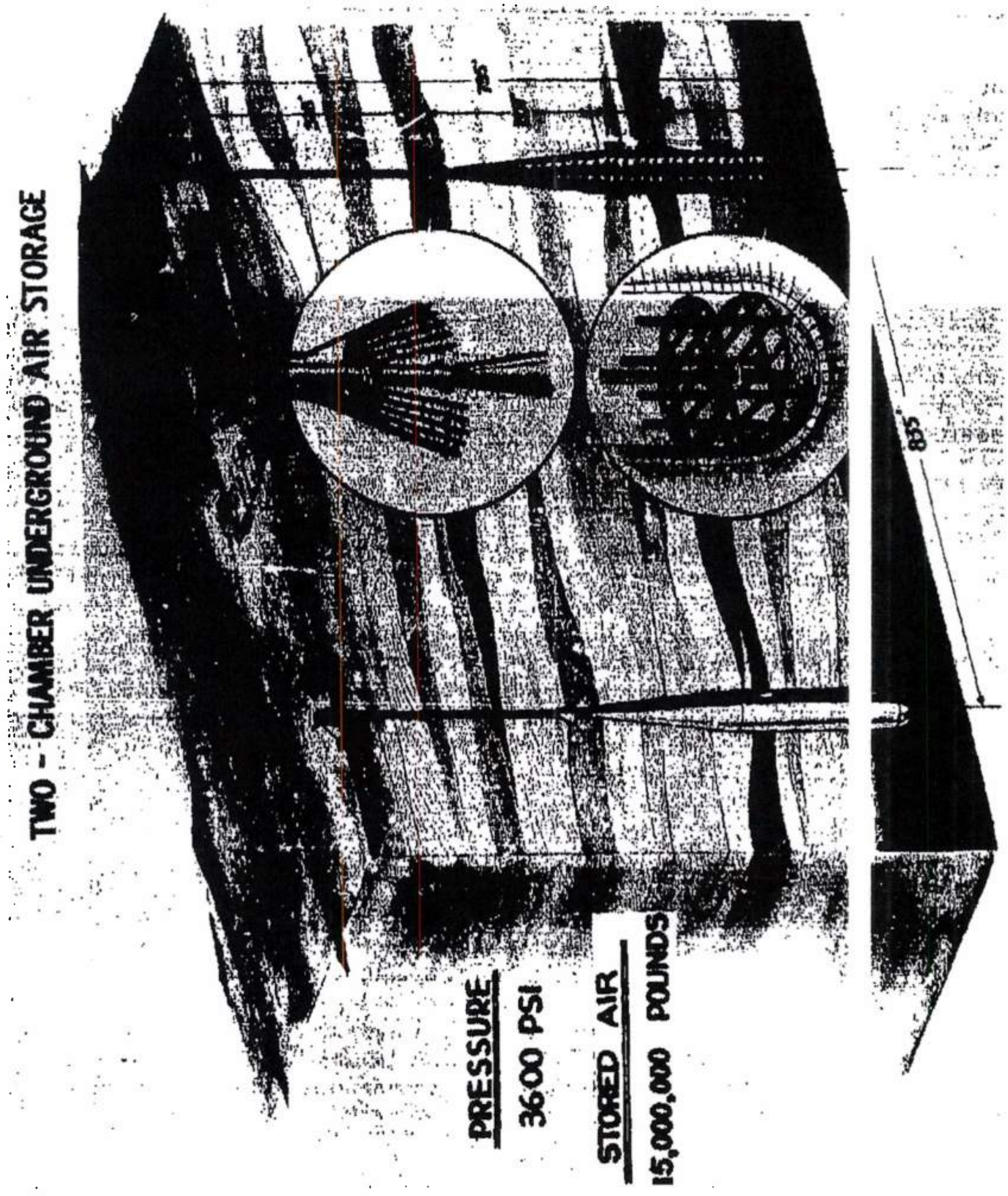

Reference: 232-4043-32B

Air Temperature Control System

The air temperature control system has been designed to fulfill fc r main objectives: (1) to permit reasonably accurate transient programming f air temperature, (2) to provide temperature stability during steady state op ra-tion, (3) to maintain uninterrupted delivery of heated air to the test item wi either manual or automatic time-temperature programming, and (4) to prev it an inadvertent heater control failure from either damaging the reactor or se i-ously disrupting the test.

The temperature control system has been designed for use with a four-burner vitiated heater. Each of the four burners is provided with a se rate automatic temperature controller, thereby assuring that the malfunction of y one burner control system will not cause all burners to malfunction or flam ut. Safety interlocks have been incorporated to assure sequential, safe, and aut matic operations during startup and shutdown procedures.

Data Acquisition and Handling

The acquisition of data during a test mission will be provided in tl form of magnetic recordings by a multiplexed pulse-duration-modulated (PI i) signal telemetering system. The data acquisition system will gather 86 cha iels of information from the test cell and 86 channels of information from the va ous controllers and monitors within the main control room. The two 86-channe groups will be simultaneously recorded on magnetic tape along with the inte phone conversation to provide permanent magnetic recordings of raw data si nals that can be edited and processed for data reduction and analysis of further p o-cessing.

Facility Cost Estimates

Revisions to the facility performance criteria required correspon ng revisions to facility cost estimates. Some of the factors affecting the costs f the facility that were varied for estimating purposes included run time, faci ty recovery time (recharge rate), and type of air supply.

Run time variations from 25 to 90 minutes, a request for the cost f a facility capable of complete trajectory simulation in one run, together wit the alternate air supplies previously reported, produced facility cost estimates summarized in Table 30.

5.2 UNDERGROUND AIR STORAGE EXPERIMENT

Significant progress has been made on the UAS Experime t during the year. The site location survey and core drilling program was com eted, chamber site location determined, chamber design finalized, data acqui tion system defined and designed, and construction specification and detail dra ngs completed.

5.2.1 Site Investigation

The USGS conducted a mapping program of the NTS 401 ea. To provide for the possibility of joint use of the full scale UAS chamber b both Pluto and Tory facilities, this site exploratory program included possibl sites close to the Tory IIC facility.

Aboveground Area Surveys

A gravity meter survey was completed by the USGS. Th survey indicated that there were no rhyolite plugs in the area under conside tion, and that the originally planned electromagnetic survey was unnecessar Compressive strength tests of several samples of surface rock in this area ive values ranging from 8,200 to 42,000 psi, considerably above the 4,000-ps strength required by the UAS chamber design. The gravity meter survey, t gether with a more detailed visual inspection of the area, detailed the area's f lting system. Due to indications of a highly altered rock zone at one of the consic red site locations 3,000 feet east of the Tory test point, core drilling was diver d to a more encouraging area.

Core Drilling Program

A contract was awarded for core drilling at the Nevada est Site. Figure 174 shows the core hole locations at which the drilling acti ty was centered. Typical core samples and views of the drilling operatio at the test site are shown in Figure 175. Unconfined compressive strengths nd unconfined moduli of elasticity were determined from core samples.

After evaluation of the core drilling program and a repo submitted by Dr. John Manning, consulting geologist, a location for the UAS xperimental Pilot Chamber was established on the centerline between Core Hol TMC No. 1 and TMC No. 3, 12 feet from the latter. This location is shown g phically in Figure 174.

UAS CHAMBER VICINITY MAP INCLUDING PLOT PLAN AND CORE HOLE LOCATIONS

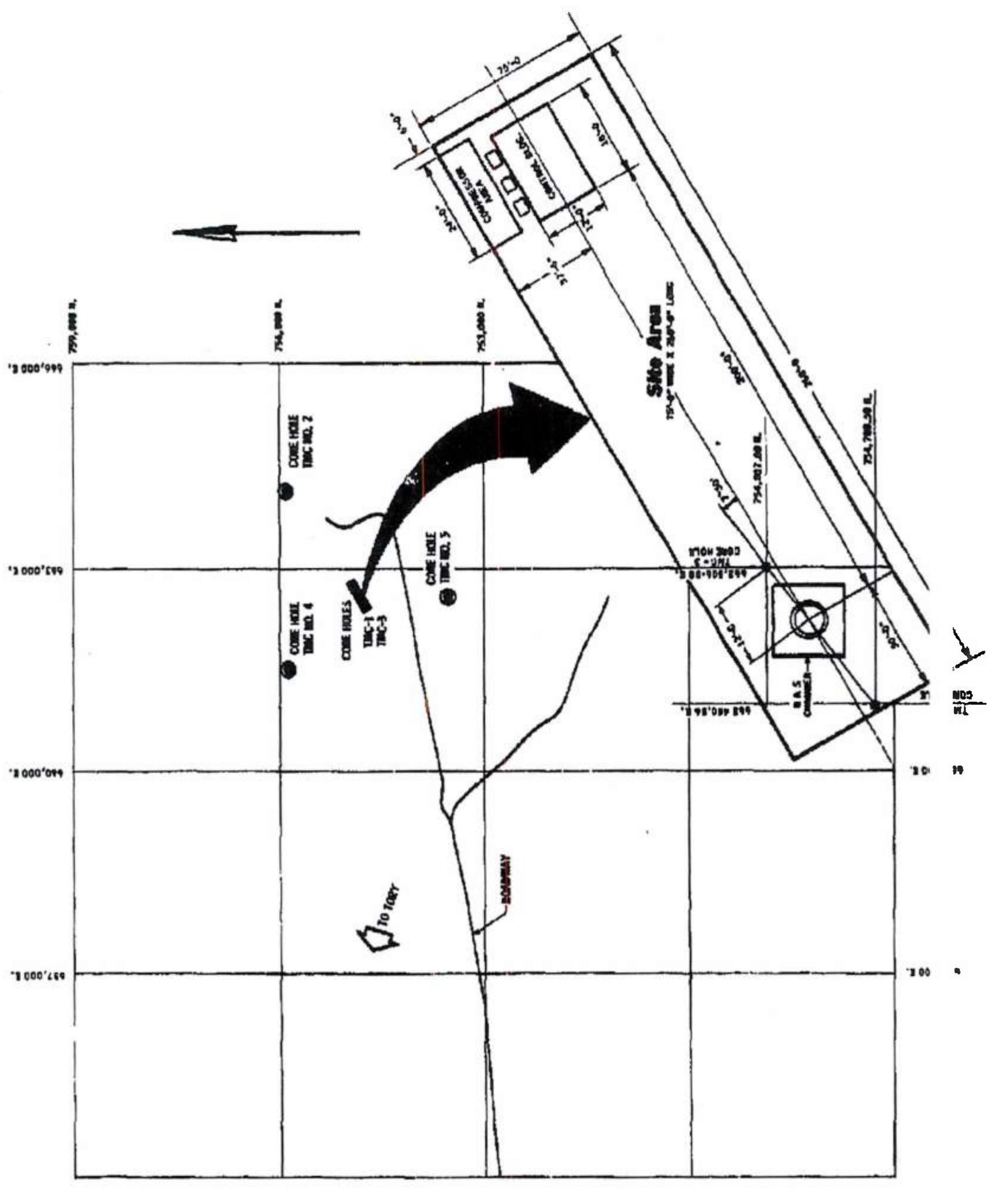

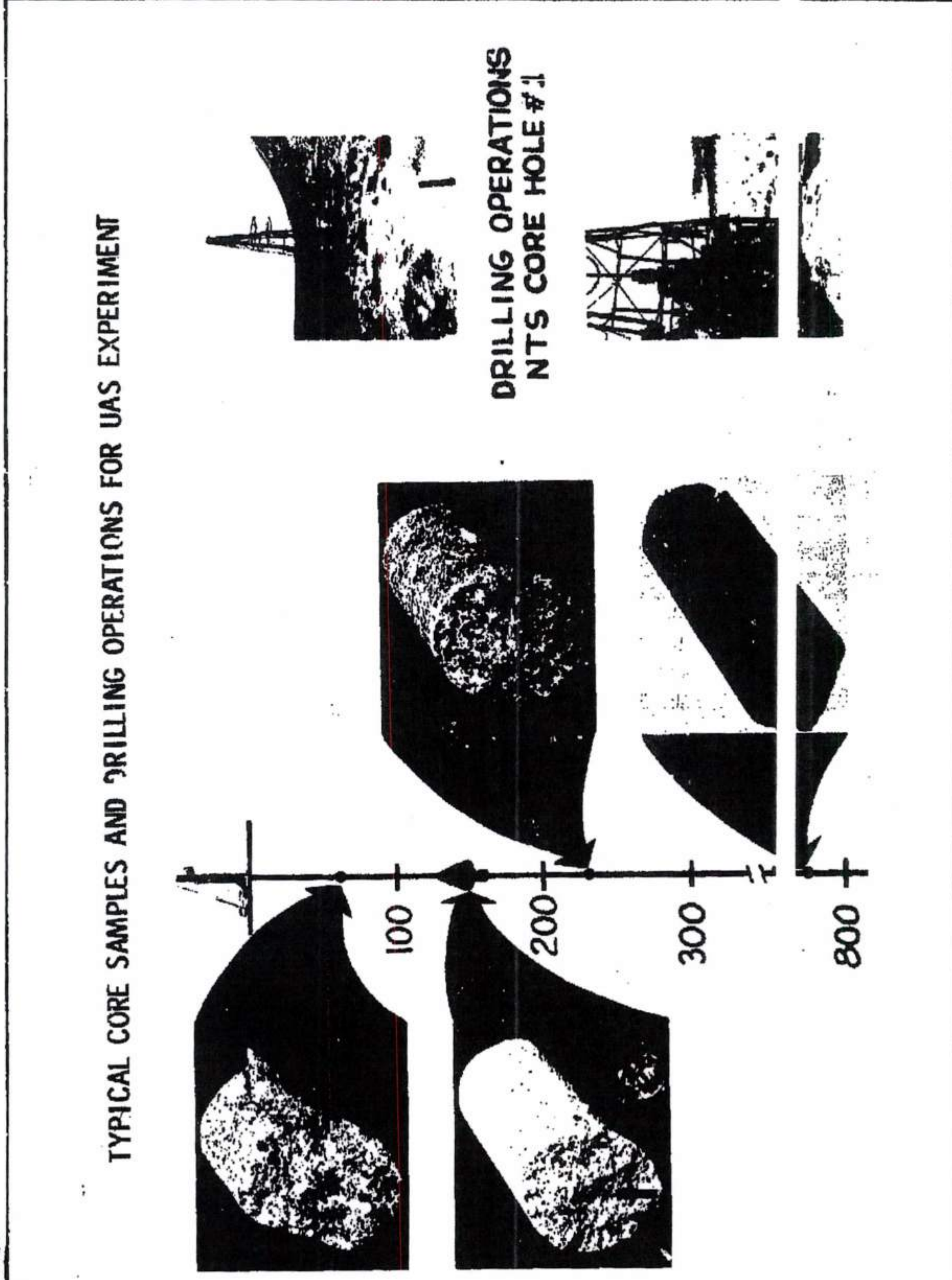

MAC A652

Reference: 232-4134-10A

Core Holes TMC No. 1 and No. 3 were drilled approximately at th recommended site for the Flight Engine Ground Test Facility. Their firm da ite roc. structure proved satisfactory for underground air storage.

Core Hole TMC No. 2 was drilled in the amphitheater at the north eastern edge of the site area. Individual pieces of rock from this hole exhibi :d high strength, but the condition of the rock indicated the existence of random oriented, uncemented joints throughout the underground rock mass in this ar .. The hole was abandoned at 112 feet because the rock was getting progressive worse with depth. In addition, the observed surface faulting in the amphithea :r confirmed its unsuitability for underground air storage.

Core Hole TMC No. 4 was drilled to explore the area northwest of he test chamber site. The rock was firm dacite down to a depth of 241 feet whe : a soft altered zone was encountered. The hole was bottomed in this soft mater l at 261 feet without any indication of the bottom of the soft zone. This zone of intensive alteration may represent the subsurface trace of a sizable fault. It lso gives indication of a major shear zone, eliminating the use of this site for ar underground air storage installation.

Core Hole TMC No. 5, drilled to explore the valley area approxim tely 1200 feet south of Core Hole TMC No. 1, penetrated coarse-grained altered dacite from the surface to the total cored depth of 322 feet. The rock cores ere firm and sound, an indication that this area, as well as the area around Core Hole TMC No. 1, should be explored further during the full scale chamber c e drilling program.

5.2.2 Chamber Design

All structural and mechanical design for the pilot chamber was co - pleted, and detail drawings were submitted to the AEC for preliminary appro al. Figure 176 shows the basic arrangement of the UAS chamber.

5.2.3 Liner-Rock Loading Analysis

During October 1961, the physical properties of the rock cores ta en during the core drilling program of the experiment became available from th laboratory tests. One of these cores, sampled in Core Hole TMC No. 1 at a depth of 309 feet indicated an unconfined elastic modulus of 1,700,000 psi. V ile this depth is considerably greater than that for the pilot chamber, but less th a

33

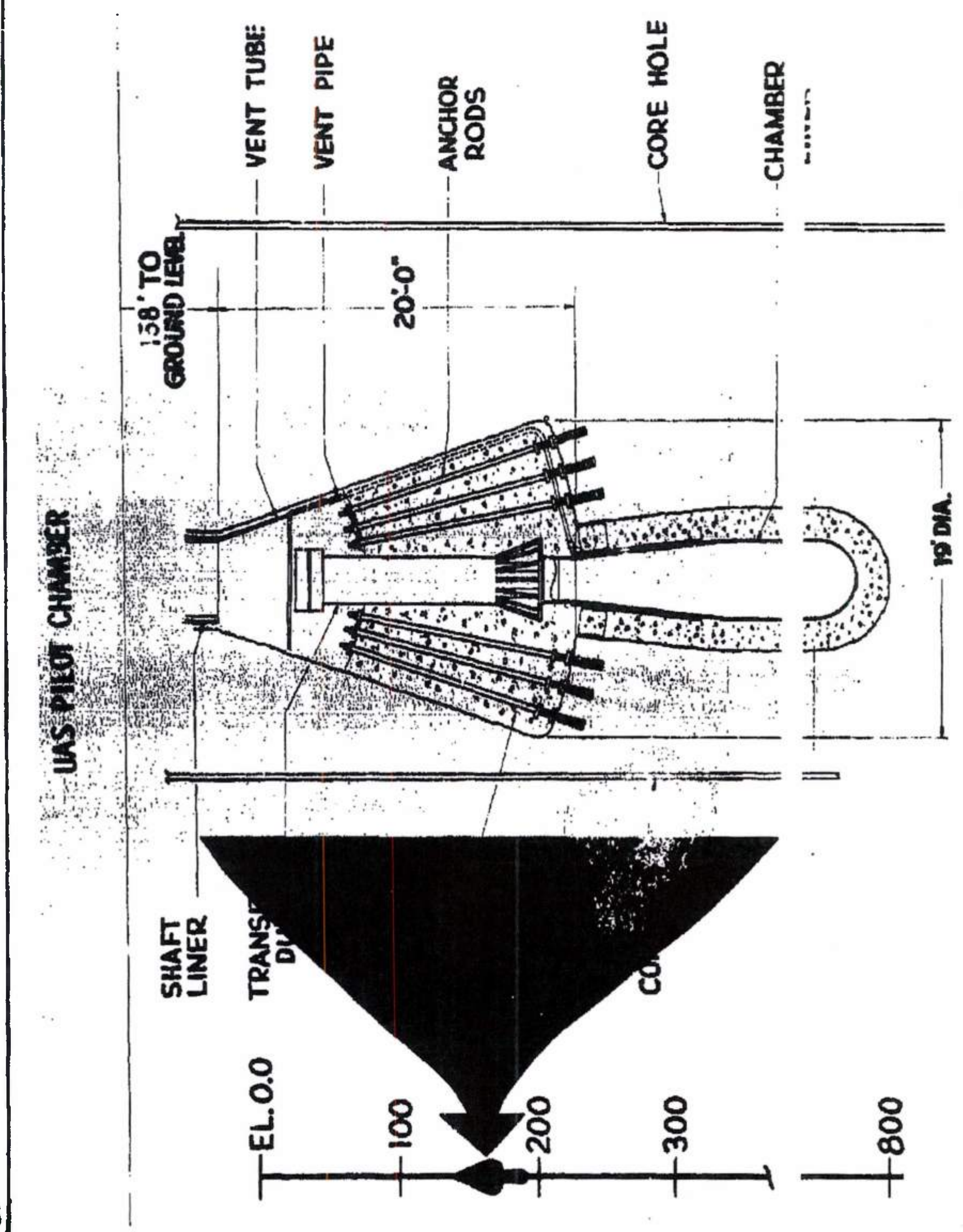

Reference: 323-4134-4A

that for the large chamber plug, it indicated that during the construction of tl pilot chamber there is a possibility of experiencing a similar modulus in a localized area adjacent to the chamber wall. Therefore, since one of the mi: sions of the experiment is to gain experience prior to full scale chamber desi n and construction, an analysis was made of the interaction of the liner and the rock in greater detail than that provided by the "cracked rock" analysis previ usly reported. The basis for this new analysis was an examination of the relative abilities of the chamber liner and the surrounding rock, as parallel load-bea ng structures, to back up the chamber pressure load imposed upon them, withou the use of the reinforced concrete liner common in tunnel design.

An analytical model (Figure 177) was set up to simulate this inter action and functional relationship. Although the anisotropic characteristics c the rock provide many more (relatively unpredictable) variables than those a counted for in the model, it contains the important functional factors. The ba ic functional characteristics shown in Figure 177 are the following:

(1) The liner will pick up a percentage of the radial chamber pres re load and convert it into liner hoop stress.

(2) The rock must resist the remainder of this load to satisfy equi - brium.

(3) Liner and rock will expand radially until equilibrium of forces prevails and a new common radius is reached.

(4) The relative percentages of load carried by liner and rock are determined by the relative stiffness of these two parallel struc tures, similar to the case of two beams, supported at both end one above the other, carrying their portion of a single central load in proportion to the ratio of their EI's.

In the case of the liner, its relative "EI" (or resitance to deflectio is a function of (1) its radius, and (2) its elastic modulus (E). The rock stiffnes is a function of its elastic modulus in confined state (in-situ E), the depth of the column of rock actually supporting the load, and the load it must bear.

ANALYTICAL MODEL OF LINER-ROCK DEFLECTION

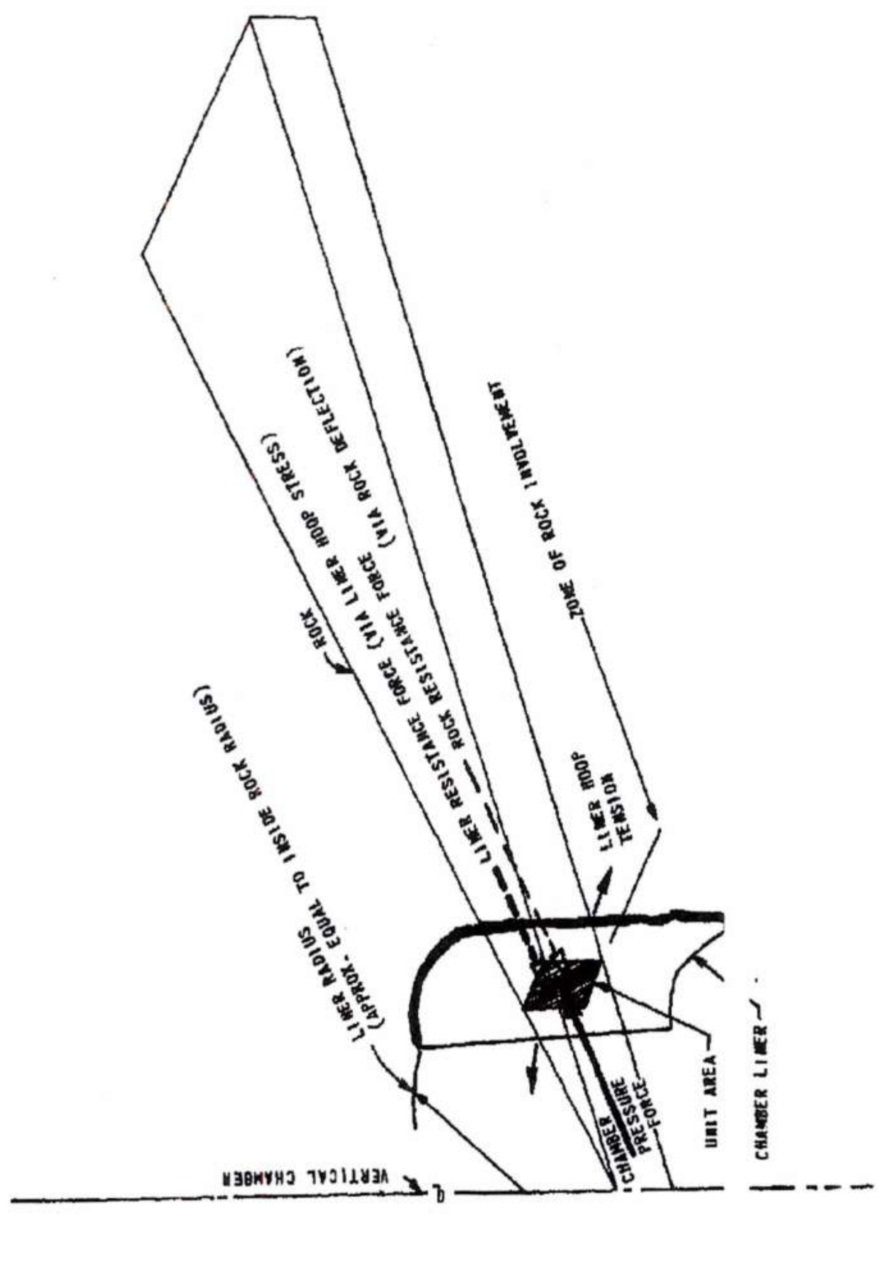

In operation, as chamber pressure increases, the thin liner defle :s (stretches circumferentially) to transmit pressure load to the rock, which d - flects radiall· As the rock deflects, the liner is forced to follow and its hc p stress builds up, thereby picking up a portion of the chamber pressure load When equilibrium is reached, both the liner and rock have moved the same s- tance radially and have shared the load between them in some proportion.

It then becomes obvious that, if the rock E is low (it deflects easi ·), it will increase the stress experienced by the liner. Therefore the design thickness of the liner of a UAS chamber is determined in part by the lowest ɔck E (in-situ) to be experienced during operation. Thickening the liner decrea :s its hoop stress by making it relatively more rigid, thereby picking up a gre er portion of the pressure load, and in turn reducing the load on the rock and i subsequent deflection. In addition, the larger the diameter of the chamber, he more capable the liner is of resisting the effects of a softer rock, since the radial deflection at the rock and liner is distributed over a larger liner circ m- ference.

The pilot chamber liner thickness of 0.187 inches was selected oı the basis of the analysis summarized in Figures 178 through 181. For the analytical model previously described, Figure 179 shows the relationship i - tween the effective pressure load the rock experiences (at equilibrium) vs. ıam- ber pressure. The unconfined E of the analytical model corresponds to the ı- situ E that the experiment will reveal. This relationship is plotted for a se c- tion of rock E's from the lowest E anticipated through the largest. At 4000 sig chamber pressure, the liner stress is also designated for each rock E. Sir s the liner material (T-1 steel) has a minimum yield point of 100,000 psi and a ultimate tensile strength of 135,000 psi, this curve shows that during the ex er- iment the rock can be made to experience a pressure of 3450 psi at a chamb r pressure of 4000 psi (if the rock E is 2,500,000 psi) without stressing the li er beyond its elastic limit. This rock loading, though occurring in a 5-foot dia ne- ter pilot chamber, closely approximates the loading in the full scale chamb . Figures 178, 180, and 181 provide similar rock pressure vs. chamber res- sure data for liners of thicknesses above and below the 0.187 inches selecte .

5.2.4 Chamber Construction Specification

The construction specification prepared for the experiment incluc d chamber excavation, structural work, concrete, instrumentation installatio control building, and electrical work. Drawings and specifications were su .

ROCK LOADING FOR UNDERGROUND AIR STORAGE CHAMBER
STEEL LINER THICKNESS = 0.161 inch

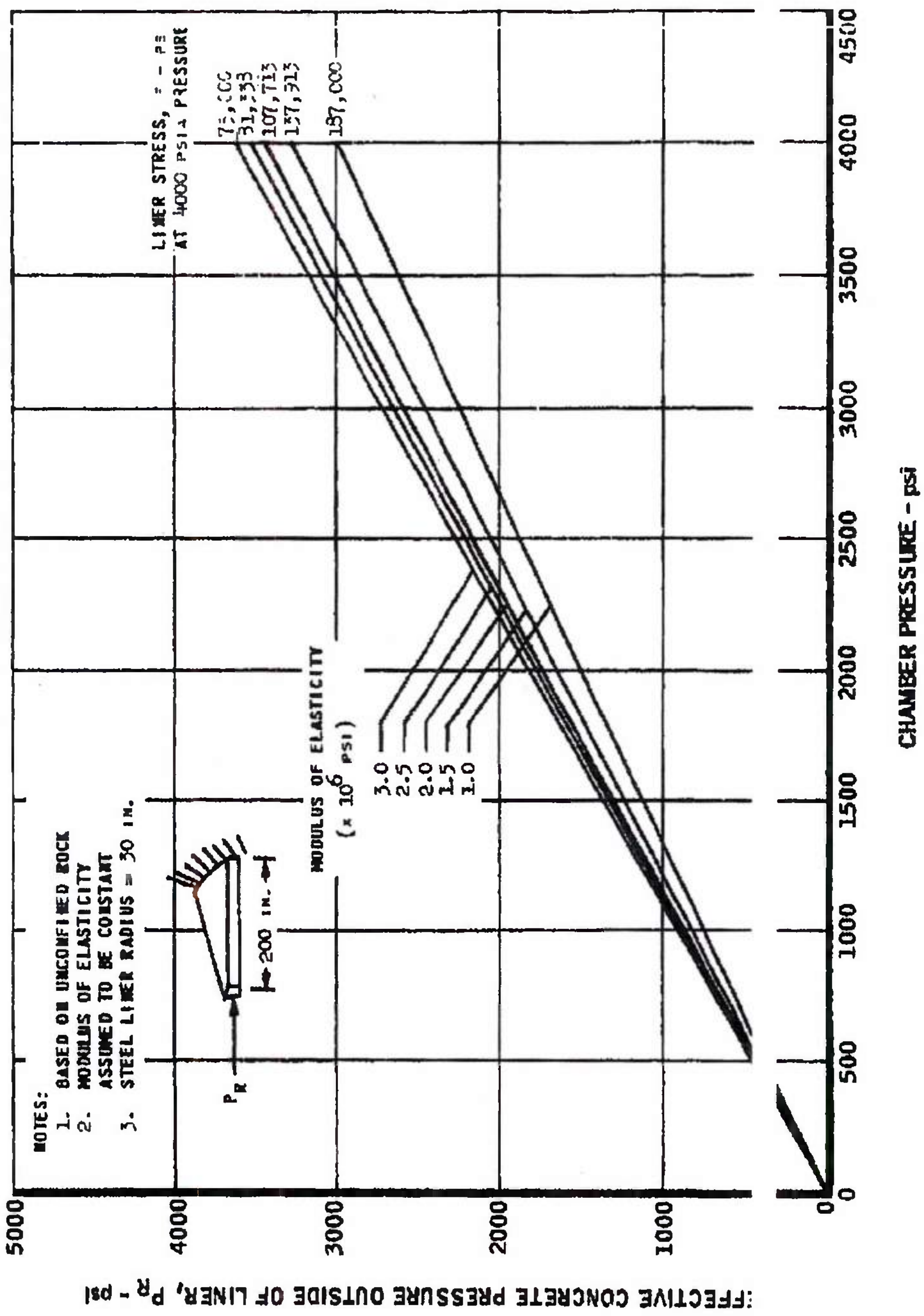

ROCK LOADING FOR UNDERGROUND AIR STORAGE CHAMBER
STEEL LINER THICKNESS = 0.187 inch

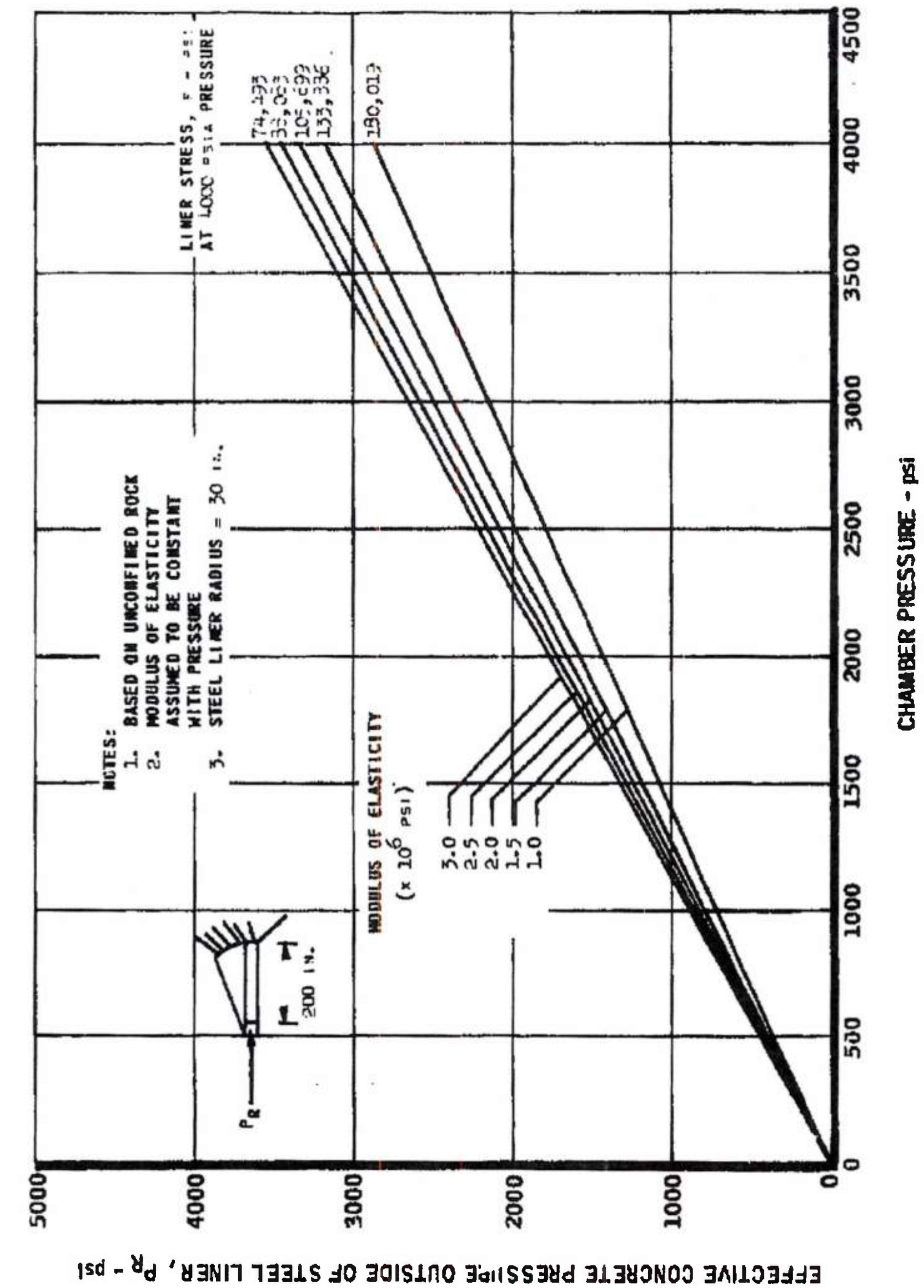

ROCK LOADING FOR UNDERGROUND AIR STORAGE CHAMBER
STEEL LINER THICKNESS = 0.438 inch

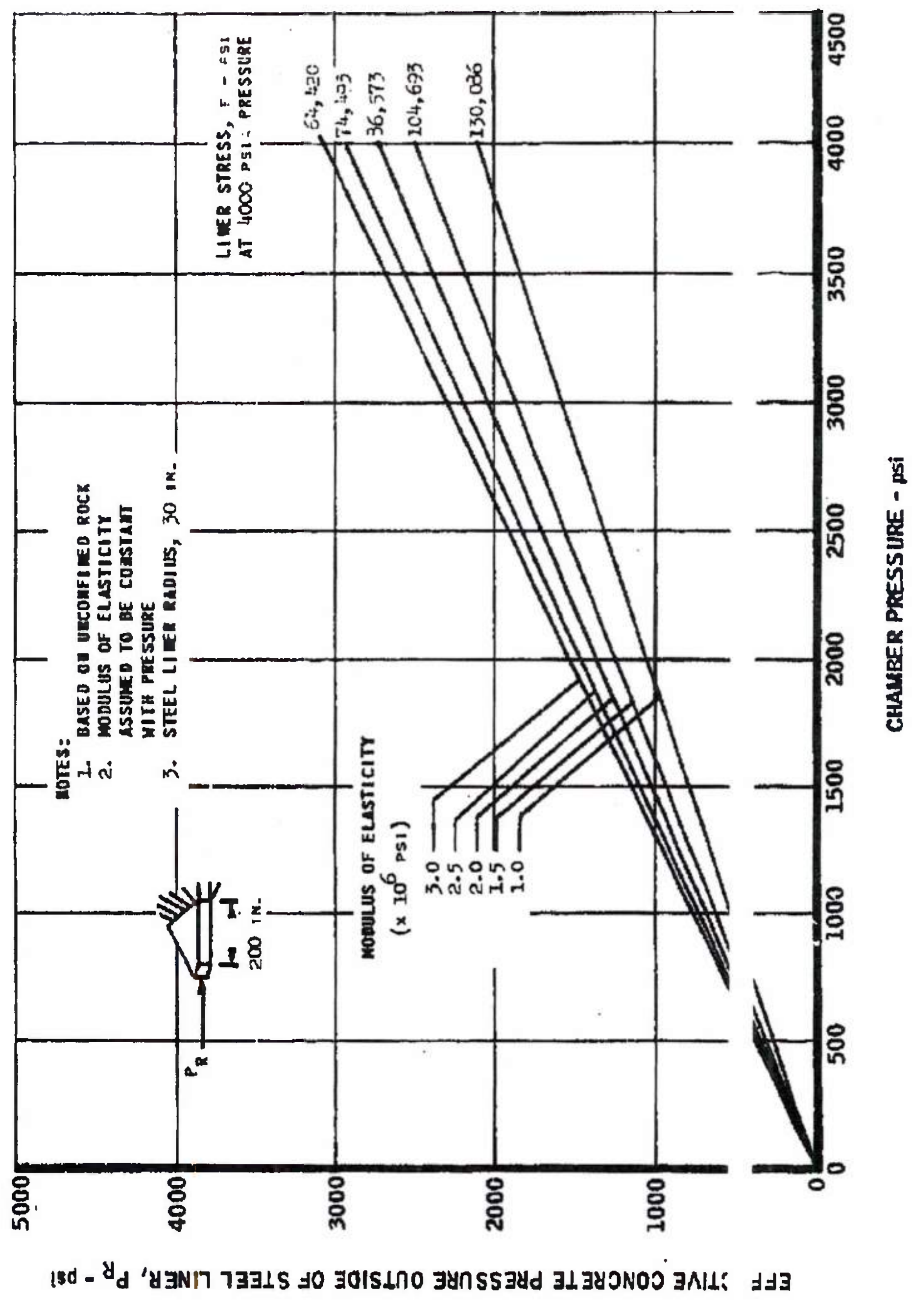

ROCK LOADING FOR UNDERGROUND AIR STORAGE CHAMBER
STEEL LINER THICKNESS = 1.12 inches

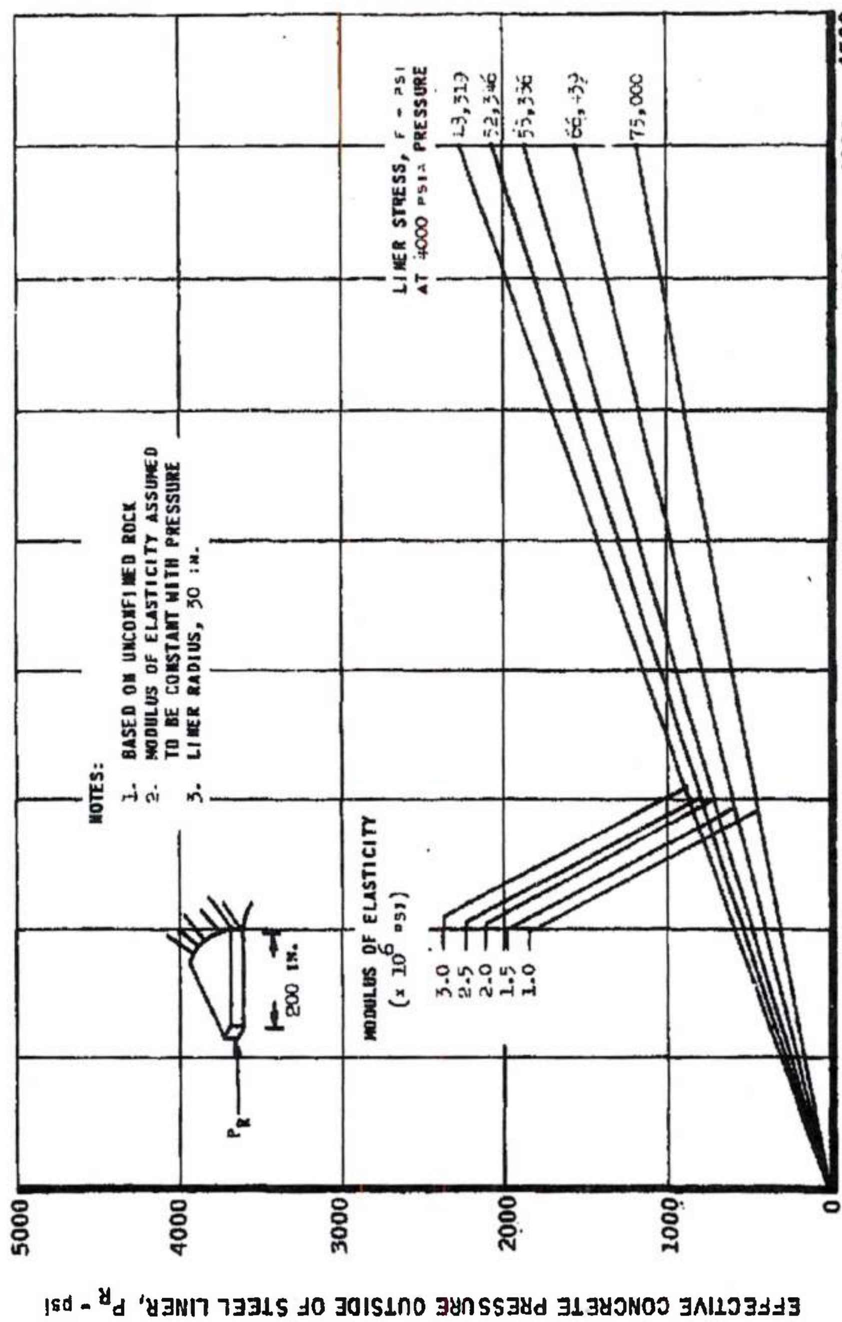

mitted to AEC-LVAO for preliminary approval. The construction pecification and detail drawings were then finalized, bound, and resubmitted fc final AEC approval prior to release for bidding.

5.2.5 Instrumentation

The instrumentation system, revised according to lates :indings, is designed to provide performance data on the chamber liner, surro ıding rock, the concrete plug, and the chamber overburden.

Figure 182 graphically displays the types and locations : the various strain and temperature transducers to be installed on the chamber iner, in the concrete, in the rock, and on the anchor rods.

Chamber Liner Coating

To help detect evidence of possible nodes in the rock an liner radial deflection during pressurization, three grades of stress-revealing :oatings will be applied to the liner inside surface. These coatings will be appl ıd to three separate longitudinal segments of the liner and will cover the antic ɔated chamber air temperature range from 60°F to 130°F, approximately. I addition to visibly revealing hysteresis in the chamber liner after cycling, th ;e coatings will provide a rough check on strain gage data.

Diametral and Axial Strain Measurement

A separate strain measuring subsystem to provide spot- heck confirmation of data being accumulated by the liner strain gages has been esigned and incorporated into the experimental chamber. The subsystem will onsist of diametral and axial strain rods equipped with high sensitivity line: potentiometers. Continuous monitoring of a null balance indicator, capable f being switched between the several strain rods, will provide evidence o: ıtrains during all phases of pressurization or pressure cycling of the chamber. he design of the strain rod system has been completed and is as shown in Figu: 183.

Page determined to be Unclassified
Reviewed Chief, RDD, WHS
IAW EO 13526, Section 3.5
Date: MAY 29 2015

UAS CHAMBER INSTRUMENTATION

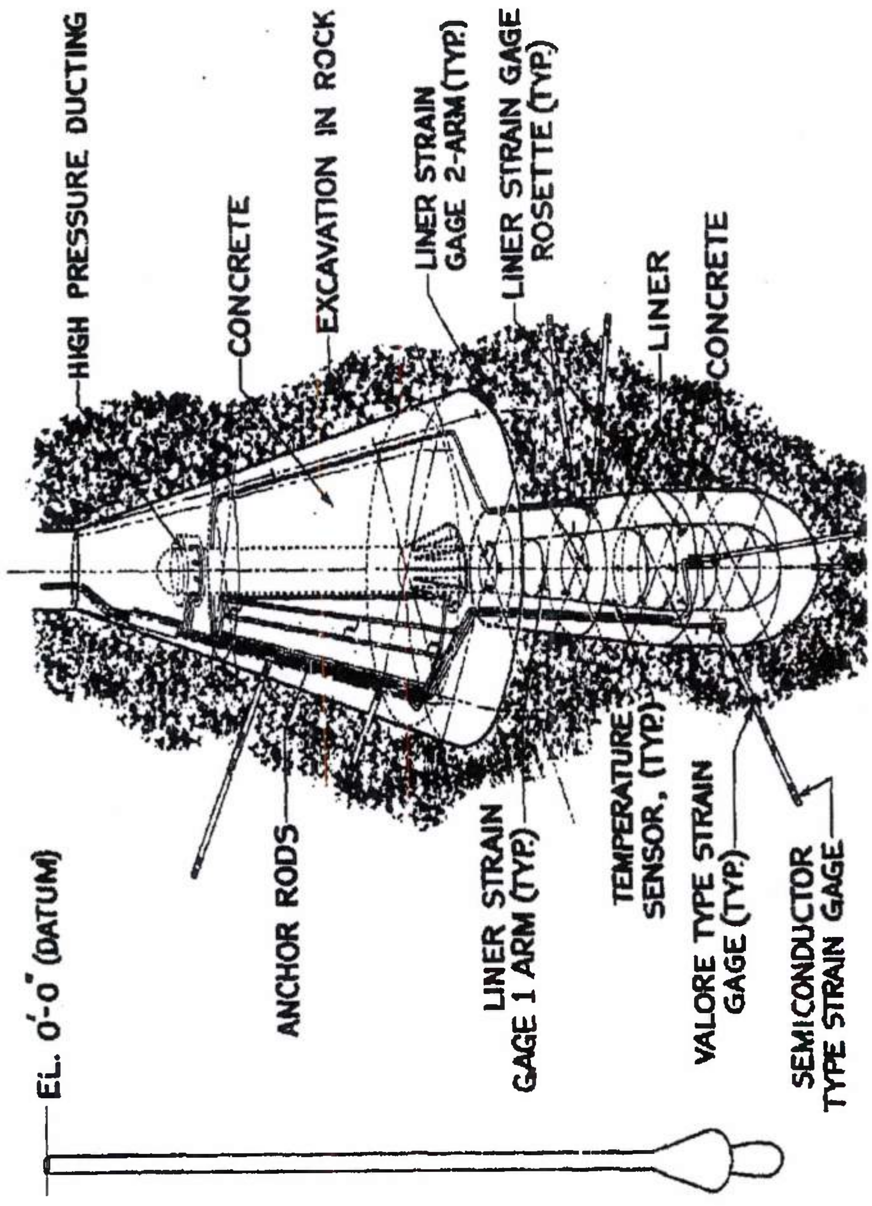

Reference: 232-4248-5A

TRANSDUCER RODS OF UAS CHAMBER INSTRUMENTATION

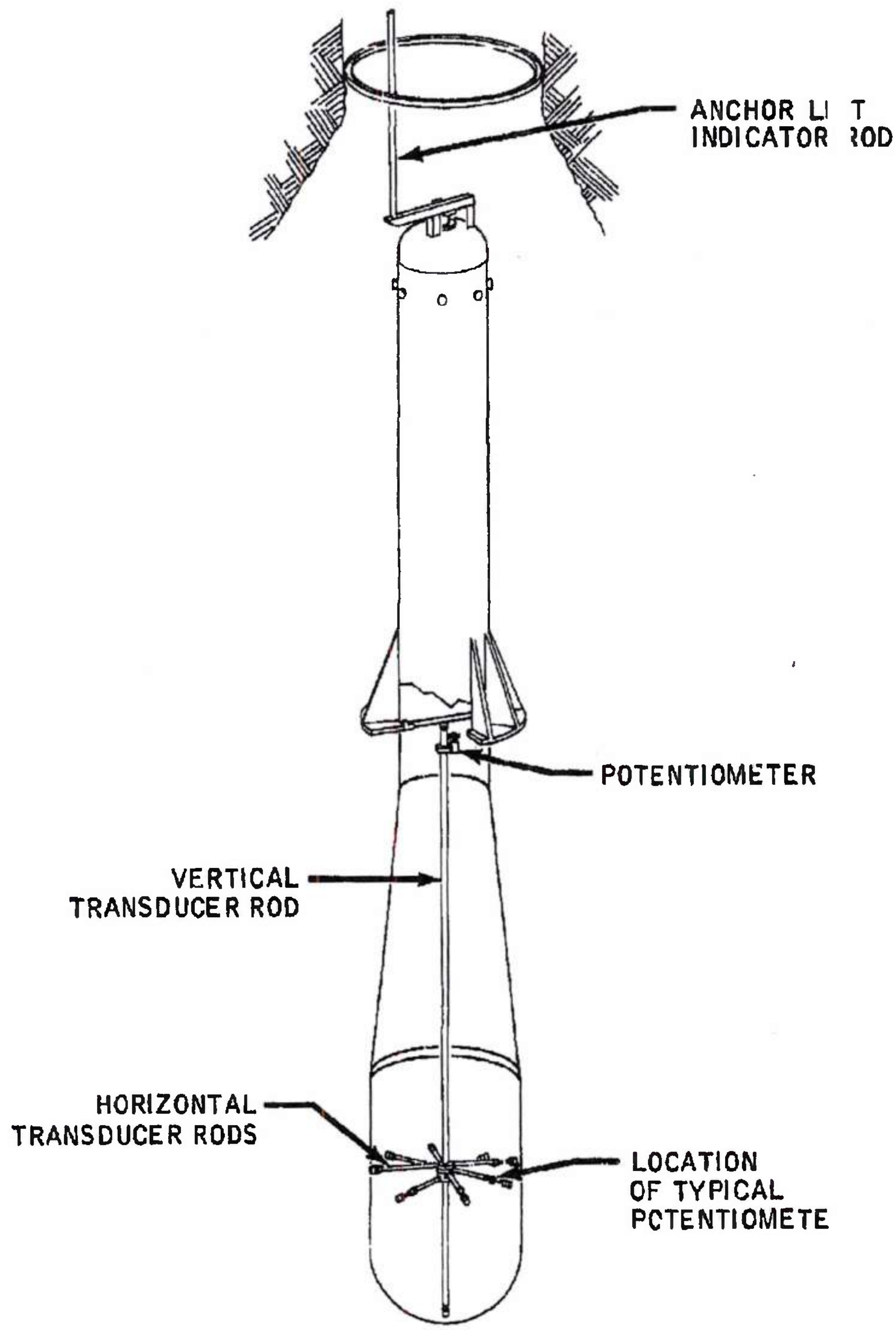

Chamber Anchor Lift Indicator

During pressurization of the chamber, the pressure loads will be transmitted to the surrounding rock formation. These loads will be transm ted downward through the bottom hemispherical section of the liner, radially th ugh the cylindrical and conical sections of the liner, and upward through the tra i-tion section of the liner assembly. The upward load will be through the anc r (plug) to a core of rock above the chamber.

To indicate vertical movement of the anchor, a mechanical indica ng device has been designed for attachment at the top of the transition section. This device (shown in Figure 183), elevating a fluid container at the top of the c m-ber access shaft, will actuate a draft gage type indicator in the control build ng.

REFERENCES

1. Lawrence Radiation Laboratory, "Tory IIC Data Book," Liver iore, California, Revised 12 October 1961, SECRET RESTRICTED ATA.

2. Marquardt Report 5854, "Preliminary Performance Bulletin f · the Marquardt Model MA50-XCA Ramjet Engine," 17 July 1961, S CRET RESTRICTED DATA.

3. Marquardt Report 5863, "Preliminary Performance Bulletin I ., 2 for the Marquardt Model MA50-XCA Ramjet Engine," 22 September 1 61, SECRET RESTRICTED DATA.

4. Marquardt Report 5872, "Preliminary Performance Bulletin I ., 3 for the Marquardt Nuclear Ramjet Engine," 1 December 1961, SECR: [RE-STRICTED DATA.

5. Marquardt Report P3015B, Book I of II, "Aircraft Nuclear Pr pulsion System Research and Development for 1961," SECRET RESTI CTED DATA.

6. NASA Report TMX-145, "Performance of a Mach 3.0 Externa Internal-Compression Axisymmetric Inlet at Mach Numbers from 2.0 › 3.5," by L. E. Stitt and R. J. Salmi, Washington, January 1960, CON: DENTIAL.

7. Marquardt Report PR 254-19Q, "Aircraft Nuclear Propulsion /stems, Project Pluto, Nineteenth Quarterly Progress Report," 29 Ap 1 1961, SECRET RESTRICTED DATA.

8. Marquardt Report PR 254-20Q, "Aircraft Nuclear Propulsion /stems, Project Pluto, Twentieth Quarterly Progress Report," 31 Jul 1961, SECRET RESTRICTED DATA

9. Marquardt Report PR 254-21Q, "Aircraft Nuclear Propulsion /stems, Project Pluto, Twenty-first Quarterly Progress Report," 31 : ecember 1961, SECRET RESTRICTED DATA

10. Chance Vought Report ARDC-TR-59-13, "Final Report, SLAM Nuclear Powered Missile Weapon System Study," Part XIII, "Propulsi 1," 28 February 1959, SECRET RESTRICTED DATA

REFERENCES (Continued)

11. Chance Vought Report AER/SLAM-S-250, "Aerothermodynamics for Pl[illegible]; Interim Summary Report," 3 October 1961, SECRET RESTRICTED DAT[illegible].

12. NACA Report TN2973, "Theoretical Pressure Distributions and Wave D[illegible]gs for Conical Boattails," by J. R. Jack, Washington, July 1953.

13. University of Illinois, Mechanical Engineering Dept. Report ME TN392-[illegible] "A Theory for Base Pressures in Transonic and Supersonic Flow," by H. H. Korst, R. H. Page, and M. E. Childs, March 1955.

14. Marquardt Report P3015B, Book II of II, "Aircraft Propulsion System R[illegible]-search and Development for 1961," SECRET RESTRICTED DATA.

15. NASA Report TN D-130, "Use of a Theoretical Flow Model to Correlate [illegible]ata for Film Cooling or Heating an Adiabatic Wall by Tangential Injection of Bases of Different Fluid Properties," J. E. Hatch and S. S. Papell, November 1959.

16. Marquardt Report 5873, "Preliminary Analysis of Lateral Vibrations of [illegible]he Pluto Reactor," 15 December 1961, SECRET RESTRICTED DATA.

17. Den Hartog, J. P., "Mechanical Vibration," 3rd Edition, McGraw-Hill [illegible]ook Company, Inc., New York, 1947.

18. Wachpress, E. L., "Thin Regions in Diffusion Theory Calculation," NU SCI ENGRG, Vol. 3, pp 186-200, February 1958.

19. Lawrence Radiation Laboratory, Tory IIC Memorandum No. 36, H. Rey[illegible]lds and M. Uthe, October 1960, SECRET RESTRICTED DATA.

20. AEC Report NYO-3075, "Calculation of the Penetration of Gamma Rays[illegible] by H. Goldstein and J. E. Wilkins, New York, 30 June 1954.

21. General Electric Report XDC 61-1-149, "Measured and Calculated Radi[illegible]ion Levels Within and Behind Beryllium Oxide," by P. W. Schrieber and F. D. Kodras, 15 December 1960, CONFIDENTIAL RESTRICTED DAT[illegible].

22. Nuclear Development Corporation of America Report NDA 2058-10, "Ga[illegible]ma Ray Penetration in Composite Slabs," M. H. Kalos, March 1957.

REFERENCES (Continued)

23. Atomics International Report NAA-SR-3719, "Grace-I, an IBM)4-709 Program Designed for Computing Gamma Ray Attenuation and leating in Reactor Shields," D. S. Duncan and A. B. Spier, April 1959.

24. Marquardt Report MR 20,140, "Radiation Analysis and Shieldi ; for the Nuclear Ramjet Engine System," 1 June 1961, SECRET REST :CTED DATA.

25. Marquardt Report PR 254-18Q, "Aircraft Nuclear Propulsion rstems, Project Pluto, Eighteenth Quarterly Progress Report," 19 No :mber 1960, SECRET RESTRICTED DATA.

26. Marquardt Report MR 5847, "Analysis of the In-Flight Contro: System for the Project Pluto Engine for the Year 1960," 15 April 1961, SECI :T RE-STRICTED DATA.

27. BuAer Report AE-61-411, "Dynamics of the Airframe," Septe iber 1952.

28. Marquardt Report MR 20,142, "Temperature Sensers," June '61.

29. Marquardt Report S-209, "Operation of Thermocouples Under Conditions of High Temperature and Nuclear Radiation," 15 June 1961.

30. Marquardt Report S-222, "Performance of Radiation Resistar Magnetic Amplifier Controls Under Fast Neutron and Gamma Irradiatic ," 30 August 1961.